

17TH

INTERNATIONAL SYMPOSIUM

**Water Management and Hydraulic
Engineering**


WMHE
2022

5055

14–18 SEPTEMBER 2022, SOPOT, POLAND

GDAŃSK UNIVERSITY OF TECHNOLOGY PUBLISHERS

CHAIRMAN OF EDITORIAL BOARD

Dariusz Mikielewicz

EDITOR OF SCIENTIFIC PUBLICATIONS

Michał Szydłowski

REVIEWERS

Lea Čubanová

Dalibor Carević

Katerina Donevska

Bojan Đurin

Magdalena Gajewska

Dariusz Gąsiorowski

Violeta Gjeshovska

Ivan Halkijević

Josif Josifovski

Milorad Jovanovski

Tomáš Julínek

Tomasz Kolerski

Katarzyna KołECKA

Neven Kuspilić

Goran Lončar

Stevco Mitovski

Domagoj Nakić

Eva Ocvirk

Ljupcho Petkovski

Jaromír Říha

Andrej Šoltész

Michał Szydłowski

Vladimir Vitanov

Katarzyna Weinerowska-Bords

Zbyněk Zchoval

Piotr Zima

LAYOUT AND COVER DESIGN

Ireneusz Jelonek

Published under the permission of the Rector of Gdańsk University of Technology Gdańsk University of Technology

The monograph “Water Management and Hydraulic Engineering – WMHE 2022” edited by Prof. Michał Szydłowski provides immediate open access to its content under the [Creative Commons BY 4.0 license](#).

Gdańsk University of Technology Publishing House, Gdańsk 2022

ISBN 978-83-7348-874-8

Symposium Chairmen

- Michał Szydłowski, Gdansk University of Technology, Faculty of Civil and Environmental Engineering, Gdansk, Poland
- Josif Josifovski, Ss. Cyril and Methodius University, Faculty of Civil Engineering, Skopje, North Macedonia
- Damir Bekić, University of Zagreb, Faculty of Civil Engineering, Zagreb, Croatia
- Andrej Šoltész, Slovak University of Technology, Faculty of Civil Engineering, Bratislava, Slovak Republic
- Helmut Habersack, University of Natural Resources and Life Sciences, Vienna, Austria
- Jaromír Říha, Brno University of Technology, Faculty of Civil Engineering, Brno, Czech Republic

Scientific Advisory Committee

- Adam Szymkiewicz, Magdalena Gajewska, Piotr Zima, Gdansk University of Technology, Faculty of Civil and Environmental Engineering, Gdansk, Poland
- Neven Kuspilić, Goran Lončar, Eva Ocvirk, Ivan Halkijević, University of Zagreb, Faculty of Civil Engineering, Zagreb, Croatia
- Petko Pelivanovski, Milorad Jovanovski, Ljupcho Petkovski, Katerina Donevska, Ss. Cyril and Methodius University, Faculty of Civil Engineering, Skopje, North Macedonia
- Andrej Šoltész, Silvia Kohnová, Štefan Stanko, Jana Frankovská, Slovak University of Technology, Faculty of Civil Engineering, Bratislava, Slovak Republic
- Petr Lichtneger, Hubert Holzmann, University of Natural Resources and Life Sciences, Vienna, Austria
- Jaromír Říha, Brno University of Technology, Faculty of Civil Engineering, Brno, Czech Republic

International Organizing Committee

- Michał Szydłowski, Alina Wargin, Dominika Kalinowska, Natalia Gietka, Patrycja Mikos-Studnicka, Andam Mustafa, Poland
- Damir Bekić, Dražen Vouk, Dalibor Carević, Croatia
- Vladimir Vitanov, Josif Josifovski, Zlatko Zafirovski, Stevcho Mitovski, Goce Taseski, North Macedonia
- Lea Čubanová, Slovak Republic
- Petr Lichtneger, Austria
- Tomáš Julínek, Czech Republic

Spis treści

PROGRAMME	8
PREFACE	10
Michał Szydłowski	
Climate Change and its Effect on Water Resources in Iraq	12
Nadhir Al-Ansari	
Water Resources and Challenging Issues in Agricultural Water Use in Turkiye	13
MAHMUT CETIN	
ABSTRACTS	15
I INTEGRATED WATER RESOURCES MANAGEMENT	
Efficiency of Methods for Solving System of Non-Linear Algebraic Equations in Numerical Solution of Diffusive Wave Equation.....	16
Wojciech Artichowicz, Dariusz Gąsiorowski	
Impact of Spatial Distribution of Precipitation in an Urban Catchment on the Quality of Rainfall-Runoff Hydrological Modeling	17
Patrycja Mikos-Studnicka, Michał Szydłowski	
Protection of the Baltic Sea by Processing Beach Wrack in the Reed Bed System	18
Alicja Kupczyk, Katarzyna Kotecka, Magdalena Gajewska	
II HYDRAULIC ENGINEERING AND ENVIRONMENTAL IMPACT	
Beach Construction and Nourishment in Croatia	19
Dalibor Carević, Tonko Bogovac, Damjan Bujak, Suzana Ilić, HANNA MILIČEVIĆ	
Calibration of the 3D Numerical Model for Scour around Riprap Sloping Structure	20
Antonija Harasti, Gordon Gilja	
Coastal Dynamics of the 233.6 a 282.4 km under Changing Climatic Conditions	21
Krzysztof Piłczyński	
Hydraulic Design of the Settling Basin for Irrigation System	22
Ante Kovač, Gordon Gilja, Robert Fliszar	
Ice-Structure Interaction in Photovoltaic Solar Panels Influencing by the Wind Velocity	23
Parisa Radan, Tomasz Kolarski	
Physical Models in Hydraulic Engineering	24
Jarosław Biegowski, Zuzanna Cuban, Jakub Malicki, Małgorzata Robakiewicz	
III SANITARY ENGINEERING AND SUSTAINABLE WATER USE	
Composition of the Urban Wastewater in Drainage Systems	25
Marta Kiraga, Oscar Herrera-Granados, Maurycy Naliwajko, Aleksander Staar, Laura Majewska, Adrianna Kluj, Michał Sieczych	
Prediction of Water Quality Index for Processes Improvement on Drinking Water Treatment Plant	26
Goran Volf, Ivana Sušanj Čule, Elvis Žic, Sonja Zorko	
IV HYDRAULIC STRUCTURES	
Bootstrap Resampling in Hydraulic Modelling Research.....	27
Aleksander Staar, Laura Majewska, Adrianna Kluj, Michał Sieczych, Maurycy Naliwajko, Marta Kiraga	
Filling Algorithm Proposals Using 3D Numerical Modelling for the Proper Exploitation of Navigation Shiplocks.....	28
Oscar Herrera-Granados, Marta Kiraga	
Hydraulic Research on Physical Weir Model	29
Maurycy Naliwajko, Michał Sieczych, Marta Kiraga, Aleksander Staar, Laura Majewska, Adrianna Kluj	
Hydrodynamics in the Presence of Groynes – Physical and Numerical Modelling	30
Jakub Malicki, Jarosław Biegowski, Zuzanna Cuban, Małgorzata Robakiewicz	

Impact of the Bridge Piers Shape on Hydraulic Flow Conditions – an Experimental Study	31
Tomasz Tymiński	
V ECOHYDROLOGY AND WATER BODY PROTECTIONS	
Differentiation of Hydrochemical Conditions of Surface Waters and Groundwater in Selected Peatlands of the Slowinski National Park (Northern Poland)	32
Marlena Pawłowska, Zuzanna Lipińska, Iwona Bubak, Roman Cieśliński	
Short and Long-Term Hydrological Forecasts for Agricultural Basins Based on the Swat Model	33
Dominika Kalinowska, Paweł Wielgat, Piotr Zima	
The Importance of Controlling Point Sources of Pollution within Small Catchment Areas	34
Marija Leko-Kos, Tamara Brleković, Lidija Tadić	
Traces Studies of Exchange Water in Breeding Pools	35
Paweł Wielgat	
VII CLIMATE CHANGE AND FLOOD RISK MANAGEMENT	
Climate Change and the Occurance of Floods in Gdańsk.....	36
Jacek Barańczuk, Katarzyna Barańczuk, Martina Zeleňáková, Hany F. Abd-Elhamid	
Flood Simulation Model and Risk Analysis of Huaihe River (Lutaiz to Huainan) China.....	37
Umar Farooq, Tian Fuchang, Yuan Ximin	
Modeling Urban Flood with HEC-RAS 6.1 in Erbil Kurdistan, Iraq	38
Andam Mustafa, Michał Szydłowski	
VIII GEOTECHNICAL ASPECTS OF HYDRAULIC ENGINEERING	
Simulation of Water Table Fluctuations and Lateral Outflow from a Soil Profile Using a 1D Vadose Zone Model.....	39
Anna Gumuła-Kawęcka, Vipin Kumar Oad, Adam Szymkiewicz, Jirka Šimůnek, Beata Jaworska-Szulc	
EXTENDED ABSTRACTS	40
I INTEGRATED WATER RESOURCES MANAGEMENT	
The Effect of Dem Resolution on the Calculation of the LS Factor Entering the Universal Soil Loss Equation	41
Matúš Tomaščík, Michaela Danáčová, Milica Aleksić, Roman Výleta	
II HYDRAULIC ENGINEERING AND ENVIRONMENTAL IMPACT	
Discussion on the Uncertainties in Flood Zoning on the Example of the Rusava River.....	44
Jaromir Říha, David Duchan	
Evaluation of Wind Energy Potential in South Baltic Sea	47
Michał Bojan, Piotr Szmytkiewicz	
Mathematical Model of the Eutrophication of the Baltic Sea in the Bay of Puck Region	49
Piotr Zima	
Scour around Breakwater – Canal through Vistula Spit. Preliminary Analysis of Causes. Lesson Learned	52
Bartosz Zabłocki, Piotr Szmytkiewicz	
Sensitivity Analysis of Acoustic Doppler Velocimeter Parameters for Flume Experiments	54
Robert Fliszar, Luka Drandić, Gordon Gilja	
IV HYDRAULIC STRUCTURES	
Sensitivity Analysis of DL Breach Model for Simulation Embankment Dam Breaching Due to Internal Erosion	57
Stanislav Kotaška, Jaromír Říha	
V ECOHYDROLOGY AND WATER BODY PROTECTIONS	
Dispersion Analysis Using Dye Test at a Small Stream.....	59
Jaromír Říha, Tomáš Julínek, Stanislav Kotaška	

VII CLIMATE CHANGE AND FLOOD RISK MANAGEMENT

Future Change in Low Flow Characteristics in Selected Gauging Stations of Slovakia	61
Zuzana Sabová, Silvia Kohnová, Zuzana Némětová	
Improvement of Surface Erosion Resistance of Silty Sand Soil by Biopolymer-Based Treatment	64
Aleksandra Nikolovska Atanasovska, Josif Josifovski, Bojan Susinov	
Rainwater Management in Gdansk – Meteorological and Hydrological Monitoring.....	66
Wojciech Szpakowski	

ARTICLES 68

I INTEGRATED WATER RESOURCES MANAGEMENT

Application of Simulation Models for Management of Complex Water Resources System.....	69
Stevo Mitovski, Frosina Panovska, Ljupcho Petkovski	

II HYDRAULIC ENGINEERING AND ENVIRONMENTAL IMPACT

Dependency of the Whitemapping Parameter on Model Resolution Settings in the Eastern Adriatic Sea.....	80
Damjan Bujak, Dalibor Carević, Tin Kulić, Tonko Bogovac	
Estimating Changes in Gravel Beach Slope Using a Video Monitoring System – a Case Study of the Ploče Beach in Rijeka, Croatia	88
Hanna Miličević, Damjan Bujak, Dalibor Carević, Tin Kulić	
Fish Pass on the Turiec River, Slovakia	96
Lea Čubanová, Peter Dušička, Ján Rumann, Vladimír Polák	
Flood Protection Measures in Lowland Regions	103
Andrej Šoltész, Jakub Mydla, Martin Orfánus	
Hydraulic Capacity Analysis of an Existing Combined Sewer System Using Storm Water Management Model.....	109
Nikola Krstovski, Goce Taseski	
Positive Effects of Variable Frequency Driven Pump.....	115
Tin Kulić, Hanna Miličević, Ivan Halkijević, Hana Posavčić	
Wind Wave Induced Impulsive Pressure Load on Reinforced Concrete Deck Structure	124
Tin Kulić, Hanna Miličević, Goran Lončar, Katarina Licht	

III SANITARY ENGINEERING AND SUSTAINABLE WATER USE

Comparison of Efficiency Two Polyaluminiumchloride Coagulants at Surface Water Treatment	133
Danka Barloková, Ján Ilavský	
Numerical Analysis to Determine the Technical Water Losses in a Water Supply System	139
Goce Taseski, Nikola Krstovski	
Optimization of Circulating Flow Sono-Electrochemistry for Mineral Oil Removal	146
Hana Posavčić, Dražen Vouk, Katarina Licht	
Removal of Chlorinated Pesticides From Water Using Granular Activated Carbon	151
Ján Ilavský, Danka Barloková, Michal Marton, Michal Kunštek	
The Influence of Different Process Parameters on the Efficiency of Organic Load Removal from Oily Wastewater Using Electrochemical Treatment	159
Dražen Vouk, Morana Drušković, Sara Banovec, Dajana Kučić Grgić	
The Influence of Particle Size Distribution of Sewage Sludge Ash and Clay on the Compressive Strength of Bricks	167
Dražen Vouk, Anđelina Bubalo, Domagoj Nakić, Nina Štirmer	
The Influence of the Initial Concentration of Heavy Metals and the Electrode Material on the Efficiency of Electrocoagulation Water Treatment	174
Katarina Licht, Hana Posavčić, Ivan Halkijević, Mislav Markić, Josipa Zlomislíć	
Ultrasound Assisted Electrocoagulation Removal of Heavy Metals from Water	184
Diana Smoković, Hana Posavčić, Katarina Licht, Ivan Halkijević	

IV HYDRAULIC STRUCTURES

- Optimization of the Operation of the Gabčíkovo Ship Locks Filling and Emptying System
by Differential Evolution 191
Peter Šulek, Daniel Buček
- Prognosis Analysis of Arch Dam Behavior by Hybrid Model 198
Frosina Panovska, Stevcho Mitovski, Ljupcho Petkovski

V ECOHYDROLOGY AND WATER BODY PROTECTIONS

- Hydrometric and Water Quality Properties of the Medulin Pond (Republic of Croatia)..... 205
Ivana Sušanj Čule, Goran Volf, Nevenka Ožanić, Igor Ružić

VI RIVER BASIN RESTORATION STRATEGIES AND EXPERIENCES

- Deep Water – Managed Aquifer Recharge (Mar) in Slovakia 214
Andrej Šoltész, Michaela Červeňanská, Jakub Mydla, Dana Baroková
- Development of Green Zones on Technical University of Kosice 222
Martina Zeleňáková, Mária Hlinková

VII CLIMATE CHANGE AND FLOOD RISK MANAGEMENT

- Analysis of the Change of Precipitation with Short Duration in Macedonia 227
Violeta Gjeshovska, Goce Taseski, Bojan Ilioski
- Climate Change, Water Resources and Tourism 234
Antonio Dekanić, Barbara Karleuša, Ivana Sušanj Čule
- Hydrologic Regime of the Torysa River Basin 243
Patrik Nagy, Martina Zeleňáková, Katarzyna Barańczuk, Jacek Barańczuk
- Slope Instability for Different Rainfall Intensities 249
Bojan Susinov, Josif Josifovski, Vladimir Vitanov

Programme

DATE	TIME	TOPICS AND THEMES	PRESENTATION TITLE	AUTHORS
15 SEPTEMBER 2022	8:00–09:00	Registration of participants		
	9:00–09:30	Opening ceremony		
	9:30–10:30	Keynote lecture – Prof. Nadhir Al-Ansari, Iraq, Sweden		
	10:30–11:00	Coffee break		
	11:00–13:00	First session (oral presentations), Chairman: Prof. Jaromír Říha		
	11:00–11:15	Integrated Water Resources Management	<i>Application of Simulation Models for Management of Complex Water Resources System</i>	Stevcho Mitovski, Frosina Panovska, Ljupcho Petkovski
	11:15–11:30	Hydraulic Engineering and Environmental Impact	<i>Physical Models in Hydraulic Engineering</i>	Jarosław Biegowski, Zuzanna Cuban, Jakub Malicki, Małgorzata Robakiewicz
	11:30–11:45		<i>Beach Construction and Nourishment in Croatia</i>	Dalibor Carević, Tonko Bogovac, Damjan Bujak, Suzana Ilić, Hanna Miličević
	11:45–12:00		<i>Evaluation of Wind Energy Potential in South Baltic Sea</i>	Michał Bojan, Piotr Szmytkiewicz
	12:00–12:15		<i>Coastal Dynamics of the 233.6 a 282.4 km under Changing Climatic Conditions</i>	Krzysztof Piłczyński
	12:15–12:30		<i>Flood Protection Measures in Lowland Regions</i>	Andrej Šoltész, Jakub Mydla, Martin Orfánus
	12:30–12:45		<i>Scour around Breakwater – Canal through Vistula Spit. Preliminary Analysis of Causes Lesson Learned</i>	Bartosz Zablocki, Piotr Szmytkiewicz
	12:45–13:00		<i>Positive Effects of Variable Frequency Driven Pump</i>	Tin Kulić, Hanna Miličević, Ivan Halkijević, Hana Posavčić
	13:00–14:30		LUNCH (full and one-day participants are invited)	
	14:30–16:30	SECOND SESSION (oral presentations), Chairman: Prof. Andrej Šoltész		
	14:30–14:45	Hydraulic Engineering and Environmental Impact	<i>Estimating Changes in Gravel Beach Slope Using a Video Monitoring System – a Case Study of the Ploče Beach in Rijeka, Croatia</i>	Hanna Miličević, Damjan Bujak, Dalibor Carević, Tin Kulić
	14:45–15:00		<i>Fish Pass on the Turiec River, Slovakia</i>	Lea Čubanová, Peter Dušička, Ján Rumann, Vladimír Polák
	15:00–15:15		<i>Dependency of the Whitecapping Parameter on Model Resolution Settings in the Eastern Adriatic Sea</i>	Damjan Bujak, Dalibor Carević, Tin Kulić, Tonko Bogovac
	15:15–15:30		<i>Wind Wave Induced Impulsive Pressure Load on Reinforced Concrete Deck Structure</i>	Tin Kulić, Hanna Miličević, Goran Lončar, Katarina Licht
	15:30–15:45		<i>Discussion on the Uncertainties in Flood Zoning</i>	Jaromír Říha, David Duchan
15:45–16:00	Hydraulic structures	<i>Hydrodynamics in the Presence Of Groynes – Physical and Numerical Modelling</i>	Jakub Malicki, Jarosław Biegowski, Zuzanna Cuban, Małgorzata Robakiewicz	
16:00–16:15		<i>Sensitivity Analysis of DI Breach Model for Simulation Embankment Dam Breaching Due to Internal Erosion</i>	Stanislav Kotaška, Jaromír Říha	
16:15–16:30	Ecohydrology and Water Body Protections	<i>Dispersion Analysis Using Dye Test at A Small Stream</i>	Jaromír Říha, Tomáš Julínek, Stanislav Kotaška	
16:30–17:00	Coffee break			
17:00–18:00	Poster session			
20:00–00:00	Dinner (full participants are invited)			

DATE	TIME	TOPICS AND THEMES	PRESENTATION TITLE	AUTHORS	
16 SEPTEMBER 2022	8:00–09:30	REGISTRATION OF PARTICIPANTS			
	9:30–10:30	KEYNOTE LECTURE – Prof. Mahmut Cetin, Turkey			
	10:30–11:00	COFFEE BREAK			
	11:00–13:00	FIRST SESSION (oral presentation), Chairman: Josif Josifovski			
	11:00–11:15	Sanitary Engineering and Sustainable Water Use	<i>The Influence of Different Process Parameters on the Efficiency of Organic Load Removal From Oily Wastewater Using Electrochemical</i>		Dražen Vouk, Morana Drušković, Sara Banovec, Dajana Kučić Grgić
	11:15–11:30		<i>The Influence of Particle Size Distribution of SSA and Clay on the Compressive Strength of Bricks</i>		Dražen Vouk, Anđelina Bubalo, Domagoj Nakić, Nina Štímer
	11:30–11:45		<i>The Influence of the Initial Concentration of Heavy Metals and the Electrode Material on the Efficiency of Electrocoagulation Water Treatment</i>		Katarina Licht, Hana Posavčić, Ivan Halkijević, Mislav Markić, Josipa Zlomislčić
	11:45–12:00		<i>Optimization of Circulating Flow Sono-Electrochemistry for Mineral Oil Removal</i>		Hana Posavčić, Dražen Vouk, Katarina Licht
	12:00–12:15	Ecohydrology and Water Body Protections	<i>Differentiation of Hydrochemical Conditions of Surface Waters and Groundwater in Selected Peatlands of the Slowinski National Park (Northern Poland)</i>		Marlena Pawłowska, Zuzanna Lipińska, Iwona Bubak, Roman Cieśliński
	12:15–12:30		<i>Hydrometric and Water Quality Properties of the Medulin Pond (Republic of Croatia)</i>		Ivana Sušanĳ Čule, Goran Volf, Nevenka Ožanić
	12:30–12:45	Hydraulic structures	<i>Hydraulic Research on Physical Weir Model</i>		Maurycy Naliwajko, Michał Sieczyk, Marta Kiraga, Aleksander Staar, Laura Majewska, Adrianna Kluj
	12:45–13:00		<i>Prognosis Analysis of Arch Dam Behavior by Hybrid Model</i>		Frosina Panovska, Stevcho Mitovski, Ljupcho Petkovski
	13:00–14:30	LUNCH (full and one-day participants are invited)			
	14:30–16:30	SECOND SESSION (oral presentation), Chairman: Dalibor Carević			
	14:30–14:45	River Basin Restoration Strategies and Experiences	<i>Deep Water – Managed Aquifer Recharge (Mar) in Slovakia</i>		Andrej Šoltész, Michaela Červeňanská, Jakub Mydla, Dana Baroková
	14:45–15:00		<i>Development of Green Zones on Technical University of Košice</i>		Martina Zeleňáková, Mária Hlinková
	15:00–15:15	Climate Change and Flood Risk Management	<i>Improvement of Surface Erosion Resistance of Silty Sand Soil by Biopolymer-Based Treatment</i>		Aleksandra Nikolovska Atanasovska, Josif Josifovski, Bojan Susinov
	15:15–15:30		<i>Modeling Urban Flood with Hec-Ras 6.1 in Erbil Kurdistan, Iraq</i>		Andam Mustafa, Michał Szydłowski
	15:30–15:45		<i>Hydrologic Regime of the Torysa River Basin</i>		Patrik Nagy, Martina Zeleňáková
	15:45–16:00		<i>Climate Change, Water Resources and Tourism</i>		Antonio Dekanić, Barbara Karleuša, Ivana Sušanĳ Čule
	16:00–16:15		<i>Climate Change and the Occurance of Floods in Gdańsk</i>		Jacek Barańczuk, Katarzyna Barańczuk, Martina Zeleňáková, Hany F. Abd-Elhamid
	16:15–16:30		<i>Rainwater Management in Gdansk – Meteorological and Hydrological Monitoring</i>		Wojciech Szpakowski
	16:30–17:00	Coffee break			
17:00–18:00	Poster session				
18:00–18:30	Closing ceremony				
20:00–00:00	Gala dinner (full participants are invited)				

PREFACE

MICHAŁ SZYDŁOWSKI¹

¹ Gdańsk University of Technology (Gdańsk Tech), Faculty of Civil and Environmental Engineering
e-mail: mszyd@pg.edu.pl

The 17th International Conference on Water Management and Hydraulic Engineering (WMHE 2022) is organized by the Faculty of Civil and Environmental Engineering at the Gdańsk University of Technology (Gdańsk Tech), from 14–18 September 2022, in Sopot, Poland. The WMHE 2022 conference is the next in the series of International Symposiums in the field of Water Management and Hydraulic Engineering, organized with the participation of the Gdańsk University of Technology (Poland), University of Zagreb (Croatia), Slovak University of Technology in Bratislava (Slovak Republic), Ss. Cyril and Methodius University in Skopje (North Macedonia), University of Natural Resources and Applied Life Sciences in Vienna (Austria) as well as Brno University of Technology (Czech Republic).

The main goal of the conference is to share transboundary and interdisciplinary knowledge and experience between scientists and experts from Central Europe, from older and new EU member states as well as from South-East European candidate countries. In 1976 the first conference of this type was organized as a bilateral activity between the faculties of Gdańsk University and Zagreb University. Since 1998, the Slovak University of Technology, the Ss. Cyril and Methodius University in Skopje and the BOKU University of Natural Resources and Applied Life Sciences, Vienna, have joined this biannual conference series. In 2013 Brno University of Technology, Czech Republic, joined the steering group of WMHE.

The aim of the symposium is to encourage and facilitate communication between scientists, engineers and professionals involved in work related to the multidisciplinary tasks of water management. This Conference provided a setting for discussing recent developments in a wide variety of topics including: Integrated Water Resources Management, Hydraulic Engineering and Environmental Impact, Sanitary Engineering and Sustainable Water Use, Hydraulic structures, Ecohydrology and Water Body Protections, River Basin Restoration Strategies and Experiences, Climate Change and Flood Risk Management, Geotechnical aspects of Hydraulic Engineering. During the conference, two plenary lectures were delivered by invited professors from Iraq and Turkey. The purpose of inviting lecturers from outside Europe was to raise the significance and range of the symposium, as well as to establish new scientific contacts.

The conference was announced on the Internet via the creation of a dedicated web site <http://wmhe2022.wilis.pg.edu.pl>. All accepted abstracts and papers are published in Proceedings of WMHE 2022 in digital form. The conference has Patronage of Rector of the Gdańsk University of Technology. The conference fee is co-financed by Gdańsk Tech program *Carbonium Supporting Conferences*.

Symposium Chairmen

- Michał Szydłowski, Gdańsk University of Technology, Faculty of Civil and Environmental Engineering, Gdańsk, Poland
- Josif Josifovski, Ss. Cyril and Methodius University, Faculty of Civil Engineering, Skopje, North Macedonia
- Damir Bekić, University of Zagreb, Faculty of Civil Engineering, Zagreb, Croatia
- Andrej Šoltész, Slovak University of Technology, Faculty of Civil Engineering, Bratislava, Slovak Republic
- Helmut Habersack, University of Natural Resources and Life Sciences, Vienna, Austria
- Jaromír Říha, Brno University of Technology, Faculty of Civil Engineering, Brno, Czech Republic

The Editors and WMHE 2022 Chairmen would like to express their warm gratitude to the members of the **International Organizing Committee**: Alina Wargin, Dominika Kalinowska, Natalia Gietka, Patrycja Mikos-Studnicka, Andam Mustafa (Poland), Dražen Vouk, Dalibor Carević (Croatia), Vladimir Vitanov, Zlatko Zafirovski, Stevcho Mitovski, Goce Taseski (North Macedonia), Lea Čubanová (Slovak Republic), Tomáš Julínek (Czech Republic).

To manage the tasks related to this Conference an **International Scientific Advisory Committee** was set up: Adam Szymkiewicz, Magdalena Gajewska, Piotr Zima (Poland), Neven Kuspilić, Goran Lončar, Eva Ocvirk, Ivan Halkijević (Croatia), Petko Pelivanovski, Milorad Jovanovski, Ljupcho Petkovski, Katerina Donevska (North Macedonia), Andrej Šoltész, Silvia Kohnová, Štefan Stanko, Jana Frankovská (Slovak Republic), Petr Lichtneger, Hubert Holzmann (Austria), Jaromír Říha (Czech Republic).

Special thanks should go to Prof. Krzysztof Wilde, the Rector of Gdańsk Tech, and to Prof. Joanna Żukowska, the Dean of the Faculty of Civil and Environmental Engineering, for their support which has greatly aided the preparation of the

conference on the University grounds. The members of the Organizing Committee are also grateful to all members of the staff of the Faculty of Civil and Environmental Engineering for their efforts in preparing the conference and technical visit. Finally, special acknowledgements are extended to the reviewers of submitted papers for their aid in producing the Conference Proceedings. All abstracts and papers have been double peer reviewed before final publication. Initially, the abstracts were read and selected by the conference Scientific Committee as possible papers for the conference.

CLIMATE CHANGE AND ITS EFFECT ON WATER RESOURCES IN IRAQ

NADHIR AL-ANSARI¹

¹ Lulea University of Technology, Department of Civil, Environmental and Natural Resources Engineering; Sweden
e-mail: nadhir.alansari@ltu.se

Abstract

Iraq is in the north-eastern part of the Middle East. This area is considered as arid to semi-arid region. Iraq relies in its water resources on the waters of the Tigris and Euphrates Rivers and their tributaries, and it is located at the lower part of the catchment area of these rivers. Long term records of the average annual flow that enters Iraq from these rivers is about 84 BCM. About 30 BCM from the Euphrates, 22.2 BCM from the Tigris, 24.78 BCM from tributaries and about 7 BCM from side valleys between Iraq and Iran. The flow of these rivers is decreasing now due to climate change and hydrological projects established in the upper parts of the catchment. It is expected that precipitation will decrease 15–25% during this century and therefore, the flow of the Tigris and Euphrates Rivers will be reduced by 29–73%. The decrease of precipitation and flow of rivers will cause a grave depletion of ground water resources. Turkey is trying to finish building 22 dams and 19 hydropower stations within a project known as GAP. Iran built 12 dams and diverted the flow of some tributaries inside Iran and blocked all the valleys that contributes water from its land to Iraq. For these reasons, Iraq is experiencing shortages in its water resources and there is some sort of friction and conflict between riparian countries within the Tigris and Euphrates basins because each country tries to secure its water resources. The factors affecting the water resources within these basins are Water scarcity, Climate change and Hydrological projects, population growth rate, Energy issues, Water mismanagement, Economic changes, Expansions of projects and technology, Political issues, international water laws and public awareness. To solve the problem of water scarcity in Iraq they should reach an agreement with riparian parties and develop Long-term Strategy that should take care of: Rehabilitating of dams, barrages & pump stations, Improving the efficiency of diversion and supply, Using of Nonconventional Water Resources, Irrigation modernization using suitable techniques, developing a public awareness program and establishing an agenda for training.

Keywords: Tigris River, Euphrates River, water management, Iraq.

WATER RESOURCES AND CHALLENGING ISSUES IN AGRICULTURAL WATER USE IN TURKIYE

MAHMUT CETIN¹

¹ University of Cukurova, Faculty of Agriculture, Department of Agricultural Structures and Irrigation; Adana, Turkiye
e-mail: mcet64@cu.edu.tr

Abstract

Turkiye occupies geographically a unique place and connects the two continents, viz., Europe and the Middle East. It has a varied landscape as well as climate, which, in turn, reflects various spatiotemporal characteristics of its water resources. These diverse characteristics present a challenge and an opportunity to researchers, policymakers, practitioners and the agencies responsible for water resource management, the agricultural sector, the energy sector, the municipalities, the departments of tourism as well as those involved in environmental and ecosystem management. Due to its location, Turkiye is known as the realm of ecologies since there exist seven distinct climatological regions in the country. In this context, the Marmara, Aegean, Mediterranean, and South-eastern Anatolia regions of Turkiye are characterized mainly by the dry summer of sub-tropical Mediterranean climate. However, the humid-temperate climate type prevails only in the Black Sea region, but the continental inland climates in Central Anatolia and Eastern Anatolia regions. Since Turkiye is situated in a transition zone, it is under the influence of various atmospheric disturbances and weather types originating from polar and tropical regions. In addition to the influence of various atmospheric disturbances and weather types originating from polar and tropical regions; among others, the complexity of topographical features, rapid elevation changes within short distances, land-sea interactions, and finally thermodynamic influences and modifications are the primary causes of evident climate diversity in Turkiye. Therefore, the spatial and temporal distribution of precipitation is all the time uneven across the country, changing from 325 mm (in Konya, Central Anatolia) to 2312 mm (in Rize, Eastern Black sea region) at the point scale.

Until recently, areal mean precipitation was recorded as 642 mm. Current studies have shown that areally averaged precipitation is about 574 mm, indicating an almost 12% decrease in average precipitation. In addition to this reduction, with the increase in the population and demand, water scarcity has further accelerated, making water a more vital and/or critical element, particularly in some river basins such as Akarcay and Konya basins. The decrease in precipitation may have resulted from both the phenomenon of climate change and the calculation technique of mean areal rainfall over the country.

Surface water hydrology in Turkiye is a greatly challenging problem as it has a share of 84% of the total exploitable water potential of the country. However, the share of groundwater resources is only 16%. In this context, the surface water resources of Turkiye are divided between 25 river basins; most stay within the country. Five of the 25 river basins are transboundary where Turkiye is either the upstream country or the downstream country. Due to uneven precipitation distribution over the basins, the topography, morphometry, climatology, meteorology and land use-land cover characteristics of the basins and many other factors, not surprisingly, catchment yield (min-max: 1.29-22.85 l/s-km²), run-off coefficient (0.085-0.837) and water potential (40.6 mm-720.6) of the river basins differ from each other. Nonetheless, Turkiye's water resources potential was estimated by aggregating hydrometric network data -provided by the national water agency State Hydraulic Works (DSI)- acquired in the river basin level in the long term. As seen in Fig. 1, the gross surface water potential of Turkiye is 186.6 km³ (238.0 mm) of which 5.8 km³ (7.4 mm) is the contribution from neighbouring countries, resulting in a runoff coefficient (SW/P) of 0.40. However, until 2018, it was recorded officially that the runoff coefficient of Turkiye was about 0.37. This indicates an increase in the runoff volume. Recently, the frequency and magnitude of extreme values such as floods and heavy precipitation have tended to increase. Therefore, the increase in runoff coefficient might be due to the effects of climate change. Although the gross water potential of Turkiye is 231.4 km³, due to technical reasons, it was reported that only a total of 112.0 km³ of the potential is exploitable, 95.0 km³ from surface water and 18.0 km³ from groundwater.

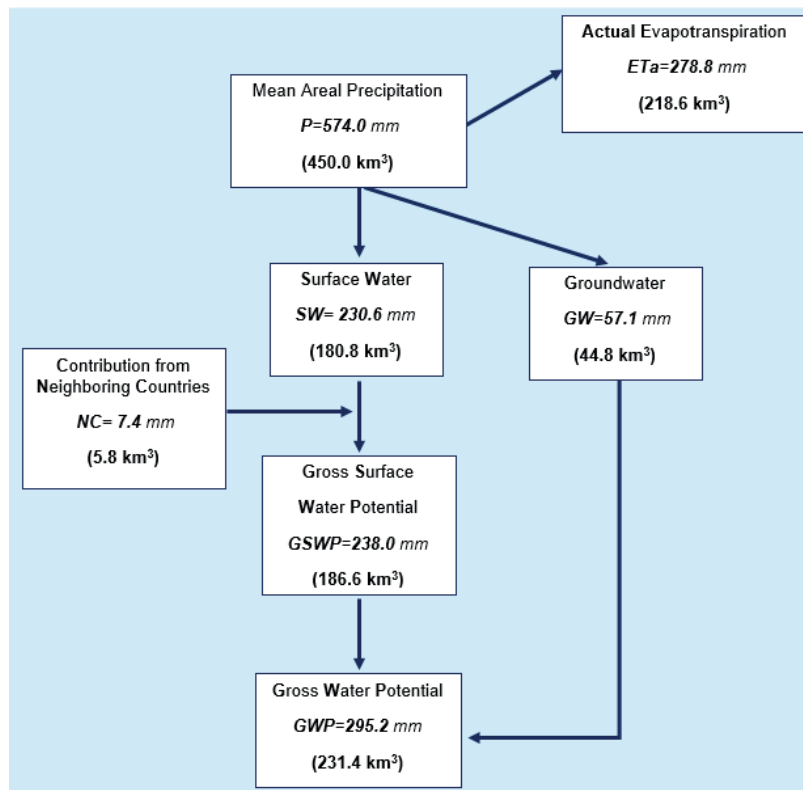


Figure 1. Surface and groundwater potential of Turkiye

Due to the considerably large size of the country and the spatial and temporal uneven distribution of water resources, water demand in some regions exceeds the available water for a period which creates a water shortage in the agricultural sector. Therefore, spatial and temporal variabilities in temperature and precipitation values hinder the year-round production of field and horticultural crops under natural conditions. In this context, precipitation is the most limiting factor for consumptive use. Sunflower, cereals and pulses are the main field crops, which can be economically grown under rain-fed conditions over the country, except for the Black Sea region. However, the Turkish government has made remarkable achievements in developing soil and water resources for irrigation, drinking, industrial and municipality water supply. As of the end of 2021, the total amount of area equipped with irrigation and drainage infrastructures has reached approximately 6.85 hectares ($\approx 30\%$ of economically and technically irrigable areas (22.6 Mha) under today's conditions). Cropping patterns in irrigation schemes vary considerably from each other due to variable climatic conditions and water availability in the river basins. Totally 58.4 BCM, viz. km^3 , water was consumed in irrigation, domestic and industrial sectors. Of this, a total of 77% (45.05 km^3) was consumed by irrigation such that 59% (34.3 BCM) was supplied from surface water resources and 18% (10.8 BCM) from groundwater resources.

Although irrigation farming makes rather significant contributions to the Turkish economy, there exist some problems to be solved in the progress of time. Accelerating the implementation of land consolidation (LC) projects in agricultural areas is inevitable to render at least 40% savings in expropriation and construction costs. Improving the very low irrigation efficiencies (average 37%) as well as irrigation ratios (42% in DSI operated, 66% in water user associations operated irrigation schemes), rehabilitation and rejuvenation of the dilapidated irrigation facilities, popularization of pressurized irrigation methods are some of the issues that need immediate action.

Keywords: rainfall distribution, irrigation, drainage, water user association, land use, drip irrigation.



Abstracts

I Integrated Water Resources Management

EFFICIENCY OF METHODS FOR SOLVING SYSTEM OF NON-LINEAR ALGEBRAIC EQUATIONS IN NUMERICAL SOLUTION OF DIFFUSIVE WAVE EQUATION

WOJCIECH ARTICHOWICZ¹, DARIUSZ GAŚSIOROWSKI¹

¹ Gdańsk University of Technology, Faculty of Civil and Environmental Engineering, Department of Geotechnical and Hydraulic Engineering; Poland

e-mail: wojartic@pg.edu.pl, gadasar@pg.edu.pl

Abstract

Two-dimensional diffusive wave equation is a popular model of flood inundation. One of the most promising solution methods of the two-dimensional equation is the splitting method. As a result of such approach the two-dimensional problem reduces to the solution of the set of one-dimensional diffusive wave equations. To increase the efficiency and to assure the stability of the numerical solution the implicit approximation schemes should be used. However, such proceeding leads to formulation of large systems of non-linear algebraic equations. The choice of the proper solution method of the non-linear system is a very significant part of the solution process influencing stability, accuracy and efficiency. In this study an analysis of different methods on the solution of the arising non-linear algebraic equations is performed. The Newton's method, Picard's method and their combination are used to solve the arising non-linear algebraic system. In order to test the performance and an efficiency of the considered methods two assumed flow scenarios were considered. The first scenario was the wave propagation over a horizontal plane, the second one was a wave propagation over an obstacle and depression. The depression and an obstacle had the rectangular shape reaching -0.5 m and 0.5 m respectively. In both cases the spatial solution domain with constant roughness coefficient was equal to $L=1$ km whereas the simulation times were 6000 s and 8000 s respectively. The initial conditions used in both scenarios assumed the dry bottom. At the $x = 0$ m the Dirichlet boundary condition in the form of linear function was imposed, whereas at $x = L$ the von Neumann boundary condition was imposed. The spatial steps were equal 1, 2, 10, 20 m whereas the time steps were equal to 1, 5, 10, 20, 50 s. The tests were carried out for all mentioned pairs of time and spatial step values resulting in total 20 numerical tests performed for each scenario. The characteristics used for solver comparisons were the total number of iterations required by each method to fulfil the criterion of convergence, the total time of computation, and the mean square error computed with respect to reference solution computed with very fine spatial and time step. The performed numerical tests showed that the most efficient method for solving non-linear system arising during the solution process of one-dimensional diffusive wave model is the modified Picard's method. In all cases this method required the most iterations to obtain the required solution accuracy. However, it was the fastest one with regard to the time of computation requirements. This is due to fact that the Picard's method doesn't require calculation of the computationally expensive Jacobian matrix. The Newton's method converged in smaller number of iterations, but it required the computation of the Jacobian matrix which eventually made the computations slower. The combination of the Picard's and the Newton's solver did not seem to be beneficial in terms of the computation time. It provided the better performance than Newton's solver, but it was slower than the pure the Picard's method. However, it assured the best prevention from computations breakdown in difficult cases.

Keywords: diffusive wave equation, system of non-linear algebraic equations, Picard's method, Newton's method, computational efficiency.

I Integrated Water Resources Management

IMPACT OF SPATIAL DISTRIBUTION OF PRECIPITATION IN AN URBAN CATCHMENT ON THE QUALITY OF RAINFALL-RUNOFF HYDROLOGICAL MODELING

PATRYCJA MIKOS-STUDNICKA¹, MICHAŁ SZYDŁOWSKI¹

¹ Gdańsk University of Technology, Faculty of Civil and Environmental Engineering, Department of Geotechnical and Hydraulic Engineering; Poland

e-mail: patstudn@pg.edu.pl, mszyd@pg.edu.pl

Abstract

Information on the spatial distribution of precipitation in the urban catchment is crucial for proper and reliable simulation of the outflow computed with rainfall-runoff hydrological models. In the paper authors present the case study of the Strzyża Stream catchment in Gdańsk (Poland), where rainfall recorded by hydrological monitoring system located throughout the catchment, should be assigned with care to individual elementary catchments for effective rainfall-runoff modeling. The problem is particularly visible in the matter of very local precipitation observed in the urban area, which is also characterized by high intensity and short duration. In the agglomeration of Gdańsk a large diversity of precipitation is observed, and their sums registered at rain gauges located in close vicinity from each other can vary significantly, even within one district of the city and at distance just of 5 km. In the work hydrological model created in the HEC-HMS (Hydrological Modeling System) was used to simulate the outflow based on SCS CN method. The results were compared with the water stage elevations (WSE) noted in the outlet control cross-sections during intensive rainfalls. Moreover, the sensitivity of the rainfall-runoff hydrological model to the method of determining the spatial distribution of precipitation in the analyzed catchment was examined.

Keywords: spatial distribution of precipitation, rainfall-runoff simulation, urbanized catchment.

I Integrated Water Resources Management

PROTECTION OF THE BALTIC SEA BY PROCESSING BEACH WRACK IN THE REED BED SYSTEM

ALICJA KUPCZYK¹, KATARZYNA KOŁECKA¹, MAGDALENA GAJEWSKA¹

¹ Gdańsk University of Technology, Faculty of Civil and Environmental Engineering, Department of Environmental Engineering Technology; Poland

e-mail: alikupcz@pg.edu.pl, katkolec@pg.edu.pl, mgaj@pg.edu.pl

Abstract

The area of dead zones in the Baltic Sea is constantly growing. The cause of the formation of oxygen deserts is the eutrophication process, which is intensified by many factors. One of them is so-called beach wrack (BW). It is a material washed ashore by waves, wind and tides. This phenomenon is natural and occurs all over the world. The algae decomposes on shore, releasing nutrients that recirculate to the Baltic Sea, deepening phenomenon of water blooming and thus contributing to an increase in oxygen deficit and growth of dead zones. In order to protect the Baltic Sea, the supply of nutrients reaching it should be limited, which poses the problem of managing the beach wrack material (Figure 1).



Figure 1. Beach wrack accumulated on the beach in Gdańsk (M. Gajewska)

Beach wrack is characterized by high water and nutrients content, similar to sewage sludge. Due to the resemblance of both materials, the idea of processing beach wrack in reed bed system (RBS) was born, which will enable the change of nuisance - heaps of rotting algae on the beaches, which exacerbate the condition of the Baltic Sea, into a resource - fertilizer that will allow to close the circulation of nutrients in an environmentally beneficial way. This solution is being tested in a pilot reed bed system located in the WWTP in Swarzewo. Preliminary results show that this technology in case of algae substrate, works properly and the possibility of producing valuable fertilizer is real (Table 1).

Table 1. Changes of basic parameters in beach wrack processing in reed bed system

parameters	water content [%]	dry matter [%]	mineral substance [%]	organic substance [%]	N [% dm]	P [% dm]
raw BW	92,2	7,9	63,9	36,1	1,1	1,0
BW after a month processing in RBS	38,1	61,9	90,3	9,7	0,6	0,9

Investigating the possibilities of these systems in relation to beach wrack seems right because of its environmental friendliness, low emissivity, and aesthetic appearance that can be easily incorporated into the existing seaside landscape.

Keywords: beach wrack, eutrophication, Baltic Sea, reed bed system, fertilizer.

II Hydraulic Engineering and Environmental Impact

BEACH CONSTRUCTION AND NOURISHMENT IN CROATIA

DALIBOR CAREVIĆ¹, TONKO BOGOVAC¹, DAMJAN BUJAK¹, SUZANA ILIĆ²,
HANNA MILIČEVIĆ¹

¹ University of Zagreb, Faculty of Civil Engineering; Croatia

² Lancaster University, Lancaster Environment Centre, Lancaster, United Kingdom

Abstract

The Croatian Adriatic coast is rich in a large number of gravel and sandy beaches about which there is no published data. The total number of beaches, sediment composition, average length, area and other relevant data are unknown. The lack of data also makes it difficult for managing the coastal area where local authorities are in charge. Beaches on the Croatian coast are under pressure from growing tourism industries, but also under the influence of climate change, which leads to an increase in the number of stormy events and rising sea levels, which all together result in erosion. As a measure to control erosion caused by storms, the practice of nourishing beaches prevails. Most European countries regularly carry out nourishing procedures on their mostly sandy beaches, and the practice is also present in Croatia. Beach nourishment is a procedure that falls under the regular maintenance of the beach, and involves the addition of materials to the beach in order to compensate for material previously lost by erosion or abrasion. Nourishment as a procedure is the dominant measure for beach maintenance for several reasons: it is adaptable to conditions on the coast that can change relatively quickly, the process of supplementation is non-invasive and does not disrupt the existing dynamics of the process on the coast, it also has a low environmental impact if performed properly. Coastal erosion can be monitored by various methods, and new, more technologically advanced coastal monitoring systems are emerging. One of the main goals of the Beachex project (<http://grad.hr/beachex/language/en/frontpage-beachex/>) is to develop a database on nourishment and construction of beaches and to educate the public and local self-government units. This article provides basic data relevant to assessing the current state of construction and nourishment of beaches, and in the future, defining sustainable coastal zone management practices.

Keywords: beach nourishment, gravel beaches, beach management, erosion.

II Hydraulic Engineering and Environmental Impact

CALIBRATION OF THE 3D NUMERICAL MODEL FOR SCOUR AROUND RIPRAP SLOPING STRUCTURE

ANTONIJA HARASTI¹, GORDON GILJA¹

¹ University of Zagreb, Faculty of Civil Engineering; Croatia
e-mail: antonija.harasti@grad.unizg.hr, gordon.gilja@grad.unizg.hr

Abstract

River flow through the bridge opening interacts with the bridge elements located in the active flow area, locally increasing turbulence and causing scour. A widely used countermeasure against scour at bridge piers is riprap sloping structure, in which launchable stones form a conical shape around the pier. Under such conditions, scour hole shifts downstream of the toe of the riprap sloping structure. Scour simulations are usually performed using three-dimensional numerical models representing natural environment with variable boundary conditions. The 3D model requires calibration of numerical parameters to accurately simulate the prototype conditions. The aim of this paper is to calibrate the Free surface model within the Flow-3D software using the flow field measurements. The model parameters selected for calibration are cell mesh size, turbulence model, and roughness associated with natural riverbed and riprap sloping structure. Flow field measurements were collected with ADCP (Acoustic Doppler current profiler) instrument on 20 transects along the river section around the bridge for two independent surveys. Surveys were conducted for 30% flow duration and 60% flow duration (mean flow conditions). The numerical modeling results such as cross-sectional velocities in 3 characteristic transects (upstream, downstream and bridge opening) were analyzed. The model has shown good agreement with the measured flow field across all transects.

Acknowledgments

This work has been supported in part by Croatian Science Foundation under the project R3PEAT (UIP-2019-04-4046).

Keywords: bridge, scour, riprap, calibration, flow-3D.

II Hydraulic Engineering and Environmental Impact

COASTAL DYNAMICS OF THE 233.6 A 282.4 KM UNDER CHANGING CLIMATIC CONDITIONS

KRZYSZTOF PIŁCZYŃSKI¹

¹ Institute of Hydro-Engineering of Polish Academy of Sciences; Poland
e-mail: krzysztofpilczynski@ibwpan.gda.pl

Abstract

The objective of this study was to analyse hydrodynamic and lithodynamic phenomena and processes in the seashore zone (Figure 1). An assessment of hydrological conditions was also conducted. An analysis of extreme sea levels, including those associated with storm surge, was conducted using historical datasets and numerical simulations to determine the probability of seaward flood risk.

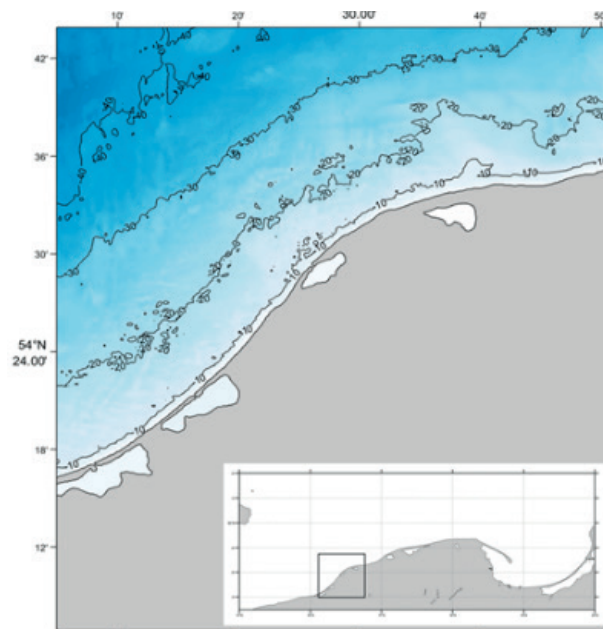


Figure 1. The Map of the region under study

As part of the study, work was performed to determine the wave-current field parameters, i.e. the wave transformation and calculation of current velocity distributions in the coastal zone. Wave data were derived from the Baltic Sea Wave Hindcast model, the results of which are available on the Copernicus Marine Environment Monitoring Service (<https://resources.marine.copernicus.eu/>). Statistical-stochastic analyses of wave parameters were carried out based on time series for period January 1, 1993 – December 31, 2020. In this study, the calculation of maximum wave heights significant were carried out for offshore wave directions W, WNW, NW, NNW, N, NNE, NE, ENE and E with recurrence interval TR = 5, 50 and 100 years. The probability density function of the three-parameter Weibull distribution was used to describe the distributions of random event variability with respect to maximum wave height significant (Lockhart and Stephens, 1994). An assessment of hydrological conditions was also conducted. An analysis of extreme sea levels, including those associated with storm surge, was conducted using historical datasets and numerical simulations to determine the probability of seaward flood risk. Sea levels were obtained from the Center for Hydrological Protection of the Country IMGW PIB (<https://hydro.imgw.pl/>) from hydrological stations located in Kołobrzeg and Ustka. Analyses and model studies of lithodynamic processes in the marine coastal zone using historical data allowed determination of sediment transport rates, seabed and shoreline rebuilding, and estimation of the expected magnitude of shoreline changes in the analysed section.

The paper deals with sediment migration in the coastal zone, which is a problem that occurs with both natural and artificial coasts (beaches). It is a very interesting and still insufficiently studied topic.

Keywords: coastal dynamics, climate change, South Baltic coastal zone, wave climate, longshore sediment transport.

II Hydraulic Engineering and Environmental Impact

HYDRAULIC DESIGN OF THE SETTLING BASIN FOR IRRIGATION SYSTEM

ANTE KOVAČ¹, GORDON GILJA¹, ROBERT FLISZAR¹

¹ University of Zagreb, Faculty of Civil Engineering; Croatia

e-mail: ante.kovac@student.grad.unizg.hr, gordon.gilja@grad.unizg.hr, robert.fliszar@grad.unizg.hr

Abstract

Siltation is one of the most common problems in irrigation systems, where sediment particles can cause clogging and reduce irrigation efficiency, thus reducing system's operational efficiency. Settling basins are integral part of the traditional irrigation pumping systems that abstract high volumes of water from the watercourses with high suspended sediment concentration. In order to fully exploit their main advantages, versatility and low maintenance requirements, they need to be efficiently designed to reduce their footprint and overall cost, at the same time retaining hydraulic efficiency for sediment removal. The objective of this study was to investigate the influence of the basin layout on the siltation rate for fine sand particles. A CFD model was applied to simulate the flow pattern in the settling basin subject to water withdrawal by pumping station. A total of six selected settling type basins were selected for simulating of short-term continuous flow through the basin for two flow boundary conditions, replicating operational prototype conditions. Evaluation of the hydraulic efficiency through identification of the intensive sedimentation areas was done using settling velocity approach and particle trajectories within the settling basin characteristic for each basin layout. Calculated spatial sediment concentration and deposition rate are further used to investigate the siltation volume and distribution pattern within the siltation basin, optimizing the basin section width. Result show that deposition generally exhibits decreasing pattern from the forebay to the pump intake. For further optimization, settling volume can be used to control system operation without adjusting the settling basin layout.

Keywords: settling basin, irrigation system, CFD.

II Hydraulic Engineering and Environmental Impact

ICE-STRUCTURE INTERACTION IN PHOTOVOLTAIC SOLAR PANELS INFLUENCING BY THE WIND VELOCITY

PARISA RADAN¹, TOMASZ KOLERSKI¹

¹ Gdańsk University of Technology, Faculty of Civil and Environmental Engineering, Department of Geotechnical and Hydraulic Engineering; Poland

e-mail: parisa.radan@pg.edu.pl, tomasz.kolerski@pg.edu.pl

Abstract

In northern regions, owing to the rise in energy and its transformation prices, solar power is more frequently used, due to the preference for the green energy. Floating photovoltaic structures (FPV) are one of the efficient substitute types for the fossil fuels, due to their advantages in land occupation. The study investigated the imposed ice forces on this structure type affected by the wind velocity in Łapino Reservoir located in Radunia River (Poland). Based on the low flow velocity and designed thermal expansion space, the static ice load is the principal force placed on the floating type of the structure. In Łapino Reservoir, ice cover is shoved under the influence of wind, thickened, and pushed towards the structure. DynaRICE model, a two-dimensional mathematical model for simulation dynamic of ice and location of the structure, was implemented. Different wind velocities, representing low to high velocity magnitudes in the region, were applied for the study. Moreover, the pool level reduction was considered as an extra parameter for changing the loads enforced on the structure. It was observed that varying wind velocity, changed the maximum ice thickness, which in turn, affected the loads on the structure. The wind direction is determinative for the inclination and formation of secondary ice layer. Not noticeable influences were observed in the applied ice load, from changing the pool level of the dam. It was also indicated that the maximum normal force was put onto the left side of the northern edge. Furthermore, a tilting at the south-east direction could be predicted since western and southern edges carry negligible forces.

Keywords: ice cover force, DynaRICE model, FPV structure, Łapino reservoir, wind drag.

II Hydraulic Engineering and Environmental Impact

PHYSICAL MODELS IN HYDRAULIC ENGINEERING

JAROSŁAW BIEGOWSKI¹, ZUZANNA CUBAN¹, JAKUB MALICKI¹,
MAŁGORZATA ROBAKIEWICZ¹

¹ Institute of Hydro-Engineering, Polish Academy of Sciences; Poland
e-mail: marob@ibwpan.gda.pl

Abstract

Construction of hydrotechnical facilities requires site specific solutions adjusted to local conditions. To reach the optimum solution two approaches, i.e., numerical, or physical models can be in use. Historically physical models have been commonly used, especially in case of large constructions. However, development of numerical methods and increase in computation power to carry out complex calculations changed the preferences. At the beginning of the 21st century, numerical models have largely displaced physical models. In practise, application of numerical models due to their limitations was not always successful. Due to limitations of both approaches, the most recommended is to apply both methods complementary in the design process. Following this trend, in 2021 Institute of Hydro-Engineering PAS re-opened the hydraulic laboratory.

First experiments were carried out in a prismatic channel ($L = 60$ m, $W = 5$ m, $H = 0.6$ m) partly occupied by a system of groynes (5 pairs spaced 2.5 m). These experiments were dedicated to an analysis of hydrodynamic conditions in the main channel and in groyne fields. Experiments were carried out both for emerged and submerged groynes for various discharge conditions (e.g., 0.05, 0.08, 0.11 m³/s). They were conducted in case of a fixed bottom. Direct velocity measurements carried out using ADCP current meter delivered information on flow characteristics in the water column, excluding the upper-most 10-centimeter layer. Video records of the surface layer, with flowing regular plastic elements applied as tracers, were used to analyse velocity patterns in the surface layer using the PTV (Particle Tracking Velocimetry) method. These two complementary methods delivered quite detailed information on velocity patterns in the study area.

The collected data enabled comparison of velocity patterns in case of emerged and submerged groynes. In case of emerged groynes distinct differences between unidirectional flow in the main channel and water circulations in groyne fields were observed. In case of submerged groynes, with the increasing flooding of groyne top, water circulations in groyne fields disappeared and resembled situation without groynes.

In the next step, experiments with the emerged groynes and moveable bed were carried out. They allow to work out methodology of bottom scanning, and analysis of bottom changes due to flow.



Figure 1. Exemplary photo from experiments with plastic tracer (left) and results from the PTV analysis (right)

Keywords: physical models, hydraulic structures, hydrodynamics, sediment transport, ice transport.

III Sanitary Engineering and Sustainable Water Use

COMPOSITION OF THE URBAN WASTEWATER IN DRAINAGE SYSTEMS

MARTA KIRAGA¹, OSCAR HERRERA-GRANADOS², MAURYCY NALIWAJKO³,
ALEKSANDER STAAR⁴, LAURA MAJEWSKA³, ADRIANNA KLUJ³, MICHAŁ SIECZYCH³

¹ Warsaw University of Life Sciences, Faculty of Civil and Environmental Engineering, Institute of Civil Engineering; Poland

e-mail: marta_kiraga@sggw.edu.pl

² Wrocław University of Science and Technology, Faculty of Civil Engineering; Poland

e-mail: oscar.herrera-granados@pwr.edu.pl

³ Warsaw University of Life Sciences, Faculty of Civil and Environmental Engineering, Civil Engineering (engineering studies); Poland

e-mail: s200264@sggw.edu.pl

⁴ Warsaw University of Life Sciences, Faculty of Civil and Environmental Engineering, Water Engineering and Management (engineering studies); Poland

e-mail: s203445@sggw.edu.pl

Abstract

The water flow in closed pipeline systems is almost always turbulent. Laminar flow may only occur when water flows in a thin layer on smooth surfaces. Turbulent flow is characterized by velocity components perpendicular to the main flow direction, the irregularity of current lines, and the velocity distribution across the flow cross-section. This results in intensive mixing of currents, characterized by various temperatures, chemical admixtures, or solids.

In the flow conditions prevailing in the large-diameter pipelines and their connecting chambers, such factors can be listed as crucial: longitudinal channel gradient, cross-sectional shapes, or materials roughness. Surface runoff can be divided into three groups: from urbanized areas; from traffic routes; from agricultural areas and forests. In Warsaw the key role is played by runoff from urbanized areas and from traffic routes. Rainwater runoff from roofs alone may be classified as relatively clean (Tab. 1), however, in the stage of surface runoff there occurs essential pollution of rainwater and its transformation into rainwater sewage during catchment flushing.

Table 1. Concentration of pollutants in rainwater, runoff from roofs, outflows to rainwater sewers (research conducted in 1987–1991 at the Warsaw University of Technology)

TYPE OF SAMPLE	BOD [mgO ₂ /l]	SUSPENSION [mgO ₂ /l]
Rainwater – precipitation	2,4–31	0–58
Roof runoff	19–74	0–440
Outflow to the rainwater drainage system	20–500	5–40 000

Due to many factors affecting the composition of rainwater runoff and its probabilistic nature, in the case of Warsaw sewage there is no unambiguous information concerning the composition of rainwater after it passes through the phase of surface runoff. The second characteristic of runoff water generated in the surface runoff phase is the irregularity of pollutant load discharge per time unit. Only 1 to 18% of the total hydrocarbon load mass is discharged as dissolved or unbound (oils, greases, and fuels which are separated from the rainwater through the flotation process). The remaining part is absorbed in suspension in the form of hydrocarbon cover of mineral sand or clay particles; the main component of sediment are mineral substances whose content ranges from 73.1 to 97.1% of dry mass. This study summarizes our own research related to the identification of the load transported in the urban stormwater drainage system in order to model the process of sediment transport in chambers and pipelines of the urban drainage system.

Keywords: wastewater, drainage systems, erosion, corrosion, accumulation, oils, road pollution.

III Sanitary Engineering and Sustainable Water Use

PREDICTION OF WATER QUALITY INDEX FOR PROCESSES IMPROVEMENT ON DRINKING WATER TREATMENT PLANT

GORAN VOLF¹, IVANA SUŠANJ ČULE¹, ELVIS ŽIC¹, SONJA ZORKO²

¹ University of Rijeka, Faculty of Civil Engineering; Croatia
e-mail: goran.volf@uniri.hr; isusanj@uniri.hr; elvis.zic@uniri.hr

² Istarski Vodovod d.o.o. Buzet; Croatia
e-mail: sonja.zorko@ivb.hr

Abstract

To improve drinking water treatment plant processes on the Butoniga reservoir in Istria (Croatia), the prediction of the Water Quality Index (WQI) is performed.

Based on parameters such as temperature, pH, turbidity, KMnO_4 , NH_4 , Mn, Al and Fe, the calculation of WQI is conducted, while for the prediction models of WQI along with mentioned parameters, additionally O_2 , TOC and UV254 are used.

All data are pre-processed concerning modeling and research goal. For the WQI prediction models, the entire span of the measured daily data was used, from 2011 to 2020, while missing data were filled in by usage of cubic spline interpolation.

Four models were built to predict WQI with a time step of one-, five-, ten-, and fifteen days in advance to improve certain processes in the drinking water treatment plant regarding changes in raw water quality in the Butoniga reservoir which could influence the treatment processes. Therefore, these models can help optimize certain processes depending on the quality of raw water.

For the experiment, the machine learning algorithm M5P for rule-based models integrated into the WEKA modeling software was used. Predicted WQI (one, five, ten-, and fifteen-days' time step) was set as a target (dependant) variable, whereas water temperature, pH, turbidity, KMnO_4 , NH_4 , Mn, Al, Fe, O_2 TOC and UV254 were set as independent variables (descriptors) from which the predicted WQI was modeled. The above parameters were used because they represent the parts of the system (drinking water treatment plant) on top of which the target variables depend.

To achieve the highest correlation coefficient (R), and the optimal number of rules default values of parameters for building models were used in WEKA modeling software. The model that was performing most accurately, according to the validation method, was selected as a representative model for prediction purposes.

Obtained results from models showed that one-day prediction model for WQI has only one rule which is related to a linear equation predicting the WQI and a very high correlation coefficient of 0.93, while five-day prediction model is consists of 12 rules with a correlation coefficient of 0.81. Ten-day prediction model has 14 rules and a correlation coefficient of 0.79. Finally, fifteen-day prediction model has five rules and a correlation coefficient of 0.71. As expected, obtained correlation coefficient decreases as the number of prediction days increases, while the number of rules, and related linear equations depend on the parameters set in WEKA modeling software which give the highest values of the correlation coefficient. Also, all models have high accuracy compared to the measured data, with a good prediction of the peak values.

Therefore, obtained models through the prediction of WQI could help to manage certain drinking water treatment plants depending on the quality of raw water in the Butoniga reservoir.

Keywords: WQI, prediction model, machine learning, processes improvement, drinking water treatment plant, Butoniga.

IV Hydraulic structures

BOOTSTRAP RESAMPLING IN HYDRAULIC MODELLING RESEARCH

ALEKSANDER STAAR¹, LAURA MAJEWSKA², ADRIANNA KLUJ², MICHAŁ SIECZYCH², MAURYCY NALIWAJKO², MARTA KIRAGA³

¹ Warsaw University of Life Sciences, Faculty of Civil and Environmental Engineering, Water Engineering and Management (engineering studies); Poland
e-mail: s203445@sggw.edu.pl

² Warsaw University of Life Sciences, Faculty of Civil and Environmental Engineering, Civil Engineering (engineering studies); Poland
e-mail: s200264@sggw.edu.pl

³ Warsaw University of Life Sciences, Faculty of Civil and Environmental Engineering, Institute of Civil Engineering; Poland
e-mail: marta_kiraga@sggw.edu.pl

Abstract

Development of the river bed with pillars and bridge abutments causes narrowing of its cross-section. This influences variations in flow conditions, which can be seen primarily during catastrophic floods. Then there is an increase in the velocity of the flow and the accumulation of water in front of the bridge. These changes depend on the geometry of the stream bed and the bridge cross-section, especially the degree of narrowing of the stream under the bridge. Hydraulic conditions under the bridge depend on the flow velocity, the dimensions and shape of the supports, the granulometric composition of the debris, which can be quantitatively characterized by hydraulic resistance coefficients.

The scouring under the bridge was calculated using one of the known empirical formulas, and compared with laboratory results. The local scour shape was measured using a sound probe with the accuracy of 0.1 mm on supercritical flow conditions. The aim of the study was to optimize the coefficients of the formulas using bootstrap resampling in a Monte Carlo simulation (Fig. 1).

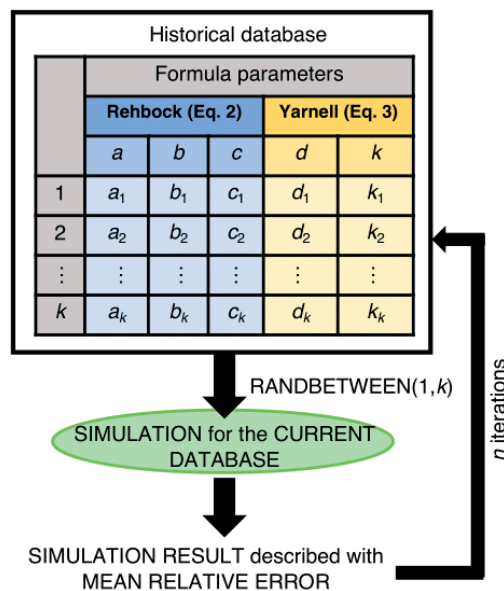


Figure 1. The bootstrap resampling algorithm

The analysis showed that the optimization of the chosen formula allows for a calculation error reduction relative to observations. It was concluded that the bootstrap resampling method in Monte Carlo simulation is a useful engineering tool for optimizing formulas in hydraulic research, also as a procedure for confirming the form of formulas previously used in practice. A particularly valuable feature of the paper is the use of a historical data set. The results demonstrated that the formula's calculation error could be diminished even with the whole order of magnitude.

Keywords: local scour, pier, bridge, erosion, optimization, verification.

IV Hydraulic structures

FILLING ALGORITHM PROPOSALS USING 3D NUMERICAL MODELLING FOR THE PROPER EXPLOITATION OF NAVIGATION SHIPLOCKS

OSCAR HERRERA-GRANADOS¹, MARTA KIRAGA²

¹ Wrocław University of Science and Technology, Faculty of Civil Engineering; Poland
e-mail: oscar.herrera-granados@pwr.edu.pl

² Warsaw University of Life Sciences, Faculty of Civil and Environmental Engineering, Institute of Civil Engineering; Poland
e-mail: marta_kiraga@sggw.edu.pl

Abstract

Inland navigation is not only one of the oldest, but also economical, environmentally friendly and energy efficient means of transport. Therefore, the European Union is promoting the improvement of its existing waterway infrastructure, which includes the existing ship-locks along its waterways. In this contribution, computational fluid dynamics (CFD) was applied to analyze the behavior of water flow through culverts inside a two-chambered ship lock (Fig. 1 left side) during different filling lock operation algorithms. Two different algorithms (gate opening timing) were analyzed for the filling operation from the upper pond to the chambers (Fig. 1. A-sudden opening of the gates inside the culverts and B-slow/paused opening of the gates). Due to the model's output, one can state the pros and cons of both proposals. The 3D numerical model is based on the modification of the continuity and momentum equations, the commonly used Reynolds-average Navier-Stokes (RANS) equations. The commercial software Flow3D was used to discretize the RANS equations, which is sufficient for practical purposes.

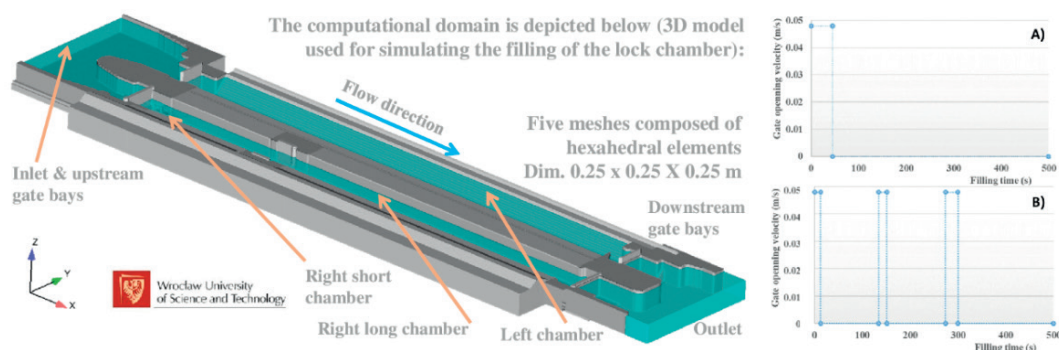


Figure 1. The computational domain and the filling/locking algorithms that were analyzed using CFD

Table 1. CFD results for the filling operation analysis

Flow and exploitation parameters	Algorithm A	Algorithm B
FILLING TIME (S)	410	480
CRITICAL FILLING TIME (S)	25	30
MAX. WAVE DEPTH (M)	0.23	0.20

In Tab. 1, a summary of some of the results of the CFD analyses is presented. Algorithm A is more efficient to accelerate the filling time process of the right subchamber but also is riskier because the collision between water and small shipping units can be stronger (the maximum wave depth is higher). However, for exploitation purposes, it is always convenient to accelerate the filling process to reduce the travel time of large ships with large containers. This fact can neglect the stronger flow behavior at the beginning of the filling process (critical filling time). Therefore, both algorithms present benefits and trade-offs and thanks to the usage of CFD, other algorithms can be used and analyzed to find an efficient solution for the proper exploitation of this kind of hydraulic structures.

Keywords: computational fluid dynamics (CFD), inland navigation, hydraulic structures, turbulence modelling, Flow3D, chamber lockage time.

IV Hydraulic structures

HYDRAULIC RESEARCH ON PHYSICAL WEIR MODEL

MAURYCY NALIWAJKO¹, MICHAŁ SIECZYCH¹, MARTA KIRAGA², ALEKSANDER STAAR³,
LAURA MAJEWSKA¹, ADRIANNA KLUJ¹

¹ Warsaw University of Life Sciences, Faculty of Civil and Environmental Engineering, Civil Engineering (engineering studies); Poland

e-mail: s200264@sggw.edu.pl

² Warsaw University of Life Sciences, Faculty of Civil and Environmental Engineering, Institute of Civil Engineering; Poland

e-mail: marta_kiraga@sggw.edu.pl

³ Warsaw University of Life Sciences, Faculty of Civil and Environmental Engineering, Water Engineering and Management (engineering studies); Poland

e-mail: s203445@sggw.edu.pl

Abstract

Stream channels become transmuted due to fluvial processes which involve two basic processes: water flow and soil structure elements' movement caused by it – a sediment transport. Both of these processes proceed according to the so-called feedback rule, which means that the hydraulic conditions of the water flow and the channel's morphology formed by it mutually adjust so that the river can reach a dynamic balance between the waterflow discharge and the bedload's transport intensity.

The material of bed in rivers comes from different sources. The main source could be described as soil erosion. Under the influence of weathering, drying, wetting, freezing, etc. processes there could be observed land management effects: non-cohesive (alluvial) and cohesive soils. Alluvial soils undergo erosion by water and the main type of erosion in case of cohesive soils is erosion by wind.

The research comprises field and laboratory works, database analysis, and computational part of the investigation. The model of the weir was recreated maintaining the geometric scale of the real object, sited on the Radomka River. Laboratory works were conducted in physical model of the flume with partially scourable bed, with rectangular 0.58-meter width cross-sections. The main dimensions of the flume were: 11.00 m of total length L_c and 0.60 m of lateral glass panels width H (Figure 1 a, b).



Figure 1. The researched weir, a) real object, b) laboratory model

The conditions of water flow and the formation of the local scour phenomenon at the water structure were studied. During initial data analysis it was demonstrated that the stream velocity increment was translated into scour hole deepening.

Keywords: local scour, clear water conditions, erosion, accumulation, weir, hydraulic structures.

IV Hydraulic structures

HYDRODYNAMICS IN THE PRESENCE OF GROYNES – PHYSICAL AND NUMERICAL MODELLING

JAKUB MALICKI¹, JAROSŁAW BIEGOWSKI¹, ZUZANNA CUBAN¹,
MAŁGORZATA ROBAKIEWICZ¹

¹ Institute of Hydro-Engineering, Polish Academy of Sciences; Poland
e-mail: jakubmalicki@ibwpan.gda.pl

Abstract

Groynes are commonly used structures for river regulation. Their goal is to concentrate flow in the main channel and protect riverbanks against erosion. Groynes can work as emerged or submerged constructions, depending on their height and water level in a channel. Mostly groynes are constructed as impermeable, however it is possible to find permeable ones. It is well known that flow parameters depend on bottom configuration, characteristic of sediment in the channel and can be modified by the presence of vegetation. To analyse river hydrodynamics in the presence of groynes numerical and physical models can be used.

Recently, in the open-air hydraulic laboratory of the Institute of Hydro-Engineering PAS series of experiments in a prismatic channel (width – 5 m; length – 60 m; depth – 0.5 m) with a system of groynes (5 pairs spaced 2.5 m) has been carried out. Experiments were done for various values of discharge ($Q = 50, 80, 110$ l/s) in case of emerge groynes. Velocity in selected cross-sections of the chosen groyne field were measurements using the ADCP current meter.

The numerical model was set-up using Delft3D-FLOW. The computational domain discretized using in horizontal plane regular grid while in vertical 10 layers in sigma co-ordinates were applied.

Laboratory experiments were used to calibrate numerical model set-up using Delft3D-FLOW. Analysis of measurements, and comparison with results from the numerical model will be presented.

Comparison between measured and modelled results confirmed applicability of the proposed model to reproduce recirculation in the groyne field.

Keywords: hydrodynamics, groyne, laboratory experiments, numerical modelling.

IV Hydraulic structures

IMPACT OF THE BRIDGE PIERS SHAPE ON HYDRAULIC FLOW CONDITIONS – AN EXPERIMENTAL STUDY

TOMASZ TYMIŃSKI¹

¹ Wrocław University of Environmental and Life Sciences, Faculty Of Environmental Engineering And Geodesy, Institute of Environmental Engineering; Poland
e-mail: tomasz.tyminski@upwr.edu.pl

Abstract

In the Water Laboratory of the WUELS hydraulic research has been carried out on 1:20 models of flow around pier for various shapes typical for selected bridges on the Odra river in Opole (Poland/Lower Silesia). The principal idea behind this research was to consider a pier an obstacle that causes local backwater and attempt to identify the most streamlined bridge pier shape. Streamlines of individual piers was investigated by means of measurements, observations of local velocity distribution for water fluxes and observations of water swelling in front of the pier. Results of hydraulic parameter measurements were used to calculate, for each pier, the local loss coefficients ζ , the flow-around drag coefficients c_w and the shape factors in the computational formulae of Rehbock (δ) and Yarnell (K). Comparison of these coefficients was used as a criterion for streamlines of investigated 6 piers (nos. I–VI). In each case being studied local water build-up was observed in front of the pier. Measurement data analysis revealed that the biggest turbulences were caused by the pier with rectangular shape (no. I), and the smallest by the cigar-shaped pier (no. VI). Measurements have also confirmed that all rectangular piers cause the greatest changes to the velocity field. These changes are smaller for piers which are rounded and pointed and are the smallest for those which are streamlined and cigar-shaped. For rectangular piers nos. I and II turbulences around the pier were bigger than those observed for other shapes. One might expect that this shape increases the risk of soil erosion in the vicinity of piers. Measured drag and shape coefficient values quantitatively confirm the qualitative analysis of the phenomenon. The biggest drag coefficient values were obtained for the two least streamlined piers (e.g. for pier no. I with $\zeta = 2.36$), whereas the most streamlined piers produced the smallest values (e.g. pier no. VI with $\zeta = 0.31$). Laboratory measurements enabled us to verify the formulas of Rehbock and Yarnell used in hydraulic bridge calculations. For the Rehbock's formula a certain distinct regularity could be observed: the shape factor δ was almost twice too low as compared to the results of experiments. In what concerns the formula of Yarnell, results of author's experiments are in good agreement with the theory. The investigations and laboratory observations carried out confirmed a clear and significant effect of the bridge pillars on the hydraulic flow conditions in the trough.

Keywords: bridge piers, hydraulic modeling, laboratory measurements, local loss coefficients, drag coefficient.

V Ecohydrology and Water Body Protections

DIFFERENTIATION OF HYDROCHEMICAL CONDITIONS OF SURFACE WATERS AND GROUNDWATER IN SELECTED PEATLANDS OF THE SLOWINSKI NATIONAL PARK (NORTHERN POLAND)

MARLENA PAWŁOWSKA¹, ZUZANNA LIPIŃSKA¹, IWONA BUBAK¹, ROMAN CIEŚLIŃSKI¹

¹ University of Gdańsk, Institute of Geography, Department of Hydrology; Poland

Abstract

Peat bogs are unique objects on the globe, for which one of the most important functions is water retention. They give the possibility not only to better regulate water relations in the catchment (decrease the threat of flood and drought), but also to improve the quality of water flowing there. Currently, the mainstream of research is based on the assessment of their biotic state, as well as greenhouse gas emissions, forgetting that research on physico-chemical characteristics is also extremely important. In this paper, the object of study are unique raised bogs of the Baltic type, whose quality status should be closely related to rainfall conditions (the main source of supply) and local geographical conditions. Unfortunately, anthropopressure observed since the end of the 18th century has caused that their quality condition may be affected by human activity, as well as by extreme phenomena, e.g. the phenomenon of storm and accompanying sea water intrusion. The aim of this paper is to compare water quality status of selected peatbogs located in the Slowinski National Park: Kluki Peatbog, Ciemińskie Błota and Żarnowska Peatbog. The key element of this work is also identification of main determinants affecting this state and determination of hydraulic relation between investigated peatbogs, groundwater and Lake Lebsko. The main work consisted of field research. Quarterly sampling of surface and groundwater (from previously installed piezometers) was carried out in 2017–2021, followed by laboratory analyses of selected chemical indicators (total nitrogen and phosphorus, basic cations and anions) in the Hydrochemical and Hydrobiological Laboratory of the Department of Hydrology, University of Gdańsk. Additionally, specific conductivity, pH, temperature and oxygenation were measured directly in the field. As a result, high variability of chemical indices was found between the objects and within the objects themselves, as well as lack of clear temporal and spatial variability of pH. Higher values of specific conductivity were also observed in the vicinity of drainage channels and peat mines. The highest values of conductivity, exceeding $600 \mu\text{S}\cdot\text{cm}^{-1}$, were recorded at Kluki peat bog in the C9 channel. Points located in the vicinity of the Lebsko Lake were characterised by high values of i.a. chlorides, which indicates hydraulic connection of peat bogs with lake waters. Water quality of selected objects is determined by local conditions and does not show typical parameters for ombrogenic peatlands. Moreover, it can be stated that human activity in the form of drainage ditches and peat exploitation has a negative impact not only on the height of groundwater table, but also on the physico-chemical condition of waters in peat bog areas.

Keywords: Slowinski National Park, peatlands, hydrochemical conditions, anthropopression, hydrometeorological conditions, groundwater.

V Ecohydrology and Water Body Protections

SHORT AND LONG-TERM HYDROLOGICAL FORECASTS FOR AGRICULTURAL BASINS BASED ON THE SWAT MODEL

DOMINIKA KALINOWSKA¹, PAWEŁ WIELGAT¹, PIOTR ZIMA¹

¹ Gdańsk University of Technology, Faculty of Civil and Environmental Engineering, Department of Geotechnical and Hydraulic Engineering; Poland
e-mail: domszawu@pg.edu.pl

Abstract

The study included a set of simulations related to changes in agricultural land use. The result of the work is a system performing a hydrological forecast of the quality and quantity of surface water up to 3 days ahead (using the weather forecast made available by the Interdisciplinary Centre for Mathematical and Computational Modelling at the University of Warsaw), as well as long-term simulation of planned activities in the context of agricultural year (taking into account different variants of meteorological scenarios). WaterPUCK web-based service (waterpuck.pl) is used as a decision support tool, enabling local stakeholders (administration and farmers) to predict changes in local water resources. The social and economic perspective of WaterPUCK aims to increase the environmental quality of the Puck Bay ecosystems under different scenarios of economic development.

The study area is located in northern Poland on the southern coast of the Baltic Sea. The basin area is 176 km². The use of land for agriculture dominates (60%), in addition to forests (29%) and urban areas (11%). This is a young glacial area of varied relief, characterized by a large denivelation (from -0.5 to 113.5 m a.s.l.) cut by smaller valleys with steep slopes. The bottoms of the valleys contain the beds of rivers, e.g., Gizdepka, Bładzikowski Stream, and Phutnica. The geological structure consists of fluvio-glacial sediments, mainly loamy sands and sandy loams interlaced with clay.

Meteorological data from 2000 to 2009 were used for the calibration. The criteria for calibration represented the components of the hydrological budget and plant biomass. Validation of the SWAT model was performed by comparing the observed and calculated average daily outflow from the Gizdepka river. To validate the model, monitoring in the years 2018–2019 was used. The monitoring consisted of a water level measurement station. Then the water level was converted into the flow rate using a rating curve based on measurements carried out in the years 2017–2019. Additional validation criteria included the weight of the yield of the major crops in the area: winter wheat, canola, silage corn, and hay production on grassland. Realistic yield values were obtained for all scenarios, thanks to agricultural calendars containing the best dates for agricultural treatments, determined based on the guidelines and experience of the surveyed farmers.

A series of hydrological simulations have been carried out, assuming the most common types of crops, and the various possible variants of the corresponding fertilization methods (doses, fertilizer types, etc.), taking into account the variable location of the crop field (spatial variation of soil types). The impact of possible climate changes (modification of meteorological data) on the water balance was then checked. The final step was to test the feasibility of using short- and long-term meteorological forecasts in the process of planning agricultural practices to optimize their impact on the catchment area.

Keywords: Puck Bay, SWAT model, hydrological forecast.

V Ecohydrology and Water Body Protections

THE IMPORTANCE OF CONTROLLING POINT SOURCES OF POLLUTION WITHIN SMALL CATCHMENT AREAS

MARIJA LEKO-KOS¹, TAMARA BRLEKOVIĆ², LIDIJA TADIĆ³

¹ Meander M d.o.o.; Croatia

e-mail: marijalekokos@gmail.com

² Građevinski i arhitektonski fakultet Osijek; Croatia

e-mail: tamaradadic@gfos.hr

³ Građevinski i arhitektonski fakultet Osijek; Croatia

e-mail: ltadic@gfos.hr

Abstract

Many developed countries are dealing with problems of monitoring of the formation and pollution of sediment in drainage canals, as well as disposal of extracted polluted sediment. The European area is characterized by the development of monitoring strategies by individual countries. The Water Framework Directive changes the approach in the field of water systems management, and requires monitoring the quality of sediments as an integral part of aquatic systems. The Directive also changes the way of management of extracted sediment. According to the EU Water Framework Directive, each member state was obliged to identify polluted sediments that require remediation, and to take the necessary actions in order to achieve good ecological status of the water bodies. Also, the problem of sediment must and can be solved in locations where the ecological status has been violated due to polluted (degraded) sediment, which can act as a secondary source of pollution.

Control of point and diffuse sources of pollution due to its nature and the impossibility of complete control, is recognized as problem which needs special attention. Most of this pollution ends up in drainage canals through precipitation or direct discharge. There are large amounts of sediment disposal in the drainage canals of lowland areas where agriculture is the dominant activity, which is even increased by reduced canal maintenance. The amount of sediment is also affected by reduced discharge in the canals as a result of frequent droughts.

In order to analyse heavy metal pollution of sediment in canals, research was conducted in the wider area of the Vuka River Basin, which belongs to the continental area of Croatia. The obtained results showed variable concentrations of heavy metals in canal sediment, especially copper, in years 2020 and 2021. Geodetic surveys of cross-sectional canals profiles, with the aim of monitoring the change in canal geometry in years 2020, 2021 and 2022 were also performed. Weak mobility of sediment pollution due to low water discharge was proven, and the lag of pollution in the sediment and its spread along the channel was confirmed.

Such contaminated sediment is retained in the canals until its removal within the framework of technical maintenance. As part of technical maintenance, canal sediment is deposited along drainage canals, directly next to agricultural areas. One of the most important principles of the current legislation refers to the elimination of damage directly at the source. The conducted research indicates the magnitude of pollution caused by uncontrolled sources of point pollution and the need to make additional efforts to reduce its formation.

Keywords: sediment, pollution, drainage canals, heavy metals.

V Ecohydrology and Water Body Protections

TRACES STUDIES OF EXCHANGE WATER IN BREEDING POOLS

PAWEŁ WIELGAT¹

¹ Gdańsk University of Technology, Faculty of Civil and Environmental Engineering, Department of Geotechnical and Hydraulic Engineering; Poland

e-mail: pawel.wielgat@pg.edu.pl

Abstract

The study of the issue of solute transport and water exchange in hydraulic structures is an important environmental engineering problem. Water exchange is particularly important in aquatic or semi-aquatic animal breeding pools. Water quality is a key issue for animal welfare and health. Livestock pools are non-standard facilities. Due to the presence of animals, stirrers cannot be used to improve circulation. In addition, the flow rate must not be too high. In such facilities, water exchange can be detected by tracer studies using fluorescent dyes. By using a passive tracer (rhodamine WT), it is possible to track fluid movement, water exchange intensity, and estimate transport parameters necessary for mathematical modeling. The tracer measurements allow to verify the correctness of calculations of fluid flow as a carrier of solute. The methodology presented in the poster concerns tracer measurements carried out in breeding pools of grey seals at the Marine Station of the Institute of Oceanography of the University of Gdańsk in Hel. Tracer was injected into the inlet of basin being tested. The volume of the investigated pool is 495 cubic meters. The pool has one point inlet and one overflow outlet. A series of four measurements were made at different inflow rates. A CYCLOPS-7 fluorimeter from Turner Designs was used to measure rhodamine concentration. The tracer signal was measured downstream at the outlet. A short pulse injection of the tracer allowed observation tracer concentration at the outlet and efficiency of the basin hydraulics. Due to the measurements, the efficiency of water exchange in the pools was estimated, and data on solute transport were collected.

Keywords: breeding pool, pollution migration, water exchange.

VII Climate Change and Flood Risk Management

CLIMATE CHANGE AND THE OCCURANCE OF FLOODS IN GDAŃSK

JACEK BARAŃCZUK¹, KATARZYNA BARAŃCZUK¹, MARTINA ZELEŃÁKOVÁ²,
HANY F. ABD-ELHAMID^{3,4}

¹ University of Gdańsk, Faculty of Oceanography and Geography, Coastal Cities Living Lab; Poland
e-mail: jacek.baranczuk@ug.edu.pl

¹ University of Gdańsk, Faculty of Oceanography and Geography, Coastal Cities Living Lab; Poland
e-mail: katarzyna.baranczuk@ug.edu.pl

² Technical University of Košice, Faculty of Civil Engineering, Department of Environmental Engineering; Slovakia
e-mail: martina.zelenakova@tuke.sk

³ Technical University of Košice, Faculty of Civil Engineering, Center for Research and Innovation in Construction; Slovakia
e-mail: hany_farhat2003@yahoo.com

⁴ Zagazig University, Faculty of Engineering, Department of Water and Water Structural Engineering; Egypt
e-mail: hany_farhat2003@yahoo.com

Abstract

The aim of the speech is to present how the floods in Gdańsk have shaped over the years and what impact the climate has on them. The climate of Gdańsk is mainly shaped by air masses approaching from the North Atlantic Ocean. The city has moderately cold and cloudy winters and mild summers with frequent rains and thunderstorms. Gdańsk is a city on the Baltic coast of northern Poland with a population of almost 629 ths and covers an area of 262 square kilometers. Gdańsk is the capital and largest city of the Pomeranian Voivodeship and the most important city in the geographical region of Pomerania. Gdańsk lies at the mouth of the Motława River, connected to the Leniwka, a branch in the delta of the nearby Vistula River. The city is located at an altitude of 0 m above sea level up to 180 m above sea level. The climate variability is a feature of processes and phenomena that take place in the natural environment. This variability is determined by different kinds of factors resulting from both cyclical natural processes and increasing anthropopression. In order to properly interpret the course of parameters describing the variability of the environment, it is necessary to analyse data obtained for the longest possible period of time. For this reason, data concerning flooding in Gdańsk from the 14th century to the present day (2017 year) was analyzed. The material for analysis regarding data on flooding was obtained from the Regional Water Management in Gdansk (RZGW), the Institute of Meteorology and Water Management (IMGW), Regional Atmosphere Monitoring Agency Gdańsk–Gdynia–Sopot (ARMAG) and Water Gdańsk municipal water company. Over the centuries, the following types of floods have occurred in Gdańsk: flood waves on the River Vistula (pluvial floods), blockage floods (ice jams), snow melt floods, storm floods, anthropogenic floods and fluvial urban floods. The type of flood in Gdańsk depends on the prevailing climate. When the climate cools down, floods related to ice jam on the Vistula prevail. In turn, along with a warming of the climate, the most frequent are urban flash floods.

Keywords: climate change, flooding, Gdańsk, urban flash floods, historic floods.

This work has received support from the SCORE (Smart Control of the Climate Resilience in European Coastal Cities) project, funded by the European Union's Horizon 2020 research and innovation programme under grant agreement No 101003534.

VII Climate Change and Flood Risk Management

FLOOD SIMULATION MODEL AND RISK ANALYSIS OF HUAIHE RIVER (LUTAIZ TO HUAINAN) CHINA

UMAR FAROOQ¹, TIAN FUCHANG², YUAN XIMIN²

¹ Gdansk University of Technology, Faculty of Civil and Environmental Engineering; Poland,
e-mail: umar.farooq@pg.edu.pl

^{1, 2} State Key Laboratory of Hydraulic Engineering Simulation and safety, Tianjin University; No 92 Weijin Road
Tianjin, 300072, China
e-mail: tianfuchang@tju.edu.cn, yxm@tju.edu.cn

Abstract

The present study is conducted on the Huaihe river, aiming to quantify multiple aspects of flood risks across their influence in the Cinan Feizuo vulnerable region. The DHI Mike 1D model was used for the river, while the 2D model was applied to the Cinan Feizuo flood protection area. The Finite volume method (FVM) is used for discrete grid problem and the models are coupled through the weir equation to find the volume of flow from the 1D domain to the 2D domain to investigate water level changes. A remote sensing interpretation approach is used to estimate complex roughness that has a significant impact on the flood. The 2D model has been refined so that ground topography and flooding dry and wet water depth boundary conditions were taken into account to optimize the model and perform the risk analysis. The refined data was combined and used to generate inundation maps for the Cinan Feizuo flood protection area for 20, 50, and 100 year return periods. The results evaluate maximum discharge, velocity, and submerged depth for 50 and 100-year flood events were compared with flood risk factors, while for 20-year flood event there is no probability of risk. Flood risk analysis and loss assessment were calculated based on theoretical and practical approaches by using inundated land, submerged water depth, and geographic information and social economic indicators. Finally, statistical analysis of socio-economic indicators for flood impacts and loss assessment is compared with the site survey and the Huaihe river Commission report, which show a high degree of agreement with the data. The risk analysis results showed significant damage caused by the flood over the target regions. The study provides technical support for flood risk analysis and loss assessment of the flood protection area and has important reference value for regional flood control, disaster reduction decision-making, and constructive planning.

Keywords: risk analysis, flood protection area, Huaihe river.

VII Climate Change and Flood Risk Management

MODELING URBAN FLOOD WITH HEC-RAS 6.1 IN ERBIL KURDISTAN, IRAQ

ANDAM MUSTAFA¹, MICHAŁ SZYDŁOWSKI¹

¹Gdańsk University of Technology, Faculty of Civil and Environmental Engineering, Department of Geotechnical and Hydraulic Engineering; Poland

e-mail: andam.mustafa@pg.edu.pl, mszyd@pg.edu.pl

Abstract

Flooding is a major threat to urban infrastructure, particularly in residential areas, even more so, in rapidly developing districts. Flood hydraulic modelling assists in identifying areas that are especially vulnerable to flooding and in improving the resiliency of mitigation plans. Urban floods present a unique set of challenges because the flow conditions are unpredictable due to rapidly changing topography and a lack of comprehensive raw data. Erbil (also known as Hawler in the Kurdish language) is the capital city of the Kurdistan Region in northern Iraq, and it is the region's largest city by population. Erbil, Iraq's second-largest city in the north of the country after Mosul, is the region's economic hub (Figure 1). In general, Erbil Province has a semi-arid continental climate, which is characterized by hot and dry summers and cold and wet winters, owing to its geographic location on the Arabian Plate. The investigation will be focused on the central district of Erbil. In the hydraulic modeling using HEC-RAS 2D, the area that was considered was within the 120 m ring road, which is approximately (102.38 km²).

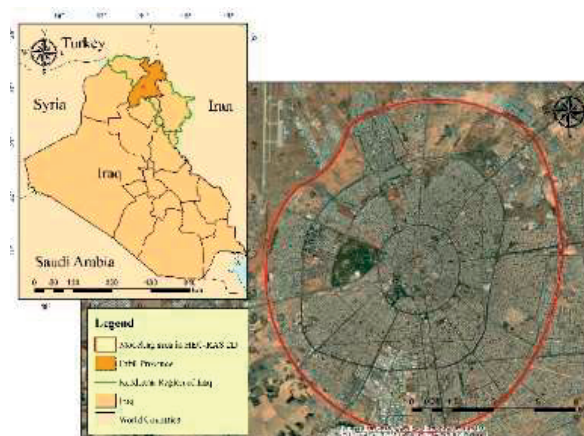


Figure 1. Study area

Rapid urbanization is one of the main causes of flash floods in Erbil. As a result, the patterns of Land Use Land Cover (LULC) in Erbil have changed significantly over the last two decades, particularly in the urban areas. Another important factor that increases the risk of flash flooding is the wrong way that land is used for urbanisation, where waterways have been blocked. Using a GIS-based modeling interface, the terrain was pre-processed and input files for the hydraulic model were generated. Determining characteristics of the physical basin was accomplished through the use of soil map data, LULC maps, and a digital elevation model. This way, HEC-RAS 2D hydraulic model was created, and it was used to assess the flood susceptibility, vulnerability, and impact on socio-economics in Erbil, Iraq. The case study pays specific attention to the quality of the flood modeling results obtained using Digital Elevation Model (DEM) of different precision. Faced with the challenge, this study provides insights to two different building representation techniques: Building Block (BB) and Building Resistance (BR). Given this backdrop, this work puts forward a novel in order to model an urban flash flood in the heart of Erbil. In the end, we were successful in employing the BR technique to construct a model with cell size (10 * 10). In point of fact, we were able to draw the conclusion, on the basis of our observations, that the BR technique is adequate for modelling flash floods in regions where there is a scarcity of data. Despite the modeling, this study attempts to identify flood-prone areas. Fill in some of the gaps regarding stormwater management in Erbil. The findings of this study can be applied to planning and the design of flood control structures, as the study identified flood-prone areas throughout the city.

Keywords: extreme rainfall, flash floods, data scarcity, HEC-RAS 6.1, flood modelling, Erbil, Iraq.

VIII Geotechnical aspects of Hydraulic Engineering

SIMULATION OF WATER TABLE FLUCTUATIONS AND LATERAL OUTFLOW FROM A SOIL PROFILE USING A 1D VADOSE ZONE MODEL

ANNA GUMUŁA-KAWĘCKA¹, VIPIN KUMAR OAD¹, ADAM SZYMKIEWICZ¹, JIRKA ŠIMŮNEK², BEATA JAWORSKA-SZULC¹

¹ Gdańsk University of Technology, Faculty of Civil and Environmental Engineering, Department of Geotechnical and Hydraulic Engineering; Poland

e-mail: annkawec@pg.edu.pl, vipin.oad@pg.edu.pl, adams@pg.edu.pl, bejaw@pg.edu.pl

² University of California Riverside, CA; USA

e-mail: jsimunek@ucr.edu

Abstract

1D models of vertical flow through vadose zone are often used to estimate groundwater recharge or contaminant travel time from the ground surface to the aquifer. In order to provide meaningful results, vadose zone models must be calibrated and validated against field measurements. Groundwater level measurements are a good alternative for vadose zone data or evapotranspiration (ET) measurements because they are simpler to obtain and usually readily available. However, if groundwater levels are used as calibration data, the 1D vertical vadose zone flow model must be able to reproduce the observed groundwater table fluctuations, which requires an appropriate choice of the bottom boundary condition (BC). In our study, we combine vadose zone flow modeling based on the Richards equation (HYDRUS-1D [1]) with the pressure head-dependent flux as the bottom boundary condition. This condition typically represents flow to horizontal drains, but it can also be applied to simulate natural horizontal flow occurring in the shallow aquifer [2]. The bottom of the soil profile is below the groundwater table, and the outflow rate from the saturated zone is calculated as a function of the current water table position using an analytical formula describing flow to drains implemented in HYDRUS-1D:

$$q_{dr} = \frac{4K_h}{L_{dr}^2} (H - H_{dr})^2 \quad (1)$$

where q_{dr} is the lateral outflow (discharge to drains) per unit area, K_h is the horizontal saturated hydraulic conductivity, L_{dr} is the drain spacing, H is the water table elevation in the soil profile, H_{dr} is the water table elevation in the drains. The parameters in Eq. (1) (the ratio $4K_h/L_{dr}^2$ which can be considered as a single parameter, and H_{dr}) can be calibrated either manually or automatically to fit the observed groundwater levels. We apply this method to a shallow sandy aquifer on the Brda outwash plain in northern Poland. The presented approach allows to (i) use easy-to-obtain water table measurements to calibrate parameters for unsaturated zone flow simulations, (ii) significantly reduce uncertainty in recharge estimation in the absence of reliable data on ET, (iii) reproduce lateral discharge to adjacent surface water bodies from 1D saturated/unsaturated soil profiles, which can be substantial for shallow groundwaters in humid regions.

Keywords: water table fluctuations, lateral outflow, groundwater, soil profile, 1D vadose zone model.

References:

- [1] Šimůnek, J., Šejna, M., Saito, H., Sakai, M., & van Genuchten, M.Th., (2013). *The HYDRUS-1D Software Package for Simulating the One-Dimensional Movement of Water, Heat, and Multiple Solutes in Variably-Saturated Media. Version 4.17*. Department of Environmental Sciences, University of California Riverside, Riverside, CA, USA.
- [2] Gumuła-Kawęcka, A., Jaworska-Szulc, B., Szymkiewicz, A., Gorczewska-Langner, W., Pruszkowska-Caceres, M., Angulo-Jaramillo, R., Šimůnek, J., (2022). Estimation of groundwater recharge in a shallow sandy aquifer using unsaturated zone modeling and water table fluctuation method. *J. Hydrol.*, 605, p. 127283.

Extended abstracts

I Integrated Water Resources Management

THE EFFECT OF DEM RESOLUTION ON THE CALCULATION OF THE LS FACTOR ENTERING THE UNIVERSAL SOIL LOSS EQUATION

MATÚŠ TOMAŠČÍK¹, MICHAELA DANÁČOVÁ¹, MILICA ALEKSIĆ¹, ROMAN VÝLETA¹

¹ Slovak University of Technology in Bratislava, Faculty of Civil Engineering, Department of Land and Water Resources Management; Slovakia

e-mail: matus.tomascik@stuba.sk

Abstract

Soil erosion is a relief-forming activity currently defined as a complex process involving the destruction and degradation of the soil surface by transporting and sedimentation of released soil particles by water, wind, ice, and other so-called erosion agents, including human activity. The application of models to calculate soil erosion allows a quick assessment with a reliable result. One of the most used models for the calculation of erosion risk respectively soil erosion is also the Universal Soil Loss Equation (USLE).

In this paper, a small experimental area that is threatened by water erosion was selected. It is located in western Slovakia, in the town of Myjava in the Turá Lúka district. The total area is approximately 30 ha, characterized by clay soils with an average slope of 6° (ArcMap). It belongs to mildly humid to warm climates with mild winters and an average annual rainfall of 650 to 700 mm. The area is used for agriculture. In the middle of the experimental catchment is a permanent erosion pit, which is stabilized by seven wooden dams.

The aim of this paper is to use USLE2D to determine the erosion risk in a small experimental catchment area. The modelling took place in the environment of the ArcMap program, where the method of calculating the LS factor was also investigated, and several algorithms for calculating the topographic factor (LS) were compared. We pointed out the influence of Digital Elevation Model (DEM) resolution (0.25m, 1m and 10m). Other USLE factors by default and their overview are given in Table 1.

Table 1. Description of input parameters (factors) entering Universal Soil Loss Equation (USLE)

Factor	Description		Value	Unit	
R	Location – Myjava, station 15020 according to the original methodology from minute data from 1995–2009 (summer months)		59.9	[MJ ⁻¹ .ha.cm.h ⁻¹]	
K	Map – areas divided by type of soil unit	BPEJ	0793672	0.3	
			0787413	0.39	
			0787232	0.39	
			0872212	0.25	
C	Map with information on vegetation coverage (in this case)	Wheat	0.12	[-]	
		Grass	0.005		
P	Without the influence of anti-erosion measures		1	[-]	
LS	Topographic factor with using different resolution (10×10m, 1×1m, 0.25×0.25)	Overview			[-]
		DEM 10×10m	McCool's algorithm [2] [3]		
		DEM 1×1m	Wischmeier & Smith algorithm [5]		
			McCool's algorithm [2] [3]		
			Govers algorithm [1]		
DEM 0.25×0.25m	Nearing algorithm [4]				
		DEM 0.25×0.25m	McCool's algorithm [2] [3]		

For the correct determination of soil loss in this small experimental catchment, it was necessary to determine it precisely within the total area due to the water erosion of the soil. In the first step, the switchboard was determined using hydrological analysis in the ArcMap software. The second step was followed by calculating the LS topographic factor in the environment of the USLE2D model, where parcel maps and DEM for the selected area served as input values. For DEM 1x1m, a comparison of algorithms was performed, namely according to Wischmeier & Smith [5], McCool's algorithm [2] [3], Govers's algorithm [1], and Nearing's algorithm [4]. Subsequently, based on unique algorithms, the average annual soil loss was calculated using USLE (Table 2, Figure 1).

Table 2. USLE calculation for Digital Elevation Model (DEM) with resolution 1×1m

Universal Soil Loss Equation - USLE: $G = R.K.LS.C.P$			
G – average annual loss of soil [$t.ha^{-1}.year^{-1}$]		R – rainfall and runoff factor [$MJ^{-1}.ha.cm.h^{-1}$]	
K – soil erodibility factor [$t.ha^{-1}.year^{-1}$]		LS – topographic factor [-]	
C – vegetation protection factor [-]		P – impact factor of anti-erosion measures [-]	
Calculation			
Algorithm	DEM	USLE result	Unit
Wischmeier & Smith [5]	1×1m	16.1767	$t.ha^{-1}.year^{-1}$
McCool [2] [3]		18.3787	
Govers [1]		34.6541	
Nearing [4]		17.5173	

Wischmeier & Smith algorithm (1978)

McCool's algorithm (1987, 1989)

Govers algorithm (1991)

Nearing algorithm (1997)

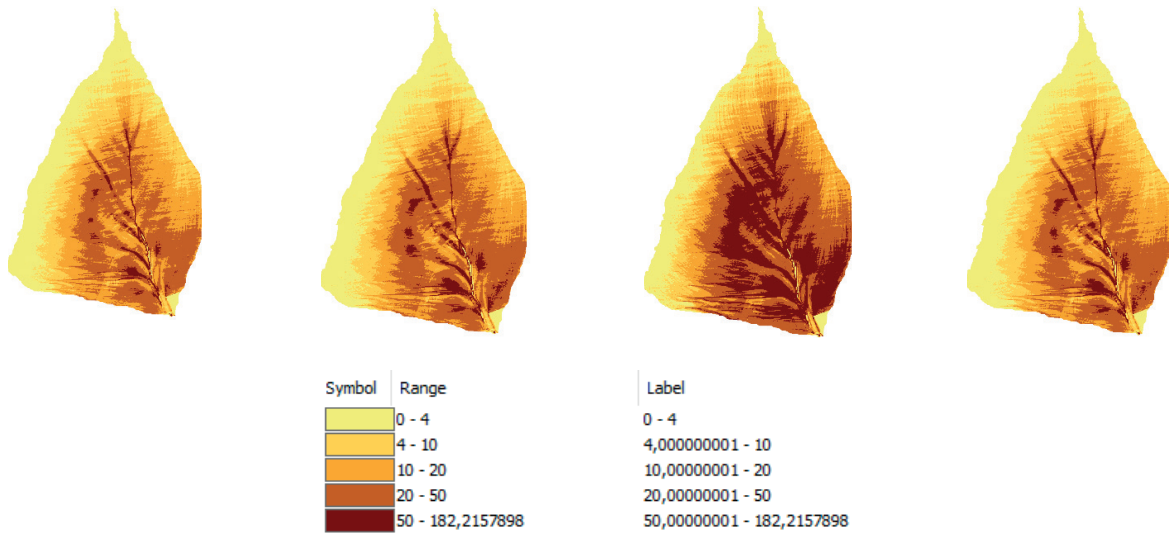


Figure 1. Graphical representation of USLE calculation results for DEM 1×1m resolution

Within Slovakia, the algorithm for calculating the LS factor according to McCool [2] [3] is mainly used, and therefore it was selected for comparisons of the effect of DEM resolution. Using this algorithm, the USLE calculation was performed in DEM 10×10m resolution (Table 3, Figure 2).

Table 3. USLE calculation for Digital Elevation Model (DEM) with resolution 10×10m

Algorithm	DEM	USLE result	Unit
McCool [2] [3]	10×10m	22.1598	$t.ha^{-1}.year^{-1}$

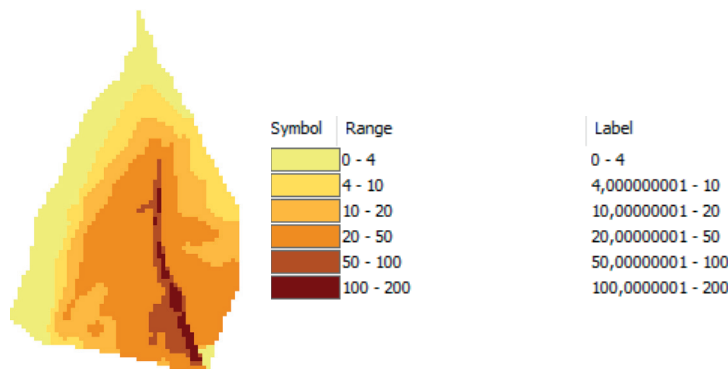


Figure 2. Graphical representation of USLE calculation results for DEM 10×10m resolution

Subsequently, the effect of a DEM resolution of 0.25×0.25 m was to be compared similarly. However, the interface of the USLE2D model was unable to calculate the LS topographic factor in such a high resolution. For this reason, it was necessary to calculate the factors L and S individually and numerically calculated according to the equations of the chosen algorithm. The results are presented in Table 4 and Figure 3.

Table 4. USLE calculation for Digital Elevation Model (DEM) with resolution 0.25×0.25 m

Algorithm	DEM	USLE result	Unit
McCool [2] [3]	0.25×0.25 m	36.7416	$\text{t} \cdot \text{ha}^{-1} \cdot \text{year}^{-1}$

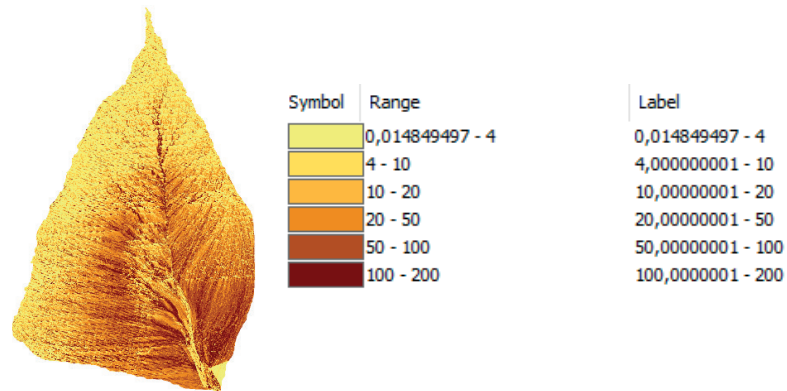


Figure 3. Graphical representation of USLE calculation results for DEM 0.25×0.25 m resolution

Based on the results obtained by USLE and USLE2D in the ArcMap software environment, it was concluded that it is not practical to use DEM in too high (0.25×0.25 m), but also in relatively low resolution (10×10 m), given the size of the river basin, to model the average annual soil loss in a small area. In the case of DEM resolution 0.25×0.25 m, the results are overestimated. On the contrary, when using DEM 10×10 m, the amount of transported soil was distorted because a more complicated relief of the formation of erosive furrows, especially in its middle and upper slopes, was not captured. For this pilot basin, modelling water erosion in DEM resolution 1×1 m proved suitable. In conclusion, it can be stated that the influence of DEM resolution was demonstrated, and the topographic factor LS was also compared, which significantly influenced the calculation of the average annual soil loss.

Acknowledgement

This work has been funded by the VEGA grant agency under the contract numbers VEGA 1/0632/19.

This work has been funded by the APVV grant agency under the contract numbers APVV-20-0374.

The authors are grateful for their financial support.

References

- [1] Govers, G. 1991. Rill erosion on arable land in Central Belgium – Rates, Control and Predictability. In: Catena, vol. 18, 1991, no. 2, p. 133–155.
- [2] McCool, D.K. et al. 1987. Revised slope steepness factor for the Universal Soil Loss Equation. In: Transaction of the American Society of Agricultural Engineers, vol. 30, 1987, no. 5. p. 1387–1396.
- [3] McCool, D.K. et al. 1989. Revised slope length factor for the Universal Soil Loss Equation. In: Transaction of the American Society of Agricultural Engineers, vol. 32, 1989, no. 5. p. 1571–1576.
- [4] Nearing, M.A. 1997. A single, continuous function for slope steepness influence on soil loss. In: Soil Science Society of America Journal, vol. 61, 1997, no. 3, p. 917–919.
- [5] Wischmeier, W.H., Smith, D.D. 1978. Predicting rainfall erosion losses. Agricultural Handbook, no. 537. Washington D.C.: U. S. Department of Agriculture, 1978. 58 p.

II Hydraulic Engineering and Environmental Impact

DISCUSSION ON THE UNCERTAINTIES IN FLOOD ZONING ON THE EXAMPLE OF THE RUSAVA RIVER

JAROMIR ŘÍHA¹, DAVID DUCHAN¹

¹ Brno University of Technology, Faculty of Civil Engineering, Institute of Water Structures; Czech Republic
e-mail: riha.j@fce.vutbr.cz, duchan.d@vutbr.cz

Abstract

Flood zones as an output of the hydraulic modelling are projected into maps and serve for emergency planning, flood risk analysis and urban planning in areas along rivers. As they constitute an important basis for conceptual decision-making, flood zones need to be determined with a high degree of accuracy. However, the input data and hydraulic calculations suffer from numerous uncertainties which should be taken into account when defining the extent of flood zones. The uncertainties are discussed in the paper.

1. Flood zoning in the Czech Republic

In the Czech Republic (CR), flood zones are defined for river floods with the return period $N = 5, 20, 100$ and 500 years. Hydraulic modelling of the corresponding discharges is carried out via appropriate software like HEC-RAS [Brunner 2016]. The Czech river authority performs the hydraulic modelling and the proposal of flood zones for the mentioned flood scenarios. The local authority provides flood zones with geographical identifiers, declare the zones and makes them public [Fojtík et al 2022]. Due to possible changes in the hydrological data, flood zones should be periodically revised every 5 years. Risk analysis is carried out for flood-prone areas based on the declared flood zones, calculated water depths and velocities according to the methodology [Drbal et al 2012].

2. Uncertainties in flood zones

2.1. General considerations

The extent of flood zones may be influenced by hydrological, geometrical, hydraulic and other uncertainties [Koivumäki et al 2010], [Bharath, Elshorbagy 2018], [Bales, Wagner 2009], [Brandt et al 2021], [Winter et al 2018], [Willis et al 2019]. They arise mostly from incomplete and inaccurate input data. The uncertainties should be carefully discussed during data analysis and hydraulic modelling, and when incorporating the results of calculations into the flood zones. Due to gaps in the data and the nature of uncertainties, it is usually impossible to express them probabilistically: their quantification can be feasibly achieved via the interval of uncertain variables. Very often they are incorporated into the resulting flood zones through the application of an engineering approach and the extending of the flood zone by adding a safety margin.

2.2. Hydrological uncertainties

The peak discharges and flood hydrographs are provided by the Czech Hydrometeorological Institute (CHMI) which declares that the data are valid for 5 years and may change due to new knowledge, namely in the case of the extension of measured hydrological series. Aside from this, the provided data are fraught with inaccuracies in the rating curves at gauging stages and due to the interpolation of the data between stations. The CHMI specified the expected error in the Czech national standard ČSN 75 1400, which is dedicated to hydrological data on surface water and its uncertainties (see Table 1).

Table 1. Expected error according to ČSN 75 1400

Return period	ACCURACY CLASS			
	I	II	III	IV
	Expected error [%]			
$N = 1 - 10$	10	20	30	40
$N = 20 - 100$	15	30	40	60

2.3. Digital terrain model uncertainties

The digital terrain model is often a combination of the floodplain terrain and the riverbed terrain [Kiczko, Mirosław-Świątek 2018], [Lim 2018]. The geodetic survey of the riverbed is available as a geodetic survey (profile points) or more recently as a sonar survey. The floodplain is available as a point geodetic survey, photometric survey and laser scanning (LIDAR) by aircraft or drone. Digital model terrain of the 5th Generation (DMR5G) from LIDAR by aircraft is available in the Czech Republic [CUZK 2022]. DMR5G in the place of the river represents part of the river banks and part of the water surface due to the inability of the laser to penetrate the water. The accuracy of DMR5G ranges from 0.18 m to 0.3 m depending on the vegetation. For the Rusava River, a combination of DMR5G and point geodetic survey for the riverbed was used for every variant of the hydraulic model. The most problematic part is the crossing of the river banks and the floodplain. These locations need to be addressed with the highest possible precision, as they are often the critical point of flood zone occurring.

A difficult source of uncertainty in this context is the possible changes in floodplain morphology and flow with time. For example, during a flood event, there is the transport of sediment, movement of floating objects (e.g. silting of bridge profiles and culverts) and other similar phenomena.

2.4. Hydraulic modelling

The uncertainties in hydraulic modelling lie in:

- inputs such as hydrological data, the geometry of the channel and the floodplain, structures (weirs, bridges) and hydraulic characteristics (roughness, contraction, expansion, etc.),
- the simplifications adopted and the model applied (1D, 2D, steady, unsteady, mesh size, etc.).

2.5. Uncertainties in the interpretation of flood zones

The calculated water levels corresponding to the mentioned flood scenarios are interpreted into the floodplain along the stream. The method of projection depends on the model used; usually Geographical Information Systems are employed. When unsteady flow models are utilised, the maximum water levels are used for the flood zoning. In the case of 1D models, water levels related to individual cross-sections are projected into the floodplain. This brings uncertainties in the direction of the river cross-section and the configuration of the adjacent inundation area, namely if several separate flows occur. If 2D models are used, the water levels are taken from the pixels of the 2D mesh. An inaccuracy may occur at the edge of the flood zone when an incomplete “filling” of cells occurs and the minor flow propagates to cells with an interpolated terrain level.

A study of the Rusava River in the Czech Republic included a comparison of the flood zone extent when taking into account four different types of models, namely a combination of steady/unsteady flow simulations with a 1D/2D approach. The different models provided significant differences in discharge distribution between the main channel and the floodplain, as well as in the extent of flood zones when steady and unsteady flow models were used (Fig. 1). The largest flooding corresponds to the 1D steady state model when water levels from river cross sections were projected into the floodplain. This creates an outer envelope to all other results obtained from other model types. The lowest extent was achieved by the 2D unsteady flow model when a relatively small theoretical flood hydrograph was used.

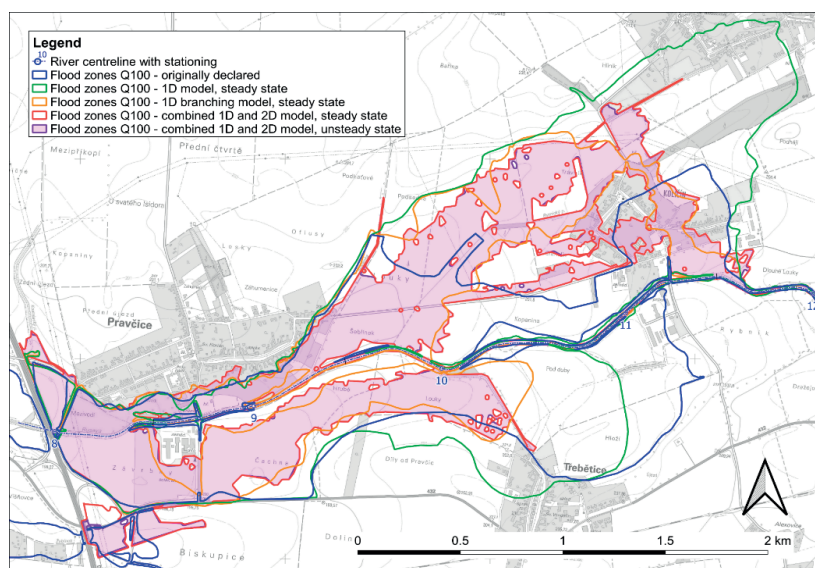


Figure 1. Comparison of the flood zones resulting from different hydraulic models

3. Conclusions

The performance of an uncertainty analysis is still not a routine procedure at flood zoning. The current practice is to introduce an adequate safety margin, which usually consists of the use of a steady flow model with a discharge increased by the expected error according to Table 1. Sometimes current hydraulic data are compared with those from historical flood events, if available. The conceptual challenge is the rate of extending the flood zone by adding a safety margin, which should be advocated against the wishes and desires of land owners, especially when construction development restrictions are declared based on risk zones.

4. References

- [1] Bales, J., Wagner, C. (2009) Sources of uncertainty in flood inundation maps. *Journal of Flood Risk Management*, 2, pp. 139–147.
- [2] Bharath, R., Elshorbagy, A. (2018) Flood mapping under uncertainty: a case study in the Canadian prairies. *Nat Hazards* 94, pp. 537–560.
- [3] Brandt, S.A., Lim, N.J., Colding, J., Barthel, S. (2021) Mapping Flood Risk Uncertainty Zones in Support of Urban Resilience Planning. *Urban Planning*. 2021, Volume 6, Issue 3, pp. 258–271.
- [4] Brunner, G. (2016) HEC-RAS River Analysis System: Hydraulic Reference Manual, Version 5.0.; US Army Corps of Engineers Hydrologic Engineering Center (HEC): Davis, CA, USA, pp. 1–538.
- [5] ČSN 75 1400 (2014) Hydrological data on surface water, Czech national standard. Czech Office for Standards, Metrology and Testing, Prague (In Czech).
- [6] CUZK. Czech Office for Surveying, Mapping and Cadastre (2022) Digital Terrain Model of the Czech Republic of the 5th Generation.
- [7] Drbal, K. et al. (2012) Methodology of flood hazard and flood risk mapping. Prague: VÚV TGM, Ministry of the Environment of the Czech Republic, 84 p.
- [8] Fojtík, T., Jašíková, L., Kurfířtová, J., Makovcová, M., Mařašová, V., Mayer, P., Nováková, H., Zavřelová, J., Zbořil, A. (2022) GIS and cartography at VÚV TGM. *Water Technical and Economic Information*, vol. 64, no. 1, pp. 47–52. ISSN 0322-8916
- [9] Kiczko A, Mirosław-Świątek D. (2018) Impact of Uncertainty of Floodplain Digital Terrain Model on 1D Hydrodynamic Flow Calculation. *Water*, 10(10):1308. <https://doi.org/10.3390/w10101308>
- [10] Koivumäki, L., Alho, P., Lotsari, E., Käyhkö, J., Saari, A., Hyyppä, H. (2010) Uncertainties in flood risk mapping: A case study on estimating building damages for a river flood in Finland. *Journal of Flood Risk Management*. 3, pp. 166–183.
- [11] Lim, N.J. (2018) Modelling, mapping and visualisation of flood inundation uncertainties. Doctoral thesis. Gävle University. 130 p.
- [12] Willis, T., Wright, N., Sleight, A. (2019) Systematic analysis of uncertainty in 2D flood inundation models. *Environmental Modelling & Software*, 122. ISSN 1364-8152
- [13] Winter, B., Schneeberger, K., Huttenlau, M. (2018) Sources of uncertainty in a probabilistic flood risk model. *Nat Hazards* 91, pp. 431–446. <https://doi.org/10.1007>

Keywords: flood, uncertainties, modelling.

II Hydraulic Engineering and Environmental Impact

EVALUATION OF WIND ENERGY POTENTIAL IN SOUTH BALTIC SEA

MICHAŁ BOJAN¹, PIOTR SZMYTKIEWICZ¹

¹ Institute of Hydro-Engineering, Polish Academy of Sciences; Poland
e-mail: P.Szmytkiewicz@ibwpan.gda.pl

Abstract

Wind energy is among the fastest growing renewable energy sources, growing 29% in 2008 alone to reach 1.21 GW of installed capacity worldwide. Offshore wind energy grew at an even faster rate of 32% in 2008, with Europe alone reaching 1.47 MW installed in offshore wind farms. Still, wind energy only accounts for 1.2% of the world's total installed power capacity. The construction of wind farms offshore is significantly more expensive than those onshore. The costs of connecting cables to the national power grid and the costs of turbine maintenance are also considerably higher. These costs depend to a large extent on the distance from shore and the depth at which the turbines are to be located.

Plans to construct wind energy farms in the Polish economic zone are being carried out and are meant to reach the total generated capacity of 6 GW by 2030. The plan to achieve this capacity, involves construction of approximately 430 offshore wind turbines with a unit capacity of 14 MW (ibidem). Poland's energy policy assumes that the country will have 11 GW of capacity from offshore wind turbines by 2040.

Before setting up a wind farm, factors such as wind energy potential, feasibility and operating costs must be evaluated in order to avoid investment risks and maximize turbine efficiency. The goal of this paper is to present a comprehensive methodology for determination of statistical wind characteristics and wind energy potential. An exemplary calculation was performed for a single forecasting point located within the Polish exclusive economic zone, in the vicinity of Slupsk shoal. The starting point for such calculations is the determination of a reliable statistical distribution function to describe the measured wind speeds. The Weibull distribution function is commonly used in the world, including Poland, as the standard method. This distribution is a function characterized by two parameters: shape and scale. The scale parameter controls the range, and the shape parameter determines the width of the data distribution. A wider data distribution implies a smaller shape parameter and a lower maximum value of the data distribution. Independent of the Weibull distribution, the statistical distribution functions were also determined by the maximum likelihood method, GEV, lognormal distribution, and compared with the Weibull distribution.

1. Data

Given the large scope of available data, wind data has been acquired from an 11-year period of January 2008-December 2018. The point for which data has been acquired (marked yellow on the map) is located at 54.99° N, 17.29° E. The point is located 27 km away from the coast. The data comes from MESCAN-SURFEX system in UERRA regional reanalysis for Europe on single levels from 1961 to 2019, courtesy of Copernicus Climate Change Service (<https://cds.climate.copernicus.eu/cdsapp#!/dataset/reanalysis-uerraa-europe-single-evels?tab=overview>). MESCAN-SURFEX is a surface analysis system that provides 6-hourly wind speed and wind direction at 10 m above sea level, with analysis available each day at 0.00, 6.00, 12.00 at 18.00 UTC. The projection of this model is a Lambert conformal conic grid with 1069 × 1069 grid points, with a horizontal resolution of 5.5 km × 5.5 km.

2. Results and discussion

The mean wind power densities are at their highest in late fall and in winter, with the maximum in December (809.96 W/m²). Those values are significantly smaller in the summer period, with the lowest mean power density calculated in July (273.92 W/m²), sitting at only about half of the average value (535.71 W/m²).

The wind climate exhibits substantial variation, with wind speeds in winter months high enough to put the region into the “very good” category of wind power classification, while summer months have low enough wind power density values to place them below the “fairly good” rating. This particular result is of note as generally, the maintenance of wind farms tends to be harder and more expensive during the winter period while the wind farms themselves are also the most busy with producing energy during that time.

3. Conclusions

Main conclusions are as follows:

1. The Weibull distribution is proven to be a very useful tool of estimating wind power potential from available numerical or observational data.
2. Among the suggested wind turbine hub height variants, the height of 150 m seems to be close the threshold of reaching good efficiency of harvesting energy from wind in marine conditions.
3. High seasonal variation of wind speeds exists in the region, and the variation is even more exemplified when it comes to wind power density values.

References

- [1] A.R. Henderson, C. Morgan, B. Smith, H.C. Sørensen, R.J. Barthelmie, B. Boesmans, 2003. Offshore wind energy in Europe – a review of the state-of-the-art, *Wind Energy* 6 (1), pp. 35–52.
- [2] Alkhalidi M, Shoug Kh. Al-Dabbous, Neelamani S, Hassan A. Aldashti, 2018. Wind energy potential at coastal and offshore locations in the state of Kuwait. *Renewable Energy* 135 (2019), pp. 529–539.
- [3] Fazelpour F., Markarian E., Soltani N., 2017. Wind energy potential and economic assessment of four locations in Sistan and Balouchestan province in Iran. *Renewable Energy*, 2017, vol. 109, issue C, 646–667.
- [4] McKinsey & Company 2016. Developing offshore wind power in Poland. Available at: www.mckinsey.com/pl/~media/McKinsey/Locations/Europe%20and%20Middle%20East/Polska/Raporty/Rozwoj%20morskiej%20energetyki%20wiatrowej%20w%20Polsce [Accessed 14 April 2022]
- [5] Palutikof J, Brabson B, Lister D., Adcock S.T., 1999. A review of methods to calculate extreme wind speeds. *Meteorol. Appl.* 6, 119–132.
- [6] Peter Enevoldsen, Mark Z. Jacobson, 2020. Data investigation of installed and output power densities of onshore and offshore wind turbines worldwide. *Applied Energy* 156 (2015), pp. 362–373.
- [7] Z.R. Shu, Q.S. Li, P.W. Chan, 2015. Investigation of offshore wind energy potential in Hong Kong based on Weibull distribution function. *Applied Energy* 156, 362–373.

Keywords: offshore wind farms, South Baltic Sea, wind energy potential.

II Hydraulic Engineering and Environmental Impact

MATHEMATICAL MODEL OF THE EUTROPHICATION OF THE BALTIC SEA IN THE BAY OF PUCK REGION

PIOTR ZIMA¹

¹ Gdańsk University of Technology, Faculty of Civil and Environmental Engineering, Department of Geotechnical and Hydraulic Engineering; Poland
e-mail: piotr.zima@pg.edu.pl

Abstract

The quality of coastal waters depends mainly on the pollution discharged along the tributaries of rivers [1]. The genesis of these pollutants is usually associated with the runoff of rainwater from developed agricultural catchments. This may be the cause of eutrophication and water hypoxia.

The Baltic Sea is considered to be one of the most polluted seas in the world [2]. One main cause of this condition is pollution supplied by rivers. This problem particularly affects areas in the Gulf of Gdańsk, where water exchange is impeded. The paper presents mathematical model of eutrophication of the Puck Bay waters which is a part of the Gulf of Gdańsk (southern Baltic). This model is based on the solute transport equation with regard to the Monod eutrophication equations. The inflow of pollutants was assumed point-by-point at the mouth of the main watercourses: Plutnica, Gizdepka, Bładzikowski Creek and Reda River. The hydrodynamic conditions in the bay were adopted for several scenarios regarding wind force and direction. As a result, the extent of pollution in the area of the Bay of Puck was obtained in relation to Natura 2000 – the EU's protected areas.

A mathematical model of coastal waters in the area of the Bay of Puck was made. For this purpose, a two-dimensional, partial differential, advection-dispersion equation describing the migration of dissolved matter was used in the following form [3–5]:

$$\frac{\partial(hc_i)}{\partial t} + \frac{\partial(hu_x c_i)}{\partial x} + \frac{\partial(hu_y c_i)}{\partial y} = \frac{1}{h} \frac{\partial}{\partial x} \left(hD_{xx} \frac{\partial c_i}{\partial x} + hD_{xy} \frac{\partial c_i}{\partial y} \right) + \frac{1}{h} \frac{\partial}{\partial y} \left(hD_{yx} \frac{\partial c_i}{\partial x} + hD_{yy} \frac{\partial c_i}{\partial y} \right) + \sum_{j=0}^J S_{i,j} \quad (1)$$

where: t – time, x, y – space coordinates, h – depth, u_x, u_y – velocity vector components, c_i – concentration of dissolved matter of component i , D_{xx}, D_{xy}, D_{yy} – coordinates of the dispersion tensor. The coordinates of the dispersion tensor \mathbf{D} are defined as follows:

$$D_{xx} = D_L n_x^2 + D_T n_y^2, \quad D_{xy} = D_{yx} = (D_L - D_T) n_x n_y, \quad D_{yy} = D_L n_y^2 + D_T n_x^2 \quad (2)$$

where $\mathbf{n} = (n_x, n_y)$ is the directional velocity vector:

$$n_x = \frac{u_x}{|\mathbf{u}|}, \quad n_y = \frac{u_y}{|\mathbf{u}|} \quad (3)$$

Longitudinal D_L [$m^2 \cdot s^{-1}$] and transverse D_T [$m^2 \cdot s^{-1}$] coordinates of the dispersion tensor (Eq. (2)) are described by the Elder formulas [6].

The term $\sum S_{i,j}$ in equation (1) defines the eutrophication model in the following form [7]:

$$\begin{aligned} S_{CT} &= -\alpha_0 C_T - \frac{K_1 C_T C_B}{K_{12} + K_{11} C_T} \\ S_{CB} &= \frac{\lambda_1 K_1 C_T C_B}{K_{12} + K_{11} C_T} - \alpha_1 C_B - \alpha_{10} C_B^2 \\ S_n &= -\alpha_2 n - \frac{\beta_1 C_n C_a}{\beta_{12} + \beta_{11} C_n} \\ S_a &= \frac{\theta_1 \beta_1 C_n C_a}{\beta_{12} + \beta_{11} C_n} - \alpha_3 C_a - \beta_{10} C_a^2 \\ S_S &= \pi_1 \alpha_1 C_B + \pi_2 \alpha_3 C_a - \delta C_S \end{aligned} \quad (4)$$

$$S_{O_2} = C_{sat} - \alpha_4 C_{O_2} - \lambda_{12} \frac{K_1 C_T C_B}{K_{12} + K_{11} C_T} - \lambda_{11} \alpha_1 C_B + \lambda_{22} C_a - \delta_1 C_S$$

where C_T is a cumulative concentration of organic pollutants, C_B is the density of bacteria, C_n is the cumulative concentration of various nutrients, C_a is the density of algae, C_S is the density of detritus and C_{O_2} is the concentration of the dissolved oxygen (DO). It is further assumed that the cumulative rate of depletion of C_T due to bacteria is given by monod type of interaction. As bacteria wholly depend on organic pollutants, the growth rate of bacteria is proportional to this monod type interaction term. The depletion rate of bacteria due to natural factors is assumed to be proportional to C_B while that due to crowding is proportional to C_B^2 . The depletion of nutrients by algae is given by monod type of interaction. The growth rate of algae is assumed to be wholly dependent on the nutrient and is therefore proportional to this monod type interaction. The natural depletion rate of algae is assumed to be proportional to its density C_a , and its depletion rate due to crowding is proportional to C_a^2 . Since some part of natural depletions of bacteria and algae is converted into detritus, the growth rate of detritus is assumed to be proportional to C_B and a and its natural depletion rate is assumed to be proportional to the density of detritus, C_S . We consider that the rate of growth of DO by various sources is C_{sat} (assumed a constant) and its natural depletion rate is proportional to its concentration C_{O_2} . It is also considered that the rate of growth of DO by algae is proportional to density of algae a , and the depletion rate of DO caused by eutrophication is proportional to the detritus concentration C_S . It is further considered that the depletion of DO is proportional to the monod terms (representing growth and depletion of bacteria). All remaining constants were taken according to the reaction kinetics.

This equation was solved numerically using the finite volume method [8], and a continuous area of the solution was discretized and covered with a mesh of triangular elements (Fig.1). In order to obtain a solution, the distribution of surface velocity in the Gulf caused by wind stresses was adopted in accordance with the Ekman model [9]. The inflow of pollution was assumed on the edge of the area (as a point), taking into account the multi-year average flow in the river and a constant concentration of 100% of C_T . 0% was assumed as background in the bay. Sample results for the north-west wind (NW – most common in this area) are shown in Fig.1.

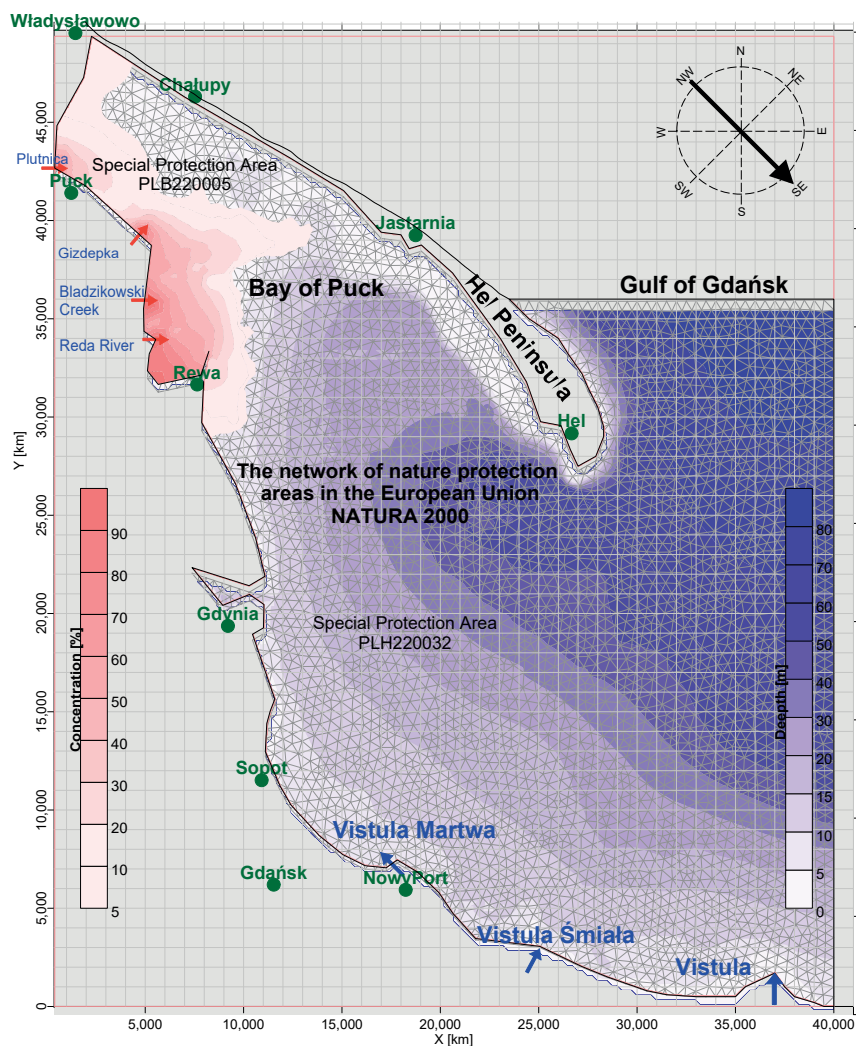


Figure 1. The influence of water courses on the eutrophication of the Bay of Puck

The conducted research has shown that watercourses discharging water from areas adjacent to the Puck Bay have a significant impact on the eutrophication of its water. Taking into account the growing pressure of agriculture on the environment, an increase in the costs of the mitigation of eutrophic processes in the Baltic Sea is expected. In addition, the attractiveness for tourists of the Bay of Puck, which is one of the most popular places for water sports in Poland, especially kitesurfing, is decreasing.

References:

- [1] Clark, R.: Marine pollution, Oxford University Press, 2001.
- [2] HELCOM BSEP No. 115B: Eutrophication in the Baltic Sea An integrated thematic assessment of the effects of nutrient enrichment in the Baltic Sea region, 2007.
- [3] Chapara, S.C.: Surface water-quality modelling. MacGraw Hill Company, New York, 1994.
- [4] Zima, P.: Mathematical Modeling of the Impact Range of Sewage Discharge on the Vistula Water Quality in the Region of Włocławek. Chapter in book: Free Surface Flows and Transport Processes. Verlag: Springer International Publishing, 489-502, 2018.
- [5] Zima, P.: Simulation of the impact of pollution discharged by surface waters from agricultural areas on the water quality of Puck Bay, Baltic Sea. Euro-Mediterr J Environ Integr 4, 16, 2019.
- [6] Elder, J.W.: The dispersion of marked fluid in turbulent shear flow. J Fluid Mech 5:544–560, 1959.
- [7] Rinaldi, S., Soncini-Sessa, R., Stehfest, H., Tamura, H.: Modeling and Control of River Quality, McGraw-Hill, UK, 1979.
- [8] LeVeque, R.J.: Finite Volume Method for Hyperbolic Problems. Cambridge University Press, New York, 2002.
- [9] Dyke, P.P.G.: Coastal and Shelf Sea Modelling. Series Title: Topics in Environmental Fluid Mechanics, Vol. 2, Springer US, 2001.

Keywords: Baltic Sea, Puck Bay, coastal waters, pollution migration, eutrophication.

II Hydraulic Engineering and Environmental Impact

SCOUR AROUND BREAKWATER – CANAL THROUGH VISTULA SPIT. PRELIMINARY ANALYSIS OF CAUSES. LESSON LEARNED

BARTOSZ ZABŁOCKI¹, PIOTR SZMYTKIEWICZ²

¹ NDI SA; Poland
e-mail: bzablocki@ndi.com.pl

² Institute of Hydro-Engineering, Polish Academy of Sciences; Poland
e-mail: P.Szmytkiewicz@ibwpan.gda.pl

Abstract

In 2020, construction works for the project “Construction of a waterway connecting the Vistula Lagoon with the Gulf of Gdańsk” (hereinafter referred to as the Spit Canal) have started at the Vistula Spit in the Nowy Świat district of the city of Gdańsk (Fig. 1). The waterway under construction is a connection between the Vistula Lagoon and the Gulf of Gdańsk. The first stage involves the construction of a breakwater harbour facing the Gulf of Gdańsk and consisting of eastern and western breakwaters, a wave breaker and berthing quays located respectively on the eastern and western side of the entrance to the ship canal through the Vistula Spit. A lock is currently under construction in the canal according to the project.



Figure 1. Approximate location of the scour (gray stain) near the head of the eastern breakwater (bright lines).
Satellite image from September 2020

After construction of the eastern breakwater body, gradual seabed scour was observed around its head between September 2021 and February 2022. This paper describes the development of this process over the course of time based on systematic bathymetric measurements. To determine the causes of this phenomenon, data on both water levels and wave parameters were analysed for this period. These data were compared with corresponding data from the period 1993–2021 and with the adopted design parameters for water levels and wave heights. In addition, current velocities were estimated in the area of the eastern breakwater head during the storm peak on 30 January 2022. Based on these analyses, main possible hydro- and lithodynamic scenarios that could lead to the development of scours around the eastern breakwater head were determined and are as follows:

1. In the situation when the direction of wave approach to the breakwater is approximately perpendicular, a vortex is formed at the breakwater head, which induces scour formation around the structure. The relationship between wave parameters, head geometry and vortex characteristics is described by the Keulegan–Carpenter (KC) number:

$$KC = \frac{U_M T}{B}$$

where:

- U_M – oscillatory velocity at the sea floor,
- T – wave period,
- B – head width.

For $KC < 1$ a vortex does not occur, for $1 < KC < 12$ a moderate vortex develops, for $KC > 12$ a strong vortex develops.

For the wave conditions that occurred during the very strong January storms, the calculated Keulegan–Carpenter number was $KC \approx 5$.

2. The severe storms that occurred between November 2021 and January 2022 were propagating from W and NW directions. Under such conditions as well as with the existing spatial arrangement of breakwaters and the exposure of the port entrance towards these directions, the water was “pumped” into the port by waves and wind. When the water level inside the port is higher than outside, water is discharged outside the port. The water is moved inside the port through the surface layers and discharged outside the port through the near-bottom layers. In such a case, the resulting near-bottom velocities lead to seabed scour.

Indirect confirmation of this concept is provided by the differential bathymetric map which shows that erosion processes occurred throughout the study area. No sediment accumulation processes were identified inside the port, which indicates that bottom sediment is carried outside the port perimeter under such wave conditions.

3. At the present stage of breakwater construction under storm conditions with high sea levels, waves overtopped the body of the structure, mainly in its near-head section, due to the lack of parapet walls. The overtopping water increases the level of turbulence in the vicinity of the head resulting in additional sediment transport. However, the impact of this phenomenon on the size of scour in the present case is difficult to clearly and quantitatively determine. It can be assumed that water overtopping is one of the possible additional sources of increased shear stresses at the bottom.

References:

- [1] Lin, I-Fu; Tseng, I-Fan; Lee, Chung-Pan; and Chen, Guan-Yu (2015). SEABED SCOUR AROUND A BREAK-WATER A CASE STUDY IN MAILIAO HARBOR, *Journal of Marine Science and Technology*: Vol. 23: Iss. 6, Article 2. DOI: 10.6119/JMST-015-0610-1.
- [2] Myrhaug D., Rue H., Torum A. (2004). Tentative engineering approach to scour around breakwaters in random waves. *Coastal Engineering* 51, 1051–1065.

Keywords: scour around breakwaters, South Baltic Sea, breakwater failure, climate changes.

II Hydraulic Engineering and Environmental Impact

SENSITIVITY ANALYSIS OF ACOUSTIC DOPPLER VELOCIMETER PARAMETERS FOR FLUME EXPERIMENTS

ROBERT FLISZAR¹, LUKA DRANDIĆ¹, GORDON GILJA¹

¹ University of Zagreb, Faculty of Civil Engineering; Croatia

e-mail: robert.fliszar@grad.unizg.hr, luka.drantic@student.grad.hr, gordon.gilja@grad.unizg.hr

Abstract

This paper describes the sensitivity analysis of an acoustic Doppler velocimeter (ADV) under various flow conditions to determine the best configuration for a particular laboratory environment. ADV instruments used for the experiments were two Vectrino Profilers calibrated to measure velocity in x, y, and z coordinates in a profiling range of 40–70 mm height from the central transducer. Experiments were conducted on a physical model of bridge pier scour placed in a rectangular hydraulic flume. The Vectrino Profilers were positioned at the inlet and outlet of the physical model and measured in a raster of points defined in the transverse direction and by flow depth (as shown in Figure 1).

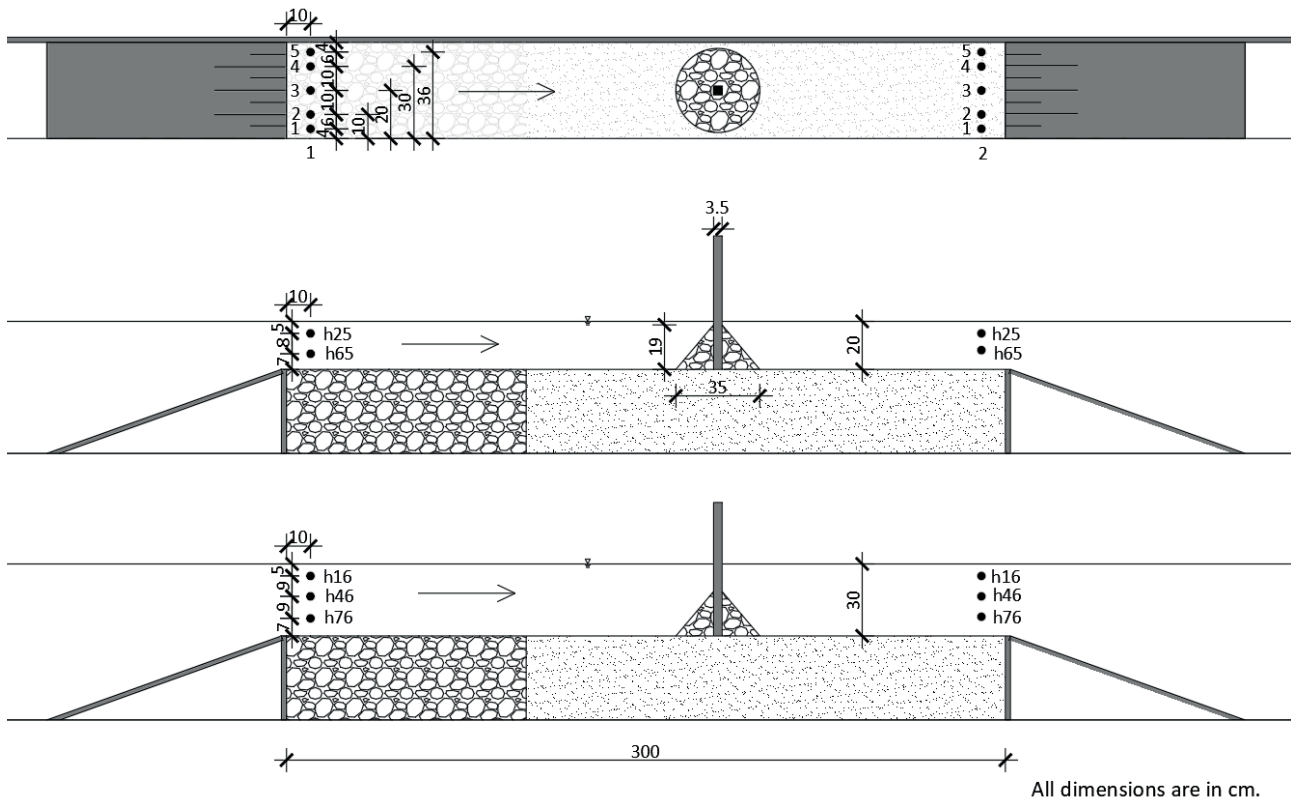


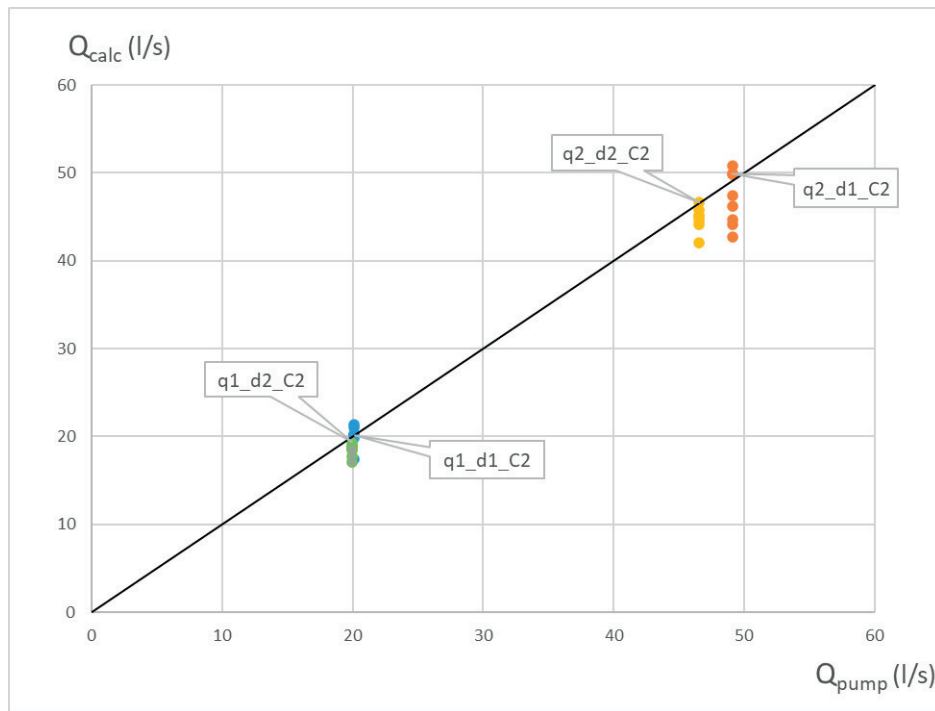
Figure 1. Raster of measurement points on the physical model

The parameters of the two Vectrino Profilers that were varied were the Ping algorithm, the Transmit pulse size, and the Cell size. Ping algorithm was varied between max interval and adaptive, while cell size and transmit pulse size were varied from 1–4 mm (Table 1). A total of 32 experiments were performed with the combination of 2 different flow rates as well as 2 flow depths ($q1_d1$, $q1_d2$, $q2_d1$, $q2_d2$).

Table 1. Parameters configurations

Configuration	Ping algorithm	Cell size [mm]	Transmit pulse size [mm]
C1	max interval	1	1
C2	max interval	1	4
C3	max interval	4	1
C4	max interval	4	4
C5	adaptive	1	1
C6	adaptive	1	4
C7	adaptive	4	1
C8	adaptive	4	4

The effects of each combination of these parameters on the accuracy of the results were evaluated. Data quality was based on the signal-to-noise ratio (SNR) and correlation, which can be viewed in real time during the experiment. The accuracy of the results was evaluated by comparing the two discharge values – the first was calculated using the flow velocities measured in the model (Q_{calc}), and the second was the adjusted pump discharge measured with the pump flow meter (Q_{pump}). The comparison of the results is shown in Figure 2.

**Figure 2.** Difference between calculated and measured flow rate

As can be seen in Figure 2, configuration C2, the combination of the max-interval ping algorithm, cell size of 1 mm, and transmit pulse size of 4 mm, proved to be the most accurate, which is why it is used for the experimental measurements and the verification of the physical model.

The physical model must accurately represent the prototype bridge to obtain reliable flow velocity data. Verification of the geometry and scale of the physical model was performed using field ADCP measurements. Comparison between the ADCP and ADV velocity measurements was performed on the same cross-sections used for ADV parameter's calibration. Five vertical velocity profiles across each cross-section were compared (Figure 3).

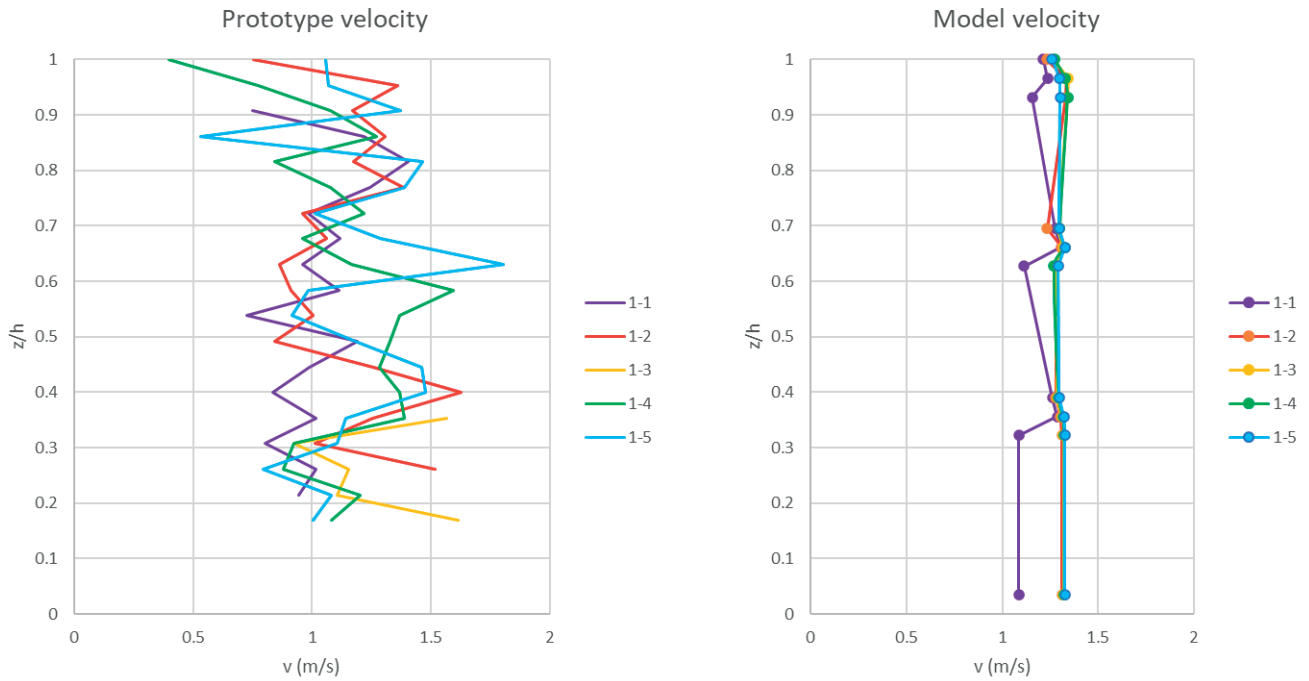


Figure 3. ADCP measured velocity (left), ADV measured velocity (right)

Verified physical model will be used to measure flow velocities around the bridge pier protected with riprap for the R3PEAT (Remote Real-time Riprap Protection Erosion AssessmentT on large rivers) project.

Keywords: ADV, physical model, Vectrino Profiler, ADV parameters, verification, R3PEAT.

Acknowledgments

This work has been supported in part by Croatian Science Foundation under the project R3PEAT (UIP-2019-04-4046).

IV Hydraulic structures

SENSITIVITY ANALYSIS OF DL BREACH MODEL FOR SIMULATION EMBANKMENT DAM BREACHING DUE TO INTERNAL EROSION

STANISLAV KOTAŠKA¹, JAROMÍR ŘÍHA¹

¹ Brno University of Technology, Faculty of Civil Engineering, Institute of Water Structures; Czech Republic
e-mail: kotaska.s@fce.vutbr.cz, riha.j@fce.vutbr.cz

Abstract

One of the most frequent failure mode of embankment dams is internal erosion. For the simulation of the breaching process DL Breach model was used (also implemented into HEC-RAS code). DL Breach is one-dimensional numerical 1D model containing both hydraulic and transport modules [1].

For the simulation numerous input parameters have to be specified such as inflow hydrograph, reservoir bathymetry, hydraulic data (roughness), characteristics of the dam, soil properties (density, porosity, grain size, strength) and erodibility characteristics, etc. Initial conditions are represented by initial reservoir water level H_0 , characteristics of seepage path such as initial pipe diameter d_0 and elevation of the pipe outlet Z_0 . While some of the input values can be specified with reasonable accuracy, the other are subject to significant uncertainty.

To assess an impact of uncertainty of input variables on the resulting breach discharge Q and final breach width B , one at a time (OAT) parameter sensitivity analysis was applied. The method consists in repeatedly changing one selected input parameter (5 values were set – 0.6, 0.8, 1.0, 1.2 and 1.4 of average value) while the others are fixed. The procedure is repeated for all selected uncertain input variables. The simulations were carried out for the parameters of the dam subjected to the field test of the piping dam breach conducted as part of the IMPACT project in Norway in 2004 [2]. From the test fixed input values were specified (soil particle density $\rho_b = 2650 \text{ kg/m}^3$, bathymetry of the reservoir, dimensions of the dam, H_0 , d_0 , Z_0), the other are subject to significant uncertainty (erodibility k_d , cohesion c , critical shear stress τ_c , internal friction angle φ , porosity p , sediment diameter d_{50} and roughness n).

The set of generated variables serve as an input for the deterministic model (DL Breach) providing resulting Q and B values. The evaluation of results was carried out by normalizing input variables (horizontal axes in Fig. 1).

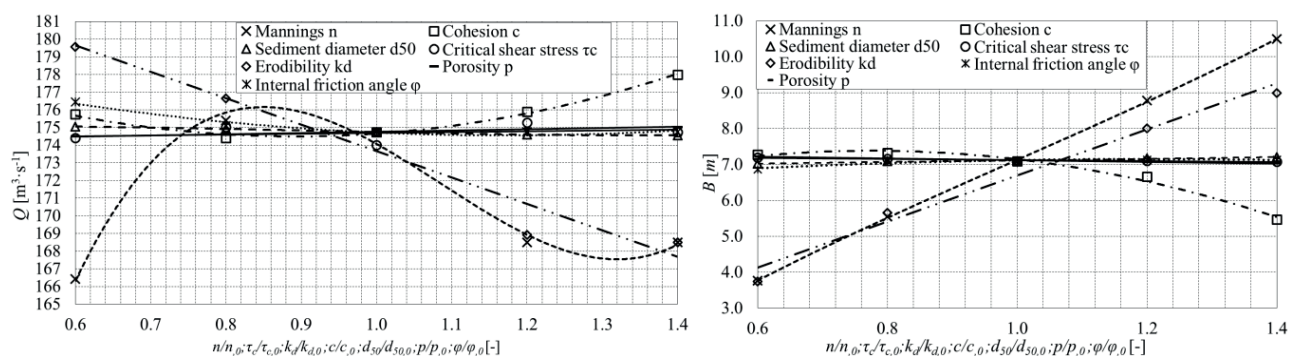


Figure 1. The results of the sensitivity analysis. Influence on the peak discharge (left) and breach width (right)

The sensitivity analysis indicates that resulting Q and B is mostly sensitive to changes in the erodibility coefficient k_d and the roughness factor according to Manning s n . Fig. 1 shows that the critical shear stress τ_c , internal friction angle φ , porosity p , sediment diameter d_{50} doesn't have any meaningful influence on the final results. For that reason it can be selected deterministically.

Acknowledgements

The paper is a part of the project FAST-J-21-7486 *Sensitivity analysis of parameters of internal erosion dam breach models* and TH04020154 *Optimization of the construction, repair and operation of asphalt-concrete linings*.

References

- [1] Wu, W. 2016. Introduction to DL Breach – A simplified physically based dam/levee breach model. Clarkson University, NY, 119 p.
- [2] Vaskinn, K.,A.; Lovoll, A.; Morris, M.; Hassan M.,A.,A., M. Physical modelling of Breach formation: Large scale field test. IMPACT project, (www.floodsite.net), 2004.

V Ecohydrology and Water Body Protections

DISPERSION ANALYSIS USING DYE TEST AT A SMALL STREAM

JAROMÍR ŘÍHA¹, TOMÁŠ JULÍNEK¹, STANISLAV KOTAŠKA¹

¹ Brno University of Technology, Faculty of Civil Engineering, Institute of Water Structures; Czech Republic

e-mail: riha.j@fce.vutbr.cz, julinekt@fce.vutbr.cz, kotaska.s@fce.vutbr.cz

Abstract

The modelling of pollution transport processes in open channels requires good knowledge about parameters such as hydrodynamic dispersion, advection and decay rates. Such parameters can be determined by dye tests. Number of tracer studies have been done on large rivers. In this study the dye test was realized on the local small stream using Rhodamine WT fluorescein dye as a tracer. Four tests were carried out in order to obtain longitudinal and transversal dispersion. For this purpose, analytical solution of transport dispersion equation was used. The results indicated dispersion coefficients $D_L = 0.065 \text{ m}^2/\text{s}$ (longitudinal) and $D_{PH} = 0.0006 \text{ m}^2/\text{s}$ (horizontal transversal).

1. Description of the locality

Dye tests were carried out at the Lipkovsky stream in the north of the Czech Republic. The selected reach of the stream was about 63 m long with constant discharge $Q = 0.225 \text{ m}^3/\text{s}$ and with average profile velocity $v = 0.42 \text{ m/s}$. The vertical velocity in the central part of the cross section subject to dye transport was approximately constant counting $v_p = 0.65 \text{ m/s}$. The average water depth was $h = 0.21 \text{ m}$, the width of the stream was about 2.6 m. The discharge in the stream and also the velocity distribution was determined by hydrometric measurement in two profiles 0 and D (Fig. 1).

2. Dye tests

To determine transport parameters, four dye tests were carried out. Data about the clouds' positions and dimensions were collected at 6 time instants and related to the profiles 0 – D (Fig. 1). 2 grams of Rhodamine WT dye was applied as an instantaneous injection in the centreline of the stream in the profile 0. Approximately elliptical extent of the dye cloud in the stream was recorded by the measuring staff at individual instants (Fig. 1). Following data were recorded simultaneously during the experiment:

- arrival time of the cloud front in 7 profiles,
- position of the centre of the cloud,
- width of the central part of the cloud,
- position of the cloud end.

Based on the recorded data the isolines characterizing the dye cloud visibility limit were expressed by ellipses for 6 time instants and four tests. In Figure 1 the results for the tests No. 3 are shown.

3. Backward analysis

In this study the longitudinal dispersion coefficient D_L and horizontal transversal dispersion coefficient D_{PH} in the stream were quantified by the comparison of the dye extent identified during the dye test and obtained from the calculation. For the solution, constant water depth and velocity in vertical were assumed at the central section of the stream where the dye propagated. The problem was solved as symmetrical according the vertical plane following the axis of the stream. Due to the small depth of the stream, ideal mixing along the vertical was taken into account. For the case mentioned above the concentration distribution along the stream holds [Holly, Usseglio-Polareta 1984]:

$$c(x, y, t) = \frac{M_V}{4 \cdot \pi \cdot t \cdot h \cdot \sqrt{D_L \cdot D_{PH}}} \cdot \exp - \left(\frac{[x - v_p \cdot t]^2}{4 \cdot D_L \cdot t} + \frac{y^2}{4 \cdot D_{PH} \cdot t} \right) \quad (1)$$

where M_V is the mass of injected dye (here $M_V = 1 \text{ g}$), $v_p = 0.65 \text{ m/s}$ and $h = 0.21 \text{ m}$ is the vertical velocity and water depth in the central part of the cross section, D_L and D_{PH} are coefficients of the longitudinal and horizontal transversal dispersion, x, y are coordinates (0,0 corresponds to the injection point) and t is the time.

For the backward analysis the “no dye” zone was represented by the concentration smaller than 10^{-4} mg/l , which corresponds about to 0.1 per mile of peak concentration at the last measured section. From Equation (1) it comes that the constant concentration at given time is represented by the ellipse. The comparison of measured and calculated results

for the test No. 3 are in Figure 1, the resulting concentration distribution for the times 34 s and 67 s are shown in 3D diagram in Figure 2.

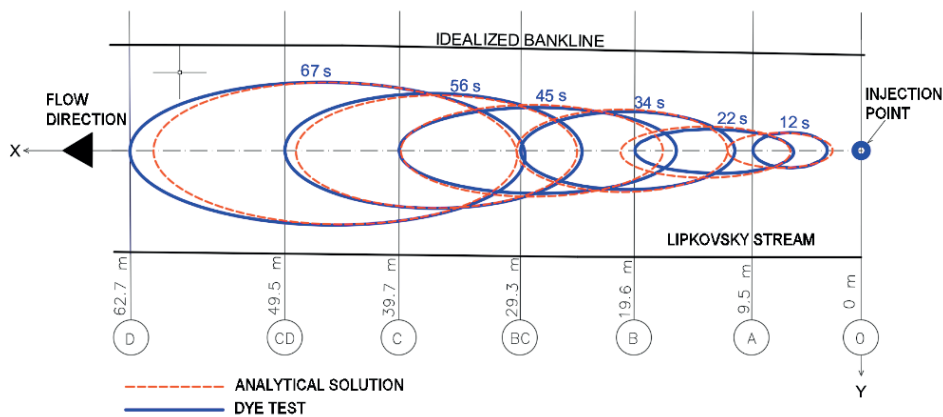


Figure 1. The results of the backward analysis (blue ellipses – dye test, red axes of ellipses – calculation)

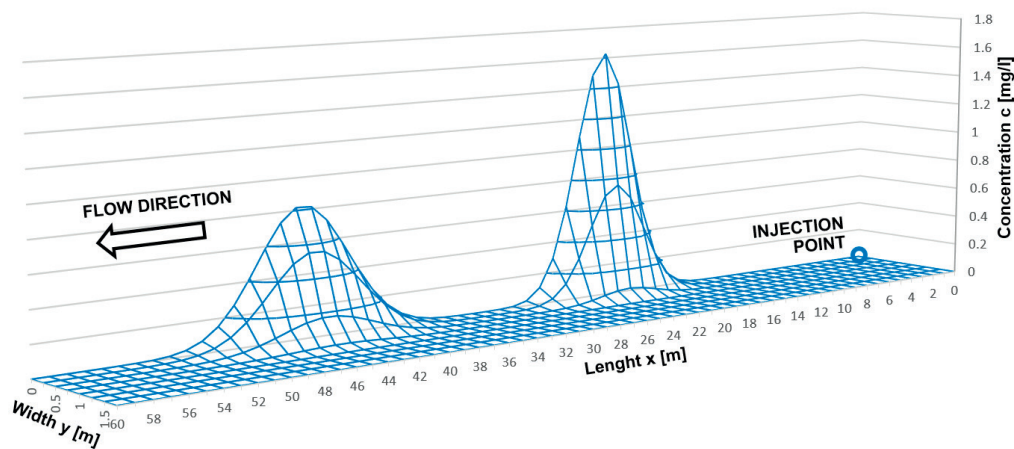


Figure 2. Resulting concentration distribution obtained from the analytical solution at times 34 s and 67 s

4. Conclusions

In the paper the backward analysis of the dye test in a small stream is carried out using analytical solution. Even if simplifications of the real flow domain and regime were adopted the results show acceptable agreement between observed and calculated extents of the dye cloud. The simplified method was based on the comparison of the cloud extent, no measurement of concentration was necessary. The concentration distribution may be obtained from the numerical calculations. The dispersion coefficients $D_L = 0.065 \text{ m}^2/\text{s}$ and $D_{PH} = 0.0006 \text{ m}^2/\text{s}$ are within the range of published values [Sayre, Chang 1968].

Acknowledgements

The paper is a part of the project TH04020154 *Optimization of the construction, repair and operation of asphalt-concrete linings*.

References

- [1] Holly, Jr., F.M., Usseglio-Polatera, J.-M. 1984. Dispersion Simulation in Two-Dimensional Tidal Flow. *Journal of Hydraulic Engineering*, vol. 110, No. 7, July, 1984, ASCE, paper no 18997, p. 905–926.
- [2] Sayre W.W., Chang F.M. 1968. A Laboratory Investigation of Open-Channel Dispersion Processes for Dissolved, Suspended, and Floating Dispersants. U.S. Geological Survey. Prof. Paper 433-E, 71 p.

Keywords: hydrodynamic dispersion, backward analysis, dye test, transport, rhodamine.

VII Climate Change and Flood Risk Management

FUTURE CHANGE IN LOW FLOW CHARACTERISTICS IN SELECTED GAUGING STATIONS OF SLOVAKIA

ZUZANA SABOVÁ¹, SILVIA KOHNOVÁ¹, ZUZANA NĚMETOVÁ¹

¹ Slovak University of Technology in Bratislava, Faculty of Civil Engineering, Department of Land and Water Resources Management; Slovakia

e-mail: zuzana.sabova@stuba.sk

Abstract

During recent decades the attention is increasingly focusing on the issue of drought. Drought is associated with water scarcity and occurs more often in Slovakia like in the past. Drought is one of the many extremes that are caused by climate change. Using various climate scenarios is possible to predict the future development of minimum discharge characteristics affected by climate change and anthropogenic influences. The present study used two regional climate scenarios: the Dutch KNMI and the German MPI, to detect the future changes in low flow characteristics in the eight River basins of Slovakia.

The research area is the territory of the Slovak Republic, where following River basins with these gauging stations (Fig. 1), i.e. Myjava – Jablonica (No. 5022), Váh – Liptovský Mikuláš (No. 5550), Turiec – Martin (No. 6130), Nitra – Nitrianska Streda (No. 6730), Hron – Banská Bystrica (No. 7160), Poprad – Chmeľnica (No. 8320), Laborec – Humenné (No. 9230), and Topľa – Hanušovce nad Topľou (No. 9500).

The available data were observed data from gauging stations (OBS) from 1981 to 2010. Modelled data created by the Department of Water Management of the Slovak University of Technology in Bratislava using the rainfall-runoff HBV model (MODEL HBV) were simulated for the period 1981–2010. The input to the HBV model was actual (real) precipitation and total temperature. Parameters from the model calibration were also used for simulated data according to both climatic scenarios (KNMI and MPI) from 1981 to 2100. All data were in the form of daily discharges.

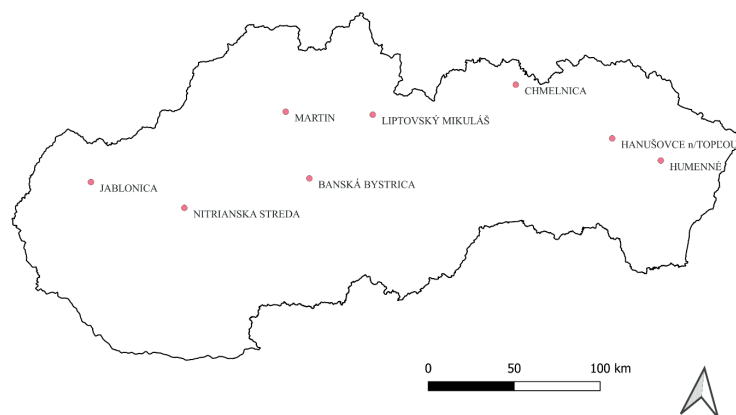


Figure 1. Location of the selected gauging stations in Slovakia

The program The Indicators of hydrologic Alteration (IHA) was used to calculate hydrological statistics to assess the degree of hydrological change. The program outputs consist of 67 parameters, which are available in graphical or tabular form. Analyzes were performed by nonparametric statistics at the level of the hydrological year. The analyzed period was from 1981 to 2100 and was divided into four 30-year periods. The analyzed characteristics of the minimum discharges are the occurrence of the minimum discharges, baseflow index, and 7- to 90-day minimum discharges.

First, the occurrence of the minimum discharge can be seen in Table 1a for the KNMI climate scenario data and Table 1b for the MPI climate scenario data. All the gauging stations generally have the occurrence of the minimum discharge between September and March. For the simulated data according to the KNMI climate scenario, the shift of the occurrence of the minimum discharge is in October by 2100. For the simulated data according to the MPI climate scenario, the occurrence of the minimum discharge is in October and November by 2100.

Table 1a. Summary of the occurrence of the minimum discharge for the simulated data according to the KNMI climate scenario

ID	River	Gauging station	OBS	MODEL HBV	KNMI	KNMI	KNMI	KNMI
			1981–2010				2011–2040	2041–2070
5022	Myjava	Jablonica	September	November	November	October	November	October
5550	Váh	Liptovský Mikuláš	February	February	March	February	December	November
6130	Turiec	Martin	October	November	November	October	October	August
6730	Nitra	Nitrianska Streda	September	November	October	October	November	October
7160	Hron	Banská Bystrica	November	January	November	November	November	October
8320	Poprad	Chmeľnica	January	January	January	November	November	October
9230	Laborec	Humenné	September	November	November	November	November	October
9500	Topľa	Hanušovce nad Topľou	October	January	January	November	November	October

Table 1b. Summary of the occurrence of the minimum discharge for the simulated data according to the MPI climate scenario

ID	River	Gauging station	OBS	MODEL HBV	MPI	MPI	MPI	MPI
			1981–2010				2011–2040	2041–2070
5022	Myjava	Jablonica	September	November	November	November	October	November
5550	Váh	Liptovský Mikuláš	February	February	March	March	February	February
6130	Turiec	Martin	October	November	November	November	November	October
6730	Nitra	Nitrianska Streda	September	November	November	November	November	October
7160	Hron	Banská Bystrica	November	January	December	November	November	October
8320	Poprad	Chmeľnica	January	January	January	December	November	November
9230	Laborec	Humenné	September	November	November	November	November	November
9500	Topľa	Hanušovce nad Topľou	October	January	January	January	November	November

The results of the baseflow index (Table 2) indicate that for the Váh – Liptovský Mikuláš (No. 5550) gauging station, the increase of the baseflow index for the future. The growth is also visible for the Poprad – Chmeľnica (No. 8320) and Topľa – Hanušovce nad Topľou (No. 9500) gauging stations. These basins are in mountain areas and have dominant low flows in the winter months. Other gauging stations are characterized by decreasing values of the baseflow index.

Table 2. The results of the baseflow index development by 2100 in selected gauging stations

ID	River	Gauging station	OBS	MODEL HBV	KNMI	MPI	KNMI	MPI	KNMI	MPI	KNMI	MPI
			1981–2010				2011–2040		2041–2070		2071–2100	
			[-]									
5022	Myjava	Jablonica	0.26	0.17	0.12	0.15	0.14	0.13	0.11	0.13	0.10	0.10

5550	Váh	Liptovský Mikuláš	0.34	0.42	0.40	0.37	0.46	0.38	0.48	0.45	0.48	0.47
6130	Turiec	Martin	0.40	0.38	0.36	0.37	0.34	0.35	0.32	0.37	0.28	0.29
6730	Nitra	Nitrianska Streda	0.32	0.30	0.24	0.29	0.23	0.24	0.21	0.23	0.18	0.21
7160	Hron	Banská Bystrica	0.33	0.33	0.35	0.35	0.32	0.32	0.30	0.32	0.28	0.29
8320	Poprad	Chmeľnica	0.25	0.24	0.24	0.20	0.25	0.24	0.29	0.33	0.28	0.30
9230	Laborec	Humenné	0.14	0.20	0.17	0.18	0.16	0.17	0.14	0.17	0.11	0.12
9500	Topľa	Hanušovce nad Topľou	0.22	0.30	0.23	0.25	0.26	0.26	0.25	0.27	0.21	0.24

The analysis of the 7-day minimum discharges in selected Slovak River basins does not show extreme future changes. The most significant increase in the 7-day minimum discharge is recorded in the Váh – Liptovský Mikuláš (No. 5550) gauging station for the simulated data according to both climate scenarios.

The 90-day minimum discharges demonstrate more extensive changes according to both climate scenarios by 2100. The most significant decrease in the values of the 90-day minimum discharges in the future can be seen in the Myjava – Jablonica (No. 5022) and Laborec – Humenné (No. 9230) gauging stations. Data from the Váh – Liptovský Mikuláš (No. 5550) gauging station show increased values of the 90-day minimum discharge.

Finally, we can conclude that the highest changes in low flows are registered for the Váh – Liptovský Mikuláš (No. 5550) gauging station by 2100. This River basin may be affected by its location, in the north of Slovakia, where the upper part lies in the high mountain areas of the High and Low Tatras region, where the snow regime is dominant. The Hron – Banská Bystrica (No. 7160) gauging station has similar conditions. A decrease in the investigated hydrological characteristics applies to selected gauging stations. Analyses have shown that drought will be a more significant problem for the territory of Slovakia in the lowlands in the west and east of the country.

Acknowledgements

This work has been funded by the VEGA grant agency under the contract numbers VEGA 1/0632/19. This work has been funded by the APVV grant agency under the contract numbers APVV-20-0374. The authors are grateful for their financial support.

Keywords: climate change, the KNMI climate scenario, the MPI climate scenario, IHA method, minimum discharges, base flow index.

VII Climate Change and Flood Risk Management

IMPROVEMENT OF SURFACE EROSION RESISTANCE OF SILTY SAND SOIL BY BIOPOLYMER-BASED TREATMENT

ALEKSANDRA NIKOLOVSKA ATANASOVSKA¹, JOSIF JOSIFOVSKI¹, BOJAN SUSINOV¹

¹ Ss. Cyril and Methodius University in Skopje, Faculty of Civil Engineering; Republic of North Macedonia
e-mail: nikolovskaaleksandra189@gmail.com, josifovski@gf.ukim.edu.mk, susinov@gf.ukim.edu.mk

Abstract

Nowadays, the consequences of climate change are becoming more visible and almost impossible to ignore. Climate change has a significant influence on the slope stability of the existing infrastructure. Exposed to atmospheric perturbations such as higher temperature and rainfall, they can become unstable with deformation, cracking, water infiltration, shallow (local) sliding and erosion.

In general, the cut-slope design is not taking into account the phenomenon of soil-atmospheric interaction. In practice, there are a lot of examples where the erosion and local instabilities with time escalate into global instabilities that eventually cause a collapse of the slope. To overcome these problems, it is necessary to take adequate measures to improve the erosion resistance on the slopes by using naturally-based solutions, hence in this case the biopolymer solution. In geotechnical engineering worldwide, natural polymer compounds are used to improve and stabilize the soil. The natural enhancers to some extent improve the soil mechanical and hydrological properties. Hence, the natural biopolymer solutions form a solid gel matrix with a strong bond with the soil grains and also fill the soil pores, which produce high resistance to deformation, cracking and erosion as well they restrict the surface water infiltration into the soil. This measure can be enhanced by using vegetation which will provide long-term protection.

This paper presents a study where the effects of the biopolymer solution are investigated through a series of laboratory tests. A concentration of 1.0% of the Xanthan gum compound was used on a sample of silty sand soil. In the first test phase, the material was characterized through the standard classification tests, after which the strength parameters and water permeability were determined. The soil strength was obtained through the Uniaxial compressive test and Direct shear test. Hence, the measured strength of the treated samples on the 1st day was 257 kPa but due to the curing of the admix an increase of 1744 kPa was reached on the 28th day. Thus if compared to the strength of the untreated sample which was 435 kPa, the biopolymer additive seems to be responsible for a 4.6 times increase in strength. The Oedometer test was used to determine the compressive modulus of the treated sample which for the pressure of 240 kPa was 4648 kPa, in contrast to the value of 2945 kPa of the untreated soil sample, or an increase of 1.6 times. The coefficient of water permeability of the treated soil is 2.20×10^{-6} m/s, while of the natural soil is 3.47×10^{-7} m/s.

In the second test phase, an experimental investigation on a small-scale model was performed, where a 1:1.5 slope had been exposed to 10 l/h rainfall in 180 minutes. The test results showed that the biopolymer solution reacted very well with the soil particles creating a surface crust, stabilizing the particles, had restricted the water infiltration, thus proving that the biopolymer solution admixes offers higher resistance to erosion. The amount of eroded soil in the untreated sample was 1900 gr/m² or 9.5% loss of the soil content while the biopolymer-treated sample had almost zero loss of the soil content which is depicted in Figure 1.

Finally, it can be concluded that naturally-based solutions, such as biopolymers, offer an efficient, environmentally-friendly and economically viable engineering solution for surface stabilization of the soil slopes. This study will continue in the next period with the third test phase where the methodology and efficiency of the biopolymer solution will be proved in in-situ conditions on infrastructure cut-slopes.

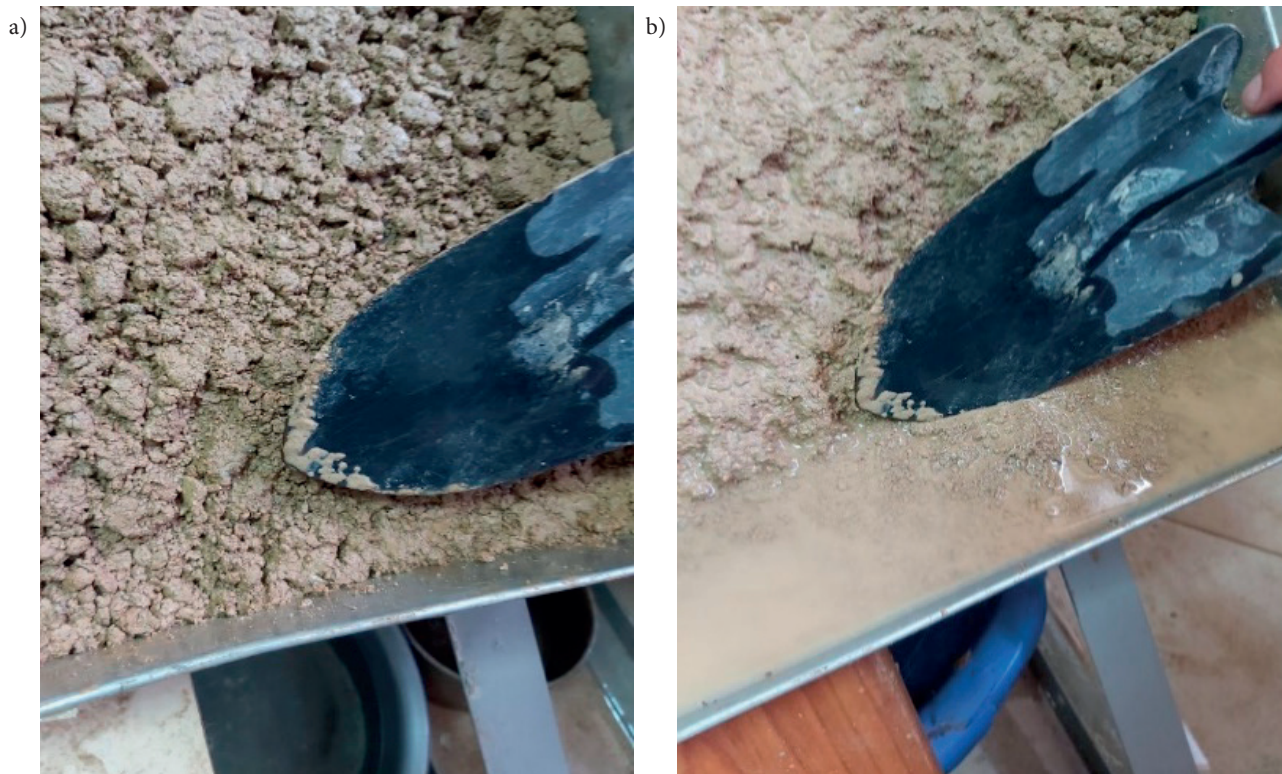


Figure 1. Slope erosion of a) biopolymer-treated and b) untreated soil after 180 minutes of rainfall exposure

Keywords: slope stability, erosion resistance, biopolymer binder, xanthan gum, experimental study.

VII Climate Change and Flood Risk Management

RAINWATER MANAGEMENT IN GDANSK – METEOROLOGICAL AND HYDROLOGICAL MONITORING

WOJCIECH SZPAKOWSKI^{1, 2}

¹ Gdańsk University of Technology, Faculty of Civil and Environmental Engineering, Department of Geotechnical and Hydraulic Engineering; Poland
e-mail: wszp@pg.edu.pl

² Gdansk Water, Poland
e-mail: w.szpakowski@gdanskiewody.pl

Abstract

Gdansk is located in the North of Poland in the Vistula River mouth. The west part of the city is situated on a moraine hills up to 180 m a.s.l. The east part of the city is a depression land of the Vistula Delta Plain. Such a location of the city results in the changeability of meteorological conditions, among which precipitation is the most important.

Gdansk has a separate sewage system. For this reason, almost 30 years ago, the management of these systems was separated. The company Gdansk Water is responsible for the municipal rainwater management system.

The first rain gauge and a water level sensor were installed in 2001. After a few months in July, Gdansk experienced the largest rainfall flood due to losses (main rainfall about 6 hours with daily sum of rainfall of about 130 mm). Such an event occurred again in July 2016 (main rainfall about 8 hours with daily sums of rain up to 170 mm). Since 2001, Gdansk has built or modernized over 50 retention reservoirs with a total retention volume of approximately 800,000 cubic meters. Therefore, in 2016 the losses caused by the precipitation flood were much lower compared to 2001. (Szpakowski, Szydłowski 2017 and 2018a)

The longest rain data in Gdańsk is collected by the IMGW-PIB (National Meteorological and Water Management Institute-Polish Scientific Institute) near the Gdansk Lech Walesa Airport located in the Rebiechowo district. Basing this data, probably daily sum of rainfall were established (Szpakowski, Szydłowski 2018b). But the Climate change has shown the need for accurate measurements both of meteorological elements in the different parts of the Gdansk city and the knowledge of current water levels.

Several rain gauges were built until 2007. Later, as a result of cooperation between the city of Gdansk and the Gdańsk University of Technology, measurement of the Strzyza stream catchment area was performed, which allowed for a detailed analysis of the rainfall-runoff processes in this catchment area. The largest increase in the system with rainfall sensors (and other meteorological parameters) and water level sensors took place in 2017. Currently, there are 26 meteorological sensors (mainly precipitation) and almost 80 water level sensors (retention reservoirs, streams, ditches and rainwater sewage system) located in the city. The neighbouring communes (Gdynia, Sopot) and municipal companies from outside Gdańsk join the system with their sensors. Such activities made this measurement system the largest local meteorological system in Poland (Fig. 1).

The system is used in various ways. It is used to optimize crisis management in municipalities. Up-to-date information on precipitation allows you to select districts in which the intervention of emergency services will be necessary. The system allows for the analysis of the catchment response to various precipitation patterns. As a result of these activities, various activities are carried out to improve safety in the catchments. Based on the collected rainfall data, it will be possible to establish and update local rainfall formulas.

An important advantage of the system is the cooperation of the municipality of Gdansk (the Gdansk Water company) with scientific units – the main one with the Gdańsk University of Technology. As a result of cooperation, scientific publications and technical expertise are created. The most important publications concern the analysis of rainfall phenomena, rainfall-runoff analysis in Gdansk catchments, and aspects related to the quality of surface waters. In recent years, important publications related to the implementation of the nature based solution policy in Gdansk have been published, in this issue Gdansk is also a leader in Poland (Kasprzyk M. et al 2022).

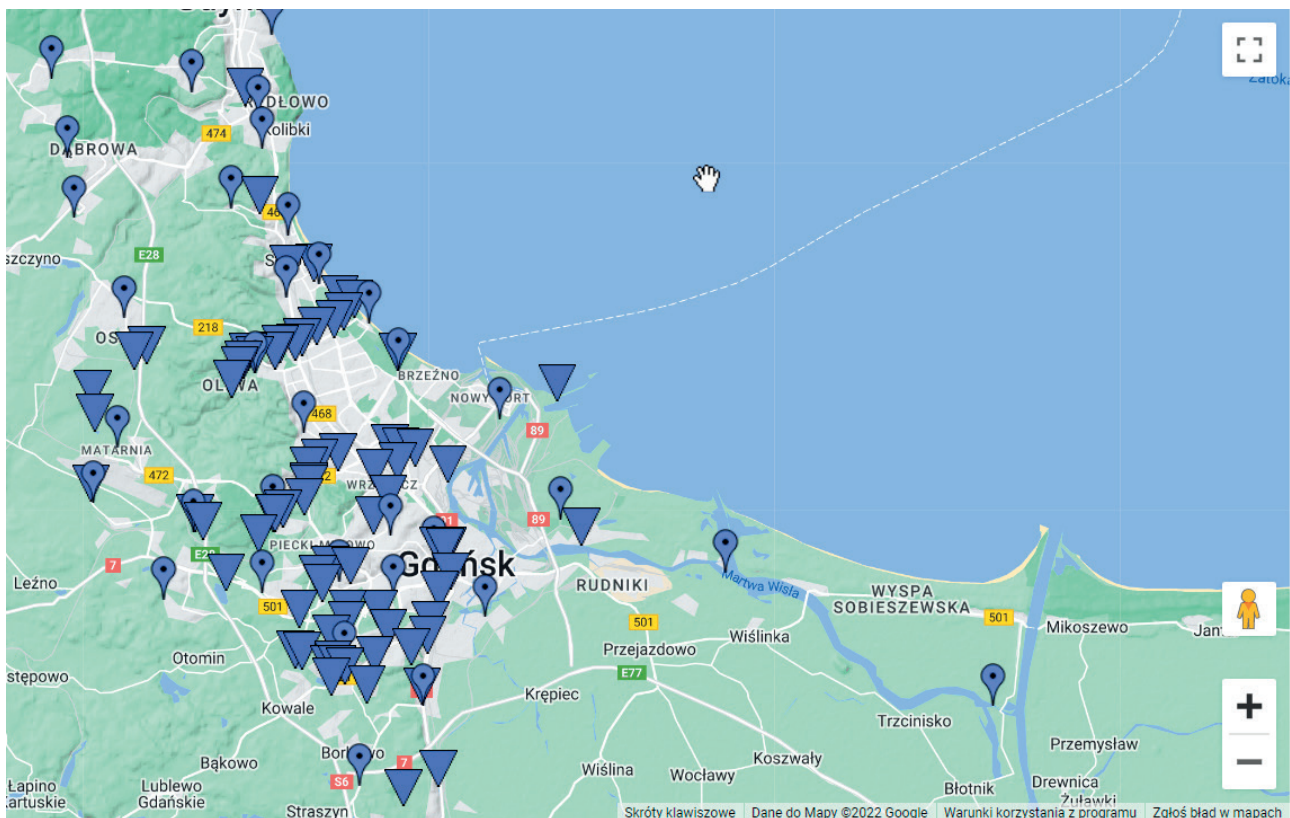


Figure 1. Localisation of the sensors of meteorological and hydrological monitoring system
(source: <https://pomiar.gdanskiewody.pl/map>)

The Gdansk Water company deals mainly with the management of rainwater and snowmelt in the city of Gdansk. Precipitation is analysed on an annual basis (monthly totals). Since 2018, days with precipitation above 10 mm that occurred in the warm half-year (May–October) have been analysed in detail. For such episodes, the type of rainfall was determined using the Chomicz scale. The maximum rainfall intensity for 10 minutes to 24 hours is also analysed.

In recent years, short episodes lasting up to 120 minutes have definitely dominated in Gdansk. Temporary rainfall during such events could exceed 25 mm in 10 minutes or 45 mm in 30 minutes and caused perturbations in the operation of the city infrastructure in selected city districts.

Keywords: monitoring system, rainwater management, rain gauge, crisis management; flash floods, torrential rain.

References:

- [1] Szpakowski, W., & Szydłowski, M. (2017). Extraordinary Rainfalls in Gdansk (Northern Poland) in the 21st Century. *PROCEEDINGS of the 15th International Symposium Water Management and Hydraulics Engineering*, pp. 2–11.
- [2] Szpakowski, W., & Szydłowski, M. (2018a). Evaluating the Catastrophic Rainfall of 14 July 2016 in the Catchment Basin of the Urbanized Strzyza Stream in Gdańsk, Poland. *POLISH JOURNAL OF ENVIRONMENTAL STUDIES*, 27(2), 861-869. <https://doi.org/10.15244/pjoes/75962>
- [3] Szpakowski, W., & Szydłowski, M. (2018b). PROBABLE RAINFALL IN GDAŃSK IN VIEW OF CLIMATE CHANGE. *Acta Scientiarum Polonorum Formatio Circumietus*, 3(18(3)), 175-183. <https://doi.org/10.15576/asp.fc/2018.17.3.175>
- [4] Kasprzyk, M., Szpakowski, W., Poznańska, E., Boogaard, F., Bobkowska, K., & Gajewska, M. (2022). Technical solutions and benefits of introducing rain gardens – Gdańsk case study. *SCIENCE OF THE TOTAL ENVIRONMENT*, 835, 155487. <https://doi.org/10.1016/j.scitotenv.2022.155487>

The background features a solid blue color. In the center, the word "Articles" is written in a large, white, sans-serif font. Behind this text, there are several faint, light blue letters 'A' scattered across the page. In the top-left corner, there is a faint, light blue graphic of a globe showing latitude and longitude lines.

Articles

I Integrated Water Resources Management

APPLICATION OF SIMULATION MODELS FOR MANAGEMENT OF COMPLEX WATER RESOURCES SYSTEM

STEVCHO MITOVSKI¹, FROSINA PANOVSKA¹, LJUPCHO PETKOVSKI¹

¹ Ss. Cyril and Methodius University in Skopje, Faculty of Civil Engineering; Republic of North Macedonia
e-mail: smitovski@gf.ukim.edu.mk, fpanovska@gf.ukim.edu.mk, petkovski@gf.ukim.edu.mk

Abstract

The increasing water demands as well as unfavourable climate changes in the past decades have led to increased pressure to existing water resources systems worldwide and in our country. The priority is to maintain, manage and upgrade the existing water resources systems so they can successfully match the increased water demand for various purposes.

In the following paper, acknowledgments are commented obtained from simulation analysis of complex water resources system of cascade type, composed of existing two dams with reservoirs and planned water resources system with single dam and reservoir, as upgrade of the existing system, by application of simulation models. The input data are recorded hydrology time series of discharge for a period of 40 years, considered as sufficient amount of data to carry out reliable simulation analysis. In addition, the available data for the water demand are taken into consideration within the analysis.

Primary purpose of the existing two-reservoir water resources system is matching the water demand for water supply of the population and irrigation needs. In order to assess the state and capacity of the existing cascade water resources system, firstly, is prepared simulation model for such purpose. Based on the accomplished simulation experiment for the existing water resources system, another simulation model is prepared including the planned single water resources system. Namely, the simulation modeling and analysis run are carried out for both water resources systems – the existing and planned. The simulation models are prepared with application of HEC ResSim software, released by the USACE Army Corps of Engineers.

Keywords: complex water resources systems, simulation models, water demand, HEC ResSim.

1. Introduction

Scarcity of fresh water throughout the world as well as in RN Macedonia demands complex planning and management of available water resources. Mathematical models are created in order to comprehend the behaviour of complex water resources systems under different hydrology input as well as different operation policies applied to the system. Such analyses are done by simulation models, type of mathematical models that reproduce the behaviour of the system under certain hydrological input (inflows) and physical parameters of the system (1). Simulation model is a mathematical replica of the original system, describing the system with logical relations and mathematical equations (1). Namely, the model calculates output results of the system using the balance equation, having in consideration the input hydrographs, physical limitations of the system and the operation rules. The convenience of simulation models is the possibility of applying different input parameters, physical parameters or operation rules, and analysing the response of the system without implementing them on the real system, i.e. the simulation model is a simplified replica of the original system. Simulation models have been developed since mid 90's and are improved by the day – alongside digital technology development. Many software are available for the purpose of water resources simulation and analysis, such as MIT-SIM, WEAP, HEC ResSim, RIBASIM.

With application of simulation models, two different alternatives are analysed within the paper. The first alternative comprises of hydro system 'Lipkovo' and 'Glaznja', located in the north of RN Macedonia on river Lipkovska, north from the city of Kumanovo. The main purpose of this cascade hydro system is water supply for the city of Kumanovo and water for irrigation needs

The second alternative comprises of the hydro system 'Lipkovo' and 'Glaznja' upgraded with hydro system 'Slupchanka' wherefrom water is diverted to 'Lipkovo' in order to improve its water balance.

The goal of the analyses is to overview the capacity of the hydro system 'Lipkovo' and 'Glaznja', and the necessity of including hydro system 'Slupchanka' in order to fully suffice water needs in this region.

The first alternative represents the current state of the hydro system since ‘Lipkovo’ and ‘Glaznja’ are in operation, whereas ‘Slupchanka’ is in the process of commencement of the construction.

2. Case study

The analysed hydro systems are located in the north of RN Macedonia, close to the city of Kumanovo.

The hydro system ‘Lipkovo’ is comprised of two reservoirs with dams ‘Lipkovo’ and ‘Glaznja’ on river Lipkovska (Fig. 1). This configuration is alternative 1. ‘Lipkovo’ dam was built in 1958 as the downstream dam, whereas ‘Glaznja’ is located 5km upstream from ‘Lipkovo’ dam, built in 1972.

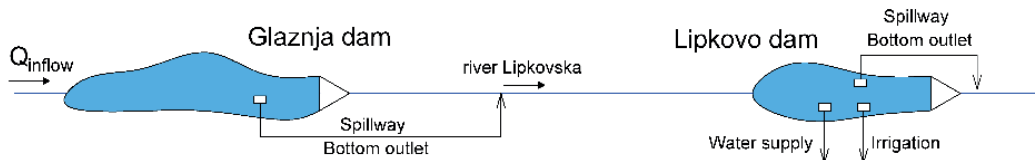


Figure 1. Layout of the cascade system ‘Lipkovo’

‘Lipkovo’ dam is concrete arch dam 40m high from the lowest point in the central cross section (Fig. 2), closing a reservoir with total volume capacity of $2,25 \times 10^6 \text{ m}^3$. The normal operating water level in the reservoir is 478 masl, whereas the minimal operating water level is 468 masl. Water from ‘Lipkovo’ reservoir is used for water supply of the city of Kumanovo (approximately 200 l/s throughout the whole year), as well as irrigation of agricultural fields in total area of 2754 ha (currently 1300 ha are being actively irrigated).

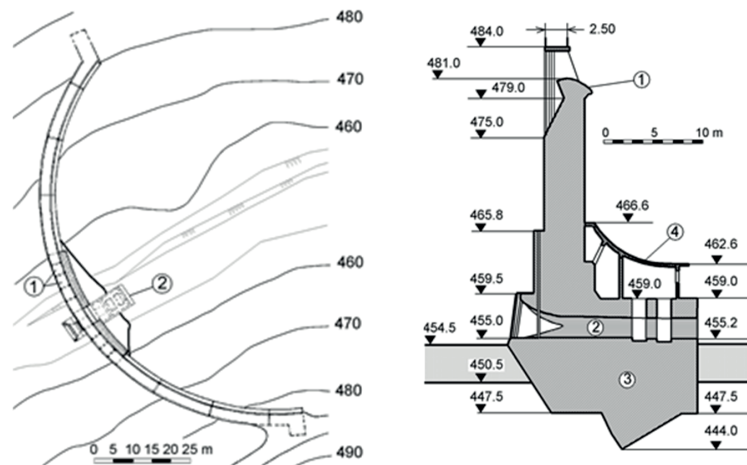


Figure 2. Layout and typical cross section of the arch dam ‘Lipkovo’

‘Glaznja’ dam is the highest concrete arch dam in RN Macedonia, 80m high, built 5km upstream from ‘Lipkovo’ reservoir (Fig. 3). ‘Glaznja’ reservoir has total volume capacity of $22 \times 10^6 \text{ m}^3$ ($\times 10$ times larger than ‘Lipkovo’ reservoir) where the main water management is conducted for this hydro system. The normal operating water level in the reservoir is 588 masl, whereas the minimal operating water level is 547,6 masl. Water from this reservoir is directly released into ‘Lipkovska’ river i.e. in the downstream ‘Lipkovo’ reservoir.

The hydro system ‘Lipkovo – Slupchanka’ is comprised of the previously described and built dams with reservoirs ‘Lipkovo’ and ‘Glaznja’, upgraded with dam and reservoir ‘Slupchanka’. Water from ‘Slupchanka’ reservoir will be diverted to ‘Lipkovo’ reservoir in order to improve its water balance and provide more reliable water supply flow (Fig. 4). This configuration, is hereafter, alternative 2. The connection between ‘Slupchanka’ and ‘Lipkovo’ is a pipeline. This pipeline is modelled as a ‘diverted outlet’ with assigned release of $0,2 \text{ m}^3/\text{s}$ at all times during the simulation analysis, hence, other physical characteristics of the pipeline are not of paramount importance to the model.

‘Slupchanka’ dam is located approximately 2 km upstream from the village ‘Slupchane’ – village in the region of Kumanovo city (Fig. 5). The dam is at stage of construction commencement, by prepared technical documentation at level of Basic Design, and it is planned as a concrete face rockfill dam, with height of 54m (2). The topographic curves for dam Slupchanka are displayed on Fig. 6.

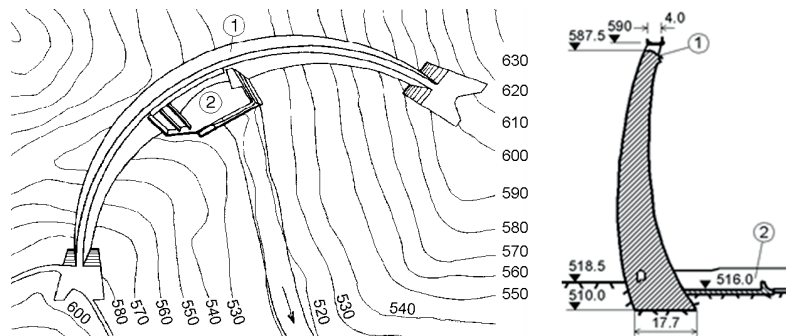


Figure 3. Layout and typical cross section of the arch dam 'Glaznja'

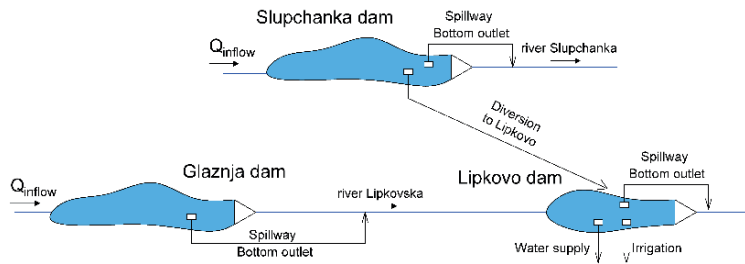


Figure 4. Layout of the cascade system 'Lipkovo - Slupchanka'

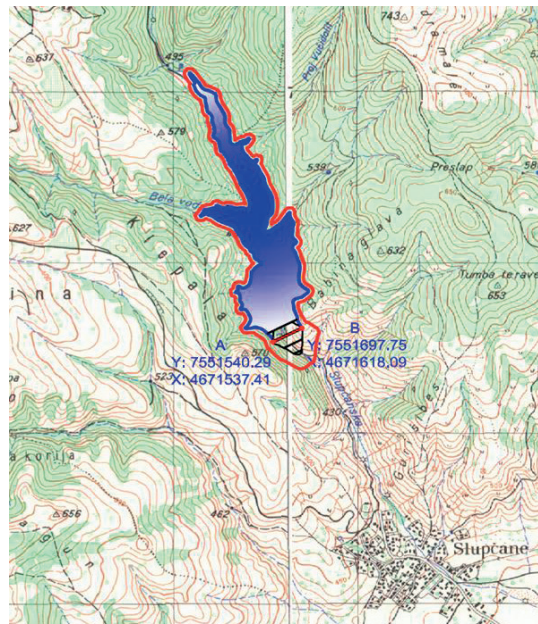


Figure 5. Location of 'Slupchanka' dam (2)

The normal operating level in the reservoir is 491 masl, and the minimal operating level is 468 masl. Total reservoir volume capacity is $2,89 \times 10^6 \text{ m}^3$.

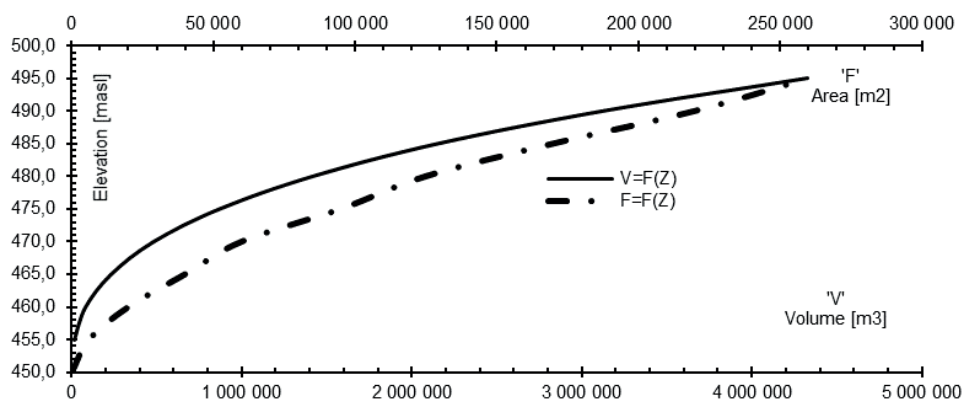


Figure 6. Topographic curves for reservoir 'Slupchanka' (2)

3. Simulation model

Simulation model is applied to perform the analyses of the complex water resources system. More precisely, the model was created by HEC ResSim software, that offers the possibilities for simulation analysis of complex water resources systems. The software consists of three basic modules: (1) Watershed setup, (2) Reservoir network, and (3) Simulation module (3). In the first module, the model is set up and relationships between the elements is defined. In the second module, physical parameters of the elements and operation rules for the whole systems are defined. In the third, defined configurations are called upon and analyses are conducted, with an overview of the results (4).

Two simulation models are analysed. Alternative 1 is comprised of ‘Lipkovo’ and ‘Glaznja’ reservoirs, whereas alternative 2 is comprised of ‘Lipkovo’, ‘Glaznja’ and ‘Slupchanka’ reservoirs.

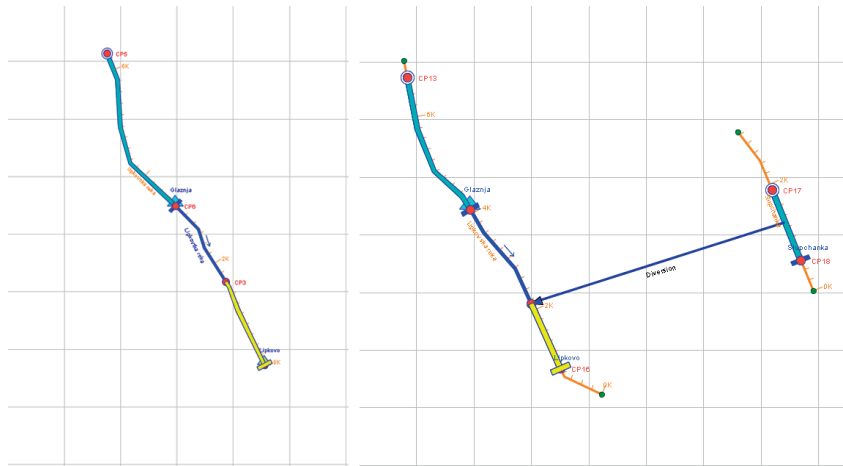


Figure 7. Display of schematics for simulation models for alternative 1 (left) and alternative 2 (right)

As input parameters, gauged flow hydrographs of Lipkovska and Slupchanka river are entered. Both hydrographs are over 40-years long (measured data from 1961 to 2000) and are used with the presumption that in future similar dry and wet periods will repeat – as gauged in the 40-year timeline. Reservoir parameters are defined through Volume-Surface curves, whereas physical parameters of the appurtenant structures are entered through their maximal capacity curves. The time step of simulation run is 1 Day, common for analyses of this type.

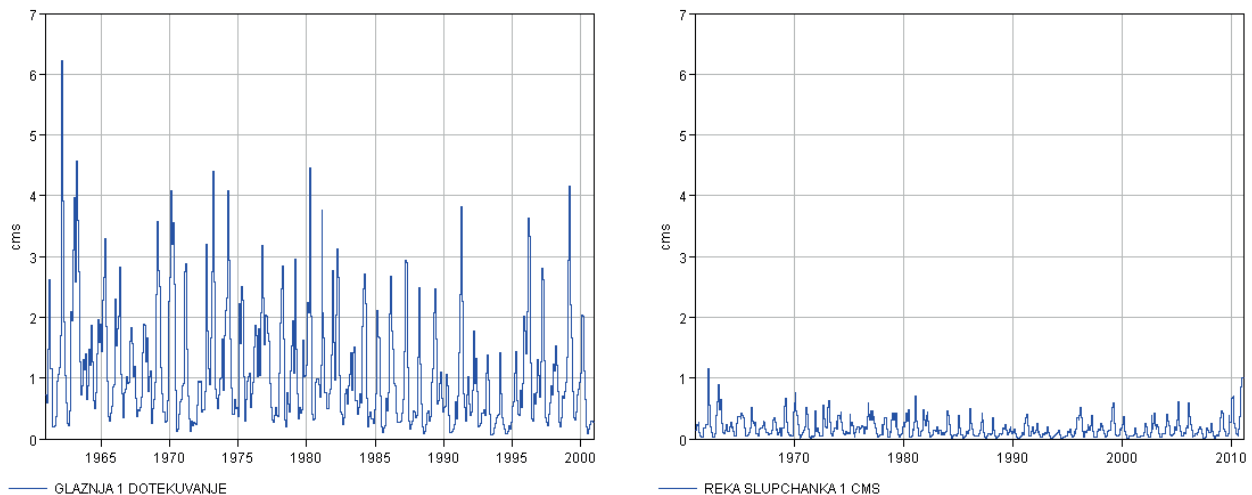


Figure 8. Hydrographs of inflow at ‘Glaznja’ and ‘Slupchanka’ reservoirs

Water supply and irrigation needs are entered as average monthly needs, derived from reference data (5).

Table 1. Monthly water needs for the city of Kumanovo

Q_{aver} [m ³ /s]	January	February	March	April	May	June	July	August	September	October	November	December
	0.260	0.220	0.230	0.230	0.250	0.260	0.270	0.260	0.240	0.230	0.220	0.200

Table 2. Monthly irrigation needs.

Q_{aver} [m ³ /s]	January	February	March	April	May	June	July	August	September	October	November	December
	0.000	0.000	0.290	0.290	0.290	0.290	0.290	0.290	0.000	0.000	0.000	0.000

In HEC ResSim it is mandatory to divide the reservoir in different zones. Each zone has its one, specific characteristics and rules that apply only for the zone itself. When creating a basic model, three zones are automatically generated: (1) Flood Control zone, (2) Conservation zone, and (3) Inactive zone. Flood control zone is normally the zone above normal operating water level, when the elevation in the reservoir rises above the normal level and spills out. Conservation zone is the zone where all operation rules are applied, such as rules for irrigation, water supply or whatever the purpose of the reservoir is. Basically, the volume of water in the conservation zone is the available water, that will be managed. Conservation zone is located between Flood control and the Inactive zone. Below the Inactive zone no rules can be applied since this water levels are considered to be below the physical capacities of the outflow structures. In Table 3, all three different zones and elevations for each reservoir is shown, as modelled in both alternatives.

Table 3. Definition of elevations for zones at the reservoirs for alternative 1 and 2

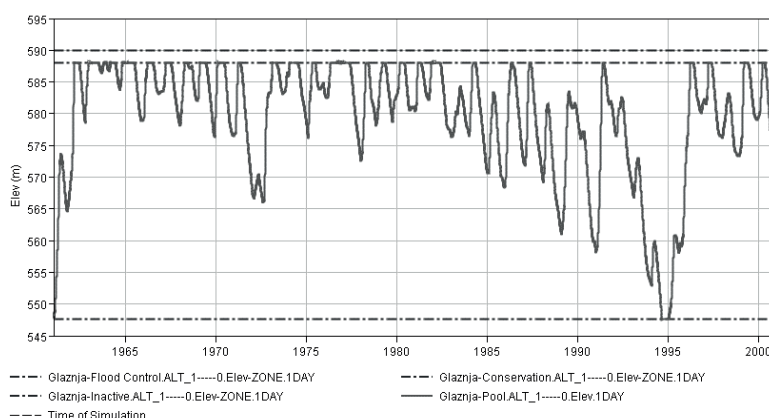
Reservoir / Zone [masl]	Glaznja	Lipkovo	Slupchanka
Flood control	590,00	482,80	495,00
Conservation	588,00	481,00	493,00
Inactive	547,60	468,00	468,00

4. Results and discussions

Two models are prepared for the capacity analyses, one for alternative 1 and second for alternative 2. Results on reservoir water level fluctuation and delivered water is commented as follows.

4.1. Alternative 1 – hydro system ‘Lipkovo’

For alternative 1, a simulation run was carried out for hydro system ‘Lipkovo’ comprised of both ‘Lipkovo’ as downstream and ‘Glaznja’ as upstream reservoir, for a simulation period from 1961 to 2000. The main purpose of this hydro system is delivering water quantities for water supply for the city of Kumanovo and for irrigation of the region. By analysing the output results for alternative 1, it can be noticed significant oscillation of the water level for reservoir Glaznja (Fig. 9), especially in the period of low water from 1988–1996. There is also variation of the input flow and output flow from the Glaznja reservoir (Fig. 10), according to overall reservoir capacity. The average controlled release towards ‘Lipkovo’ reservoir is $Q_{aver}=1,1 \text{ m}^3/\text{s}$.

**Figure 9.** Water level fluctuations in ‘Glaznja’ reservoir during the analyses period, for alternative 1

By analysing the output results for alternative 1 in case of Lipkovo reservoir, there is some oscillation of the water level (Fig. 11) typical for the period of low water from 1988–1996. There is also variation of the input flow and output flow from the Lipkovo reservoir (Fig. 12), according to overall reservoir capacity. The average controlled release from Lipkovo reservoir is $1,09 \text{ m}^3/\text{s}$ – much of which is due to spillway overflow.

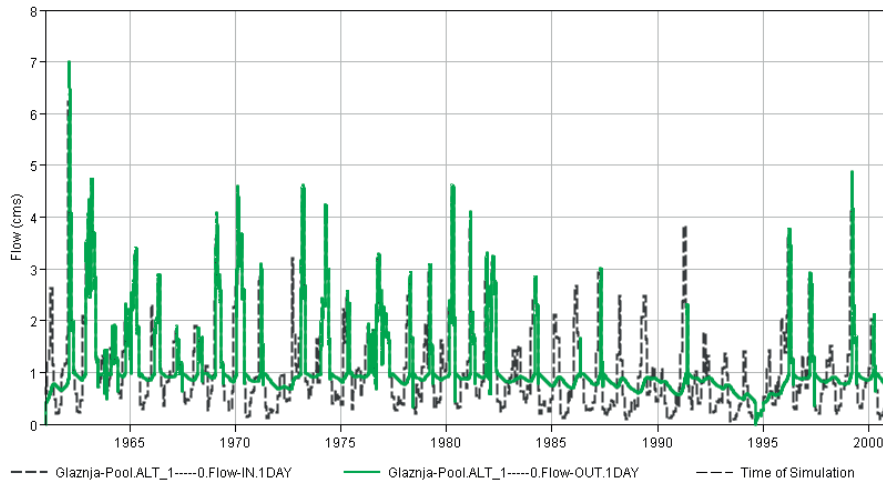


Figure 10. Inflow and outflow hydrographs for 'Glaznja' reservoir

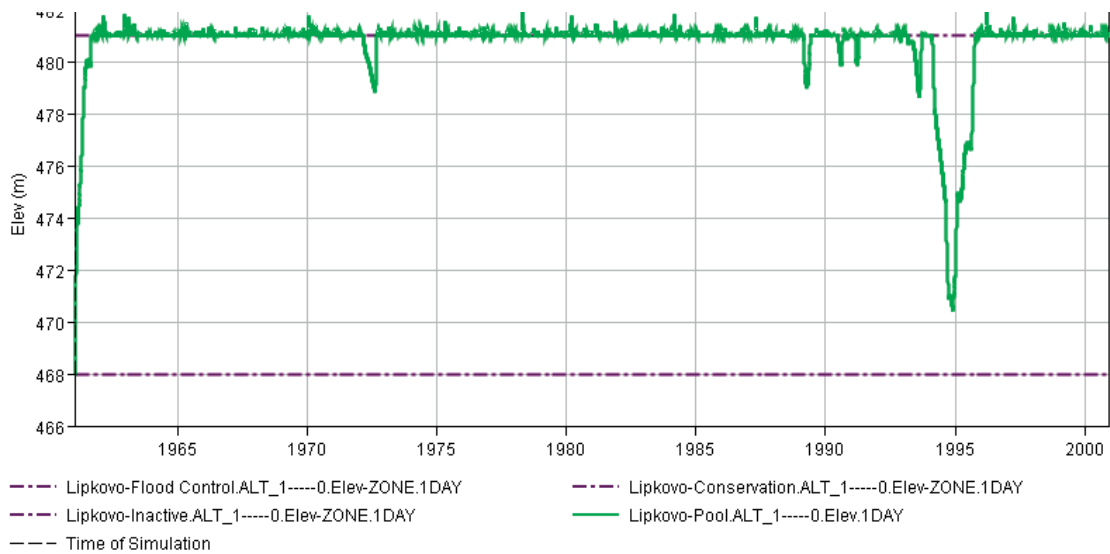


Figure 11. Water level fluctuations in 'Lipkovo' reservoirs during the analyses period, for alternative 1

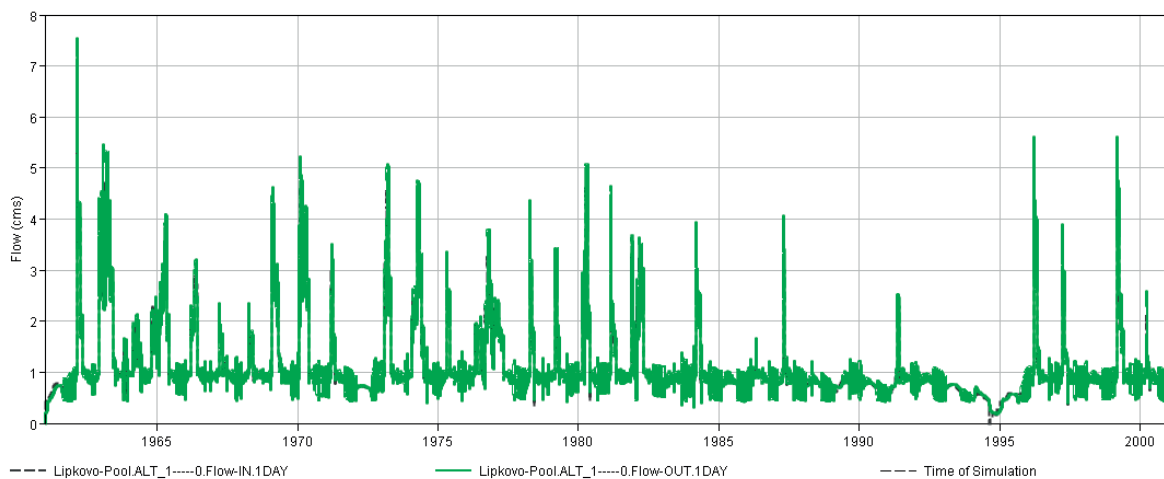


Figure 12. Inflow and outflow hydrographs for 'Lipkovo' reservoir

On Fig. 13 are displayed output values from reservoir Lipkovo for water supply, irrigation and environmental discharge, as well and spillway overflow. The environmental flow in the operation scenario is set as priority and it is matched during the full analysis period. The water supply and irrigation discharge are mainly matching the specified water demands. However, there is overflow from reservoir Lipkovo, that is minimized by the applied operation policy.

According to the results, with average release of $1,1 \text{ m}^3/\text{s}$ from 'Glaznja' reservoir and set tandem operation with 'Lipkovo', covering the target water needs is in range between 69% (January) to 100% for most of the other period

during the year (Figure 14, left), whereas 88% to 95% of the irrigation needs are covered during the vegetation period with this operation policy (Figure 14, right). Both water supply as primary, and irrigation as secondary water purposes are meeting the specified water demands according to the output results from alternative 1. It should be noted that the analyses are conducted with water needs for irrigation taken into consideration as average delivered water derived from 10-years long recorded data. The current irrigated fields using water from this hydro system are approximately 50% of the planned agricultural land for irrigation.

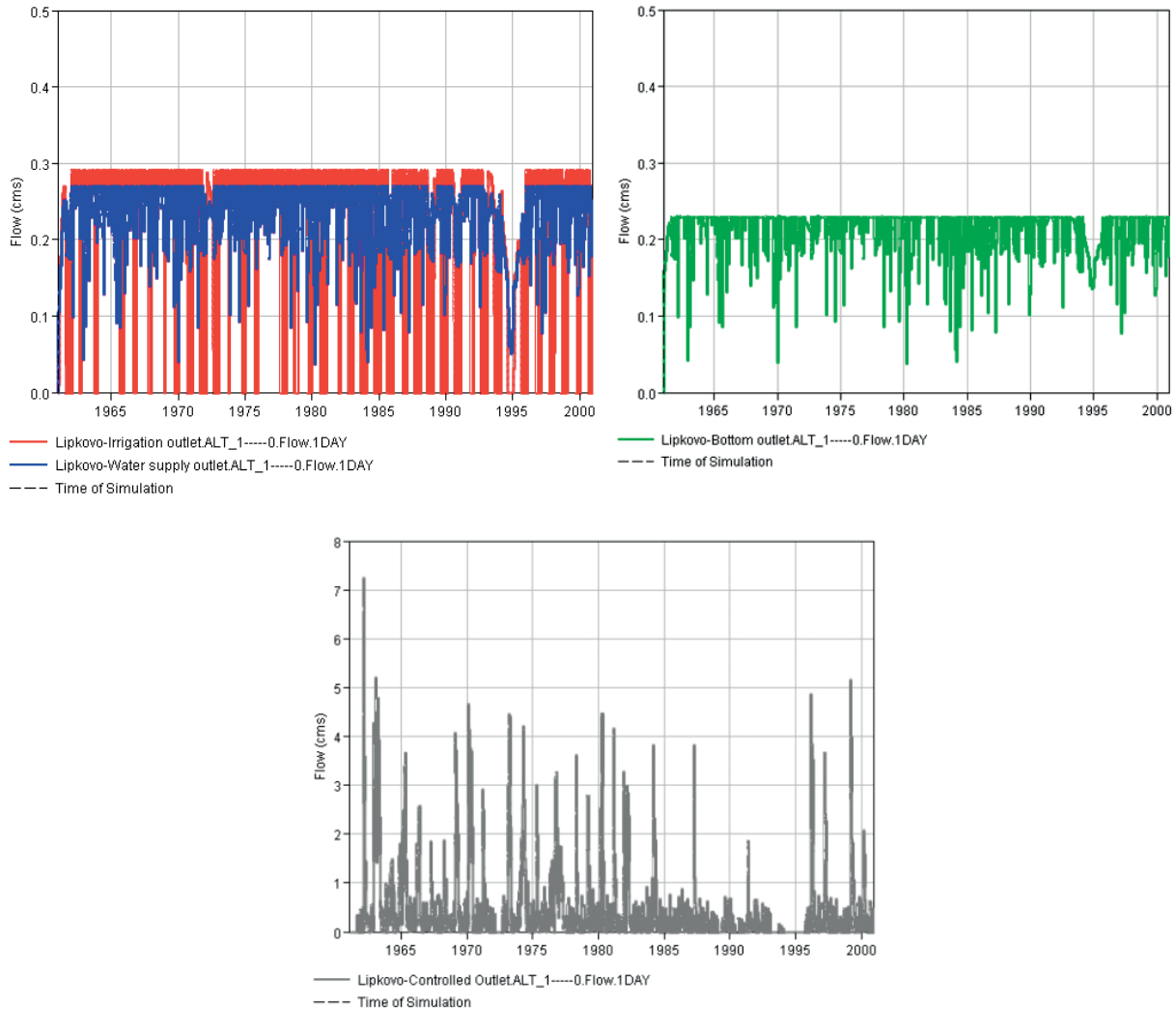


Figure 13. Releases from ‘Lipkovo’ reservoir for water supply, irrigation, (upper left), spillway release (upper right) and environmental flow (bottom) during the whole simulation period for alternative 1

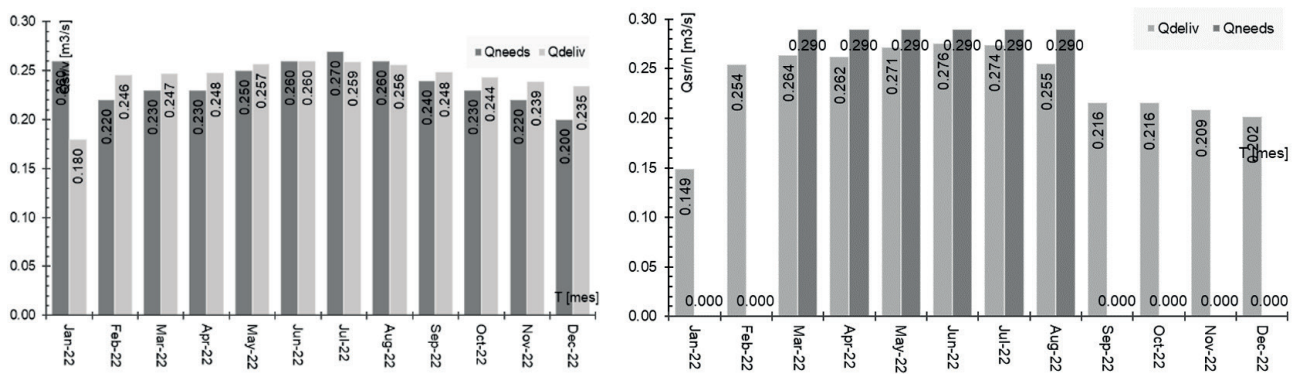


Figure 14. Water demands and delivered water in m³/s for water supply (left) and irrigation (right), results from alternative 1

4.2. Alternative 2 – hydro system ‘Lipkovo’ with ‘Slupchanka’

As planned in the Water master plan from 1973, as addition to the ‘Lipkovo’ hydro system another dam with reservoir is planned – hydro system ‘Slupchanka’. The following alternative – alternative 2 is an upgraded alternative. The main purpose of ‘Slupchanka’ hydro system is to improve water balance of the ‘Lipkovo’ hydro system and provide water when increased demands of water – for both irrigation and water supply. For alternative 2, a simulation run was conducted for hydro system ‘Lipkovo’ and ‘Slupchanka’ comprised of both ‘Lipkovo’ as downstream and ‘Glaznja’ as upstream reservoir, as well as ‘Slupchanka’ reservoir with water deviation to ‘Lipkovo’ reservoir, for a simulation period from 1961 to 2000. ‘Slupchanka’ reservoir is located on a different watershed than ‘Lipkovo’ and ‘Glaznja’, and water from this hydro system is planned to be deviated to ‘Lipkovo’ reservoir through a deviation canal, with approximately $0,2 \text{ m}^3/\text{s}$ of water to be transferred to ‘Lipkovo’ reservoir.

By analysing the output results for alternative 2, it can be noticed significant oscillation of the water level for reservoir Slupchanka (Fig. 15), specially in the low water periods from 1988–1996, where the water level is approximaltey at elevation of dead storage. On average, according to the applied operation policies and tandem operation of all reservoirs, a discharge of $0,17 \text{ m}^3/\text{s}$ is conveyed to reservoir ‘Lipkovo’ reservoir ‘Slupchanka’ through the water conveyer (Fig. 16). Controlled release from ‘Lipkovo’ reservoir is increased compared to alternative 1, to $1,23 \text{ m}^3/\text{s}$. The average controlled release from ‘Glaznja’ remains the same as in alternative 1, by value of $1,10 \text{ m}^3/\text{s}$.

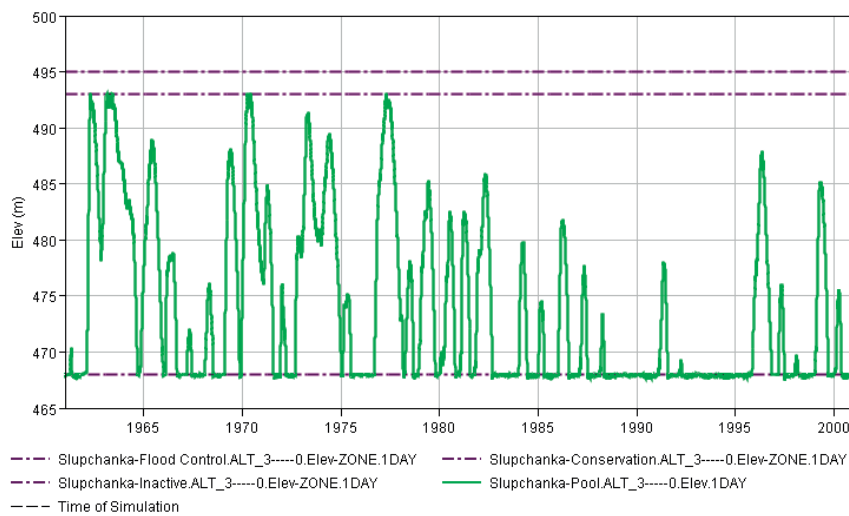


Figure 15. Water level fluctuations in ‘Slupchanka’ reservoir during the analyses period, for alternative 2

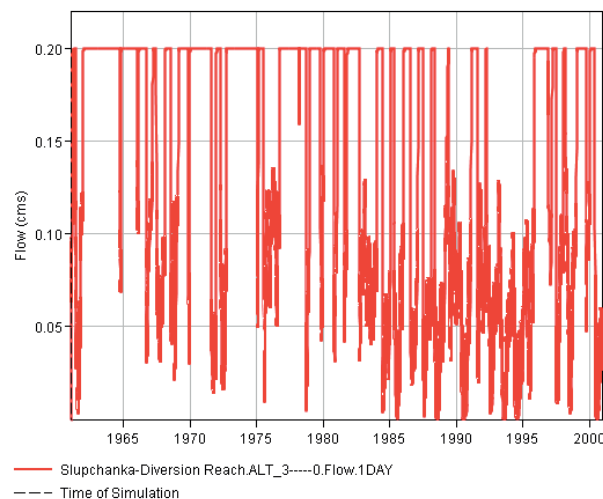


Figure 16. Intake flow through the water conveyer from ‘Slupchanka’ to ‘Lipkovo’ reservoir

By analysing the output results for alternative 2 in case of Lipkovo reservoir, there is similar oscillation of the water level (Fig. 17) as in alternative 1, with increased spillway flow. There is also variation of the input flow and output flow from the Lipkovo reservoir (Fig. 18), according to overall reservoir capacity. The average controlled release from Lipkovo reservoir is $1,09 \text{ m}^3/\text{s}$ – much of which is due to spillway overflow.

On Fig. 18 are displayed output values from reservoir ‘Lipkovo’ for water supply, irrigation and environmental discharge, as well and spillway overflow. The environmental flow in the operation scenario is set as priority and it is matched during the full analysis period.

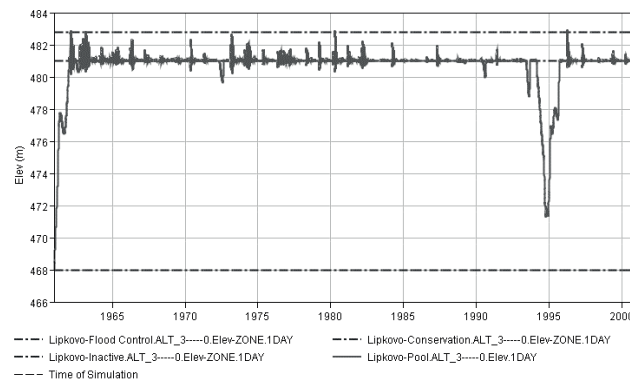


Figure 17. Water level fluctuations in ‘Lipkovo’ reservoir during the analyses period, for alternative 2

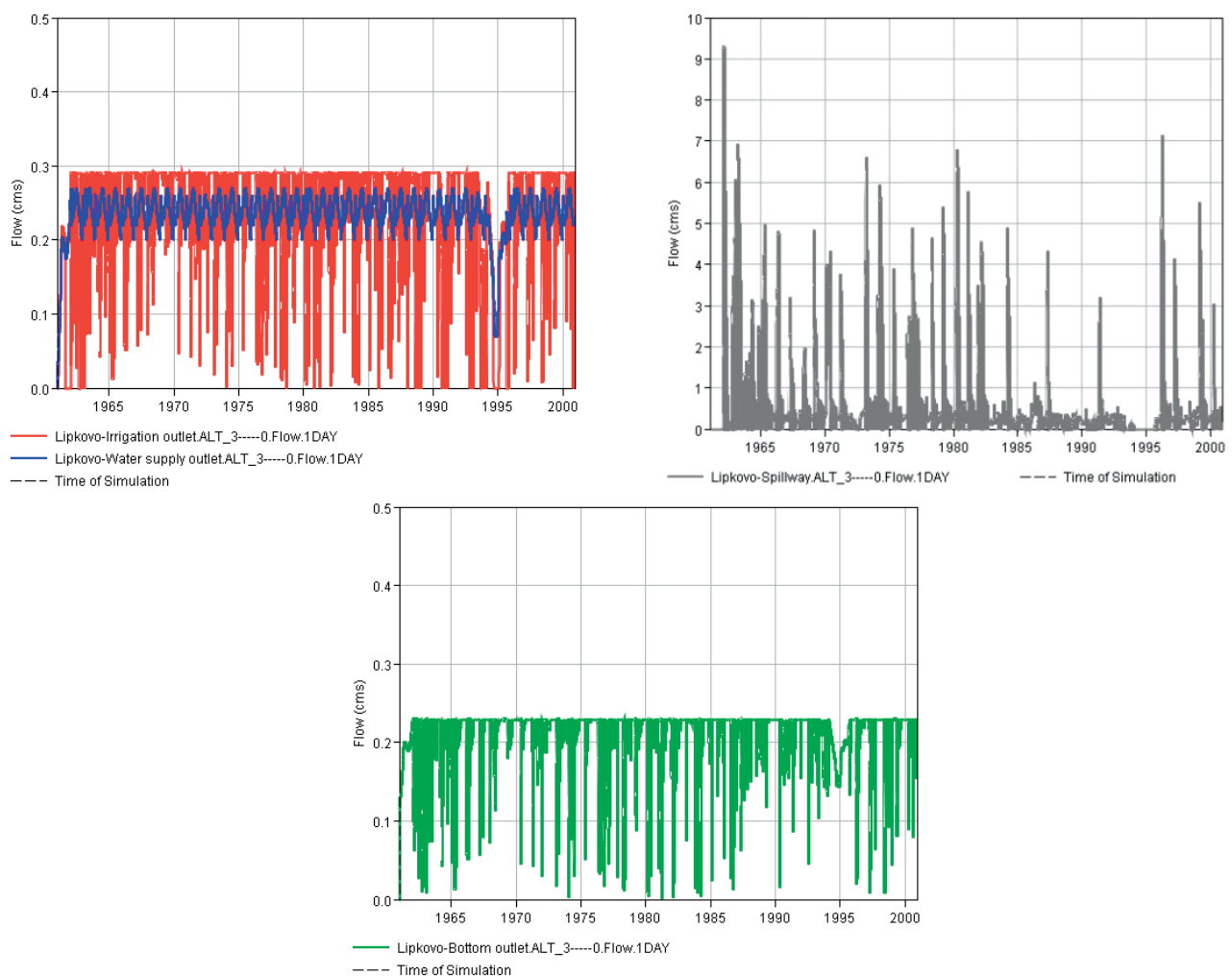


Figure 18. Releases from ‘Lipkovo’ reservoir for water supply, irrigation, (upper left), spillway release (upper right) and environmental flow (bottom) during the whole simulation period for alternative 2

According to the results, with average release of 1,1 m³/s from ‘Glaznja’ reservoir and 0,17 m³/s from ‘Slupchanka’ including a tandem operation with ‘Lipkovo’, almost every month during the analyzed period covering the target water needs in range between 68% (January) to 100% for most of the other period during the year (Figure 19, left), whereas 85% to 89% of the irrigation needs are covered during the vegetation period with this operation policy (Figure 19, right). Both water supply as primary, and irrigation as secondary water purposes are meeting the specified water demands according to the output results from alternative 2. From Figure 18 (right) it can be noted that there is increase in spillway release from ‘Lipkovo’ reservoir which is due to the increased inflow from ‘Slupchanka’ – approximately

0,500 m³/s. These quantities of water can be counted on for future planning of expansion of the water supply and the irrigation system.

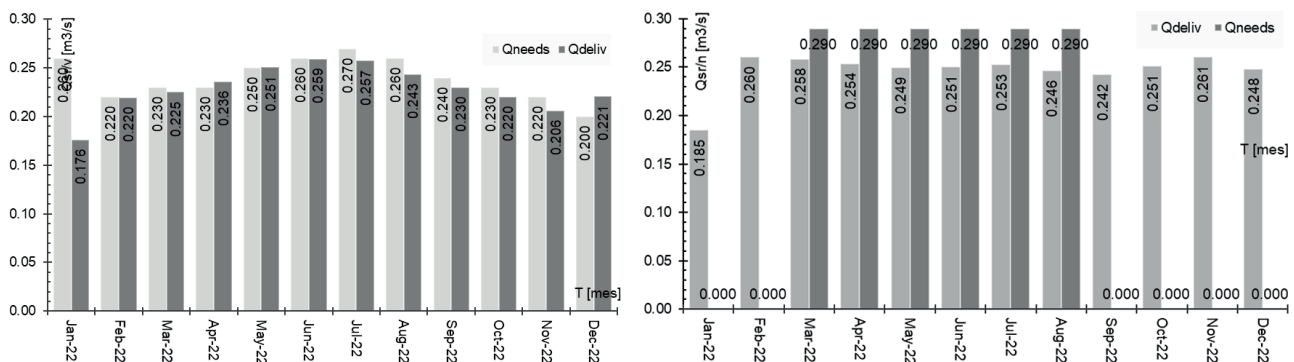


Figure 19. Water demands and delivered m³/s for water supply (left) and irrigation (right) for alternative 2

5. Conclusion

With application of simulation models, two alternatives are analysed for ‘Lipkovo’ hydro system – alternative 1 (existing state with Glaznja and Lipkovo reservoirs) and alternative 2 – hydro system Lipkovo’ upgraded with ‘Slupchanka’ hydro system. The main purpose of the analyses is to assess the reservoirs capacity and matching of the water demands for water supply of Kumanovo city and irrigation of the Kumanovo region, for input flow hydrographs for period of 40 years of measured data.

According to the output results from the analyses, the following conclusions can be derived:

1. The current state of the operation of hydro system ‘Lipkovo’ (reservoirs ‘Glaznja’ and ‘Lipkovo’), modelled as alternative 1 in HEC ResSim, can suffice at great scale both water supply and irrigation needs in the Kumanovo region, covering the target water needs in range between 69% (January) to 100% for most of the other period during the year, whereas 88% to 95% of the irrigation needs are covered during the vegetation period with the adopted operation policy.
2. For both alternatives, irrigation needs are derived from a longer period of recorded delivered water quantities to Kumanovo from ‘Lipkovo’ hydro system, differencing every month – as expected, higher during the summer period, and lower during the winter period. These quantities account for 1300 ha of land – approximately 50% of the planned agricultural land to be irrigated with this hydro system. This means that in future, shall agricultural land increase, water needs will also increase compared to the current available data for this water user. On the other hand, water supply needs for Kumanovo region are approximately 0,2 m³/s.
3. All reservoirs are modelled using the ‘tandem operation’ rule which forces upstream reservoirs to provide sufficient water quantity for the downstream reservoirs’ accommodation of needs. This is a real representative of the current state of operation with the system, where water releases from ‘Lipkovo’ reservoir is much regulated through the 10-times-larger ‘Glaznja’ reservoir. Such operation rule, set in HEC ResSim applies for cascade reservoirs’ management.
4. Since ‘Lipkovo’ is a much smaller reservoir compared to ‘Glaznja’, there is quite some water flow overflowing the spillway. On average, for alternative 1 this quantities are 0,38 m³/s and 0,50 m³/s for alternative 2. These quantities of water can be accounted for future planning of development of the hydro systems – whether for increasing water supply, irrigation of agricultural fields, or adding a hydro power plant to harvest the potential energy of water.
5. According to the results, with average release of 1,1 m³/s from ‘Glaznja’ reservoir and 0,17 m³/s from ‘Slupchanka’ including a tandem operation with ‘Lipkovo’, almost every month during the analyzed period covering the target water supply needs is in range between 68% (January) to 100% for most of the other period during the year, whereas 85% to 89% of the irrigation needs are covered during the vegetation period with the adopted operation policy in alter. 2.
6. By inclusion of the hydro system ‘Slupchanka’ in the existing hydro system ‘Lipkovo’, an improved management is achieved. Namely, there is possibility for more flexible management of the hydro system ‘Lipkovo’, especially in critical periods of low water such as the period from 1998–1996 in the analysed timeline.

References:

- [1] Votruba, L. Analysis of water resources. Prague: Technical University of Prague, 1988.
- [2] Disposition of dam and appurtenant structures on river Slupchanka. Igor Nikoloski, Slavcho Mihajlovski. Struga: Macedonian Committee of Large dams, 2017. 4th Congress of large dams.

- [3] Center, USACE Hydrologic Engineering. User's Manual HEC ResSim 3.1. 2013.
- [4] Application of simulation model in case of multi-reservoir system planning. Frosina Panovska, Stevcho Mitovski, Ljupcho Petkovski. SKopje: WMHE, 2019. WMHE.
- [5] Радевски, А. Системите за наводнување во Република Македонија. Скопје: s. l: РАДИНГ, 2009. 978-9989-690-06-8, 2009.
- [6] P. Novak, A.I.B. Moffat, C. Nalluri. Hydraulic structures, 3rd edition. London, UK: Taylor&Francis Group, 2007.
- [7] Tanchev, Ljubomir. Dams and appurtenant structures, 2nd edition. London, UK: A.A. Balkema Publ., CRC press, Taylor&Francis Group plc, 2014.

II Hydraulic Engineering and Environmental Impact

DEPENDENCY OF THE WHITECAPPING PARAMETER ON MODEL RESOLUTION SETTINGS IN THE EASTERN ADRIATIC SEA

DAMJAN BUJAK¹, DALIBOR CAREVIĆ¹, TIN KULIĆ¹, TONKO BOGOVAC¹

¹ University of Zagreb, Faculty of Civil Engineering; Croatia

e-mail: damjan.bujak@grad.unizg.hr, dalibor.carevic@grad.unizg.hr, tin.kulic@grad.unizg.hr, tonko.bogovac@grad.unizg.hr

Abstract

The white-capping parameter plays a crucial role in wave numerical models for wind wave growth and dissipation. Despite the importance and physical nature of the white-capping parameter, this source term is often considered a calibration parameter. This paper discusses the influence of resolution settings on the calibrated white-capping parameter in complex coastal areas, such as the eastern Adriatic coast. The SWAN model is forced with the MEDSEA reanalysis wave data on the open boundary and the ECMWF reanalysis wind grid data on the entire domain. This paper provides good initial guess values for resolution settings in limited fetch domains, while keeping the computational costs low.

Keywords: white-capping, surrogate model optimization, SWAN, numerical modelling, complex coastal areas.

1. Introduction

Long-term wave climate data are critical to ensure sustainable coastal structure design [1], morphodynamics studies [2], or to force regional nearshore wave numerical models [3], etc. A long time series of significant wave height is critical for providing confident wave forecasting, (e.g. to define the return period of significant wave height) [4]. Because in-situ wave observations are mostly limited to occasional campaigns in most regions due to operational costs [3, 5], numerical simulations are used to provide a long-term wave hindcast [6, 7]. Numerical wave models are a great tool for studying waves, because they enable the extension of available wave data in a flexible manner [8]. Using third-generation spectral wind wave models to simulate waves has progressed from state-of-the-art to state of practice in the last decade [9]. The accuracy of wave model forecasts has been fundamentally further developed recently [9, 10]. These advances are mainly due to further developed source term definitions and more precise wind fields from environmental models [9]. Given these points, the ability to access a reliable long-term wave database using reliable wave numerical models is of great value to ocean and coastal engineers.

For wind wave-generating numerical models, wind data are an essential boundary value [10, 11]. As already observed in previous research, the quality of the wind forcing greatly impacts the accuracy of wave modeling output [12, 13]. The atmospheric reanalysis wind model, ERA5 [14], from the European Centre for Medium-Range Weather Forecasts showed great performance when used in the coastal region [3, 15]. For example, Bellotti, *et al.* [3] showed the applicability of ERA5 in the Mediterranean Sea in coastal situations without islands to shelter the measuring location. Nevertheless, ERA5 could provide promising wind hindcast forcing data even in complex shoreline basins, such as the eastern Adriatic Sea.

Granted that wind data in a region is available, other physical parameters are also required for accurate wave modeling, which include: a detailed bathymetry of the modeled region, difficult to know coefficient inputs (such as white-capping parameters, bed frictional dissipation, depth limited wave breaking etc.), and boundary wave data for forcing regional nearshore models [3]. To obtain boundary forcing wave data for a locally based numerical model, data from a global or regional scale reanalysis wave models can be applied [3, 16]. This methodology is called downscaling [17–19].

An integral part of the wave generation method employed in GEN3 wave models (for instance, SWAN and WAVE-WATCH III) includes a white-capping dissipation term. The white-capping parameter is commonly adjusted to calibrate the numerical model according to measurements, even though it is a physical term [20, 21]. The white-capping dissipation parameter is often chosen for calibration because it is considered the least known in wave generation numerical models [22]. This nonphysical method is quite effective in fitting wave simulation outputs to wave measurements [23]. This engineering solution compensates for errors between the forcing wind field and the white-capping dissipation term. The optimal value is often determined by a detailed sensitivity analysis, one case at a time. The C_{ds} value, which is part of the white-capping formulation by [24, 25], is the most common value adjusted in this method (if more tunable coefficients are tuned simultaneously, then C_{ds} is surely included in the set). For instance, Amarouche, Akpinar,

Bachari, Çakmak, Houma [26] determined the C_{ds} value for the western Mediterranean Sea in this way. The paper reported a calibrated value for C_{ds} of 1.0 as the best for the western Mediterranean. Using the same popular methodology, the numerical model in this paper is also calibrated using the C_{ds} value.

The tunable white-capping coefficient, C_{ds} , is commonly reported and cited in research papers for various wave climates and basin geography. However, rarely do papers conduct a sensitivity analysis of their reported white-capping physical calibration parameters to different numerical settings, such as grid resolution, directional wave resolution, etc. Furthermore, some studies do not even report the chosen numerical resolution themselves.

If the calibrated white-capping parameter is dependent on any numerical parameter, the calibration procedure should highlight the numerical parameter as well. Considering the recent SWAN studies done in the Mediterranean Sea, 36 bins are often chosen for the directional wave resolution, the number of frequency bins varies between 28–35, the spectrum frequency range starts at 0.033–0.0521 Hz to 1 Hz, and the directional wave spreading is applied at 30 degrees or as a cosine power value of 4 [3, 26, 27]. In general, the numerical solution should preferably converge to a fixed solution as the numerical resolution is refined [28]. On the other hand, the modeler tries not to excessively increase the numerical resolution settings, to avoid exponentially increasing the computational time of the model. Even for moderately small basins such as the Mediterranean Sea, finding the right balance between numerical resolution and available processing resources is difficult. Paper conducting detailed sensitivity studies of SWAN numerical model settings are common (e.g. [29], [16]), however studies are rarely done in basins with limited fetch such as the eastern Adriatic Sea.

This paper aims to evaluate the effect of the size of the mesh element and the wave resolution settings on the calibrated white-capping value in complex shoreline basins. This is part of an ongoing project to establish a framework for wave downscaling to obtain wave hindcasting data in complex shoreline basins, whilst a downscaling proof-of-concept study has already been done in the western Mediterranean Sea [3] for a less sheltered basin. Through a sensitivity analysis of relevant numerical resolution parameters, the numerical setting recommendations are presented for a reliable physical white-capping value calibration.

1.1. Study site

The study site is located in the eastern mid-latitude Adriatic Sea, particularly in the vicinity of Split, as can be seen in Figure 1. The study area is shown on an orthophoto background in Figure 1, whilst Figure 2 shows the mesh extent. Because several small islands in the south-east and two large islands in the south-east (Brač and Hvar) surround the Split basin, the coastline of the basin is relatively variable and complex. The coastal area has developed economically, particularly in terms of beaches and marinas, and has a rich environmental and archaeological value.

The wave climate in the region is predominately forced by both Bora (NE) and Scirocco (SE) winds. The wave buoy, which provides wave measurements used in this study, is in front of the Split waterfront (43.48833° N, 16.46500° E) (shown in Figure 1 with a red dot).

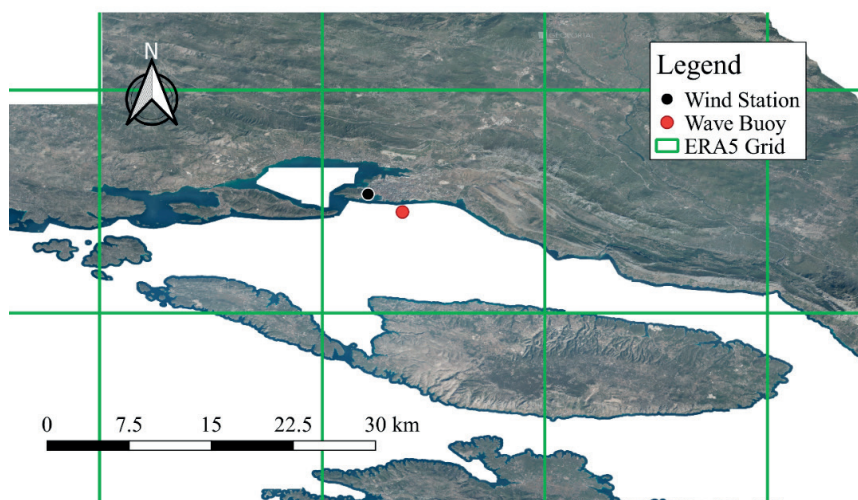


Figure 1. Map of the Split region that is modeled in SWAN, with the locations of the wave buoy and wind station shown

1.2. Model description and boundary conditions

The third generation SWAN spectral wave model (version 41.31AB in this study) developed at the TU Delft is known for its excellent performance in shallow wave propagation simulation. SWAN is based on the governing equation of the spectral action balance and is represented in Cartesian coordinates as follows:

$$\frac{\partial N}{\partial t} + \frac{\partial C_x N}{\partial x} + \frac{\partial C_y N}{\partial y} + \frac{\partial C_\sigma N}{\partial \sigma} + \frac{\partial C_\theta N}{\partial \theta} = \frac{S}{\sigma}, \quad (1)$$

$$N = \frac{E}{\sigma}, \quad (2)$$

where the left-hand side represents the kinematic component, showing the derivatives of the action density N in the geographical and spectral space. C_x and C_y are the Cartesian coordinate components of wave group velocity in geographical space, whereas C_θ and C_σ are the spectral components of wave group velocity. The N action density is the ratio of the wave energy spectrum $E(\sigma, \theta)$ and frequency σ . The term S on the right-hand side represents the total source of wave energy. The total source term comprises the following terms:

$$S = S_{in} + S_{ds} + S_{bot} + S_{br} + S_{nl3} + S_{nl4}, \quad (3)$$

where S_{in} is the energy input by wind, S_{ds} is the dissipation induced by white-capping, S_{nl4} is the nonlinear wave energy transfer between quadruplets, S_{nl3} is the triad nonlinear interaction, S_{fric} is the dissipation due to bottom friction (JONSWAP formulation in this study [30]), and S_{brk} is the dissipation due to depth-induced wave breaking (Battjes formulation in this study [31]). Since our study is focused in intermediate and shallow waters, the term for triads is also included in the source term.

In this study, the Janssen [25] white-capping formulation is used, which showed success in the western Mediterranean basin with a value of $C_{ds} = 1.0$ [26]. The white-capping formulation includes tunable coefficients in the form of C_{ds} and δ . The white-capping dissipation rate coefficient, C_{ds} , has default value of 4.5, whereas δ can hold a value between 0 and 1, and the default value is 0.5. Since we were interested in the impact of the calibration process on C_{ds} , the δ term is fixed at the default value.

To automate the white-capping calibration procedure, a surrogate model was established. The surrogate model algorithm uses Radial Base Functions (RBF) to construct a cost-effective model for the objective function interpolation, while the SWAN model itself is occasionally called by the surrogate model for verification of incumbent points. The maximum number of calls to the SWAN numerical model that the surrogate model could make is set to 15, after which the calibration algorithm stops. The surrogate model searches for the best possible value to minimize the loss function defined by the error equation – this is shown in section 4.1, Figure 1. The search range for the white-capping parameters S_{ds} is limited to 0 at the lower bound and 5 at the upper bound.

The wind forcing boundary condition was given from the novel fifth generation atmospheric reanalysis ERA5 dataset [14], which showed improvements compared to other reanalysis products when forcing numerical wave models. The ERA5 reanalysis provides high spatial resolution (31 km), hourly temporal output, and 3-hour uncertainty information. The ERA5 grid size is overlaid on the map in green in Figure 1.

We imposed wave reanalysis data, namely MEDSEA from the Copernicus database [32], on the open boundary (Figure 2). MEDSEA is a fine resolution ($1/24^\circ$) wave model of the Mediterranean Sea, providing wave hindcast as far back as 1993. Even though the MEDSEA reanalysis model is the most detailed wave numerical model reanalysis in the Mediterranean Sea provided by the Copernicus project, the authors found low accuracy when verifying the reanalysis data to buoy measurements in well-sheltered locations. According to their report [32], the Adriatic Sea has the weakest model accuracy.

The tests are performed on a stationary model, which is justified when the residence time of the simulated waves is small relative to the time scale of the changes [33]. The main advantage of this method is shorter run times of the numerical models. Hence, the boundary forcing data and the measurement data were extracted for 08.04.2008. at 08:00. The significant wave height at the time was measured at 1.07 m at the wave buoy in front of the Split waterfront (Figure 1), which the numerical model will hindcast with the appropriately tuned white-capping dissipation coefficient. The magnitude of the ERA5 wind velocity magnitude interpolated at the location of the meteorological wind station in Split is 10.86 m/s ($u = -9.03$ m/s, $v = 6.05$ m/s) in the SE direction.

1.3. Mesh and wave resolution

The mesh element size and wave resolution settings, which are tested in this study, are described in this section. The effect of resolution on the calibrated value of the white-capping parameter can be investigated using the test results.

We adopted an unstructured mesh for an accurate description of the complex shoreline geometry in the Split region (Figure 2). Similarly, research that used coarser grids than 2 km advocates using unstructured grids to accurately resolve complex coastal features, particularly in the presence of islands due to their sheltering effect [34]. The Mediterranean basin is a sea with a complicated morphology and environment, including a severely complex coastline, highly variable bathymetry, and limited fetches. Hence, an unstructured mesh enables flexible local refinement that can improve the accuracy of wave simulation for a specific area. The domain of the numerical model covers a part of the eastern Adriatic Sea, spanning 117° E – 128° E in longitude and 29° N – 41° N in latitude. The grid domain is composed of 53630 and 16412 triangle elements for the 250 m and 500 m mesh, respectively (Table 1).

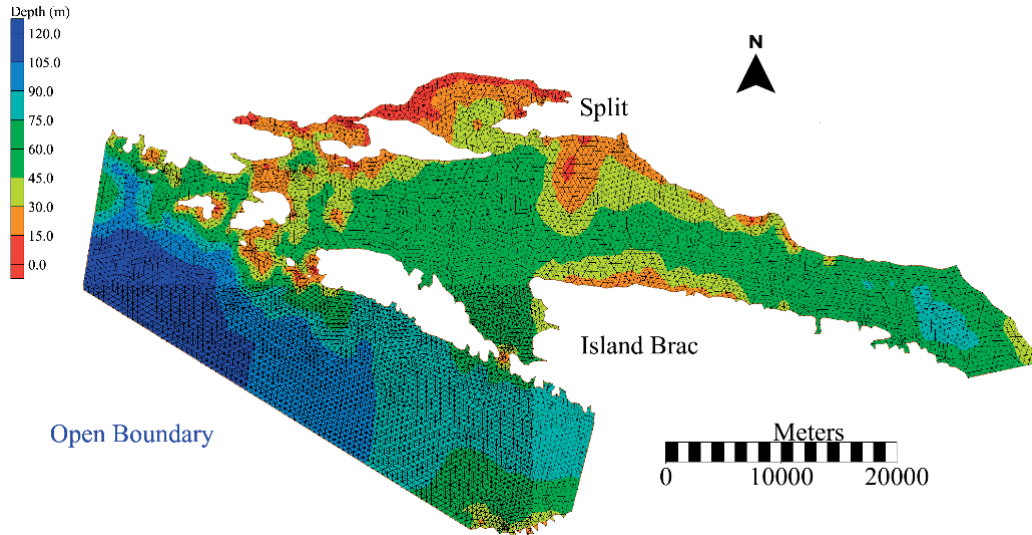


Figure 2. Mesh constructed to simulate wave in the Split region; figure shows a mesh resolution of 500 m

Base bathymetric data is sourced from the GEBCO database [35]. Additionally, local bathymetry measurements were added to the nearshore base data for a finer coastline resolution. The depth of the deepest water is approximately 120 m below the mean sea level (MSL) at the open boundary (Figure 2). The resolution of the base bathymetry data is about 200×200 m offshore, whilst the nearshore area resolution was finer at 5×5 m. To accurately present the complex shoreline geography, the spatial resolution of the shoreline data is 5 m.

The numerical resolution settings tested in this study are presented in Table 1. The ranges of tested numerical settings include the numerical settings used in [3, 26, 27] in the Mediterranean Sea and are further extended to test a wider range. A large value of power of directional wave spreading reflects a narrow spread – common for swells, whereas a low value indicates a wide spread – common for wind waves [36].

Table 1. Summary table of numerical settings tested in this study

Resolution setting	Values tested	SWAN recommended (default) values for application in coastal areas
Mesh resolution	250 m and 500 m	50 m – 1000 m
Directional resolution of waves	15° – 5°	$\Delta\theta = 15^\circ$ – 10° for wind waves $\Delta\theta = 5^\circ$ – 2° for swell
Directional wave spreading (power)	2–4	2
Number of spectral frequencies bins	20–35	minimum of 4
Frequency range	0.04–1 Hz	0.04–1 Hz

1.4. Statistical error metrics

Given the simple SWAN model output of a single value of significant wave height, the error metric is a straightforward absolute error metric described by a difference between the measured and modelled values:

$$e = \left| H_{s,SWAN} - H_{s,measured} \right|, \quad (4)$$

where $H_{s,SWAN}$ is the significant wave height modelled at the buoy location and $H_{s,measured}$ is the wave height measured by the wave buoy (Figure 1).

2. Results and discussion

2.1. Calibration results

In this section we show the result of the white-capping parameter calibration procedure discussed in section 3.2. The results are shown for a case with a directional wave resolution of 36, power wave spreading of 2, 30 wave frequency bins, and mesh resolution of 500 m.

The results of the surrogate optimization algorithm reveal a relationship between the significant wave height and the white-capping parameter (Figure 1). The relationship sharply declines to 0 m of wave height error near the white-capping of 0.57. There are no other visible locations where some other minima could be achieved, so the 0.57 minima could be taken as a global minimum. The algorithm revealed a significant difference between the calibrated white-capping parameter value for this specific case and the SWAN default value in for Janssen [24] white-capping dissipation of 4.5. For a white-capping dissipation of 4.5 the error would be more than 0.28 m – not specifically shown in Figure 1 but deduced from the relationship curve in Figure 1. When considering the recommendation given by Amarouche, *et al.* [26], the white-capping parameter of 1.0 is closer to the calibrated one in this situation. As discussed in Wu, Li, Zhai, Gu, Liu [37], the SWAN model with default settings tends to increase the underprediction of the significant wave height.

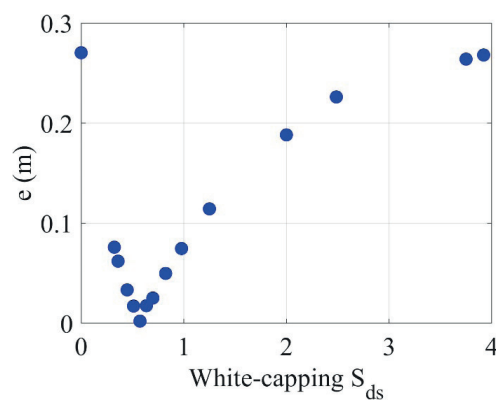


Figure 1. Comparison between the numerical error of the significant wave height and the white-capping parameter as a result of the surrogate model's optimization procedure - directional wave resolution of 36, power wave spreading of 2 and 30 wave frequency bins, mesh resolution of 500 m

2.2. White-capping parameter dependency on resolution settings

It is found that the calibrated white-capping parameter shows low sensitivity to the directional wave spreading and the number of spectral frequency bin settings of the numerical model (Figure 2 and Figure 3). In both cases, the value of the calibrated white-capping parameter is in the 0.5 – 0.6 range and is negatively related to the number of frequency bins. The results are in agreement with the sensitivity analysis conducted by Feng, Chen [16], which also showed low sensitivity of the model results to these numerical settings.

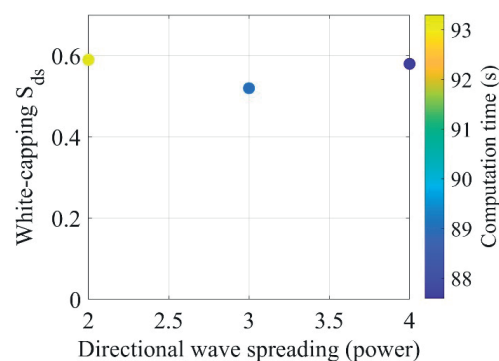


Figure 2. Comparison between white-capping parameter S_{ds} and directional wave spreading (power), with the required computation time presented using a color bar; number of directional bins – 36, mesh resolution – 500 m

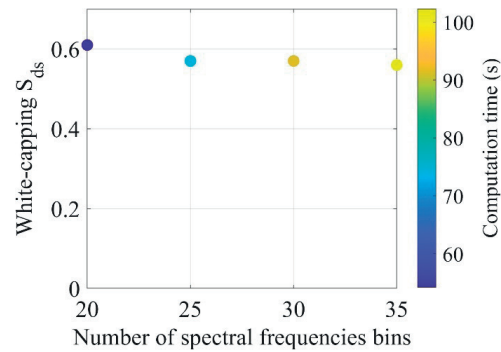


Figure 3. Comparison between white-capping parameter S_{ds} and number of spectral frequency bins, with the required computation time presented using a color bar; number of directional bins – 36, mesh resolution – 500 m

On the same note, Allandadi, *et al.* [29] stated that the white-capping parameters are more influential than numerical settings such as wave spreading, number of spectral frequency bins, number of iterations, and size of time steps. This is indirectly confirmed in this study through the calibration procedure (Figure 1), where the modeled significant wave height varies ± 0.3 m depending on the wave-capping parameter.

The computational cost, expectedly, increases with increase in the number of spectral frequency bins and decrease of the directional wave spreading. The wave spreading shows a small impact with only 5% cost increase (ratio of max and min computational costs); however, the number of spectral frequency bins shows a moderate impact of 70%.

Figure 4 shows the influence of the number of wave directional bins and mesh resolution on the white-capping parameter, S_{ds} . Interestingly, the number of wave directional bins has a great impact on the calibrated white-capping, while the mesh resolution has a negligible impact. When the number of wave directional bins is low (e.g., 24, 30 and 36), the white-capping parameter is low, indicating the numerical model's need to increase the modeled the significant wave height to match the measured. On the other hand, a high white-capping parameter has the opposite effect of damping the modeled significant wave height when a high number of wave directional bins are employed. This increase is likely due to the model's ability to increase wave energy propagation with a finer wave directional resolution, and thus increasing the calibrated white-capping through the surrogate algorithm procedure to dampen the significant wave height to match measurements.

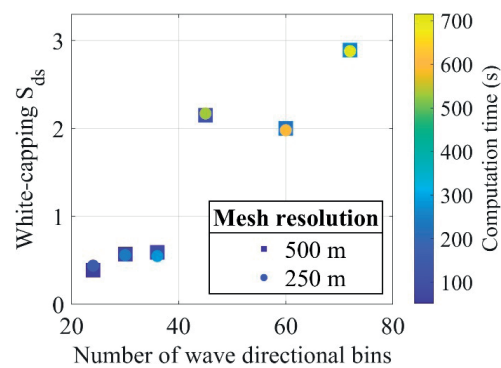


Figure 4. Comparison between white-capping parameter S_{ds} and the number of wave directional bins, with the required computation time presented using a color bar and mesh resolution presented using square scatter for 500 m and circle scatter for 250 m; number of spectral frequency bins – 30, wave spreading (power) – 2

The mesh resolution did not show an impact, probably because the lower resolution of 500 m was already fine enough for this case. The computational costs increased with the increase in both wave directional resolution and mesh resolution. The increase in computation cost is substantial and has increased almost 3-fold when comparing the 500 m and 250 m resolution (and 72 bins for wave direction). The impact of the number of directional bins is also higher for a finer resolution mesh, as expected. For the lower resolution mesh of 500 m, the increase in computational cost is 3-fold with increasing number of wave directional bins, while for the higher resolution mesh of 250 m, the increase is almost 4-fold.

3. Conclusion

We have presented the influence of several numerical settings on the calibrated white-capping parameter and computational costs in SWAN, namely wave directional resolution, mesh resolution, number of frequency bins and wave spreading on the open boundary. The case study was carried out in a basin with limited fetch, encompassing a region

around the city of Split. Overall, these results suggest that the wave direction resolution has a great impact on the calibrated white-capping parameter, probably due to a greater ability to propagate wind-wave energy in narrow channels. Studies commonly choose 36 wave directional bins, while not doing any sensitivity study for this parameter, unaware of its impact on the model outputs. It should be noted that this observation could change in basins that are not fetch limited, such as in this study. The other numerical settings showed an insignificant impact on the calibrated white-capping parameter. This is probably due to the lower bound of the tested resolution settings (mesh resolution and number of wave frequency bins) being already detailed enough for this case. Therefore, in similar limited-fetch locations, the following resolution settings are good for an initial guess while keeping the computational costs low: mesh resolution of 500 m, number of wave frequency bins of 20, and directional spreading of 2; while the wave directional resolution should be submitted to a sensitivity analysis because of its high impact on model outputs when the value is higher than 45.

It is important to note that the current study was limited to the stationary model and the results could slightly vary for transient wave numerical models. Given that the sensitivity studies in Feng, Chen [16] and Allandadi, *et al.* [29] on a transient SWAN model showed similar conclusions in most regards, this should not vary substantially. These studies did not consider the wave directional resolution in their sensitivity analysis, which proved to be the most influential numeric resolution parameter in this study, so comparison is currently not possible.

This work has highlighted that the reported white-capping parameters in cited studies should be taken with care with insight into the numerical settings used, specifically the wave directional resolution, while calibration should be conducted for each site and numerical setting separately.

References:

- [1] USACE: Coastal Engineering manual, pp. 477, 2008.
- [2] Masselink, G., Kroon, A., Davidson-Arnott, R.G.D.: Morphodynamics of intertidal bars in wave-dominated coastal settings - A review, *Geomorphology*, 73 (2006) 1–2, pp. 33–49.
- [3] Bellotti, G., Franco, L., Cecioni, C.: Regional Downscaling of Copernicus ERA5 Wave Data for Coastal Engineering Activities and Operational Coastal Services, *Water*, 13 (2021) 6.
- [4] Camus, P., Mendez, F.J., Medina, R.: A hybrid efficient method to downscale wave climate to coastal areas, *Coastal Engineering*, 58 (2011) 9, pp. 851–862.
- [5] Akpınar, A., Bingolbali, B.: Long-term variations of wind and wave conditions in the coastal regions of the Black Sea, *Natural Hazards*, 84 (2016) 1, pp. 69–92.
- [6] Music, S., Nickovic, S.: 44-year wave hindcast for the Eastern Mediterranean, *Coastal Engineering*, 55 (2008) 11, pp. 872–880.
- [7] Amarouche, K., Bachari, N.E.I., Houma, F.: Simulation of Hydrodynamic Behavior Using Data from Coastal Weather Stations at the Bejaia Bay, Algeria, *Recent Advances in Environmental Science from the Euro-Mediterranean and Surrounding Regions*, Vols I and II, (2018) pp. 1595–1598.
- [8] Wu, W., Liu, Z., Zhai, F., Li, P., et al.: A quantitative method to calibrate the SWAN wave model based on the whitecapping dissipation term, *Applied Ocean Research*, 114 (2021).
- [9] Christensen, E.D., Johnson, M., Sorensen, O.R., Hasager, C.B., et al.: Transmission of wave energy through an offshore wind turbine farm, *Coastal Engineering*, 82 (2013) pp. 25–46.
- [10] WAMDI Group: The WAM Model—A Third Generation Ocean Wave Prediction Model, *J. Phys. Oceanogr.*, 18 (1988) 2, pp. 1775–1810.
- [11] Booij, N., Ris, R.C., Holthuijsen, L.H.: A third-generation wave model for coastal regions - 1. Model description and validation, *Journal of Geophysical Research-Oceans*, 104 (1999) C4, pp. 7649–7666.
- [12] Van Vledder, G.P., Akpınar, A.: Wave model predictions in the Black Sea: Sensitivity to wind fields, *Applied Ocean Research*, 53 (2015), pp. 161–178
- [13] Stopa, J.E.: Wind forcing calibration and wave hindcast comparison using multiple reanalysis and merged satellite wind datasets, *Ocean Modelling*, 127 (2018), pp. 55–69.
- [14] Hersbach, H., Bell, B., Berrisford, P., Hirahara, S., et al.: The ERA5 global reanalysis, *Quarterly Journal of the Royal Meteorological Society*, 146 (2020) 730, pp. 1999–2049.
- [15] Amarouche, K., Akpınar, A.: Increasing Trend on Storm Wave Intensity in the Western Mediterranean, *Climate*, 9 (2021) 1.
- [16] Feng, X., Chen, X.: Feasibility of ERA5 reanalysis wind dataset on wave simulation for the western inner-shelf of Yellow Sea, *Ocean Engineering*, 236 (2021).

- [17] Camus, P., Mendez, F.J., Medina, R., Tomas, A., et al.: High resolution downscaled ocean waves (DOW) reanalysis in coastal areas, *Coastal Engineering*, 72 (2013) pp. 56–68.
- [18] Breivik, Ø., Gusdal, Y., Furevik, B.R., Aarnes, O.J., et al.: Nearshore wave forecasting and hindcasting by dynamical and statistical downscaling, *Journal of Marine Systems*, 78 (2009) pp. S235–S243.
- [19] Gaslikova, L., Weisse, R.: Estimating near-shore wave statistics from regional hindcasts using downscaling techniques, *Ocean Dynamics*, 56 (2006) 1, pp. 26–35.
- [20] Cavaleri, L., Abdalla, S., Benetazzo, A., Bertotti, L., et al.: Wave modelling in coastal and inner seas, *Progress in Oceanography*, 167 (2018) pp. 164–233.
- [21] Cavaleri, L., Barbariol, F., Benetazzo, A.: Wind–Wave Modeling: Where We Are, Where to Go, *Journal of Marine Science and Engineering*, 8 (2020) 4.
- [22] Pallares, E., Sanchez-Arcilla, A., Espino, M.: Wave energy balance in wave models (SWAN) for semi-enclosed domains-Application to the Catalan coast, *Continental Shelf Research*, 87 (2014) pp. 41–53.
- [23] Amarouche, K., Akpınar, A., Semedo, A.: Wave storm events in the Western Mediterranean Sea over four decades, *Ocean Modelling*, 170 (2022).
- [24] Janssen, P.A.E.M.: Wave-Induced Stress and the Drag of Air Flow over Sea Waves, *Journal of Physical Oceanography*, 19 (1989) 6, pp. 745–754.
- [25] Janssen, P.: Quasi-linear Theory of Wind-Wave Generation Applied to Wave Forecasting, *Journal of Physical Oceanography*, 21 (1991) pp. 1631–1642.
- [26] Amarouche, K., Akpınar, A., Bachari, N.E.I., Çakmak, R.E., et al.: Evaluation of a high-resolution wave hindcast model SWAN for the West Mediterranean basin, *Applied Ocean Research*, 84 (2019) pp. 225–241.
- [27] Lončar, G., Šreng, Ž., Miličević, H., Ostojić, S.: Increase of Wave Height Due to Transition in Wind Direction – Example: Rijeka Bay, *Elektrinički časopis građevinskog fakulteta Osijek*, (2019) pp. 57–70.
- [28] Versteeg, H.K., Malalasekera, W.: *An Introduction to Computational Fluid Dynamics*, 2007.
- [29] Allandadi, M.N., Gunawan, B., Lai, J., He, R.Y., et al.: Development and validation of a regional-scale high-resolution unstructured model for wave energy resource characterization along the US East Coast, *Renewable Energy*, 136 (2019) pp. 500–511.
- [30] Hasselmann, K.: ON THE SPECTRAL DISSIPATION OF OCEAN WAVES DUE TO WHITE CAPPING, *Boundary-Layer Meteorology*, 6 (1973) pp. 107–127.
- [31] Battjes, J.A., Janssen, J.P.F.M.: Energy loss and set-up due to breaking of random waves, Hamburg, Germany, pp. 569–587, 1978.
- [32] Korres, G., Ravdas, M., Zacharioudaki, A.: Mediterranean Sea Waves Hindcast (CMEMS MED-Waves) [Data set], pp. 2019.
- [33] Hydraulics, W.D.: Nonstationary SWAN simulation in the Wadden Sea, pp. 2008.
- [34] Perez, J., Menendez, M., Losada, I.J.: GOW2: A global wave hindcast for coastal applications, *Coastal Engineering*, 124 (2017) pp. 1–11.
- [35] Weatherall, P., Marks, K.M., Jakobsson, M., Schmitt, T., et al.: A new digital bathymetric model of the world's oceans, *Earth and Space Science*, 2 (2015) 8, pp. 331–345.
- [36] Babarit, A.: *Ocean Wave Energy Conversion*, Elsevier, 2018.
- [37] Wu, W., Li, P., Zhai, F., Gu, Y., et al.: Evaluation of different wind resources in simulating wave height for the Bohai, Yellow, and East China Seas (BYES) with SWAN model, *Continental Shelf Research*, 207 (2020).

II Hydraulic Engineering and Environmental Impact

ESTIMATING CHANGES IN GRAVEL BEACH SLOPE USING A VIDEO MONITORING SYSTEM – A CASE STUDY OF THE PLOČE BEACH IN RIJEKA, CROATIA

HANNA MILIČEVIĆ¹, DAMJAN BUJAK¹, DALIBOR CAREVIĆ¹, TIN KULIĆ¹

¹ University of Zagreb, Faculty of Civil Engineering; Croatia

e-mail: hanna.milicevic@grad.unizg.hr, damjan.bujak@grad.unizg.hr, dalibor.carevic@grad.unizg.hr, tin.kulic@grad.unizg.hr

Abstract

Beach slope is of critical importance for coastal area protection, as well as for other coastal morphodynamic research. Despite its importance, a reliable method for estimating slope is still not defined. In this paper, a new efficient method using VMS technology is presented. The beach slope is calculated by dividing the difference in the tide level with the shoreline distance along a cross-shore transect at different times. The result of calculation using this technique shows good agreement with other methods and demonstrates the potential of VMS for effective beach slope monitoring.

Keywords: video-monitoring system (VMS), coastal management, shoreline changes, gravel beaches, beach-face slope, image processing.

1. Introduction

The beach environment is subject to regular daily and seasonal changes, as well as unpredictable changes due to extreme weather conditions, unusual tides, and human influence. The beach face is the sub-aerial beach sector [1], which extends from the berm to the low tide water line and is constantly interacting with the uprush and downrush of individual waves and tidal cycles [2]. The steepness of the beach face ($\tan\beta$), or the beach-face slope, is a key parameter in coastal geomorphology and coastal engineering due to its control of important coastal processes [2]. It is one of the key parameters controlling the elevation of wave runup and total swash excursion at the shoreline, processes that are of primary concern for assessing coastal inundation hazards along the coastal boundary [3]. Despite the importance of the beach-face slope parameter in numerous empirical formulations in coastal engineering (e.g. wave run-up prediction), large-scale datasets of the beach-face slope remain unavailable along most of the world's coastlines [2]. In the 1961, coastal scientist named K.O. Emery developed simplest technique to measuring a beach profile known as the "Emery board" method (Figure 1.). Emery proposed a simple method of beach profiling based on the use of two graduated rods, whose alignment and reading of the intersection with the horizon allow for the determination of differences in level along the profile [4]. This approach may seem simple, but it provides reasonably accurate measurements of beach profiles. It also has the advantages of light and inexpensive equipment, which can be easily carried to distant survey sites, for very rapid surveys [5]. However, measurement of the difference in elevation by two people like this has the potential to have errors due to limited visibility and is considered labor intensive so that it is limited to the number of beach profile transects measured [6]. In spite of some shortcomings, and because of its simplicity and low cost [4], this method is still considered a reliable method as observation data, so it is still used as comparison data for validation of more sophisticated techniques [6]. Beach slope can also be measured using conventional survey techniques, for example GPS survey. This method has limitations because in areas where the beach is muddy or covered with coastal vegetation, measuring position and elevation is very complicated and considered ineffective. Especially in estimating the beach slope on a wide spatial scale such as global, national, and regional events, which is still a major challenge in using this method [3]. In recent decades, airborne lidar technology (LiDAR) has significantly increased the spatial coverage of coastal topographic data from individual beaches to hundreds of kilometres of coastline [7]. It can provide very detailed and accurate results, but the process is very complicated and requires high operational costs for surveying. However, in the swash zone, these active remote sensing techniques are hampered by the constant alternation of wet and dry phases as water levels fluctuate at the shoreline under the action of waves and tides [7], limiting the ability to extract beach-face slopes [2]. Today, UAV (unmanned aerial vehicles) and VMS (video monitoring system) provide data with high accuracy for a larger area. The development of imaging systems has emerged as one of the most powerful and reliable tools for monitoring shoreline changes associated with variations in key beach parameters (i.e., changes in beach slope and beach width). Video-based technology is becoming an increasingly popular low-cost method for monitoring beach, because it can be used to build a database of frequent, long-term and spatially extensive observations

of coastal changes [8]. It covers time scales from seconds to years and spatial scales from meters to kilometers. The first system that enables the controlled acquisition and return of optical remote sensing data from land-based computers observing coastal sites of interest [9] is the “Argus system” developed by the Coastal Imaging Lab (CIL) at Oregon State University. These systems are positioned at an elevated location and some distance from the beach (e.g., on the roofs of nearby buildings, headlands, etc.) to continuously collect high-frequency image data of the coastal zone [10]. Physically, an Argus Station consists of a number of video cameras attached to a host computer that serves as both system control and communication link between the cameras and central data archives [9]. The video monitoring system also uses geometric techniques to transform and rectify the oblique images captured by the camera into a plan view of the beach. These are used in algorithms developed to detect the shoreline position needed for further research (i.e. beach slope, beach area, beach width). The use of VMS and UAVs has been widely applied and has resulted in various achievements and improvements in other coastal dynamics studies, such as calculating beach volume change [11], determining erosion and accretion rates, coastal topographic surveys, and many other applications [6]. This paper has demonstrated a new method using video monitoring system technology to calculate the beach slope and monitor shoreline changes. Recent developments in shoreline mapping now make it possible to extract instantaneous shorelines from publicly available satellite imagery [3, 12, 13]. The concept of calculating the beach slope using this method is to compare the tidal elevation obtained from tide gauge in Bakar, Croatia, and the distance between the shoreline positions along a cross-shore transect at two different times. In the following section, we briefly describe the study site and explain the method used in more detail in Section 3.

In Section 4, we compare the results between two methods using video monitoring system (VMS) and unmanned aerial vehicle (UAV) surveys to test the accuracy of the results obtained between two different methods.

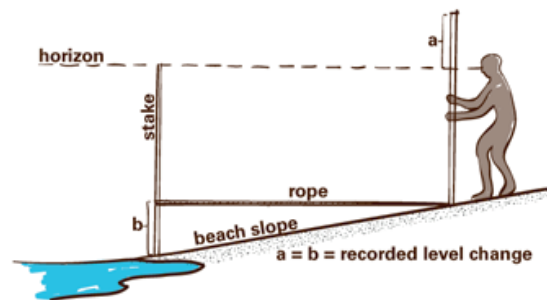


Figure 1. The simplest technique for measuring a beach profile known as the “Emery board” method, developed by K.O. Emery in 1961

2. Methods

2.1. Study site – Beach Ploče

This study was carried out on an artificial gravel beach Ploče, in the northwest part of the city of Rijeka, the Kvarner Bay. It consists of a beach area of 14 000 m², a green and illuminated walkway, and a zone above the promenade with Mediterranean plants and benches for resting. The total length of the beach is 320 m and is divided by a 30 m long central groyne into two cells of approximately equal length. Two additional groynes were constructed on the east and west sides of the beach to extend the natural headlands (Figure 2). The sediment grain size can be classified as gravel to pebble ($D_{50} = 16\text{--}32$ mm), which is typical for other gravel beaches in Croatia. Weak and moderate winds dominate throughout the year, with often calm periods, and occasional storms with wind velocities exceeding 30 m/s rarely last more than one day [14]. The prevailing winds in the Kvarner Bay are bura (NE) and jugo (SE). Most of energetic wave conditions are observed during winter season. Storm events are the dominant generator of gravel transport on beaches of the eastern Adriatic Sea. Tides in the Adriatic Sea can be described as microtidal, with mean tidal amplitudes well below 2 meters. The nearest tide gauge in Bakar, which is the longest-operating station on the Croatian coast (since 1929) shows that the mean daily amplitudes in the Kvarner Bay are 0.35 m [15]. The region is also prone to occasional extremely high-water levels (also called Acqua Alta) when there is a superposition of high tide, storm surge, seiche, and other low-frequency sea level fluctuations [16].



Figure 2. Historical coastline from aerial images from 1968 (black), the coastline of the artificial beach constructed in 2011 (green), constructed submerged sill (yellow) and groynes (orange)

2.2. Camera setup

An Argus video monitoring system was installed at the Ploče beach, which consists of two cameras mounted on the roof of the indoor swimming pool in early October 2019. The video cameras are at 13.8 m above the mean sea level (MSL) (Figure 3). Each camera covers different part of the beach, the western and eastern part of the beach respectively. However, due to location of cameras, there is a complete coverage of the western part of the beach (azimuth 277° TN) only. The eastern part is not fully visible due to trees and vegetation (azimuth 120° TN). In this project, the Blackfly S GigE camera (BFS-PGE-122S6C-C) was used with a resolution of $4,096 \times 3,000$ pixels, which provides continuous high-resolution video images captured at 4 Hz (Figure 3).



Figure 3. Position of the video monitoring system at the edge of the swimming pool complex at the beach site, one camera per beach cell (west and east in Figure 1)

The shoreline location is function of tidal elevation, wave set-up and swash. In order to enable the shoreline location comparison, images are taken during calm wave periods. Additionally, images taken when the sea level at the Bakar tide gauge was between 0 cm and 60 cm were considered. The focus of this study is on the western beach and in the rest of the paper it will be referred as the beach. During the period from September 30, 2020, to March 27, 2021, we collected 10 images using video monitoring system technology. The images were taken on the same day or ± 5 days compared to the UAV survey period. The CoastSnap software package, developed by [15], is used to derive shorelines. The package is developed for processing and analysis of the beach images. The original images are oblique, and they were georectified before shorelines were extracted. Due to the fixed location of the sensor, only the lens characteristics (radial distortion) and ground control points (GCPs) were required to create a georectified image. Six GCPs for the beach were set-up by the Geodetic Institute Rijeka. Points on fixed objects were chosen, such as concrete walkways and walls, groyne rocks, and stairs. All the GCP points were measured in the Croatian Terrestrial Reference System

HTRS96 (EPSG: 3765) in the horizontal plane and HRVS71 in the vertical direction. The RMSE error for image rectification (that is, the difference between the estimated and ground-surveyed point positions) was 3.80 pixels for this study on beach Ploče. For the extremely high-resolution images recorded, this corresponds to an 8.5 cm distance on the ground. We laid out a series of cross-shore transects at a 2 m interval along the shoreline (Figure 4). The transects were used to determine the shoreline position along the transect using the CCD method/algorithm [17].

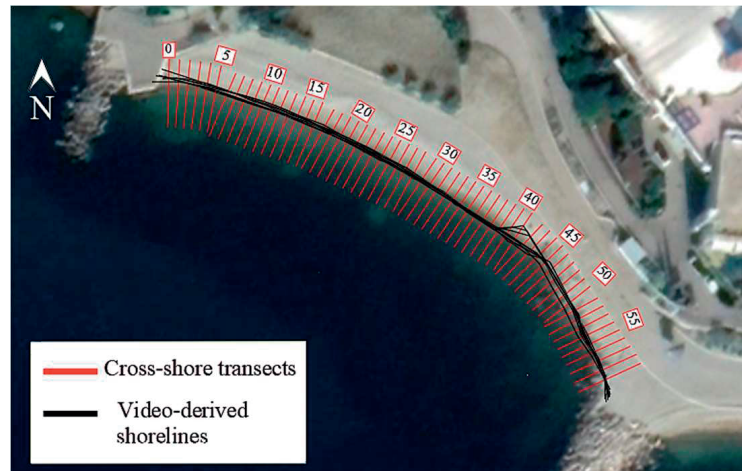


Figure 4. Alongshore variability in shoreline position between September 30, 2020, and March 27, 2021

2.3. Flight mission settings

Unmanned Aerial Vehicle (UAV) – based remote sensing techniques have demonstrated great potential for monitoring rapid shoreline changes [18] and mapping coastal environments. With image-based approaches utilizing Structure from Motion (SfM), high-resolution Digital Surface Models (DSM), and orthophotos can be generated efficiently using UAV imagery [18]. In this study, Geodetic Institute Rijeka (GZR) and the Faculty of Civil Engineering in Rijeka (GradRi) carried out the surveys. GZR used a Matrice 200 unmanned aerial vehicle (UAV) with camera Sony ILCE-7M2 and GradRi used a DJI Phantom 4 Pro e UAV for the image requisition [19]. The number of images ranged from 208 to 667 and the flight altitude ranged from 19.2 to 29 m and 100–103 m for GradRi and GZR survey [19]. Both institutions used Agisoft Metashape Professional to generate point clouds from the captured photos.

This technique has demonstrated a successful implementation and being considered as an efficient method of calculating and mapping the spatial distribution [6]. Detailed settings for the UAV flight mission can be found in [19].

2.4. Beach slope calculation (VMS)

Ideally, beach slope is measured in the area starting from the highest point reached by high tide and the lowest point reached by low tide. The timing of these conditions can occur at night when mapping with a video monitoring system cannot be carried out [6]. To simplify this, beach slope in this study is defined as the ratio of vertical elevation to horizontal distance. Based on this, the vertical elevation Δh is determined from the tidal elevation which is obtained from tide gauge at Bakar, and the horizontal distance Δx is calculated from the difference in distance between two shoreline positions along the cross-shore transect (yellow line Figure 5) with different tidal conditions at different times. The simple method to estimate beach slope from the set of the instantaneous shorelines is shown in Figure 5. It is important to choose dates when the weather conditions are calm, because then waves, storms, etc. cannot affect the shoreline changes. Once these values are obtained, the beach slope can be easily calculated using Eq. (1) if we want the result in degrees, or Eq. (2) for $\text{tg}\beta$.

$$s = \tan^{-1} \frac{\Delta h}{\Delta x} \quad (1)$$

$$\text{tg}\beta = \frac{\Delta h}{\Delta x} \quad (2)$$

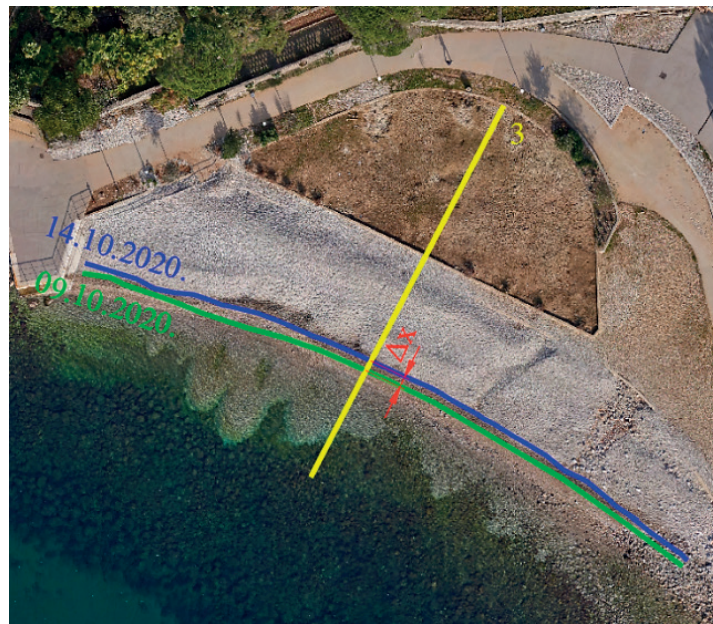


Figure 5. Beach slope calculation using video monitoring system

2.5. Beach slope calculation (UAV)

By considering the practicality of a method based on the spatial and temporal scale of interest and the use of low operating costs, the use of UAV is considered as a method with high accuracy, speed, and efficiency, hence making it suitable for beach slope spatial mapping [6]. The use of drones is expected to cover areas that are difficult to access and still provide high accuracy and resolution. Figure 6. shows the elevation changes of the beach during the UAV survey (red dots) and the process of beach slope calculation (red triangle). The concept of beach slope calculation by an unmanned aerial vehicle is the similar to the procedure performed with VMS technology, i.e., comparing different tidal conditions (blue and green line) at different times. Two parameters Δh and Δx were determined as intersection between two tidal elevations and the UAV survey on the same day or ± 5 days. After the values are obtained, the beach slope can be calculated by using the Equation 2.

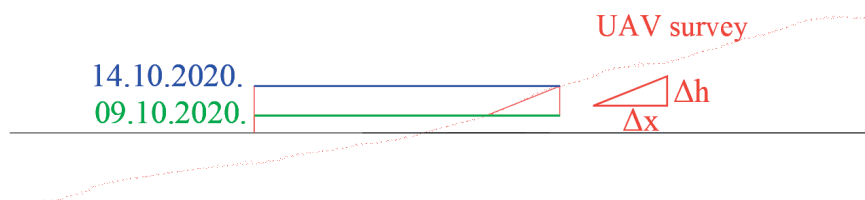


Figure 6. Beach slope calculation using unmanned aerial vehicle

3. Results and discussion

3.1. Beach slope

The objective of the method presented here is to estimate the beach slope without the requirement for field surveys, but instead relying only on remotely sensed data. Instantaneous shorelines are extracted using CoastSnap, an open source software package that allows users to obtain time series of shoreline position on any gravel coastline. For this study, 10 shorelines were extracted at different times to determine the slope of the beach surface. Only images taken during calm wave conditions were suitable for analysis, and the observation period was between October 1, 2020, and December 15, 2020, as UAV surveys. Beach slope results obtained using UAVs are useful for testing the agreement between two methods. The method of calculating beach face slope using VMS is based on the comparison of two waterlines (shoreline, extracted from a satellite image) and waterline heights (difference between two tidal elevation) which are timed to match [6]. Table 1. summarizes the key characteristics needed for the calculation of the beach slope (Δx -horizontal distance between two shoreline positions along the cross-shore transect, Δh – vertical difference between two tidal elevations, and $\text{tg}\beta$ beach-face slope, i.e., the ratio between Δx and Δh). From the obtained results, presented in the table, we could observe that the beach-face slopes varied from $\text{tg}\beta = 0.16$ to $\text{tg}\beta = 0.42$ for the video monitoring system and $\text{tg}\beta = 0.16$ to $\text{tg}\beta = 0.44$ for the unmaned aerial vehicle technology. Comparing the obtained values with research by [3] the Ploče beach can be characterized as a steep beach. Flatness or steepness of the beach also depends

on the grain size. In general, the beach slope will be steeper if the sediment grain size is larger (pebbles, cobbles) and will be gentler if the sediment grain size is smaller (sand, silt) [21], [22].

Sediment grain size at Ploče beach can be classified as gravel to pebble, and on gravel beaches the slope is often more than 10° ($\text{tg}\beta > 0.18$) [22], which we can also confirm with the obtained results.

Table 1. Beach slope values using VMS and UAV technology

Beach slope values using VMS	Date	Δx	Δh	$\beta(^{\circ})$	$\text{tg}\beta^a$
	1.10.2020	0.81	0.29	19.70	0.36
	13.10.2020	1.28	0.31	13.61	0.24
	24.11.2020	0.81	0.34	22.77	0.42
	10.12.2020	3.02	0.47	8.85	0.16
	14.12.2020	1.58	0.35	12.49	0.22

Beach slope values using UAV	Date	Δx	Δh	$\beta(^{\circ})$	$\text{tg}\beta^a$
	1.10.2020.	0.73	0.29	21.66	0.40
	13.10.2020.	1.03	0.31	16.76	0.30
	24.11.2020	0.77	0.34	23.82	0.44
	10.12.2020.	2.86	0.47	9.34	0.16
14.12.2020.	1.57	0.35	12.55	0.22	

UAV is beneficial tool for environmental surveying, mapping, and monitoring [12]. The beach was surveyed 19 times between January 17, 2020 and February 26, 2021 to observe post-nourishment changes of the Ploče beach for the purposes of [19]. For the comparison of these two methods, 5 UAV survey data without significant changes due to erosion or accretion were used for this study. After performing the procedure described in Section 3.5, we obtained the results shown in Table 1. Performance indicators such as root mean square error (RMSE) and coefficient of determination (R^2) are used to assess the accuracy between two sophisticated techniques. There is strong agreement between the UAV and VMS technologies, with a coefficient of determination (R^2) of 0.95 and a root mean square error (RMSE) of 0.05 with a small deviation in October, as shown in Figure 7. The slope estimation method performed best when $\text{tg}\beta \leq 0.22$, as we can observe in December, where the results are the same, but for steeper profiles ($\text{tg}\beta > 0.24$), the average deviation is 0.03.

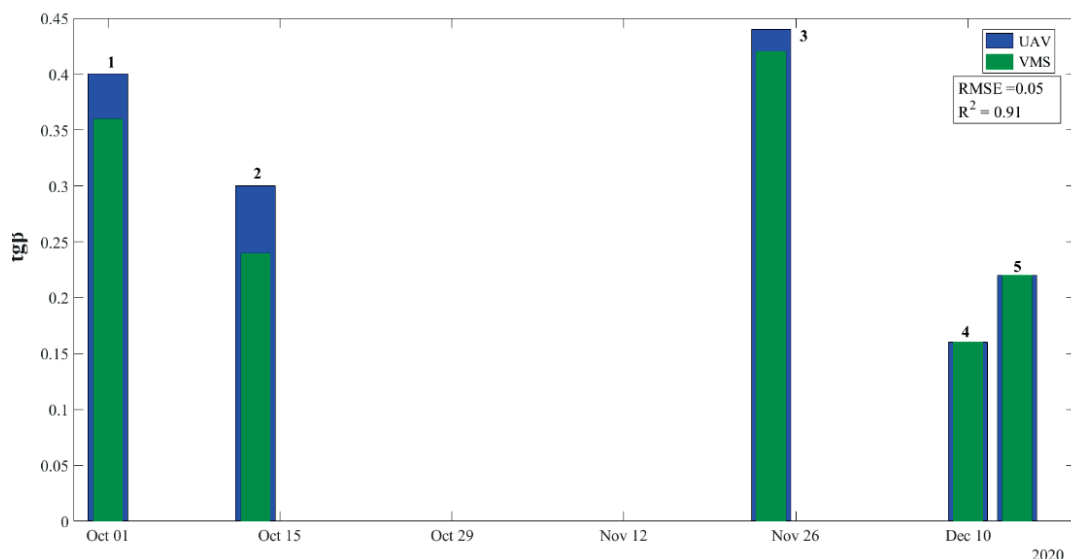


Figure 7. Alongshore variability in average beach-face slope using the methods described in Section 3.3 and 3.4

4. Conclusion

The relationship between beach-face slope with tidal range, grain size and wave energy have been studied by numerous researchers over the years. Some researches derived equations for the beach face slope, but these equations are complicated and require knowledge of the wave characteristics at a site (e.g., offshore wave height, breaking wave height, and wave period) or the sediment characteristics (grain size, average grain, sediment sorting, and porosity) [13]. Researchers also suggested some simpler methods such as the “Emery board”, which is inexpensive, quick, and easy but required field survey and unnecessary human labour. This paper presents a new method for calculating beach

slope using a video monitoring system (VMS). The concept for calculating beach slope using this method is to compare the tidal elevation and the distance between two shoreline positions along the cross-shore transect at two different times. The obtained results characterized the Ploče beach as steeper beach with beach slope between $\tan\beta = 0.16$ and $\tan\beta = 0.42$, and show good suitability with UAV mapping technology.

Shortcomings of this method can occur during the shoreline extraction because of possibility of a lot of noise and errors in the resulting data [6]. For example, misalignment occur due to sun glint, coastal winds or heavy rainfall which can cause water surface movement and thus image distortion.

This technique reveals VMS's potential for effective coastal management and provide high accuracy in beach slope calculation. The goal of the future study is to expand the data set and show agreement with the "beach-face slope estimation algorithm" developed by [20].

Acknowledgements

This work has been fully supported by the "Research Cooperability" Program of the Croatian Science Foundation funded by the European Union from the European Social Fund under the Operational Programme Efficient Human Resources 2014-2020.

References:

- [1] Reis, A.H., Gama, C.: Sand size versus beachface slope - An explanation based on the Constructal Law, *Geomorphology* 114 (2010), 3, pp. 276–283.
- [2] Vos, K., Deng, W., Harley, M.D., Turner, I.L., Splinter, K.D.M.: Beach-face slope dataset for Australia, *Earth System Science Data* 14 (2022), 3, pp. 1345–1357.
- [3] Vos, K., Harley, M.D., Splinter, K.D., Walker, A., Turner, I.L.: Beach Slopes From Satellite-Derived Shorelines, *Geophysical Research Letters* 47 (2020), 14.
- [4] Andrade, F., Ferreira, M.A.: A simple method of measuring beach profiles, *Journal of Coastal Research* 22 (2006), 4, pp. 995–999.
- [5] Florida Center for Instructional Technology: Beach Profiling with "Emery Boards" and Measuring Sand Grain Size, <https://fcit.usf.edu/florida/teacher/science/mod2/emery.board.html>, 23.06.2022.
- [6] Abdurrahman, U., Pratyaksa, I.F., Suprijo, T., Park, H.: Beach slope distribution mapping using UAV in the Cirebon coastal area, *E3S Web of Conferences* 324, 2021.
- [7] Middleton, J.H., Cooke, C.G., Kearney, E.T., Mumford, P.J., Mole, M.A., Nippard, G.J., Rizos, C., Splinter, K.D., Turner, I.L.: Resolution and accuracy of an airborne scanning laser system for beach surveys, *Journal of Atmospheric and Oceanic Technology* 30 (2013), 10, pp. 2452–2464.
- [8] Shin, B., Kim, K.: Estimation of shoreline change using high resolution images, *Procedia Engineering* 116 (2015), 1, pp. 994–1001.
- [9] Holman, R.A., Stanley, J.: The history and technical capabilities of Argus, *Coastal Engineering* 54 (2007), 6–7, pp. 477–491.
- [10] Harley, M.D., Andriolo, U., Armaroli, C., Ciavola, P.: Shoreline rotation and response to nourishment of a gravel embayed beach using a low-cost video monitoring technique: San Michele-Sassi Neri, Central Italy, *Journal of Coastal Conservation* 18 (2014), 5, pp. 551–565.
- [11] Yoo, C.I., Oh, T.S.: Beach volume change using UAV photogrammetry Songjung beach, Korea, *International Archives of the Photogrammetry, Remote Sensing and Spatial Information Sciences - ISPRS Archives, XLI* (2016), B8, pp. 1201–1205.
- [12] Drummond, C., Harley, M.D., Turner, I.L.: Predicting Shoreline Change over timescales of days to decades, *Coastal Engineering* 130 (2017), pp. 14–25.
- [13] McFall, B.C.: The Relationship between Beach Grain Size and Intertidal Beach Face Slope, *Journal of Coastal Research* 35 (2019), 5, pp. 1080–1086.
- [14] Tabain, T.: Standard wind wave spectrum for the Adriatic Sea revisited, *Brodogradnja* 45 (1997), pp. 303–313.
- [15] Pasarić, M., Orlić, M.: Long-term meteorological preconditioning of the North Adriatic coastal floods., *Continental Shelf Research* 21 (2001), pp. 263–278.
- [16] Medugorac, I., Pasarić, M., Orlić, M.: evere flooding along the eastern Adriatic coast: the case of 1 December 2008, *Ocean Dynamics* 65 (2015), pp. 817–830.

- [17] Turner, I., Leyden, V., Symonds, G., McGrath, J., Jackson, A., Jancar, T., Aarnikhof, S.G.J., Elshoff, I.E.: Comparison of observed and predicted coastline changes at the gold coast artificial (surfing) reef, 27th International Conference on Coastal Engineering, Sydney, Australia, 2000.
- [18] Lin, Y.C., Cheng, Y.T., Zhou, T., Ravi, R., Hasheminasab, S.M., Flatt, J.E., Troy, C., Habib, A.: Evaluation of UAV LiDAR for mapping coastal environments, *Remote Sensing* 11 (2019), 24.
- [19] Tadić, A., Ružić, I., Krvavica, N., Ilić, S.: Post-nourishment changes of an artificial gravel pocket beach using UAV imagery, *J. Mar. Sci. Eng* 10 (2021), 3.

II Hydraulic Engineering and Environmental Impact

FISH PASS ON THE TURIEC RIVER, SLOVAKIA

LEA ČUBANOVÁ¹, PETER DUŠIČKA¹, JÁN RUMANN¹, VLADIMÍR POLÁK²

¹ Slovak University of Technology in Bratislava, Faculty of Civil Engineering; Slovakia
e-mail: lea.cubanova@stuba.sk, peter.dusicka@stuba.sk, jan.rumann@stuba.sk

² Water Research Institute, Nábřežie arm. gen. L. Svobodu 5, 812 49 Bratislava; Slovakia
e-mail: vladimir.polak@vuvh.sk

Abstract

A weir on the Turiec River in Martin has been in operation since 1968 and belongs to the grayling fish zone. An originally included technical fish pass did not meet the new required parameters and therefore was rebuilt and modified according to the EU legislation. Hydraulic measurements in 5 different profiles were performed at the discharge of $Q = 0.87 \text{ m}^3 \cdot \text{s}^{-1}$. The results serve for verification of the design parameters and assessment of the passability for target fish species. Measurements of depths and velocities pointed out problem areas (unmet limit in the shallows, insufficient attractive outflow jet), but also the need to increase the subsidy discharge and research the outflow part of the fish pass.

Keywords: fish pass, Turiec River, depths, velocities, hydraulic measurements.

1. Introduction

Barriers built across rivers interrupt the longitudinal continuity for the migration of fish fauna. Therefore, it is necessary to build fish passes on each barrier (weir, dam) on a river or a channel. In general, fish passes are constructions that enable overcoming an obstruction on the stream for occurring fishfauna. It is designed either as a substitutive route next to the water structure, known as a biocorridor/bypass, or as a technical one in the water structure itself. The location of fish passes on the side of the hydropower plant is recommended due to the water outflow from the turbines, this outflow is attractive to fish [1, 2, 3].

A fish pass is functional when it not only meets the hydraulic parameters, but is passable in both directions for the target fish species. An efficient fish pass along the entire course of its riverbed enables upstream migration of all target fish species by provably passing both male and female individuals of each of the local target fish species, determined by the ichthyologist. Therefore, monitoring devices are placed on fish passes to monitor the migratory movements of fish, whether in the form of scanners, cameras, or the fish are directly tagged or monitored telemetrically [4].

There are numbers of water structures in the territory of the Slovak Republic, which create artificial barriers in the migration routes of the fish fauna that inhabit streams. According to the Ministry of Environment of the Slovak Republic, there are 1075 barriers on the streams; 117 of them are passable for the ichthyofauna due to the existing fish passes. The remaining 958 barriers do not have a functional fish pass or its presence or function is unknown [5]. Reconstruction, restoration or revitalization of the existed fish passes as well as proposal of new ones in Slovak Republic should be done in terms of the Methodological Guideline of the Ministry of Environment of the Slovak Republic: The determination of suitable types of fish passes according to the typology of water bodies [2] and Decree no. 383/2018, On technical conditions for the design of fish passes and the monitoring of the migration passability of fish passes [6].

An important element of the design of each fish pass is mathematical modeling (1D, 2D, or even 3D) [7], in the case of more complex proposals, physical modeling in the hydraulic laboratory is highly recommended [8]. After construction, it is necessary to check the achieved parameters by measuring in situ (hydraulic, ichthyological) and, if the limits are not reached, also possible reconstruction of the internal environment of the fish pass riverbed, because each water structure is unique and has its own boundary conditions, both in terms of operating parameters and biota.

2. Methods

The water structure where the research was carried out is located on the Turiec River (Fig. 1) in its artificially modified section at rkm 8.050 in the cadastral area of the town of Martin in the south-western part of the town of Martin. It consists of a reservoir, a two-field movable weir with flap gates, an intake structure, a fish pass, and a stilling basin under the weir. The minimum operating water level in the reservoir is 397.75 m above sea level and the maximum operating water level is 398.12 m above sea level. The long-term average annual discharge in the weir profile is $Q_a = 9.725 \text{ m}^3 \cdot \text{s}^{-1}$. The minimum residual/biological discharge in the Turiec riverbed under the weir must be ensured by the value of $Q = 0.50 \text{ m}^3 \cdot \text{s}^{-1}$, which is the discharge reached or exceeded for 365 days a year [9].

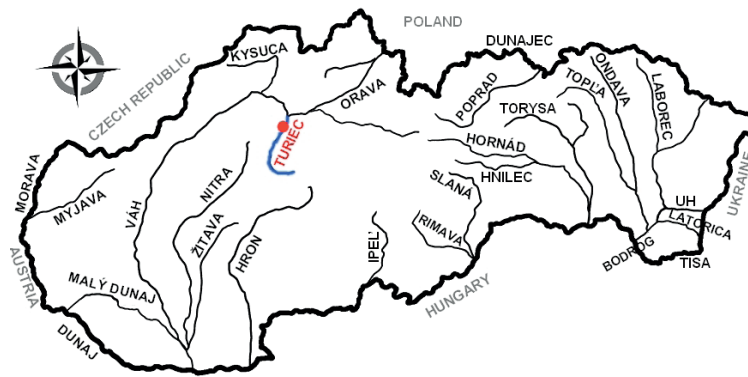


Figure 1. Map of Slovakia with the area of interest – Turiec River

The fish pass is formed by the modification of the original old inconvenient fish pass in the left bank pier and its continuation with the route on the left bank of the stream. From the point of connection to the old part, the route of the new part of the fish pass continuous in the direction of the stream flow of the Turiec River, while approximately in half of its length is rotating 180 degrees and the fish pass is returning upstream under the migration barrier to the riverbed bottom of the stilling basin of the weir (Fig. 2). The final construction permit of the rebuilt fish pass was in August 2019.

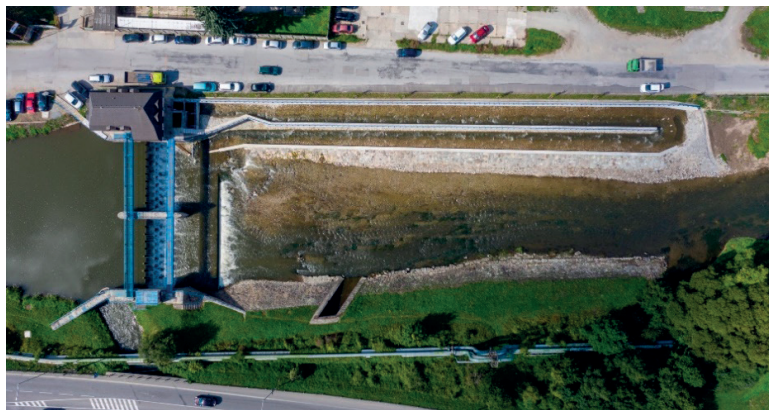


Figure 2. Aerial view of the fish pass

In the location of the barrier, it is a grayling fish zone with the following target fish species: Danubian Salmon (*Hucho hucho*), Grayling (*Thymallus thymallus*), Nase Carp (*Chondrostoma nasus*), Barbel (*Barbus barbus*), East European Bream (*Vimba vimba*), Chub (*Squalius cephalus*), the migration period was established for April and May.

The beginning of the fish pass is formed by an unattended inflow structure of the original old fish pass, which is protected at the inflow against floating objects by screenings and a suspended floating cylinder (closed steel profile DN 300). The inflow threshold is at 397.25 m above sea level. The fish pass riverbed (except the inflow part) consists of a deep and a shallow. The width of the cross section of the riverbed at the water level at the design discharge is 1.8 up to 4.5 m. The average longitudinal slope of the riverbed bottom in the modified old part of the fish pass is 1.35% (0.0% in the inflow part) and in the new part 1.25% [9].

The surface of the fish pass riverbed is almost in the whole part of the cross section formed by river stones – pebbles set in the concrete base. In the old part of the fish pass, there is a new riverbed created in the range of the original concrete walls. The outflow part of the old fish pass currently serves as a side relaxation pool for the fish. In the new section, the construction of the fish pass consists of three parallel reinforced concrete retaining walls that form the walls of the fish pass. The riverbed itself is led in the range of these retaining walls. It is a retaining wall on the side of the local road, then a retaining wall delimiting the area of the fish pass on the side of the Turiec riverbed and a middle – dividing retaining wall, which separates the two opposite sections of the fish pass. In the opposite direction of the fish pass path with an arc, there is a relaxation pool for migrating fish in its concave part [9].

The outflow from the fish pass (entrance for upstream migrating fish) is on the bottom of the stilling basin of the weir. To protect upstream fish migration across the stilling basin threshold (it forms a migration barrier) into the stilling basin, an auxiliary chute is used, which is located along the outflow line of the fish pass course. It is a boulder chute made of quarry stone set on a concrete base. The width of the chute is 4.0 m [9].

The size of the water abstraction into the fish pass depends on the level of the operating water level in the weir reservoir. The design discharge for the fish pass has a value of $Q = 1.0 \text{ m}^3 \cdot \text{s}^{-1}$ and is achieved at the maximum operating level in the reservoir. The inflow structure of the fish pass is located on the left bank pier of the weir. The size of the inflow opening is $1.0 \times 0.9 \text{ m}$. The fish pass is controlled by a sluice gate in the inflow part. Ensuring the function of the fish pass during the year [9]:

- if the current operating conditions on the water structure allow it, the water level in the reservoir is maintained throughout the year at the maximum operating level ($Q = 1.0 \text{ m}^3 \cdot \text{s}^{-1}$),
- to ensure full functionality of the fish pass (in terms of flow conditions in the fish pass), it is necessary to maintain the level in the reservoir, especially in the period from 1 April to 31 October, at the level of the maximum operating water level at 398.12 m above sea level and at least at elevation 397.97 m above sea level ($Q = 0.8 \text{ m}^3 \cdot \text{s}^{-1}$). This water level regime in the reservoir for the needs of the fish pass can be kept only depending on the current flow conditions in the Turiec River in the given period.

2.1. Hydraulic measurements and fish monitoring

After reconstruction of the fish pass, continuous water level measurement is ensured using a probe with a data logger NAM7HQ2000 [9], which is installed in front of the resting pool in the old part of the fish pass (Fig. 3).

For monitoring of fish movement in the fish pass, two DS-2CD2343G0-I underwater cameras were installed, one is placed at the inflow to the fish pass (Fig. 4) protected by rake and the other at the outflow to the stilling basin of the weir under its own protective basket [9].

After construction, there is a regular measurement of hydraulic parameters of the fish pass, which is carried out by the Water Research Institute in Bratislava (15.08.2019, 26.04.2021, 26.04.2022), while monitoring the discharge, achieved depth and velocities in different parts of the fish pass (behind the inflow, in the narrowed part, in 2 profiles in a straight course and on a chute at the outflow). Calibrated Universal Current Meter consists of hydrometric propellers type HYM (made by Water Research Institute in Bratislava) is used for the measurement, with a pitch of 0.100 m (according to the standard of fy. A.OTT type 6), the propellers diameter of the used is 30 mm. A counter with direct evaluation of the measured velocity type DENTOSAN is connected to the propellers. HYDRO 11, manufactured by Hydrometrics Ltd, is used as evaluation software.



Figure 3. Probe for continuous water level measurement (staff gauge, data logger)



Figure 4. Cameras at the inflow and outflow (construction state)

At the same time, the depths in the fish pass are recorded (Fig. 5) and the passability of the fish pass is monitored by ichthyologists by evaluating images from underwater cameras (Fig. 6). Furthermore, ichthyologists also tagged fish on 20.04.2022 using fish tags.

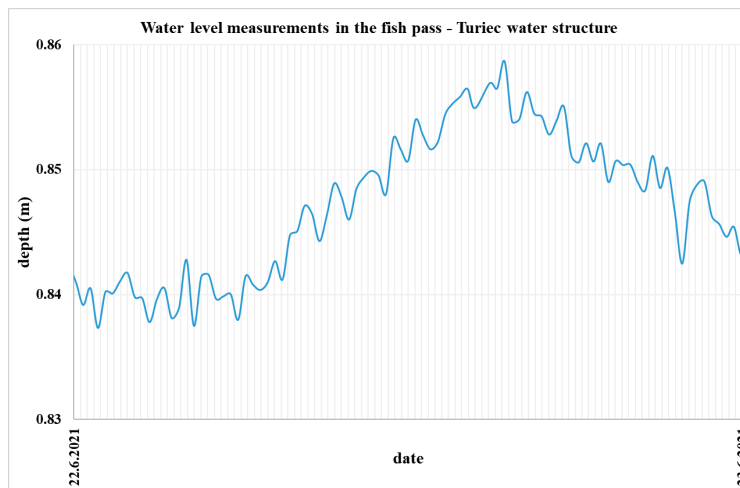


Figure 5. Record of depths in the fish pass – 22.06.2021 (0,837 – 0,859 m)

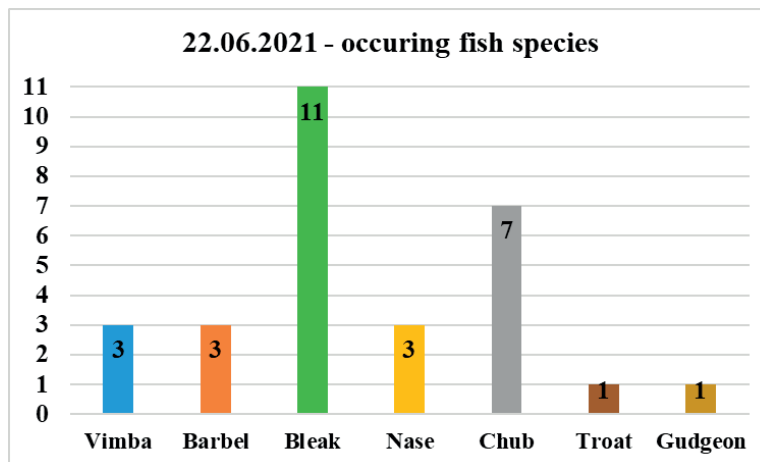


Figure 6. Evaluation of the migrants in the fish pass – 22.06.2021 (in total 29 pieces)

3. Results and discussion

The last measurement of hydraulic parameters performed (26.04.2022) (Fig. 7) was done in accordance with ecological monitoring of the fish pass during normal operation (almost 3 years after its final construction permit) in 7 profiles in different parts of the fish pass, so that all shape and hydraulic changes were covered. The current discharge in the fish pass was measured and the depths and velocity fields in each measured profile were evaluated.

The discharge in the fish pass at the water level in the reservoir at 398.12 m above sea level stated in the project [10] was $1.0 \text{ m}^3 \text{ s}^{-1}$ and at the level of 397.25 m above sea level $0.8 \text{ m}^3 \cdot \text{s}^{-1}$. During the measurement, the water level in the reservoir was 398.06 m above sea level and the measured subsidy discharge in the fish pass was $0.87 \text{ m}^3 \cdot \text{s}^{-1}$. The project referred to the average profile velocities in specific profiles $v = 0.85\text{--}1.61 \text{ m} \cdot \text{s}^{-1}$ at discharge of $Q = 0.8 \text{ m}^3 \cdot \text{s}^{-1}$ (Fig. 8) and $v = 0.93\text{--}1.78 \text{ m} \cdot \text{s}^{-1}$ at $Q = 1.0 \text{ m}^3 \cdot \text{s}^{-1}$ [10].

The evaluated velocities from the measurements were in the range of $v = 0.58\text{--}1.07 \text{ m} \cdot \text{s}^{-1}$ at the measured discharge of $Q = 0.87 \text{ m}^3 \text{ s}^{-1}$ (Fig. 9). The depths in the streamline from the project documentation are $y = 0.68\text{--}0.79 \text{ m}$ [10] and during the measurement they were $y = 0.55\text{--}0.9 \text{ m}$.



Figure 7. Measurements in the fish pass

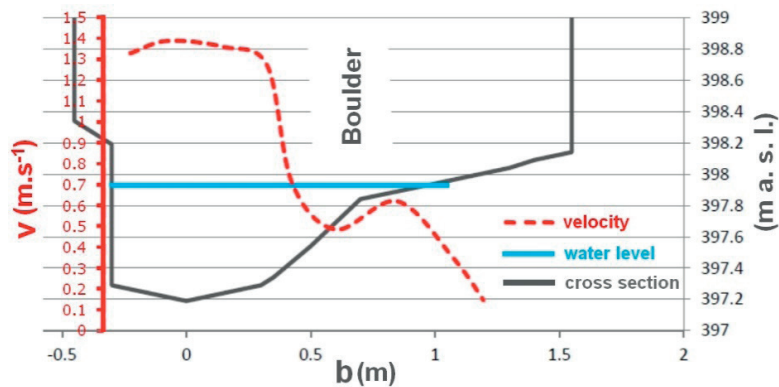


Figure 8. Vertical velocities according to the project by discharge of $Q = 0.8 \text{ m}^3 \text{ s}^{-1}$ (one chosen profile) [10]

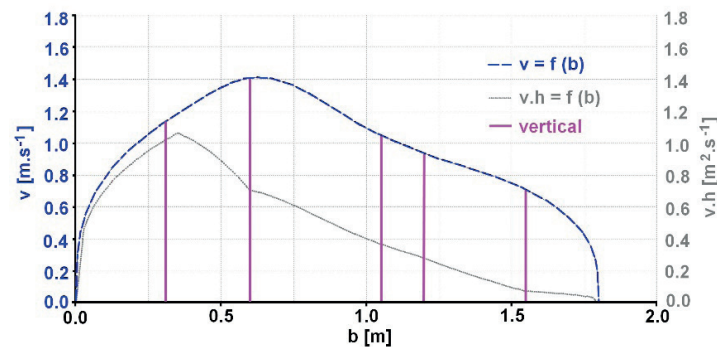


Figure 9. Measured velocities for the same profile as from the project by the measured discharge of $Q = 0.87 \text{ m}^3 \text{ s}^{-1}$

The identified shortcomings are as follows:

- for most of the year, the fish pass should be supplied with a discharge of $1.0 \text{ m}^3 \cdot \text{s}^{-1}$, the discharge of $0.8 \text{ m}^3 \cdot \text{s}^{-1}$ should flow in the fish pass only rarely (even if it meets the limit of the valid decree),
- the velocity in the shallows according to the valid decree is max. $0.5 \text{ m} \cdot \text{s}^{-1}$, the measured velocity exceeds this limit,
- insufficient attractiveness of the outflow jet, observed slow dissipation of the stream, shallow at the outflow is too wide.

Recommendations:

- ensuring the discharge of $1.0 \text{ m}^3 \text{ s}^{-1}$ over the entire year (the water level in the reservoir must be kept at the maximum allowed level) and during the migration period (end of March and April) over $1.0 \text{ m}^3 \cdot \text{s}^{-1}$, which will increase the power/robustness of the outflowing water even for the largest fish – Danubian Salmon,
- proposing to increase the velocity limit in shallow to max. $0.8 - 1.0 \text{ m} \cdot \text{s}^{-1}$, which appears to be passable even for the weakest fish species,
- reaching the flow velocity at the outflow min. $0.75 \text{ m} \cdot \text{s}^{-1}$ (according to the decree) by narrowing the shallow (especially due to the Danubian Salmon).

4. Conclusion

Making barriers passable is a highly relevant issue that is being addressed by all EU Member States, because fish migration does not know borders. Theoretical knowledge summarized in methodologies and decrees must be supplemented by continuous in situ measurements, especially during operation and several years after the final building approval. Of course, it is necessary to correlate the hydraulic parameters with the research of ichthyologists, in order to be able to make any adjustments to ensure the highest possible passability of the barriers on the streams.

The idea of reconstruction of the existed fish pass results from the assumption that it is cheaper and easier to make existing fish pass passable by rearrangement of internal environment as to build new one because of the complex property composition. This was also applied to the water structure on the Turiec River, where new and modern approach not only to the redesign but also to the monitoring of the fish pass were applied.

As shown in the article, the procedure of evaluating a proposed fish pass built in practice according to theoretical recommendations is a long-term process, requiring a large amount of data and the cooperation of several experts from different fields. In the future, on the basis of their evaluation, it will be possible to propose several changes in the design limits of the fish pass so that it meets the prescribed requirements; respectively, it will be the subject of model research of complex hydraulic phenomena that occur during the flow of water in the fish pass riverbed.

Acknowledgements

This article was created with the support of the Ministry of Education, Science, Research and Sport of the Slovak Republic within the Slovak Research and Development Agency, project no. APVV-20-0023 and project no. APVV-18-0472.

References:

- [1] Directive DVWK-Merkblatt 232/1996, Fish passes – Design, dimensions and monitoring, German Association for Water Resources and Land Improvement: Bonn, Germany, 1996.
- [2] Polák, V., Mužík, V., Druga, V., Abaffy, D., Rebenda, F., Matok, P., Mravcová, K., Hránková, R., Čomaj, M., Joštiaková, D.: Determination of suitable types of fish passes according to the typology of streams: Methodological guideline of Ministry of the Environment of the Slovak Republic, (in Slovak), Bratislava, Slovakia: Výskumný ústav vodného hospodárstva, 2015.
- [3] Schmutz, S., Mielach, C.: Measures for ensuring fish migration at transversal structures, Technical paper, Vienna, Austria: International Commission for the Protection of the Danube River, 2013.
- [4] Turek, J., Horký, P., Slavík, O., Randák, T.: Fish tagging, Edition of Methodics 154, (in Czech), Faculty of Fisheries and Protection of Waters, University of South Bohemia in České Budějovice, ISBN 978-80-7514-016-6, 2014.
- [5] Water Plan of Slovakia, Management Plan of the Danube River Basin District, Bratislava 2015, Ministry of the Environment of the Slovak Republic, (in Slovak), https://www.minzp.sk/files/sekcia-vod/vodny-plan-2015/vodny-planslovenska-2015_sup-dunaja-sup-visly.pdf, 31.05.2022.
- [6] Decree 383/2018, On technical conditions for the design of fish passes and the monitoring of the migration passability of fish passes, (in Slovak), The Ministry of the Environment of the Slovak Republic, 2018.

- [7] O'Connor, J., Stuart, I., Jones, M.: Guidelines for the design, approval and construction of Fishways. Arthur Rylah Institute for Environmental Research. Technical Report Series No. 274. Heidelberg, Victoria: Department of Environment, Land, Water and Planning, 2017.
- [8] Ocvirk, E., Gilja, G., Bujak, D., Cikojević, A., Jelić, D.: Nomograms for calculating the functionality of technical fish passes on small sills, (in Croatia), *Hrvatske vode*, Vol. 28, No. 111, pp. 9–20, 2020.
- [9] Operational manual for the water structure Weir on the Turiec River km 7.530 (in Slovak), Slovak Water Management Enterprise, Ružomberok, Slovak Republic, 2022.
- [10] Dobranský, M., Chládek, P.: Removal of barriers on the Turiec River, rkm 7.530, Hydraulic Calculations, (in Slovak), CABEX ltd, Bratislava, Slovak Republic, 2016.

II Hydraulic Engineering and Environmental Impact

FLOOD PROTECTION MEASURES IN LOWLAND REGIONS

ANDREJ ŠOLTÉSZ¹, JAKUB MYDLA¹, MARTIN ORFÁNUS¹

¹ Slovak University of Technology in Bratislava, Faculty of Civil Engineering, Department of Hydraulic Engineering; Slovakia

e-mail: andrej.soltesz@stuba.sk, jakub.mydla@stuba.sk, martin.orfanus@stuba.sk

Abstract

The goal of the contribution is to review the possibilities of flood protection of the county city Trebišov against flood situation which can occur on the Trnávka River flowing along the city. The analysis was performed by mathematical modelling using HEC-RAS software. Based on Trnávka drainage basin reconnaissance, own measurements in situ and study literature relating thereto a proposal of several technical measures for safe run-off in the Trnávka River bed has been elaborated and consequently evaluated from hydraulic point of view. Mitigation of flood discharges was ensured through lateral spillway structures directed the excessive water flow towards existing drainage system connected with the Hraň pumping station into the Ondava River. Presented contribution includes the evaluation of flood situation in 2010 and recommendation for mitigation of the flood wave.

Keywords: flood wave, protection dyke, mathematical modelling, HEC-RAS software, lowland, pumping station.

1. Introduction

The Trnávka stream is a 36,6 km long right-hand tributary of the Ondava River. Both streams are situated in the region of East Slovak Lowland (ESL) close to the Trebišov city (Figure 1). First water management modifications were carried out after establishing institution called Water society for the Ondava River in 1848 [1]. Activities of the Water society were closely connected with the development of the run-off conditions on the Trnávka River. The main problem was that flood situation occurred mostly in the period of simultaneous flood situation on the Ondava River. It has caused backwater and no possibility for the Trnávka River to drain the flood wave. For this purpose, a three field flood gate (1886) on the Trnávka River was built up in front of the mouth into the Ondava River (Figure 2) and excessive water was released through system of culverts and lateral spillways into drainage area of adjacent lowland towards the pumping station in Hraň [2].

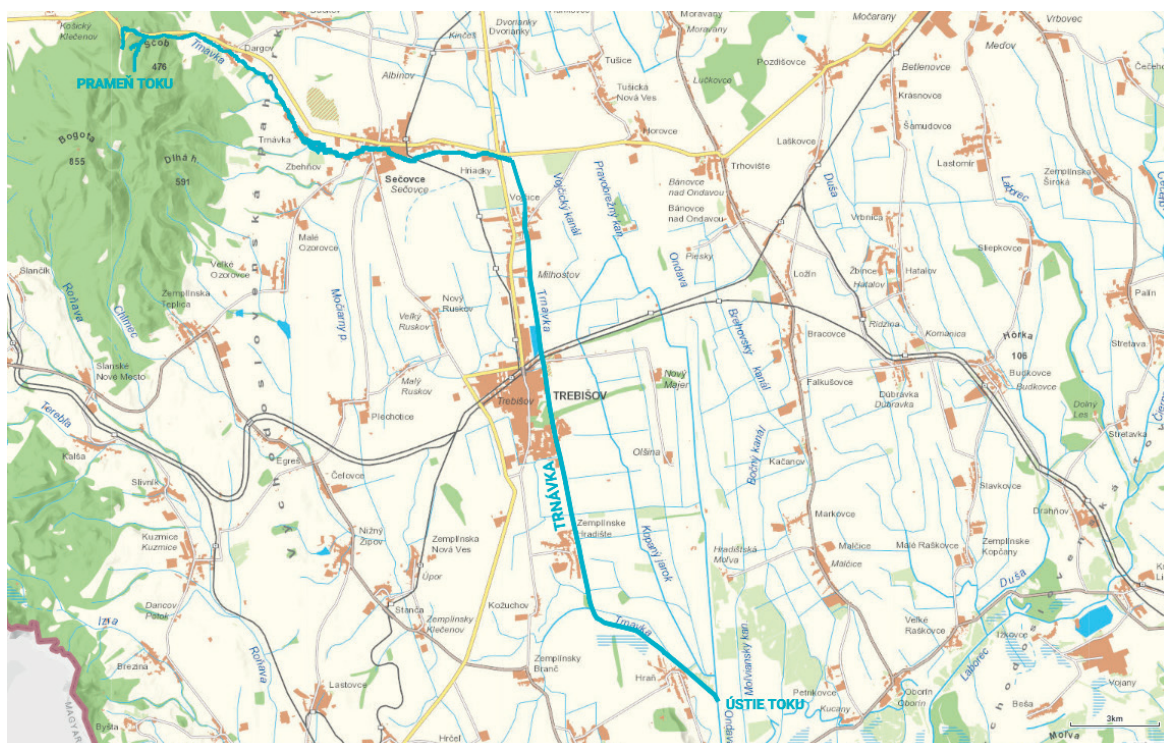


Figure 1. The area of interest – the Trnávka River

There were several floods during last years in this region, example for such critical situation was the flood in May 2010 when all neighbouring rivers and streams have reached their maximum records of water levels and discharges, as well. Critical situation during this flood occurred mainly on the Ondava River (dam breach of right-hand protection dyke (rkm 10,100 and left-hand protection dyke (rkm 12,800) as well as on the Trnávka River (number of dam breaches of left-hand protection dyke in rkm 5,500; 8,970; 9,030 and 16,100) [2].



Figure 2. The bridge with historical flood gate on the Trnávka River in Hraň, rkm 0,270 (1886)

2. Methods

For flood protection solution all necessary data were obtained from the local administrator of the Trnávka and Ondava river basins – Slovak Water Management Enterprise (SWME), direction in Trebišov. They consist of morphology of the Trnávka River as cross sections and longitudinal slope of the river bed, parameters of protection dams and all operational structures on the stream. One of them is a culvert for releasing surplus water directly into drainage channel (Figure 3). The culvert was one of the structures which was considered at the analysis of possible flood protection solution of the Trebišov city. The capacity of it is approx. $Q = 16 \text{ m}^3 \cdot \text{s}^{-1}$. Although, morphologic data were available, it was necessary to append them by own in situ measurements for proper calibration process of the utilized mathematical model. Hydrological data for the solution were obtained from Slovak Hydro-meteorological Institute (SHMI). They concerned primarily the flood situation in the year 2010. There were three flood situations, the most serious was in May 2010, (Figure 4, in the middle). The value has reached almost Q_{50} .



Figure 3. Culvert on the Trnávka River, rkm 9,380 (photo Mydla)

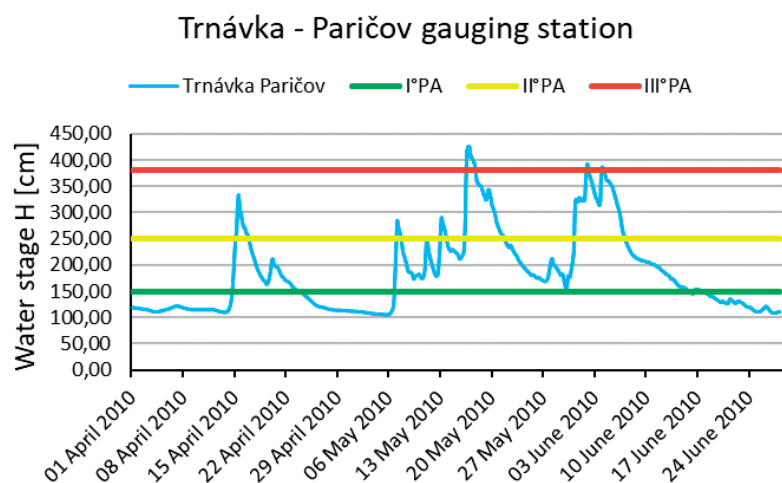


Figure 4. Water stage course in profile Trnávka – Paričov during the flood period in 2010

The green, yellow and red line in Figure 4 represents the first, second and third stage of flood protection activity on the Trnávka River. The mathematical modelling itself involved steady and unsteady calculation using HEC-RAS modelling software [3]. For water level transfer in the Trnávka river bed the 1-D version of the modelling tool in steady conditions was applied to determine the capacity of the Trnávka River bed [4], [5].

Next step was the analysis of unsteady conditions during the flood situation to determine the water level altitude with no use of flood protection measures. This analysis was consequently integrated by 2-D mathematical modelling of released surface water through mentioned lateral structures as culverts or spillways into the adjacent lowland region.

3. Results and discussion

Using the calibrated coupled 1-D and 2-D mathematical model several flood protection measures have been introduced, hydraulically analysed and evaluated from water level transformation point of view [5]. Some of the modelling results are shown in Figure 5 and Figure 6.

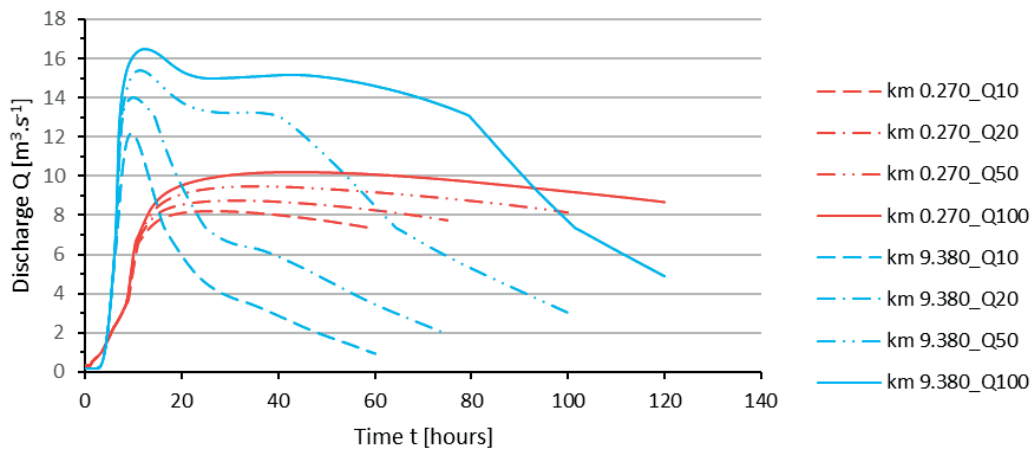


Figure 5. Discharge course through culverts – closed flood gate (**Figure 2**)

The graph in Figure 5 illustrates the course of the discharge of released water through the culvert in rkm 9,380 and the culvert in front of the flood gate (rkm 0,270, Figure 2) on the Trnávka River. The flood gate to the Ondava River is closed and the water is flowing towards the main drainage channel of the Hraň pumping station ($Q = 8,2 \text{ m}^3 \cdot \text{s}^{-1}$) as well as auxiliary pumping station Július ($Q = 5,64 \text{ m}^3 \cdot \text{s}^{-1}$). The volume of the released water was determined $V = 3,64 \text{ mil. m}^3$ and it could be pumped into the Ondava River approximately within three days.

The graph in Figure 6 illustrates the same situation, i.e. the discharge of released water through the culvert in rkm 9,380 and the culvert in front of the flood gate (rkm 0,270, Figure 2). The only difference is that the flood gate on the Trnávka River is open. The released volume of water in this case was determined $V = 1,99 \text{ mil. m}^3$. It could be pumped through Hraň pumping station into the Ondava River approximately within 1,7 days.

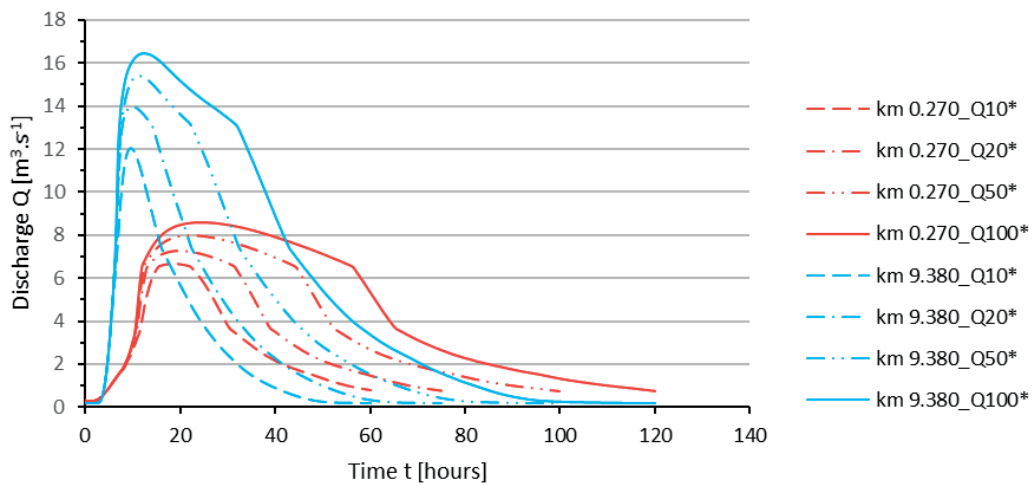


Figure 6. Discharge course through culverts – open flood gate (**Figure 2**)

The released water is stored in adjacent area and diverted towards the Hraň pumping station. Flooded area is illustrated in Figure 7.



Figure 6. Flooded area at Q_{20} flood wave, left side – open flood gate, right side – closed flood gate

According to hydraulic analysis additional flood protection measures have been introduced into the prognosis and they have been analysed and evaluated. From the results of the analysis came out alternatives of flood protection measures which seemed to be most appropriate from flood wave transformation point of view. Evaluation of all alternatives concerned the real flood wave course from year 2010 which was evaluated as a wave with culmination at $Q_{50} = 55 \text{ m}^3 \cdot \text{s}^{-1}$. When introducing the fact that protection dams of the Trnávka River are protecting the Trebišov city to maximum discharge of $Q_{20} = 34 \text{ m}^3 \cdot \text{s}^{-1}$, it is necessary really to find out proper measures for safety run-off of similar flood waves.

4. Conclusion

The Trebišov city is protected against floods of Q_{20} value what is really insufficient for a county city. Therefore, authors strive to find a solution to increase the flood protection of the city using hydraulic analysis by mathematical modelling of water level and discharge regime of the Trnávka River. For the effort the 1-D and 2-D HEC–mathematical model was used to evaluate proposed flood protection measures from hydrological point of view. The goal was to increase the flood protection at least up to Q_{50} value what was the flood situation in May 2010. Considering the possibility to release the surplus water into the lowland region on the left side of the Trnávka River (mostly with no agricultural production, Figure 1), the main effort was concentrated to such solutions. There are existing culverts and lateral spillways which can help to handle the flood situation but it seems to be insufficient. Therefore, additional lateral spillways have been introduced into the analysis with the possibility to divert the surplus water into the drainage channels in the region between the Ondava River and the Trnávka River and towards pumping stations of internal water. The proposed measures were discussed with the SWME administrator and were in full conformity with water management planning of the SWME in this region.

Acknowledgements

This article was created with the support of the Ministry of Education, Science, Research and Sport of the Slovak Republic within the Slovak Research and Development Agency, project no. APVV-19-0383 and project VEGA no. 01/0728/21.

References:

- [1] Kundrát, V., Prosba, J. et al.: Water society on the Ondava River in Trebišov, Košice, ISBN 80-7132-012-9, 1998, 83 p.

- [2] Šoltész, A.: Hydrological-hydraulic analysis of drainage of internal waters on East Slovak Lowland. FCE STU Bratislava, ISBN 80-227-2427-0, 2006, 109 p.
- [3] Brunner, W.G.: HEC-RAS River Analysis System User's Manual, version 5.0, US Army Corps of Engineers Hydrologic Engineering Centre, Davis, CA, 2016, 960 p.
- [4] Leško, P.: Possibilities of flood protection of the Trebišov. Diploma thesis, FCE STU Bratislava, 2020, 93 p.
- [5] Mydla, J., Šoltész, A., Orfánus, M.: Possibilities of design of flood protection measures on the Ondava River. Proc. Of 16th Int. Symp. on Water Management and Hydraulic Engineering, Skopje, 2019, pp. 142–149.

II Hydraulic Engineering and Environmental Impact

HYDRAULIC CAPACITY ANALYSIS OF AN EXISTING COMBINED SEWER SYSTEM USING STORM WATER MANAGEMENT MODEL

NIKOLA KRSTOVSKI¹, GOCE TASESKI¹

¹ Ss. Cyril and Methodius University in Skopje, Faculty of Civil Engineering; Republic of North Macedonia
e-mail: nikolatudence@gmail.com, taseski@gf.ukim.edu.mk

Abstract

Most of the sewerage systems in N. Macedonia is said to be separation, but in reality, they are most often combined systems where in the fecal sewerage system there are large number of connections from the storm sewer system, which practically in case of heavy rain with low intensity occurs overflow of the fecal sewage system. Also, with the increasing investment in the construction of wastewater treatment plants, the problems with mixing the sewage water are problems for the functioning of the treatment plants themselves.

The subject of this paper is to make a hydraulic model using the software package SWMM to determine the hydraulic characteristics of a combined sewer system at the appropriate intensity of rain from where will be defined: the maximum amount of water that will come to the wastewater treatment plant, bottlenecks of the existing network, amount of water that will flow through the overflows, points of overflow of the sewerage, etc. The case study that was used to create the hydraulic model is for the city of Bitola.

There are various methods for determining the amount of atmospheric water - the authoritative rain that will be used for analyzing the existing sewerage or will dimension the future sewerage, and in our country the most commonly used method is method of prof. Gorbachev because it is quite useful when the analysis does not use a sophisticated mathematical model. However, in this paper a comparative analysis will be made where besides the method of prof. Gorbachev will use the Rational Method.

Keywords: sewer network; Method of Prof. Gorbachev, Rational Method, hydraulic analysis, SWMM.

1. Introduction

The amount of water flow that appears in the stormwater drainage system is highly variable throughout the year. During dry periods, it is equal to zero, while during heavy rains its value can be very high. The maximum flow which occurs as surface runoff, depends on: hydrometeorological conditions, urban surface relief, slope, type and size of the catchment area, hydrogeological composition of the soil, groundwater etc. The stormwater drainage system collects the water flows from the natural water processes such as: rainfalls, melting snow, ground water, etc.

Accurate determination of the amount of water to be accepted by the sewer is important from a functional and economic point of view. If the network is undersized, it will not be able to fully accept surface water which would lead to water spills on the streets and the formation of watercourses that could in the worst case cause loss of human life. Whereas if sewage network is oversized, then we would have unjustifiably spent funds for its construction. That is why it is very important to accurately determine the amount of water for sizing the sewer. For that purpose, in this paper will be made comparison the results of two methods for defining amount of stormwater.

First method is method of Prof. Gorbachov. In Macedonia, it is most commonly used method because it is quite useful when the analysis does not use a sophisticated mathematical model and we have data of average annual rainfall.

Second method is Rational Method. In the SWMM software a hydraulic model of the sewerage network is made, and then the amount of atmospheric water is determined according to the Rational Method.

This comparison of the obtained results will be made on the existing sewerage system for the city of Bitola.

2. Methods

2.1. Method of Prof. Gorbachov

The method of prof. Gorbachov is an empirical form for determining the intensity of rain.

$$Q_{ATM} = \Sigma F \cdot q_r \cdot \varphi \cdot \Psi \text{ [l/s]}$$

where:

Q_{atm} – amount of atmospheric water flowing into the canal [l/s]

ΣF – total catchment area for the corresponding move [ha]

q_r – authoritative rain for channel sizing [l/s/ha]

φ – delay coefficient

Ψ – leakage coefficient

It is used in cases when we do not have data on the amount of rain and duration, but when we have only information of the average annual rainfall. This method uses the equation for technical intensity of rain

$$q = 166,7 \cdot i$$

It expresses the dependence between the height of the rain and the duration through the intensity of the rain.

$$\Delta = \sqrt{h \cdot i}$$

if $i = \frac{h}{t}$, then the expressions can be written: $\Delta = \frac{h}{\sqrt{t}}$ or $\Delta = i \cdot \sqrt{t}$

If the intensity is expressed from the last equation, it will be seen that it is inversely proportional to the square root of the duration.

$$i = \frac{\Delta}{\sqrt{t}}$$

The intensity of the rain for a given locality is determined with the help of the average annual precipitation (H_{cp}) according to the equation of prof. Gorbachev.

$$\Delta = \mu \cdot \sqrt[3]{p}; \mu = \alpha \cdot \sqrt[3]{H_{cp}^2}; \Delta = \alpha \cdot \sqrt[3]{H_{cp}^2} \cdot \sqrt[3]{p}$$

where:

α – geographical constant (correction coefficient) which for Macedonia is 0.046

μ – climatic constant that depends on the average annual rainfall

H_{cp} – average annual precipitation [mm]

p – probability of rain

$$\varphi = \frac{1}{\sqrt[n]{\Sigma F}}$$

2.2. Rational Method

A hydrograph is a graph showing the rate of flow (discharge) versus time past a specific point in a river, channel or conduit carrying flow. The peak of the hydrograph is sufficient for design and analysis of the hydraulic model of the storm water drainage system, which can be easily calculated using the Rational Method.

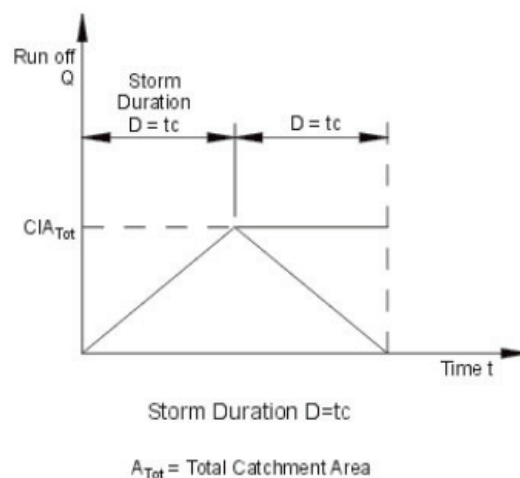


Figure 1. Rational Method runoff hydrograph

The rational method was developed about 130 years ago by Kuichling (1889). This method is applied to urban areas up to 15 km² and uses a simple equation that determines the maximum surface runoff (peak of the runoff hydrograph) in a given profile. The equation is

$$Q = C \cdot I \cdot A \quad [\text{m}^3/\text{s}]$$

C is a dimensionless runoff coefficient intended to indicate the amount of runoff generated by the catchment area. The value of this coefficient varies between 0.05-0.95, depending on the type of the catchment area.

Storm intensity i [mm/min], depends of duration of the rain and the return period. The relation between the three components – storm duration, storm intensity and storm frequency (return interval) is presented by a family of curves called the intensity-duration-frequency curves, or IDF curves.

Time of concentration T_c is the time required for rainfall landing on the farthest point of the watershed to reach the watershed outlet. T_c depends of the size, type and shape of the catchment area.

In Rational Method, storm duration is equal to time of concentration. Therefore hydrograph has triangular shape.

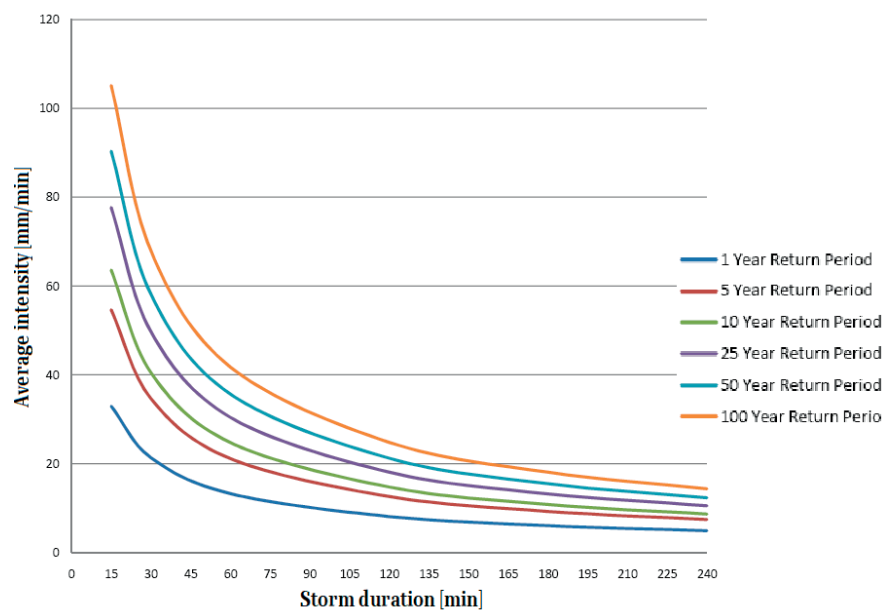


Figure 2. Example for IDF curves

Time of concentration T_c is the time required for rainfall landing on the farthest point of the watershed to reach the watershed outlet. T_c depends of the size, type and shape of the catchment area.

In Rational Method, storm duration is equal to time of concentration. Therefore, hydrograph has triangular shape.

3. Hydraulic model

As a case study that is analyzed is existing combined sewer network for the city of Bitola. The terrain in the city of Bitola consists of both steep and flat parts, which is quite convenient to see the differences in the results of the methods that will be compared.

The hydraulic model of existing sewerage network was created in the software package “Storm Water Management Model” (SWMM).

The data for the manholes and pipes were obtained from the public utility company Niskogradba. 4215 manholes were imported. The pipes diameter varies from 200mm to 500 mm for secondary network, while it varies from 500mm to 2200mm for collectors. The sewerage network consists of 7 main collectors with a length of about 21 km.

The total catchment area is 1025 ha and it is distributed over 32 catchment areas. The 32 catchment areas have a relatively large area, each catchment area is divided by the Thiessen method into a subcatchment area for each manhole, i.e. each manhole has its own catchment area to which atmospheric water flows.

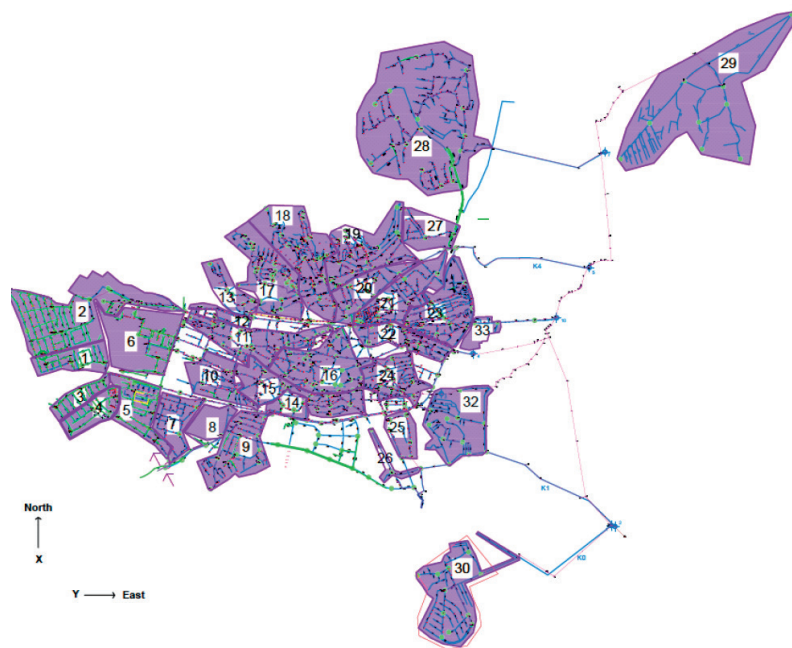


Figure 3. Hydraulic model of the sewerage network in the city of Bitola

The leakage coefficient for each catchment area is determined separately, depending on the percentage of greenery, roof, asphalt and concrete. The following leakage coefficients are adopted depending on the type of surface:

- 0.90 – leakage coefficients for roofs
- 0.80 – leakage coefficients for asphalt surface
- 0.70 – leakage coefficients for concrete surface
- 0.25 – leakage coefficients for parks

After previously received information from the public utility, three overflows were inserted in the model, two of which were placed on the collector 4, one placed on the collector 3.

The maximum amount of sanitary wastewater for each catchment area is obtained from public utility and it varies from 0.2 l/s/ha to 2 l/s/ha.

During the hydraulic analysis, rain with a return period of 2 years, intensity of 93.02 l/s/ ha and duration of 20 minutes was used.

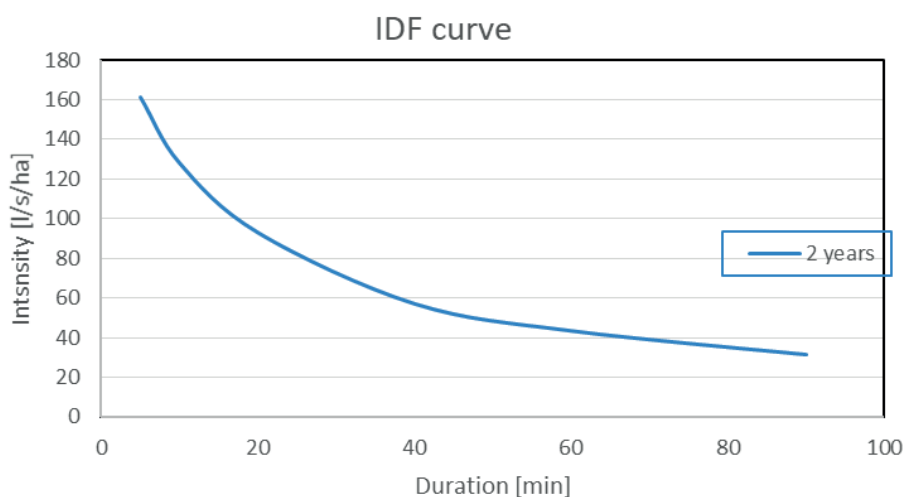


Figure 4. IDF curve used in SWMM

4. Results and discussion

The amount of atmospheric water obtained by the method of prof. The Gorbachev and SWMM methods differ due to the different complexity between these two methods and the number and nature of the input data required for input into these two methods. Namely, the SWMM method considerate the slope of the pipes and the topography of the catchment areas, while that data in the method of prof. Gorbachev is contained in the formula for the coefficient of delay

with article n, which indirectly considerate the influence of the slope, the shape, the size of the catchment area and the slope of the pipe on the size of the runoff. Therefore, for small, steep and elongated catchments, this article, although according to the recommendations should be a maximum of 10 in certain parts. The same in this hydraulic model is provided with values up to 15, while for larger and developed catchments this is adopted between 4 and 8 in depending on the type, shape, slope and size of the catchment area. For article n values above the recommended ones are adopted, in order to get as close as possible to the runoff quantities obtained according to the Rational Method

Table 1. Runoff Quantities

Method	Prof. Gorbachov					SWMM	Compare	
Collector	Manhole	Catchment	Specific Runoff l/s/ha	Area	ϕ	Quantities l/s	Quantities l/s	SWMM – Prof. Gorbachov
K00	S30	O-K00	93.02	49.97	0.61	97.5	112	14.5
K01	S26	S26	93.02	5.29	0.89	11.8	18	6.2
	S25	S25		11.24	0.74	72.6	82	9.4
	S32	S32		40.30	0.63	189.7	221	31.3
	S32	O-K01		56.83	0.36	169.5	169	-0.5
K02	S07	S07	93.02	17.59	0.70	239.7	295	55.3
	S08	S08		22.64	0.68	204.6	226	21.4
	S10	S10		20.23	0.47	336.3	382	45.7
	S09	S09		30.84	0.65	364.1	465	100.9
	S07	S08		17.59	0.70	273.7	330	56.3
	S08	S10		40.23	0.63	444.8	563	118.2
	S10	S09		60.46	0.60	857.2	908	50.8
	S09	MH-1801		91.30	0.57	1130.7	1195	64.3
	S14	S14		7.62	0.78	289.9	345	55.1
	S15	S15		28.79	0.66	936.9	1268	331.1
	S14	S15		7.62	0.78	289.9	318	28.1
	S15	MH-1801		36.40	0.64	1154.5	1457	302.5
	MH-1801	O-K02		127.71	0.55	2108.5	2499	390.5
K03	S12	S12	93.02	13.12	0.53	333.5	361	27.5
	S11	S11		22.37	0.68	752.7	905	152.3
	S16	S16		38.06	0.59	1122.5	1133	10.5
	MH-3154	O-K03		91.36	0.57	2253.0	2464	211.0
K04	S13	S13	93.02	13.96	0.84	344.7	385	40.3
	S17	S17		36.55	0.79	844.1	929	84.9
	S18	S18		45.53	0.78	1067.7	1255	187.3
	S19	S19		37.27	0.79	834.2	921	86.8
	S21	S21		29.00	0.71	741.8	810	68.2
	S23	S23		33.01	0.50	503.2	557	53.8
	S27	S27		16.88	0.83	68.0	75	7.0
	S13	S17		13.96	0.84	344.7	373	28.3
	S17	S18		50.51	0.77	493.3	611	117.7
	S18	S19		113.62	0.73	1130.2	1444	313.8
	S19	S21		150.90	0.72	1841.3	2176	334.7
	S21	S27		167.78	0.71	2326.2	2902	575.8
	S27	S23		184.66	0.71	2683.2	2948	264.8
S23	O-K04	217.67	0.51	2086.6	2483	396.4		
K05	S28	O-K05	93.02	143.96	0.19	170.8	191	20.2
K06	S29	O-K06	93.02	129.84	0.30	89.6	27	-62.6

From the obtained results it can be concluded that in the places where we have steep terrain, according to the SWMM method we have a higher flow, while in the plain parts we have a higher flow according to the method of prof. Gorbachev. These two cases are significantly more pronounced when we have a steep slope and small and elongated catchments, while large circular catchments and a slight slope produce approximately the same amount of atmospheric water.

5. Conclusion

The method of prof. Gorbachev is an old method, in which a simple formula provides the maximum amount of storm water that is needed to dimension the storm sewer. In this method, the topographic characteristics of the catchment area are not taken as a whole, but are expressed through article n of the delay coefficient, so when we analyze storm water for settlements with large variation of slope, size and shape of the catchment area, we will get unrealistic quantities of storm water at certain parts of sewer network.

SWMM is a modern method of determining the amount of storm water, which with the help of the power of computers can very quickly simulate storm water, turning it from rain into canal water, taking into account the topography of the terrain, the slope of the canals, the type of surface, etc. The advantage of this method that can solve very complex sewer networks and in a very easy way to make changes in them. The great advantage of this method is that the model can be calibrated, i.e the input parameters can be changed and thus we can get a model that works approximately the same as the real sewer network.

From the above, it can be concluded that the method of Prof. Gorbachev is an outdated method that can only be used for some preliminary calculations in order to obtain an indicative size of storm water even when we have a smaller number of input data. While the SWMM method is a modern tool that requires large data input, but therefore provides a realistic simulation of the operation of the sewer system.

References:

- [1] Nikola Krstovski, "DIFFERENT ANALYSIS METHODS FOR STORMWATER SYSTEM MODELING" Master thesis, Skopje, Macedonia, 2022.
- [2] Шкоклески Ж. "Врнежи во Република Македонија".
- [3] Rossman L.A. Storm water management model user's manual, version 5.0, EPA. United States. 2009; p. 233.
- [4] David B. Thompson "The Rational Method", September, 2006, Civil Engineering Department, Texas Tech University.
- [5] Junaidi, A.; Ermalizar, L.M. (2018): "Flood simulation using EPA SWMM 5.1 on small catchment urban drainage system".
- [6] Waikar, M.L.; Undegaonkar Namita, U. (2015): "Urban Flood Modeling by using EPA SWMM 5".

II Hydraulic Engineering and Environmental Impact

POSITIVE EFFECTS OF VARIABLE FREQUENCY DRIVEN PUMP

TIN KULIĆ¹, HANNA MILIČEVIĆ¹, IVAN HALKIJEVIĆ¹, HANA POSAVČIĆ¹

¹ University of Zagreb, Faculty of Civil Engineering; Croatia

e-mail: tin.kulic@grad.unizg.hr, hanna.milicevic@grad.unizg.hr, ivan.halkijevic@grad.unizg.hr, hana.posavcic@grad.unizg.hr

Abstract

Energy efficiency of the water pipeline system is analysed on the physical model of the water supply system through the application of the pump with nominal characteristics (unregulated pump) and the same pump controlled by variable frequency drive (frequency regulation). The functional advantage of pump frequency regulation is quantified in terms of reducing water loss due to leakage through the circular orifice (crack/opening). The occurrence of leakage was simulated by opening a 20 [mm] diameter circular orifice drilled through the pipe wall (polyethylene pipe (PE), 110/90 [mm]). The influence of pressure change on the leakage outflow in the physical model was also investigated in order to find the leakage exponent NI in the ratio $Q_i / Q_l = (h_i / h_l)^{NI}$ where Q and h represent the leakage flow and the corresponding pressure head. The results of the research showed that frequency regulation of the pump enables an average reduction of energy consumption by 16.5% in the case of water demand pattern characteristic for a larger agglomeration (city), or by 41.5% in the case of a smaller agglomeration. Furthermore, exponent NI receives a value of ≈ 0.5 , indicating only a minor influence of the elastic deformations of the pipe material in the regime of the tested pressure head range (20–70 [m]).

Keywords: pump frequency, control, intensity of leakage, water pipeline system, physical model, numerical model, pressure and flow measurements.

1. Introduction

Pumps are often used in public water supply without any motor speed control, with flow being mostly regulated by valves (dissipation of mechanical energy). The other most common ways are by using a bypass (increasing the flow rate for lower output pressure) or reducing (cutting, installing a smaller) pump rotor. The pump, according to the usual design solutions, operates at full capacity in the nominal operating mode (maximum efficiency coefficient).

Considering that water supply systems are characterized by the fluctuation of user demand throughout the day, while the prescribed minimum pressure in the system due to firefighting requirements should be achieved with the least possible temporal and spatial fluctuations in flow. Thus, the application of a speed-controlled pump enables the possibility of considerable energy savings, especially in the case of direct water supply systems (pump energy consumption proportional to the third power of pump revolutions per minute [1]). Variable frequency drive controls the motor speed in such a way that the fixed values of the input voltage and frequency are transformed into variable ones. In addition to saving energy for the operation of the pump itself, the application of frequency control also achieves indirect benefits such as reducing the intensity of water hammer and water leakage (water losses).

Water supply systems are subject to aging and usually increasing water demands at the same time. Water losses reach alarm value in agglomerations around the world, somewhere more than 70% [2]. Water losses through pipe cracks have been recognized as a major cause of mismanagement of available water resources [3], which has led to the development of leak detection techniques [4].

In the last two to three decades, detection techniques have been developed and applied for the non-stationary (acoustic detection, transient analysis) or stationary (mass balance, inverse stationary) flow regime analysis [3], [5], [6], [7], [8], [9], [10]. Also, many studies clearly indicate an increase in number of pipe cracks with an increasing pressure in the system [11].

The intensity of leakage through a small orifice is traditionally described by equation [12], [13]:

$$Q_S = C_d A_s \sqrt{2gh} \quad (1)$$

where: Q_S represents orifice leakage discharge, C_d orifice discharge coefficient, A_s size of orifice area, and g the gravitational acceleration.

The value of C_d depends primarily on the orifice shape, the pressure, and the flow velocity in the pipe. According to the results of a study [14] for a circular orifice and a wider range of velocities in the pipe (0.4 - 2.0 m/s), at pressure head

greater than 20 m, the coefficient C_d maintains approximately a constant value of 0.65. According to older study [15], for circular orifice with a surface area less than 20% of pipe flowing surface, and a flow that entirely flows out through the orifice, C_d is 0.62. Admittedly, the C_d also depends on the Reynolds number (Re), but for $Re > 8000$ in the orifice profile, C_d value remains constant.

Within the application of Eq(1), it is commonly assumed that the area of leakage orifice A_S is independent of the pressure. However, the results of laboratory testing presented in the [16], [17], [18] show that an increase in pressure above a certain value also causes an increase in the leakage surface of the crack. In view of the above, Eq(1) does not represent a suitable model for the relationship between the pressure and the flow rate through a real crack. Therefore [2], [19], [20], [21], [22] proposed the power equation, Eq(2), as a more advanced option for describing the relation $Q - h$:

$$Q_S = Ch^{N1} \quad \text{or} \quad Q_{S1}/Q_{S2} = (h_1/h_2)^{N1} \quad (2)$$

where: C is a discharge coefficient, $N1$ leakage exponent, Q_{S1} , Q_{S2} leakage discharge at pressure heads h_1 and h_2 .

Mathematically speaking, Eq(2) is a generalization of the leakage equation through a small opening (Eq(1)) with the possibility of adopting $N1$ values other than 0.5. The drawback of Eq(2) is contained in the dependence of C and $N1$ on the system pressure.

The results of individual studies [23] have shown that the corresponding $N1$ value for the real pipeline system can significantly exceed the value of 0.5, and that it usually varies between 0.5 and 2.79, with a median of 1.15. These results suggest that leakage flow rate is highly dependent on the pressure in the water supply network, and that the strategy of water loss management should concentrate on finding the possibility of maintaining minimum system pressures. For example, if the value of the exponent is $N1 = 2.5$, reducing the pressure by half will result in 82% reduction of leakage flow rate.

Pipe material significantly influences the intensity of leakage at the points of crack through the difference in the geometric shapes of the cracks and their expansion rate (elastic or elastoplastic deformation of the pipeline) at increased pressure.

The analysis of pressure effect on the water leakage loss through the crack was also performed using numerical modelling [24] assuming linear elastic behaviour of the pipe material (PVC, cast iron - ductile iron, and asbestos cement). A key conclusion of the study is to recognize the linear relationship between the leakage flow rate increase and the pressure in the pipe what is presented in Eq(3):

$$Q_S = ch^{0.5} + dh^{1.5} \quad (3)$$

where: $c = Cd A_S (2g)^{1/2}$, $d = Cd m (2g)^{1/2}$ with A_S the leakage surface of the crack at low pressure condition ($h = 0$) and m the parameter dependent on crack geometry.

In the case of pipe made of viscoelastic material, it is necessary to modify the previous equation into a form with a corresponding participation of the elastic and viscous member, thereby obtaining a viscoelastic model [25].

The aim of the research in this paper is to quantify the increase in energy efficiency and the reduction of water losses through the application of a frequency-controlled pump in a pressured pipeline system compared to the application of an unregulated pump. Details of physical model of the pressured system installed in the laboratory are given in Section 0. The Section 0 presents the results of the performed experiments, and the conclusions of the conducted research are given in the final section.

2. Materials and methods

The physical model of the pressured pipe system was made in the Hydraulic Laboratory of the Faculty of Civil Engineering, University of Zagreb. A schematic is given in Figure 1, and some photographs of the device are presented in Figure 2. The horizontally positioned pump drive shaft is chosen as reference geodetic "0" level. Water surface elevation in the underground channel is at -1.5 [m]. The suction pipe of the pump is submerged up to -1.75 [m]. The pump is installed with power $P_P = 15.55$ [kW] and nominal characteristics $Q_P = 36$ [m³/h] (10 [l/s]), $H_P = 70$ [m] at $n = 3000$ [rpm] (Etanorm ETN, 065-040-250, KSB manufacturer). The model of pressure system contains several typical fitting elements (air vents and reduction valves, plate valves, elbows ...). The pressured system is made up of a series of short pipes with a diameter of $110 = 110/90$ mm, cast iron (ductile iron), asbestos and PE (Figure 2). At the PE pipe section, a circular orifice (model crack) of diameter $d_0 = 20$ mm was drilled, and a nozzle with a built-in plate valve to regulate the leakage was applied (Figure 2). By closing the plate valve, the leakage surface of the orifice (model crack) is reduced, and its shape is changed (change in the geometry of circular opening).

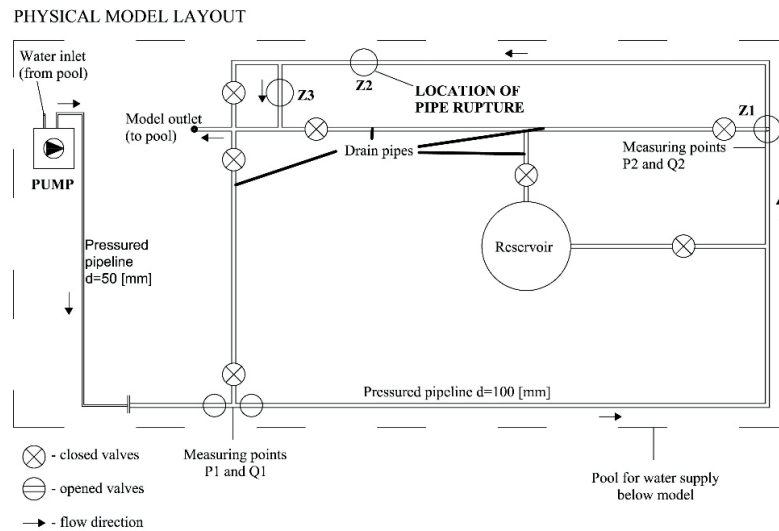


Figure 1. Schematic ground plan of the pressured pipeline system

The pump pressure head gain values H_P are read directly from the pump. Pressure head data at positions P1 and P2 (Figure 1) were obtained with pressure gauges connected to the data acquisition (logger) system of the PDL-AG manufactured by SMTech (Figure 2). The sampling frequency is 20 Hz. Flow measurement was performed with an FLUXUS F601 ultrasonic meter (manufactured by Flexim), at positions Q1 and Q2 (Figure 1, Figure 2). The data on pump motor power P_P are read directly from the pump display.



Figure 2. Pressured pipeline system installed at the Hydraulic Laboratory of the Faculty of Civil Engineering, University of Zagreb (a – pump at the inflow section of physical model, b – part of pipeline with nozzle and plate valve to regulate leakage through opening-crack, c – acquisition system controls for dynamic pressure and flow measurement)

3. Results and discussion

3.1. Measurements of pump performance

Initial (reference) measurement was performed by setting the appropriate pump speed ($n = 2100, 2400, 2700, 3000$ [rpm]) with the fully closed valve Z3 at the end of the pressure pipeline. The plate valve Z3 is then opened to

reach stationary conditions with flow rate $Q_P = 1, 2, 3, 4, 5$ and 6 [l/s] (flow rate reading at position Q1, Figure 1). Valve Z2 is closed (there is no leak at the point of model orifice – crack) and valve Z1 is open. After a constant flow through the pipeline is obtained, the values of pump height H_P and applied pump power P_P are read from the pump display. The measured values are documented in the form of characteristic $Q_P - H_P$, $P_P - Q_P$ and $\eta - Q_P$ curves (Figure 3). The efficiency coefficient was calculated as $\eta = \rho g Q_P H_P / P_P$ (adopted $\rho = 999$ [kg/m³]). The efficiency coefficient η extends from 17% at a flow rate of $Q_P = 1$ [l/s] to 53% at a flow rate of $Q_P = 6$ [l/s], approximately independent of the pump rotor speed. It should be noted that the model design of the pressured system did not allow the application of a flow rate greater than 6 [l/s], primarily due to the occurrence of a pressure head lower than -8.5 [m] of water column on the suction part of the pump.

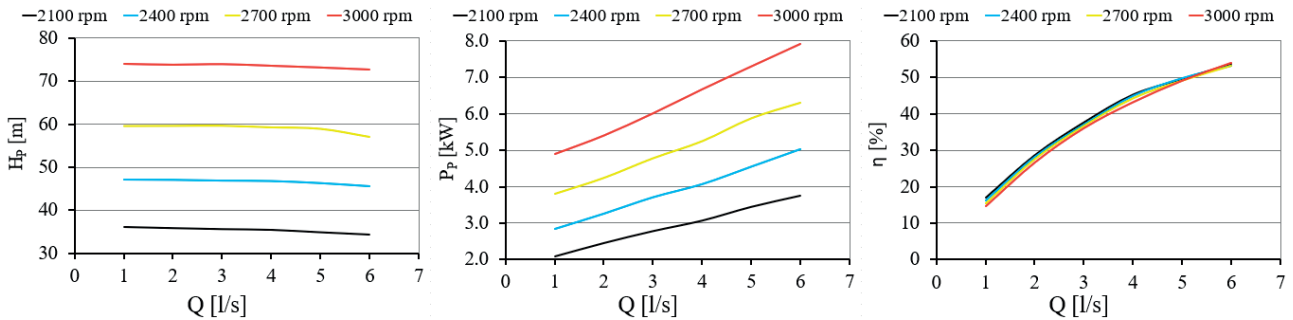


Figure 3. Performance of the Etanorm ETN pump, 065-040-250 (KSB manufacturer), in the flow range 1–6 [l/s]

3.2. Power consumption for different water demand using a pump without / with frequency control

The pump energy consumption was analysed for two characteristic water supply scenarios according to different water demand patterns, i.e., daily water consumption regimes for smaller and larger agglomeration during one day (Figure 4). In the first scenario, the pump was used without frequency control (constant pump rotor speed $n = 3000$ [rpm]), while in the second scenario, the same pump was used with frequency control. The required condition (for firefighting requirements) is that the pressure at the position of the pressure gauge P2 must not fall below 250 [m] of water column. Due to the limitation of the maximum pump flow rate (see Section 0), a discharge of 6 [l/s] was used for the peak hour of consumption, and for other hours the discharge rates were normalized to this value (Figure 5).

In Experiments 1–6 (Table 2) the pump rotor speed was constant ($n = 3000$ [rpm]) and the valve Z3 at the end of the pipeline was opened until the desired flow was achieved ($Q_P = 1, 2, 3, 4, 5$ and 6 [l/s]), respecting the condition of minimum permissible pressure head (25 [m]) at position P2. The pressure was measured at the pressure gauge positions P1 and P2. In order to simulate the friction and local losses occurring in the real pressured pipeline system, partial closure of the Z1 valve was performed. This action generates local losses of the required intensity to achieve 25 [m] pressure head at the hour of peak consumption. During experiments 1 – 6, the degree of closure of valve Z1 does not change and the valve Z2 remains fully closed (no cracks).

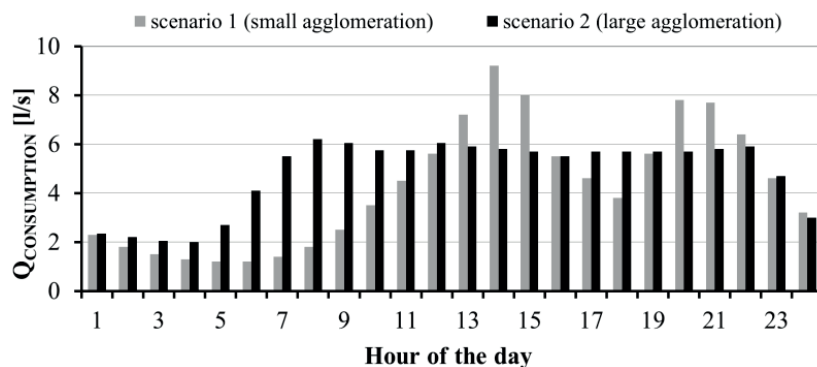


Figure 4. Characteristic distribution of consumption needs intensity during the day for a small and large agglomeration

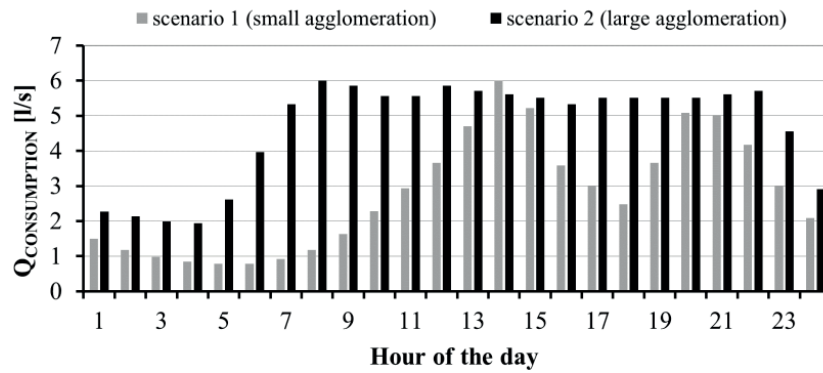


Figure 5. Characteristic distribution of consumption needs intensity during the day for a small and large agglomeration by normalizing to a peak consumption value of 6 [l/s]

In Experiments 7–12 (Table 2), the rotation speed of the pump rotor was variable ($n = 2100\text{--}3000$ rpm) and selected according to the desired discharge ($Q_P = 1, 2, 3, 4, 5$ and 6 [l/s]), maintaining the set condition of minimum pressure head (25 [m]) at the position of the pressure gauge P2. The degree of closure of valve Z1 was the same as in Experiments 1–6. The valve Z2 was completely closed (no cracks).

Applying the measured $Q_P - P_P$ ratios (Table 2, Table 3) and the previously adopted distribution of consumption intensities during the day for the two analysed scenarios (formally: scenario 1 – small agglomeration, scenario 2 – large agglomeration, Figure 5), the corresponding energy distribution for pump operation during the day was obtained (Figure 6).

Table 2. Measured pressure heads at positions P1 and P2, flow rate in pipeline Q_P and pump power P_P used for experiments 1–6 (without pump frequency control)

Exp.	n	$h_{(P1)}$	$h_{(P2)}$	Q_P	Q_S	Q_{IZ}	P_P
	[rpm]	[m]	[m]	[l/s]	[l/s]	[l/s]	[kW]
1	3000	65.0	62.0	1.00	0.00	1.00	4.91
2	3000	65.0	60.0	2.00	0.00	2.00	5.5
3	3000	65.0	55.0	3.00	0.00	3.00	6.05
4	3000	64.0	49.0	4.00	0.00	4.00	6.72
5	3000	61.0	36.0	5.00	0.00	5.00	7.34
6	3000	59.0	25.0	6.00	0.00	6.00	7.92

Figure 6 shows that the application of pump frequency control enables higher increase of energy efficiency in scenario 1 when compared to scenario 2. The reason is that in the case of larger agglomeration, consumption close to the peak occurs over a longer period (from 7h to 22h, Figure 4 and Figure 5), in which the nominal operation pump with 3000 [rpm] is required to achieve the desired pressure head of 25 [m]. The main contribution to the reduction of energy consumption is made between 22h and 6h, with a total daily reduction of energy consumption by 16.5% in scenario 2.

The benefit of applying frequency control is more pronounced in the case of scenario 1 (Figure 6), where a total daily reduction in energy consumption reaches 41.5%.

Table 3. Measured pressure heads at positions P1 and P2, flow rate in pipeline Q_P and pump power P_P used for experiments 7–12 (with pump frequency control)

Exp.	N	$h_{(P1)}$	$h_{(P2)}$	Q_P	Q_S	Q_{IZ}	P_P
	[rpm]	[m]	[m]	[l/s]	[l/s]	[l/s]	[kW]
7	2100	28.0	25.0	1.00	0.00	1	1.87
8	2100	30.0	25.0	2.00	0.00	2.00	2.43
9	2250	34.0	25.0	3.00	0.00	3.00	3.19
10	2490	41.0	25.0	4.00	0.00	4.00	4.44
11	2790	51.0	25.0	5.00	0.00	5.00	6.3
12	3000	59.0	25.0	6.00	0.00	6.00	7.92

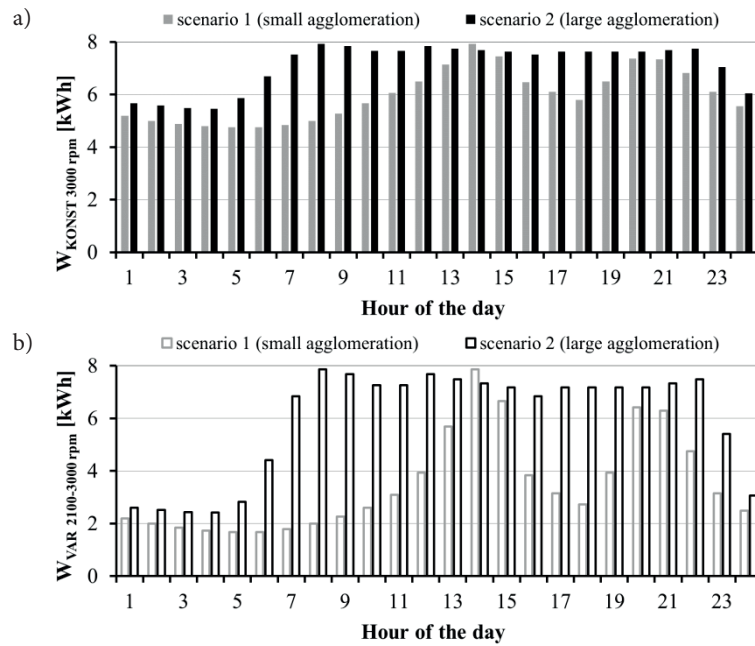


Figure 6. Daily distribution of energy consumption intensity for pump operation during the day in scenario 1 and 2 (a – without frequency control, down – b frequency control)

3.3. Measurements in the operation condition with the presence of a crack

In Experiment 13 (Table 4), hydraulic characteristics of the system were monitored for a leakage occurring at a time of low consumption of 1 [l/s] (without frequency control, pump at 3000 [rpm]). The leakage was simulated by partially opening the plate valve Z2 (see Figure 1) in the nozzle connected to a 20 [mm] diameter circular orifice (crack) by partially opening the leakage area is 1/5 of the total circular orifice area, or $6.3E-5$ [m²]. The degree of closure of valve Z1 was the same as in Experiments 1–12. The measured flowrate Q_{IZ} at position Q2 refers to the pipe section after the leakage and represents an imposed consumption of 1 [l/s]. The pump flow rate Q_P is measured at position Q1 and refers to the pipe section before leakage. It includes the leakage flowrate Q_S and outgoing flowrate at the end of model pipeline Q_{IZ} . Therefore, the leakage flow rate Q_S was calculated as the difference $Q_S = Q_P - Q_{IZ}$.

The conditions in Experiment 14 (Table 4) differ from the conditions in Experiment 13. The pump motor speed is 2100 [rpm], resulting with a pressure head of 25 m at a pressure gauge position P2. The degree of closure of valves Z1 and Z2, along with discharge Q_{IZ} are the same as in the case of Experiment 13.

Table 4. Measured pressure heads at positions P1 and P2, flow rates in pipeline QP, QIZ, QS and pump power PP for experiments 13 and 14 (leakage appearance)

Exp.	N	$h_{(P1)}$	$h_{(P2)}$	Q_P	Q_S	Q_{IZ}	P_P
	[rpm]	[m]	[m]	[l/s]	[l/s]	[l/s]	[kW]
13	3000	65.0	60.0	2.00	1.00	1.00	5.42
14	2100	30.0	25.0	1.65	0.65	1.00	2.35

The results in Table 4 show that the leakage intensity Q_S decreases with the square root of the pressure ratio at position P2 (just before the leakage point), what agrees with Eq(1). Frequency control of the pump reduces the leakage intensity by 35%. It should be noted that the measured pressure data $h_{(P2)}$ allows the calculation of the discharge coefficient for the model leakage orifice based on Eq(1) resulting in a value of $C_d = 0.47$.

In a view of the given comment on the possible occurrence of pipe and crack elastic deformations (see Section 0), additional experiments have been made to determine the appropriate value of the exponent Nl (Experiments 15–36, Table 5). If elastic deformations are present, Eq(1) is no longer valid, and it is suggested to use Eq(2) and Eq(3). Furthermore, exponent Nl in Eq(2) does not take the value 0.5. In experiments 15–36, the rotation speed of the pump varies from 1500 to 3000 [rpm], along with the damping rate on the reduction valve. Manipulation of the reduction valve enables controlled incremental variation of pressure head $h_{(P2)}$ at position P2 in the desired range 20–70 m (Table 5). The plate valve Z2 is positioned to provide a leak area of $1.6E-4$ [m²] (50% of the total drilled circular orifice). The valve Z3 at the end of the pipeline is completely closed, so the flow rate through the pipeline Q_P corresponds to the leakage flow rate ($Q_P = Q_S$). The pairs of measured leakage flow rates Q_{S-i} and the associated pressure heads $h_{(P2-i)}$

at position P2 are recorded where $i = 15, 16, \dots, 36$ represents the experiment number. Figure 4 shows the graphical interpenetration of the measured ratios $Q_{S-i}/Q_{S-15} = (h_{P2-i}/h_{P2-15})^{NI}$ for experiments 15–36. The curves obtained by using the values $NI = 0.5$ and 0.75 are also shown in addition to the measured $Q_{S-i}/Q_{S-15} = (h_{P2-i}/h_{P2-15})^{NI}$ points.

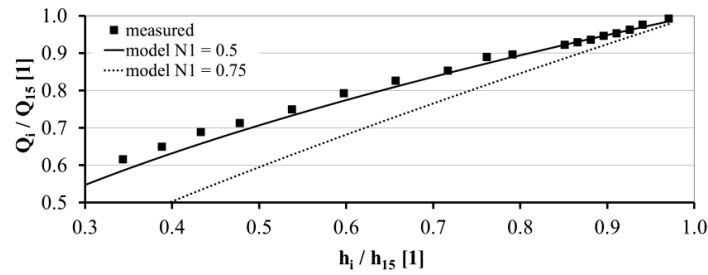


Figure 7. Measured dependence of Q_{S-i}/Q_{S-15} ratio on h_{P2-i}/h_{P2-15} ratio for experiments 15–36, and $Q_{S-i}/Q_{S-15} = f(h_{P2-i}/h_{P2-15})^{NI}$ curves with adopted values $NI = 0.5$ and 0.75

Table 5. Measured pressure heads h_{P2-i} at position P2 and pipeline flow rates Q_{P-i} for experiments 15–36

Exp.	h_{P2-i}	$Q_{P-i} = Q_{S-i}$	Q_{S-i}/Q_{S-15}	h_{P2-i}/h_{P2-15}
	[m]	[l/s]	[1]	[1]
15	67.0	3.00	–	–
16	65.0	2.98	0.99	0.97
17	63.0	2.93	0.98	0.94
18	62.0	2.89	0.96	0.93
19	61.0	2.86	0.95	0.91
20	60.0	2.84	0.95	0.90
21	59.0	2.81	0.94	0.88
22	58.0	2.79	0.93	0.87
23	57.0	2.77	0.92	0.85
24	53.0	2.69	0.90	0.79
25	51.0	2.67	0.89	0.76
26	48.0	2.56	0.85	0.72
27	44.0	2.48	0.83	0.66
28	40.0	2.38	0.79	0.60
29	36.0	2.25	0.75	0.54
30	32.0	2.14	0.71	0.48
31	29.0	2.07	0.69	0.43
32	26.0	1.95	0.65	0.39
33	23.0	1.85	0.62	0.34
34	20.0	1.74	0.58	0.30
35	18.0	1.65	0.55	0.26

4. Conclusions

The energy consumption for the operation of the pump with and without the application of variable frequency drive during the variation of daily consumption was analysed on the laboratory physical model of the pressure pipeline system. A minimum pressure head of 25 [m] has been adopted as the additional functionality criterion of the pipeline. The measurement also defines the $Q-H$, $P-Q$ and $\eta-Q$ curves for the used pump (nominal characteristics $H_n = 70$ [m], $Q_n = 10$ [l/s], $n = 3000$ [rpm]). Furthermore, experiments were conducted to analyse the influence of the pump frequency regulation and pipe pressure change on the reduction of leakage intensity.

The results of the study showed that in the case of scenario 2 (small agglomeration), the application of frequency regulation allows for an increase in energy efficiency of 16.5%, while in the case of scenario 1 (large agglomeration), the energy efficiency is increased by 41.5%. Furthermore, by applying frequency control, a 35% reduction in leakage flow rate is achieved. In addition, the measurement results showed that the exponent Nl in the relation $Q_i / Q_l = (h_i / h_l)^{Nl}$ take a value of 0.5 in the range of investigated pressures heads from 20 [m] to 70 [m], indicating a negligible effect of pipe and leakage opening elastic deformations.

Acknowledgements

This research has been supported by the Croatian Science Foundation (projects DOK-2020-01, UIP-2020-02-1160, PZS-2019-02-3081).

References:

- [1] Jović, V.: Analysis and modelling of non-steady flow in pipe and channel networks, John Wiley & Sons, 2013.
- [2] Lambert, A.: What do we know about pressure: Leakage relationship in distribution system?, Proceedings of IWA Conference on System approach to leakage control and water distribution systems management, Brno, pp. 1–8, 2001.
- [3] Colombo, A., Lee, P., Karney, B.W.: A selective literature review of transient-based leak detection methods, J. Hydro Environ. Res., 2 (4), pp. 212–227, 2009.
- [4] Araujo, L.S., Ramos, H., Coelho, S.T.: Pressure control for leakage minimisation in water distribution systems management, Water Resources Management, 20(1), pp 133–149, 2006.
- [5] Brunone, B.: A technique for leak detection in wastewater outfalls – Numerical experiments, Proceedings of Congress on ‘Wastewater Outfalls’, Naples, pp. 223–236, 1989.
- [6] Brunone, B.: Transient test-based technique for leak detection in outfall pipes, Journal of Water Resources Planning and Management, 125(5), pp. 302–306, 1999.
- [7] Brunone, B., Ferrante, M.: On leak detection in single pipes using unsteady-state tests, Proceedings of the IASTED International Conference on Modeling and Simulation, Philadelphia, pp. 268–272, 1999.
- [8] Jönsson, L.: Hydraulic transients as a monitoring device, Proceedings of the XXVIII International Association for Hydro-Environment Engineering and Research Congress, Graz, pp. 1–6, 1999.
- [9] Liggett, J.A., Chen, L.: Inverse transient analysis in pipe networks, Journal of Hydraulic Engineering, 120 (8), pp. 934–955, 1994.
- [10] Puust, R., Kapelan, Z., Savić, D., Koppel, T.: A review of methods for leakage management in pipe networks, Urban Water Journal, 7(1), pp. 25–45, 2010.
- [11] May, J.: Leakage, Pressure and Control, Proceedings of the BICS International Conference Leakage Control Investigation in underground Assets, London, 1994.
- [12] Idelchik, I.E.: Handbook of hydraulic resistance, Third edition, Cambridge University Press, 1994.
- [13] Finnemore, E.J., Franzini, J.B.: Fluid mechanics with engineering applications, Tenth edition, McGraw-Hill, 2009.
- [14] Shao, Y., Yao, T., Gong, J., Liu, J., Zhang, T., Yu, T.: Impact of Main Pipe Flow Velocity on Leakage and Intrusion Flow: An Experimental Study, Water, 11(118), pp. 1–12, 2019.
- [15] Osterwalder, J. Wirth, C: Experimental investigation of discharge behaviour of crack-like fractures in pipes, Journal of Hydraulic Research, 23(3), pp. 255–272, 1985.
- [16] van Zyl, J.E., Clayton, C.R.I.: The effect of pressure on leakage in water distribution systems, Water Management, 160(2), pp. 109–114, 2007.
- [17] Ferrante, M., Massari, C., Brunone, B., Meniconi, S.: Experimental evidence of hysteresis in the head-discharge relationship for a leak in a polyethylene pipe, Journal of Hydraulic Engineering, 137(7), pp. 775–780, 2011.
- [18] De Marchis, M., Fontanazza, C.M., Freni, G., Notaro, V., Puleo, V.: Experimental evidence of leaks in elastic pipes, Water Resources Management, 30(6), pp. 2005–2019, 2016.
- [19] Ferrante, M., Meniconi, S., Brunone, B.: Local and global leak laws – The relationship between pressure and leakage for a single leak and for a district with leaks, Water Resources Management, 28(11), pp. 3761–3782, 2014.
- [20] Giustolisi, O., Savic, D.A., Kapelan, Z.: Pressure-driven demand and leakage simulation for water distribution networks, Journal of Hydraulic Engineering, 134(5), pp. 626–635, 2008.
- [21] Gupta, R., Nair, A.G.R., Ormsbee, L.: Leakage as pressuredriven demand in design of water distribution networks, Journal of Water Resources Planning and Management, 142(6), pp. 1–14, 2016.

-
- [22] Schwaller, J., van Zyl, J.E.: Modeling the pressure-leakage response of water distribution systems based on individual leak behavior, *Journal of Hydraulic Engineering*, 141(5), pp. 1–8, 2014.
- [23] Farley, M., Trow, S.: *Losses in Water Distribution Networks – A Practitioner’s Guide to Assessment, Monitoring and Control*, IWA Publishing, 2003.
- [24] Cassa, A.M., van Zyl, J., Laubscher, R.: A numerical investigation into the effect of pressure on holes and cracks in water supply pipes, *Urban Water Journal*, 7(2), pp. 109–120, 2010.
- [25] Meniconi, S., Brunone, B., Ferrante, M., Massari, C.: Transient hydrodynamics of in-line valves in viscoelastic pressurized pipes: Long-period analysis, *Experiments in Fluids*, pp. 266–275, 2012.

II Hydraulic Engineering and Environmental Impact

WIND WAVE INDUCED IMPULSIVE PRESSURE LOAD ON REINFORCED CONCRETE DECK STRUCTURE

TIN KULIĆ¹, HANNA MILIČEVIĆ¹, GORAN LONČAR¹, KATARINA LICHT¹

¹ University of Zagreb, Faculty of Civil Engineering; Croatia

e-mail: tin.kulic@grad.unizg.hr, hanna.milicevic@grad.unizg.hr, goran.loncar@grad.unizg.hr, katarina.licht@grad.unizg.hr

Abstract

An analysis of the impulsive pressure load on the underside of the deck of a complex caisson structure caused by wind waves was conducted. The measurements obtained with the physical model are compared with the numerical FLOW-3D model simulation results and the maximum pressure values obtained by applying empirical expressions based on linear wave theory. FLOW-3D model results fit the measurements better where such an approach allows the analysis of pressure dynamics at any structure point. This opens the possibility of targeted modification of the design solutions at the early design stages.

Keywords: wind waves, impulsive pressure load, horizontal deck, physical model, numerical model, empirical model.

1. Introduction

Wind waves are subject to significant deformation during their convection through a complex caisson-type coastal structure (Figure 1.c). This deformation is primarily related to the mechanisms of viscous dissipation and wave breaking. As the wave travels along the embankment armour below the deck structure, the wave contour reaches the underside of the deck and generates the impulsive pressure load. This impulsive pressure has a local loading effect of short duration and greatly exceeds the usual hydrostatic loads [1]. Due to this local effect, the stability of the whole deck may not necessarily need to be compromised, while in the design phase it is crucial to define the parts of the element exposed to such impulsive loads [2].

This topic was discussed on a theoretical mathematical basis in [3], [4], [5], where the obtained results agreed well with experimental measurements on two-dimensional physical models. The effect of a vertical force on a flat plate generated by monochromatic waves was studied using physical models developed by ElGharmy [6], Denson and Priest [7], Broughton and Horn [8], Shih and Anastasiou [9], and Tomazis et al [10], where the latter research presented the empirical formulas with the wave heights and the vertical distance between the still water and the underside of the plate as the two inputs. Kaplan [11] extended the previous theoretical models, while Isaacson et al [12] presented the dimensionless relationships between vertical forces, wave height, period, length and steepness, and plate geometry. Tirindelli et al [13] and Cuomo et al [14] developed a physical model and analysed the relationship between quasi-static and impulsive pressure loads on the front and middle parts of the plate, while air compression affecting the wave-induced impulsive pressures was studied by Martinelli et al [15]. The results of these studies have been adopted in engineering practice to define simple formulas for design load analysis [16], [17].

In this paper, we are concerned with comparing the results of physical model measurements with numerical model simulations and those derived from empirical models for estimating the impulsive pressure load in wind waves on horizontal plates. Both the physical and numerical models were developed considering the real geometry of a deck structure integrated as part of a caisson type dock. Here, the geometry of a container terminal that is an integral part of the port of Rijeka is analysed (Figure 1.b, Zagreb Deep Sea Container Terminal [18]). It is important to note that the terminal construction shown Figure 1.c has a more complex geometry and wave field at the underside of the deck than the plates and decks discussed in the previous studies. The measured pressure field obtained from the physical model provides a reference value for analysing the performance of the newly developed FLOW-3D numerical model as well as the existing empirical or combined numerical-empirical models for the same parameter.

2. Methods

2.1. Designed terminal construction and wind wave characteristics

The Zagreb Deep Sea Container Terminal was recently built in the port of Rijeka (Figure 1) and its shoreline is 700 [m] long with a maximum width of 180 [m] perpendicular to the shoreline. A reinforced concrete deck is placed upon

a caisson structure arranged in several rows and columns. Stone armouring is installed between the caisson walls to dissipate wave energy. One of the preparatory activities in the design of the container terminal was the analysis of a deep-sea wind wave climate in the study area. In this study, the wave parameters for the critical wind wave direction is presented (Figure 1.b). These wave characteristics are adopted as boundary conditions for both physical and numerical models.

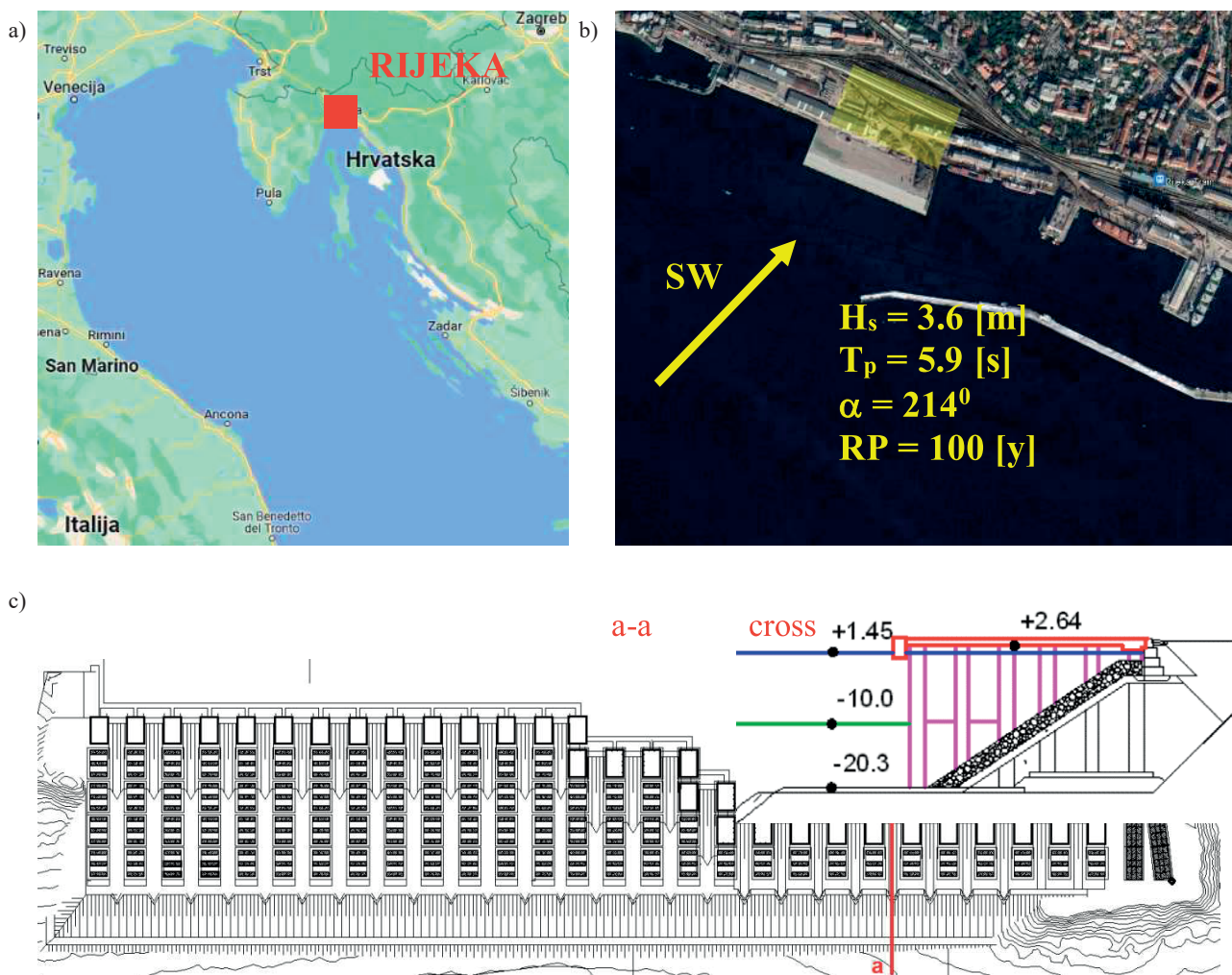


Figure 1. a) Location of Port of Rijeka on the Google Maps plan of middle and north Adriatic Sea, b) plan view of Port of Rijeka on Google Satellite with Zagreb Deep Sea Container Terminal (transparent yellow) and a critical wind wave direction (yellow arrow) with wave characteristics in deep-sea, c) design plan view and vertical cross sections of the analysed container terminal

2.1. Physical model

A physical model was built at a scale of 1:35 and placed in the flume with a piston-like wave generator that moves a 6 [m] wide plate used to form a JONSWAP wave spectrum ($\gamma = 3.3$, $\sigma_1 = 0.07$, $\sigma_2 = 0.09$). This model includes three long construction sections consisting of five caisson rows and four shorter sections with two caisson rows (Figure 2).

A total of six capacitance probes are installed in the wave flume (G01 and G02 in front of the wave-generating plate, G1-G4 parallel to the outer contour of the caisson structure placed at every 0.1 [m], Figure 2). Probes G2 and G4 are installed in front of the caisson walls, while G1 and G3 are installed in front of the spans between the caisson walls. The separation of the incident and reflected wave fields is evident from the measurement at probes G01 and G02 using the Goda method [19]. The sampling frequency is 40 [Hz] and is the same for all installed probes. The sampling time for each experiment is 10 minutes, which corresponds to one hour in real scale. Within this time span, approximately 600 wave periods are covered to adequately model the stochastic nature of a spectral process. The pressure load on the underside of a deck structure is recorded using five Honeywell 26PCBFA6D pressure gauges installed at positions P24-P29 (Figure 2). The sampling frequency of the pressure gauges is 1 [kHz] at high water level (+1.45 [m a.s.l.]).

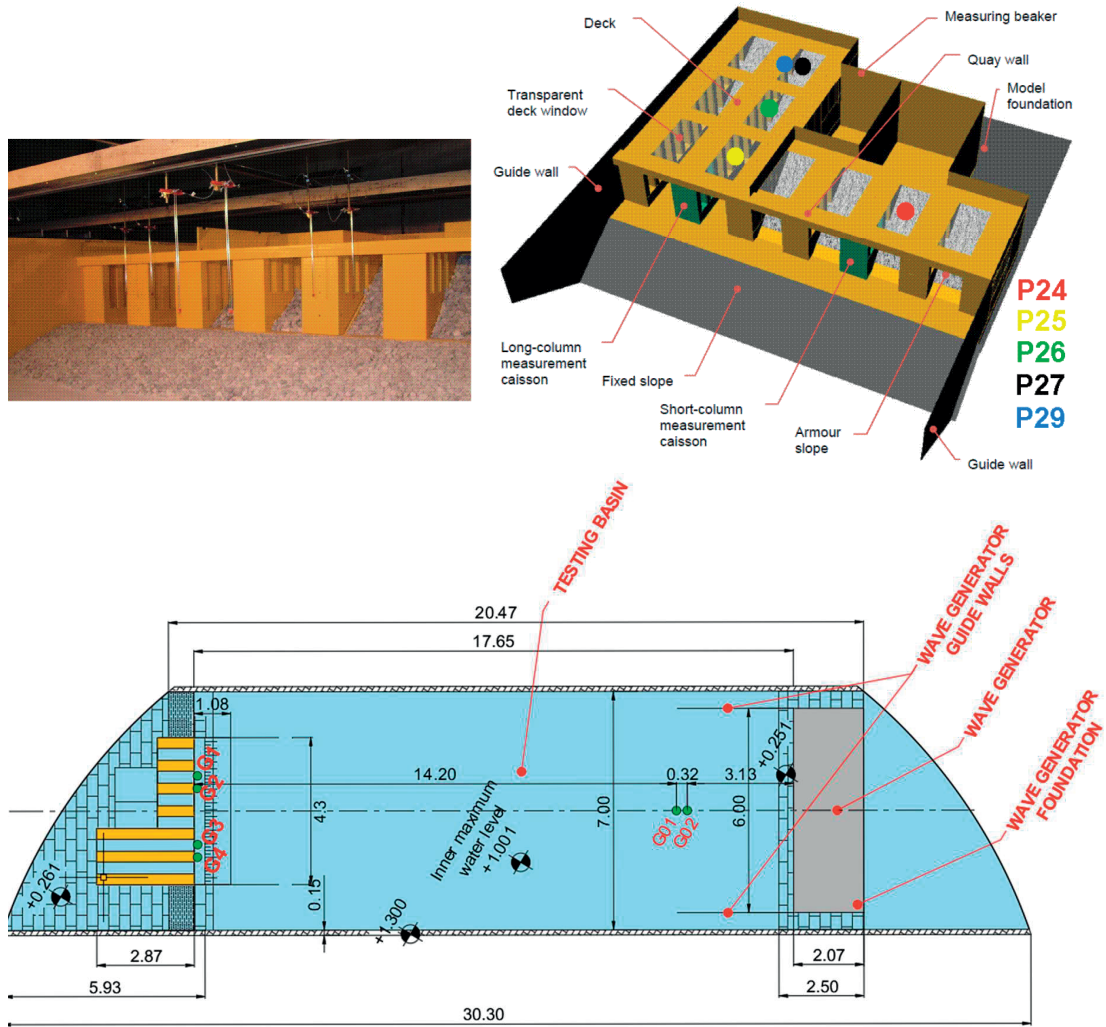


Figure 2. Physical model front view photo (upper left), 3D schematic (upper right) and a plan view (bottom)

2.2. Empirical models

Within the Kaplan model [11], the relationship between the wave height and vertical distance between the still water level and the underside of a deck is considered to be as the most significant factor for the occurrence of the impulsive pressure p_{Kap} , which is calculated according to the formula:

$$p_{kap} = \rho \frac{\pi}{8} \frac{l}{[1 + (l/b)^2]^{1/2}} a_w + \rho \frac{\pi}{4} c \frac{1 + \frac{1}{2}(l/b)^2}{[1 + (l/b)^2]^{3/2}} w + \frac{\rho}{2} C_d w |w| + \rho g a \quad (1)$$

where ρ is the density of the sea (a constant of 1028 [kg/m³]), b is the width of the deck structure perpendicular to the direction of the incident wave (a constant of 12.3 [m]), l is the width of the deck in line with the direction of the incident wave (a constant of 12.3 [m]), c is the propagation velocity of the wave, a_w represents the vertical acceleration of a fluid particle in the surface streamline, w is the vertical velocity of a fluid particle in the surface streamline, C_d is the drag coefficient (a constant equal to 2 according to [11]).

According to the design guidelines presented in [16], [17], it is recommended to use the following expression to calculate the average pressure p_{dnv} on the underside of a deck subjected to wave loading:

$$p_{dnv} = C_{d nv} \rho \frac{w^2}{2} \quad (2)$$

where $C_{d nv}$ is a dimensionless coefficient which that equals to 10 according to [17]. These empirical models also require that the vertical velocity w at the time of contact between the wave profile and underside of the deck structure be known (in this study $w = 1.44$ [m·s⁻¹]). The $p_{d nv}$ represents an average pressure value below the wetted deck surface. A more detailed calculation of this parameter can be found in [17]. The product of the $p_{d nv}$ pressure and the area of the wetted deck $A_{d nv}$ gives the total vertical force on deck underside required for the stability calculation. The ratio between the impulsive pressures p_{mng} and the mean pressures $p_{d nv}$ is calculated according to Meng [20] and is equal

to $p_{mng} / p_{dnt} = 2$. It is important to mention that according to [20] maximum pressures are expected at the beginning of the deck structure.

2.3. Numerical model for wave deformations

FLOW-3D is a general-purpose model developed by Flow Science Inc [21]. FLOW-3D uses an orthogonal structured grid system and allows multiblock grids with nested grids. The fractional area/volume method FAVOR is used for modelling complex geometric regions. Several researchers have used the application of FLOW-3D in their research on the behaviour of waves over a coastal structure, including [22], [23]. The method used to solve the equations is the limited volume method. By formulating the equations governing fluid motion, turbulent models for flow are considered when modelled in porous media. The general mass continuity equation in the three directions x , y and z is given in the following equation:

$$V_f \frac{\partial \rho}{\partial t} + \frac{\partial}{\partial x}(\rho u A_x) + \frac{\partial}{\partial y}(\rho v A_y) + \frac{\partial}{\partial z}(\rho w A_z) + \xi \frac{\rho u A_x}{x} = R_{DIF} + R_{SOR} \quad (3)$$

where V_f is the fractional volume open to flow, ρ is the fluid density, R_{DIF} is the turbulent diffusion term and R_{SOR} is the mass source. A_x is the fractional area open to flow in the x -direction, A_y and A_z are similar area fractions for flow in the y and z directions, respectively. The equations of motion for the fluid velocity components (u , v , w) in the three coordinate directions are represented with the Navier–Stokes equations with some additional terms given below:

$$\frac{\partial u}{\partial t} + \frac{1}{V_f} \left(u A_x \frac{\partial u}{\partial x} + v A_y \frac{\partial v}{\partial y} + w A_z \frac{\partial w}{\partial z} \right) = -\frac{1}{\rho} \frac{\partial p}{\partial x} + f_x - b_x \quad (4)$$

$$\frac{\partial v}{\partial t} + \frac{1}{V_f} \left(u A_x \frac{\partial u}{\partial x} + v A_y \frac{\partial v}{\partial y} + w A_z \frac{\partial w}{\partial z} \right) = -\frac{1}{\rho} \frac{\partial p}{\partial y} + f_y - b_y \quad (5)$$

$$\frac{\partial w}{\partial t} + \frac{1}{V_f} \left(u A_x \frac{\partial u}{\partial x} + v A_y \frac{\partial v}{\partial y} + w A_z \frac{\partial w}{\partial z} \right) = -\frac{1}{\rho} \frac{\partial p}{\partial z} + G_z + f_z - b_z \quad (6)$$

where, (G_x , G_y , G_z) are body accelerations, (f_x , f_y , f_z) are viscous accelerations, (b_x , b_y , b_z) represent flow losses in porous media or through porous baffles. Gravity acts in the G_z direction. Moreover, f represents the turbulent effect, and the value of b is equal to that in Eq(10), where F_d represents the drag coefficient of the porous media and U is the macroscopic flow velocity (u , v , w).

$$b = F_d U \quad (7)$$

Because of the large porosity of breakwaters and generally in the coarse-grained environments, the flow is turbulent, so the original Darcy law cannot be applied. As the Reynolds number increases and the pressure decreases, Darcy's law leaves from the linear condition state. Therefore, Forchheimer equation is used and F_d is calculated based on it:

$$F_d = \frac{\mu}{\rho} \frac{1 - V_f}{V_f} \left(A \frac{1 - V_f}{V_f} + B \frac{Re_p}{D} \right) \quad (8)$$

where Re_p is the pore Reynolds number and D is the particle diameter.

The coefficients A and B are calculated from the following equations described in [25]:

$$A = \frac{\alpha}{D_{n50}^2}, B = \frac{\beta}{D_{n50}} \quad (9)$$

$$\alpha = 1684 + 3.12 \cdot 10^{-3} \left(\frac{g}{v^2} \right)^{\frac{2}{3}} D_{n50}^2, \beta = 1.72 + 1.57 e^{-5.1 \cdot 10^{-3} \left(\frac{g}{v^2} \right)^{\frac{1}{3}} D_{n50}} \quad (10)$$

In these relations, D_{n50} is the diameter of the armour rock and v is the kinematic viscosity. The armour layer is considered to be rigid. Using the rock diameter for the armour $D_{50} = 0.5$ m (according to the project documentation) and calculating the values $\alpha = 3.1E+5$ and $\beta = 1.72$, we obtain $A = 1.2E+6$ and $B = 3.4$. The porosity coefficient of the armour layer is taken to be 0.3. In this study, the RNG model is used to solve turbulence closure problem.

The modelling is done by a mesh block and the mesh size of 0.2 [m] is assumed. The total number of cells is 2.16E+5. The total length of the model channel (mesh block) is 320 [m]. The 2D model domain includes a vertical profile between two rows of caisson walls (Figure 3, Figure 1.c). The bed of the model is defined with a constant level of -20.3 [m], while the slope stabilization (porous media) is defined with a slope of 2:3. The still water level is defined as +1.4 [m].

The boundary conditions for the net block include irregular waves at the block entrance, the boundary condition of symmetry above the block and at the lateral sides, while at the bottom and at the end of the block the boundary condition is selected as a wall. The boundary of the irregular wave input is user-defined (JONSWAP wave energy spectrum) with prescribed series of angular frequencies of the waves (in rad/time) and the corresponding energy values (Figure 4). Active absorption is used to avoid reflections at the boundary of wave generation. The model has a simulation time of 600 [s].

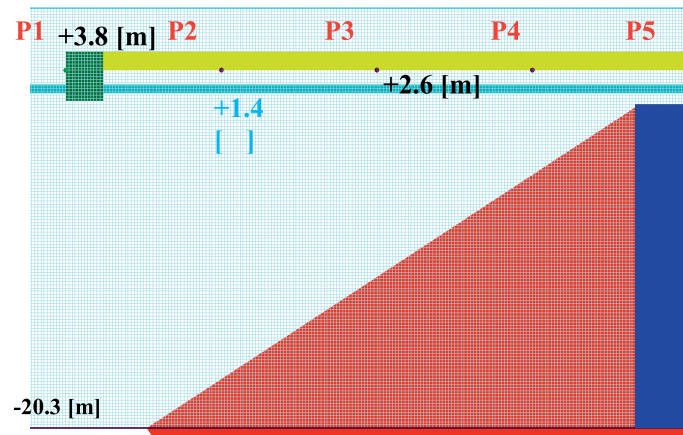


Figure 3. Numerical model mesh (vertical profile between the two rows of caisson walls) at the edge of the modelled construction

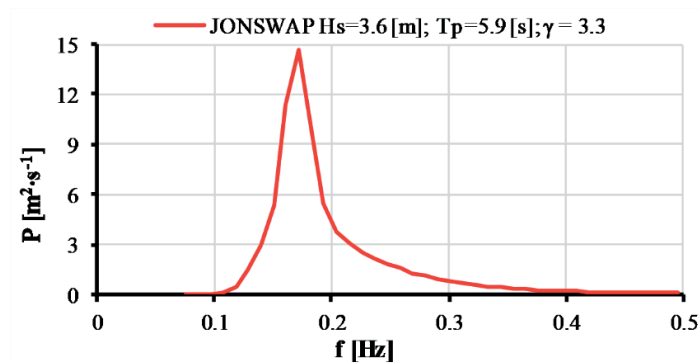


Figure 4. Used JONSWAP spectrum ($H_S = 3.6$ [m], $T_P = 5.9$ [s], $\gamma = 3.3$; $f_{min} = 0.08$, $f_{max} = 0.5$, $\sigma_1 = 0.07$, $\sigma_2 = 0.09$)

4. Results and discussion

This chapter provides an overview and comparison of results obtained from physical model measurements, empirical expressions used to calculate maximum pressure and numerical model simulations.

The physical model results are presented using the extracted reflection coefficients obtained from the measurements at probes G1-G4 (Table 2) and a sequence of measured pressure time series at gauge P24 during the wave from the SW direction in Figure 5. It can be seen that the maximum recorded pressure is 26.7 [kPa].

Table 1. Reflection coefficient obtained from measurements on G1-G4 probes (see Figure 2)

KR AT POSITION [-]			
G1	G2	G3	G4
0.23	0.30	0.26	0.29

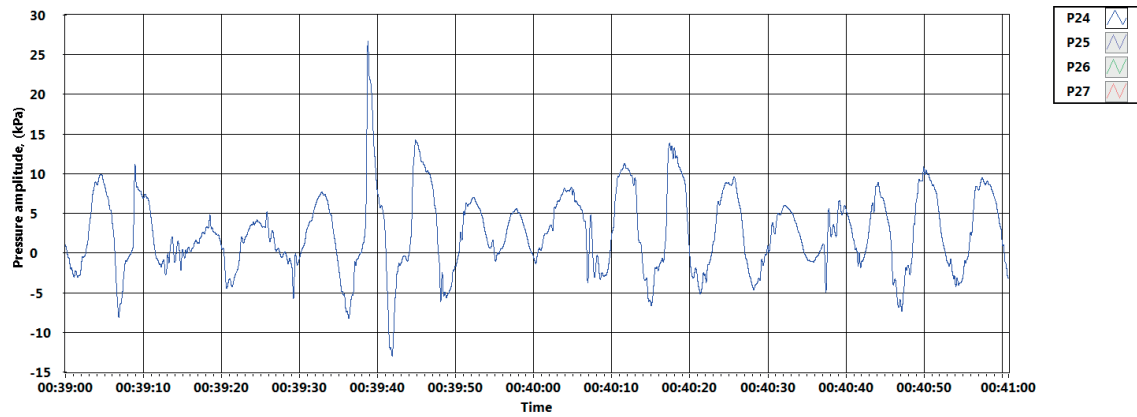


Figure 5. Pressure time series measured on P24 manometer

Within Kaplan's empirical model [11], the kinematic parameters c , w , and a_w were estimated based on linear wave theory with a wave amplitude η_S equal to $H_S/2 = 1.8$ [m] and a wave period of $T = T_P = 5.9$ [s] (see Figure 1). The vertical velocity w and acceleration a_w are calculated for the moment when the wave profile reaches the underside of a deck (+2.64 [m a.s.l.]) at a still water level of 1.45 [m a.s.l.]). The following values are considered for a wave profile:

- $\eta = 2.64 - 1.45 = 1.19$ [m],
- $c = 9.2$ [m·s⁻¹],
- $w = 1.44$ [m·s⁻¹],
- $a_w = -1.34$ [m·s⁻²].

The application of this empirical model neglects many processes that occur in a realistic physical environment of a real harbour basin (such as overtopping, the reflection off the walls and embankment armour between the elements of the caisson structure). When the above values for c , w and a_w are substituted into Eq(2), an impulsive pressure of $p_{Kap} = 22.1$ [kPa] is obtained. The second empirical model recommended by [16] and [17] yields a lower maximum pressure, referred to as the impulsive pressure p_{mng} . As explained in Section 0, the impulsive pressure p_{mng} is 21.3 [kPa] when $w = 1.44$ [m·s⁻¹] and $C_{dvw} = 10$ are substituted into Eq(5) and the ratio $p_{mng} / p_{dvw} = 2$ is considered.

The pressure change within the vicinity of the numerical model was extracted at five locations at the underside of the deck (P1–P5, +2.6 [m], Figure 3) and is shown in Figure 6. Location P3 corresponds to pressure change P24, which is installed as part of the physical model. The dynamics of the surface elevation is extracted at the coordinate $x = 50$ [m] of the modelled flume (Figure 6).

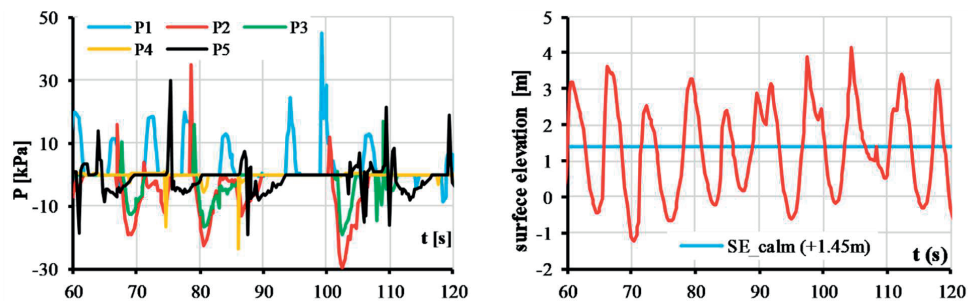


Figure 6. Pressure time series at the P1-P5 and surface elevation dynamics at the coordinate $x = 50$ [m] of the modelled flume

The same parameter is shown at $x = 250$ – 320 [m] in Figure 7. This detail shows the occurrence of wave breakage upstream of the modelled construction of the terminal, overtopping of the upper deck surface, and wave propagation in a zone below the deck. Figure 4 gives a general overview of the flow velocity field in a whole model domain at the beginning of the simulation at $t = 91$ [s].

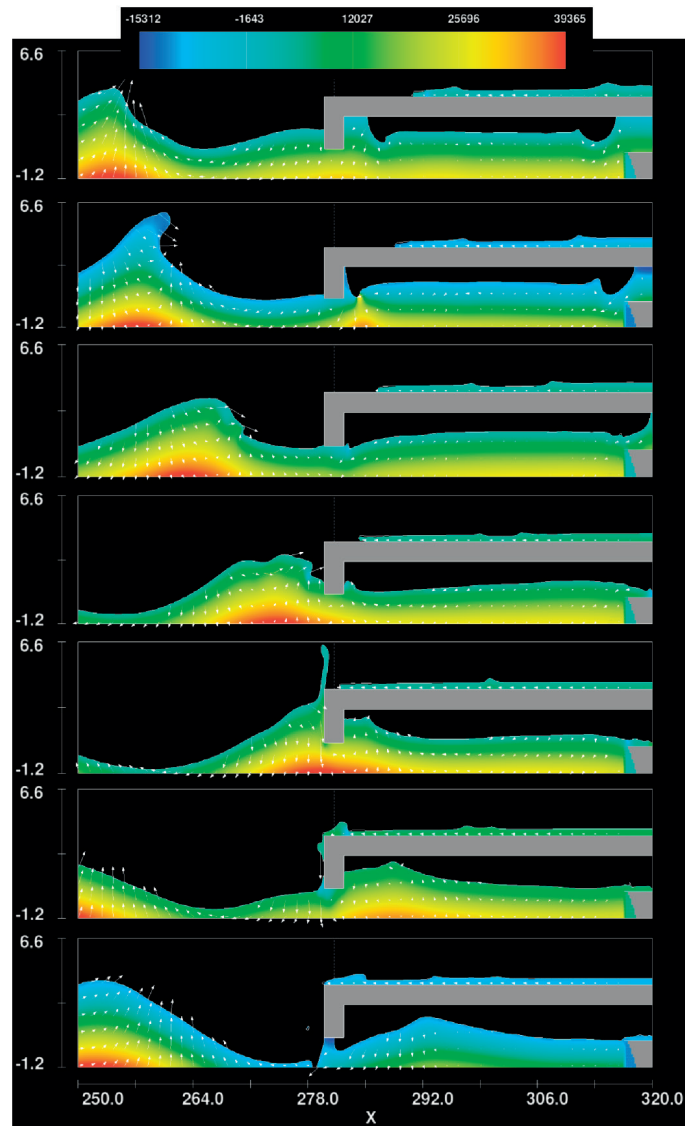


Figure 7. Pressure field expressed in [Pa] during simulation time $t = 91\text{--}97$ [s] with time step of 1 [s]

A general pattern of pressure reduction from the deck face ($x = 280$ [m]) to its contact with a wall ($x = 320$ [m]) is evident. The maximum modelled pressure at P1 is 44.1 [kPa], at P2 34.6 [kPa], at P3 26.7 [kPa], at P4 9.4 [kPa]. P5 shows the increase of the maximum pressure (29.6 [kPa]), which is due to the fact that the progression of the wave profile is prevented by a vertical wall at the end of the embankment (known as sloshing).

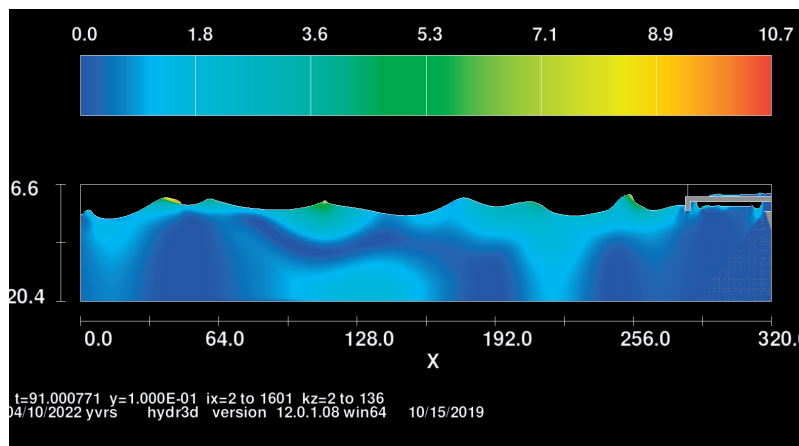


Figure 8. Flow velocity field expressed in $[m \cdot s^{-1}]$ at $t = 91$ [s]

5. Conclusion

This work addressed the problem of the effect of pulsating pressure loads generated by wind-gravity waves on the underside of a deck structure constructed as part of a container terminal. Reference values for the pressure at the underside of the deck were obtained by taking measurements on a physical model. These values were compared with the results of the two empirical models, where the kinematic parameters of a wave profile were calculated according to a linear wave theory. In addition, the measurements were compared with the results of the numerical model simulations FLOW-3D. As a result, the following conclusions can be drawn:

- The use of linear wave theory to estimate the kinematic coefficients of a wave profile allows the calculation of a single maximum momentum pressure without providing information about the spatial distribution of pressures on the underside of the deck.
- Empirical models underestimate the measured values of maximum impulsive pressure by 17% according to the empirical model of Kaplan [11] and 20% according to the recommendations of USACE [16] and Det Norske Veritas [17].
- The simulations with the numerical model FLOW-3D resulted in equivalent maximum impact pressures as the reference values from the measurements of the physical model.
- The position P1 in the numerical model shows the highest pulsating pressures (see Figure 3, Figure 7), whose values decrease with increasing position of the plate (x-coordinate in the model domain). Such mechanism is mainly influenced by the dissipation of wave energy during contact with the embankment armour. At position P5, this pressure increases due to the sloshing effect.

By developing a numerical model in software such as FLOW-3D, spatio-temporal tracking of changes in all calculated hydraulic parameters is made possible, providing insight into the wave breaking process, overtopping of a deck, and wave propagation beneath the deck. Such continuous tracking of wind wave dynamics and their interaction with rigid structures brings a great advantage, as critical areas or locations of extreme pressure loading can be easily identified during the design phase. This reduces the possibility of incorrect placement of certain structures in wave-affected environments during the construction phase and has a highly beneficial financial effect.

Acknowledgements

This research has been supported by the Croatian Science Foundation (DOK-2020-01 and PZS-2019-02-3081).

References:

- [1] Lai, C.P., Lee, J.J.: Finite Amplitude Wave Uplift on Platforms or Docks, *Journal of Waterways, Ports, Coastal & Ocean Engineering*, ASCE, 115 (1989) 1, pp. 19–39.
- [2] Bhat, S.S.: *Wave slamming on the horizontal plate*, A thesis in partial fulfilment of the requirements for the degree of master of applied science, The University of British Columbia, 1994.
- [3] Wagner, H.: *Landing of Seaplanes*, National Advisory Committee for Aeronautics, Technical Note No. 622, 1932.
- [4] Chuang, S.L.: Experiments on slamming of wedge-shaped bodies with variable dead rise angle, *J. Ship Research*, 11(4), pp. 190–198, 1967.
- [5] Verhagen, J.H.G.: The impact of flat plate on a water surface, *J. Ship Research*, 11(4), pp. 211–223., 1967.
- [6] El Gharmy, O.A.: *Wave force on a dock*, Report no. HEL-9-1, Inst. Of Engg. Research, Hydraulic Engg. Lab., University of California, Berkley, California. 1963.
- [7] Denson, K.H., Priest, M.S.: Wave pressure on the underside of a horizontal platform, *Proc. Offshore Technology Conference*, Houston, USA, pp. 555–570, 1971.
- [8] Broughton, P., Horn, E.: Ekofish Platform 2/4C: Re-analysis Due to Subsidence, *Proc. Inst. Civ. Engrs.*, 82, pp. 949–979, 1987.
- [9] Shih, R.W.K., Anastasiou, K.: A Laboratory Study of the Wave-induced Vertical Loading on Platform Decks, *Proc. ICE, Water Maritime and Energy*, 96(1), pp. 19–33, 1992.
- [10] Toumazis, A.D., Shih, W.K., Anastasiou, K.: Wave Impact Loading on Horizontal and Vertical Plates, *Proc. IAHR 89 Conf.*, Ottawa, Canada, pp. 209–216, 1989.
- [11] Kaplan, P., Murray J.J., Yu W.C.: Theoretical Analysis of Wave Impact Forces on Platform Deck Structures, *Volume 1-A Offshore Technology, OMAE – Offshore Mechanics and Arctic Engineering Conference*, Copenhagen, pp. 189–198, 1995.
- [12] Isaacson, M., Allyn, N., Ackerman, C.: Design wave loads for a Jetty at Plymouth, Montserrat, *International Symposium: Waves-physical and numerical modelling*, University of British Columbia, Vancouver, Canada, pp. 1153–1162, 1994.

- [13] Tirindelli, M., Cuomo, G., Allsop, N.W.H., Lamberti, A.: Wave-in-Deck Forces on Jetties and Related Structures, *Proceedings of The Thirteenth International Offshore and Polar Engineering Conference*, Honolulu, USA, pp. 562–569, 2003.
- [14] Cuomo, G., Tirindelli, M., Allsop, N.W.H.: Wave-in-deck loads on exposed jetties, *Coastal Engineering*, 54 (9), pp. 657–679, 2007.
- [15] Martinelli, L., Lamberti, A., Gaeta, M.G., Tirindelli, M., Alderson, J., Schimmels, S.: Wave Loads on exposed Jetties - Description of large scale Experiments and preliminary Results, *Proceedings of 32nd Conference on Coastal Engineering*, Shanghai, China, pp. 1–12, 2010.
- [16] USACE: *Coastal Engineering Manual, Part 6, Chapter 5, Fundamentals of Design*. 2006.
- [17] Det Norske Veritas: *Recommended Practice - Environmental Conditions and Environmental Loads*, DNV-RP-C205, 2010.
- [18] Brodarski institute: *Zagreb Container Terminal Pier Structure – Hydraulic investigations on physical model and numerical analysis of the wave field in front of the structure – Final report*, Technical report no. 6359-H, Zagreb, 2013.
- [19] Goda, Y., Suzuki, Y.: Estimation of incident and reflected waves in random wave experiments, *Proceedings of 15th International Conference on Coastal Engineering*, Hawaii, pp. 828–845, 1976.
- [20] Meng, Y., Chen, G., Yan, S.: Wave interaction with deck of jetty on a slope, *Proceedings of 32rd Conference on Coastal Engineering*, Shanghai, China, pp. 1–12, 2010.
- [21] Hirt, C.W. and Nicholas, B.: *Flow-3D User's Manual*, Flow Science Inc., 1998.
- [22] Dentale, F., Donnarumma, G., Carratelli, EP., Giovanni, V.: A new numerical approach to the study of the interaction between wave motion and rubble mound breakwaters. In *Proceedings of the 7th International Conference on Engineering Mechanics, Structures, Engineering Geology (EMESG'14)*, Salerno, Italy: WSEAS Press, pp. 45–52, 2014.
- [23] Vanneste, D., Altomare, C., Suzuki, T., Troch, P., Verwaest, T.: Comparison of numerical models for wave overtopping and impact on a sea wall. *34th International Conference on Coastal Engineering, Proceedings*, pp. 1–14, 2014.
- [24] Marashian, S.M., Adjami, M., Mazyak, A.R.: Numerical modelling investigation of wave interaction on composite berm breakwater. *China Ocean Eng.*, 35 (5), pp. 631–645, 2021.

III Sanitary Engineering and Sustainable Water Use

COMPARISON OF EFFICIENCY TWO POLYALUMINIUMCHLORIDE COAGULANTS AT SURFACE WATER TREATMENT

DANKA BARLOKOVÁ¹, JÁN ILAVSKÝ¹

¹ Slovak University of Technology in Bratislava, Faculty of Civil Engineering, Department of Sanitary and Environmental Engineering; Slovakia

e-mail: danka.barlokova@stuba.sk, jan.ilavsky@stuba.sk

Abstract

The efficiency of polyaluminium chloride PAX18 and PAX-XL19 coagulant agents during pilot-scale experiments in a drinking water treatment plant Rozgrund was studied. These coagulants have not been used in the Rozgrund water treatment plant till now. The original surface water treatment technology was designed for aluminium sulfate. Within coagulation tests the turbidity, colour, chemical oxygen demand (COD_{Mn}), the residual aluminium concentration and other parameters were monitored for the determination of optimal operative conditions. These values were used for the evaluation of effectiveness for each coagulant too. The determined optimal dose of coagulant indicates that the coagulant PAX-XL19 was a more efficient than PAX18 resulted to the production of treated water with lower COD_{Mn} and residual aluminium content, but optimal coagulant dose of PAX-XL19 (1,69 mg Al/L) is higher than PAX18 (0,94 mg Al/L). When we used PAX18 in Jar test, treated water had lower turbidity, higher value of pH and alkalinity. For use PAX18 says the economic aspect.

Keywords: water reservoir Rozgrund, drinking water treatment, coagulation, PAX-XL19, PAX18, residual aluminium concentration, turbidity, laboratory coagulation tests.

1. Introduction

The ground waters represent in Slovakia the dominant source for supplying the population with the drinking water. Only a 16% of the total amount of the water supplied into the public water mains present the waters retrieved from the surface sources. Based on the quality of water that is taken it is necessary in many cases to treat the water that way it meets the requirements for the drinking water that are laid by the Decree of the Ministry of Health of the Slovak Republic No. 247/2017. When it comes to the ground waters, only 22% requires to be treated – which from the total amount represents approximately 7700 L/s of these waters used for drinking purposes. The surface water sources represent 1400 L/s.

In the present day is in Slovakia operation 113 water treatment plant (WTP) and they are used for providing the treatment to the surface and also the ground water to provide the drinking water. There operates 65 WTPs for the treatment of surface waters and 48 WTPs for the treatment of ground waters. Eight water-supply reservoirs (Rozgrund, Turček, Hriňová, Klenovec, Málinec, Nová Bystrica, Bukovec and Stariná) supply the population in Slovakia (Figure 1).

Water quality in water reservoirs is constantly monitored as it has the crucial impact on the treatment technology as well as on final quality of water after the treatment. Water quality is mainly affected by turbidity, colour, pH, dissolved oxygen, water temperature, chemical oxygen demand (COD), nutrients (phosphorus and nitrogen), in the last period biological revival (blue-green algae and cyanobacteria). Conventional water treatment (coagulation, flocculation, sedimentation, filtration and disinfection) is most often used for surface water treatment. To increase the efficiency of water treatment, additional stages are gradually added, e.g. membrane processes (microfiltration, ultrafiltration and nanofiltration), filtration with activated carbon (granular or powdered), UV radiation, ozone, filtration by microsieves and recarbonization process to improve the quality of drinking water [1.2].

The Rozgrund water treatment plant (WTP) was put into operation in 1997 for supplying part of Banská Štiavnica with water. The eponymous water reservoir Rozgrund. The WTP Rozgrund serves for treatment and repumping of the treated water into the Červená studňa water tank (the water tank volume is 650 m³). The designed output of the water treatment plant is 14 L/s.

The water treatment technology was designed as single-stage and it consists of pumping water from the Rozgrund water reservoir, dosing an aluminium coagulant into the raw water pipeline but also into the treated water, slow mixing by means of 4 perforated walls, dosing calcium hydrate into the raw water pipeline but also into the treated water,

3 open sand filters, sanitary protection of the treated water by chlorine with the possibility for pre-chlorination, repumping of the treated water into the Červená studňa water tank and accumulation of the used wash water.

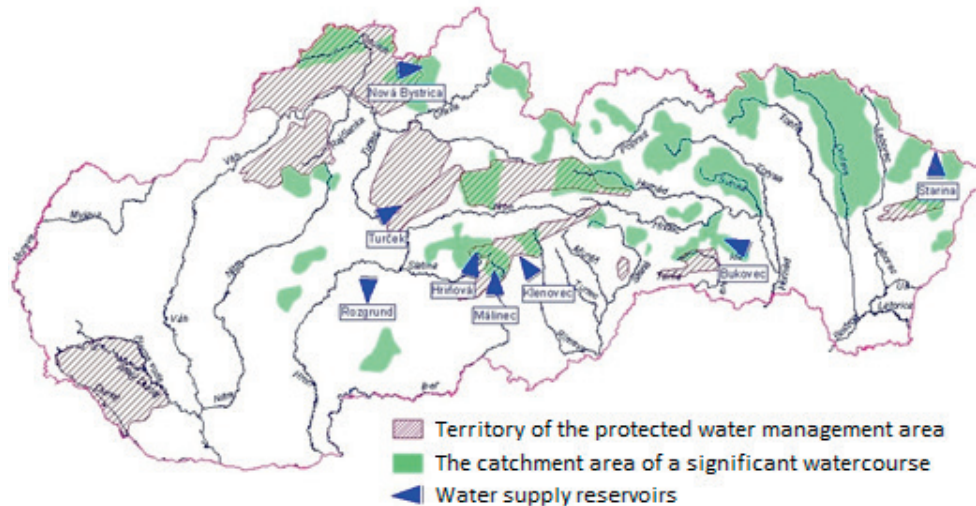


Figure 1. Map of Slovakia with marking of the protected water management area, the river basins of significant watercourses and water supply reservoirs

In 2015, the water treatment plant was taken out of operation due to the stench of the drinking water in the distribution system. Until the water treatment plant was taken out of operation, the technological line functioned only on the direct filtration principle and sanitation of the water by dosing with chlorine gas. In the critical situation regarding the stench, the operator sought to treat the water by dosing the PAX-18 coagulant and powdered active carbon into the water. Subsequently, part of Banská Štiavnica was connected to the Hron group water mains, entailing multiple repumping of the water.

Currently, an effort is being made to utilise the surface water from the Rozgrund water reservoir again for supplying Banská Štiavnica, Banka and Vyhne. The proposed modernization of the water treatment plant is required to perform pilot experiments, to test various technologies, filtration materials, coagulants etc. and to adapt the technology to the water source quality.

From the long-term perspective, the water quality does not change very much, the water is of relatively high quality; without the impact of human activity, the pH of the water between 2012 and 2019 ranged from 6.97 to 8.23, the water temperature from 2.8 to 24.1°C. The water colour on the long-term average did not exceed 20 mg/L Pt. The year 2013 was an exception, as in March and April, 69 and 26 mg/L Pt, respectively, were measured. The water turbidity ranges from 1.0 to 3.0 NTU; in 2013, the turbidity measured in March and April was 5.8 to 3.3 NTU. COD_{Mn} on the long-term average achieves 1.4 to 2.9 mg/L, but in one case the value achieved 3.56 mg/L. With regard to the ageing of the reservoir and the eutrophication process, an increase of live organisms was determined from 150 up to 400 organisms/mL

On the present surface water treatment is possible without the addition of chemical compounds only in sporadic cases. The advantage of coagulation is that addition of coagulants effects not only to colloidal and fine dispersion substances but to all others suspended solids which form flakes with high ability to settle. Iron, respectively aluminum salts [3–7] are the most widely used coagulants. Required dose of coagulant varies with the quality of raw water. The optimum dose of coagulant is possible to determine in the laboratory with coagulation test.

Aim of presented work is to make a comparison efficiency of two coagulant PAX-18 and PAX-XL19 at surface water treatment from water reservoir Rozgrund and to determine optimal dose of coagulants for a given water quality.

2. Methods

2.1. Surface water quality

The experimental part of this work compared two coagulants, polyaluminiumchlorid PAX-18 a PAX-XL19 (Kemwater) to find the optimal dose for reduction of humic substances (COD_{Mn}) and turbidity in surface water from water reservoir Rozgrund. The concentration of aluminium in the treated water was monitored too.

Tab. 1 shows the physical-chemical analysis of water on entry to the water treatment plant during the pilot tests.

Table 1. Water quality on entry to the Rozgrund water reservoir during the experiments

PARAMETER	UNIT	RAW WATER SAMPLE	PARAMETER	UNIT	RAW WATER SAMPLE
pH		7.69	chlorides	mg/L	8.01
Conductivity (EC)	mS/m	15.3	nitrates	mg/L	3.12
COD _{Mn}	mg/L	2.4	sulphates	mg/L	34.61
TOC	mg/L	0.96	fluorides	mg/L	0.27
turbidity	NTU	2.94	phosphates	mg/L	0.06
colour	mg/L	11	Fe	mg/L	0.03
ANC _{4,5}	mmol/L	0.922	Mn	mg/L	0.001
BNC _{8,3}	mmol/L	0.047	ammonia	mg/L	0.02
TDS	mg/L	120	sodium	mg/L	10.55
Undissolved solids	mg/L	1.5	calcium	mg/L	27.72
Ca+Mg (TH)	mmol/L	0.922	magnesium	mg/L	5.6

2.2. Coagulation test

The coagulation test is a common laboratory procedure used to determine the optimum operating conditions for water treatment procedure. A jar test simulates the coagulation and flocculation processes. Coagulation is the process by which colloidal particles and very fine solid suspensions initially present in water are combined into larger agglomerates that can be separated via sedimentation, flocculation, filtration, centrifugation or other separation methods. Coagulation is commonly achieved by adding different types of chemicals (coagulants) to the raw water to promote destabilization of the colloid dispersion and consequently to agglomerate the resulting individual colloidal particles [8–13].

For the coagulation test was used device with six mixers with adjustable speed and high-speed mixing. Into six flasks were added per liter of raw water. After adding a coagulant (1% solution) followed by 3 minutes rapid mixing (180 rpm) and 20 minutes slow mixing (40 rpm). After mixing followed sedimentation of sample, which took 1 hour. Thus prepared sample (without filtration through filter paper) was analysed. The following parameters were monitored: pH, ANC_{4,5}, concentration of Al, turbidity, color, and COD_{Mn} (humic substances).

PAX-18 is a concentrated solution of polyaluminum chloride. It is used as a clarifying agent in the treatment of drinking water, wastewater and industrial water. It is especially suitable for the treatment of low-mineralized waters containing humic substances. The actual coagulation takes place faster than conventional coagulants, when even at low temperatures large, well-separable flakes are formed. Due to the basicity of the product, the alkalinity of the water is minimally affected.

PAX-XL19 is an aqueous solution of polyaluminum chloride. It is used as a coagulant in the treatment of drinking water, industrial water and also wastewater. It is a special product with a significantly high value of basicity (it has minimal effect on lowering the pH values after dosing). It has an extremely high content of the active ingredient aluminium. The actual coagulation is faster compared to conventional coagulants, even at low temperatures large, well-separable flakes are formed. Due to the basicity of the product, the alkalinity of the water is minimally affected. The high content of the active ingredient ensures the cleaning effect even in heavily polluted wastewater.

Table 2. Chemical composition and basic characteristic of coagulants [14]

PARAMETER	PAX-18	PAX-XL19
Appearance	yellowish clear solution	light yellow, colorless, light grey solution
Al ₂ O ₃	17.0% ± 0.5	23.6% ± 0.6
Al	9.0% ± 0.3	12.5% ± 0.3
Fe	< 0.1 %	–
Cl ⁻	21. % ± 2.0	9.0% ± 2.0
SO ₄ ²⁻	< 0.1%	–
Density (25 °C)	1.36 ± 0.02 g/cm ³	1.35 ± 0.04 g/cm ³ (at 20°C)

Basicity (alkaline)	4% ± 5	85% ± 5
pH	1.0 ± 0.5	1.5–4.0
Freezing point	approx. 18°C	approx. 20°C

2.3. Water analysis

The water samples were analysed in triplicate for various water quality parameters such as pH, total dissolved solids (TDS), electrical conductivity (EC), turbidity, colour, Total hardness (TH), Calcium (Ca^{2+}), Magnesium (Mg^{2+}), Sodium (Na^+), Potassium (K^+), Ammonia (NH_4^+), total iron (Fe), Manganese (Mn), Aluminium (Al), Chloride (Cl^-), Sulfate (SO_4^{2-}), Alkalinity (acid neutral capacity at pH 4,5), Acidity (basic neutral capacity at pH 8,3), Nitrate (NO_3^-), Nitrite (NO_2^-), Fluorides (F^-), Phosphates (PO_4^{3-}), Dissolved oxygen (DO), Chemical oxygen demand (COD_{Mn}) and Total organic carbon (TOC) using standard classical and instrumental methods of analysis.

For analyses of base parameters of water was used spectrophotometer Hach DR3900, for analyses of cations and anions presented in water ITP analyser (isotachophoresis), for analyses of organic compounds TOC Analyzer Aurora Model 1030W, laboratory instruments Hach Lange for measuring of pH, conductivity, oxygen or HQ40D Hach Lange multi-versatile pH, oxygen, conductivity and ORP meter, determination of chemical oxygen demand in drinking water or clean surface water (COD_{Mn}) by STN EN ISO 8467:1995 with using potassium permanganate oxidation (KMnO_4) and titration with oxalic acid ($\text{Na}_2\text{C}_2\text{O}_4$). The method can be used for the determination of COD (Mn) up to 10 mg/L without dilution and COD (Mn) up to 100 mg/L with dilution. Limit for COD_{Mn} in drinking water is 3,0 mg/L (by the Decree of the Ministry of Health of the Slovak Republic No. 247/2017).

3. Results and discussion

The results of coagulation tests from surface water Rozgrund reservoir (WTP Rozgrund) are showed in Figure 2 and 3. The effectiveness of coagulation was monitored for two coagulants, polyaluminiumchlorid PAX-18 and PAX-XL19.

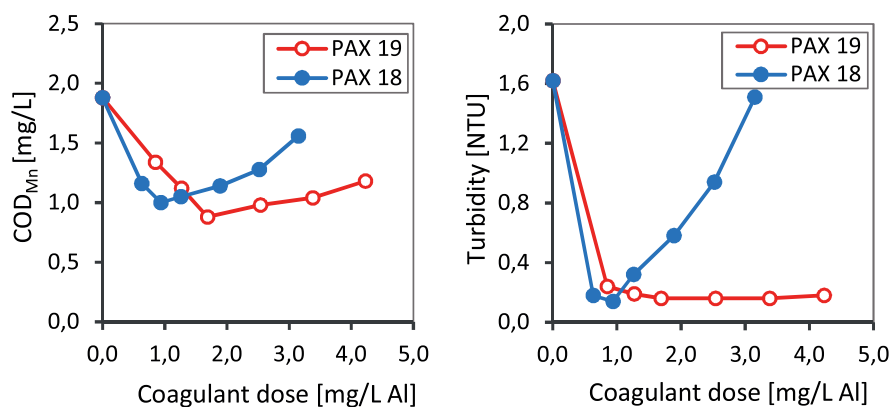


Figure 2. Course of COD_{Mn} (left) and turbidity (right) after adding 1% solution of PAX-18 and PAX-19 in coagulation tests

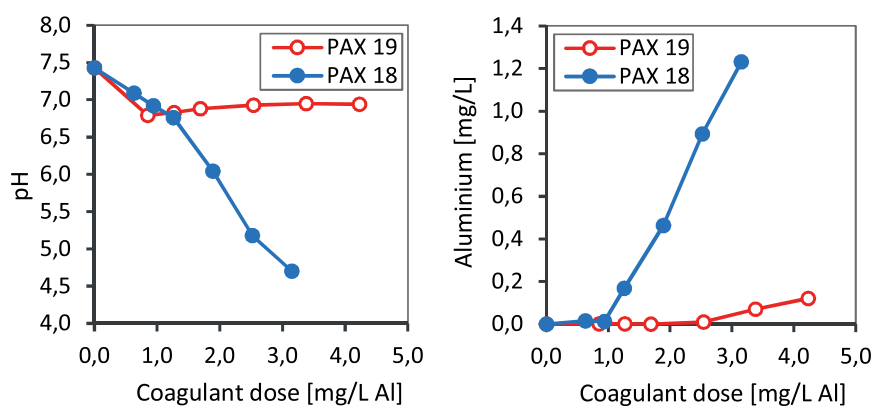


Figure 3. Course of pH value (left) and concentration of Al (right) after coagulation tests with 1% solution of PAX-18 and PAX-XL19

When comparing the technological effects based on the test performed, coagulant PAX-XL19 appears to be more suitable in terms of residual aluminium at a dose of 0.85-1.69 mg/L of Al (0.5-1.0 mL of 1% solution PAX-XL19), because the filtered water did not contain any aluminium. When using the PAX-18 optimal dose 0.94 mg/L Al (0.75 ml of 1% solution PAX-18), the quantity of aluminium in the treated water was determined as 0.012 mg/L (Table 3).

Coagulation tests showed that there are no significant differences in other monitored parameters when using coagulants PAX-18 and PAX-XL19. When using the PAX-18 or PAX-XL19 optimal dose the efficiency removal of turbidity was 91,36% or 90,12% respectively. For parameter COD_{Mn}, the COD_{Mn} (humic acid) removal efficiency using PAX-18 and PAX-XL19 was 46.81% and 53.19%, respectively. PAX-18 is more suitable in terms of residual alkalinity and pH in water after coagulation (in water after sedimentation).

Table 3. Water quality on entry to the Rozgrund water reservoir during the experiments

SAMPLE TYPE	Dose [mL]	Dose [mg/L Al]	pH	Turbidity [NTU]	Colour [mg/L Pt]	COD _{Mn} [mg/L]	Alkalinity [mmol/L]	Al [mg/L]
Raw water	–	–	7.43	1.62	4	1.88	0.82	0
PAX-18	0.75	0.94	6.92	0.14	<1.0	1.0	0.59	0.012
PAX-XL19	1.0	1.69	6.88	0.16	<1.0	0.88	0.52	0.001

4. Conclusion

The aim of the laboratory coagulation tests was to verify the possibility of using the aluminum coagulant PAX 18 and PAX-XL19 for a given water quality and determine the optimal dose for each coagulant.

The laboratory coagulation tests were performed with only two available aluminium coagulants because this treatment plant was designed and operated as a single-stage water treatment and it is a low temperature surface water. Therefore, an iron-based coagulant is not warranted. In relatively pure water, where the decisive parameters (colour <12 mg/L, turbidity 2.94 NTU, COD_{Mn} 2.56 mg/L) are below the limit values of the Slovak Republic Decree No. 247/2017 for drinking water, mechanical filtration would in principle be sufficient. However, living organisms in the number of 354 individuals are present in the raw water. This value was measured in water with which laboratory coagulation tests were performed. A test focused on the possibility of trapping microorganisms in the flakes showed that at the optimal dose of 0.70 mg to 0.75 mg of aluminium in the flakes about 70–75% of the organisms were trapped, which means that about 280–300 organisms were trapped in the flakes.

Both coagulants can be used in the treatment of surface water from the Rozgrund water reservoir. For further pilot-tests in the Rozgrund Water Treatment Plant, coagulant PAX-18 and coagulant dose 0.94 mg/L of Al was chosen (also with regard to the economic aspect and the price of coagulants).

Acknowledgements

This paper was produced thanks to support from the experiments were performed with financial support from the APVV-15-0379, APVV-18-0205 and VEGA 1/0737/19 Projects.

References:

- [1] CRITTENDEN, J., TRUSSELL, R.R., HAND, D., HOWE, K., TCHOBANOGLIOUS, G., MWH's Water Treatment: Principles and Design, third ed. John Wiley & Sons, Hoboken, NJ, USA, 2012, p. 1920.
- [2] HOWE, K., Principles of Water Treatment, John Wiley & Sons Inc. New York, United States, 2012, p. 672.
- [3] SILLANPÄÄ, M., MATILAINEN, A. NOM Removal by Coagulation. Natural Organic Matter in Water, Butterworth-Heinemann, pp. 55–80, 2015. doi:10.1016/b978-0-12-801503-2.00003-3.
- [4] HUANG, C., PAN, J. Coagulation Approach to Water Treatment, Encyclopedia of Surface and Colloid Science; Hubbard, A.T. (ed.) Marcel Dekker Inc, New York, pp. 1049–1064, 2002.
- [5] ZOUBOULIS, A., TRASKAS, G., SAMARAS, P. Comparison of Efficiency between Poly-aluminium Chloride and Aluminium Sulphate Coagulants during Full-scale Experiments in a Drinking Water Treatment Plant, Separation Science and Technology, 43:6, pp. 1507–1519, 2008.
- [6] SILLANPÄÄ, M., NCIBI, M.C., MATILAINEN, A., VEPSÄLÄINEN, M. Removal of natural organic matter in drinking water treatment by coagulation: A comprehensive review. Chemosphere 190, pp. 54–71, 2018. <https://doi.org/10.1016/j.chemosphere.2017.09.113>.
- [7] SZLACHTA, M., ADAMSKI, W., Effects of natural organic matter removal by integrated processes: alum coagulation and PAC-adsorption. Water Sci Technol 59, pp. 1951–1957, 2009.
- [8] VAN BENSCHOTEN, J.E, EDZWALD, J.K. Chemical aspects of coagulation using aluminum salts. I. Hydrolytic reactions of alum and polyaluminum chloride. Water Research 24, pp.1519–1526, 1990.
- [9] PERNITSKY, D.J., EDZWALD J. K., Selection of alum and polyaluminium coagulants: principles and applications. J. Water Supply 55(2), pp. 121–141, 2006.

- [10] YANG, Z., GAO, B., YUE, Q., Coagulation performance and residual aluminium speciation of $Al_2(SO_4)_3$ and polyaluminium chloride (PAC) in Yellow River water treatment. *Chem. Eng. J.* 165, pp. 122–132, 2010.
- [11] ZARCHI, I., FRIEDLER, E., REBHUN, M. Polyaluminium chloride as an alternative to alum for the direct filtration of drinking water, *Environmental Technology*, 34:9, pp. 1199–1209, 2013.
- [12] NTI, S.O., Richard BUAMAH, R., ATEBIYA, J., Polyaluminium chloride dosing effects on coagulation performance: case study, Barekese, Ghana. *Water Practice and Technology* 16(4), pp. 1215–1223, 2021.
- [13] ATARI, L., ESMAEILI, S., Amir ZAHEDI, A., MOHAMMADI, M.J., ZAHEDI, A., BABAEI, A.A., Removal of heavy metals by conventional water treatment plants using polyaluminium chloride. *Toxin Reviews* 38:2, pp. 127–134, 2019.
- [14] Kemwater ProChemie, 2022: <http://www.prochemie.cz/chem/tech-list-pax-18-polyaluminiumchlorid.pdf>; <http://www.prochemie.cz/chem/tech-list-pax-xl-19.pdf>

III Sanitary Engineering and Sustainable Water Use

NUMERICAL ANALYSIS TO DETERMINE THE TECHNICAL WATER LOSSES IN A WATER SUPPLY SYSTEM

GOCE TASESKI¹, NIKOLA KRSTOVSKI¹

¹ Ss. Cyril and Methodius University in Skopje; Republic of North Macedonia
e-mail: taseski@gf.ukim.edu.mk, nikolatudence@gmail.com

Abstract

In N. Macedonia for many years, even decades, decreasing the capacities of water resources has been discussed, as well as increasing the specific water consumption per individual consumer. These circumstances of increased water consumption are directly related to, and caused by increased water losses in water supply system.

The great losses in water supply systems, as well as ordered Non Revenue Water contribute to further restrict clean water supply. Namely, this contributes to increased amount of water entering the distribution system and additional unjustified investment in the capacities of supplied raw water, rather than investment into remodeling and subsequent management of the network.

Recently, technological development facilitates a more active application of all available data; namely, the amount of information collected from water supply systems is increased, as well as the number of measurement points, the type of measurement data and the frequency of readings. As a result, control of water supply networks is improved, as well as knowledge for what in fact happens in the water supply systems. By using a measurement technique and by determining measurement points, we obtain data for the amount of water in water supply systems, which can be analyzed to determine the water losses in water supply systems.

The measurements taken from the water supply system and the analysis of the experimental readings gave a full picture for the water loss state in the water supply system of Strumica.

Leakages and pressure at specific measurement spots were also analyzed, and the total water loss and real losses on a daily and yearly basis were calculated, shown in percentage in relation to the water entering the distribution system in the water supply of Strumica.

Keywords: water supply systems; water losses; measurement points; analysis water losses.

1. Introduction

Many countries that have water management strategy, water losses in water supply systems take a significant place in the successful management of water and water supply systems. Of course, the level of economic development and ecological awareness influences the modernization and management of water resources, but the reduction and management of water losses improves the existing water supply systems and makes them efficient and sustainable. However, all plumbing systems face water loss, even the best and the most modern systems cannot eliminate the occurrence of water loss. But with continuous monitoring of the system, with the introduction of new technical measures and consistent implementation of management procedures, as well as the application of institutional measures, it is enabled to effectively manage the loss of water and the rationalization of water consumption.

In all water supply systems, the impact of water losses on their sustainability is great, and therefore when sustainability and the impact of water losses are mentioned, it is necessary to highlight the following impacts: economic, technical, social, ecological, etc. While during water loss management there are several elements that can justify the measures taken and the increased cost of water loss management such as:

- efficiency of operating costs,
- efficiency of capital costs,
- improved metering and invoicing,
- reduced health risks,
- increased security of water supply,
- less infrastructure damage,
- reduced sewage load,

- improved user satisfaction,
- publicity and willingness to increase the payment,
- reduced burden on the environment

In Macedonia, as a developing country, the level of awareness about reducing water losses is still at a very low level compared to developed countries that pay great attention to the problem of rationalizing consumption and the functionality of water supply systems and make great efforts to reduce water losses.

That is why the aim of this paper is through a numerical analysis with a selection of measuring points in the water supply network of the City of Strumica, to analyze the water losses, especially how much of it is technical and how much is administrative.

2. Defining water losses

Water losses can be expressed in many ways, but the most common way to express water losses is expressed in a percentage of water produced. Since the term “water loss” is rather broad and undefined and can be interpreted differently, the scientific community has adopted the term “uninvoiced water”, that is, water that is produced and not paid for. So, we can divide water losses in water supply systems into apparent and real.

2.1. The real losses

Real losses are amounts of water lost as a result of network failures, damage to pipes and equipment, bad management and other network losses between the water entry into the distribution network and the end users’ water meters.

Real losses refer to the loss of a specified amount of water over a given period of time through all types of leaks, cracks and overflows.

The reason for the real water losses are the pipes, the shaped and connecting elements, the type of material and the age, but various other factors that are related to the environment in which the installation is placed.

2.2. Apparent losses

Apparent losses represent amounts of water that occur as a difference between incoming water and sold water. Apparent water losses are not losses that occur due to the physical leakage of water, but are due to other factors that we can divide based on their origin and specificity, namely:

- Incorrect measurements, Inaccuracy of water meters due to untimely replacements and irregular calibration, both of house and control ones
- Errors with data processing and calculations, invoicing to consumers
- Unauthorized, illegal consumption due to theft of water and unauthorized connections

2.3. Unbilled allowed consumption

Unbilled permitted consumption represents the amount of water that was delivered to the system, but was used for own needs, such as testing of the water supply network, washing and flushing of the network, leaks during repair of defects and other incidental interventions in the network, i.e. it includes all amount of water that is justifiably not invoiced.

2.4. Non-revenue water (NRW)

The real and apparent water losses together with the uninvoiced allowable consumption represent the Non-Revenue Water (NRW) in the water supply system.

2.5. Irrational consumption of water

Irrational consumption of water according to IWA recommendations is not calculated as a component of water loss and is not included in the calculations in the water balance, because this consumption occurs after the measurement of the water meters. However, this amount of water can represent a significant part of metered and unmetered consumption. Practically, it can be divided into deliberate irrational consumption of water by the consumers themselves, where the cause would be damage to the taps and their continuous flow, or when we have consumption due to a failure of the internal plumbing system or overflowing of the toilet cisterns.

Irrational water consumption can also occur in the water supply company itself through excessive or negligent use of water for operational purposes, for example: during repair of defects, when flushing the water supply network, as well as when washing filters and other needs in the same technological process of the Filter stations.

2.6. Water balance

With the correct definition and accurate determination of the water balance, we get a calculation that will be a good basis for assessing water losses in the water supply system. The water balance is a calculation of the state of produced water, consumed water and losses.

Table 1. Water balance as recommended by IWA

Quantity which enters into the system QI	Authorized consumption QA	Billed authorized consumption QBA	Billed delivered water	Income water
			Billed measured consumption	
		Unbilled authorized consumption QUA	Billed Not measured consumption	Non-revenue water
			Unbilled measured consumption	
	Water loss QL	Apparent Losses QAL	Unbilled Not measured consumption	
			Unauthorized consumption	
		Real losses QRL	Inaccuracy in consumer water meters and data handling errors	
			Leakage in main and distribution pipes	
			Leaks and overflows in tanks	
			Leakage of connections to consumers' water meters	

In the past, a variety of forms and definitions were used when calculating the water balance, but the International Water Association (IWA) provided a best practice approach that a number of countries and water supply companies have accepted and adopted the water balance, following the IWA terminology, so the basic and fundamental need is to calculate all the components of non-revenue water and terminologically to unify the individual components of the water balance.

3. Analysis of water losses on a real system in Macedonia

The aim of this paper is to determine the water losses in the water supply system of the city of Strumica using the IWA methodology.

The water supply of the city of Strumica functions as a modern water supply system that has been built and is continuously being built, expanded and constantly modernized for more than 50 years.

At first, the city was supplied with water through a pumping station in the Sofilar area until the construction of the old filter station and the pipeline from the dam Vodocha. In 1978 the new filter station was put in use through which the city of Strumica is still supplied with water today, but a pipeline from the Turia accumulation was built, from where the untreated water comes by gravity to the water processing plant through a 15 km long pipeline derived from asbestos cement pipes f600 and in the last 600m. passes into a steel pipeline f500 mm. For the need to purify and process raw water and provide clean water a Filter station with a capacity of 240 l/s was built.

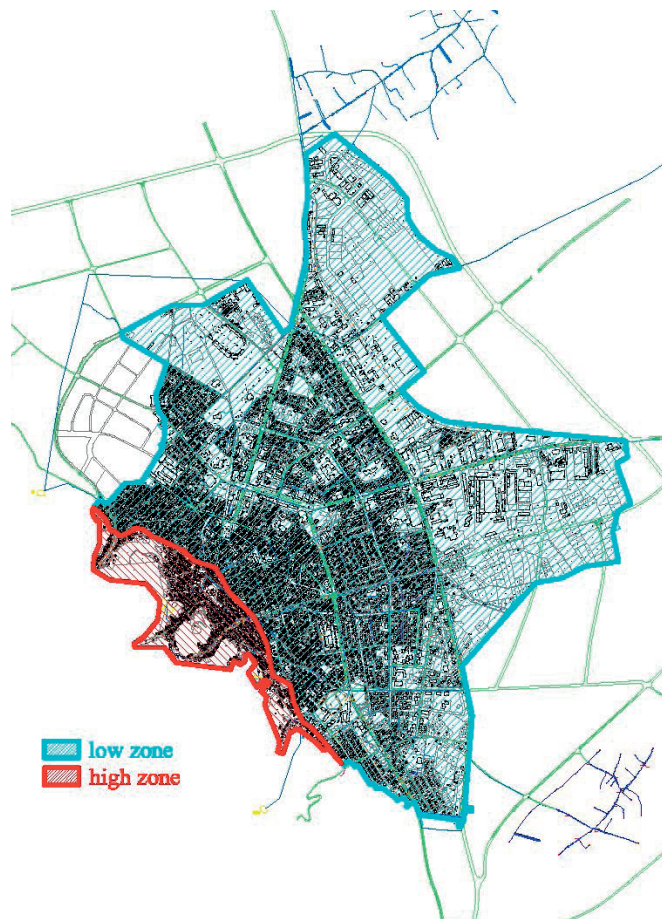


Figure 1. Map of Strumica water supply network

3.1. Analysis of water consumption in the water supply system of Strumica

The data on water consumption were provided by JPKD Komunalec for the last 30 years. These data refer to purchased raw water which is monthly read and invoiced by the Water Management Department of the Republic of Macedonia, data are also given on invoiced clean water to households and industry (business entities), as well as for the consumed technical water.

The following image shows total water losses, which are given as a ratio of invoiced water and purchased raw water expressed in percentage.

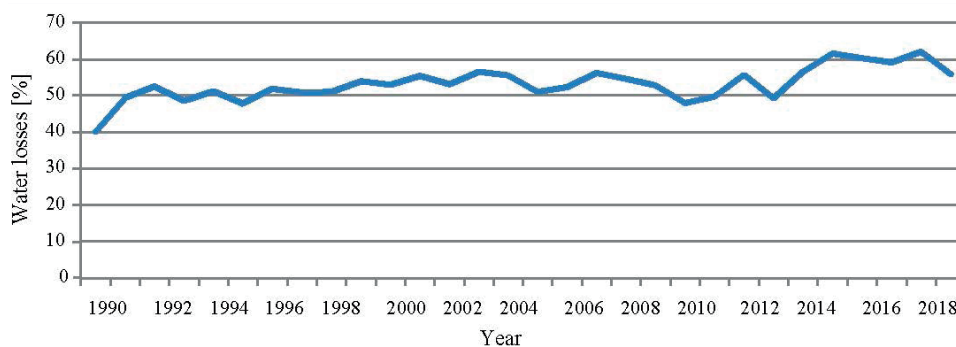


Figure 2. Total water losses in water supply system of Strumica

It should be noted that the measurement of raw water is carried out at the dam Turija at the entrance to the pipeline through which the raw water is transported to the Filter Station. This means that we present the water losses in the water supply system of the city of Strumica as total losses, which also include the losses of the pipeline to the Filter Station in a length of 15 km. and the consumption of water required for the technological process itself for the production of clean water. Of course, these data include all other losses, real and apparent, as well as authorized nonvoiced consumption.

When we look the numbers, we get a picture that in this period the total water losses range from 46% to 62%, it shows that the water losses are gradually increasing, the value of the invoiced water is gradually decreasing, while there are no

major changes in the amount of incoming water. This tells us that the impact of reported water and invoicing to citizens, along with all other administrative water losses, have a large percentage in the total water losses.

3.2. Real measurements of the total consumption of the city of Strumica

In order to define the total consumption of the city of Strumica, the total entry into the water supply system of the city of Strumica is monitored, which implies installation of ultrasonic flow meters on the two pipelines DN 300 mm and DN 400 mm that represent the entry of water into the water supply system for the city (exit from the water plant).

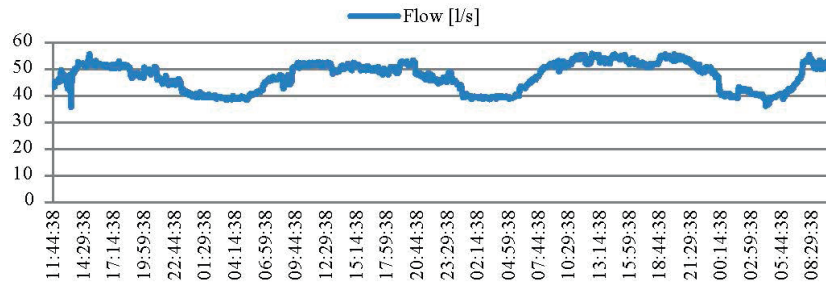


Figure 3. Flow measurement of pipeline DN300mm from filter station

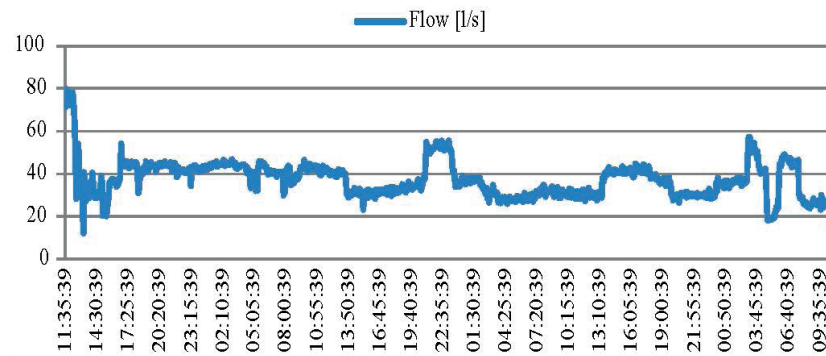


Figure 4. Flow measurement of pipeline DN400mm from filter station

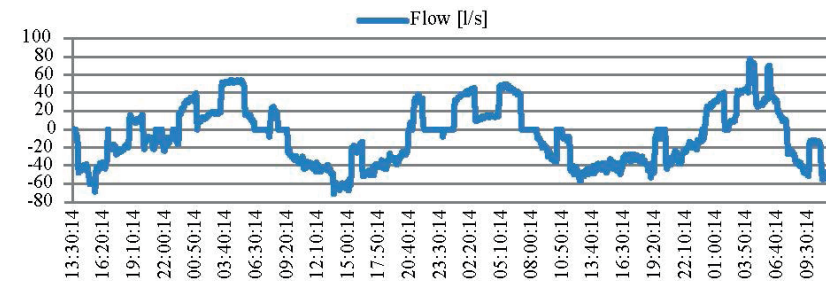


Figure 5. Flow measurement of pipeline DN600 mm in front of tank low zone 5000 m³ (Values with a negative sign are due to water flowing in the reverse direction – the measurement is in front of the tank where water goes in two directions to and from the tank)

Due to the large capacity of the low zone tank (5000m³), it was necessary to simultaneously monitor its flow by installing an additional ultrasonic flow meter on the DN600 mm pipeline, which represents the output of the low zone/input of the low zone tank. (Flow measurement with an ultrasonic flow meter is a non-invasive method, which involves installing sensors on the outer pipe wall and monitoring and memorizing the current pipe flow at pre-defined time intervals).

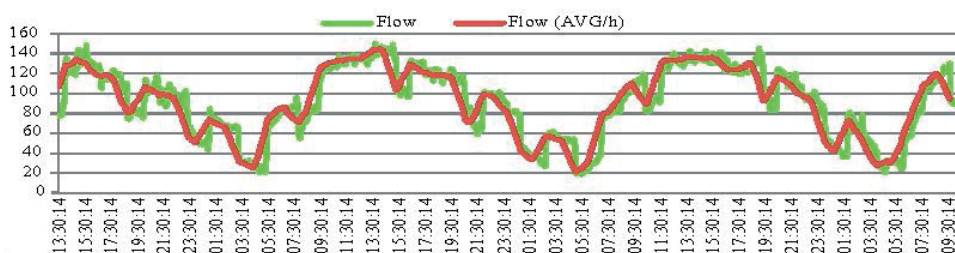


Figure 6. Total measured flow for low zone (AVG/h - The measurement was made at an interval of 10 minutes, therefore the average flow in one hour is shown)

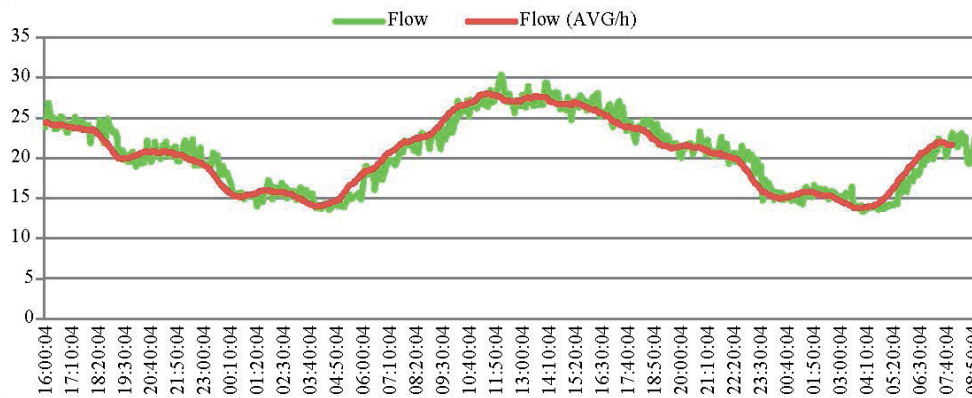


Figure 7. Total measured flow for high zone (AVG/h – The measurement was made at an interval of 10 minutes, therefore the average flow in one hour is shown)

3.3. Analysis of results of experimental measurements

The analysis of the results of the experimental measurements were used for the analysis of water losses, while according to the specificities of the water supply system of the city of Strumica, we have to make a divided analysis for the low and high zones, from where the total water losses were obtained by summarizing the results.

The actual water losses in the water supply system of the city of Strumica were determined using the following method:

This method can be applied because reliable flow data is available at time intervals of 10–15 min. What are the conditions for performing the analysis? Measuring the minimum night consumption is one of the essential activities that should be undertaken to define the level of technical water losses. With a simple examination of the night minimum, it is possible to diagnose many problems. The losses are small and the network is in a relatively good condition, if the night consumption is very low, at most 13–18% of the daily average. This is based on the assumption that the nighttime activity of the population is reduced to a minimum, and thus the need for water. However, the losses depend on the time of day, and at night they are higher due to the increased pressure.

When we talk about the measured minimum night flow, it is not appropriate that this value represents the loss of water, because there is still a part of legally consumed water by individual and commercial users (Minimum legal night consumption), although the largest percentage is accounted for by leakages, which can be major faults on the primary network or minor faults on the secondary network.

The difference between Minimum night flow (MNF) m³/hour and Legitimate night consumption (LNF) m³/hour gives the Net night flow: m³/hour (NNF). Due to the difference in pressures during night and day, the daily flow (m³/day) should be multiplied by NDF (Night Day Factor), which is a coefficient that creates the actual average 24-hour flow, which is depending on the pressure (values vary mostly from 17 to 28). In the case of gravity water supply, the values can vary from 17–18 to 24, while in the case of pumped water supply, from 23–24 to 26–28.

Based on the realized pressure measurements and using a software tool, this low zone factor was calculated at a value of 22.58. while for high zone this factor is 23.6.

Based on the previously performed calculations for real water losses in low and high zones, the total real water losses at the level of the city of Strumica with the surrounding villages amounts to:

City of Strumica = low zone + high zone

Daily flow: 1095 m³/day + 1037 m³/day = 2132 m³/day
or 26.97% of the total daily input into the system

Annual flow:

399765 m³/year + 378505 m³/year = 778 180 m³/year
or 16% of the total input of purchased raw water in the filter station

4. Conclusion

Analyzing these figures for the annual total losses for the analyzed year 2021, which are 56%, it can be concluded that the level of apparent water losses is high, about 40% in relation to the purchased raw water. The percentage of 16% of real losses in relation to the purchased raw water gives us an image that the water distribution network is in a relatively good condition, that these losses are still at a relatively low level, which with constant monitoring and taking measures to reduce losses can be even smaller.

But it is also necessary to note that the water losses along the supply pipeline to the Filter Station, as well as the water losses in the technological process of the Filter Station, are not separated as a quantity and as a percentage and were not the subject of this analysis. Although these losses should be calculated in the real losses, due to the lack of possibility to measure these quantities, they will remain as losses that enter into the 40% apparent losses.

But with these measurements and analysis, the aim was to perceive the water losses in the water distribution network, determining the real water losses at the output from the Filter Station, (entrance to the water supply system), then to the end users, and thus determined is the water balance required for the water supply system of the city of Strumica.

References:

- [1] AWWA. Computer Modeling of Water Distribution Systems Manual of Water Supply Practices M32. [ed.] American Water Works Association, Denver, Colorado, USA, 2005.
- [2] Bristol Water, Assessment of Economic Level of Leakage. Bristol, United Kingdom, 2007.
- [3] Charalambous, B., Effective Pressure Management of District Metered Areas. Proceedings of Water Loss 2007, Bucharest, Romania, 2007.
- [4] Cornell, R. and Dunphy, J., Water Distribution System Asset Management Needs and Nice to Have. Journal of the American Water Works Association. 2005.
- [5] Fanner, P., Assessing real water losses: a practical approach. Water 21 - Magazine of the International Water Association, pp. 49–50, 2004.
- [6] Fanner, P. and Thornton, J., The Importance of Real Loss Component Analysis for Determining the Correct Intervention Strategy. Proceedings of the IWA Specialized Conference 'Leakage2005', Halifax, Nova Scotia, Canada, 2005.
- [7] Farley, M., Leakage Management and Control. WHO, 2001.
- [8] Farley, M. and Trow, S., Losses in Water Distribution Networks. IWA Publishing, 2003.
- [9] Heiman, A., Meyer, N. and Liemberger, R., Tailoring the Specifications for Pressure Reducing Valves. Proceedings of the 5th IWA Water Loss Reduction Specialist Conference, Cape Town, South Africa, 2009.
- [10] Kober E. and Gangl G., New Monitoring Methodology for Water Distribution [11]Systems. Proceedings of the 5th IWA Water Loss Reduction Specialist Conference, Cape Town, South Africa, 2009.
- [12] Lambert, A.O., International Report: Water losses management and technique. Water Science and Technology: Water Supply. pp. 1–20, 2002.

III Sanitary Engineering and Sustainable Water Use

OPTIMIZATION OF CIRCULATING FLOW SONO-ELECTROCHEMISTRY FOR MINERAL OIL REMOVAL

HANA POSAVČIĆ¹, DRAŽEN VOUK¹, KATARINA LICHT¹

¹ University of Zagreb, Faculty of Civil Engineering; Croatia

e-mail: hana.posavcic@grad.unizg.hr, drazen.vouk@grad.unizg.hr, katarina.licht@grad.unizg.hr

Abstract

In this paper, the optimization of circulating flow sono-electrochemistry for mineral oil removal is investigated. The multilevel categorical design was used to study the effects of aeration, electrode distance and ultrasound intensity on mineral oil removal efficiency. According to the experimental results, the highest mineral oil removal efficiency of 97.17% was obtained when the electrodes were placed at a distance of 5 mm and with a US intensity of 9.3 kW/m². Aeration had no effect on the removal efficiency.

Keywords: sono-electrocoagulation, circulating flow, mineral oil, aeration, electrode distance, transducer.

1. Introduction

Since oily wastewaters contain high concentrations of hydrocarbons, oil, phenol, benzene, etc., and their uncontrolled discharge or inadequate treatment can cause environmental pollution [1, 2], there is an interest in searching and developing various methods for oily wastewater treatment.

The term sono-electrochemistry (sono-EC) refers to the combination of ultrasonic irradiation (US) and electrochemistry (EC). In this combination, US cavitation is generated by US transducers that are part of an US bath or horn (probe), and an electrochemical cell is used for EC [3]. According to the relevant research results, the individual EC and US processes, as well as their combination, have been shown to be effective in removing various contaminants, including suspended solids, heavy metals, oil, colour, etc. [4, 5].

In one of the previous studies [6], an optimal combination of operating parameters for the circulating flow sono-EC was determined. The effects of flow rate, current density and number of cycles on mineral oil removal were investigated in that study. The experimental results showed that sono-EC with circulating flow could effectively reduce mineral oil by 94.3% under the optimum conditions of 14.13 cycles, a current density of 53.124 A/m², and a flow rate of 0.234 L/s.

In this study, further optimization of the previously mentioned operating conditions is investigated. The optimization included the study of aeration, electrode distance and US intensity on mineral oil removal. Multilevel categorical experimental design was used to create the experimental matrix, and a total of 12 experiments were conducted.

2. Methods

2.1. Oily wastewater samples

Samples of oily wastewater were obtained from oil and grease separators used to treat stormwater from roads and some industries. Mineral oil concentrations were measured using the NEXIS GC-2030 (from Shimadzu, Japan), while pH, conductivity, total dissolved solids (TDS), dissolved oxygen (DO), and temperature were measured continuously using the HI-98194 Multiparameter Waterproof Meter (from Hanna Instruments, Romania). Initial and final wastewater characteristics are shown in table 1.

Table 1. Characteristics of wastewater influent and effluent

PARAMETER	INFLUENT	EFLEUNT
PH	7.28	7.45
CONDUCTIVITY (MS/CM)	620	235
TDS (MG/L)	310	120
DO (MG/L)	6.26	5.52
TEMPERATURE (°C)	21.89	23.27
MINERAL OIL (MG/L)	701.07	61.14±42.71

2.2. Experimental setup

In the previous study [6], an optimal combination of operating parameters for the circulating flow sono-EC was determined. In that earlier study, the effects of flow rate, current density, and number of cycles on mineral oil removal were investigated. The use of 5.1 kW/m² of US intensity in combination with four aluminium electrodes (sono-EC) was also compared to EC alone. A total of 34 experiments were conducted and the results were statistically analysed using the Box-Behnken design (Design-Expert 13 software). The experimental results showed that sono-EC with circulating flow could effectively reduce mineral oil by 94.3% under the optimum conditions of 14.13 cycles, a current density of 53.124 A/m², and a flow rate of 0.234 L/s.

This study is a continuation of testing with these defined device settings, which includes the investigation of the removal effect of aeration, electrode distance (5 and 10 mm) and US intensity (2.5 kW/m², 5.1 kW/m² and 9.3 kW/m²). The factor levels are also listed in Table 2.

Table 2. Factor levels

PARAMETER	L [1]	L [2]	L [3]
A: AERATION	WITH A	WITHOUT A	–
B: ELECTRODE DISTANCE (MM)	5	10	–
C: US INTENSTIY(KW/M²)	2.5	5.1	9.3

In the experimental setup four aluminium electrodes were placed in a rectangular Plexiglas container 5 mm above the bottom and connected to a DC power supply (from MC Power LBN-1990, Germany). The US transducers were firmly attached to the insulated 1 mm thick steel plate at the underside of the reactor. US transducers provided an intensity of 2.5 kW/m² or 5.1 kW/m², while the intensity of 9.3 kW/m² was achieved by combining US transducers and two US homogenisers (probes) SONOPULS HD 2200.2 (from Bandelin, Germany). The US homogenisers were immersed near the electrodes from above. In each experiment 8 L of raw oil wastewater circulated through the reactor according to the experimental setup defined by experimental matrix (Table 3). If necessary, TetraTec PAS 400 (from Tetris GmbH, Germany) was used for additional aeration of the wastewater samples. After each experiment, the mineral oil concentrations of the effluent were determined (Table 1 and Table 3).

2.2.1. Experimental design and Analysis of Variance (ANOVA)

Design-Expert 13 software was used for the experimental design. For this purpose, a Multilevel categorical experimental design, also known as a General Factorial design, was used. In general, categorical experimental designs are used for experiments with 1 to 12 factors, where each factor can have a different number of levels. Therefore, each factor is treated as categorical [7].

According to the number of factors, a matrix of 12 experiments was created, Table 3. The matrix included experiments with and without aeration, electrodes distances of 5 and 10 mm, and the use of different US intensities (2.5 kW/m², 5.1 kW/m² and 9.3 kW/m²). The experimentally determined results of the mineral oil removal efficiencies as well as the modelled results are also shown in Table 3.

The response of Design-Expert (effluent output) is a random variable determined by the percentage of mineral oil removed (removal efficiency, y (%)) using Eq. (1) [8]:

$$y (\%) = (C_i - C_e)/C_i \times 100 \quad (1)$$

where C_i and C_e correspond to the measures of influent and effluent concentrations, respectively.

Table 3. A Multilevel categoric design matrix with a mineral oil removal efficiencies

EXPERIMENT	A:AERATION	B: ELECTRODE DISTANCE [MM]	C:US INTENSITY [KW/M ²]	MINERAL OIL REMOVAL [%] (EXPERIM.)	MINERAL OIL REMOVAL [%] (PREDICTED)
1	with A	10	2.5	89.73	90.09
2	with A	10	5.1	88.40	90.14
3	without A	5	5.1	93.54	94.29
4	without A	10	5.1	91.88	90.14

5	with A	10	9.3	96.03	96.18
6	with A	5	9.3	97.17	97.14
7	without A	10	9.3	96.34	96.18
8	without A	5	2.5	82.65	79.90
9	with A	5	5.1	95.04	94.29
10	with A	5	2.5	77.15	79.90
11	without A	5	9.3	97.12	97.14
12	without A	10	2.5	90.46	90.09

Significance tests were performed to build the model where P-value of each parameter or interaction must be less than 0.05 [9]. Analysis of Variance (ANOVA), Table 4, showed that the model was significant ($P < 0.001$), with factor C (US intensity) being the most significant ($P = 0.0004$). Although not significant ($P = 0.1812$), factor B (electrode distance) was included in the analysis because it was required to calculate the BC interaction, which was significant ($P = 0.0046$). Aeration (factor A) was found to have no significant effect on the removal efficiency of mineral oils and therefore was not included in further analysis. This is because water circulation generates a sufficient amount of air bubbles in the flow device. Electrodes, US probes and transducers also generate additional gases (oxygen and hydrogen), so aeration with an air pump in addition to all this does not contribute significantly to the overall process [10, 11, 12]. Moreover, the coefficient of determination (R^2) is 0.9464, indicating that the model reproduces well the experimentally obtained results.

Table 4. ANOVA

	SUM OF SQUARES	MEAN SQUARE	F-VALUE	P-VALUE
MODEL	399.63	79.93	21.19	0.001
B: ELECTRODE DISTANCE	8.63	8.63	2.29	0.1812
C: US INTENSTIY	277.49	138.74	36.78	0.0004
BC	113.52	56.76	15.05	0.0046

The mathematical relationship in terms of actual factors between the independent variables (A, B and BC) and their responses (mineral oil removal) can be stated as follows:

$$y (\%) = 91.29 + 0.85B - 6.30C[1] + 0.96C[2] + 4.25BC[1] - 2.92BC[2] \quad (2)$$

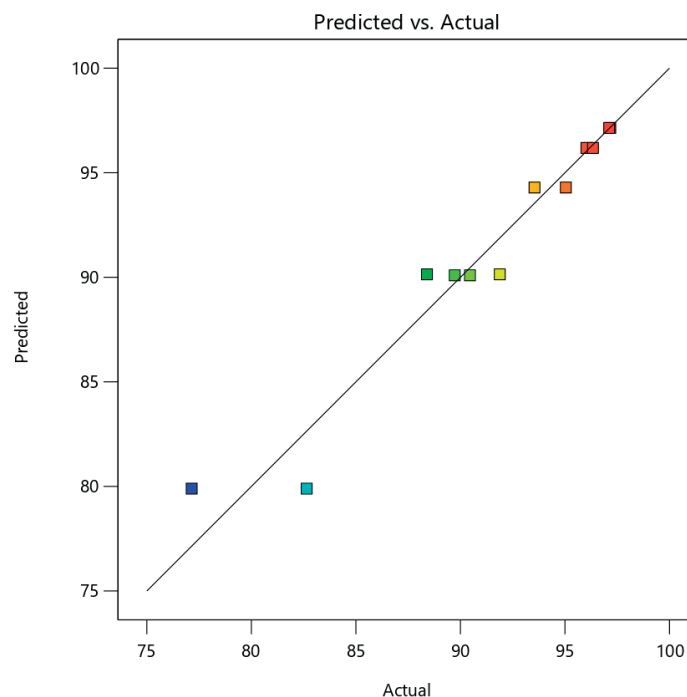


Figure 1. Comparison of model prediction of mineral oil removal [%] with experimental (actual) observations (scatter plot)

The equation in terms of coded factors (Eq. (2)) can be used to make predictions about the response for specific levels of each factor. By default, the high values of the factors are coded +1 and the low values are coded -1. The coded equation is useful to determine the relative influence of the factors by comparing the factor coefficients [7].

The mineral oil removal predictions (Table 3) are compared with the experimental (actual) observations in Fig. 1. The obtained data were sufficiently close to the linear values, and it can be concluded that the predictions using the above equation agree well with the actual observations with an acceptable error.

3. Results and discussion

The interaction between electrode spacing and US intensity is shown in Figure 2. In general, as the electrode distance increases, the electrical resistance of the water increases and therefore a higher voltage must be applied [13, 14]. Since the voltage was corrected to achieve the required current density (53.124 A/m^2), the electrode distance did not affect the removal efficiency significantly. At a distance of 5 mm, the voltage was 8 V, and at a distance of 10 mm between the electrodes, the voltage was 15 V.

The highest removal efficiency (97.17%) was obtained when the aluminum electrodes were spaced 5 mm apart and US transducers and homogenizers were used together (US intensity of 9.3 kW/m^2). Thus, the increase in removal efficiency was a result of the higher US intensity. The concentration of free radicals increased with the increase of US intensity, so the rate of organic matter degradation increased [15]. At a US intensity of 9.3 kW/m^2 , the use of 10 mm electrode spacing instead of 5 mm resulted in negligibly lower efficiency (96.18%). In both cases, mineral oil concentrations were experimentally lower than 30 mg/L , which is in compliance with the European standard for wastewater discharge to public sewers [16].

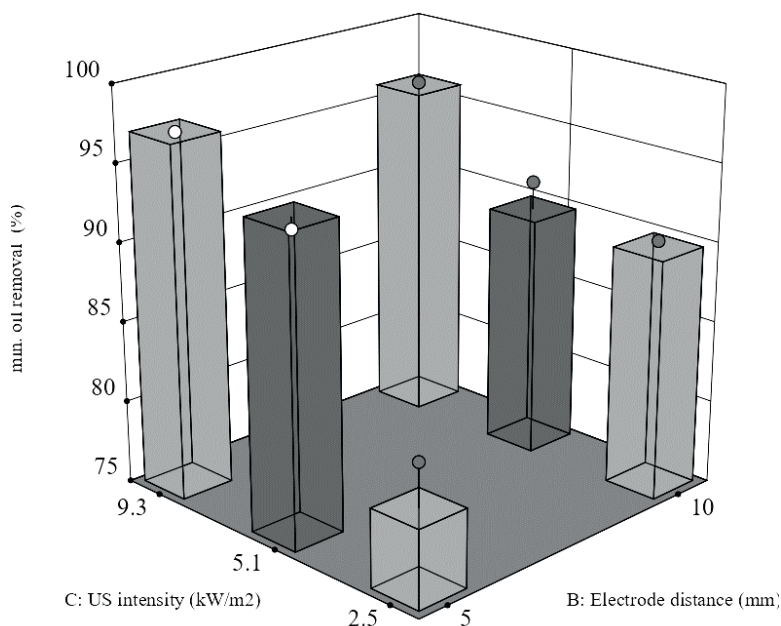


Figure 2. Interaction of US intensity and electrode distance

4. Conclusion

In this study, an innovative hybrid circulating reactor based on EC and US was optimised to reduce mineral oil concentration, and the influence of three categorical factors (aeration, electrode distance, and US intensity) on mineral oil removal was analysed.

A matrix of 12 trials was constructed using a multilevel categorical experimental design, and the results from ANOVA showed that the experimental design model was significant. US intensity was found to be the most significant factor, and the use of aeration had no significant effect on mineral oil removal efficiency. Aeration did not affect the overall process because a sufficient amount of air bubbles are already generated due to the flow rate and the electrodes, US probes, and transducers which are already producing oxygen and hydrogen.

The highest removal efficiency (97.17%) was achieved when the aluminium electrodes were spaced 5 mm apart and with a US intensity of 9.3 kW/m^2 . It can be concluded that the increase in removal efficiency was mainly due to the increase in US intensity, which led to cavitation and the formation of free radicals, which in turn caused the decomposition of organic matter.

Acknowledgements

This work has been fully supported by Croatian Science Foundation under the project “IP-2019-04-1169 – Use of treated oily wastewater and sewage sludge in brick industry – production of innovative brick products in the scope of circular economy”.

References:

- [1] Tir M., Moulai-Mostefa N.: Optimization of oil removal from oily wastewater by electrocoagulation using response surface method. *J Hazard Mater*, 158(1), pp. 107–115, 2008.
- [2] Safari S., Azadi Aghdam M., Kariminia H.R.: Electrocoagulation for COD and diesel removal from oily wastewater. *Int J Environ Sci Technol*, 13(1), 231–242, 2016.
- [3] Radi M.A., Nasirizadeh N., Rohani-Moghadam M., Dehghani M.: The comparison of sonochemistry, electrochemistry and sonoelectrochemistry techniques on decolorization of C.I Reactive Blue 49. *Ultrason Sonochem*, 27, pp. 609–615, 2015.
- [4] Kabdaşlı, I., Arslan-Alaton, I., Ölmez-Hancı, T., Tünay, O.: Electrocoagulation applications for industrial wastewaters: a critical review, *Environmental Technology Reviews*, 1(1), pp. 2–45, 2012.
- [5] Moradi, M., Vasseghian, Y., Arabzade, H., Mousavi Khaneghah, A.: Various wastewaters treatment by sono-electrocoagulation process: A comprehensive review of operational parameters and future outlook“, *Chemosphere*, 263, 2021.
- [6] Posavcic, H., Halkijevic, I., Vouk, D., Cvetnic, M.: Circulating flow Hybrid Ultrasonic and Electrochemical Process for the Treatment of Mineral Oil Wastewaters, 2022, in the process of publication
- [7] Anderson M.J., Whitcomb P.J.: DOE simplified: practical tools for effective experimentation. Third edit. Taylor & Francis Group, 2007.
- [8] Praveen, K.C., Radha, K.V., Balasubramanian, N.: Electrochemical Treatment of Plating Effluent: Kinetics and Statistical Modeling, *Water Sci. Technol.*, 5, pp. 17–24, 2011.
- [9] Tak, B., Tak, B., Kim, Y., Park, Y., Yoon, Y., Min, G.: Optimization of color and COD removal from livestock wastewater by electrocoagulation process: Application of Box-Behnken design (BBD), *J. Ind. Eng. Chem.* 28, pp. 307–315, 2015.
- [10] Babu, S.G., Muthupandian A., Bernaurdshaw, N.: The role of ultrasound on advanced oxidation processes. *Topics in Current Chemistry*, 374(5), pp.1–32, 2016.
- [11] Doosti, M.R., Kargar, R., Sayadi, M.H.: Water treatment using ultrasonic assistance: A review, *Ecology*, 2(2), pp. 96–110, 2012.
- [12] Ghernaout, D.: Advanced oxidation phenomena in electrocoagulation process: a myth or a reality?, *Desalination and Water Treatment*, 51(40–42), pp. 7536–7554, 2013.
- [13] Al-Rubaiey, N.A., Al-Barazanji, M.G.: Electrocoagulation Treatment of Oily Wastewater in the Oil Industry, *Journal of Petroleum Research & Studies*, 20, pp. 274–89, 2018.
- [14] Andrade, A., da Costa Marques, M.C.: Electrolytic Treatment of Wastewater in the Oil Industry, *New Technologies in the Oil and Gas Industry*, pp. 3–28, 2012.
- [15] Wang, J., Wang, Z., Vieira, C., Wolfson, J.M., Pingtian, G., Huang, S.: Review on the treatment of organic pollutants in water by ultrasonic technology, *Ultrasonics Sonochemistry*, 55, pp. 273–78, 2019.
- [16] EU. 2018. Commission Implementing Decision (EU) 2018/1147 of 10 August 2018 establishing best available techniques (BAT) conclusions for waste treatment, under Directive 2010/75/EU of the European Parliament and of the Council (notified under document C(2018) 5070), 2018.

III Sanitary Engineering and Sustainable Water Use

REMOVAL OF CHLORINATED PESTICIDES FROM WATER USING GRANULAR ACTIVATED CARBON

JÁN ILAVSKÝ¹, DANKA BARLOKOVÁ¹, MICHAL MARTON¹, MICHAL KUNŠTEK²

¹ Slovak University of Technology in Bratislava, Faculty of Civil Engineering, Department of Sanitary and Environmental Engineering; Slovakia

e-mail: jan.ilavsky@stuba.sk, danka.barlokova@stuba.sk, michal_marton@stuba.sk

² Water Research Institute, Nábřežie arm. gen. L. Svobodu 5, 812 49 Bratislava, Slovakia

Abstract

The effectiveness of removal the chlorinated pesticides (simazine, atrazine and terbuthylazine) from drinking water with adsorption using two types of granular activated carbon (Filtrisorb 400 and WG12) was monitored.

The experiments were performed in laboratory conditions with pH value of water 7.6, stable temperature 22–23°C and dose of adsorbent. The experiments were performed in the glass bottles with the volume of 400 mL stock model water (drinking water spiked with pesticide standard) with concentration approximately 0.5 µg/L, granular activated carbon (400 mg) was added to the bottles. Subsequently these bottles were regularly stirred at 400 rpm. Samples were taken at 30, 60, 120 and 240 minutes, after which they were analysed. Analyses of target pesticides were performed in laboratories of ALS Czech Republic in Prague.

The removal efficiencies for both types of activated carbon reached over 90%, which can be considered a very effective adsorption process for removal of pesticides from water. The adsorption efficiency depending on the contact time of water with the material and concentration of pesticides in water.

Keywords: drinking water treatment, chlorinated pesticides, granular activated carbon, adsorption efficiency, adsorption capacity, laboratory tests.

1. Introduction

In the last decade, traces of micropollutants (pharmaceuticals, drugs, pesticides and their metabolites, microplastics, etc.) typically at levels in the nanograms to micrograms per litre range, have been reported in the water cycle, including surface waters, wastewater, groundwater and, to a lesser extent, drinking water. Advances in analytical technology have been a key factor driving their increased detection.

Pesticide substances are one of the major pollutants of water. They are among the undesirable substances that have a negative effect on the human health and the aquatic ecosystem. The behaviour of pesticides after their application to the environment and the possible presence of their residues in groundwater and surface water depends on the physicochemical properties of the particular 'substance active' as well as on the whole product itself, the way of application (dose, time period) and on the agro-climatic conditions. Metabolites of these pesticides are relevant and irrelevant while their relevance is considered within the approval process of the 'substance active' [1–3].

Important factors determining the pesticide's potential for water pollution are as follows: solubility of the pesticide, distance of application from a body of water or watercourse, type of soil, gradient, presence, density of crop, agrochemical application method and technique.

Pesticides are chemicals of inorganic or organic type, used to destroy plant and animal pests as preparations for the protection of plants. They are categorised as insecticides, fungicides and herbicides on the basis of their intended purpose. Insecticides are used against insects which damage agricultural plants, fungicides against harmful parasitic fungi and herbicides against weeds. Other groups include acaricides (against mites), nematicides (against nematodes), molluscicides (against molluscs) and rodenticides (against rodents) [4–6].

There is recorded about 1300 'substances active' within the European Union – the pesticides for plant health protection. Among this total number, 350 of the active substances is listed as admitted active substances (which represents 28,6%) and their use in the EU is allowed. Other 59 substances are under ongoing evaluation (4,8%) in order to placement to the list of admitted substances and 814 substances is not listed and their use in the EU is not allowed (66,6%). There was registered about 250 pesticides for plant health protection in the Slovak Republic [7].

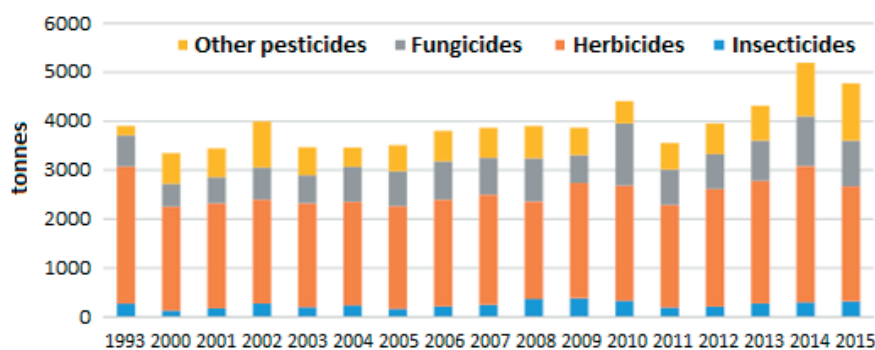


Figure 1. Pesticide consumption in Slovakia in 1993, 2000–2015 in tonnes according to preparation category (environmental, ÚKSUP)

Regarding the human health the chlorinated pesticides are the most used and most dangerous pesticides due to their toxicity, carcinogenicity and mutagenicity. Chlorinated pesticides have a high persistence in the environment. They accumulate mainly in the fat tissue, liver, kidneys, muscles, brain and in the heart as well. Acute intoxication is usually manifested in loss of the weight and paralysis of the system central nervous afterwards. Apepsy, headache, hyperphonia and total exhaustion occur in relation with the chronic intoxications while the nervous and mental defects occur later on. There are the reasons why the use of them had been prohibited in many of the countries or permitted only in exceptional cases [8].

The content of pesticides in water environment and agricultural products increases by their regular application. Their presence in water is quite frequent and that means these substances are used in a large amounts. The great issue related to pesticides represents their low biodegradability and their long persistence in water environment – as the original substances, as their metabolites (approx. 1–2 years). As having a good solubility they can be easily transported in the water or from the soil into the watered horizons [9].

The concentration of pesticides in drinking water is regulated by the Decree of the Ministry of Health of the Slovak Republic No. 247/2017. A maximum limit value of 0.1 $\mu\text{g}/\text{l}$ is determined for each defined pesticide; at the same time, a maximum limit value of 0.5 $\mu\text{g}/\text{l}$ is stipulated for the sum of pesticides, whereby the limit value represents the sum of concentrations of all pesticides in the analysed sample. A limit value of 0.03 $\mu\text{g}/\text{l}$ applies to aldrin, dieldrin, heptachlor and heptachlor epoxide. Pesticides comprised: organic insecticides, herbicides, fungicides, nematocides, acaricides, algicides, rodenticides, slimicides, related products (e.g. growth regulators) and their relevant metabolites. Only those pesticides are determined that might be anticipated as present in drinking water [10].

Due to groundwater contamination by atrazine, simazine and their metabolites, these were removed from the List of Active Substances (i.e. those which may be applied) by Commission Decisions 2004/248/EC and 2004/247/EC. Cyanazine, prometryne, propazine and terbuthylazine were also excluded from the List of Active Substances, by Commission Regulation 2076/2002/EC and Commission Decision 2008/934/EC. Despite this, we still find them in underground and surface waters.

The analytical determination of chlorinated pesticides depends on the possibilities of the workplace (equipment available, availability of chemicals and standards), purpose of the analysis, type of sample and overall level of their content in the sample. Currently, chromatographic methods, high-performance liquid chromatography (HPLC) and gas chromatography (GC) in association with mass spectrometry (MS) are used most frequently. Current analytical methods enable determination of the concentration at the level of ng/l [11–13].

Several methods can be used for removing the pesticides from the water, e.g. coagulation, precipitation, filtration combined with coagulation, biodegradation, ozonisation, adsorption, ion exchange, nanofiltration, reverse osmosis and advanced oxidative processes. Their efficiency varies significantly and depends mainly on the chemical nature of pesticide to be removed [14–16].

Mostly used sorption material to remove the organic pollution (pesticides, micropollutants) from the water is the activate carbon (powder, granules, extruded, with a treated surface). There is a large number of publications within which the efficiency of removal of various pesticides and their metabolites from the water and by the use of activated carbon was examined [17–22].

Activated carbon is the best-known sorption material for the removal of organic pollution (pesticides, micro-pollutants). Activated carbon is a highly porous carbon with a large inner surface. It is a set of graphite platelets wherein the mutual distance creates micropores (diameter < 2 nm), where the adsorption of pollutants on the surface of the activated carbon takes place (micropores constitute 90 to 95% of the adsorbent's total surface), mesopores (with a diameter of 2 to 50 nm) which secure the transport of the pollutant molecules into the internal area of carbon towards the micropores, and which also have a small adsorption capacity, and transport pores (macropores) with a diameter > 50 nm, which enable access of

the adsorbate molecules to the adsorbent's inner space; they have no adsorption properties. The quantity of micropores and transport pores determines the properties of the activated carbon and its suitability for the treatment of drinking water. The material the activated carbon is produced from is decisive for the "correct" micropores to transport pores ratio – black coal, coconut shells, wood, lignin, brown coal and others. Activated carbon made from black coal usually possesses a suitable ratio of micropores to transport pores, while in activated carbon made from coconut shells micropores predominate, and in activated carbon made from wood macropores predominate. The pore size, specific surface, and chemical reactivity of the surface determine the adsorption properties.

Activated carbon used in a powdered form is applied in the first water treatment stages, especially in surface waters when an emergency deterioration of the quality of the treated water may occur. Powdered activated carbon (PAC) is used only in emergency cases (prior to flocculation). Its disadvantage entails the adsorption also of substances which can be removed by coagulation, hence its adsorption capacity is more readily exhausted.

Granular activated carbon (GAC) is usually used in filters at the end of the water treatment process as the filtration medium of open or pressure filters with a grain size of 0.5–2 mm. Open filters are designed for a filtration rate of 5 to 10 m/h, pressure filters for up to 20 m/h. The activated carbon layer in open filters is 0.6 to 1.0 m, in closed filters 1 to 2 m, depending on the filtration rate. Activated carbon is layered in open and closed filters on a sand layer base of 30 to 40 cm. The activated carbon grain size should be 4 to 5 times the size of the efficient sand grain [23,24].

Filters filled with activated carbon are washed in the same way as conventional sand filters, i.e. by backflow of air and water. The shortest filtration cycle is approximately 14 days. About 5 to 10% of the original volume of activated carbon is consumed during the washing (by abrasion, washing out, chemical reaction). The capacity of the activated carbon is exhausted over the course of 1 to 3 years of continuous operation, depending on the quality of the water treated.

Pesticides are a diverse group of chemicals, with varying physical and chemical properties. Treatment efficacy depends on these physical and chemical characteristics (e.g. hydrophobicity, molecular weight, polarity, volatility, chemical nature), their reactivity towards different treatment processes and process control, such as solids retention time, temperature, pH value, and hydraulic retention time. Treatment processes can therefore achieve some level of removal.

Pesticides and their metabolites pose a potential risk of contamination of the environment, aquatic ecosystem and human health. Contamination of groundwater, surface water and soil by pesticides and herbicides is a serious problem today.

The aim of presented work is to compare the efficiency of removal of selected chlorinated pesticides (s-triazines) from the water by using the granulated activated carbon made by two producers (Cabot Corporation, Gryfskand, Poland).

2. Methods

Pesticides standard was purchased from company ALS Czech Republic in Prague, which also provided us with the sample vials and analysis of pesticides in samples. From the wide range of were chosen simazine, atrazine and terbutylazine. Granular activated carbon WG12 (Gryfskand, Poland) and Filtrasorb 400 (Cabot Corporation) was used for experiments. Filtrasorb F 400 was submitted by Jako Ltd. and WG12 by EnviPur Ltd. from Czech Republic. Basic properties of used materials are introduced in the Tab. 1.

Table 1. Properties of activated carbons WG12 a F400 [25,26]

PROPERTY	WG12	F400
Iodine number [mg/g]	min. 1000	min. 1050
Particle size [mm]	1.0–1.5	0.42–1.68
Specific surface area (BET) [m ² /g]	min. 1000	min. 1100
Operating density [g/cm ³]	450±30	425
Uniformity coefficient	max. 1.3	max. 1.9
Hardness [–]	min. 95	min. 95
Abrasion [–]	min. 85	min. 75
Moisture by weight [%]	max. 2	max. 2

Stock solution of selected chlorinated pesticides with initial concentration of approximately 0,5 µg/L was prepared by mixing 50 mL of the pesticide standards with 5 L of drinking water. This solution was then properly mixed and was used in the experiments. Experiments were performed in the Erlenmeyer's flasks with the initial volume of 400 mL model water. 400 mg of the adsorbent was added to the flasks. These flasks were then stirred for the duration of 4 hours

by using OHAUS Orbital Shaker at 400 rpm. During this time samples were taken from the flasks at specific times of 0, 30, 60, 120 and 240 minutes. The samples were taken to glass vials with 40 mL of volume, in which a preservation substance was put (0,32 ml 1% sodium thiosulfate). The vials were stored in a refrigerator and subsequently transferred to the ALS laboratory for analysis. The determination of pesticides was done by the HPLC method (US EPA 535 and 1694) with a direct inject of sample and by the method of internal standard.

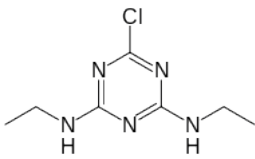
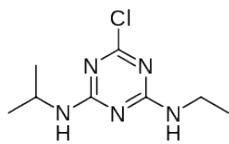
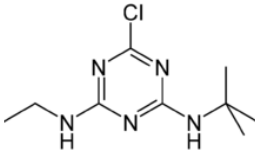
All three chemicals used in this work belong to the group of chlorinated triazine herbicides. Basic characteristics of selected herbicides are in Tab. 2. Atrazine is used for broadleaf weeds both before and after they sprout. It is also used on some grassy weeds. There are over 300 products that contain atrazine. In many countries, after application in agricultural areas, atrazine has been found in groundwater at levels of 0.01–6 µg/litre. It has also been detected in drinking water in several countries at levels of 0.01–5 µg/litre. Atrazine is broken down slowly by water, sunlight, and microorganisms. Without oxygen, atrazine has a half-life of around 578 days in water and 168 days in water exposed to sunlight. Atrazine has a low to moderate solubility in water. It does not bind well to soil, from this reason it has a high potential to reach ground and surface water. Atrazine is classified as a potential carcinogen by the International Agency for Research on Cancer (IARC). Studies shows, that atrazine is an endocrine disruptor, which can changed the natural hormonal system in animals [27,28].

Simazine is a herbicide used to control broad-leaved and grass weeds in artichokes, asparagus, berries, broad beans, citrus fruits, coffee, cocoa, hops, maize, oil palms, olives, orchards, ornamentals, sugar-cane, tea, tree nurseries, turf, and vineyards, as well as in non-crop areas. Its half-life in soil has been reported as 46–174 days. Typical levels of 1–2 µg/litre have been reported in groundwater in the USA. Contamination of groundwater by simazine has also been reported in Italy and Germany. IARC has classified simazine in Group 3 [29].

Terbutylazine (TBA) is commonly used as an herbicide (an algicide, a microbicide) to control broad-leaved weeds and grass and prevent non-desirable grow of algae, fungi and bacteria in many agricultural applications. TBA is an herbicide that belongs to the chloro-triazine family. In plants, it acts as a powerful inhibitor of photosynthesis. The substance is taken up through both roots and leaves and is distributed throughout the plant after being taken up through the roots. This enables it to be used in both pre- and post-emergence treatment. TBA is a selective herbicide for weed control in maize, sorghum, potatoes, peas, sugar cane, vines, fruit trees, citrus, coffee, oil palm, cocoa, olives, rubber, asparagus, and also at treatment of roads, industrial areas and railways. TBA has a very high soil persistence, it can be present up to 17 months after the field treatments [30,31].

Terbutylazine is used as a substitute for atrazine, which has been banned in EU countries. It has lower water solubility (8.5 vs 33.0 mg/L) and lower persistence in soil. The half-life of terbutylazine in the soil has been reported to vary between 5 and 116 days depending on the soil characteristics and temperature. In 2011, the European Food Safety Authority (EFSA) provided an extensive peer review of data concerning the environmental behavior and fate, ecotoxicology and mammalian toxicology, and risk assessment of terbutylazine [32]. Based on these conclusions the European Commission approved the inclusion of terbutylazine in Annex I of Council Directive 91/414/EEC and its use only as a herbicide until December 2021 [33].

Table 2. Basic characteristics of selected chlorinated pesticides [34–36]

Chlorinated pesticide	Chemical formula	CAS	IUPAC	Molecular formula	Solubility in water
Simazine		122-34-9	6-chloro-2-N,4-N-diethyl-1,3,5-triazine-2,4-diamine	C ₇ H ₁₂ ClN ₅	6.2 [mg/L]
Atrazine		1912-24-9	6-chloro-4-N-ethyl-2-N-propan-2-yl-1,3,5-triazine-2,4-diamine	C ₈ H ₁₄ ClN ₅	33.0 [mg/L]
Terbutylazine		5915-41-3	2-N-tert-butyl-6-chloro-4-N-ethyl-1,3,5-triazine-2,4-diamine	C ₉ H ₁₆ ClN ₅	8.5 [mg/L]

3. Results and discussion

The efficiency of pesticides removal from the water by using the sorption materials Filtrasorb 400 and WG12 was observed at the pH 7,6, laboratory temperature (22–23°C) and initial concentration of pesticides of 0,5 µg/L. The time of the contact of water with the sorbent was 30–240 minutes. Results of the adsorption efficiency and the immediate adsorption capacity for sorption materials Filtrasorb 400 and WG12 are shown in figures 2 and 3.

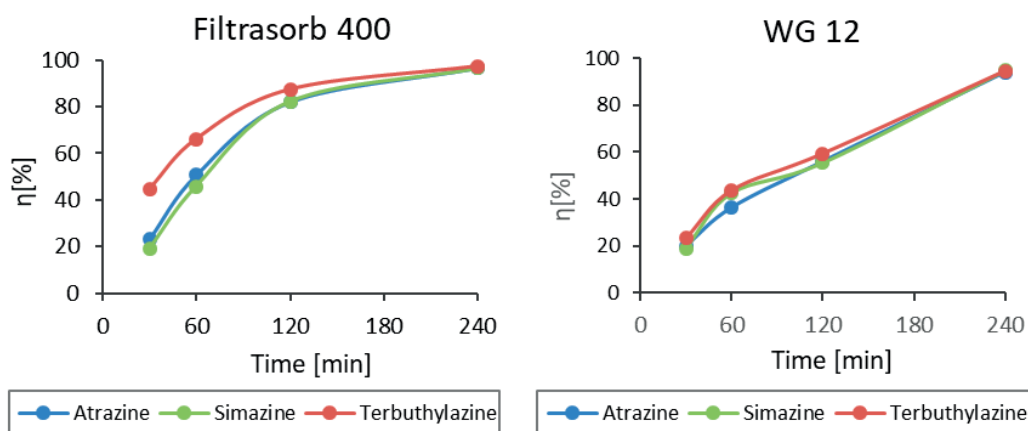


Figure 2. Adsorption efficiency [%] of activated carbon for selected chlorinated pesticides removal from the water in relation with the contact time

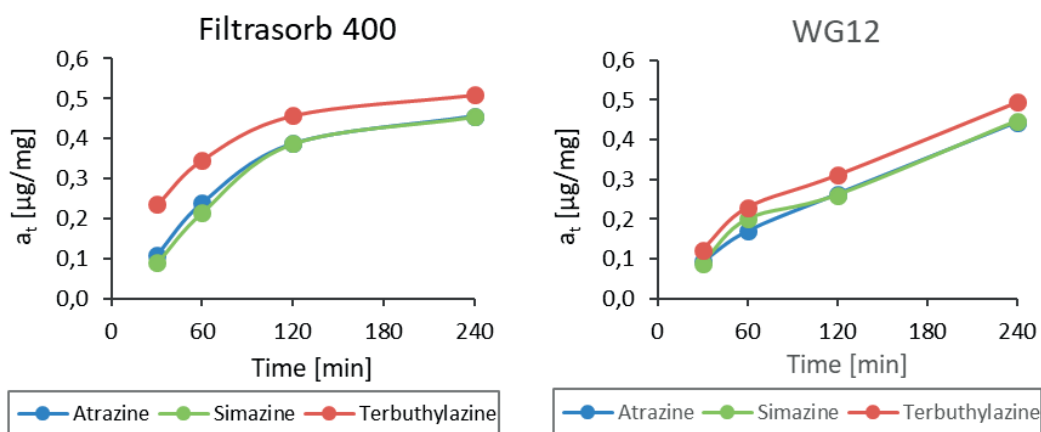


Figure 3. Adsorption capacity [µg/mg] of activated carbon for selected chlorinated pesticides and various contact times

The adsorption efficiency (in %) and immediate adsorption capacity (in µg/g) of activated carbons F400 and WG12 were calculated for the individual chlorinated pesticides depending on the water – material contact time on the base of the measured concentrations of the individual organic compounds. Based on the defined values, the efficiency of chlorinated pesticides removal η [%] and immediate adsorption capacity of selected sorption materials – at [µg/g] were calculated.

$$\eta = \frac{(c_0 - c_m) \cdot 100}{c_0} \text{ [%]} \quad (1)$$

$$a_t = \frac{(c_0 - c_m) \cdot V}{m} \text{ [µg/g]} \quad (2)$$

where η is the adsorption efficiency in %, a_t is the immediate adsorption capacity in µg/g, c_0 or c_m are the concentration of pesticides before and after the adsorption of pesticide at the time t [µg/L], V is the volume of water solution of 0.4 litre, m is the weight of sorption material, 0.4 g.

As we can see from the figures 1 and 2, the removal efficiencies for both types of activated carbon reached over 90%, which can be considered a very effective adsorption process. However, adsorption on the granular activated carbon Filtrasorb 400 took place with higher efficiency than on the granular activated carbon WG12. For the adsorption of chlorinated pesticides with the Filtrasorb 400 adsorption material, we can see that after 2 hours of adsorption, more than 80% removal efficiency of the monitored pesticides from the model water was achieved. In contrast to the adsorption material WG12, where only a maximum of 60% removal efficiency occurred after 2 hours of adsorption. For the

triazine group of pesticides, Terbutylazine was adsorbed best on used granular activated carbon F400 and WG12 with an efficiency removal from water of 97.3% or 94.5% respectively.

The adsorption capacity materials Filtrasorb 400 and WG12 was for Terbutylazine between 0.235–0.510 µg/mg or 0,122–0.495 µg/mg respectively, adsorption capacities for Atrazine were in range 0,109–0,456 µg/mg for sorbent F400 and 0,094–0,444 µg/mg for WG12. The Simazine adsorption capacity were between 0,090–0.454 µg/mg for sorbent F400 and 0,089–0.447 µg/mg for WG12. Adsorption capacity depend on the contact time of water with the material.

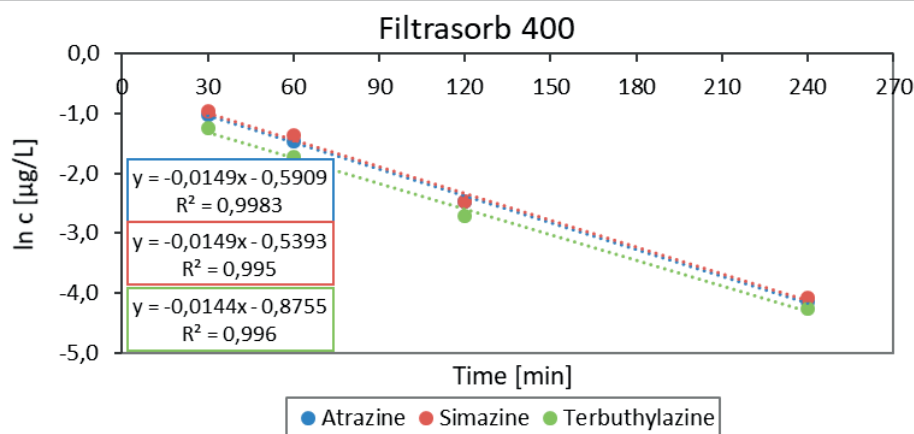


Figure 4. Kinetic equation of the 1st order for the adsorption of Atrazine, Simazine and Terbutylazine on granulated activated carbon Filtrasorb 400

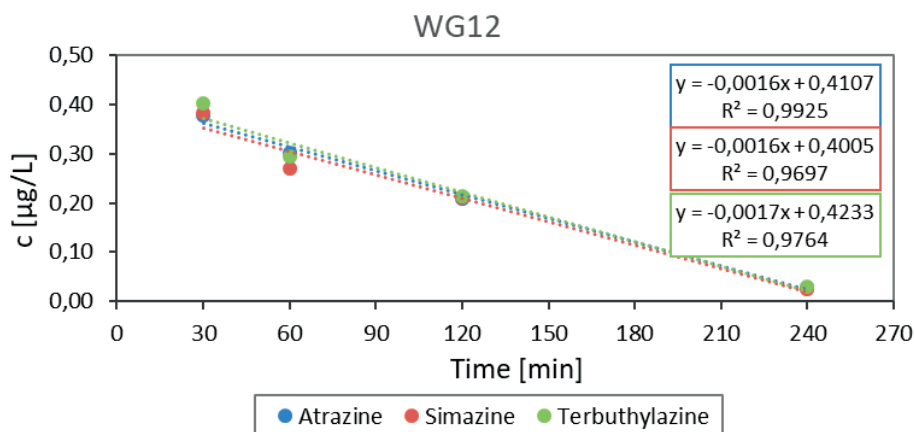


Figure 5. Kinetic equation of the 0th order for the adsorption of Atrazine, Simazine and Terbutylazine on granulated activated carbon WG12

Reaction kinetics was studied for the adsorption of used chlorinated pesticides. Reaction kinetics of 0th, 1st, 2nd and 3rd order were studied. In figure 4 to 5 are illustrated calculated values of kinetic reactions in linearised shape ($y = a \cdot x + b$) for used activated carbons.

As the figures 4 and 5 presents, 0th order kinetics has been shown to best describe adsorption process for adsorbent WG12. For the adsorbent F400, the 1st order kinetics is the best describe the process of adsorption. R² factor represents how accurate and precise kinetic equation is. The closer the number is to 1, the better kinetic equation describes the process. These equations are acquired by linearization of the kinetic equations.

4. Conclusion

The chlorinated pesticides (s-triazines) are among the most commonly used herbicides worldwide, which contaminate aquatic environments. This article studies adsorption of chlorinated s-triazines from water on the two granular activated carbons Filtrasorb 400 and WG12.

Based on the obtained data, we can conclude that the adsorption of pesticides is effective for both types of adsorption material. Nevertheless, it is still true that certain substances are better adsorbed on a specific type of adsorption material.

The efficiency and adsorption capacity of the adsorption materials used was different. Filtrasorb 400 proved to be a better sorption material than WG12, the efficiency for Terbutylazine removal ranged between 44.8–97.3%, the efficiency

of WG12 ranged between 23.2–94.5%, depending on the contact time of water with the material. Terbutylazine was adsorbed best on used granular activated carbon F400 and WG12, Atrazine and Simazine have a slightly lower removal efficiency from water with the studied sorbent materials. The efficiency for Atrazine removal for F400 ranged between 23.0–96.6%, the efficiency of WG12 ranged between 19.8–94.1%, the Simazine removal efficiency was 19.1–96.4% for materials F400, the efficiency of WG12 ranged between 18.9–94.9%

The adsorption efficiency (%) and immediate adsorption capacity ($\mu\text{g}/\text{mg}$) for the individual pesticides depending on the water – material contact time, pH value of water, and concentrations of the individual pesticides in water.

Kinetic model parameters were adjusted to find the best values fitting experimental data with simulation results. 1st order kinetics has been shown to best describe adsorption process for adsorbent Filtrasorb 400 and 0th order kinetics for adsorbent WG12.

Acknowledgements

This paper was produced thanks to support from the experiments were performed with financial support from the APVV-18-0205, VEGA 1/0825/21 and VEGA 1/0737/19 Projects.

References:

- [1] <https://www.cepta.sk/index.php/sk/pesticity-a-potraviny>.
- [2] <https://www.safewater.org/fact-sheets-1/2017/1/23/pesticides>
- [3] <https://www.eea.europa.eu/ims/pesticides-in-rivers-lakes-and>
- [4] Srivastava, M., Malin B., Srivastava, A., Yadav, A., Banger, A.: Role of Pesticides in Water Pollution. *Agri Sci Food Res.* 13(3), 1000495, 2022.
- [5] Agrawal, A., Pandey, R., Sharma, B.: Water Pollution with Special Reference to Pesticide Contamination in India, *Journal of Water Resource and Protection*, 2(5), pp. 432–448, 2010.
- [6] Akash, S., Sivaprakash, B., Rajamohan, N., Pandiyan, C.M., Vo, D.-V.N.: Pesticide pollutants in the environment – A critical review on remediation techniques, mechanism and toxicological impact. *Chemosphere*, 301, 134754, 2022.
- [7] https://water-resources.sazp.sk/wp-content/uploads/2019/06/20_PATSCOVA_Pesticidy_DusicnanyVPodzemnychVodach_WRPConference2019_Bratislava.pdf.
- [8] Rosenfeld P., Feng L. 2011 Risk of Hazardous Wastes. Elsevier Inc., USA, 472 p.
- [9] WHO 2010 The WHO Recommended Classification of Pesticides by Hazard: Guidelines to Classification 2009. WHO Library Cataloguing-in-Publication Data. World Health Organization Geneva, 81 p.
- [10] <https://www.epi.sk/zz/2017-247>.
- [11] Fenoll J., Hellín P., Martínez C. M., Flores P., Navaro S.: 2011 Determination of 48 pesticides and their main metabolites in water samples by employing sonication and liquid chromatography-tandem mass spectrometry. *Talanta* 85, 975–982.
- [12] Krutz L.J., Senseman S.A., Sciumbato A.S.: 2003 Solid-phase microextraction for herbicide determination in environmental samples – Review. *J. Chromatogr. A.* 999, 103–121.
- [13] Barchańska, H., Baranowska, I.: Procedures for Analysis of Atrazine and Simazine in Environmental Matrices. *Reviews of environmental contamination and toxicology.* 200, pp. 53–84, 2009.
- [14] Crittenden J. C., Trussell R. R., Hand D. W., Howe K., Tchobanoglous G.: *Water Treatment: Principles and Design.* 3rd ed. John Wiley and Sons, New Jersey 2012, 1920 p.
- [15] Ormad M.P., Miguel N., Claver A., Matesanz J. M., Ovelleiro J. L.: Pesticides removal in the process of drinking water production. *Chemosphere* 71, 97–106, 2008.
- [16] Cosgrove S., Jefferson B., Jarvis, P.: Pesticide removal from drinking water sources by adsorption: a review. *Environ. Technol. Rev.* 8, 1–24, 2019.
- [17] Areerachakul N., Vigneswaran S., Ngo H.H., Kandasamy J. Granular activated carbon (GAC) adsorption photocatalysis hybrid system in the removal of herbicide from water. *Separation and Purification Technology* vol. 55, pp. 206-211, 2007.
- [18] Nam S.W., Choi D.-J., Kim S. K., Her N., Zoh K.-D.: Adsorption characteristics of selected hydrophilic and hydrophobic micropollutants in water using activated carbon. *Journal of Hazardous Materials* vol. 270, pp. 144–152, 2014.

- [19] Suo F., Liu X., Li Ch., Yuan M., Zhang B., Wang J., Ma Y., Lai Z., Ji M.: Mesoporous activated carbon from starch for superior rapid pesticides removal. *International Journal of biological Macromolecules* vol 121, pp. 806–813, 2019.
- [20] Corwin C. J., Summers R. S. Controlling trace organic contaminants with GAC adsorption. *Journal of AWWA*, vol. 104, pp. E36- E47, 2012.
- [21] Kyriakopoulos G., Doulia D. Adsorption of Pesticides on Carbonaceous and Polymeric Materials from Aqueous Solutions: A Review. *Separation & Purification Reviews*, 35, pp. 97–191, 2006.
- [22] Katsigiannis, A., Noutsopoulos, C., Mantziaras, J., Gioldasi, M.: “Removal of emerging pollutants through granular activated carbon,” *Chem. Eng. J.* vol. 280, pp. 49–57, 2015.
- [23] Kopecký, J. Aktivní uhlí – technologie pro úpravu pitných a bazénových vod. *Vodní hospodářství* 53 (7), pp. 185–187, 2003.
- [24] Beneš, O., Bartoš, L., Hušková R. Aktivní uhlí a možnosti odstraňování mikropolutantů. *SOVAK Časopis oboru vodovodů a kanalizací*, č. 7–8, pp. 29/241–32/244, 2012.
- [25] Envi-pur, granulované aktivní uhlí [Online] 2022. Available at: [doc_108_granulovane_aktivni_uhli_wg12_cz.pdf](#) (in Czech).
- [26] Calgon Carbon, FILTRASORB® 400 Granular Activated Carbon [Online] 2022. Available at: <https://www.calgoncarbon.com/app/uploads/DS-FILTRA40019-EIN-E1.pdf>.
- [27] WHO. Atrazine in Drinking-water. WHO Guidelines for Drinking-water Quality, WHO/SDE/WSH/03.04/32, pp. 1–5, 2003.
- [28] <http://npic.orst.edu/factsheets/atrazine.pdf>.
- [29] WHO. Simazine in Drinking-water. WHO Guidelines for Drinking-water Quality, WHO/SDE/WSH/03.04/42, pp. 1–9, 2003.
- [30] US EPA. Terbutylazine. Prevention, Pesticides and Toxic Substances, EPA-738-F-95-006A, 1995.
- [31] Meseldžija, M., Dudić, M. (2018). Terbutylazine application with herbicides of different mode of action in maize crop. In: *Book of Proceedings. The IX International Scientific Agricultural Symposium “Agrosym 2018”, Jahorina October 04-07,2018, University of East Sarajevo, Faculty of Agriculture, Republic of Srpska, Bosnia*, pp. 1019–1025, 2018. [online].
- [32] European Food Safety Authority (EFSA). Peer review of the pesticide risk assessment for the active substance terbutylazine in light of confirmatory data submitted. *EFSA Journal* 15(6):4868, 2017. doi: 10.2903/j.efs.2017.4868 (Accessed 13 June 2018).
- [33] Commission Implementing Regulation (EU) No. 540/2011, 2011. Implementing Regulation (EC) No 1107/2009 of the European Parliament and of the Council as regards the list of approved active substances. Off. J. Eur. Union. <http://extwprlegs1.fao.org/docs/pdf/eur103357.pdf>. (Accessed 18 June 2018).
- [34] <https://pubchem.ncbi.nlm.nih.gov/compound/Atrazine> [online]
- [35] <https://pubchem.ncbi.nlm.nih.gov/compound/Terbutylazine> [online]
- [36] <https://pubchem.ncbi.nlm.nih.gov/compound/Simazine> [online]

III Sanitary Engineering and Sustainable Water Use

THE INFLUENCE OF DIFFERENT PROCESS PARAMETERS ON THE EFFICIENCY OF ORGANIC LOAD REMOVAL FROM OILY WASTEWATER USING ELECTROCHEMICAL TREATMENT

DRAŽEN VOUK¹, MORANA DRUŠKOVIĆ², SARA BANOVEC¹, DAJANA KUČIĆ GRGIĆ³

¹ University of Zagreb, Faculty of Civil Engineering; Croatia
e-mail: drazen.vouk@grad.unizg.hr, sbanovec@student.grad.hr

² Indeloop d.o.o.; Croatia
e-mail: morana.druskovic@dok-ing.hr

³ University of Zagreb, Faculty of Chemical Engineering and Technology; Croatia
e-mail: dkucic@fkit.hr

Abstract

During the treatment process of exhaust gasses produced by gasification of sewage sludge oily wastewater is generated which contains high concentrations of organic load and solid particles created by the contact of the contaminated gas with the liquid through which it passes during its treatment. Sewage sludge was generated as a by-product at the wastewater treatment plant (WWTP) in Zagreb (Croatia). For the purpose of this paper oily wastewater was further treated by hybrid electrochemical process. Applied electrochemical treatment is based on the flow of electric current through electrodes immersed in wastewater. In the process, metals are released from the electrodes and form flocs that coagulate the pollutants present in the wastewater and produce sludge that settles down in the reactor during the sedimentation phase. This research is focused on the influence of different process parameters such as electrode materials (stainless steel, iron, aluminum), pH of raw wastewater, and current on the efficiency of the treatment process. The objective was to eliminate chemical oxygen demand (COD) and total hydrocarbons (mineral oils) from wastewater below the limits prescribed for discharge to the environment or public sewer system. The laboratory tests were carried out in batches with a wastewater volume of 10 liters in one batch. The wastewater is characterized by a light brown color, fine soot particles, unpleasant odor, slightly alkaline pH (8.95) and high levels of COD (790 mg/L) and total hydrocarbons (14.20 mg/L). The experimental results show that the hybrid electrochemical treatment process that combines electrooxidation and electrocoagulation processes effectively reduces the concentration of COD and total hydrocarbons from wastewater generated during the treatment process of exhaust gas from sewage sludge gasification unit, proving the application of this process for the treatment of this type of oily wastewater.

Keywords: oily wastewater, exhaust gas treatment, electrochemical treatment, electrodes, COD, hydrocarbons, mineral oil.

1. Introduction

Wastewater is all potentially polluted industrial, sanitary, storm, and other water. Legal entities and individuals may discharge wastewater within prescribed emission limits. Water for human consumption is all water, either in its original state or after treatment (conditioning), intended for drinking, cooking, food preparation, or other domestic purposes, regardless of its origin and whether it comes from the public water supply system, from cisterns, or from bottles or water containers [1]. With the growth of population, water consumption is also increasing, so it is necessary to ensure sufficient quantity and quality of water. This also becomes one of the biggest problems of the present century. The solution to this problem may lie in wastewater treatment. The quality of drinking water in the future depends mainly on how seriously the laws and regulations for the protection of water are observed in order to preserve water resources [2].

Any composition of polluted water has a high content of colloidal particles. Colloidal particles are particles of small dimensions that are not affected by gravity and therefore do not settle. The removal of colloidal particles from water can be achieved by the processes of coagulation and flocculation, which are performed by adding so-called flocculants. Flocculants that form larger agglomerates – flocs – with colloiddally dispersed particles, which can then be removed from the water by sedimentation, flotation or filtration. To destabilize the colloidal suspension, the electrostatic repulsion between the particles must first be reduced, i.e., the charges on the surface of the particles must be neutralized. This process is called coagulation and is achieved by the addition of multivalent cations, which reduce the zeta potential by binding to colloidal particles. The coagulation process should be carried out as quickly as possible and with vigorous

stirring to distribute the added multivalent cations evenly throughout the suspension before hydroxide precipitates form during the flocculation process [3].

In this work, an experimental study was carried out to test the efficiency of electrocoagulation as an electrochemical process for the treatment of oily wastewater of mineral origin. The applied technological process is based on the use of two types of electrodes (iron and aluminum). In this study, the influence of various technological parameters on the efficiency of treatment of oily wastewater was investigated, i.e. the removal of organic matter expressed by chemical oxygen demand (COD) indicators. At the same time, the influence of different reaction times on individual electrodes (Fe and Al) and the influence of different pH values in the raw wastewater were studied.

1.1. Oily wastewater

Wastewater containing oil are mainly generated in oil processing, petrochemical, metallurgical and mechanical industries, processing of various types of wastes, and maritime transport. Oily wastewater is a mixture of wastewater and oil in varying proportions. In such wastewater, fats and oils are often classified as hazardous wastes and must be removed before the water is reused or disposed in the environment [4], [5], [6], [7]. Oil includes the following substances: light and heavy hydrocarbons, oil, tar, grease, wax, soaps, and others. It is estimated that industrial production of 1 t of oil for refineries generates 0,5–1 t of wastewater [8].

Parameters that characterize potential pollution of refinery and petrochemical wastewater include general variables that also apply to municipal wastewater and variables that apply specifically to the oil and petrochemical industries (hydrocarbons, sulfur compounds, etc.). General characteristics that also apply to municipal wastewater include: Suspended solids (SS), biological oxygen demand (BOD₅), COD and ammonium (NH₄⁺-N). Parameters characteristic of pollution control in the oil industry are hydrocarbons, phenols, sulfides, nitrogen compounds, heavy metals, etc. [9]. COD is the mass concentration of oxygen required to oxidize substances dissolved and suspended in 1 liter of water under certain conditions. The specified concentration is expressed in milligrams of oxygen per liter of wastewater (mg O₂/L). The determination method COD is based on the determination of the proportion of oxygen consumed for the oxidation of a substance in water, using the reduction of a bichromate solution under special conditions [10].

2. Description of the electrocoagulation process

In the last decade, research on the application of electrochemical methods in the treatment of drinking water and wastewater has intensified [2]. The research deals with different types of wastewater: domestic wastewater, industrial wastewater, with heavy metals, organic and inorganic contaminants, dyes, underground contaminated water, leachate, etc. For each wastewater, the effect of electrochemical processes (EC), independently or in combination with advanced oxidation processes (AOP), on its composition is observed, as well as the percentage of pollution that can be removed to make the water safe for use or discharge to the environment, and whether it is within the above regulations for wastewater emission limits [11]. The following water quality indicators are most commonly observed: chemical oxygen consumption (COD), total suspended solids (TSS), total dissolved solids (TDS), total nitrogen (TN), total phosphorus (TP), mineral oils, heavy metals such as copper, nickel, zinc, manganese, etc.

Electrochemical processes involve applying an electric field to one or more groups of electrodes, with or without the use of semipermeable membranes or additional electrolytes, to remove inorganic, organic, and microbiological contaminants in water. Depending on the concept of the system, a distinction is made between electrocoagulation, electroflotation, electrooxidation and electrodialysis. Electrochemical processes are not distinguished by the treatment mechanism, but by the fact that the substances required to carry out the process are generated in situ in a reaction vessel designed as an electrochemical cell [2].

The essence of electrocoagulation is that in the reaction vessel (electrochemical reactor) under the influence of the electric field, cations (e.g. Fe²⁺, Al³⁺), which are necessary for the process of coagulation of the pollutants present in the water, are released from the anodes and simultaneously oxidize the water to oxygen and H⁺ ions. At the same time, the water is reduced at the cathode, producing hydrogen and OH⁻ ions. Stable hydroxides of iron and aluminum are formed by the reaction of cations and OH⁻ ions. Suspended and dissolved impurities are removed by coagulation with electrochemically generated iron and aluminum cations, by coprecipitation with iron and aluminum hydroxides, and by precipitation of the corresponding metal hydroxides [2].

The change in pH is much greater at the beginning of the EC experiment than at the end, where an equilibrium state is normally reached. After the EC treatment, the pH of the wastewater increases due to the acidic influence, but decreases due to the alkaline influence. In previous studies, an increase in solution pH was also observed when Fe anodes were used compared to Al anodes. It is believed that the decrease in solution pH is due to the formation of aluminate (Al(OH)₄), which consumes alkalinity [13], [14], [15], [16], [17], [18].

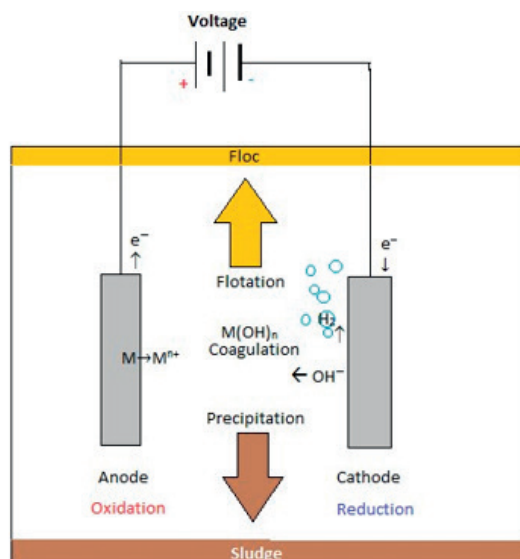


Figure 1. Scheme of a bipolar cell with direct and indirect anodic oxidation processes [12]

One of the most important factors affecting the formation of metal complexes is the pH of the solution and the anion concentration. Metal cations undergo a series of hydrolysis reactions and various forms of charged multidimensional hydroxide particles Al^{3+} or Fe^{3+} may be present in the solution. Fe^{2+} is a very weak coagulant and therefore in most cases is oxidized to the Fe^{3+} form during the coagulation process to ensure greater coagulation efficiency. Neutral amorphous metal hydroxides, $\text{Al}(\text{OH})_3$ and $\text{Fe}(\text{OH})_3$, are poorly soluble species. The distribution of mononuclear metal species can be illustrated by the solubility diagrams in Figure 2. At lower pH values, the positive charge of the Al and Fe species is greater and the primary mechanism of coagulation is the reduction of surface charge. At higher pH values, the dominant Al and Fe species are larger, less charged, and tend to form polymers, so the primary mechanisms of coagulation are adsorption, mutual bridging, and final entanglement in the precipitate. Therefore, pH is a key parameter that determines how the coagulant destabilizes colloidal suspensions. It was found that during the coagulation process, the most effective pH range is 5.0–6.5 for Al and 4.5–6 for Fe [19], [20].

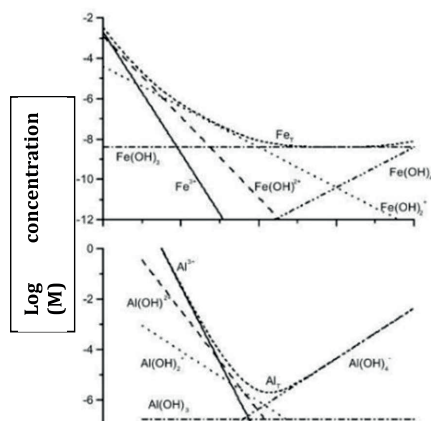


Figure 2. Concentrations of soluble monomeric hydrolysis products of Fe^{3+} and Al^{3+} in equilibrium with amorphous hydroxides at zero ionic strength and 25° [19]

The influence of the pH of the water or wastewater on the coagulation process is shown both in the use of electricity and in the effect of dissolution of metal hydroxides. In a reactor with an aluminum electrode, the electricity consumption is high in both acidic and alkaline environments, while the treatment effect in a neutral environment depends on the nature of the impurities.

A characteristic element affecting electrocoagulation is also current density. It is known that the amount of adsorbent (floc) produced depends mainly on the electrode material, time and current density. Faraday's law of electrolysis provides a theoretical estimate of the amount of dissolved Fe^{2+} or Al^{3+} ions produced by the operation of the anode. The law defines the relationship between the strength of the current (I) and the electrolytically generated mass (m) in the electrochemical cell (1):

$$m = \phi \frac{It}{ZF} M \quad (1)$$

where: m is the mass of the metal (g), t is the working time of the electrode (h), I is the current (A), M is the molecular mass for Al or Fe (g/mol), z is the number of electrons transferred (2 or 3), F is Faraday's constant (96.487 C/mol), the correction coefficient of the dissolution efficiency. It should be noted that the resolution efficiency can be higher than 100%, i.e. higher than the value determined by Faraday's law.

The size of the electrocoagulation device is also determined by the current density. This relationship is inversely proportional. High current density applications require smaller device dimensions. In addition, at high current densities, most of the energy is converted to heat energy, greater energy losses occur, and the water being treated is heated, which is considered a negative phenomenon. The recommended current density for prolonged operation without extended interruptions is in the range of 20 to 25 A/m². However, compared to the scientific research results published so far, there is still a lot of room for further research and new findings in this area. The choice of current density also depends on the pH, temperature and speed of water flow through the device. The characteristics of the treated water depend on the amount of ions produced (mg) or the amount of electrification, the product of current and time (Ah).

The most commonly used materials for the production of electrodes are aluminum or iron in the form of plates or compact waste material of the same elements. Regardless of whether waste material is used, applied to the electrode supports or the plates, care should be taken to prevent sludge from settling between the parts that make up the electrode. Therefore, it is necessary to rinse the electrodes.

The effect of the electrocoagulation process itself can be influenced by the arrangement of the electrodes as well as the distance between them. The arrangement of the electrodes can be simple, if it consists of one anode and one cathode, or complex, if it consists of several anodes and cathodes within the electrocoagulation device. The complex arrangement of electrodes can be classified as either monopolar (Figure 3 a) or bipolar (Figure 3 b).

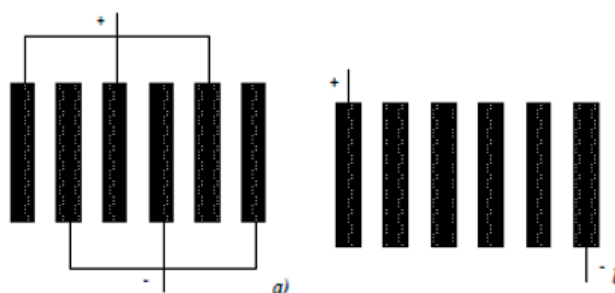


Figure 3. Electrode arrangement in a thin cell: a) monopolar electrode arrangement; b) bipolar arrangement of electrodes [14]

In addition to rectangular electrodes, round and cylindrical electrodes are also in use and can be placed either horizontally or vertically. Although the use of horizontal electrodes is rare in practice, such an arrangement of electrodes allows higher efficiency of mixing in the reactor of the electrocoagulation device [14].

3. Methods

3.1. Oily wastewater of mineral origin

The oily wastewater was taken from a wet scrubber, i.e. from a flue gas cleaning system from the process of a thermal treatment of sewage sludge (gasification) produced in wastewater treatment plants (WWTP). Within the framework of the scientific research project BRAVOBRICK, carried out at the University of Zagreb, Faculty of Civil Engineering, a certain amount of sewage sludge generated at WWTP Zagreb was thermally treated in a pilot plant for sewage sludge gasification. Gasification produces waste gases that must be cleaned before they are released into the atmosphere. In addition to the pilot plant for sludge gasification, a pilot plant for flue gas cleaning was installed as a wet scrubber. Wastewater from flue gas cleaning plants is referred to as oily wastewater of mineral origin, which must be treated in accordance with regulatory requirements before discharge to the environment or public sewer [11]. The collected oily wastewaters were treated in the hydrotechnical laboratory at the Faculty of Civil Engineering, University of Zagreb, as part of this research.

3.2. Experimental research

In this study, 24 experimental tests were performed on the treatment of oily wastewater by electrocoagulation, which belongs to the group of electrochemical methods. Iron or aluminum electrodes were placed vertically on the bottom of the reaction vessel, into which 10 liters of wastewater were placed for each test.

The first part of the experiment starts at the iron electrode, as the first phase of the applied electrocoagulation process. After the completed cycle (reaction) on the iron electrode for different durations of 10, 15 or 20 minutes, depending on

the experiment, an aluminum electrode is introduced into the same sample, whose effectiveness was also tested with different durations of 10, 15 or 20 minutes. The oily water in the tank is continuously mixed with electrochemically generated gases (H_2 , O_2) that transport impurities to the surface and form a thick foam, after which electroflotation takes place. In addition, the suspension was stirred mechanically with a wooden stick and air bubbles with a pump. In order to optimize the process, the effectiveness of the electrode type (iron, aluminum), contact time (10, 15 and 20 minutes) and current intensity (15–60 A) were observed, as well as the influence of different pH values in the raw wastewater. During the experiment, the input values of each water quality indicator and their values were measured during and at the end of the experiment. The values of pH, dissolved oxygen (DO), electrical conductivity (EC), dissolved solids (TDS), temperature (T) and chemical oxygen consumption (COD) were monitored. In each experiment, the initial parameters of the incoming oily wastewater were observed. After the initial values were determined, HNO_3 and $NaOH$ are added to lower or raise the pH of the raw wastewater (within the pH range of 4 to 9). In this way, an attempt was made to study the influence of different pH values in the raw wastewater on the treatment efficiency.

During the electrocoagulation process, i.e., operation of the electrodes, the current intensity was controlled by a 900 W laboratory rectifier (MC Power LBN-1990) with a current intensity range of 0 to 60 [A]. Multimeter (multiparameter) HI98194 pH / EC / DO (manufacturer HANNA) was used to measure certain water quality indicators, such as: Water temperature, pH (resolution and accuracy: 0.001 pH, ± 0.002 pH), DO (resolution and accuracy: 0.01 mg/L, ± 0.2 mg/L), EC (resolution and accuracy: 0.05% FS & $\pm 1\%$ FS + 1 LSD) and TDS. Spectrophotometer The heating block NANOCOLOR VARIO C2 (manufactured by Macherey Nagel) was used to determine the COD values. The reagents used are NANOCOLOR COD HR 1500 (for determination of COD in the range 20–1500 mg/L O_2) and NANOCOLOR COD 600 (for determination of COD in the range 50–600 mg/L O_2).

4. Results and discussion

The values of physical and chemical indicators determined in the raw wastewater from the wet scrubber for flue gas cleaning and in the wastewater after the cleaning process EC, as well as the permissible upper limit prescribed by Croatia regulation, are listed in Table 1. In each gasification test 10-20 kg of sludge were processed, therefore the incoming wastewater streams are different. The organic load values are not as high because a smaller amount of waste sludge was processed. The load concentrations depend on the way the process was performed during gasification and the amount of input material (sludge) processed. Wastewater containing oil is characterized by a very intense odor and a slightly alkaline pH of about 8.8. The wastewater contains soot particles that settle on the bottom of the tank over time.

Table 1. Physico-chemical parameters determined in raw water and EC treated oily water for each parameter and upper permissible limit prescribed by Croatia regulation (UPL_{cro})

PARAMETER	RAW	AFTER EC PROCESS	UPL_{cro}
PH	7.4–8.8	8,4	6.5–9.5
DO (PPM)	0.3–3.1	0,84	–
EC (MS/CM)	1,246–7,330	2,995	2.5
TDS (PPM)	363–3,637	1,420	–
KPK (MG/L)	310–688	332	700
T (°C)	22.8–28.1	31.5	40

Figure 4 shows the efficiency of removal of COD from oily wastewater at pH 9 to pH 4 for different current durations at the electrodes. From the graphical representation, it can be seen that the efficiency initially increases with increasing duration at the electrodes.

Figure 4a shows the efficiency of removal of COD from oily wastewater at pH 9 for different reaction durations at the electrodes. The most efficient COD removal was achieved with 20 minutes of current duration at the electrodes. It is necessary to perform further experiments in future research with longer reaction times at the electrodes to determine the further behavior of the efficiency.

Figure 4b shows the efficiency of removal of COD from oily wastewater at pH 8 for different reaction durations at the electrodes. An efficiency of 50% is achieved with reaction times of 15 minutes at the iron electrode and 15 minutes at the aluminum electrode. A daily increase in time leads to a decrease in efficiency to 20%.

The efficiency of COD removal at pH 7 is shown in Figure 4c. The efficiency increases with increasing duration of the reaction at the electrodes. The efficiency of removal of COD at 10 minutes on iron and aluminum electrodes is 15%, and with increase in time to 15 minutes for iron and aluminum electrodes, an efficiency of 50% is achieved.

With further increase in time to 20 minutes, the efficiency drops to 16%. It is still necessary to test times of more than 20 minutes of reaction time for both electrodes to see if even higher efficiency can be achieved.

Figure 4d shows the effectiveness of COD removal at pH 6 and different reaction times. From the graphical representation, it can be seen that the efficiency increases with increasing duration of the reactions at the electrodes. The highest efficiency was obtained at a reaction time of 15 minutes for the iron and aluminum electrodes, 52%. At a reaction time of 20 minutes for the iron and aluminum electrodes, the efficiency drops to 11%.

The effectiveness of removing COD at a pH 5 is shown in Figure 4e. From the graphical representation, it can be seen that the highest efficiency of 26% was obtained at a reaction time of 15 minutes for iron and aluminum electrodes. When the reaction time is increased to 20 minutes for iron and aluminum electrodes, the efficiency reaches 23%.

Figure 4f shows the efficiency for COD at pH 4. The highest efficiency of 19% was obtained with a reaction time of 15 minutes for the iron and aluminum electrodes. With further increase in time, the efficiency drops to 6%.

From Figure 4 it can be seen that the highest efficiencies were obtained with reaction times on iron and aluminum electrodes of 15 minutes.

Figure 5 shows the efficiencies of COD removal at different pH values from 4 to 9. The highest COD efficiencies were obtained at pH 6, 7 and 8, namely 52%, 50% and 49%.

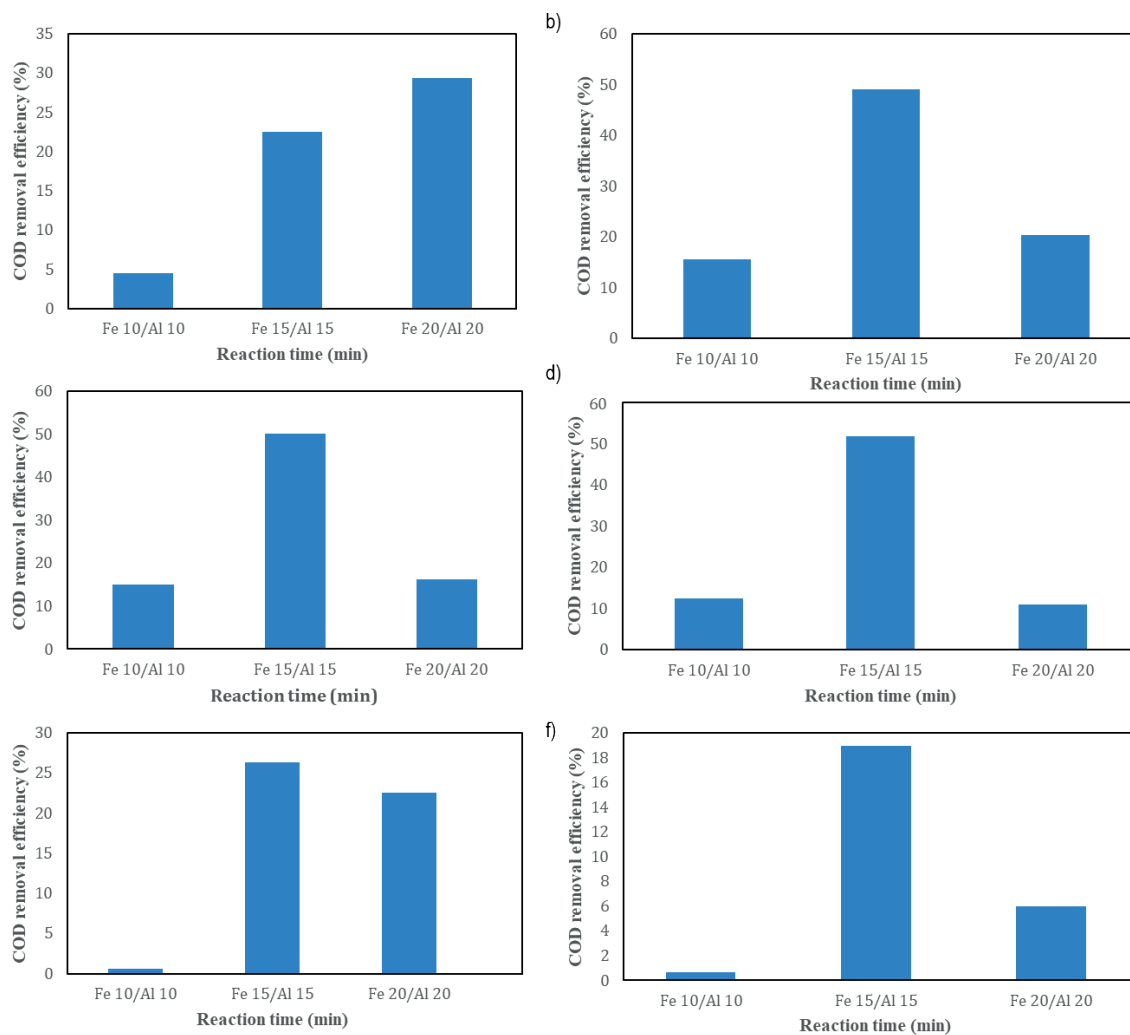


Figure 4 Efficiency of COD removal from oily wastewater at different initial pH values for different time durations of the current on the electrodes: a) pH 9, b) pH 8, c) pH 7, d) pH 6, e) pH 5, f) pH 4

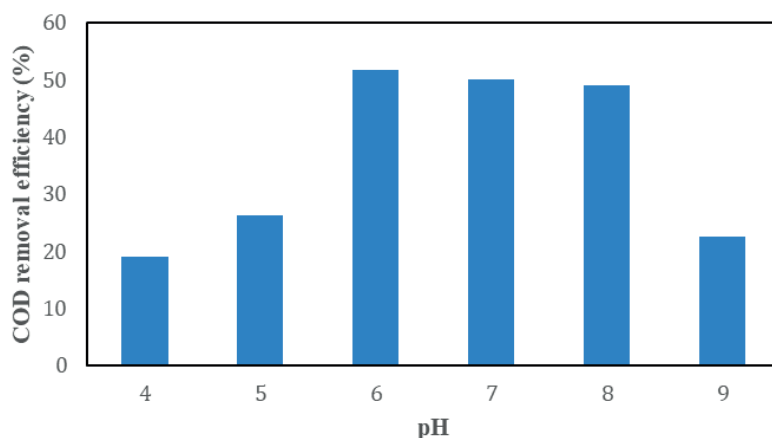


Figure 5 Efficiency of COD removal from oily wastewater in the range of pH value 4–9 and reaction times on iron electrode 15 minutes and aluminum electrode 15 minutes

5. Conclusion

This paper presents the results of an experimental laboratory research testing the effectiveness of electrocoagulation as an electrochemical process in the treatment of oily wastewaters of mineral origin (oily wastewater generated during the treatment process of exhaust gasses produced by gasification of sewage sludge). The efficiency of removal of individual pollutants from wastewater was tested under laboratory conditions with the aim of optimizing various parameters. A total of 24 experimental tests were carried out and the influence of different input settings (pH of raw wastewater) and technological parameters (reaction time) on the operation of the whole process and its efficiency was observed. The values of COD as well as technological/operational parameters (pH, current, electrical conductivity, dissolved oxygen, temperature) were observed. An analysis of the results was carried out with the aim of finding the optimal technological process, which depends on the type of electrodes, current intensity and reaction time, as well as the concentration of input loads and the time and method of deposition. The results of the research confirm that with the formation of an electrochemical process (based on electrocoagulation) for the treatment of oily wastewater, 50% efficiency of COD treatment can be achieved. The results of the conducted research show an efficiency of COD removal of about 50% at pH values of 6 to 8 and a reaction time of 15 minutes. A slightly lower COD treatment efficiency was achieved at a reaction time of 20 minutes, and the lowest at a reaction time of 10 minutes.

Acknowledgements

This work has been fully supported by Croatian Science Foundation under the project „IP-2019-04-1169 – Use of treated oily wastewater and sewage sludge in brick industry – production of innovative brick products in the scope of circular economy”.

References:

- [1] Zakon o vodama, članak 58, čl.4 stavak 1. točka 58., čl.70 (Narodne novine br. 66/2019)
- [2] Nad K.: Razvoj sustava za pripremu pitke vode primjenom elektrokemijskih metoda i naprednih oksidacijskih procesa, doktorska disertacija, Sveuciliste u Rijeci, Tehnicki fakultet, 2015.
- [3] Mijatović, I., Matosic M.: Tehnologija vode, interna skripta, 2019.
- [4] Trobic Baric, I.: Otpadne vode u naftnoj industriji, Završni rad, Veleuciliste u Karlovcu, Karlovac, 2020.
- [5] Rajakovic, V., Ljubisavljevic, D., Skala, D.: Fizicke metode za preciscavanje otpadnih voda – primena metode naizmeničnog mržnjenja i hlađenja i mikrotalasnog zagrevanja za obradu zauljenih voda, Vodoprivreda, 2005.
- [6] Coca, J., Gutierrez, G., Benito, J.: Treatment of oily wastewater, in: Coca-Prados, J., Guitierrez-Cervello, G. (eds): Water Purification and Management, NATO Science for Peace and Security Series C: Environment Security. Springer, Dordrecht, 2011.
- [7] Jamaly, S., Giwa, A., Hasan, S.W.: Recent improvements in oily wastewater treatment: Progress, challenges, and future opportunities, J. Environ. Sci., 16, 2015.
- [8] Hui, L., Yan, W., Juan, W., Zhongming, L.: Recent Advances in Oily Wastewater Treatment, Recent Innovations in Chemical Engineering, 7, 1, 2014.
- [9] Vouk, D., Druskovic, M., Halkijevec, I., Posavcic, H., Siljeg, M., Nad, K., Kollar, R., Izvjestaj br. 1, Pregled stanja znanja na podrucju istrazivanja zauljenih otpadnih voda i elektrokemijski procesi prociscavanja, 2021.
- [10] Tusar, B.: Prociscavanje otpadnih voda, Zagreb, Geotehnicki fakultet, 2009.

- [11] Pravilnik o granicnim vrijednostima emisija otpadnih voda (NN 26/20)
- [12] Druskovic, M., Vouk, D., Posavcic, H., Halkijevic, I., Nad, K.: The application of electrochemical processes in oily wastewater treatment: a review, *J. Environ. Sci. Health – Toxic/Hazard. Subst. Environ. Eng.*, 56, 13, 1373–1386, 2021.
- [13] Chen, G.: Electrochemical technologies in wastewater treatment. *Separation and Purification Technology*, 38, 1, 11–41, 2004.
- [14] Publication, V, Kuokkanen, V, Kuokkanen, T, Rämö, J., Lassi, U.: Electrocoagulation treatment of peat bog drainage water containing humic substances. *Water Research*, 79, 79–87, 2015.
- [15] Sillanpää, M.: *Natural Organic Matter in Water: Characterization and Treatment Methods*. Oxford, Butterworth-Heinemann 83, 84–85, 2014.
- [16] Zongo, I, Leclerc, J, Maïga, H.A., Wéthé, J., Lapique, F.: Removal of hexavalent chromium from industrial wastewater by electrocoagulation: A comprehensive comparison of aluminum and iron electrodes. *Separation and Purification Technology*, 66, 1, 159–166, 2009.
- [17] Katal, R., Pahlavanzadeh, H.: Influence of different combinations of aluminum and iron electrode on electrocoagulation efficiency: Application to the treatment of paper mill wastewater, *Desalination*, 265, 1–3, 199–205, 2011.
- [18] Publication, I.I., Karhu, M., Kuokkanen, V., Kuokkanen, T., Rämö, J.: Bench scale electrocoagulation studies of bio oil-in-water and synthetic oil-in-water emulsions, *Sep. Purif. Technol.*, 96, 296–305, 2012.
- [19] Vepsäläinen, M., Sillanpää, M.: *Electrocoagulation in the treatment of industrial waters and wastewaters*, Espoo, VT Science, 19, 96-146, 2012.
- [20] Drušković, M., Vouk, D., Šiljeg, M., Maldini, K.: Treatment of wastewater from separators for rainfall runoff using electrochemical oxidation processes, *En. Eng.*, 8, 1–2, 2021.

III Sanitary Engineering and Sustainable Water Use

THE INFLUENCE OF PARTICLE SIZE DISTRIBUTION OF SEWAGE SLUDGE ASH AND CLAY ON THE COMPRESSIVE STRENGTH OF BRICKS

DRAŽEN VOUK¹, ANĐELINA BUBALO¹, DOMAGOJ NAKIĆ², NINA ŠTIRMER¹

¹ University of Zagreb, Faculty of Civil Engineering; Croatia

e-mail: drazen.vouk@grad.unizg.hr, andelina.bubalo@grad.unizg.hr, ninab@grad.unizg.hr

² University North, Civil Engineering Department; Croatia

e-mail: dnakic@unin.hr

Abstract

Bricks were made from sewage sludge ash (SSA) fired under laboratory conditions at a temperature of 1000°C from sewage sludge (SS) originating from the wastewater treatment plant (WWTP) in Karlovac. Mechanical properties of bricks are influenced by different factors such as texture, particle size distribution, type of minerals and chemical composition of the clay and SSA. Literature results of the fineness analysis of SSA together with the particle size distribution curves show that the material is predominantly composed of fine sand and silt particles, indicating its natural suitability as a filler material in brick production or as a substitute for clay after grinding. The particle size distribution of SSA and clay was determined using Malvern Mastersizer 2000 instrument. The sand content of SSA was slightly higher than that of clay soil, while clay soil contained much more clayey and silty material compared to SSA. The results of the tests showed that the SSA content is the determining factor for the quality of the bricks. An increase in the SSA content leads to a decrease in the compressive strength of the bricks. When up to 20% SSA was added to the bricks, the compressive strength was 38.7 Nmm⁻². The conditions for production of good quality bricks are 10% SSA in the moulding compounds and firing at 950°C with a heating rate of 5°C min⁻¹ and the resulting compressive strength was 52.9 Nmm⁻². The compressive strength for bricks with 5% SSA was 47.4 Nmm⁻², while the compressive strength of the control brick (100% clay) was 50.4 Nmm⁻².

Keywords: sewage sludge, sewage sludge ash, particle size distribution, brick production, compressive strength.

1. Introduction

The production of sewage sludge (SS) in wastewater treatment plants (WWTP) is constantly increasing worldwide. Sewage sludge ash (SSA) is an inorganic waste material produced by the incineration or gasification of SS. However, methods for energy recovery from SS and the use of SSA as a substitute raw material for clay in the manufacture of bricks, mortar and cement are increasingly being explored [1–5]. This is in line with the principles of the circular economy, which is increasingly being promoted by the European Union. Waste recycling has recently gained importance in the field of construction materials [1,3]. The use of SSA as a substitute material in the production of clay bricks is considered as a disposal solution. Many studies show that the admixture of waste to the composition of fired clay bricks has positive effects on the performance of the bricks. The use of SSA for the production of recycled bricks is of great importance for the complete reuse of SSA resources.

2. Methods

2.1. Origin of the SSA and clay

Since there is not a single incineration plant in the Republic of Croatia, SSA was obtained in a laboratory process by burning in a muffle furnace at a temperature of 1000°C. SSA was obtained from the incineration of SS from the sewage treatment plant in Karlovac. The WWTP Karlovac has tertiary wastewater treatment with nitrogen and phosphorus removal. SS samples were collected from SS after anaerobic digestion and mechanical dewatering. About 70% of the remaining moisture was removed by drying in a laboratory dryer at 105°C for 24 hours and then burned in a muffle furnace at a temperature of 1000°C. The recovered SSA was then crushed using an electric mill and sieved through a 707 µm screen. The obtained SSA was stored in plastic containers at room temperature.

The basic raw material for brick making – clay – was taken from the brick factory in Topusko (Croatia). Due to the moisture contained in it, the collected clay samples were dried in the dryer in the same way as the SS. After drying, they were also sieved through a sieve of the same size as the SS. The raw materials prepared in this way were subjected to further analysis.

2.2. SSA and clay characterization

Characterization was performed with SSA prepared according to the previously described procedure, except for the determination of particle size distribution (without grinding). Morphology was examined using a scanning electron microscope (SEM). Samples were analysed at FE-SEM, Mira, Tescan, Czech Republic, and the evaporator was a Q150T, Quorum Technologies, England (samples were evaporated with chromium for 100 s).

The results of particle size distribution measurements by laser diffraction using a Malvern Mastersizer 2000 instrument. The particle size distribution of clay and SSA was determined by the laser light scattering method. The results are presented as plots of the percentage of particles of a given size in the particle volume (mass) distribution. Sample preparation for analysis was as follows: A representative sample was crushed, lightly tamped with a pestle in a porcelain mortar (note: all samples except clay could be crushed with fingers), and then dispersed in water (about 100 mg in 1 ml) while an ultrasonic probe (44 kHz) was preheated, 190 W, steel tip, 3×20 s). Then the dispersed sample was added to the flow cell of the instrument and the particle size distribution was measured. A value of 1.65, characteristic of aluminosilicate, was used as a reference refractive index.

X-ray diffraction (XRD) analysis of the clay and SSA samples was performed. The powder samples were reduced by quantification to the amount required for analysis, homogenised, placed in a carrier, and subjected to X-ray diffraction (XRD) analysis on a Shimadzu XRD-6000 diffractometer using CuK α -radiation with an accelerating voltage of 40 kV and a current of 30 mA in the range of $2-90 2\theta^\circ$ with a step of $0.02 2\theta^\circ$ and a retention time of 0.6 s. The X-ray diffraction (XRD) analysis was performed on the samples. The results are shown in (Figures 8–10) as a function of the intensity of the diffraction maxima around the diffraction angle.

Chemical analysis of SSA and clay includes the content of metal oxides and the content of heavy metals. Oxides present in clay and SSA were determined by atomic absorption spectroscopy using an Analyst 200 instrument (Perkin-Elmer, Inc., Waltham, MA, USA). Samples were first dissolved by boiling in an acid mixture in steel autoclaves with a Teflon cartridge, then diluted to the desired amount and measured. Results are reported as mass percent of each oxide in the sample (K_2O , MgO , Fe_2O_3 , CaO , Na_2O , SiO_2 , Al_2O_3 , and TiO_2). Heavy metals in clay and SSA were determined by X-ray fluorescence (XRF) recorded with a molybdenum tube and a molybdenum secondary target under vacuum at 1000 s and 45 kV/35 mA and compared with IAEA SL -1.

2.3. Preparation of laboratory SSA brick

The preparation of brick production on a laboratory scale was as follows. A 100% clay brick was made as a control brick for comparison. Other bricks were made with the substitute material SSA in proportions of 5 and 10%. For each batch, the general dry raw materials were mixed in the proportions indicated and then tap water was added to maintain the plasticity of the mixture. The proportions of water for each mixture are shown in Table 1. After the mixture was mixed and its workability was achieved, it was shaped into disks using metal moulds. The obtained moulded parts were air dried in the moulds for about 4 hours, after which the mould was removed. The next day, the moulded part was dried in a dryer at $105^\circ C$ until the weight loss stopped. After natural cooling, it was fired in a muffle furnace at a temperature of $950^\circ C$, increasing the temperature by $5^\circ C$ per minute, and remained at the desired temperature for 3 hours.

Table 1. Brick recipes used in this work (% by weight)

Substitution ratio with SSA [%]	Clay [%]	Water [%]
0	100	31
5	95	31
10	90	30

The following tests were carried out on the bricks produced:

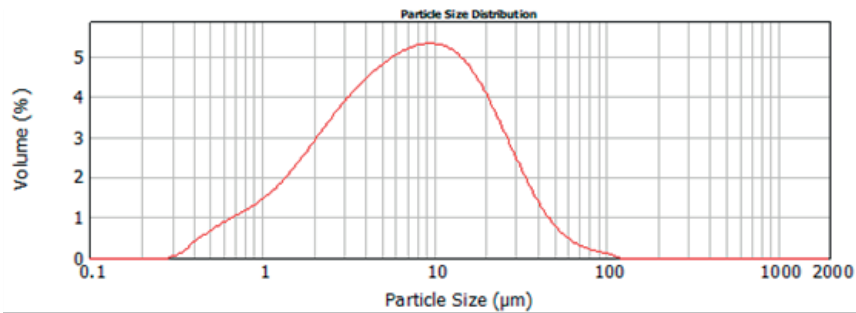
Tests	Methods
Compressive strength	HRN EN 772-1; 2015.
24-h cold-water submersion tests	HRN EN 772-21, 2011.
5-h Boiling tests	HRN EN 772-7; 2003.
Saturation coefficient	Saturation coefficient = $(W_{c(24)} - W_d) / (W_{b(5)} - W_d)^*$
Heavy metals	XRF

* W_d = dry weight of the specimen, $W_{c(24)}$ = saturated weight of the specimen after 24-h submersion in cold water, and $W_{b(5)}$ = saturated weight of the specimen after 5-h submersion in boiling water.

3. Results and discussion

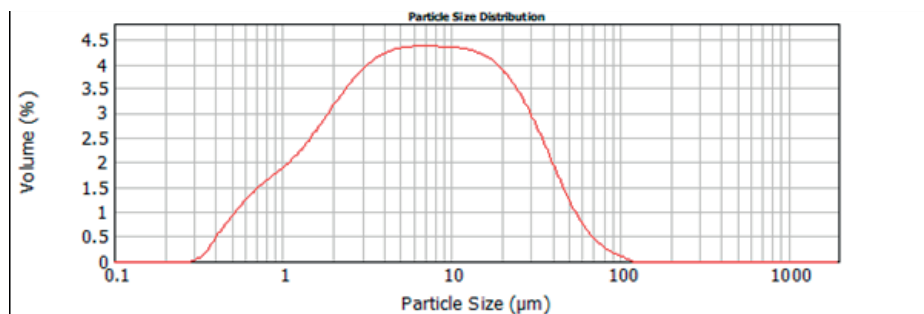
3.1. SSA and clay characterization

3.1.1. Particle size distribution of SSA and clay



—Glinasto_u60_80%

Figure 1. Particle size distribution in clay sample



—Ka1000_u60s_80%

Figure 2. Particle size distribution in SSA sample

The combustion of SS produces fine particles that, when completely burned, may contain some sand-sized particles with insignificant organic residues and low moisture content. Figure 2 shows that the particle size distribution of SSA is very similar to that of clay (Figure 1). Particles less than 2 µm in size are extremely fine-grained clay that appears plastic. Particles between 2 and 60 µm are silt size. They are not plastic or have very low plasticity. Particles between 50–2000 µm are sand-sized particles that have no plasticity.

3.1.2. Morphology of sewage sludge and clay samples

The microstructures of the specimens were studied by scanning electron microscopy (SEM). SEM allows characterization of the morphology, shape, size, and particle distribution in materials. A SEM image of a clay sample shows mostly quartz flakes. The spongy, porous structure indicates the presence of illite.

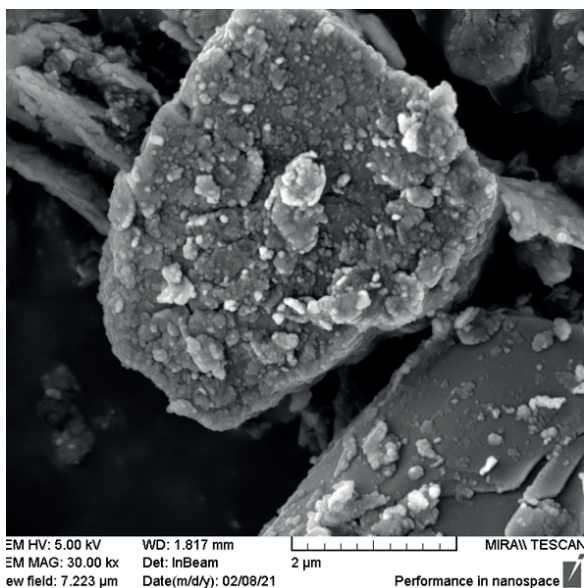


Figure 3. SEM image of clay sample showing

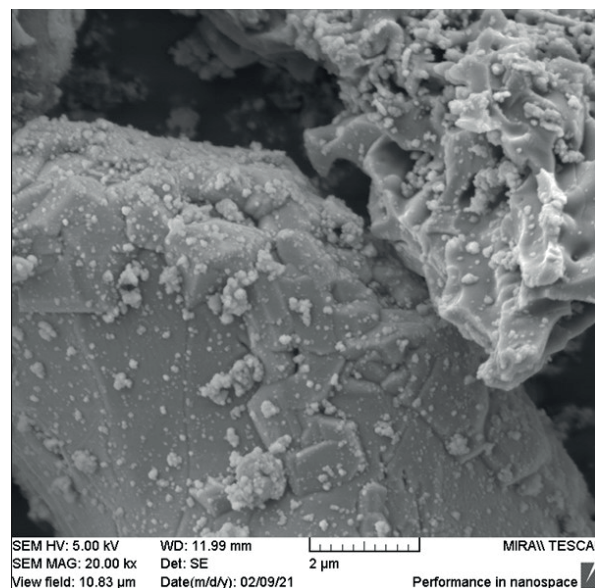


Figure 4 SEM image of SSA sample showing their their morphological variations morphological variations

In the SSA sample, the presence of glassy aluminosilicate structures is also observed, sometimes forming characteristic shapes with a spherical shape and much more often in the form of irregular clusters. The mineral structure also contains quartz, as in the clay sample.

3.1.3. XRD analysis of SSA and clay

In the clay sample, the main phases are quartz and illite, while cristobalite is present only in traces (Figure 5). The presence of stevensite and birnessite is also possible but cannot be confirmed with certainty. An amorphous phase is also present in the sample, but in very small amounts.

SSA contains clay mineral phases regardless of the high production temperature. Thermal decomposition of clay leads to crystallization of aluminosilicate phases at high temperatures. SSA also contains quartz and cristobalite, while illite is barely visible (Figure 6). Secondary phases in SSA are calcium aluminosilicate, anorthite, and calcium aluminium phosphate. Hematite is also visible in the sample, while there is no amorphous phase.

3.1.4. Chemical analysis of SSA and clay

According to the results of the analysis, it is obvious that the SSA originating from Karlovac consists mainly of oxides of silicon, aluminum and calcium (Figure 7 and 8). The proportion of oxides in the replacement raw material SSA largely matches the composition of the oxides in the clay from Topusko.

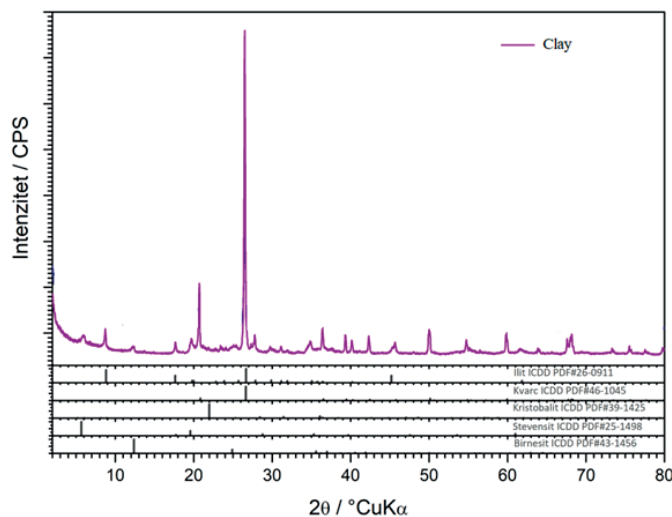


Figure 5. XRD diffractograms of the clay sample

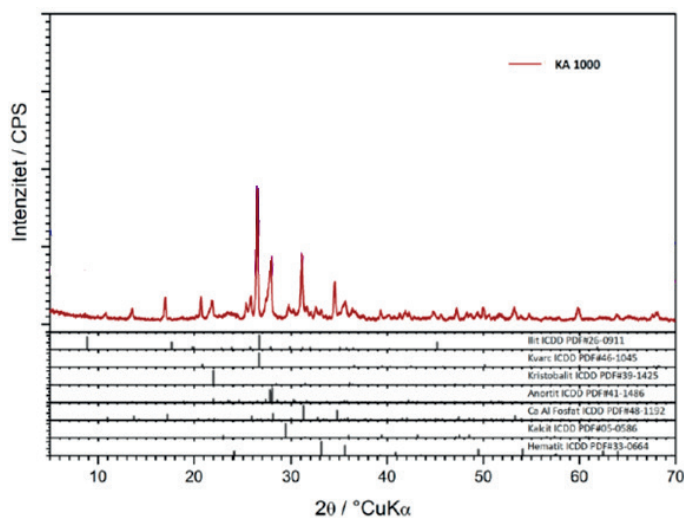


Figure 6. XRD diffractograms of the SSA sample

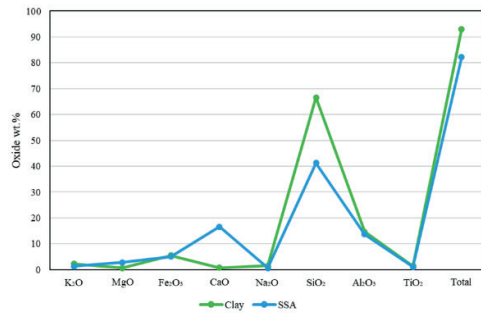


Figure 7. Oxide content in SSA and clay

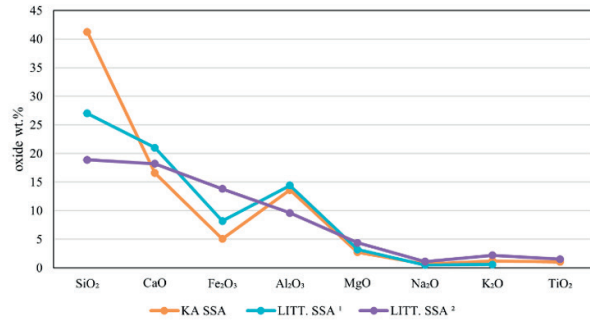


Figure 8 SSA KA Oxides compared to literature results [5, 6]

However, the graphical representation in Figure 8 shows the proportion of oxides in the SSA of Karlovac compared to the proportion of oxides in the SSA of the other researchers. Therefore, it can be said that the composition of SSA can vary greatly and depends on the type of wastewater treatment process and additives used for SS conditioning, as well as the type of thermal treatment of SS (type of reactor, selected temperature, process, etc.).

The chemical composition of SSA compared to clay indicates a high proportion of calcium in SSA, while the proportions of potassium and iron in clay are higher than in SSA (Figure 9). The content of heavy metals such as lead, cadmium, zinc and copper in SSA is usually higher than in clay or some additives such as sand or sawdust. Therefore, the use of SSA as a substitute raw material for clay should be taken with great caution. In fact, the specific results of this study indicate elevated concentrations of zinc, copper, and chromium in SSA compared to clay, but slightly lower concentrations of lead, arsenic, and vanadium are also found in SSA compared to clay. However, many studies using leaching tests indicate that heavy metal concentrations in brick leaching tests are significantly lower compared to allowable limits.

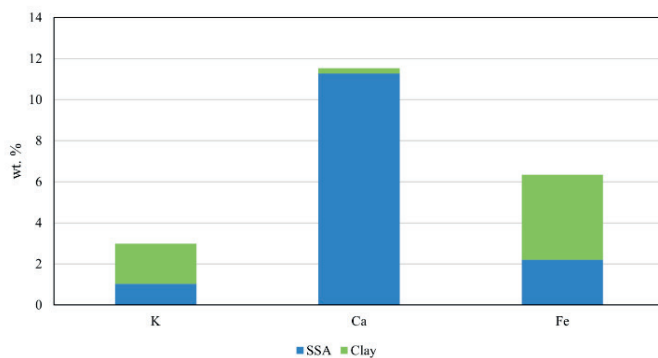


Figure 9. Content of major metals in the samples of SSA

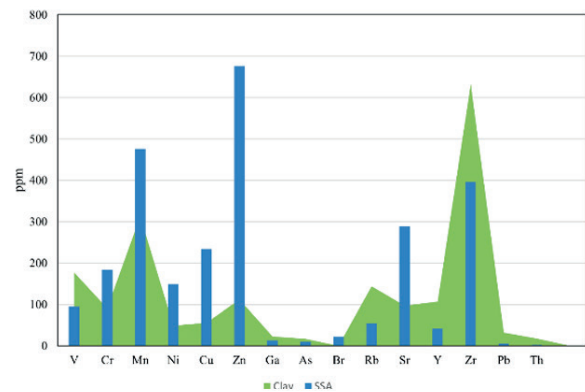


Figure 10. Content of heavy metals in the and clay samples of SSA and clay

3.2. Test on produced bricks

Figure 11 shows that the brick made with 10% SSA has the best compressive strength. The graphical representation of the water absorption tests in cold water increased with the increase of the percentage of SSA in the brick, Figure 12. According to the American standards for test materials ASTM C67-94, it should not exceed 18%, but most standards tolerate up to 20%. Therefore, all produced bricks, including the control brick, meet this requirement.

Boiling water absorption tests also showed an increase with increasing percentage of SSA waste in the brick. Figure 13 shows the average percent weight increase of the bricks after 5 hours of boiling water absorption. From this figure, it can be seen that more water was forced into the brick by the boiling water than by the 24-hour water intake. The highest 5-hour boiling water uptake occurred in bricks with 20% SSA.

The coefficient of saturation is the ratio between the amount of water a brick absorbs after being in cold water for 24 hours and the amount of water it absorbs after being in boiling water for 5 hours. When the saturation coefficient is low, the brick generally has good freeze-thaw resistance because it contains enough voids to keep freezing water out.

In this case of Figure 14, the saturation coefficient decreased with the increase of the proportion of SSA in the brick. The coefficient of saturation is a good indicator of resistance to freezing and thawing.

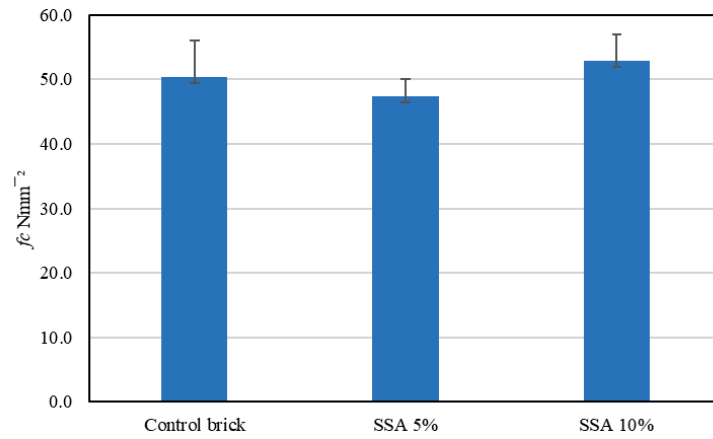


Figure 11. Compressive strength

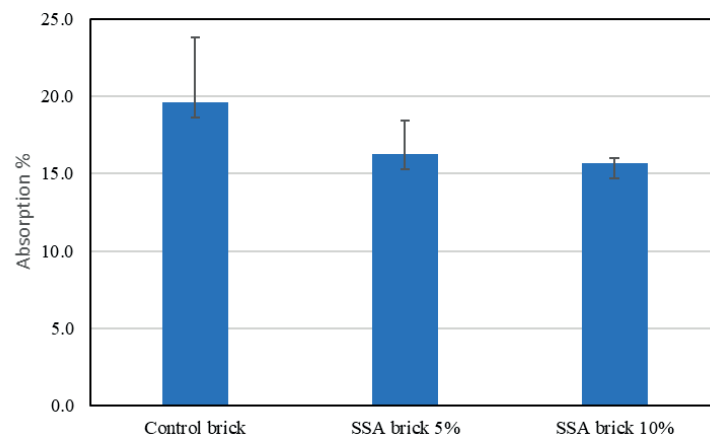


Figure 12. 24-h cold-water submersion tests

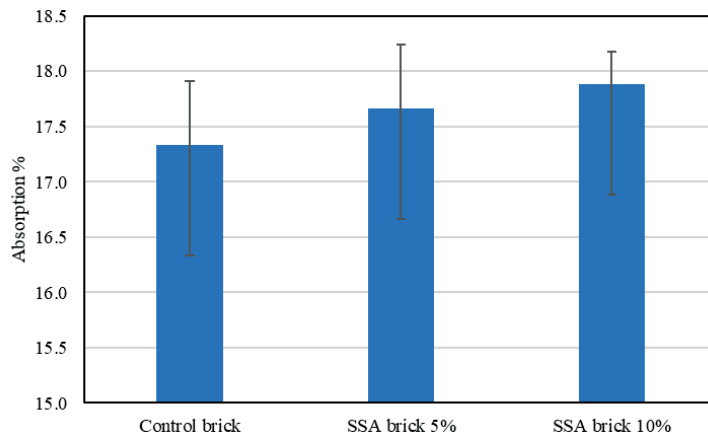


Figure 13. 5-h Boiling tests

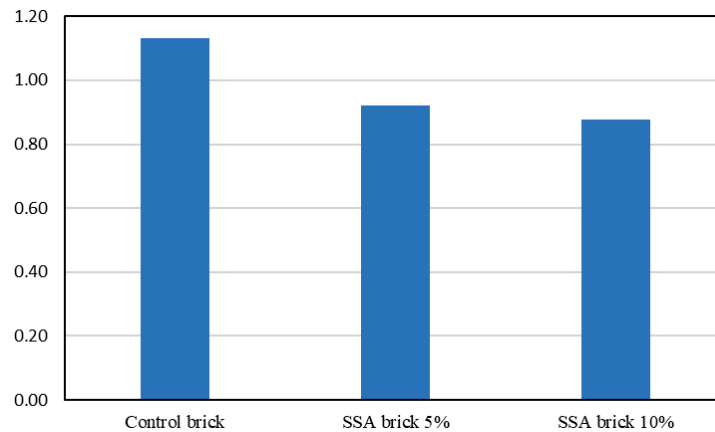


Figure 14. Saturation coefficient

4. Conclusion

SSA obtained by firing SS from Karlovac at 1000°C proved to be a suitable substitute raw material for brick production. The morphology, particle size, mineral and chemical composition of SSA proved to be very similar to the natural raw material – clay. The strength of the specimens fired at 950°C was improved by the addition of 10% SSA. It was concluded that the reactive amorphous nature of the SSA particles locally enhanced the sintering effect and this resulted in better strength behaviour. The water absorption tests also show an increase in the absorption rate at a proportion of 10% SSA. However, all brick durability factors showed good values, although the quality of the bricks decreased compared to the control and to bricks with lower SSA content. The research results in this paper are of interest to the water management sector with the aim of disposing of sewage sludge and for the construction materials industry with the aim of reducing the use of raw materials, but also reducing CO₂ emissions. Regardless of the results on the bricks, this research is applicable even more widely, and open a new gate for further research on how to integrate different types of wastes in construction industry.

Acknowledgements

This work has been fully supported by Croatian Science Foundation under the project “IP-2019-04- 1169 – Use of treated oily wastewater and sewage sludge in brick industry – Production of innovative brick products in the scope of circular economy”.

References:

- [1] Bories, C., Aouba, L., Vedrenne, E., and Vilarem, G: Fired clay bricks using agricultural biomass wastes: Study and characterization, *Constr. Build. Mater.*, 91, pp. 158–163, 2015.
- [2] Bories, C., Borredon, M.E., Vedrenne, E., and Vilarem, G: Development of eco-friendly porous fired clay bricks using poreforming agents: A review. *J. Environ. Manage.*, 143, pp. 186–196, 2014.
- [3] Zhang, L: Production of bricks from waste materials—A review. *Constr. Build. Mater.*, 47, pp. 643–655, 2013.
- [4] Karim M.A, Hassan AS, Hawa A.: Enhancement of soil engineering properties with sewage sludge ash. *MOJ Eco Environ Sci.*, 5(5), pp. 230–236, 2020. DOI: 10.15406/mojes.2020.05.00198.
- [5] Al-Sharif, M.M., Attom M. F.: A geoenvironmental application of burned wastewater sludge ash in soil stabilization, *Environ Earth Sci.*, 71, pp. 2453–2463, 2014. <https://doi.org/10.1007/s12665-013-2645-z>.
- [6] Krejcirikova, B, Ottosen, L., M., Kirkelund, G.M, Rode, C, Peuhkuri, R. H: Characterization of sewage sludge ash and its effect on moisture physics of mortar, *Journal of Building Engineering*, 21, pp. 396-403, 2019. <https://doi.org/10.1016/j.jobee.2018.10.021>.

III Sanitary Engineering and Sustainable Water Use

THE INFLUENCE OF THE INITIAL CONCENTRATION OF HEAVY METALS AND THE ELECTRODE MATERIAL ON THE EFFICIENCY OF ELECTROCOAGULATION WATER TREATMENT

KATARINA LICHT¹, HANA POSAVČIĆ¹, IVAN HALKIJEVIĆ¹, MISLAV MARKIĆ¹, JOSIPA ZLOMISLIĆ¹

¹ University of Zagreb, Faculty of Civil Engineering; Croatia

e-mail: klicht@grad.hr, hposavcic@grad.hr, ihalkijevic@grad.hr, mislav.markic@student.grad.hr, josipa.zlomislic@student.grad.hr

Abstract

In this study, the influence of the electrode material and the initial concentration of heavy metals on the efficiency of their removal from water by the electrocoagulation process is investigated. The experiments were carried out in a batch reactor with aluminium, iron, copper and graphite electrodes at three different contaminant concentrations. For the conditions that yielded the highest efficiency, a set of experiments was conducted with perforated electrodes. The process was more successful at lower concentrations, and the material of the electrodes had the greatest influence.

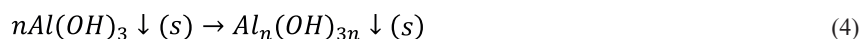
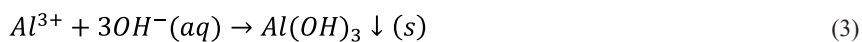
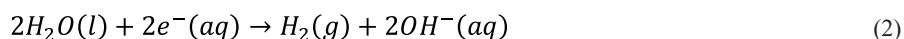
Keywords: water treatment, heavy metals, electrocoagulation, kinetics, design of experiment.

1. Introduction

Pollution by heavy metals has become one of the most important environmental issues in recent years. The term “heavy metals” refers to all metals and metalloids with relatively high density such as iron (Fe), manganese (Mn), aluminium (Al), mercury (Hg), zinc (Zn), cadmium (Cd), arsenic (As), antimony (Sb), boron (B), thallium (Tl), chromium (Cr), copper (Cu), lead (Pb), and nickel (Ni) [1]. In nature, they are widely distributed as components of the earth’s crust and as trace elements in living organisms. Although they occur naturally in soils and sediments, significant sources of heavy metals in the environment are human activities (agricultural, pharmaceutical, municipal, mining and metal processing waste and wastewater, fossil fuels consumption, etc.) and atmospheric sources like volcanic emissions and atmospheric dust [2]. Even though low concentrations of heavy metals are necessary for metabolism and normal growth and development of the organism, higher concentrations can have toxic and harmful effects, so the continuous release of heavy metals into the aquatic environment and increased human exposure are of concern [3], [4]. A major problem is the observed bioaccumulation in living organisms. Heavy metals enter the aquatic environment through natural or anthropogenic pathways and enter the food chain [1]. Since they are not biodegradable, they accumulate in living tissues, and pose a hazard with chronic exposure [5]. Arsenic, cadmium, chromium, lead, and mercury, for example, are considered systemic toxins because they can cause damage to several different organs, even at low levels of exposure [6]. They are also classified as carcinogens by the U.S. Environmental Protection Agency. Cadmium has been linked to “itai-itai” disease, respiratory and kidney problems, liver damage, anaemia, digestive issues, and inhibition of calcium control in the body [7]. Chromium can cause allergic dermatitis, nausea, vomiting and alopecia [8]. Excessive nickel consumption can result in anaphylaxis, red blood cell damage, chronic bronchitis, liver and kidney damage [9]. Exposure to high concentrations of cobalt can lead to hearing, vision, nerve, and thyroid problems [10]. The toxicity of heavy metals depends on the dose, route of administration, chemical form, as well as gender, age, weight, and genetics of the exposed individuals [5],[11].

To meet the growing demand for lower heavy metal levels in drinking water and wastewater, various water treatment processes are being investigated and developed. One of the promising technologies is electrocoagulation (EC). Although it is similar to chemical coagulation, EC is characterized by in situ generation of coagulants by passing an electric current through sacrificial electrodes. The most commonly used electrodes are electrodes made of iron and aluminium [12]. Under the influence of the electric current, the anodes dissolve, oxygen is released, and metal cations (Al^{3+} , Fe^{2+}) are formed [13],[14]. At the same time, hydrogen and hydroxide ions are released at the cathode. The hydroxide ions migrate to the anode, where they form polymeric iron and aluminium hydroxides with the metal cations, which act as coagulants. The reaction at the aluminium anode is given in Eq(1). The reaction at the cathode proceeds according to Eq(2). In the alkaline medium, aluminium hydroxide is formed as shown in Eq(3), while Eq(4) shows its polymerization.[15], [16]





The removal of pollutants from water occurs by chemical reactions and precipitation or by physical and chemical binding to colloidal metal hydroxides [17]. Thus, the process consists of dissolution of the sacrificial anode, formation of hydroxide ions and hydrogen at the cathode, electrolyte reactions at the electrode surface, adsorption of coagulants onto colloidal contaminants, and removal of the formed flocs by precipitation or flotation [18]. The flocs formed by this process are significantly larger, more stable, and contain less bound water, which greatly facilitates the separation of the resulting sludge, e.g., by filtration [18], [19]. Electrocoagulation is considered an environmentally friendly technology because it avoids the addition of chemical reagents and additives, thus preventing the formation of secondary contaminants [18],[20].

The following parameters affect the efficiency of EC in removing heavy metals from water: electrode material, solution pH, current density, treatment time, electrode potential, pollutant concentration, anion concentration, and temperature [21]. In this study, the influence of electrode material and initial pollutant concentration on the efficiency of electrocoagulation process was investigated. The experiments were statistically designed using the Design of Experiments approach (DOE). This approach can be used to determine the most important factors affecting the process and the values of these factors that allow optimization of the electrocoagulation process. These factors are independent variables, while response is a dependent variable. The main advantage of DOE is the significant reduction in the number of experiments to be performed, since the behavior of the interrelated factors can be predicted over a wide range of values. Thus, it is possible to obtain maximum information from a relatively small number of experimental data.

2. Methods

2.1. Design of experiments

Stat-Ease's Design Expert 12 software was used for experiment design and statistical analysis. The factors studied were the electrode material (Al, Fe, Cu, C) and the initial concentration of heavy metals (0.1, 1, 10 ppm), while the efficiency of the process was the response. The efficiency of the process was evaluated by measuring the change in heavy metals concentrations at the end of the process. It was calculated according to Eq(5), where C_0 is the initial concentration of the metal and C_t is the concentration of the metal measured at time t . The concentrations were measured by ICP-OES analysis.

$$\eta(\%) = \frac{C_0 - C_t}{C_0} * 100 \quad (5)$$

The experiments were carried out following the multi-level categoric experimental design. The obtained run matrix and responses are shown in Table 1.

Table 1. Experimental design matrix

Std	Run	Factor 1 A: material	Factor 2 B: concentration	Response 1 Mn, %	Response 2 Ni, %	Response 3 Cd, %	Response 4 Cr, %	Response 5 Co, %
6	1	Al	1	29.49	36.89	76.27	99.77	54.00
3	2	Cu	0.1	55.07	68.57	90.12	100	67.48
5	3	Fe	1	21.34	16.10	21.60	98.90	13.00
7	4	Cu	1	42.31	58.19	85.12	99.90	57.96
8	5	C	1	17.05	5.67	6.15	56.15	6.10
2	6	Al	0.1	35.80	53.20	78.52	100	68.00
1	7	Fe	0.1	41.02	57.93	89.63	99.60	64.71
9	8	Fe	10	6.89	8.95	13.09	97.80	7.76
10	9	Al	10	9.48	28.18	31.06	97.9	33.17
12	10	C	10	7.76	9.19	6.77	57.28	7.00
4	11	C	0.1	16.67	2.38	4.90	55.37	2.68
11	12	Cu	10	32.56	44.89	59.79	99.30	45.28

2.2. Experimental setup and procedure

Experiments were carried out in a 3-litre plexiglass batch reactor with two plate electrodes connected to the laboratory power supply. Mixing was achieved using a magnetic stirrer (set at 300 rpm) placed under the reactor. The experimental setup is shown in Figure 1. Four different electrode pairs (Figure 2) were used: Al/Al, Fe/Fe, Cu/Cu, and C/C. The active surface area or total immersed surface area of each electrode was 119 cm² and the distance between the electrodes was 1 cm. The experiments were performed with synthetic solutions containing Cd, Cr, Co, Mn, and Ni. Three different concentrations were tested: 0.1, 1, and 10 ppm. All other parameters were kept constant. A current density of 15 mA cm⁻² was used and all experiments were conducted at a room temperature of 25°C. The initial pH of the solution varied between 6.7 and 7.1. The anion concentration was not measured but is expected to be similar for experiments performed with the same concentration. Furthermore, no additional electrolyte was added. The duration of each experiment was 2 minutes, with samples taken every 15 seconds with a syringe.

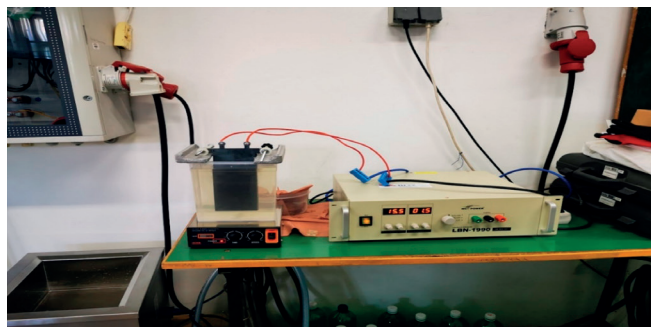


Figure 1. Experimental set-up

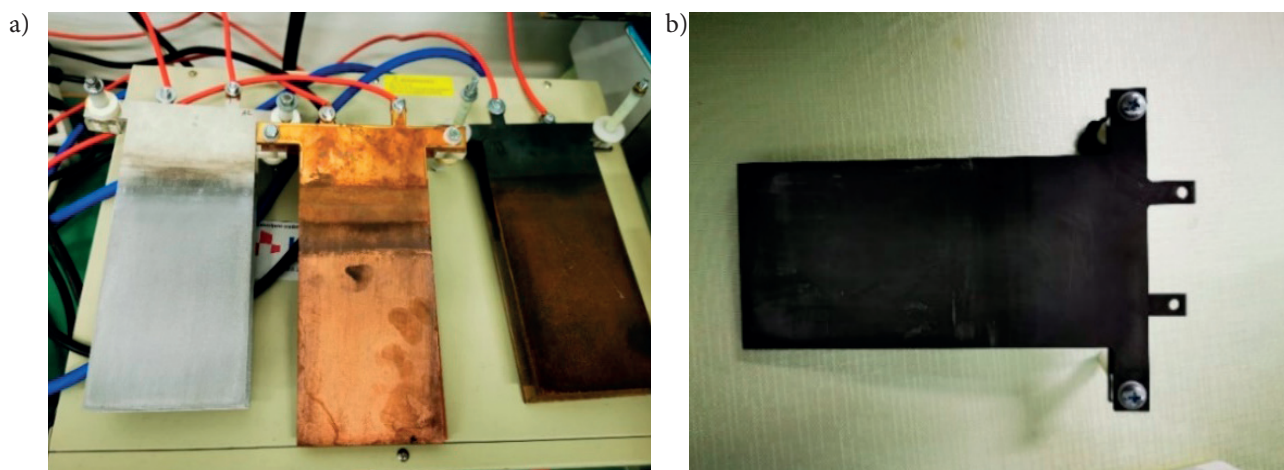


Figure 2. A) Aluminium, copper and iron electrodes B) graphite electrodes

A set of experiments was performed under the same conditions with perforated Al, Cu and Fe electrodes of the same dimensions as those originally used. The perforated electrodes are shown in Figure 3. The efficiencies of these experiments were compared with those obtained with non-perforated electrodes.

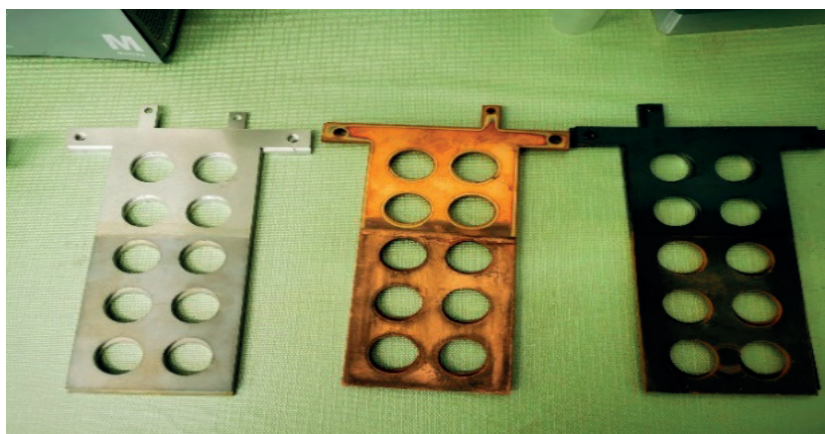


Figure 3. Perforated electrodes

3. Results and discussion

3.1. The results of statistical analysis

The three-level categorical design resulted in suitable factorial models. Using ANOVA, the quantitative significance of the models and each factor was calculated. A quantitative measure of model significance is the p-value or level of significance. The statistical significance level, P, indicates how likely it is that the difference between the experimentally tested value of removal efficiency and the value predicted by the model is due to chance. The P-value describes the probability that an error occurred in the prediction of the result (predicted removal efficiency). If the P-value is below the permitted level of significance, which is usually 5% ($P < 0.05$), the probability of an error in the prediction is less than 5%, i.e., there is a statistically significant difference. The models obtained for the removal nickel, cadmium, chromium, and cobalt indicated that the only significant factor is the electrode material with p-values ranging from 0.0001 to 0.0234. For manganese, both electrode material and initial concentration had a similar effect, with p-values of 0.0049 and 0.0045, respectively. All models showed reasonable agreement between the predicted and adjusted R^2 with a difference of less than 0.2. Table 2 shows the results of the experiments compared to the predicted values. Graphs of the predicted versus the actual values and normal plots of the residuals confirm the good fit of the model, as seen in Figure 4 in the case of manganese removal. Figure 5 shows the best solution for process optimization, i.e., the combination of factors that leads to maximum efficiency.

Table 2. The comparison between predicted (*) and observed efficiencies

Material	C	Cd	Cd*	Co	Co*	Cr	Cr*	Ni	Ni*	Mn	Mn*
Fe/Fe	0.1	89.63	60.31	64.71	43.61	99.60	99.01	57.93	40.67	41.02	33.93
Fe/Fe	1	21.60	41.81	13.00	25.66	98.90	98.95	16.10	24.36	21.34	24.34
Fe/Fe	10	13.09	22.20	7.76	16.20	97.80	98.34	8.95	17.95	6.88	10.96
Al/Al	0.1	78.52	80.82	68.00	66.84	100.00	99.47	53.20	52.43	35.80	35.77
Al/Al	1	76.27	62.32	54.00	48.89	99.77	99.41	36.89	36.13	29.49	26.19
Al/Al	10	31.06	42.71	33.17	39.43	97.90	98.79	28.18	29.71	9.48	12.81
Cu/Cu	0.1	90.12	97.22	67.48	72.03	100.00	99.98	68.57	70.23	55.07	54.17
Cu/Cu	1	85.12	78.71	57.96	54.08	99.90	99.92	58.19	53.92	42.31	44.58
Cu/Cu	10	59.79	59.10	45.28	44.62	99.30	99.31	44.89	47.51	32.56	31.20
C/C	0.1	4.90	24.82	2.68	20.38	55.37	56.51	2.38	18.76	16.67	24.68
C/C	1	6.16	6.31	6.10	2.43	56.16	56.45	5.67	2.45	17.05	15.09
C/C	10	6.77	-13.30	7.01	-7.03	57.28	55.84	9.19	-3.96	7.76	1.71

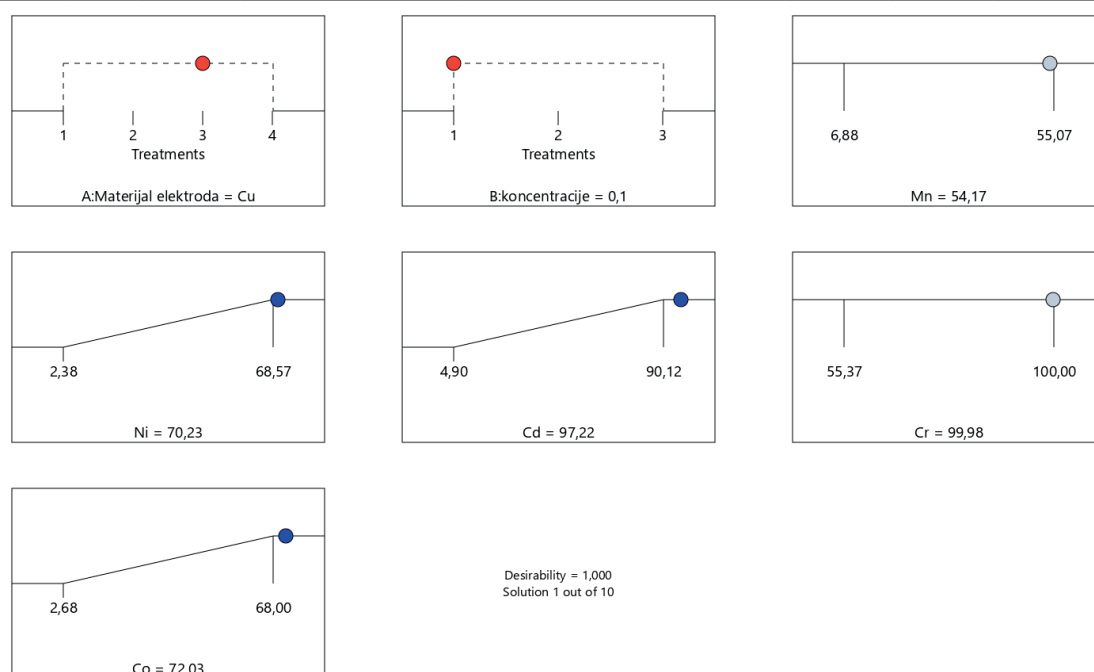


Figure 5. Ramp graphs presenting the results of process optimization

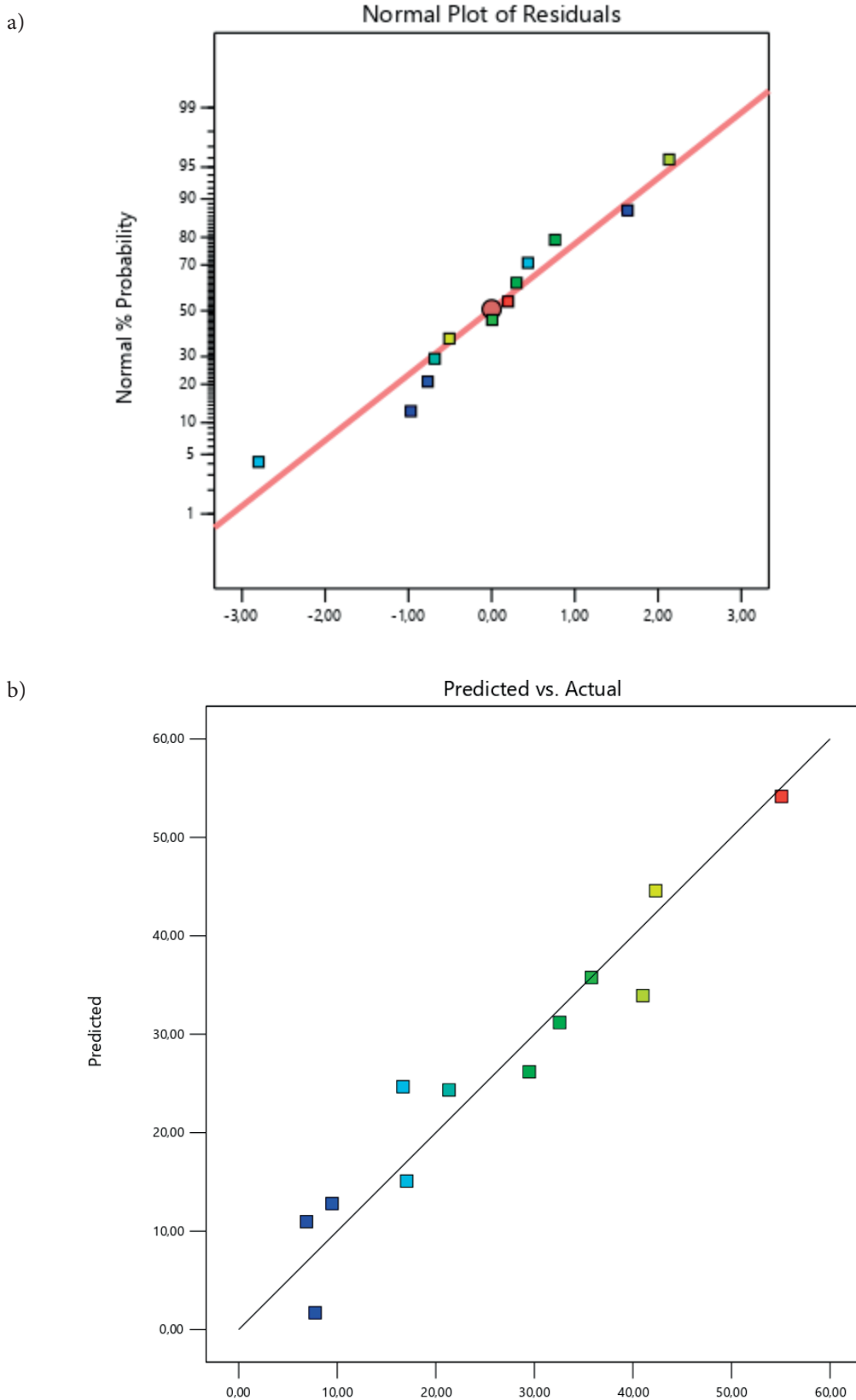


Figure 6. Normal plot of residuals (A) and predicted vs. actual graph (B) for manganese model

3.2. The effect of electrode material

The electrode material determines which electrochemical reactions occur in the EC system and the material selection depends on the pollutants to be removed and the chemical properties of the electrolyte [21]. In this study, three metallic electrode materials were tested: aluminium, iron and copper. These elements differ in many chemical and physical properties such as ion size, ion charge, oxidation potential, and polarity of the ion-OH bond [22]. The size and the

structure of the resulting metal hydroxide compound also differ, resulting in different adsorption capabilities of each hydroxide [23]. Graphite electrodes have also been tested. Although they are insoluble anodes, these electrodes show high oxygen evolution over-potential [22].

As expected, and confirmed by the model, the electrode material is the most influential factor in an EC process. All metal electrodes were found to be efficient, while graphite electrodes proved to be unsuitable for heavy metal removal and partially removing only chromium ions. It is also very important to note, that the composition of the electrodes and possible impurities can greatly affect the process. For example, manganese is a common impurity in metal electrodes and can be leached out of from the electrodes during the EC process resulting in diminished overall efficiency. In general, attention should be paid to the concentration of the electrode material in the outlet stream. For example, although copper electrodes resulted in the highest efficiency, due to the electrode potential of copper, a significant amount of copper was present in the solution after the EC treatment. Figure 7 shows how the concentration of the different electrode materials changed through the processes under the same experimental conditions.

To determine the effect of electrode geometry on the process, the experiment that yielded the highest efficiencies was repeated with perforated electrodes. Perforations reduce the active surface area of the electrode and, consequently, result in lower current density. However, perforations allow better mixing of the solution and could also reduce the effect of electrode passivation [24]. In this case, there was little difference between the overall efficiencies of perforated and non-perforated electrodes. In the experiment with Cu electrodes at 1 ppm, perforated electrodes resulted in 92.6%, 64.3%, 99.7%, 68%, and 51.9% removal of Cd, Co, Cr, Ni, and Mn, respectively. Figure 8 compares these two processes.

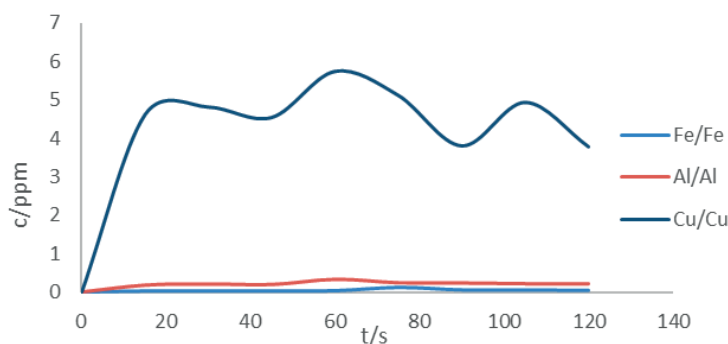


Figure 7. The change in concentration of Fe, Al and Cu during the process with corresponding electrodes

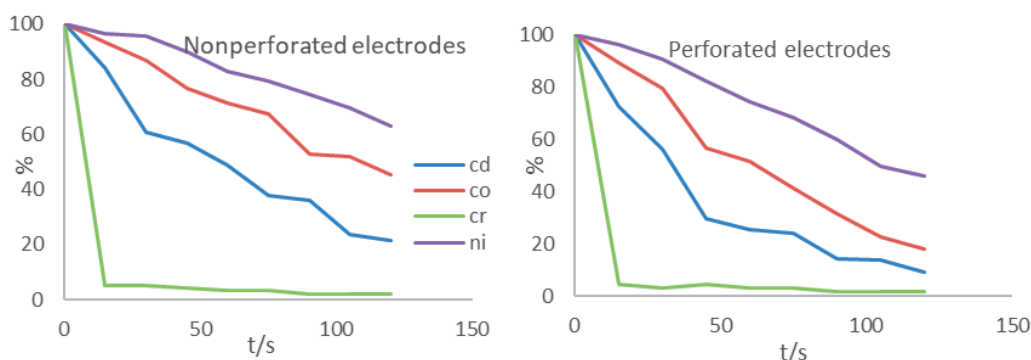


Figure 8. The comparison of the removal rate for the process with perforated and non-perforated electrodes

3.3. The effect of initial concentration of contaminants

There are several studies indicating that the removal efficiency of heavy metals from water by the EC process is higher at lower initial concentrations of the contaminating metals [25], [26],[27]. The results of our study are consistent with these findings. When the initial concentration was increased, the removal efficiency for nickel, cadmium, manganese, and cobalt ions decreased. This could be explained by Faraday's law, according to which a constant amount of metal dissolves from the anode and passes into solution for the same current density and electrolysis time [25]. This means that regardless of the initial concentration of heavy metals, the same amount of metal hydroxides was formed in the solution, and in the case of higher concentrations, that amount was not sufficient to absorb all heavy metal ions. In addition, lower efficiencies at high initial concentrations of the metals may be associated with saturation of the electrode due to the formation of an oxide layer on the electrode surface. The only exception was chromium. In this case, the initial concentration had very little effect on the removal rate, and in almost all cases, with the exception of the graphite electrodes, an efficiency greater than 99% was achieved. This can be attributed to the fact that chromium is

removed quickly and almost all of it is removed in the first 30 seconds. The effects on chromium removal for graphite electrodes are shown in Fig 9.

In general, for higher concentrations, a longer time is required for removal, and the electrocoagulation process is more effective at the beginning when the concentration is higher than at the end when the concentration is low [28]. For example, in the study by Dermentzis et al. [28], 99% of Ni was removed from 250 mL of a 100 ppm solution in 10 min using aluminium electrodes and a current density of 30 mA cm⁻². In our study, using a much larger volume of solution (3 L) and a lower current density (15 mA cm⁻²), the Ni concentration decreased by 28% from the initial concentration of 10 ppm in only 2 minutes.

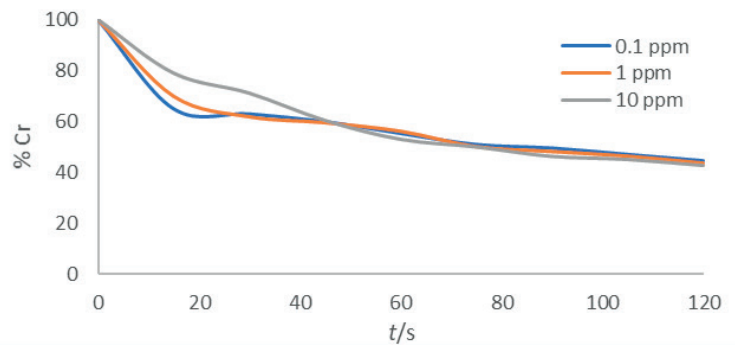


Figure 9. Removal of chrome using graphite electrodes

3.4. The kinetics of heavy metals removal

A kinetic study was carried out to describe the removal process of Ni, Co, Mn and Cd under optimal operating conditions that resulted in the highest efficiency (Cu, 0.1 ppm). There are several kinetic models used to describe the kinetics of the EC process for the removal of heavy metals. These models include first order, second order, pseudo-first order, pseudo-second order, and Elovich models[22]. For an EC batch process, the mass conservation of heavy metal ions follows the Eq (6), where the r_D is the rate of metal ion removal, C is the concentration of the metal ion, and t is the time (min).

$$-\frac{dC}{dt} = -r_D \quad (6)$$

For the zeroth order, the removal rate is defined in the Eq (7), where k is the zeroth rate constant.

$$r_D = -k \quad (7)$$

For the first-order kinetics the model is described by Eq (8), where k_1 is the first order rate constant. The integrated equation for the initial conditions of $C(0)=C_0$, at $t=0$ is given in Eq (10).

$$r_D = -k_1 C \quad (9)$$

$$C(t) = C_0 e^{-k_1 t} \quad (10)$$

The second order model is described by the Eq(11), where k_2 is the second order rate constant. Upon integration with the same initial conditions as above, the time dependant concentration is obtained in Eq (12).

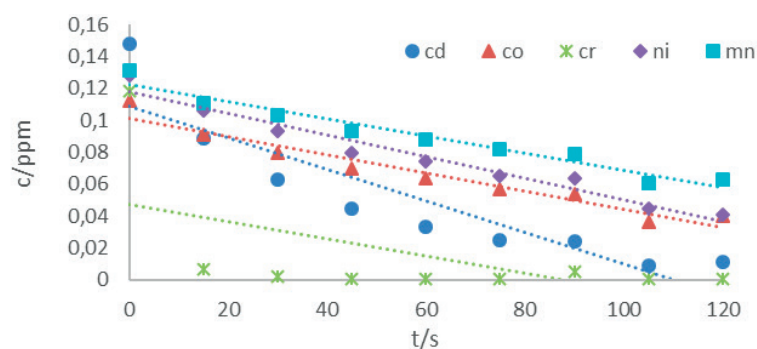
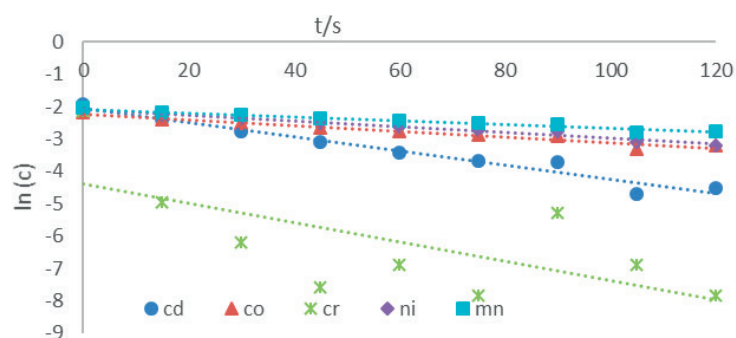
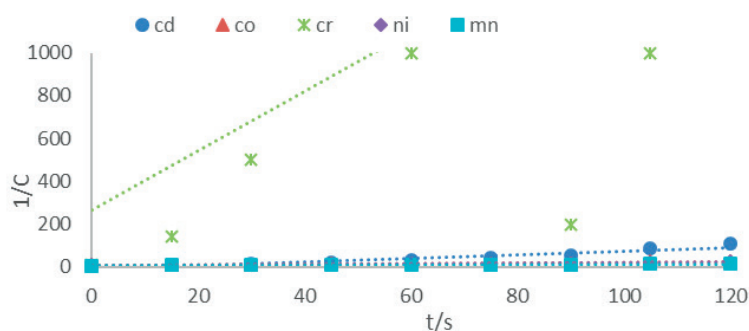
$$r_D = -k_2 C^2 \quad (11)$$

$$\frac{1}{C(t)} = \frac{1}{C_0} + k_2 t \quad (12)$$

To determine the appropriate reaction order, the concentrations of Ni, Co, Mn and Cd were plotted against time and modeled as zero, first and second order reaction kinetics. The most appropriate model was selected based on their R^2 values. The closer the R^2 value is to 1, the better the model fit. The kinetic parameters of zero-, first- and second-order models together with the R^2 values are given in Table 3. Although it can not be used to describe our process, zero order kinetics was tested because of studies such as one by Garcia-Carrillo et al. [29] in which it is used to describe silver and gold removal by EC. A graphical comparison of the kinetic models is shown in Figures 10-12. As it can be seen, cobalt, nickel, cadmium and manganese removal follows the first-order kinetic. None of the models can appropriately describe chromium removal. These results vary from studies in which heavy metal removal by EC process is described by either second-order or pseudo-first order kinetics [23],[30]. However, these differences can be due to electrode type and the current density that was used.

Table 3. Predicted rate constants and corresponding R^2 values for kinetic models

Metal	k_0 (ppm min ⁻¹)	R^2	k_1 (min ⁻¹)	R^2	k_2 (ppm ⁻¹ min ⁻¹)	R^2
Cd	0.0013	0.849	0.0189	0.973	0.3818	0.901
Co	0.0007	0.851	0.0084	0.982	0.1124	0.885
Cr	0.0006	0.330	0.0271	0.592	7.0779	0.851
Ni	0.0008	0.924	0.0086	0.972	0.1022	0.932
Mn	0.0006	0.937	0.0060	0.972	0.0615	0.889

**Figure 10.** Zero-order kinetics model**Figure 11.** First-order kinetics**Figure 12.** Second order kinetics

4. Conclusion

The most influential factor in the EC process for heavy metal removal is the material from which the electrode is made. The efficiency of the EC process increases as the initial concentration of the metal decreases. To achieve the same removal efficiency for higher initial concentrations of pollutants, a longer treatment time is required. Perforated and non-perforated electrodes showed similar behavior and overall efficiencies. In most cases, the kinetics of heavy metal removal followed first-order kinetics. While the EC process is effective in reducing heavy metals in water, further research and optimization of the process is needed, especially for highly contaminated waters.

Acknowledgements

This work was supported in part by the Croatian Science Foundation under the project PRIMEUS (UIP2020-02-1160).

References:

- [1] Gautam R.K., Sharma S.K., Mahiya S., Chattopadhyaya M.C.: Contamination of Heavy Metals in Aquatic Media: Transport, Toxicity and Technologies for Remediation (Chapter), Heavy Metals In Water: Presence, Removal and Safety, ed. Sharma, S.K., Royal Society of Chemistry, Cambridge, pp. 1–24, 2014.
- [2] He Z.L., Yang X.E., Stoffella P.J.: Trace elements in agroecosystems and impacts on the environment, *Journal of Trace Elements in Medicine and Biology*, 19, 2–3, pp. 125–140, 2005.
- [3] Tchobanoglous G., Burton F.L., Stensel D.H.: *Wastewater Engineering: Treatment and Reuse*, Fourth edition, McGraw-Hill, 2004.
- [4] Yu G., Wang X., Liu J., Jiang P., You S., Ding N., Guo Q., Lin F.: Applications of Nanomaterials for Heavy Metal Removal from Water and Soil: A Review, *Sustainability*, 13, 2, pp. 1–15, 2021.
- [5] Tchounwou P.B., Yedjou C.G., Patlolla A.K., Sutton D.J., *Molecular, clinical and environmental toxicology – Volume 3: Environmental Toxicology*, First edition, Springer Basel, 2012.
- [6] Chowdhury P., Elkamel A., Ray A.K.: Photocatalytic Processes for the Removal of Toxic Metal Ions (Chapter), Heavy Metals In Water: Presence, Removal and Safety, ed. Sharma, S.K., Royal Society of Chemistry, Cambridge, pp. 25–43, 2014.
- [7] Sud D., Mahajan G., Kaur M.P.: Agricultural waste material as potential adsorbent for sequestering heavy metal ions from aqueous solutions – A review, *Bioresource Technology*, 99, 14, pp. 6017–6027, 2008.
- [8] Carolin C.F., Kumar P.S., Saravanan A., Joshiba G.J., Naushad M.: Efficient techniques for the removal of toxic heavy metals from aquatic environment: A review, *Journal of Environmental Chemical Engineering*, 5, 3, pp. 2782–2799, 2017.
- [9] Sharma S., Bhattacharya A.: Drinking water contamination and treatment techniques, *Applied Water Science*, 7, 3, pp. 1043–1067, 2017.
- [10] Joseph L., Jun B.M., Flora J.R.V., Park C.M., Yoon Y.: Removal of heavy metals from water sources in the developing world using low-cost materials: A review, *Chemosphere*, 229, pp. 142–159, 2019.
- [11] Shrestha R., Ban S., Devkota S., Sharma S., Joshi R., Tiwari A.P., Kim H.Y., Joshi M.K.: Technological trends in heavy metals removal from industrial wastewater: A review, *Journal of Environmental Chemical Engineering*, 9, 4, 2021.
- [12] Qasem N.A.A., Mohammed R.H., Lawal D.U.: Removal of heavy metal ions from wastewater: a comprehensive and critical review, *Clean water*, 4, pp. 1–15, 2021.
- [13] Mollah M.Y.A., Schennach R., Parga J.R., Cocke D.L.: Electrocoagulation (EC) – Science and applications, *Journal of Hazardous Materials*, 84, 1, pp. 29–41, 2001.
- [14] Chen G.: Electrochemical technologies in wastewater treatment, *Separation and Purification Technology*, 38, pp. 11–41, 2004.
- [15] Tran T.-K., Leu H.-J., Chiu K.-F., Lin C.-Y.: Electrochemical Treatment of Heavy Metal-containing Wastewater with the Removal of COD and Heavy Metal Ions, *Journal of the Chinese Chemical Society*, 64, pp. 493–502 2017.
- [16] Pulkka S., Martikainen M., Bhatnagar A., Sillanpää M.: Electrochemical methods for the removal of anionic contaminants from water – A review, *Separation and Purification Technology*, 132, pp. 252–271, 2014.
- [17] Liu H., Zhao X., Qu J.: Electrocoagulation in water treatment, *Electrochemistry for the Environment*, pp. 245–262, 2010.
- [18] Khandegar V., Saroha A.K.: Electrocoagulation for the treatment of textile industry effluent – A review, *Journal of Environmental Management*, 128, pp. 949–963, 2013.
- [19] Gupta V.K., Ali I.: *Water Treatment by Electrical Technologies*, Environmental Water, pp. 155–178, 2013.
- [20] Azimi A., Azari A., Rezakazemi M., Ansarpour M.: Removal of Heavy Metals from Industrial Wastewaters: A Review, *ChemBioEng Reviews*, 4, 1, pp. 37–59, 2017.
- [21] Sillanpää M.E.T., *Advanced water treatment: electrochemical methods*, First edition, Cambridge, 2020.
- [22] Al-Qodah Z., Al-Shannag M.: Heavy metal ions removal from wastewater using electrocoagulation processes: A comprehensive review, *Separation Science and Technology*, 52, 2649–2676, 2017.

- [23] Al-Shannag M., Al-Qodah Z., Bani-Melhem K., Qtaishat M.R., Alkasrawi M.: Heavy metal ions removal from metal plating wastewater using electrocoagulation: Kinetic study and process performance, *Chemical Engineering Journal*, 260, pp. 749–756, 2015.
- [24] Ibrahim M.H., Moussa D.T., El-Naas M.H., Nasser M.S.: A perforated electrode design for passivation reduction during the electrochemical treatment of produced water, *Journal of Water Process Engineering*, 33, pp. 101–091, 2020.
- [25] Chou W.L., Huang Y.H.: Electrochemical removal of indium ions from aqueous solution using iron electrodes, *Journal of Hazardous Materials*, 172, 1, pp. 46–53, 2009.
- [26] Thella K., Verma B., Srivastava V.C., Srivastava K.K.: Electrocoagulation study for the removal of arsenic and chromium from aqueous solution, *Journal of Environmental Science and Health – Part A Toxic/Hazardous Substances and Environmental Engineering*, 43, 5, pp. 554–562, 2008.
- [27] Hashim K.S., Kot P., Zubaidi S.L., Alwash R., Al Khaddar R., Shaw A., Al-Jumeily D., Aljefery M.H.: Energy efficient electrocoagulation using baffle-plates electrodes for efficient *Escherichia coli* removal from wastewater, *Journal of Water Process Engineering*, 33, pp. 1–7, 2020.
- [28] Dermentzis K., Valsamidou E., Lazaridou A., Kokkinos N.C.: Nickel removal from wastewater by electrocoagulation with aluminum electrodes, *Journal of Engineering Science and Technology*, 4, 2, pp. 188–192, 2011.
- [29] Garcia-Carrillo C., Parga-Torres J. Moreno-Casillas H., Sellschopp-Sanchez F.S.: Kinetics and energy consumption for a three-stage electrocoagulation process for the recovery of Au and Ag from cyanide leachates, *Metals*, 9,7, pp. 1–10, 2019.
- [30] Moersidik S.S., Nugroho R., Handayani M., Kamilawati, Pratama M.A.: Optimization and reaction kinetics on the removal of Nickel and COD from wastewater from electroplating industry using Electrocoagulation and Advanced Oxidation Processes, *Heliyon*, 6, 2, pp. 303–319, 2020.

III Sanitary Engineering and Sustainable Water Use

ULTRASOUND ASSISTED ELECTROCOAGULATION REMOVAL OF HEAVY METALS FROM WATER

DIANA SMOKOVIĆ¹, HANA POSAVČIĆ¹, KATARINA LICHT¹, IVAN HALKIJEVIĆ¹

¹ University of Zagreb, Faculty of Civil Engineering; Croatia

e-mail: diana.smokovic@student.grad.hr hposavcic@grad.hr, klicht@grad.hr, ihalkijevic@grad.hr

Abstract

In this paper, ultrasonic treatment, electrocoagulation and the combinations of these treatments were compared for the removal of manganese, nickel, cobalt, cadmium and chromium from a synthetic solution. Experiments were conducted using aluminium electrodes in a modified ultrasonic bath. The experimental design approach (DOE) and multi-level categorical design were used to design the experiments and optimize the results. The results show that ultrasound largely affects the EC heavy metals removal process and leads to higher efficiencies than EC alone.

Keywords: electrocoagulation, ultrasound, water treatment, heavy metals, sonoelectrocoagulation, DOE.

1. Introduction

Heavy metal pollution of drinking water is a current problem with potentially serious consequences. Due to their toxic, biodegradable, and persistent nature, heavy metals pose a serious threat to aquatic ecosystems, as well as to human health [1,2]. In response to the challenge of reducing the concentration of heavy metals in water, various technologies have been developed. Conventional methods include physicochemical processes such as chemical precipitation, ion exchange, adsorption on various materials, electrochemical processes such as electrocoagulation, electroflotation and electrodeposition, and membrane filtration processes [3–5].

Electrocoagulation (EC) is characterized by the formation of coagulants in situ by oxidation of the metal anode due to the application of electric current. The process consists of dissolution of the sacrificial anode, formation of hydroxide ions and hydrogen at the cathode, electrolyte reactions at the electrode surface, adsorption of coagulants on colloidal contaminants and removal of the resulting flocs by precipitation or flotation [6–9]. Parameters effecting the efficiency of the EC in removing heavy metals from water are: electrode material, solution pH, current density, treatment time, electrode potential, pollutant concentration, concentration of anions, and temperature [10].

Ultrasound is a longitudinal wave with a frequency range between sonic and mega sonic region (20–600 kHz) [11]. Ultrasonic waves transmit energy through the vibration of molecules in the environment in which the wave is being spread [12]. Most commonly, ultrasonic waves are generated by the piezoelectric effect. Piezoelectric crystals are used to convert high frequency electrical energy to mechanical vibrations. The vibrating part can be made in different forms and different ultrasonic devices are commercially available. Ultrasonic devices, usually, operate at frequencies from 20k Hz to 10 MHz. High power ultrasound at low frequencies (<100 kHz) has the ability to cause cavitation [13]. Cavitation is a rapid physical phenomenon caused by sudden drop in pressure. It starts with formation of small vapour bubbles inside a liquid medium [14]. Pressure changes cause bubble propagation and eventually a violent collapse. The energy released from the bubble collapse causes extreme local increases in temperature and pressure. “Hot spots” with temperatures over 1000 K can form in the centre of the collapsing bubble, leading to formation of highly reactive hydroxyl radicals [15]. In ultrasonic baths, transducers are attached to the side or bottom of the tank and this cavitation is considered low intensity due to the large surface area through which the energy is transmitted. In ultrasonic baths, sometimes the bubbles do not actually collapse, but oscillate for many sonic cycles. This means that the extreme conditions caused by bubble collapse do not happen, but micro eddies occur causing shear stress. This type of cavitation is named “stable cavitation” and cavitation with bubble collapse is called “transient cavitation” [16].

Electrocoagulation is an effective method for removing heavy metals and has many advantages. However, the main disadvantage of the EC process is the polarization and passivation of the electrodes [10]. Passivation is the formation of a passive film forming on the electrode surface over time, which results in diminishing of the process efficiency [10]. Polarization can be caused also by gas accumulation near to the electrode surface and as a result depletion of pollutant in the electrode’s boundary layer [17]. To overcome that drawback, it is possible to couple the treatment with ultrasound. Ultrasonic waves break up the deposits formed at the electrode surface. In addition, ultrasound can generate radical species

through the cavitation phenomenon, resulting in better contaminant removal and making sono-electrocoagulation a promising technology for water and wastewater treatment [18].

2. Methods

2.1. Experimental design

In this work, the Design of Experiment approach was used for experiment design and statistical analysis. For this purpose, Design Expert 12 software from Stat-Ease was used. The multi-level categorical design was selected. The factors studied and their characteristics are presented in Table 1. There were 4 treatment options included in the design (US, US/EC, EC/US, sono-EC). US frequency was tested at 2 levels (25 and 45 kHz) and US intensity at 3 levels (10, 50, 100%). The efficiencies of the process for each heavy metal were treated as responses. The efficiency of the process was evaluated by measuring the change in heavy metals concentrations at the end of the process. It was calculated according to Eq(1), where C_0 is the initial concentration of the metal and C_t is the concentration of the metal measured at time t .

$$\eta(\%) = (C_0 - C_t) / C_0 * 100 \quad (1)$$

Table 1. Selected parameters for multilevel categorical design

Factor	Name	Units	Type	SubType	Minimum	Maximum	Levels
A	frequency	kHz	Categorical	Nominal	25	45	2
B	intensity	%	Categorical	Nominal	10	100	3
C	treatment		Categorical	Nominal	US	EC/US	4

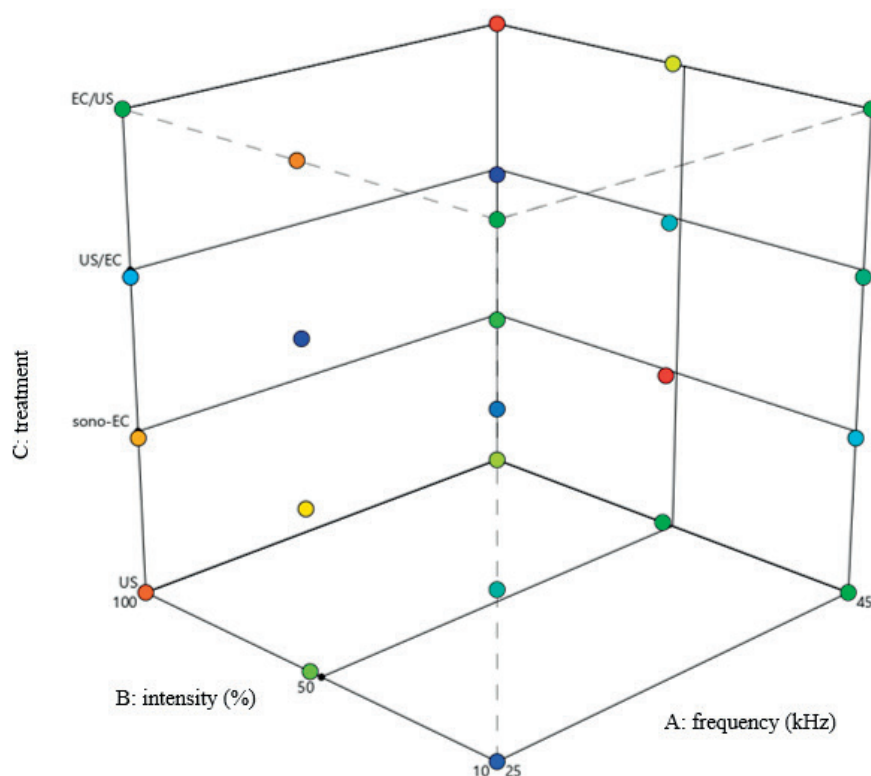


Figure 1. Scatterplot of three-level categorical design used in this study

2.2. Experimental method

The experiments were carried out in a modified ultrasonic bath (Elma Ultrasonics TI-H 10 MF2) with 2 frequency settings (25/45 kHz) and adjustable intensity (10–100%). The mixing of the treated solution was achieved by recirculation using a peristaltic pump set to 0.51 /s flow rate. For electrocoagulation treatment, 4 aluminium electrodes connected to the laboratory power supply were used. Electrodes were arranged as follows: anode/cathode/anode/cathode with the interelectrode distance of 1 cm. The electrodes were completely submerged with active surface area of 91.32 cm². The power supply was set to 60 V voltage and kept constant. An aqueous solution containing 1 ppm of Ni, Cd, Cr and Co and Mn was used as a model solution. pH value, temperature and conductivity of the solution was not altered.

Five different types of treatments were tested: EC as a standalone treatment for 2 minutes, US as a standalone treatment for 2 minutes, 2 minutes of simultaneous EC and US treatment (sono-EC), 1 minute of US followed by 1 minute of EC and 1 minute of EC followed by 1 minute of US. The frequency and intensity of ultrasound were varied according to the experimental plan in the experiments including US treatment.



Figure 2. Modified ultrasonic bath with recirculation, laboratory power supply and aluminium electrodes

The samples were taken at the beginning and the end of every experiment, using a syringe. They were filtered using a 45 μm PES filter and acidified before analysis. The concentration of heavy metals was measured using ICP-OES analysis. All chemicals used were of analytical grade, and sample containers were previously soaked in 10% nitric acid for 24 hours. The electrodes and the reactor were thoroughly rinsed between experiments.

3. Results and discussion

The electrocoagulation experiments carried out in this experimental setup resulted in the removal of 84.41% Cd, 71.84% Co, 93.60% Cr, 52.47% Ni and 38.80% Mn in a treatment time of 2 minutes. The results of the other treatments (1 minute of US treatment followed by 1 minute of EC, 1 minute of EC followed by 1 minute of of US, 2 minutes of simultaneous US-EC treatment, and 2 minutes of US treatment) are presented in Table 2.

Table 2. The experimental matrix with factors and responses

Std	Run	Factor 1	Factor 2	Factor 3	Response 1	Response 2	Response 3	Response 4	Response 5
		A:freq. kHz	B:inten. %	C:treatm.	Mn %	Ni %	Cd %	Cr %	Co %
18	1	45	100	US/EC	39.47	55.79	79.92	96.38	72.73
15	2	25	50	US/ EC	35.09	53.42	88.00	98.34	70.55
1	3	25	10	US	0.49	9.11	20.76	36.29	10.38
13	4	25	10	US/ EC	24.18	38.42	79.75	98.94	55.34
17	5	25	100	US/ EC	30.69	44.75	81.55	94.42	63.44
8	6	45	10	sono-EC	46.46	64.62	77.23	85.53	68.37
16	7	45	50	US/ EC	29.52	48.07	80.63	98.24	67.06
7	8	25	10	sono-EC	32.85	49.73	88.59	73.33	67.43
14	9	45	10	US/ EC	31.98	52.01	87.00	99.59	68.21
4	10	45	50	US	0.00	6.66	48.77	89.74	9.30
23	11	25	100	EC/US	27.80	47.60	82.01	94.66	63.02
19	12	25	10	EC/US	24.56	40.60	76.27	88.00	56.07
20	13	45	10	EC/US	26.22	42.33	79.42	95.56	59.09
2	14	45	10	US	0.68	1.28	9.77	56.70	1.37

12	15	45	100	sono-EC	23.13	40.63	78.73	98.50	60.56
3	16	25	50	US	0.00	3.74	35.06	72.26	6.25
6	17	45	100	US	0.52	8.20	27.95	75.83	11.19
22	18	45	50	EC/US	21.10	36.89	74.70	96.90	52.41
9	19	25	50	sono-EC	27.45	47.64	80.81	99.21	69.24
11	20	25	100	sono-EC	29.18	46.27	83.97	99.08	62.51
21	21	25	50	EC/US	22.84	38.72	77.06	92.47	55.02
5	22	25	100	US	0.11	1.02	5.04	32.20	1.03
24	23	45	100	EC/US	22.48	41.48	76.35	97.95	56.02
10	24	45	50	sono-EC	23.32	36.35	77.92	99.07	52.07

The significant effect of process variables on electrocoagulation efficiency has been verified by analysis of variance (ANOVA). The P value is used to estimate whether the F test values are large enough to indicate statistical significance. The F test values of the present model is significant at the 5% level (i.e. $P < 0.05$). It shows the model match with experimental values and can explain the significance of individual parameter. Furthermore, the closer the R^2 value is to 1, the better the model fits. As it can be seen in Table 3, selected factorial models show a good fit to the experimental values with p values less than 0,05. The P-values of the individual terms in the model are, also, shown in Table 3. It is evident that the only significant term is Factor C – treatment. The only exception is the chromium removal model, in which all of the main effects (A, B, C), as well as interactions AC and BC, appear to be significant. This suggests that unlike the removal of Mn, Ni, Cd and Co, the efficiency of the Cr removal depends, not only on the type of treatment, but also on the frequency and ultrasound intensity used. The normal plot of the residuals is shown in Figure 2, while Figure 3 shows graphical comparison between actual and predicted values.

Table 3. Results of ANOVA analysis

	model			p-value					
	F-value	p-value	R2	A	B	C	AB	AC	BC
Mn	13.3400	0.0021	0.9742	0.6666	0.3379	0.0001	0.1991	0.7520	0.1544
Ni	10.3688	0.0042	0.9671	0.7050	0.6435	0.0001	0.4310	0.7284	0.4380
Cd	14.6700	0.0016	0.9765	0.9904	0.3114	0.0000	0.7824	0.4698	0.1974
Cr	13.7700	0.0019	0.9750	0.0094	0.0100	0.0001	0.5539	0.0300	0.0361
Co	23.8150	0.0004	0.9854	0.9505	0.9383	0.0000	0.4193	0.4045	0.6447

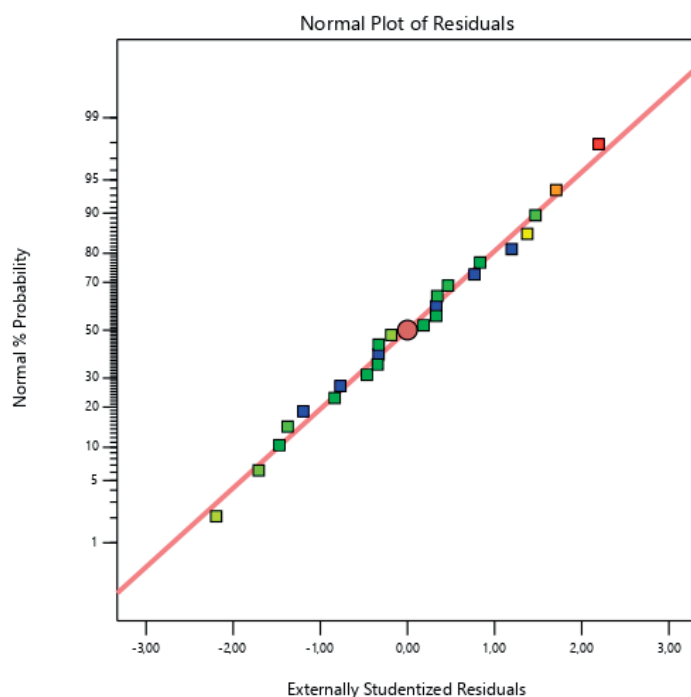


Figure 3. Normal plot of the residuals for manganese removal

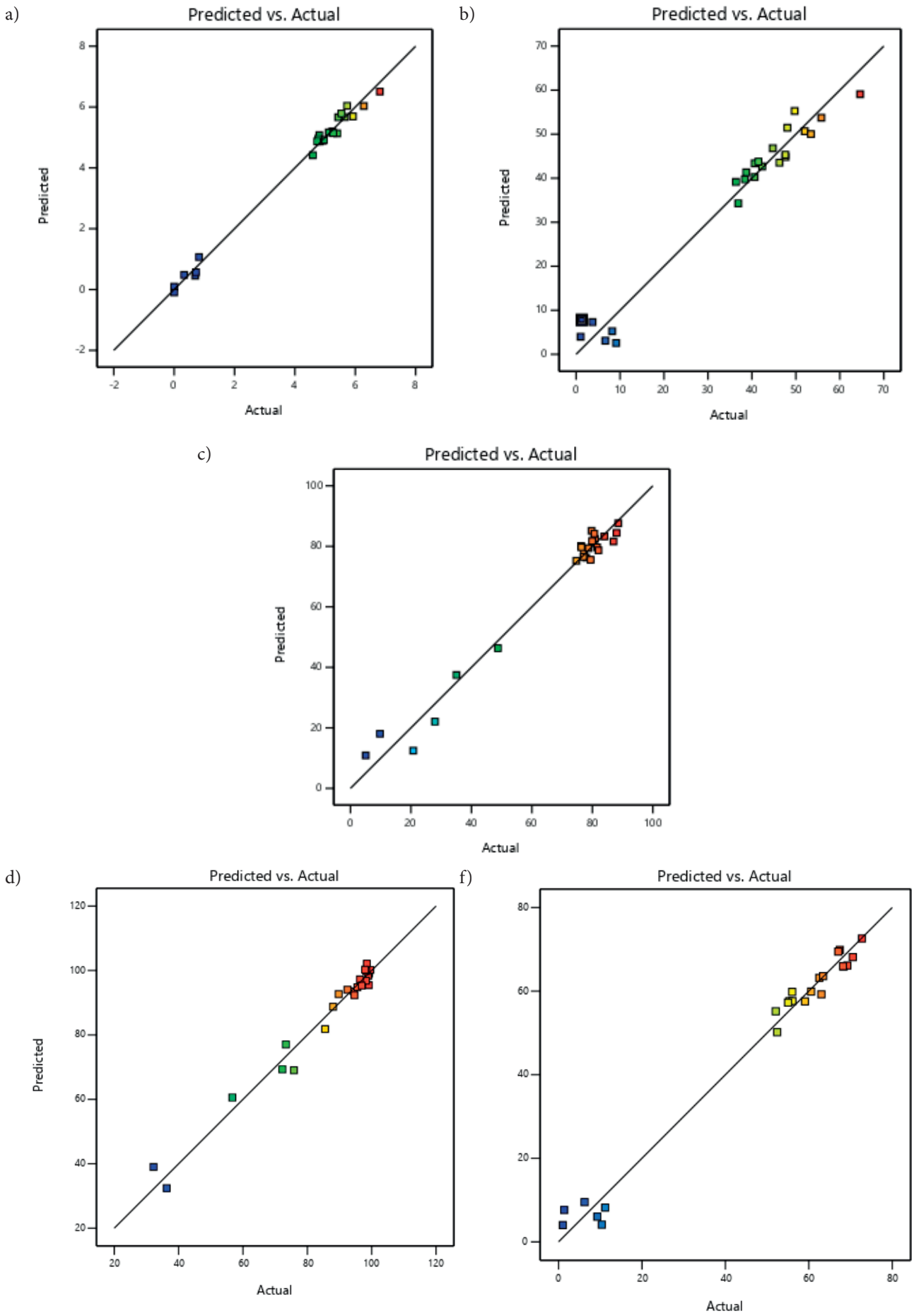


Figure 4. Predicted versus actual values for the removal of A) manganese B) nickel C) cadmium D) chromium E) cobalt

US treatment as a standalone process was found to be unsuitable for the removal of heavy metals, as it gave the lowest efficiencies for all of the investigated metals. For manganese and nickel removal, the highest efficiency was obtained during the sono-electrocoagulation treatment at 45 kHz and 100% US intensity. Sono-EC was, also, the most efficient treatment for cadmium, but at 25 kHz. Chromium was the easiest heavy metal to remove, with the highest efficiency of 99.59% in the case of US treatment at 45 kHz and 100% intensity followed by EC. The best choice for cobalt removal was the same process but at 100% US intensity. Considering the differences in the removal of each heavy metal, Design Expert software was used to determine the optimal conditions (Figure 5). The best compromise is US treatment at 45 kHz and 100% intensity followed by EC resulting in 36.24%, 53.73%, 81.76%, 97.23% and 72.59% efficiency for the removal of Mn, Ni, Cd, Cr and Co, respectively. It is interesting to note that EC treatment followed by US, resulted in the highest aluminium concentrations in the effluent, possibly due to ultrasound disrupting the flocs formed in the EC process.

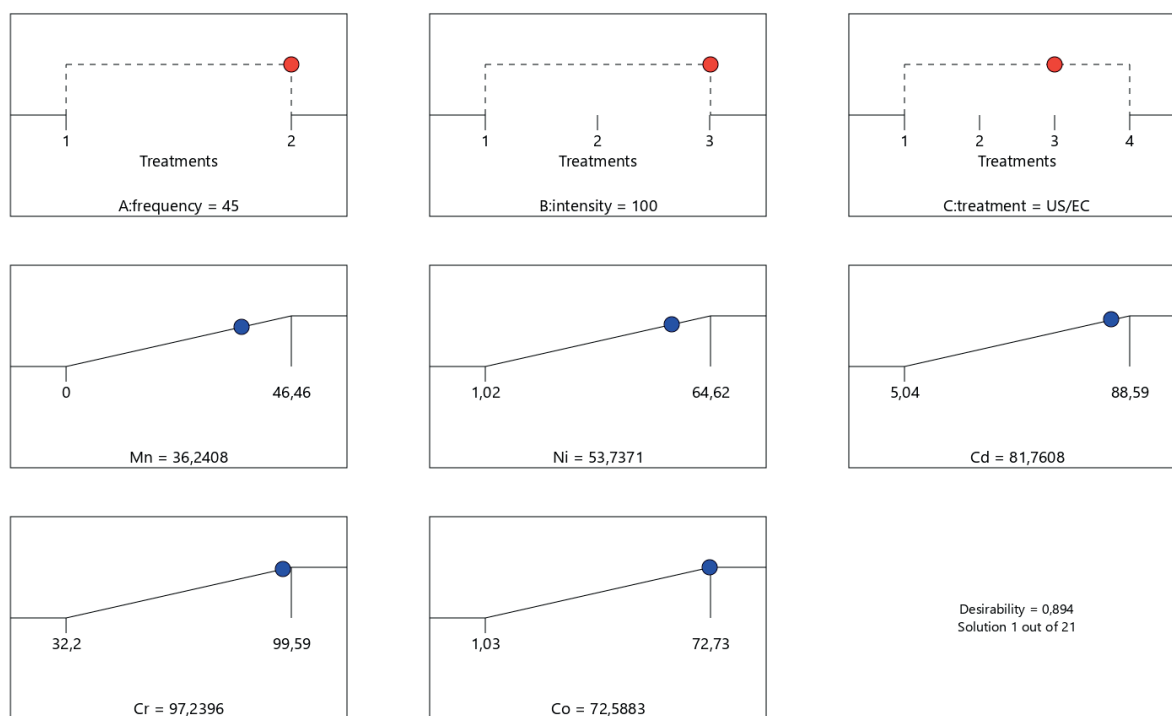


Figure 5. Ramp graphs showing the best solution obtained through process optimization

4. Conclusion

Unlike the ultrasonic treatment, the electrocoagulation process as a standalone treatment is efficient at removing heavy metals from water. However, combining EC with ultrasound results in higher efficiency. The US treatment at 45 kHz and 100% intensity followed by EC resulted in 36.24%, 53.73%, 81.76%, 97.23% and 72.59% efficiencies for the removal of Mn, Ni, Cd, Cr and Co, respectively. Similarly high efficiencies were obtained in the simultaneous US-EC process, proving that sono-electrocoagulation is a promising alternative to conventional treatment methods for heavy metal contaminated water.

Acknowledgements

This work was supported by the Croatian Science Foundation under the project PRIMEUS (UIP2020-02-1160).

References:

- [1] Gautam R.K., Sharma S.K., Mahiya S., Chattopadhyaya M.C.: Contamination of Heavy Metals in Aquatic Media: Transport, Toxicity and Technologies for Remediation (Chapter), Heavy Metals In Water: Presence, Removal and Safety, ed. Sharma, S.K., Royal Society of Chemistry, Cambridge, pp. 1–24, 2014.
- [2] Tchounwou P.B., Yedjou C.G., Patlolla A.K., Sutton D.J., Molecular, clinical and environmental toxicology – Volume 3: Environmental Toxicology, First edition, Springer Basel, 2012.
- [3] Azimi A., Azari A., Rezakazemi M., Ansarpour M.: Removal of Heavy Metals from Industrial Wastewaters: A Review, ChemBioEng Reviews, 4, 1, pp. 37–59, 2017.
- [4] Gunatilake, S.K.: Methods of Removing Heavy Metals from Industrial Wastewater, 1, pp. 12–18, 2015.

- [5] Hubicki, Z., Koodynsk, D.: Selective Removal of Heavy Metal Ions from Waters and Waste Waters Using Ion Exchange Methods (Chapter), *Ion Exchange Technologies*, ed. Kilislioglu, A., InTech, pp. 193–246, 2012.
- [6] Mollah M.Y.A., Schennach R., Parga J.R., Cocke D.L.: Electrocoagulation (EC)- Science and applications, *Journal of Hazardous Materials*, 84, 1, pp. 29–41, 2001.
- [7] Chen, G.: Electrochemical technologies in wastewater treatment, *Separation and Purification Technology*, 38, pp. 11–41, 2004.
- [8] Tran T.-K., Leu H.-J., Chiu K.-F., Lin C.-Y.: Electrochemical Treatment of Heavy Metal-containing Wastewater with the Removal of COD and Heavy Metal Ions, *Journal of the Chinese Chemical Society*, 64, 493–502 2017.
- [9] Pulkka S., Martikainen M., Bhatnagar A., Sillanpää M.: Electrochemical methods for the removal of anionic contaminants from water – A review, *Separation and Purification Technology*, 132, pp. 252–271, 2014.
- [10] Sillanpää M.E.T., *Advanced water treatment: electrochemical methods*, First edition, Cambridge, 2020.
- [11] Leighton, T.G., Apfel, R.E.: The Acoustic Bubble, *The Journal of the Acoustical Society of America*, 96, pp. 2616–2616, 1994.
- [12] Doosti, M. R., Kargar, R., Sayadi, M. H. Water treatment using ultrasonic assistance : A review. *Ecology*, 2, pp. 96–110, 2012.
- [13] Piyasena, P., Mohareb, E., McKellar, R. C.: Inactivation of microbes using ultrasound: A review. *International Journal of Food Microbiology*, 87, pp. 207–216, 2003.
- [14] Franc, J., Michel, J., *Fundamentals of Cavitation*, First edition, Springer, 2004.
- [15] Suslick, K. S., Eddingsaas, N. C., Flannigan, D. J., Hopkins, S. D., Xu, H.: Extreme conditions during multibubble cavitation: Sonoluminescence as a spectroscopic probe, *Ultrasonics Sonochemistry*, 18, pp. 842–846, 2011.
- [16] Zupanc, M., Pandur, Ž., Stepišnik Perdih, T., Stpar, D., Pektovšek, M., Dular, M.: Effects of cavitation on different microorganisms: The current understanding of the mechanisms taking place behind the phenomenon. A review and proposals for further research, *Ultrasonics Sonochemistry*, 57, pp. 147–165, 2019.
- [17] Lee, B.S., Park, H.Y., Choi, I., Cho, M.K., Kim, H.J., Yoo, S.J.: Polarization characteristics of a low catalyst loading PEM water electrolyzer operating at elevated temperature, *Journal of Power Sources*, 309, pp. 127–134, 2016.
- [18] Moradi, M., Vasseghian, Y., Arabzade, H., Mousavi Khaneghah, A.: Various wastewaters treatment by sono-electrocoagulation process: A comprehensive review of operational parameters and future outlook, *Chemosphere*, 263, pp. 128314, 2021.

IV Hydraulic structures

OPTIMIZATION OF THE OPERATION OF THE GABČÍKOVO SHIP LOCKS FILLING AND EMPTYING SYSTEM BY DIFFERENTIAL EVOLUTION

PETER ŠULEK¹, DANIEL BUČEK¹

¹ Slovak University of Technology in Bratislava, Faculty of Civil Engineering, Department of Hydraulic Engineering; Slovakia
e-mail: peter.sulek@stuba.sk, peter.sulek@stuba.sk

Abstract

Ship locks are part of the Gabčíkovo Project on the Danube. Ship locks make it possible to overcome the height difference between the headwater and tailwater in the range of 16–24 meters. Both of them have usable dimensions of 275×34 m. Due to their parameters, they are among the largest ship locks, not only on a regional scale, but on a global scale. Part of the ship locks is a complex filling and emptying system located in the bottom of the ship locks. Its management represents a complex optimization problem, where on the one hand there is an effort to make the Gabčíkovo Project operation efficient (e.g. to minimize the crossing time through the ship locks and to achieve the maximum possible transport capacity of the ship locks) and, on the other hand, the reliability of the ship locks operation is not limited (e.g. destruction of construction or technological components of the ship locks due to extreme pressures of the filling and emptying system components caused by non-permitted parameters of flowing water). One of the most used tools nowadays, for the complex optimization of problems are heuristic methods. Among the most popular heuristic method is differential evolution that belong to the evolutionary algorithms. This method is able to handle difficult, extensive problems with numerous parameters i.e., the optimization of the complex filling and emptying system of the large ship locks. The paper presents the application of the differential evolution technique in optimization of an expert system controlling the Gabčíkovo ship locking process. The optimization objective is minimization of ship's delay while waiting to transit and minimization of destruction parameters due to fast flowing water in the filling and emptying system.

Keywords: ship lock, optimization, heuristic methods, differential evolution, the Gabčíkovo Project.

1. Introduction

The Gabčíkovo Project (GP) is a multi-purpose waterworks. It provides international navigation, flood protection and is used for energy generation through a hydropower plant (HPP) with installed capacity of 720 MW and peak discharge of 5000 m³.s⁻¹ – see Fig. 1 and 2. Due to the specifics of GP, enormous demands are placed on its operation, especially on its reliability and safety.

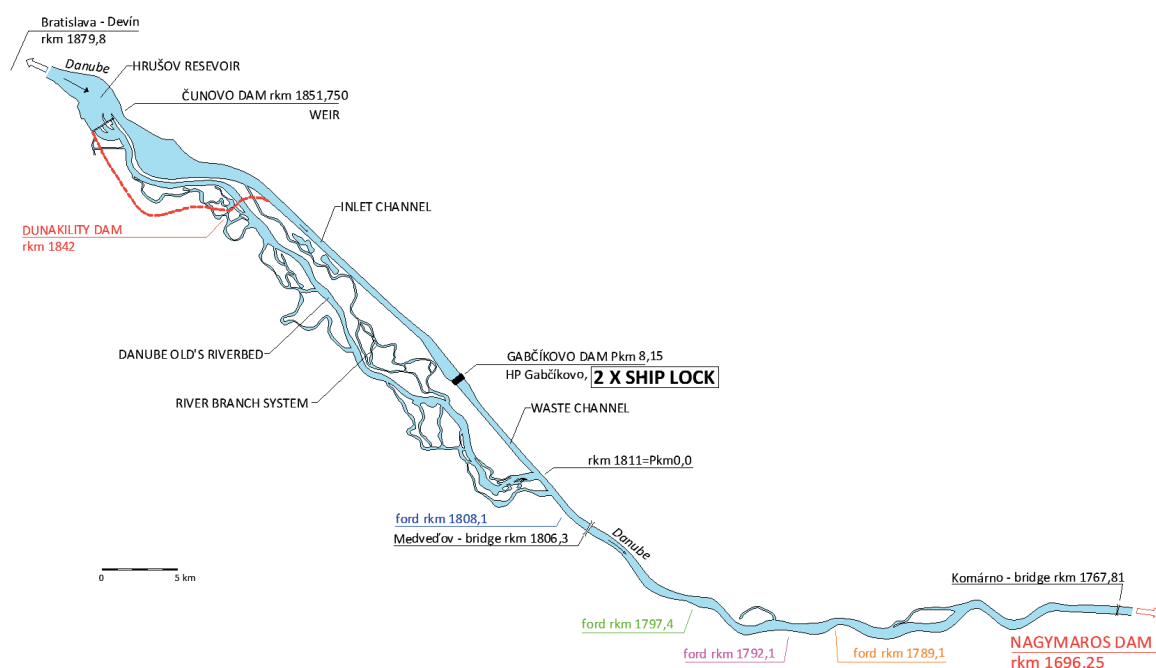


Figure 1. The Gabčíkovo project – scheme

During operation, (on GP facilities) the reliability and safety are mainly affected by the operation of the ship locks. Part of the ship locks is a complex filling and emptying system (FES) of channels located in the bottom of the ship locks – see. Fig. 3. Currently, only 2 or 1 channel out of a total of 4 is routinely used for operation. The opening of the channel valves takes about 4 min. Based on measurements and calculations presented in [1] it is clear, **that such a method of filling / emptying of ship lock causes flow velocities to exceed the operational limits in the filling and emptying system of ship lock by more than 50%**. Such high velocities have demonstrably destructive implications on the technological components of the Gabčíkovo ship lock – see. Fig. 4. On one hand, the efficiency of navigation is increased by minimizing the time of the crossing cycle, on the other hand, its reliability is significantly reduced by an increased number of outages of ship lock with subsequent interruption or restriction of navigation on the Danube.

Therefore, it is necessary to find a way of operation in order to:

1. achieve the fastest passage of vessels through the ship lock and at the same time
2. achieve minimal pressure on the construction and technological parts of the FES, in other words, **to optimize the course of filling and emptying of the Gabčíkovo ship locks.**

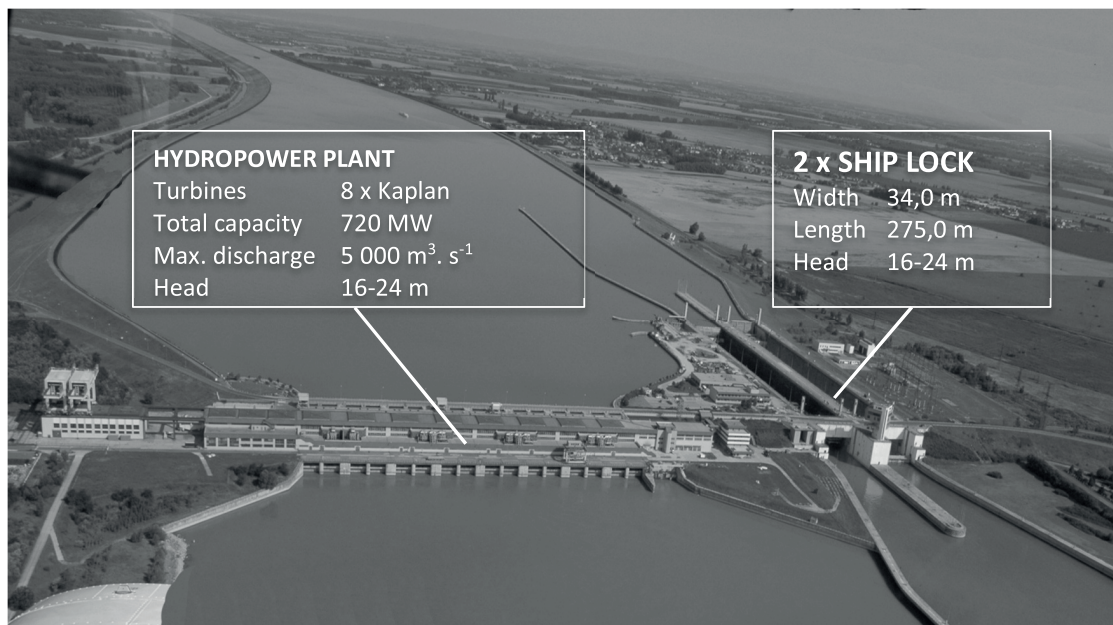


Figure 2. The Gabčíkovo Dam

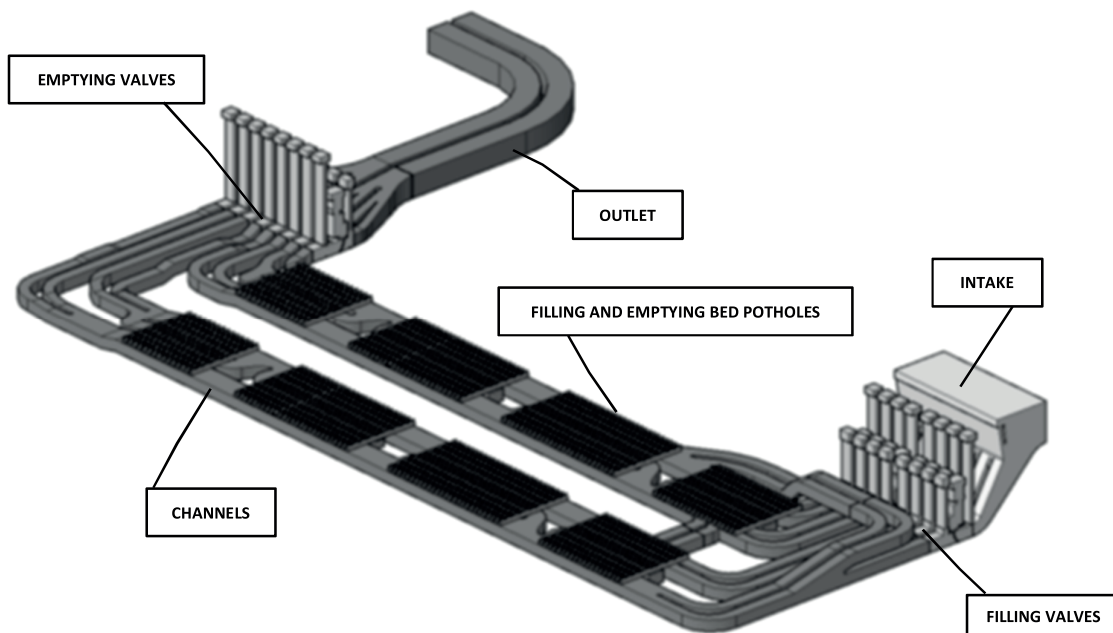


Figure 3. Filling and emptying system of the Gabčíkovo ship locks



Figure 4. Damage in channels of FES (eroded canal surface with exposed reinforcement steel)

2. Methods

2.1. Optimization of the filling and emptying of ship lock

The flow parameters in the FES are affected by multiple parameters: type of FES used, FES parameters such as geometry of individual components, dimensions of individual components (cross-section of channels, channel path, channel interconnection, number, area and distribution slits in the channel ceiling, number, dimensions and arrangement of transverse pipes and dimensions of slits, resistance characteristics). From the physical principle of filling/emptying of ship lock **it is obvious that the course of filling / emptying of ship lock**, in addition to the above-mentioned parameters, **is also significantly influenced by the course of opening the inlets or outlets** [2].

2.2. Formulation of the optimization problem

The mathematical description of the optimization model of filling and emptying of the Gabčíkovo ship lock formulated by function (1) must be based **on the theory of filling and emptying of locks with outlet below the initial water level in ship lock and with nonlinear opening of inlets and outlets**. Due to the parameters of FES, it is necessary to consider the effect of water inertia in the channels, which has dampening effect on accelerating and decelerating of the water body at the beginning and end of filling respectively.

The consequence of the influence of water inertia in the FES is that initially water inflows / outflows and the water level rises / decreases slower and later, after the start of the flow in the channels, faster in comparison with the course of filling resp. emptying calculated without considering the effect of inertia. In the case of performance, the so-called inertia can swing the level in the ship lock above the level of headwater. In the case of emptying, the inertia can “downswing” the level in the ship lock below the level of tailwater. In both cases, there may be an unusual load on the upper or lower gates of ship lock, which may result in a threat to the safety of navigation on the GP.

Regarding the above, the operation of FES of the Gabčíkovo ship lock can be seen as a complex optimization task, the aim of which is to pass the vessel(s) through ship lock as fast as possible, while minimizing the loads of FES and at the same time maintaining safety of passage by eliminating non-standard loads on construction and technological parts of the Gabčíkovo ship locks.

The result of optimization is finding the optimal course of opening the valves, in which the maximum permissible flow rates in the filling and emptying system will not be exceeded, the maximum permissible “upswing” / “downswing” will not be exceeded and at the same time the crossing time will be as short as possible.

2.3. Optimization model of filling and emptying of ship lock

The calculations of the emptying course of the Gabčíkovo ship lock are based on the expression of the elementary volume of water dV , which flows from one “compartment” to another during the time interval dt . According to [3] this phenomenon is expressed by two differential equations, namely the dynamic equation (1) and the continuity equation (2).

$$dV = \mu \cdot f \cdot \sqrt{2 \cdot g \cdot \left(y - \frac{\lambda}{g} \cdot \frac{dv}{dt} \right)} \cdot dt \quad (1)$$

$$dV = F_{SL} \cdot dy \quad (2)$$

where μ is loss coefficient for emptying, f is flow area of outlet [m²], y is immediate head in ship lock [m], λ is the virtual channel length; the path travelled by the water in the channel(s) up to the point of inflow into the ship lock taking into account the effect of the change in flow velocity caused by the change in flow rate [m], $\frac{dv}{dt}$ is the acceleration of water flow in the channels [m.s⁻²], F_{SL} is the surface area of ship lock [m²] a dy is the rise/fall of the water level in ship lock over time dt .

The emptying time of ship lock during nonlinear manipulation with outlet valves can be described by a differential equation:

$$T = \int_{H_{fin}}^{H_{in}} \frac{F_{SL} \cdot dy}{\mu \cdot f(t) \cdot \sqrt{2 \cdot g \cdot (y - \frac{\lambda}{g} \cdot \frac{dv}{dt})}} \rightarrow \min \quad (3)$$

where H_{in} is the initial hydraulic head [m] and H_{fin} is the final hydraulic head in ship lock.

The target function (3) must be supplemented by restrictive conditions:

$$v \leq v_{max} \quad f(t) \leq f_{max} \quad |H_{fin}| \leq |\Delta H_{max}| \quad (4)$$

where v_{max} is the maximum permissible flow velocity in the channels of emptying system of ship lock, f_{max} is the maximum area of the outlet valves opening and ΔH_{max} is the maximum water level “downswing” in ship lock.

Analogously, it is possible to derive relations for the filling of ship lock according to relations (1) and (2).

2.4. Optimization methods

The objective function (3) can be defined as a nonlinear optimization problem with nonlinear constraints and with a complex form. The complexity is mainly caused by the nonlinear course of the criteria function and the interconnection between the loss coefficients μ , the inflow/outflow from ship lock and the target function for valve opening $f(t)$. Various methods of operational analysis can be used to solve the problem formulated in this way.

In the case of solving large-scale and complex problems, classical (numerical) optimization methods can get into many difficulties (e.g. the so-called “curse of the dimensionality” of problems), although they show high efficiency in solving less complex problems. Possibilities for optimization of filling of ship lock using Mixed Integer Linear Programming (MILP) are published e.g., in [4, 5]. To solve multi-parameter optimization functions with a “chaotic” course, with a number of extremes or with an unknown gradient for which there is no adequate specific algorithm or a straightforward numerical method, mainly **heuristic optimization methods** are used (e.g., partical-swarm optimization (PSO), ant colony optimization (ACO), simulated annealing (SA) and others). These are search algorithms that are characterized by a certain intelligence, and therefore we classify them more among the methods of artificial intelligence. The possibilities of optimizing filling of ship lock with PSO have been demonstrated in [6]. ACO was used in [7] and the method of simulated annealing in [8]. The solution based on the combination of SA and MINLP was used to optimize the ship lock of the waterworks Three Gorges in [9]. The use of genetic algorithms (GA) in optimizing of filling/emptying of ship lock has been published in [10]. Differential evolution (DE) is currently one of the promising heuristic optimization methods.

2.4.1. Differential Evolution

DE is originally introduced by Storn and Price [11]. Gradually, this method became more applied in scientific fields, predominantly because of its good convergence properties and is in general easy to understand. The DE method’s function is to combine simple arithmetic operators with the classical events of crossover, mutation, which generate new vectors (trial vectors) and selection, which vectors will be included in the next final generation [12]. Basically, a scheme that generates trial parameter vectors which are iteratively combined and updated using simple formulas to form new vectors.

It differentiates an evolutionary strategy from creation of a new individual using a differential vector, which is considered the difference of two randomly selected individuals. Then two additional individuals join the creation of the subject and eventually the new individual consists of four individuals. The way DE works with a population is almost indistinguishable from other EA. However, crossing and mutation run in the reverse order different from other EA.

The basic parameters of DE are F_{DE} the mutation factor, CR the crossover parameter and NP the population size.

In the case of solving the function (3) using DE, it is necessary to transform the function into a pseudo fitness function φ , which can be written in the form:

$$\varphi = - \left(\int_{H_{fin}}^{H_{in}} \frac{F_{SL} \cdot dy}{\mu \cdot f(t) \cdot \sqrt{2 \cdot g \cdot (y - \frac{\lambda}{g} \cdot \frac{dv}{dt})}} \right) - W_{pen} \sum_{j=1}^A s_j \cdot pen_j \rightarrow max \quad (5)$$

where pen_j are the penalty functions replacing the limiting conditions of the solution, W_{pen} is the weighting factor of the penalty, A is the number of restrictions and s_j is the factor expressing the weight of the strictness of compliance with individual restrictions. By the mutual ratio of individual weights, it is possible to “stiffen” or “loosen” individual task boundaries. An example of a block diagram of filling/emptying of SL optimization using DE is shown in Fig. 5.

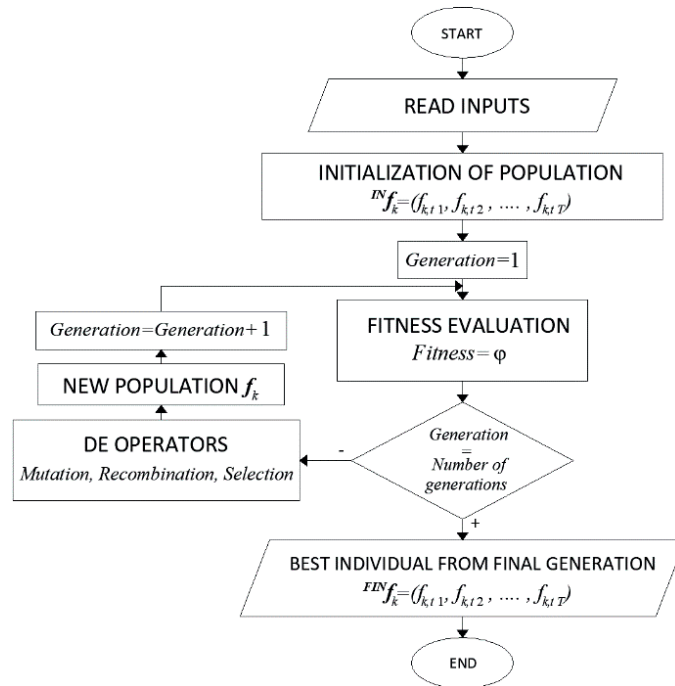


Figure 5. Block scheme of the filling and emptying optimization of the ship lock using by DE

In the case of performance or emptying SL with several closures is the solution of the pseudo fitness function φ (5) represented by the matrix of vectors $^{FIN}f_k$, which can be written in the form:

$$^{FIN}f_k = \begin{pmatrix} f_{1,t_1} & f_{1,t_2} & \dots & f_{1,t_i} & \dots & f_{1,t_{T_1}} \\ f_{2,t_1} & f_{2,t_2} & \dots & f_{2,t_i} & \dots & f_{2,t_{T_2}} \\ \vdots & \vdots & & \vdots & & \vdots \\ f_{k,t_1} & f_{k,t_2} & \dots & f_{k,t_i} & \dots & f_{k,t_{T_k}} \\ \vdots & \vdots & & \vdots & & \vdots \\ f_{N,t_1} & f_{N,t_2} & \dots & f_{N,t_i} & \dots & f_{N,t_{T_k}} \end{pmatrix} \quad \text{pre } \forall k \in \langle 1, N \rangle, \forall i \in \langle 1, T \rangle \quad (6)$$

where k is the index of the valve, $k = 1, 2, \dots, N$, N is the number of valves involved in the optimization, f_{k,t_i} is the optimal outflow area of the k -th valve at time t_i and t_{T_k} is the maximum opening time of the k -th valve.

3. Results

Fig. 6 shows the result of optimizing the emptying of the right the Gabčíkovo ship lock, optimized course of opening/closing for 4 valves using *DE/rand/1/bin* algorithm. Maximum insertion speed of the servo piston of 32 mm/s was considered, with a maximum extension speed of the servo piston of 26 mm/s, with a maximum allowed average cross-sectional flow velocity in the FES channels of 8 m/s, with a maximum allowed water level drop 2.5 m/min, with an initial hydraulic head 23.6 m and a maximum permitted “downswing” of the water level compared to the water level in tailwater of 60 mm.

The computational step for the calculation of the optimal course of the manipulation with the inlet/outlet valves ($f_k(t)$) was set to $\Delta t = 10$ sec. From the preliminary calculations it was clear that the optimal solution of the pseudo fitness function φ (5) is obtained by synchronous manipulation with valves. This significantly reduces the number of searched variables from the original 400 to 100. This results in a significant reduction in the computation time of the optimization and at the same time reduces the risk of the solution getting stuck in the local extremes of the problem. In the sense

[11, 12], the population size NP was set to a value of 10 times the dimensionality of the problem, i. e. $NP = 1000$. The parameters CR and F_{DE} were considered to be 0.5 according to the recommendations in [13~21].

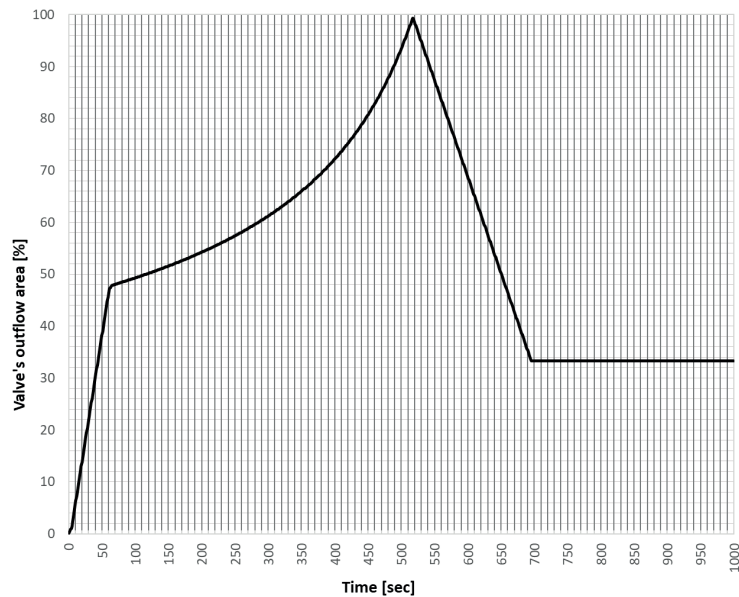


Figure 6. Optimal manipulation for 4 valves;
 $f_1(t)=f_2(t)=f_3(t)=f_4(t)$

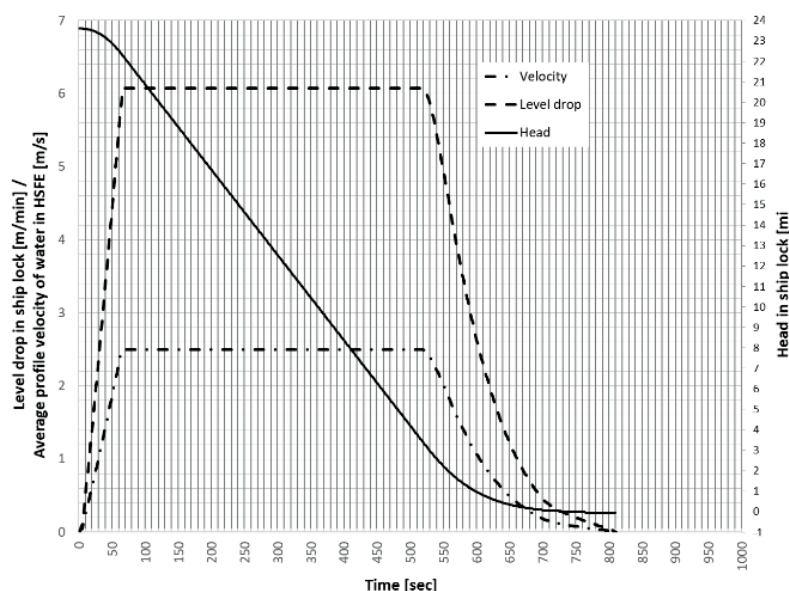


Figure 7. Parameters of ship lock emptying

Calculated parameters for emptying of right the Gabčíkovo ship lock are shown in Fig. 7, precisely the time course of the water level in the ship lock during emptying, the time course of the average cross-sectional velocity in the FES channels and the time course of the water level decrease in the ship lock. From the results of the optimal solution, it is clear that all limiting conditions were met, in other words, the average profile velocity in the FES channels is less than 8 m/s, the rate of water level drop in the ship lock is not greater than 2.5 m/min and the “downswing” of the water level in the ship lock at the end of the emptying is not greater than 60 mm. The emptying time of ship lock is about 13 minutes, which is a time that fully meets the navigation requirements on the Danube.

4. Conclusion and discussion

From the results published in Chap. 4, it is clear that DEs are a suitable method for solving the problem of optimizing the course of filling or emptying of ship locks with a relatively large head and with complex filling and emptying system. The heuristic approach makes it possible to solve this complex optimization problem with a “wild” course with a number of extremes and with an unknown gradient, even though there is no straightforward numerical solution method. The disadvantage of using DE is the relatively complex determination of the weight(s) of the W_{pen} penalty function in relation (5). However, the advantage is that after their determination, it is possible to use them to determine the optimal handling of closures for other input parameters of the task. Another disadvantage of the use of DE (and this

applies to heuristic methods in general) is their problematic use in real world conditions of the ship lock operation. This is mainly due to the relatively long calculation time (approx. several tens of minutes). The solution is the use of optimization model of ship lock filling/emptying using the DE method for the so-called pre-calculation of optimal closure manipulations and their subsequent use in the process of real operation using data models.

Acknowledgements

The paper was developed within the frame of and based on the financial support of the APVV-18-0472 project.

References:

- [1] Možiešik, L., Šulek, P., Orfánus, M., Hruštinec, L. Upgrade of Gabčíkovo locks – Feasibility study. Hydrotechnika STU, s.r.o., Bratislava. 2017.
- [2] Kašpar, T., Fošumpaur, P., Králík, M., Zukal, M. Parametric study of direct filling system of medium-head navigation locks. *Pollack Periodica*. Volume 16, Issue 2, pp. 43–49, ISSN: 17881994, August 2021
- [3] Čábelka J.: Waterways and navigation. SVTL, SNL, Praha, Bratislava 1963.
- [4] Hermans, J. Optimalisatie van binnenscheepvaart. Master's thesis, KU Leuven. 2008.
- [5] Mundy, R., Campbell, J. Management systems for inland waterway traffic control. Technical report. Retrieved from http://www.ctre.iastate.edu/mtc/reports/inland_waterway/volume1.htm. 2005
- [6] Kanović, Ž., Bugarski, V., Bačkalić, T., Jeličić, Z., Petković, M., Matić, D. Optimization Of Ship Lock Control System Using Swarm-Based Techniques. *Journal on Processing and Energy in Agriculture* 18; 1; p 30–35, ISSN: 1821–4487. 2014.
- [7] Liu, R.J., He, D.D., Wang, L.J., Xu, H.Y. Ant Colony Optimization Applied to the Three Gorges Ship Lock Arrangement Optimization. *Applied Mechanics and Materials*. Vols. 543–547, pp. 1663–1666. 2014.
- [8] Kosmas, O.T., Vlachos, D.S. Simulated annealing for optimal ship routing. *Computers & Operations Research*. 39, pp. 576–581. 2012.
- [9] Zhang, X., Qi, H., Fu, X., Yuan, X. Hybrid algorithm to minimize total weighted wait-time of ships for navigation co-scheduling in the three Gorges project. In: *International Conference on Transportation, Engineering* (pp. 2759–2764). 2007.
- [10] Kanović, Ž., Bugarski, V., Bačkalić, T. Ship Lock Control System Optimization using GA, PSO and ABC: A Comparative Review. *Promet – Traffic&Transportation*, Vol. 26, No. 1, 23–31. ISSN: 1848-4069. 2014.
- [11] Storn R., Price K. Differential evolution – a simple and efficient heuristic for global optimization over continuous spaces, *Journal of Global Optimization*, Vol. 11, No. 4, pp. 341–359. 1997.
- [12] Price K., Storn R., Lampinen J. *Differential evolution – A practical approach to global optimization*, Springer, 2005.
- [13] Šulek, P., Kinczer, T. Impact of differential evolution parameters on optimization of hydro-thermal coordination. In *Pollack Periodica*. Vol. 14, no. 3, s. 121–130. 2019.
- [14] Liu, J., Lampinen, J. On setting the control parameter of the differential evolution method, *Proceedings of the 8th International Conference on Soft Computing*, Brno, Czech Republic, pp. 11–18, 5–7 June 2002.
- [15] Zaharie, D. Critical values for the control parameters of differential evolution algorithms, *Proceedings of the 8th International Conference on Soft Computing*. Brno, Czech Republic, pp. 62–67, 5–7 June 2002.
- [16] Liu, J., Lampinen, J. A fuzzy adaptive differential evolution algorithm, *Soft Computing*, Vol. 9, No. 6, pp. 448–462. 2008.
- [17] Qin, A.K., Suganthan, P.N. Self-adaptive differential evolution algorithm for numerical optimization, *Proceedings of the IEEE Congress on Evolutionary Computation*, Edinburgh, Scotland, UK, pp. 1785–1791. 2–5 September 2005.
- [18] Qin, A.K., Huang, V.L., Suganthan, P.N. Differential evolution algorithm with strategy adaptation for global numerical optimization, *IEEE Transactions on Evolutionary Computation*, Vol. 13, No. 2, pp. 398–417. 2009.
- [19] Brest, J., Greiner, S., Boskovic, B., Mernik, M., Zumer, V. Self-adapting control parameters in differential evolution: A comparative study on numerical benchmark functions, *IEEE Transactions on Evolutionary Computation*, Vol. 10, No. 6, pp. 646–657. 2006.
- [20] Pedersen, M.E.H. Tuning and simplifying heuristical optimization, PhD Thesis, School of Engineering Sciences, University of Southampton, England, 2010.
- [21] Pedersen, M.E.H., Chipperfield A.J. Tuning differential evolution for artificial neural networks, *Artificial neural networks*, Nova Publishers, 2011.

IV Hydraulic structures

PROGNOSIS ANALYSIS OF ARCH DAM BEHAVIOR BY HYBRID MODEL

FROSINA PANOVSKA¹, STEVCHO MITOVSKI¹, LJUPCHO PETKOVSKI¹

¹ Ss. Cyril and Methodius University in Skopje, Faculty of Civil Engineering; Republic of North Macedonia
e-mail: fpanovska@gf.ukim.edu.mk, smitovski@gf.ukim.edu.mk, petkovski@gf.ukim.edu.mk

Abstract

The assessment of the structural stability and behavior of the dam during construction, at full reservoir and during the service period is of paramount importance for such structures. Each dam, in dependence of the type and dimensions, has installed system for technical monitoring that enables tracking of the dam behavior and assessment of the dam state throughout registration and interpretation of various data such as displacements, stresses, seepage etc.

The case study is double curvature concrete arch dam, with asymmetric shape due to the valley topography. In the paper are systemized acknowledgments for the comparison of the recorded data from technical monitoring of the dam and output results from spatial (3D) numerical model, created by application by application of SOFiSTiK code, based on Finite Element Method. In addition, a Neural Network model is created by recorded data from the technical monitoring. The both models create the so called hybrid model.

For both models are used input parameters such as variation of water level in the reservoir and air temperature, and the output results are compared with recorded values for water level in piezometers at specified nodes of the dam. The aim of the task is to compare and calibrate the output results from the both models and recorded values from the technical monitoring of the dam and to carry out prognosis modeling for the future behavior of the dam.

Keywords: arch dam, numerical model, FEM, SOFiSTiK, neural network, prognosis modelling.

1. Introduction

The dams, having in consideration their importance, dimensions, complexity of the problems that should be solved during the process of designing and construction along with the environmental impact are lined up in the most complex engineering structures (1) (2). The assessment of the structural stability and the behavior of the dam during construction, at full reservoir and during the service period is of paramount importance for such structures.

In this paper are systemized acknowledgments from the analysis of piezometer levels in the rock foundation of an concrete arch dam, obtained with application of numerical methods, based on Finite Element Method, with the code SOFiSTiK, as well as artificial neural networks model based on general regression neural networks. As follows, data on piezometer level obtained by both models for calibration and prediction piezometer levels in the rock foundation of an arch dam, located in France, will be commented. The aim of the task is to predict the dam behavior, that includes calibration (based on monitoring data) and prognosis stage (short-term and long-term) focusing on variable such as piezometer level.

2. Case study

The analysed dam is a double curve arch dam with asymmetric shape located in southern France (Fig. 1), constructed in the period between 1957–1960. The foundation of the dam is laminated metamorphic slate with high compressive strength, with present anisotropy in the left bank. The dam height above foundation is 45m, with crest width of 2m and width of the dam at the foundation of 6m (Fig. 2).

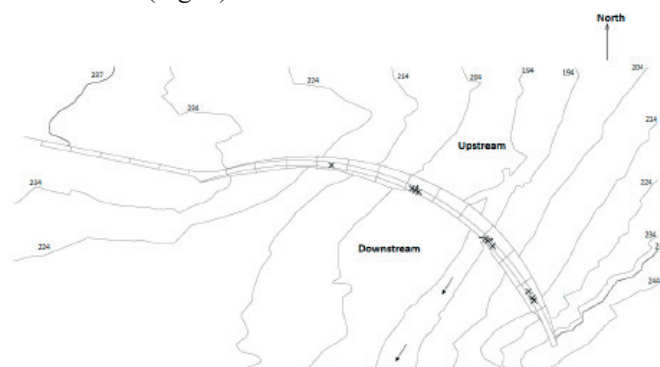


Figure 1. Layout of the case study dam

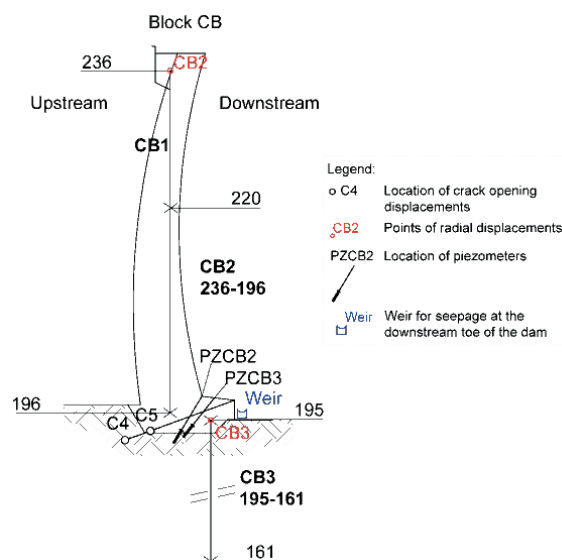


Figure 2. Central block section with display of monitoring instruments (right) (3) (4)

3. Numerical modelling by Finite Element Method

The numerical analysis of the dam is carried out with application of SOFiSTiK, a software developed in Munich, Germany. The software analyses are based on finite element method. It is a powerful numerical tool for analysis of specific phenomena, important for realistic simulation of dam's behavior, such as: discretization of the dam and foundation taking into account the irregular and complex geometry of the structure, simulation of stage construction, simulation of contact behavior by applying interface elements and etc. in order to assess the dam behavior and evaluate its stability.

The numerical experiment includes following steps: (1) choice of material properties and constitutive laws (concrete and rock); (2) discretization of the dam and the rock foundation and (3) simulation of the dam behavior for the typical loading states.

The linear material properties for the dam body (concrete) and the foundation (rock) are given in Tab.1.

Table 1. Material parameters.

Zone		dam body (concrete)	rock	Comment
γ_{spec}	kN/m ³	24.0	27.0	Unit weight
k_s	m/s		2.0e-05	Permeability coefficient
ν		0.350	0.450	Poisson coefficient
Alpha	1/C°	7.0E-06		Thermal expansion coefficient
E	GPa	22	3	Young's modulus of elasticity

Numerical analysis of piezometric levels at the foundation of the arch dam is carried out by plane (2D) model, where foundation with included grout curtain is modeled with plane elements. A powerful and reliable finite element should be applied in case where an analysis of structure with complex geometry and behavior is required, having in consideration that the correctly calculated deformations and stresses are of primary significance for assessment of the dam stability. In this case, for discretization of the dam body and the rock foundation is applied quadrilateral finite element, by 4 nodes. Namely, the model is composed of the rock foundation with included zone of grout curtain. The plane (2D) model has geometrical boundaries, limited to horizontal and vertical plane (Fig. 3), adopted according to the specified data. The discretization is conveyed by including zones of various hydraulic parameters in the model – rock foundation and grout curtain, approximately modelling the rock foundation per 75m upstream and downstream of the dam.

However, the hydraulic properties for the material in the rock foundation were not available. So, two-step calibration (in case of homogeneous and heterogeneous rock foundation) has been carried out for the value of the permeability coefficient k in accordance with the seepage values from the monitoring process. The estimated permeability coefficient for laminated metamorphic slate ranges in interval $k=(10^{-7} \div 10^{-9})\text{m/s}$ (5) (6). The permeability coefficient additionally is calibrated by the value of the full seepage flow directly below the dam, specified as measured values in weir at gallery located at the downstream toe of the dam. So, according to the available measuring data for water level at

232.0 m the average registered seepage flow is 8 l/min. From the registered reservoir water levels and seepage flow it can be noticed general correlation, however in some periods there is discrepancy in the measured values that could be indication that the seepage flow is caused by additional influences then the seepage process in the rock foundation. The seepage analysis was carried out for $H=232.0$ m as upstream boundary condition and $H=0$ m as downstream boundary condition, by applying Darcy flow rule adopting the rock foundation as heterogeneous flow medium, composed of rock material (laminated metamorphic slate) and two sections (vertical and inclined) of grout curtain, by assumed permeability coefficient in first iteration $k_r=1\times 10^{-7}$ m/s for the rock zone. By the first-step (initial) calibration calculation of the permeability coefficient for homogeneous rock foundation was obtained value of $k=2.89\times 10^{-8}$ m/s, applied in the calculation for the full calibration and prognosis analysis of the piezometric levels and seepage. Due to the grout curtain in the rock foundation (heterogeneous zone), additional calibration were carried out, in order to match the measured seepage flow $Q_m=8$ l/min and thus obtaining value of permeability coefficient for the rock foundation $k_{rf}=12.5\times 10^{-8}$ m/s and permeability coefficient for the grout curtain $k_{gc}=2.5\times 10^{-8}$ m/s, used as input parameters for the seepage calibration and prognosis stage, for the FEM model (Fig. 3).

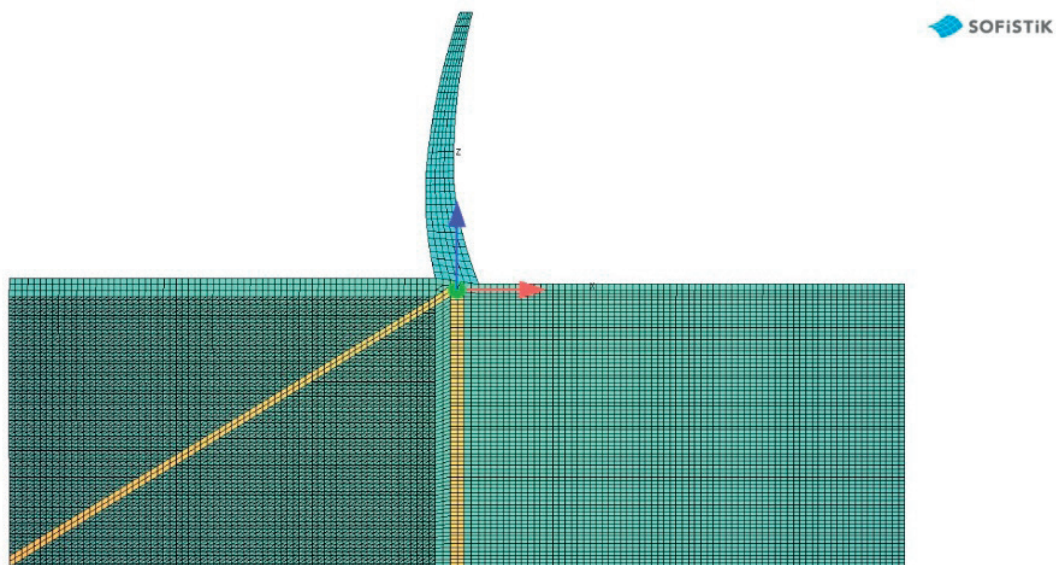


Figure 3. View of the plane numerical model, material distribution and FEM, discretized with total of 15511 elements and 11252 nodes

4. Neural networks modelling

Artificial neural networks are typical example of a advanced interdisciplinary tool that helps solving various different engineering problems which could not be solved by the classical modelling and statistical methods (7). Neural networks are capable of collecting, memorizing, analyzing and processing large number of data gained from some experiments or numerical analyses. They are an illustration of sophisticated modelling technique that can be used for solving many complex problems. The trained neural network serves as an analytical tool for qualified prognoses of the results, for any input data which were not included in the learning process of the network. Their operation is reasonably simple and easy, yet correct and precise. The artificial neural networks, together with the fuzzy logic and genetic algorithms, belong to the group of symbolic methods of intelligent calculations and data processing that operate according to the principles of soft computing. Neural networks are developed as a result of the positive features of a few different research directions: data processing, neuro-biology and physics (7). Researches around the world showed that neural networks have an excellent success in prediction of data series and that is why they can be used for creating prognostic models that could solve different problems and tasks (7; 8). For practical application of artificial neural networks, it is not necessary to use complex neuron models. Therefore, the developed models for artificial neurons only remind us to the structure of the biological ones and they have no pretension to copy their real condition (9). The artificial neuron receives the input signals and generates the output signals. Every data from the surrounding or an output from other neurons can be used as an input signal.

ANN neural networks functioning is analog to the way human neuron networks function. The neuron in the human body is consisted of axon, soma and dendrite. The soma is the body, dendrites are connections to other neurons and axon transfer electric signals among cells. ANN is also consisted of neurons, and they practically imitate biological processes that normally happen in the neuron network of a living organism. The mathematical model of artificial neural networks is basically a network comprised of a large amount of neurons interconnected with connection links of specifically defined weight coefficients. ANN consists of: (1) input data layer, (2) weight coefficients, (3) hidden layer/s and

(4) output data layer. Weight coefficients are key elements in neural networks. Their value represents the relative importance of each neural input and they define the ability of input activation of neurons. Neural networks have the ability of ‘training/learning’. This process occurs as a result of adjustments in the value of weight coefficients, based on the array of input and output data. Activation function defines the output of a neuron given an input or set of inputs. Linear or non – linear functions serve as activation functions, however, one of the most commonly used one is sigmoid function:

$$Y_t = \frac{a}{1 + e^{-y}}$$

As follows, by applying Generalized Regression Neural Network (GRNN) specifically NeuralTools software from Palisade corporation, data prediction in case of arch dam are shown. The data set used for training is basically values of the given measured data. In the training process, 70% of the data is used for training and 30% is used for validation. The variables are classified as independent or dependent, depending on their role in the prediction process. The dependent variable is the variable to be predicted. The independent variables are the “explanatory” variables used to predict the dependent variable. Cases where the dependent variable values are known are used to train and test a neural network.

The modeling by application of GRNN is based on the following variables: (1) water level in piezometer PZCB2 as dependent numeric value and water level in the reservoir as independent numeric value, and (2) water level in piezometer PZCB3 as dependent numeric value and water level in the reservoir as independent numeric value.

5. Calibration process

The calibration process is carried out by comparison of the measured and calculated piezometer levels for a time series of 12 years (2000–2012), for both the FEM and neural networks (NN) model.

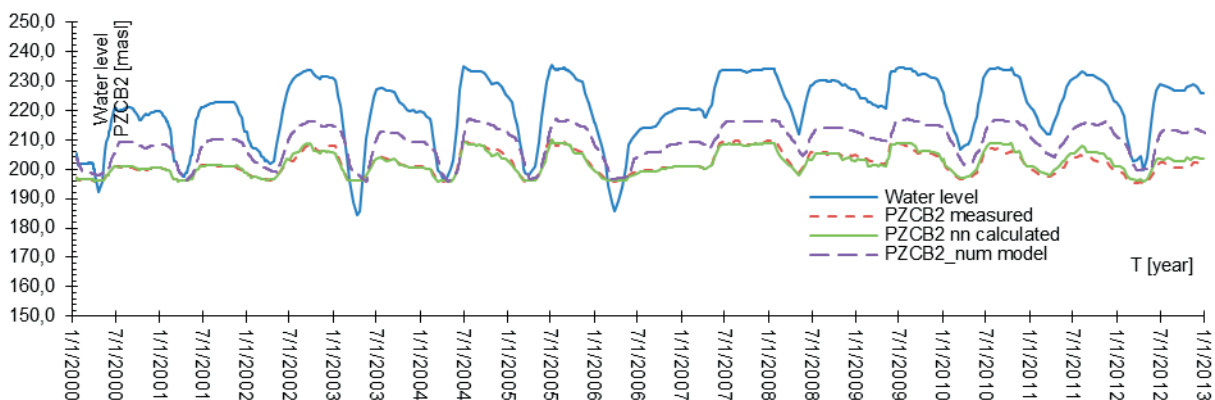


Figure 4. Display of measured and calculated time series of piezometer levels in piezometer PZCB2 for 2000–2012

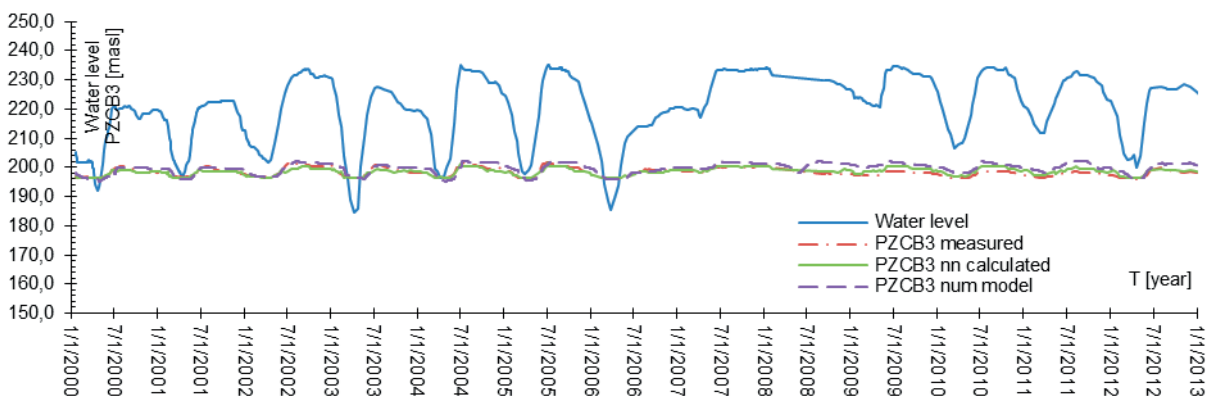


Figure 5. Display of measured and calculated time series of piezometer levels in piezometer PZCB3 for 2000–2012

In Fig. 4 and Fig. 5 graphs are shown from output results of the calibration process for measurements in piezometers PZCB2 and PZCB3, for a time series of 12 years of measured data. The calibration process modelling is done by both FEM and neural networks (NN) model.

By comparison of the piezometric levels for piezometers PZCB2 and PZCB3, calculated by NN model (Fig. 4 and Fig. 5) it can be noticed excellent matching of the measured and calculated data regarding the distribution and the values and some less good matching by the FEM model. The calculated piezometric levels by NN model, in analogy of the calculated values from the FEM model for seepage analysis, are in full correlation with the reservoir water level.

The timeline of 12 years in the calibration process is used as data for training the neural networks. The trained neural networks are afterwards used for prediction of the behavior of the water level in the piezometers for short and long term.

As follows, accuracy generated parameters for the NN models are given for both piezometer PZCB2 (Table 2) and piezometer PZCB3 (Table 3).

Table 2. Accuracy parameters for the neural networks model for PZCB2, for both the training and testing period

Parameter	Training	Testing
Root Mean Square Error	0.8597	1.072
Mean Absolute Error	0.5619	0.7393
Std. Deviation of Abs. Error	0.6507	0.7761

Table 3. Accuracy parameters for the neural networks model for PZCB3, for both the training and testing period

Parameter	Training	Testing
Root Mean Square Error	0.7792	0.7581
Mean Absolute Error	0.5574	0.5484
Std. Deviation of Abs. Error	0.5445	0.5234

6. Prognosis process

The prognosis stage consists of short-term and long-term prediction of the specified variables. Namely, the short-term prediction includes period January, 2013-June, 2013, while the long-term prediction captures period July, 2013-December, 2017. The prediction analyses are conducted for both the numerical and neural networks model, for piezometer levels in PZCB2 and PZCB3.

The calculated piezometric levels for piezometers PZCB2 and PZCB3 for the short-term and long term prognosis, as expected, are varying in correlation with the water level in the reservoir (Fig. 6 and Fig. 7) apropos are in accordance with the hydraulic loading.

The maximal and minimal calculated values for the piezometer levels in PZCB2 are varying between 205.5 masl and 195.5 masl, whereas piezometer levels in PZCB3 are varying in a tight range approximately to 200.0 masl.

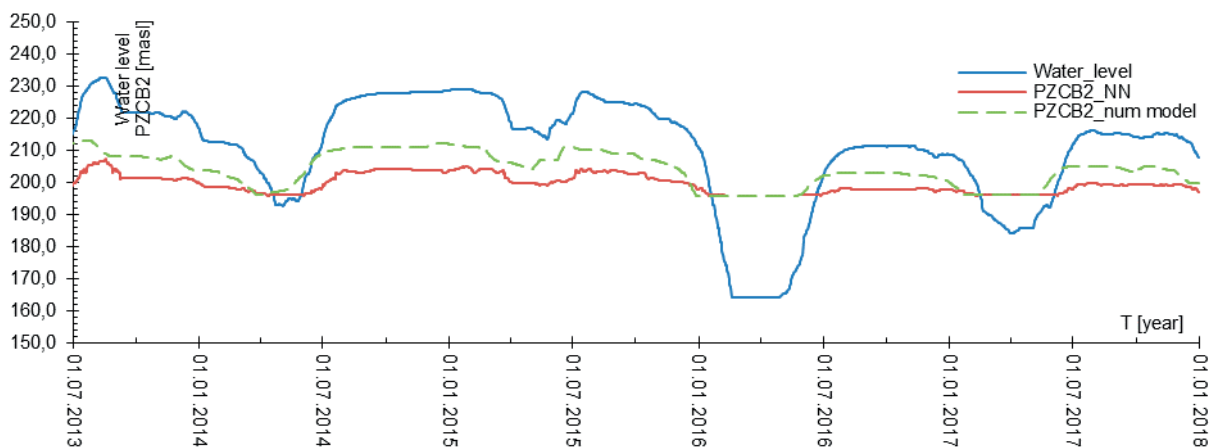


Figure 6. Prognosis calculated time series of piezometer levels for PZCB2 for 2013-2017 by NN and numerical model

Using the accuracy parameters from the calibration period derived from the neural networks model, a warning level corridor of permissible variation of piezometer levels is defined. This corridor represents boundaries of safe variation of the piezometer water level. The corridor is defined with added value ($3 \cdot$ Standard Deviation of Abs. Error) to the predicted values for piezometer level. Such levels are defined in order to establish corridors for the permissible piezometric levels for piezometer PZCB2 and PZCB3, that are not to be exceeded by the monitoring values for the future period. Any excidance of the specified coridor values would indicate to iregular occurence in the dam foundation behaviour, that will need to be investiguated additionally.

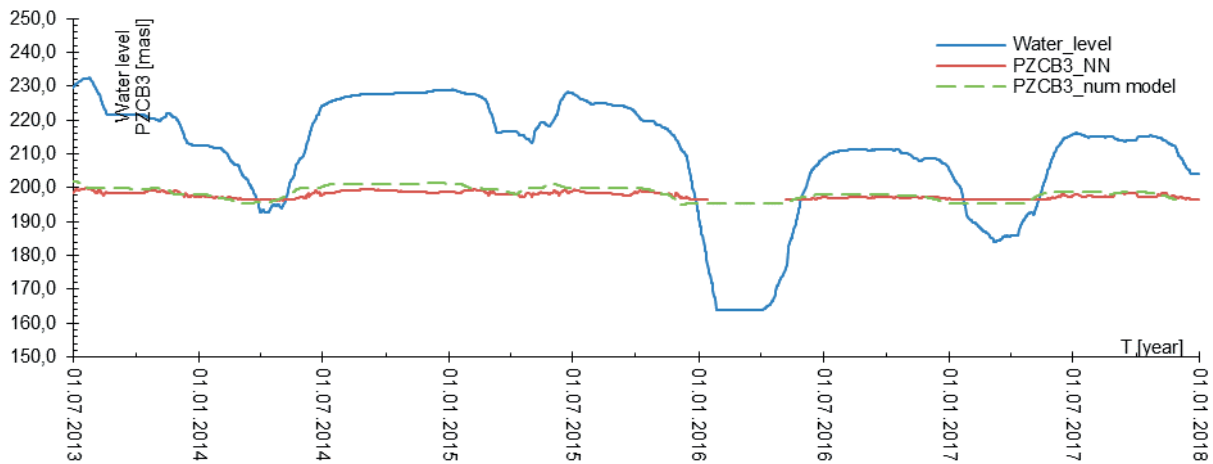


Figure 7. Prognosis calculated time series of piezometer levels for PZCB3 for 2013-2017 by NN and numerical model

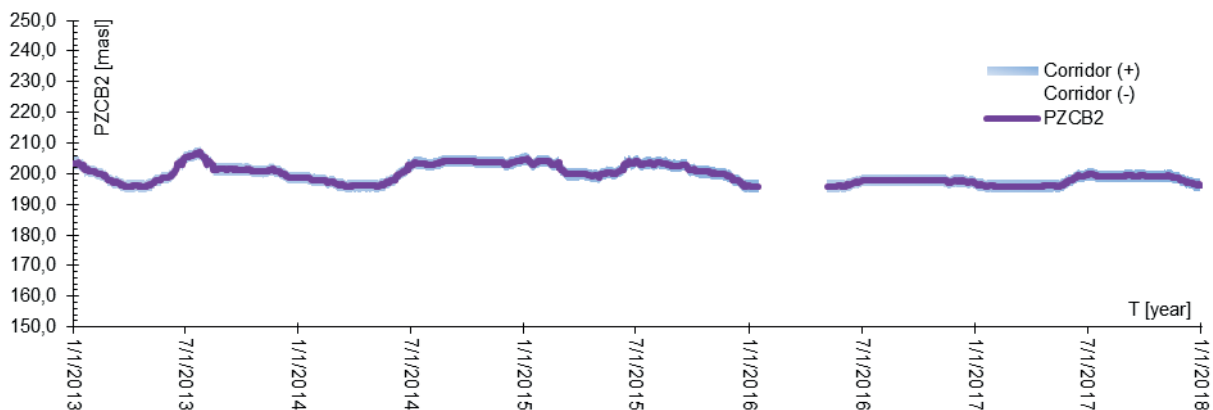


Figure 8. Warning level corridor of permissible variations for piezometer level in PZCB2

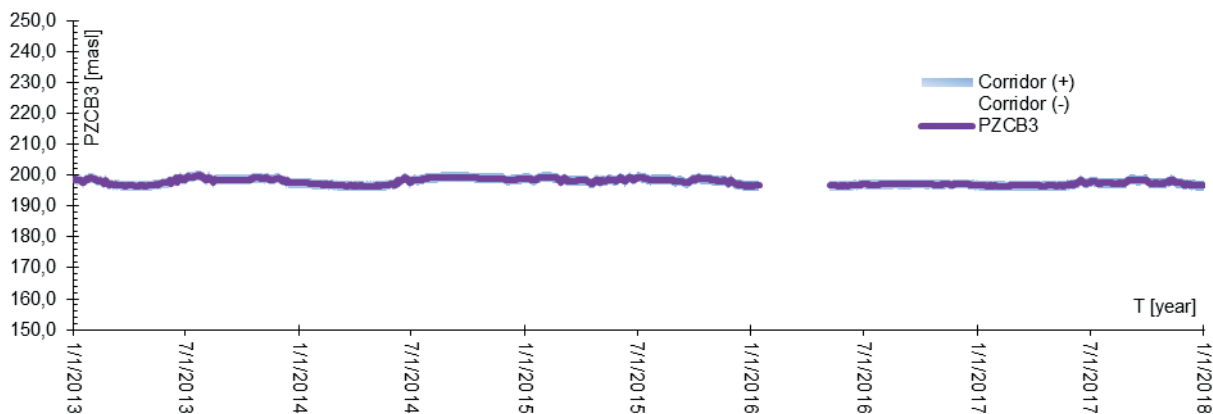


Figure 9. Warning level corridor of permissible variations for piezometer level in PZCB3

7. Conclusions

The piezometer level at the foundation of the dam during the service period for variation of the water levels in the reservoir was simulated by application of the Finite Element Method with plane (2D) numerical model and Neural Networks model.

The numerical analysis was carried out by taking in consideration the specified data for the numerical model and variations of the reservoir water level.

The prediction of the piezometer levels was analyzed in two stages – calibration and prognosis stage. From the carried out numerical experiment of simulation for analysis and prediction of the piezometer levels, following conclusions are derived:

1. For the calibration stage in the FEM numerical model, by comparison of the calculated and measured piezometric levels for piezometers PZCB2 and PZCB3 good matching of the records is obtained regarding the distribution and less good matching regarding the values.

2. For the calibration stage in case of NN model, by comparison of the calculated and measured piezometric levels for piezometers PZCB2 and PZCB3 excellent matching of the records is obtained regarding both the distribution and the values.
3. For the prediction stage, by comparison of the calculated values for piezometric levels from the FEM model and neural networks model, piezometric levels for piezometer PZCB2 shows good matching of the records regarding the distribution and less good regarding the values.
4. For the prediction stage, by comparison of the calculated levels from the FEM model and neural networks model, piezometric levels for piezometer PZCB3 shows very good matching of the records regarding both the distribution and the values.
5. The overall calculated piezometer levels in the piezometers PZCB2 and PZCB3 in the arch dam foundation, taking in consideration the findings from the calibration and the prognosis stage, are within the expected mode for such structure and applied hydraulic loading.
6. According to the measured and calculated values for the variables by NN model, warning levels corridors are established by applying criteria of $3 \times \sigma$, where σ is standard deviation of absolute error, generated by the Neural-Tools code, that would indicate of irregular occurrence in the dam foundation in case of their exceedance.
7. General conclusion can be drawn out for the analysis task that Neural Network model provided improved comparison and matching of the calculated vs measured data for both variables compared with the FEM model.

References:

- [1] Tanchev, Ljubomir. Dams and appurtenant structures, 2nd edition. London, UK: A.A. Balkema Publ., CRC press, Taylor&Francis Group plc, 2014.
- [2] P. Novak, A.I.B. Moffat, C. Nalluri. Hydraulic structures, 3rd edition. London, UK: Taylor&Francis Group, 2007.
- [3] Calibration analysis of seepage flow at arch dam foundation – a case study. Stevcho Mitovski, Ljupcho Petkovski, Frosina Panovska. Ohrid: Macedonian Association, 2022. 5th Symposium of the Macedonian Association for Geotechnics.
- [4] Behavior prediction of a concrete arch dam. Stevcho Mitovski, Gjorgji Kokalanov, Ljupcho Petkovski, Frosina Panovska. 2022. ICOLD Benchmark Workshop 2022.
- [5] Lianyang, Zhang. Engineering properties of rocks. Elsevier Ge-Engineering Book Series. 2016, Vol. 4.
- [6] Robbin Fell, Patric McGregor, David Stapledon, Graeme Bell, Mark Foster. Geotechnical engineering of dams. London, UK: Taylor&Francis Group, 2015.
- [7] Neural networks in civil engineering II: Systems and application. I. Flood, K. Nabil. 1994. Computing in Civil Engineering.
- [8] Modeling construction processes using artificial neural networks. I. Flood, C. Paul. 4, 1996, Automation in Construction, Vol. 4, pp. 307–320.
- [9] Simulating the construction process using neural networks. Flood, I. Bristol: s.n., 1990. Proceedings of the 7th ISARC – International association for Automation and Robotics in Construction.
- [10] Lazarevska, Marijana. Modeling of management of construction projects with implementation of fuzzy neural networks. Podgorica: Univerzitet Crne Gore, Gradzevinski fakultet, 2014.
- [11] Adeli, H. Neural networks in civil engineering: 1989–2000. Computer-aided civil and infrastructure engineering 16, no. 2. 2002, pp. 126–142.

V Ecohydrology and Water Body Protections

HYDROMETRIC AND WATER QUALITY PROPERTIES OF THE MEDULIN POND (REPUBLIC OF CROATIA)

IVANA SUŠANJ ČULE¹, GORAN VOLF¹, NEVENKA OŽANIĆ¹, IGOR RUŽIĆ¹

¹ University of Rijeka, Faculty of Civil Engineering, Department of Hydrotechnics and Geotechnics; Croatia
e-mail: isusanj@uniri.hr, goran.volf@uniri.hr, nozanic@uniri.hr, igor.ruzic@uniri.hr

Abstract

The objective of this paper is to present the first hydrometric and water quality properties research data of the naturally formed small lake called Medulin pond (*cro. Medulinska lokva*) in order to provide methodology foundations for the development of the procedure aimed toward water quality and ecological potential evaluation of small urban water resources. Medulin pond is placed in an urban area of the Medulin municipality in Istria County (Republic of Croatia), and is considered a public water resource under the jurisdiction of the Croatian waters, and is not characterized as a highly protected, vulnerable, or landscape significant area according to any Croatian or European Union laws and directives or local authority urban plans. In this paper, first preliminary hydrometric and water quality data in order to assess the current condition of the pond including the bathymetry of the pond, temperature stratification, and standard water quality parameters will be presented.

Keywords: Medulin pond, hydrometric, water quality, small urban water resource, evaluation.

1. Introduction

The Republic of Croatia can be considered rich in natural beauty, especially in the area of water resources. Water resources in urban and non-urban areas are under the jurisdiction of Croatian waters and are declared as protected, vulnerable, or landscape significant areas according to which local municipalities have to plan the development of their space. The Beforementioned is mostly aimed toward specific water resources that are also protected by Natura 2000. But there are a lot of urban waters, for example, small rivers, lakes, or ponds, that are on the list of the Croatian waters resources but they are not recognized as significant or special in any way. Usually, they are not considered to have any harmful water effect on the surrounding urban area. Reasons for that can maybe be found in their size or anthropological impact on some of them. Because of that, some of these “water pearls” are sometimes forgotten or not recognized as valuable which can cause many problems in the urban planning process. If some water resource is not recognized, by excessive urban planning in that area, water resource can be irretrievably destroyed. Also, if the water resource is not used for the drinking purpose (water protection zones), usually Croatian waters have jurisdiction only on the area of water resource by itself and not on the catchment area.

Because of the beforementioned problems, it would be purposive to have some kind of procedure aimed toward the evaluation of small urban water resources in order to provide guidelines for the urban planning process. By simple hydrometric, water quality, ecological potential evaluation, and hydrological analyses, the catchment area of water resource can be easily protected and a small ecological system can be set in the balance. For example, if the water resource catchment system depends mainly on surface runoff, the overall percentage area of construction on the lot can be lower to provide better soil permeability. Also, if the water resource receives water from underground, by urban planning restriction considering underground floors can be provided. Besides these two examples, there is a long list of additional simple measures by which small urban water resources can be preserved.

This whole idea of analysis and evaluation of small urban water resources became interesting in a moment when we discover that in the middle of the Medulin municipality urban area, a small natural pond is placed, and its lacks any hydrometric, hydrological, or water quality measurements.

2. Methods

In this section, the location of the research area, as well as hydrological characteristics, biodiversity, and urban significance of the Medulin pond, are going to be described. In continuation, the hydrometric, and water quality measurement procedure is going to be presented.

2.1. Location of the research

Medulin pond is placed in an urban area of the Medulin municipality in Istria County (Republic of Croatia) as is shown in Figure 1.

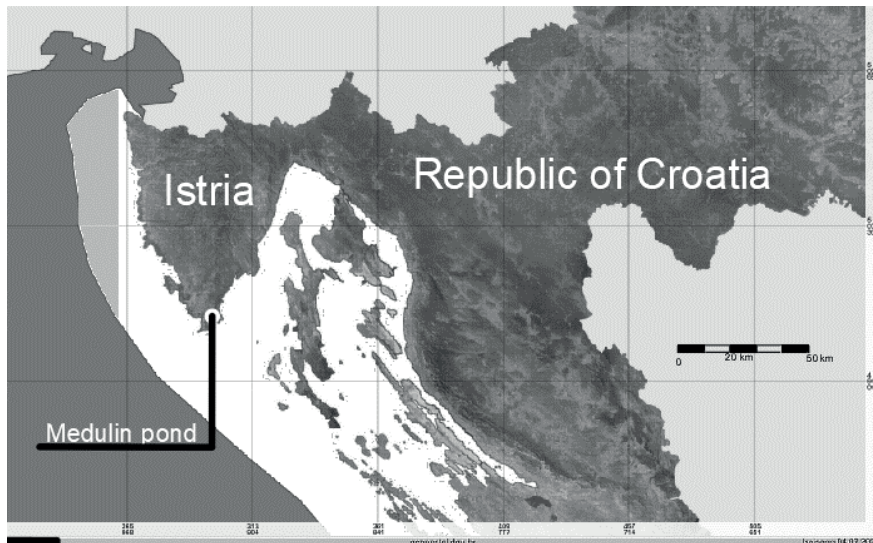


Figure 1. Location of the Medulin pond in Istria County (Republic of Croatia) [1]

On the north, west, and south side the pond is surrounded by buildings, and on the east side agricultural area is located. According to the areal map, the size of the pond in the condition of the maximum water level is approximately around 80 m wide and 100 m long and takes over the area of around 7000 m² as is shown in Figure 2. The pond contains fresh water and is placed around 650 meters from the Sea coastal line.

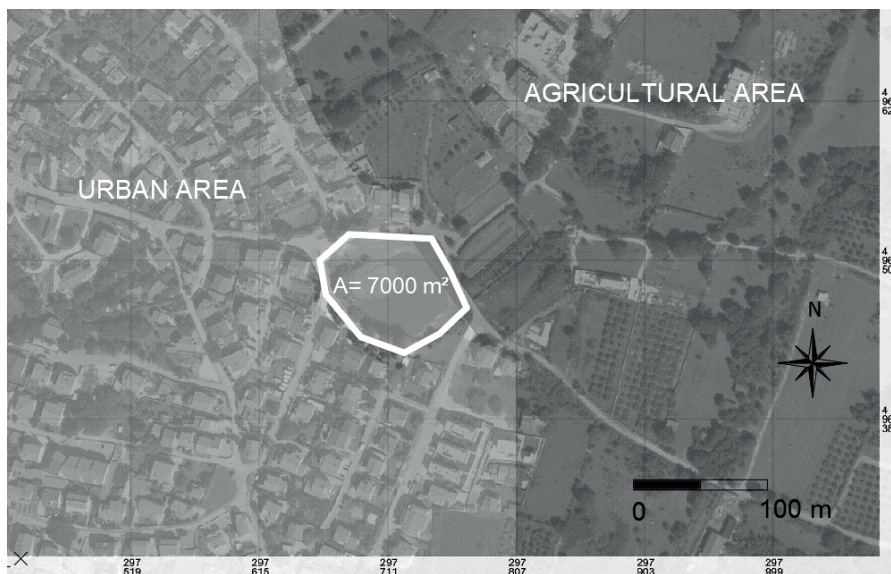


Figure 2. The Medulin pond on the areal map [1]

2.2. Hydrological characteristics

The Medulin pond topographical catchment has an area of approximately 3,08 km², and encompasses parts of the Medulin and Ližnjan municipalities as shown in Figure 3. The runoff characteristics are not yet explored, but it is visible that they are subjected to changes due to spreading of the urbanization. The water level in the pond is at the moment around 12,80 m.a.s.l. and the maximum elevation on the catchment is around 68 m.a.s.l.

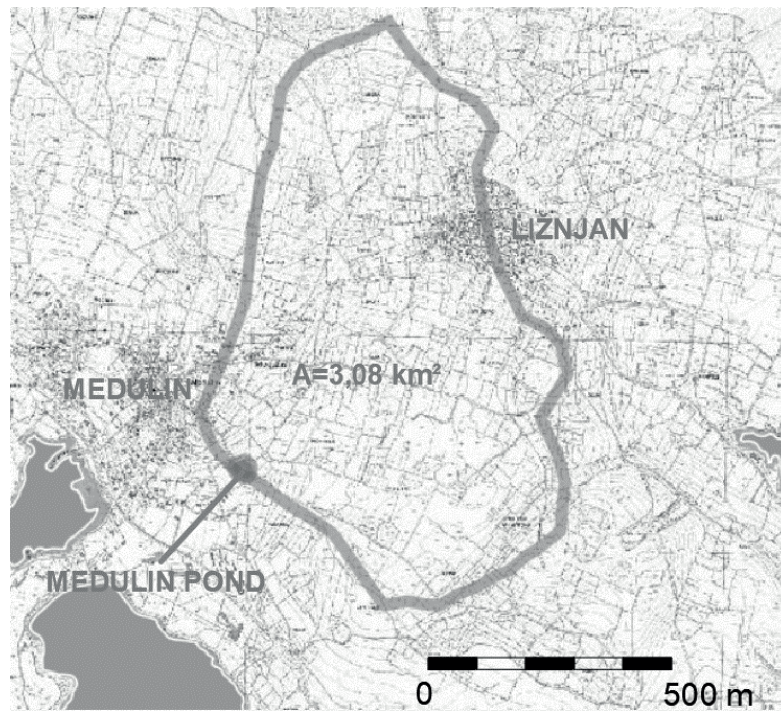


Figure 3. The Medulin pond topographical catchment [1]

According to local news, there were two rain events that caused an overflow of the pond. The first one happened on the 8. January 2010. year when rainfall over several days caused the overflow [2], and the second one is recorded in the night on 29. May 2019. year induced by the 45 mm of rainfall with big rainfall intensity [3]. There is an overflow object placed in the pond but considering problems with overflow it has apparently too small a flow capacity.

The pond is under a significant anthropological impact considering not only the pond by itself but also the catchment area. Since the anthropological impact on the catchment area is constant and constantly changing by urbanisation it can be considered a reason for overflow occurrence.

According to local people, there is always some water in the pond and it has never dried up, although they emphasize that the water levels are constantly dropping down in the last two decades.

According to all abovementioned, it can be concluded that the Medulin pond is filled with water booths from underground water aquifer and surface runoff.

2.3. Biodiversity and urban significance of the Medulin pond

Historically, there is only a little information about the Medulin pond past. The first records are from 1563 year, mentioning that this pond was connected with the Sea by the canal and was used for eel fishing [4]. Nowadays, the pond is not visibly connected to the Sea and is naturally filled with fresh water. Also, the area is recognized as a small oasis in the urban area that attracts both a local and tourist recreational population.

Since the pond is not characterized as a highly protected, vulnerable, or landscape significant area according to any Croatian or European Union laws and directives or local authority urban plans, the local people started to take care of the pond. Those nature enthusiasts artificially inhabited the pond with fish species, plants, and birds. Although their interference in natural water resources cannot be considered the right way to preserve and save the Medulin pond, it looks like they managed to establish one very stable ecosystem. One could expect that anthropological impact will have a negative impact on that small water resource as the Medulin pond, but in this case, it seems that people developed a biodiverse ecosystem as is shown in Figure 4. By artificial inhabitation of flora and fauna in the pond, they developed a place that attracts more wildlife because of which today the area of the pond can be seen more than 50 different bird species throughout the whole year as well as a lot of insects and amphibians [5].



Figure 4. The Medulin pond biodiversity

Urban significance of the Medulin pond is apparent from the fact that local people and nature enthusiasts are taking care about the pond [6]. Also, it is a place where both local people and tourists love to spend time.

2.5. Hydrometric and water quality measurement

The aim of this paper is to conduct the first preliminary hydrometric and water quality measurements on the Medulin pond, and the overall objective, in the future of this research, is to provide methodology foundations for the development of the procedure aimed toward the evaluation of small urban water resources. It is important to provide preliminary hydrometric and water quality data in order to assess the current condition of the pond.

Hydrometric measurement under this research encompasses bathymetry and temperature stratification in the Medulin pond. Bathymetry is provided by usage of the CTD – diver (Van Essen Instruments B.V., Nederland), Topcon positioning system HiPer V for geodetic surveying, and a small inflatable boat. With an inflatable boat it is possible to navigate on the surface of the pond, and with geodetic surveying equipment it is possible to take precise georeferenced points on which the depth of the water is measured by the CTD-diver [7]. CTD-diver also provides information about the temperature of the water and its conductivity. Used equipment in hydrometric measurement is shown in Figure 5.



Figure 5. Equipment used for the bathymetry measurement (from left to right): Inflatable boat, Topcon positioning system HiPer V and CTD – diver [7]

Water quality measurements are carried out by water sampling and water analyses in Hydrotechnical Laboratory at the Faculty of Civil Engineering in Rijeka. The water quality parameters are measured by the Spectrophotometer – Hach DR 3900 as shown in the Figure 6 [7].



Figure 6. Equipment used for water quality measurement: Spectrophotometer – HACH DR 3900 [7]

In this paper physical and chemical properties are provided as follows: pH, Total dissolved solids [ppm], Conductivity [$\mu\text{S}/\text{cm}$], Nitrates [mg/L ; $\text{NO}_3^- - \text{N}$], Ammonium [mg/L ; $\text{NH}_4^+ - \text{N}$], Chloride [mg/L ; Cl^-], Nitrites [mg/L ; $\text{NO}_2^- - \text{N}$], Total nitrogen [mg/L ; TNb], Orthophosphate [mg/L ; $\text{PO}_4^{3-} - \text{P}$], Total phosphorus TP [mg/L ; $\text{PO}_4^{3-} - \text{P}$], and Chemical oxygen demand COD [mg/L ; O_2], in order to assess overall quality and ecological potential of the water. All of these water quality parameters have quality ranges, and scales by which the natural water resources can be evaluated. Evaluation is going to be conducted according to the Regulation on the water quality standard (NN 96/2019) [8] issued by Republic of Croatia government.

3. Results and discussion

The bathymetry data was recorded on the 20 June 2022, on the same day when water quality sampling is done. The bathymetry was measured by usage of the small inflatable boat on which the Topcon positioning system HiPer V for geodetic surveying was attached. Also, the CTD diver was attached to the aggrigator and rope, and the depth measuring was conducted by constantly immersing the CTD diver in the water. Since the CTD diver is equipped with a temperature sensor, by moving all around the pond it was possible to take 122 depth and temperature points. In the

area where water lilies have grown very densely, conduction of the measurement was not possible. The route of depth measurement points is shown in Figure 7.

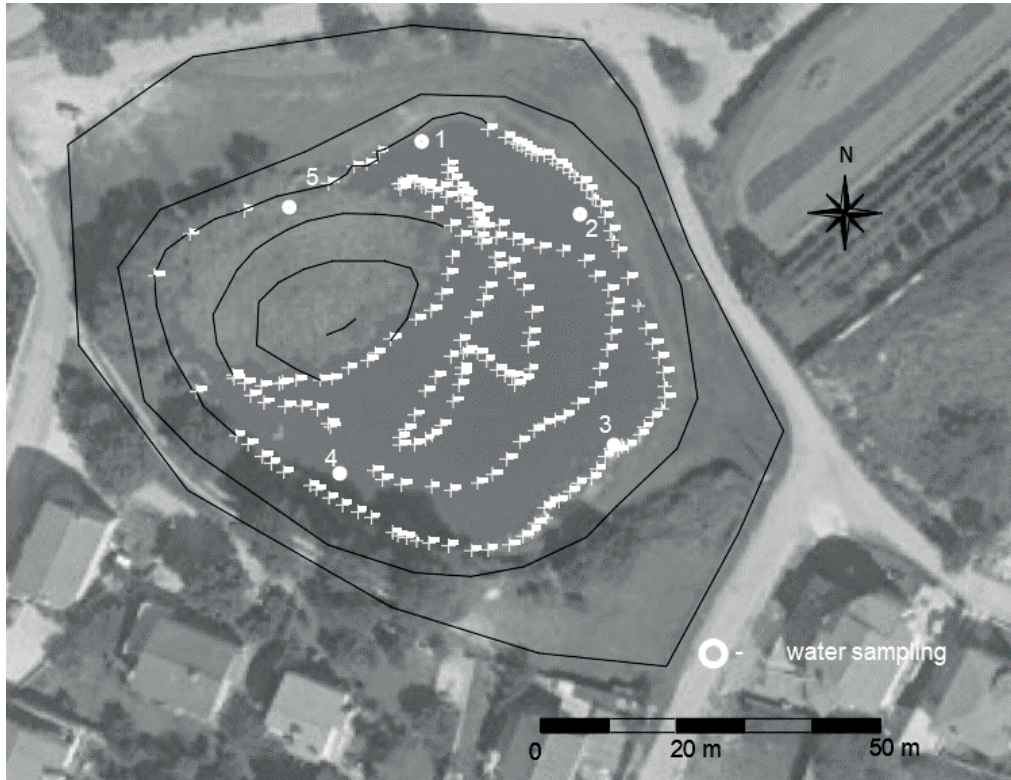


Figure 7. The route of the water depth and temperature measurements and water sampling points

Since on the north-west part of the pond was not possible to measure depth because of water lilies, the collected data was processed with help of the software Matlab 7.11.0 (R210b) from MathWorks in order to approximate the depths in that area. In the same software 2D visualization of the bathymetry is prepared and shown in Figure 8.

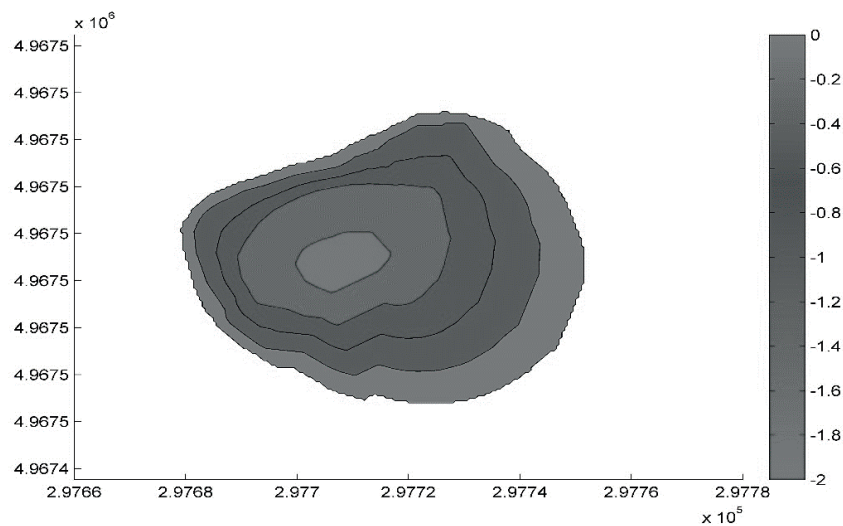


Figure 8. The 2D representation of the Medulin pond bathymetry

Also, by usage of the same recorded and processed depth and location data, the 3D visualization is done and shown in Figure 9.

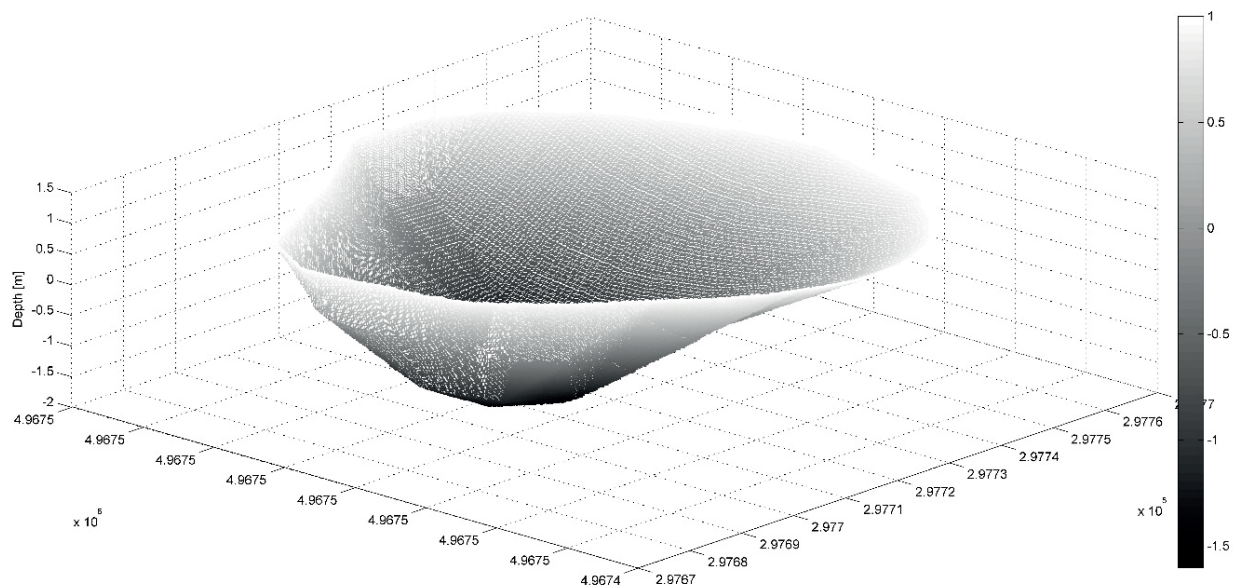


Figure 9. The 3D representation of the Medulin pond bathymetry

The collected depth and geodetic data points have shown that the water surface area at the time of measurement was 3237,8 m² and the water level is placed at 12.80 m.a.s.l. The maximum measured depth is 1,57 m and placed around the middle of the pond. The pond is very shallow, and there is no vertical temperature stratification. The measured temperature of water at the surface and bottom of the pond was 27°C while the air temperature was at the time of measurement 33°C.

According to the Regulation on the water quality standard (NN 96/2019) [8] water samples should be taken four times per year, one for every season of the year. The first preliminary water quality measurement was conducted on 20. June 2022. (summer measurement) at the same time when the bathymetry data was collected, and five surface water samples were taken. The next water sampling should be done in autumn, and then in winter and springtime. At the time of water sampling, significant turbidity is noticed. Also, the surface pollution, and not pleasant smell are noted. Water samples were taken to the laboratory at the Faculty of Civil engineering in Rijeka, and water quality parameters were measured by usage of the Spectrophotometer – Hach DR 3900. The results of laboratory water quality parameters tests are shown in Table 1.

The results of the analysis are compared with threshold values in order to evaluate the ecological potential that is specified in the Regulation on the water quality standard (NN 96/2019) [8], and shown in Table 1. According to mentioned regulation, the Medulin pond is a part of the Dinarid ecoregion (coastal sub-region) and belongs to a group of very shallow reservoirs, and a group of lowland, medium-deep, small lakes (Crypto depressions on the carbonate substrate).

The results of the water quality parameters are quite surprising. According to the results, Medulin pond is evaluated with good ecological potential. The only parameter that is characterized as marginally acceptable is total dissolved solids (TDS), and this result was expected since the noticeable turbidity is observed at the time of water sampling. Also, the temperature of the water, as mentioned above, is considerably high because of ponds' shallowness, and can affect the water ecosystem. For the natural water resource with a high anthropological impact, it is great to see the positive ecological impact. It is unknown if the purpose of local people was to preserve or to improve the ecological system, but as is beforementioned, the pond has good water quality and potential for biodiversity enrichment and seems that it is in ecological balance.

Table 1. Results of the water quality parametrs laboratory analisis and ecological potential evaluation

Water quality parameter	Label/Unit	Water sample					AVERAGE:	Evaluation of ecological potential [8, 9]
		1	2	3	4	5		
pH	[-]	7,2	7,2	7,2	7,3	7,3	7,24	Good: 7<pH<7,4
Total dissolved solids (TDS)	[ppm]	265	263	262	262	263	263	Marginally acceptable: 200 <TDS<300

Conductivity (C)	[$\mu\text{S}/\text{cm}$]	466	461	457	457	462	460,6	Fresh water
Nitrates	$\text{NO}_3^- - \text{N}$ / [mg/L]	0,344	0,311	0,388	0,327	0,3	0,334	Good
Ammonium	$\text{NH}_4^+ - \text{N}$ / [mg/L]	0,228	0,165	0,126	0,153	0,33	0,2004	Good: Cyprinid water <1)
Chloride	Cl^- / [mg/L]	0	0	0	0	0	0	Good: <0,005
Nitrites	$\text{NO}_2^- - \text{N}$ / [mg/L]	0,026	0,022	0,024	0,022	0,026	0,024	Good for water life: < 0,03
Total nitrogen	TNb / [mg/L]	2,52	1,77	2	1,71	1,85	1,97	Good: > 1,24
Orthophosphate	$\text{PO}_4^{3-} - \text{P}$ / [mg/L]	0	0,021	0,019	0,005	0,046	0,0182	Good: <0,1
Total phosphorus (TP)	$\text{PO}_4^{3-} - \text{P}$ / [mg/L]	0	0,08	0,123	0,063	0,141	0,0814	Good: <0,3
Chemical oxygen demand (COD)	O_2 / [mg/L]	40,6	48,2	49,9	33,6	45,3	43,52	Good: 20<COD<200

4. Conclusion

Medulin pond is placed in an urban area of the Medulin municipality and is considered a public water resource under the jurisdiction of the Croatian water. It is not characterized as a highly protected, vulnerable, or landscape significant area according to any Croatian or European Union laws and directives or local authority urban plans. The pond is under a significant anthropological impact considering not only the pond by itself but also the catchment area. Since the impact on the catchment area is constant and constantly changing by urbanisation the change in hydrological function can be expected in the future and is already noticed by the lowering of water level in the pond through the years according to local people.

Hydrometric or water quality measurements for the pond do not exist, and therefore first preliminary hydrometric and water quality measurements data for the Medulin pond (Istria) are introduced within this paper in order to evaluate the condition of the pond. Research has included measurement of bathymetry, water temperature, and water quality sampling. Analyses of collected data have shown that Medulin pond is a small shallow natural lake with a maximum depth of 1,57 m in present condition, and because of its shallowness, vertical temperature stratification does not exist. Also, the temperature of the water is quite high (27°C on 20 June 2022) and can have a negative impact on the water quality and biodiversity.

The water quality analyses encompassed pH, Total dissolved solids [ppm], Conductivity [$\mu\text{S}/\text{cm}$], Nitrates [mg/L; $\text{NO}_3^- - \text{N}$], Ammonium [mg/L; $\text{NH}_4^+ - \text{N}$], Chloride [mg/L; Cl^-], Nitrites [mg/L; $\text{NO}_2^- - \text{N}$], Total nitrogen [mg/L; TNb], Orthophosphate [mg/L; $\text{PO}_4^{3-} - \text{P}$], Total phosphorus TP [mg/L; $\text{PO}_4^{3-} - \text{P}$], and Chemical oxygen demand COD [mg/L; O_2]. For the purpose of preliminary analyses 5 water samples were analysed. According to the results, the Medulin pond is evaluated as having good water quality, and good ecological potential. The only parameter that is characterized as marginally acceptable is total dissolved solids (TDS).

For the natural water resource with high anthropological impact on the catchment area with urbanization, and direct impact on the pond by artificial inhabitation of fish species, plants, and birds done by local people it is quite surprising to see good water quality results. Medulin pond is a balanced ecological system, with potential for biodiversity enrichment.

Regardless of good evaluation results in water quality, Medulin pond can be considered as vulnerable considering water levels and inflow water quantities, caused by a significant impact on the Medulin pond catchment area. Already, urbanization disturbs a natural function of the pond water inflow and causes an overflow of the pond after two significant rainfall events.

The overall conclusion is that the Medulin pond can be considered a small “water pearl” and it has to be protected in some kind of way. Since the pond itself has a good balanced ecological system, in order to preserve this pond, better urbanization management in the catchment area is required. This means that one part of the responsibility in the preservation of the pond should be placed on the local municipality authority by providing guidelines for the urban planning process.

Because of all the beforementioned, future research plans will go in two directions. One is to provide more relevant measurement data for all year seasons, and the other is to develop a methodology for the small urban water resources evaluation in order to prepare guidelines for the preservation or revitalization of the water resources. It is clear that every single water resource can not be protected, but if its ecological or cultural significance can be proven then we all have obligation to save it.

Acknowledgements

The preparation of this paper was financially supported by the University of Rijeka projects: Implementation of Innovative Methodologies, Approaches and Tools for Sustainable River Basin Management, UNIRI-TEHNIC-18-129, and Hydrology of Water Resources and Identification of Flood and Mudflow Risk in Karst, UNIRI-TEHNIC-18-54).

References:

- [1] Digital map: <https://geoportal.dgu.hr/> 29.06.2022.
- [2] Rain event: <https://www.vecernji.hr/vijesti/lokva-poplavila-medulinske-podrume-i-setnice-76655> 29.06.2022.
- [3] Rain event: <https://www.glasistre.hr/istra/video-obilna-kisa-naglo-se-srucila-na-rovinj-i-medulin-gdje-je-palocak-45-mm-589573> 29.06.2022.
- [4] Medulin pond: <https://www.istriago.net/hr/medulinska-lokva/> 29.06.2022.
- [5] Medulin pond: <https://m.facebook.com/groups/4333729936653118/> 29.06.2022.
- [6] Medulin pond: <https://mapio.net/images-p/11548548.jpg> 29.06.2022.
- [7] LABORATORY EQUIPMENT CATALOGUE OF THE FACULTY OF CIVIL ENGINEERING: https://www.gradri.uniri.hr/files/Katalog_laboratorijske_i_terenske_opreme_GF_Rijeka.pdf 29.06.2022.
- [8] Republic of Croatia Government: The Regulation on the water quality standard (NN 96/2019), https://narodne-novine.nn.hr/clanci/sluzbeni/2019_10_96_1879.html, 2019.
- [9] Chapman, D. (1992). Water quality assessment. In D. Chapman (Ed.), (p. 585). London: Chapman & Hall (on behalf of UNESCO, WHO and UNEP).

VI River Basin Restoration Strategies and Experiences

DEEP WATER – MANAGED AQUIFER RECHARGE (MAR) IN SLOVAKIA

ANDREJ ŠOLTÉSZ¹, MICHAELA ČERVEŇANSKÁ¹, JAKUB MYDLA¹, DANA BAROKOVÁ¹

¹ Slovak University of Technology in Bratislava, Faculty of Civil Engineering, Department of Hydraulic Engineering; Slovakia

e-mail: andrej.soltesz@stuba.sk, michaela.cervenanska@stuba.sk, jakub.mydla@stuba.sk, dana.barokova@stuba.sk

Abstract

Coming from the literature sources Managed aquifer recharge (MAR) is defined as the intentional infiltration of water into aquifers with the purpose of either later recovering the water for different purposes like agricultural, industrial, urban or obtaining an environmental benefit. It has replaced the term “artificial recharge” which maybe evoked something what seemed to be unnatural in the environment.

There are different types of MAR methodologies and examples. Presented paper is the part of research effort of the team from the Department of Hydraulic Engineering, Faculty of Civil Engineering at the Slovak University of Technology in Bratislava in frame of the DEEPWATER-CE project. The main objective from the Slovak side in frame of the project was to induce infiltration from surface water body created by drainage channel system and to analyse the interaction between surface and subsurface (groundwater) in conditions of intensive agricultural activities in chosen territory of the upper Rye Island.

Keywords: managed aquifer recharge, drainage channel system, interaction of surface and ground water, Rye Island.

1. Introduction

Fast water transfer to rivers during flood situations causes a water deficit during dry periods. For long-term retention of water in aquifers and its subsequent use in drier or heavier demand periods, the Managed Aquifer Recharge (MAR) techniques are studied and implemented in 4 pilot areas of the DEEPWATER-CE project funded by the Interreg CENTRAL EUROPE programme [1]. In Slovakia, the pilot study is the area used for agricultural purposes bounded by irrigation channels – the Rye Island. The Rye Island is located in the Podunajska lowland, in the South-western part of the country. There are 4 channels located in the investigated area – S VII (the Gabčíkovo-Topoľníky primary channel) and secondary channels A VII (Vojka-Kračany), B VII (Šul’any-Jurová) and C VII (Baka-Gabčíkovo) [2].

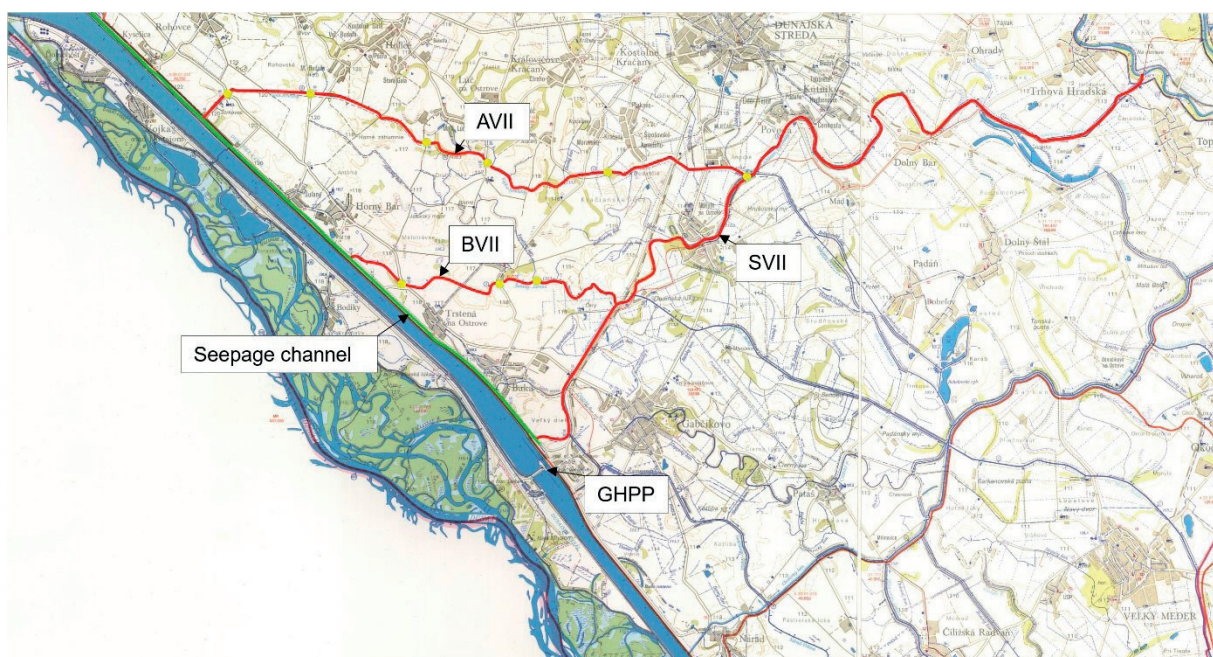


Figure 1. Illustration of the upper Rye Island area of interest in Slovakia for MAR purposes

The main objective for the Slovak side in frame of the project was to analyse the interaction of surface and subsurface (groundwater) in conditions of intensive agricultural activities in chosen territory of the upper Rye Island. The

groundwater recharge through Managed Aquifer Recharge (MAR) techniques was realised using the mentioned former drainage system (S VII) which was built up in the second half of the last century.

Nowadays, after putting Gabčíkovo hydropower plant (GHPP) into operation in 1992, this system was cut off the Danube River and is supplied by water from the seepage channel of the GHPP (Figure 1). This process enabled the second – very important function of the channel – to supply the aquifer as well as supply the unsaturated zone with water by using several irrigation systems.

2. Methods

The local geology is characterized by fluvial Quaternary sediments, which determine the hydrogeological conditions. The hydrological conditions are strongly affected by the construction of the GHPP. After construction of the GHPP, decrease of groundwater level in the adjacent area of the Danube River was observed. Groundwater regime as well as the water level regime in drainage channels changed. To improve and to control the groundwater regime in the flood-plain area, a water supply structure situated on the left-hand side of the seepage channel was constructed. This structure allows an artificial water supply into the branch system and consequently into the groundwater [2], [3], [4].

The procedure was divided into two parts. Firstly, field measurements were performed to provide data for setting up boundary conditions for numerical modelling of the surface-groundwater flow interaction. During the period from October 2020 to May 2021, several field measurements were carried out in order to determine the course of water levels in drainage channels (Figure 2). The longitudinal profiles of all modelled channels were constructed using the data from the Slovak Water Management Enterprise and the field measurements. Example of the profile is in Figure 3.

Secondly, for retention of surface water in aquifer and for recharge of groundwater and its subsequent using for irrigation during dry periods, the Recharge Dam MAR type was investigated using the numerical modelling technique.

Three hydrological years have been selected for the data analysis:

- 2008 as the year which can be characterized as the precipitation normal year for the regions of western Slovakia (100 to 109% of the long-term normal);
- 2010 as the year extremely above normal in terms of precipitation (159% of the long-term normal);
- and 2018 with extremely low precipitation totals recorded in April, May, July and October.



Figure 2. Water levels in channel system measured on May 1, 2021 [m a. s. l.]

For numerical modelling of the interaction of surface and groundwater flow expressing the possible recharge of water into aquifer a numerical model was developed using the MODFLOW program in the Groundwater Modeling System (GMS) environment, which allows us to use the conceptual model approach. MODFLOW is a computer program that numerically solves the three-dimensional groundwater flow equation for a porous medium by using a finite-difference method [5]. MODFLOW uses a modular structure. The three-dimensional movement of groundwater of constant density through porous earth material may be described by the partial-differential equation (1) [5]:

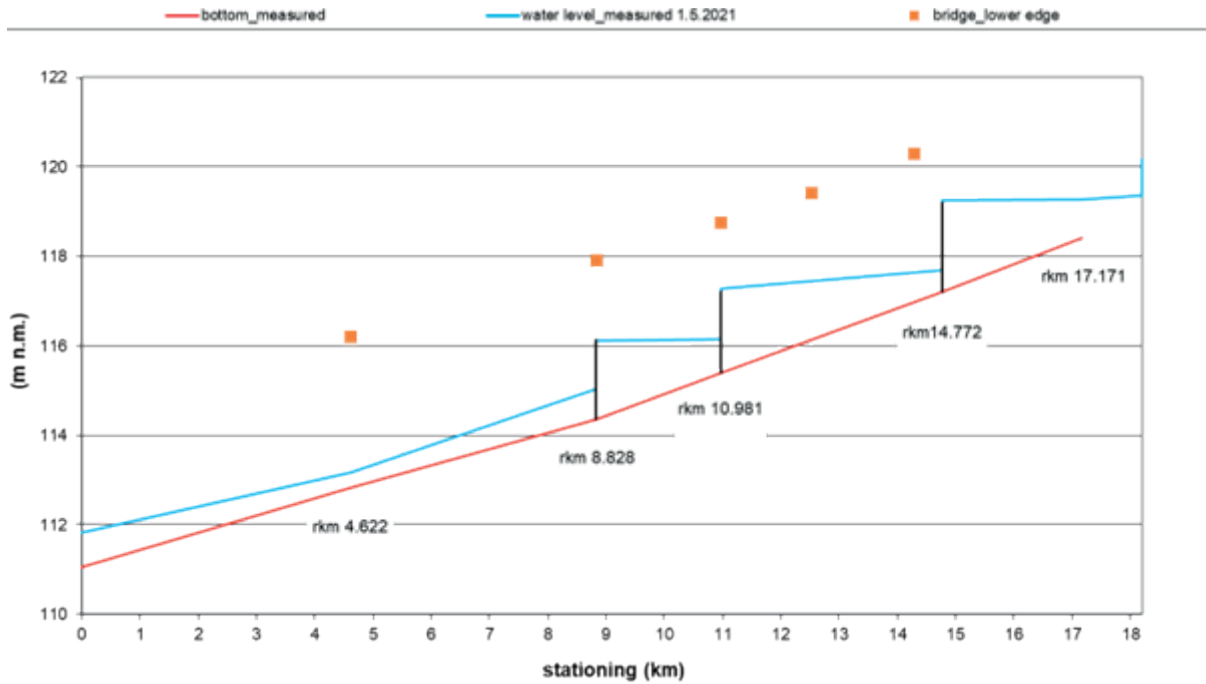


Figure 3. Longitudinal profile of the A VII drainage channel (water levels measured on May 1, 2021)

$$\frac{\partial}{\partial x} \left(K_{xx} \frac{\partial h}{\partial x} \right) + \frac{\partial}{\partial y} \left(K_{yy} \frac{\partial h}{\partial y} \right) + \frac{\partial}{\partial z} \left(K_{zz} \frac{\partial h}{\partial z} \right) - W = S_s \frac{\partial h}{\partial t} \quad (1)$$

where K_{xx} , K_{yy} , and K_{zz} are values of hydraulic conductivity along the x , y and z coordinate axes, which are assumed to be parallel to the major axes of hydraulic conductivity (Lt^{-1}); h is the potentiometric head (L); W is a volumetric flux per unit volume and represents sources and/or sinks of water (t^{-1}); S_s is the specific storage of the porous material (Lt^{-1}); and t is time (t).

Eq. (1), together with specification of flow and/or head conditions at the boundaries of an aquifer system and specification of initial-head conditions, constitutes a mathematical representation of a ground-water flow system. A solution of Eq. (1), in an analytical sense, is an algebraic expression giving $h(x, y, z, t)$ such that when the derivatives of h with respect to space and time are substituted into Eq. (1), the equation and its initial and boundary conditions are satisfied. Except for very simple systems, analytical solutions of Eq. (1) are rarely possible, so various numerical methods must be employed to obtain approximate solutions. One of the approaches is the finite-difference method, wherein the continuous system described by Eq. (1) is replaced by a finite set of discrete points in space and time, and the partial derivatives are replaced by terms calculated from the differences in head values at these points. The finite-difference analogy of Eq. (1) may be derived by applying discretization conventions described in [5].

The modelled area is bounded by the left-hand side seepage channel of the supply channel of the GHPP and 13 observation wells of the State Hydrological Network of groundwater quantity monitoring of the Slovak Hydro-meteorological Institute (SHMI). For defining the boundary condition as well as for the calibration of the model, data from 32 groundwater level monitoring boreholes (Figure 4) (or observation wells) were evaluated. Data from 19 of these boreholes were used as point observation, where the elevation of the groundwater level (the head) was set using the calibration targets. The rest 13 observation wells were used for specifying the value of the boundary condition.

The Dirichlet (or first-type) boundary condition was specified on the entire edge (vertical section) of the model boundary – the combination of *IBOUND* (identifying specified head boundaries) and *STRT* (giving the head at those boundaries) in the *Basic package* was used. The value of the boundary condition was computed as the mean value of groundwater levels measured in every individual observation well during the modelled period. At the top and bottom of the aquifer, the Neumann boundary condition was used. The drainage channels, which are represented by the Cauchy boundary condition, were modelled using the *River package*. Two elevations were specified – the elevation of the bottom of the river (channel) bed and the head in the river. Also, the conductance (in GMS entered in terms of conductance per unit length) was specified as one of the calibration parameters. For calibration of the model, the period from May 26, 2010 to September 9, 2010 (extremely wet year) was selected.

A 3D grid cell centered was created with 23 210 cells, each of 100×100 m. The dimension of the cell in the vertical direction varies approximately 50 to 75 m. The number of nodes is 32 889.



Figure 4. Groundwater level monitoring boreholes of SHMI located in the modelled area

3. Results and discussion

The entire Rye Island, and thus also the investigated part, lies in the Gabčíkovo depression. Quaternary sediments form three complexes – lower, middle and upper. The lower complex is characterized by the cyclic alternation of layers of sandy-gravel-like sediments of smaller thickness with clay and loam layers of greater thickness. The thickness of the lower complex ranges from 10 to 350 m. The middle complex is formed by Danube gravels. It is separated from the lower complex by loam-clay layers. The thickness of this formation spatially varies, in the vicinity of Komárno it is about 8–12 m, in the middle of the depression about 160 m. The upper complex is formed by loam and sandy-loam sediments with a thickness from 0.5 to 3.0 m [6].

The variation of the thickness of the Quaternary sediments led us to study final reports and reviews of the Geofond digital archive of the State Geological Institute of Dionýz Štúr [6]. The bottom elevation was adopted from these reports and reviews. Due to insufficient coverage of deep exploratory wells in the investigated area, the value of the bottom elevation of the aquifer was considered as an average value of 60 m a. s. l.

Results of the model calibration are illustrated in Figure 5. It captures the contours of the calculated groundwater head for the steady-state model of the period from May 26, 2010 to September 9, 2010. Calibration targets display a calibration error at each borehole. The centre of the target represents the observed value, a top of the target is equal to the observed value + an interval (0.10 m) and a bottom of the target is the difference of the observed value and the interval. If the colour of the calibration target is green, the bar lies entirely within the target. A yellow colour means the bar is outside the target, but the error is less than 200%. For a red colour of the calibration target, the error is greater than 200%.

As can be seen from the Figure 5, all targets (except of two targets) have the green colour, what means that the difference between the observed and computed head is less than 0.10 m in every observation borehole. The difference between the observed and calculated head in the two yellow calibration targets is 0.17 (12.04% of the difference between the maximum and minimum value in the observation well, or a variance) and -0.11 m (12.94% of the variance). The model can be assumed to be calibrated in the accepted level of accuracy. The verification of the model, which uses the set of calibrated parameter values and stresses to reproduce a second set of field data, was focused on the period from the March 13, 2018 to May 2, 2018 (extremely dry year).

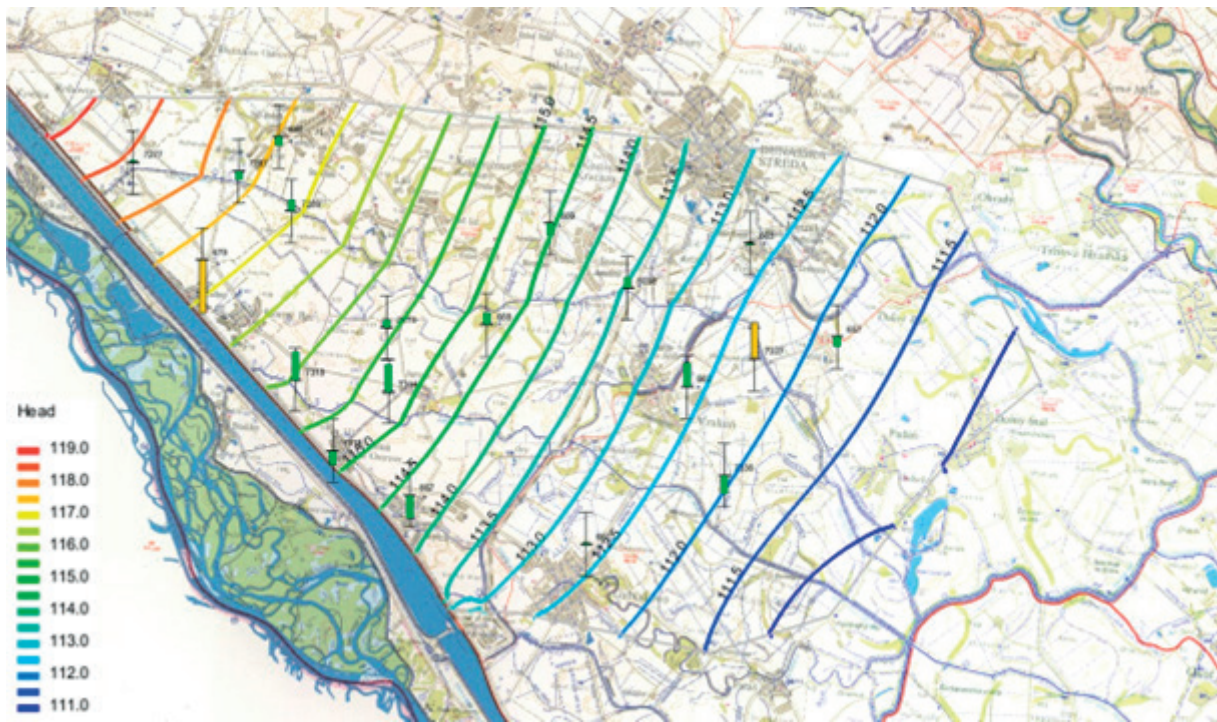


Figure 5. The calculated groundwater head for the period from May 26, 2010 to September 9, 2010

After calibration and verification process a prediction represents a response of the system to future events. Two scenarios (prognosis) have been examined on the A VII channel for both modelled periods:

- Prognosis 1 – water level corresponds to the maximum levels at each existing gate (for the period from 2018 or to the maximum level during the flood situation in 2010). All existing gates on the whole reach of the A VII drainage channel in the rkm 0.000 – 17.171 are closed (Figure 6);
- Prognosis 2 – water level corresponds to the maximum levels at each gate (for the period from 2018 or to the maximum level during the flood situation in 2010). All existing gates are closed + additional proposed gates in the rkm 2.270, rkm 7.060 and rkm 12.530 are in operation (Figure 7).

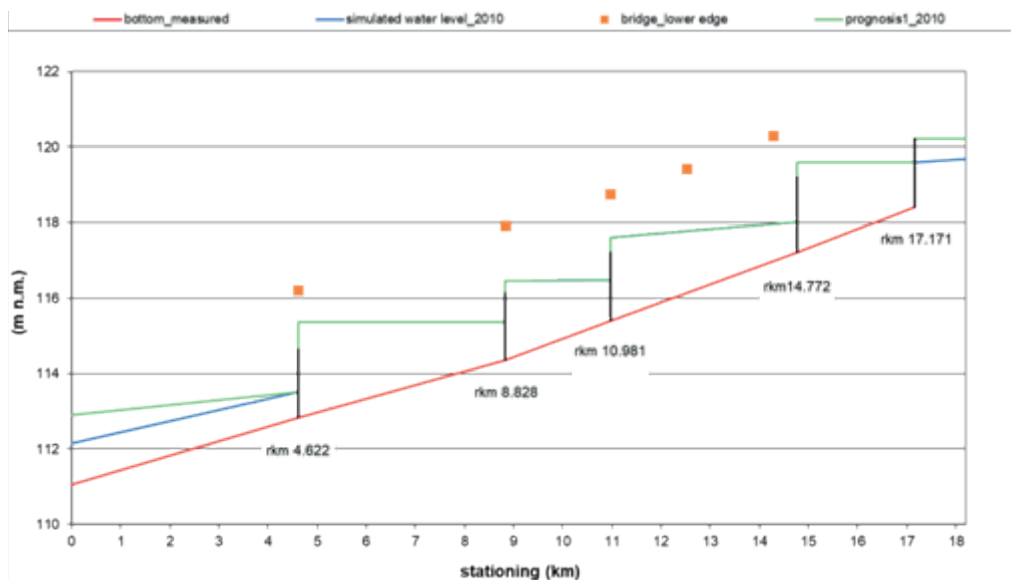


Figure 6. Longitudinal profile of the A VII drainage channel – simulated water level (prognosis 1, 2010)

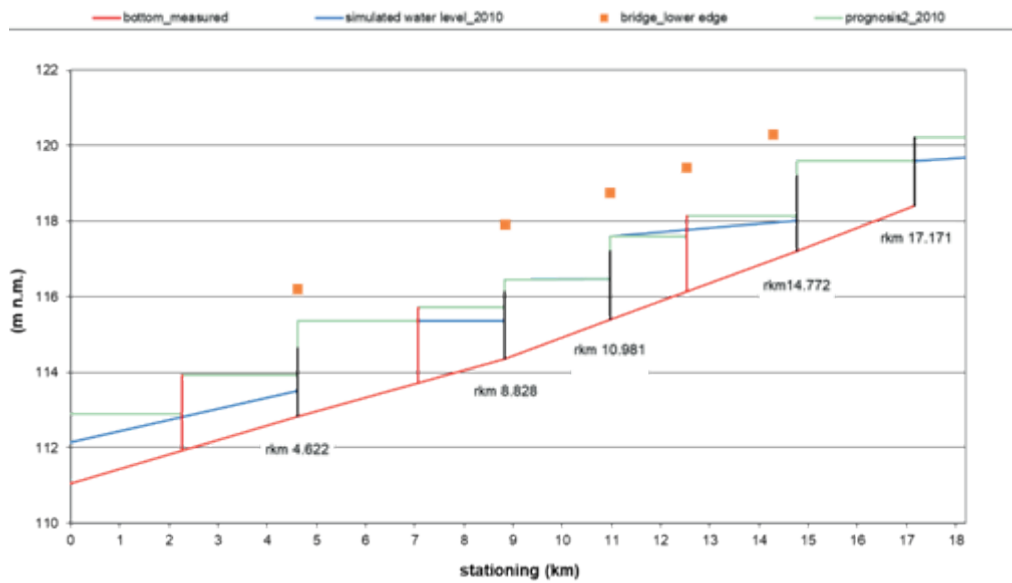


Figure 7. Longitudinal profile of the A VII drainage channel – simulated water level (prognosis 2, 2010)

The isolines of calculated groundwater heads for the steady-state models capturing the prognosis 1 for the flood year 2010 are illustrated in Figure 8, the prognosis 2 of the same period are illustrated in Figure 9.



Figure 8. Prognosis 1: calculated groundwater head for extremely wet year 2010 [m a. s. l.]

The same procedure was performed for the dry year 2018. Maybe, the results do not show significant increase of ground water level. The differences in groundwater levels vary from 0.0 to 0.25 m in the modelled period 2010 (wet year) and from 0.0 to 0.35 m in the modelled period in 2018 (dry year) and therefore the Table 1 is illustrating the balance of groundwater flow in the area of interest. Increased groundwater level affects the volume of water infiltrated into the aquifer (Table 1) but does not cause the flooding of the adjacent area. Due to the slight increase in water level, the groundwater gets closer to the roots of cultivated crops.

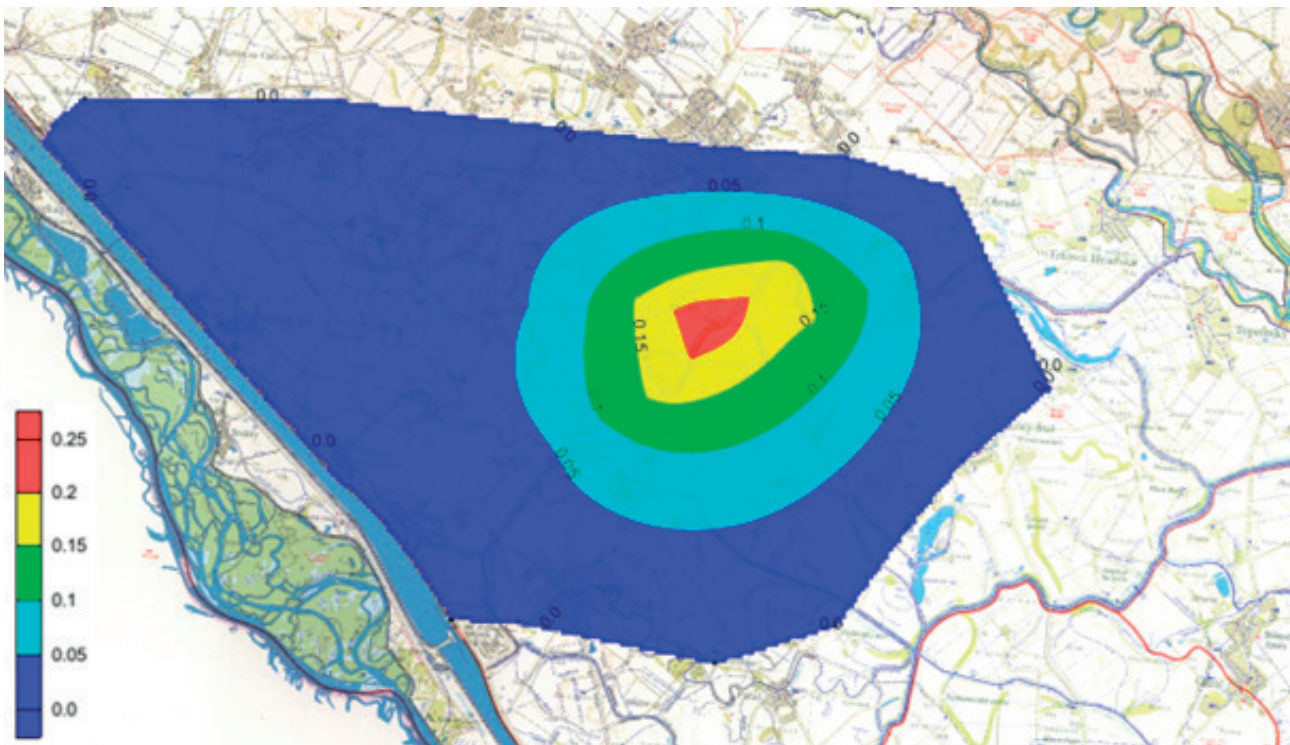


Figure 9. Difference between the prognosis 1, 2010 and the “zero variant” (natural state, no gates)

Table 1. River leakage [$\text{m}^3 \cdot \text{d}^{-1}$]

Scenario	2010			2018		
	In	Out	Total	In	Out	Total
„Zero variant”	46 648	-19 767	26 881	45 318	-30 959	14 359
Prognosis 1	48 053	-10 143	37 910	50 784	-27 186	23 598
Prognosis 2	49 946	-8 733	41 213	58 029	-25 240	32 789

4. Conclusion

The reason for elaboration of this study was the fact that the MAR system can be utilized in agricultural condition, as well. The idea of using former drainage channels for groundwater supply and for irrigation purposes was suggested already before putting GHPP into operation, but nobody expressed benefits or possible handicaps for the adjacent area. It has to be mentioned that there is more than 2 500 km of drainage channels in the Rye Island region of. The selected S VII channel system is just one part of them but maybe one of those where the surface water control can be a significant tool for water supply into aquifer. The advantage of the S VII channel system is the stable and controlled supply of water from the seepage channel of the SHPP which is of the groundwater quality [7].

It is apparent from the Table 1 that the amount of water infiltrated into aquifer after operation on existing gates (Prognosis 1) increased in both investigated years more than 40% (wet year 2010) and more than 60% (dry year 2018). The present operation on water structures of the S VII channel system by SWME enables the realisation of “managed groundwater supply into aquifer”. It could be increased by realisation of additional gates (Prognosis 2) up to more than 50% (wet year 2010) and more than 75% (dry year 2018) in comparison with the natural surface water level regime (Zero variant).

Acknowledgements

This article was created with the support of the Ministry of Education, Science, Research and Sport of the Slovak Republic within the Slovak Research and Development Agency, project no. APVV-19-0383 and project VEGA no. 01/0728/21.

References:

- [1] Stachniak, K.: DEEPWATER-CE. Workpackage WPC, Activity D.C.2.1. Press release. Final (summary from all PPS). PP4, University of Selesia in Katowice, 2020, 8p.

- [2] Šoltész, A.: Water Management in Regions Affected by Water Structure Construction and Operation. In *Advances in Hydro-Science and –Engineering. Abstracts. Proceedings of the 5th International Conference on Hydro-Science and – Engineering*, Warsaw, University of Technology, 2002, p. 127–136.
- [3] Sikora, A., Slota, R.: Research of discharge and water level regime in left-hand side branch system of the Danube by method of physical modelling. Bratislava: Water Research Institute, 1992, 42 p.
- [4] Červeňanská, M., Šoltész, A., Baroková, D., Janík, A.: Evaluation of Water Management in Regions Affected by Water Structure Construction and Operation. In “Ovidius” University Annals – Constanta, Year XVIII – Issue 18, Series: Civil Engineering. Constanta, Romania, ISSN 1584–5990, 2016, pp. 17–24.
- [5] Harbaugh, A.W., Banta, E.R., Hill, M.C., McDonald M. G.: MODFLOW-2000, The U.S. Geological Survey Modular Ground-Water Model – User Guide to Modularization Concepts and the Ground-Water Flow Process. Open-File Report 00-92. Reston, Virginia: U.S. Geological Survey, 2000, 130 p.
- [6] Benková, K., Bodiš, D., Nagy, A., Maglay, J., Švasta, J., Černák, R., Marcin, D. Explanations to the basic hydro-geological and hydrogeochemical map of the Danube Plain – Rye Island and the right bank of the Danube at a scale of 1: 50,000. Bratislava: Štátny geologický ústav Dionýza Štúra, ISBN 978-80-89343-82-9. 2013, 184 p.
- [7] Šoltész, A. et al.: Interreg CE – DEEPWATER. Final report on cooperation on activities implementation of the project. Final research report., Slovak University of Technology in Bratislava, 2021, 29 p.

VI River Basin Restoration Strategies and Experiences

DEVELOPMENT OF GREEN ZONES ON TECHNICAL UNIVERSITY OF KOSICE

MARTINA ZELEŇÁKOVÁ¹, MÁRIA HLINKOVÁ²

¹ Technical University of Kosice, Faculty of Civil Engineering, Institute for Sustainable and Circular Construction; Slovakia
e-mail: martina.zelenakova@tuke.sk

² Technical University of Kosice, Faculty of Civil Engineering, Institute of Technology, Economics and Management in Construction; Slovakia
e-mail: maria.hlinkova@tuke.sk

Abstract

Green university project is aimed to build up a centre of sustainability and water retention measures good practice example. The city of Košice is the university city with great impact to young people who can contribute by their action to make the world more suitable for life. Universities bring together people whose goal is to prepare for life in a world where it will be possible to live fully. That is why the university campus is chosen as one of the most suitable locations for the proposed measures. The roof of TUKE is the largest roof in Kosice city in terms of area, which is why it has been transformed to “green” is justified. In combination with other green elements, it can create a complex future. Water retention is also part of the concept facilities, the “green wall” segment and related information activities. The area of green roof is approximately 2 000 m². The roof contains numerous shafts, ventilation chimneys, drains and roof plane transitions and numerous antennas and test towers. There is also a dome with an observatory, which is a suitable architectural element for the application of green measures. Other proposed measures include bio retention lake and vegetation facades. The construction of lakes and vegetation walls significantly contributes to prevents the surrounding objects from overheating, the captured rainwater will be suitable for watering, thus saving money on rainwater drainage and the risk of local floods will be mitigated, and the groundwater supply will be increased. Bioretention systems that are not only able to collect water, but also have the ability self-cleaning are autonomous elements of the green infrastructure that will be further developed in the future develop and streamline. An element of an autonomous rainwater management system will be incorporated into the realization of the lake itself so that it can also provide new perspectives at management and maintenance of such facilities.

Keywords: green university, water retention, green campus.

1. Introduction

Water retention measures remain topical and increase their importance in these days. Most cities become more sustainable and “greener” due to increasing climate change [1,2]. By building new green zones in urban areas there can be ensure healthier environment for the citizens, but also the natural water balances contribute to sustainable water mitigation measures [3].

In general, universities can provide a model example of green sustainable measures implementation. Good practice examples can be found in the campuses across North America. Their applied measures allow to consider these universities to become key leaders in the promotion of sustainable development [4,6]. Also, integration green climate change mitigation measures can bring many economic benefits to the environment [5].

The concept of the “green university project” is designed to increase and strengthen capacity across the board water retention, which is very low in urban agglomerations such as Košice. The goals of the project are also aimed at raising awareness of climate change, which is for young people – students at Technical University of Košice (TUKE), but also primary and secondary school’s indispensable.

The target state can be defined in three areas:

- green roof – realized on the main campus building,
- interception of precipitation – in the form of retention measures,
- creating elements of public awareness of climate change, green roofs, bio retention systems and green facades.

2. Methods

The campus of TUKE has a huge potential for the implementation of measures to create and protect the environment and the transformation of the university into a “green university”. The roof of TUKE is the largest roof in Kosice city in terms of area, which is why it has been transformed to “green” is justified. In combination with other green elements, it can create a complex future, as seen in examples from abroad. Water retention is also part of the concept facilities, the “green wall” segment and related information activities. Functionally, it is a flat roof structure with additional reinforced concrete arches roofs above the plane of the roof. The roof contains numerous shafts, ventilation chimneys, drains and roof plane transitions and numerous antennas and test towers. There is also a dome with an observatory, which is a suitable architectural element for the application of “green measures”.

For the implementation of the project, it is necessary to completely repair roof gutters, sheeting, surface waterproofing layer and additional insulation of the roof cladding. Overall, it is the main roof structure in satisfactory condition, arched roof in emergency condition.

As part of the measures, it will be necessary to remove non-functional elements and carry out a complete cleaning from vegetation and building debris, to strengthen the pillars of the arched roof, immediate repair of waterproofing layers on the arched roofs and to implement project measures to strengthen and repair of the supporting structure of the arched roof.

3. Results and discussion

3.1. Green roof as an example of building’s nature cooling

The issue of climate change is the world’s number 1 issue today. It’s up to us, what city, country, or we will leave the planet to future generations. Many are currently emerging in the face of climate change initiatives that could slow down or stop these processes.

TUKE is an area of reducing energy intensity and building green infrastructures deals not only in the educational process of thematic study programs, but also the implementation prototype demonstrations, e.g., green vegetation shelters for bicycles, recycling waste management, Smart city systems and demonstrations of secondary resource processing.

We propose a pilot example of the implementation of a green roof on the main building university. The building was built in the 70s of the 20th centuries and is still one of the largest buildings in the city, where only the main part of the roof is over 3,500 m². It therefore has a major impact on the environment of the university and the city. For this reason, the proposal to implement a green roof on the university’s is the highest green priority of TUKE. In addition to ecological, it fulfills this intention architectural, urban, hygienic, climatic, protective, and psychological function. The area of green roof is approximately 2 000 m² (Figure 1).

Among the main aims of the green roof’s realization belong:

- rainwater retention,
- reducing the air temperature around the object,
- prevent the object from overheating,
- increased oxygen production, aesthetic (visual) function,
- reduction of costs for air conditioning and heating of the building,
- reduction of sewerage costs,
- prevention of damage to the roof insulation by UV radiation and protection of roofs layers.

The foundation area of the roof of the main TUKE building before the installation of the green roof itself must meet important criteria, which include resistance to moisture, microorganisms, required the load – bearing capacity and the base must be resistant to overgrowth of roots, perennials, annuals, or trees.

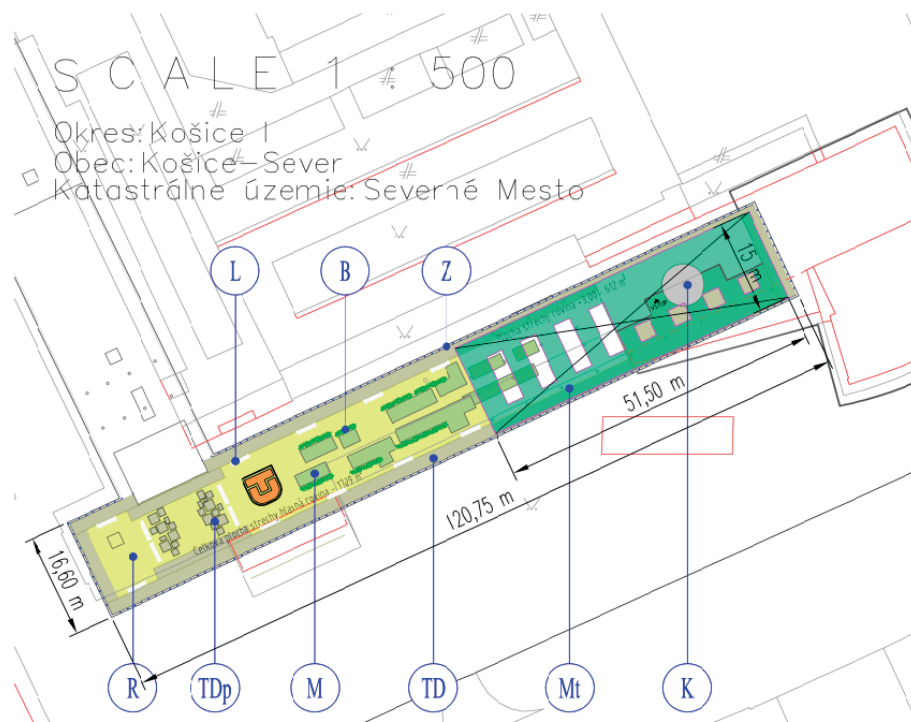


Figure 1. The proposed TUKE green roof

The construction implementation of the roof consists of the following steps:

- necessary reconstruction works, including insulation and waterproofing of the base layer,
- solutions of the formations of the extensive green roof,
- made-up ground of vegetation areas with selected river stone,
- assemblage of vegetation pots and associated structures,
- drip irrigation of vegetation pots,
- installation of walkways and terraces,
- fitting and installing security elements and railings around the entire perimeter of the area roofs,
- related electrical installation, cabling work and lighting of the roof area.

3.2. Interception of precipitation

Due to climate change, extreme weather events are currently taking place which are often manifested by frequent increases in shock temperatures, which have an adverse effect on water supplies in the country. This phenomenon is even more pronounced in the urban agglomeration, where there is a majority rainwater is immediately discharged into the form of a sewer network. This debt to the environment we use can be reduced by capturing rainwater in the form of rain gardens, collection lakes or other alternatives as efficient and at the same time an aesthetic way of mitigating the effects of drought. The implementation of different types of water retention measures is one of the options for adapting to climate change.

The aim is to build a bio retention lake (Figure 2) and vegetation facades. The main positive effects include:

- evaporated / collected rainwater will lower the air temperature during the summer months,
- water is retained in the landscape,
- it prevents the surrounding objects from overheating,
- oxygen production and humidity will increase,
- dust and the occurrence of allergens will be reduced,
- the captured rainwater will be suitable for watering, thus saving money on rainwater drainage,
- the risk of local floods will be mitigated, and the groundwater supply will be increased.

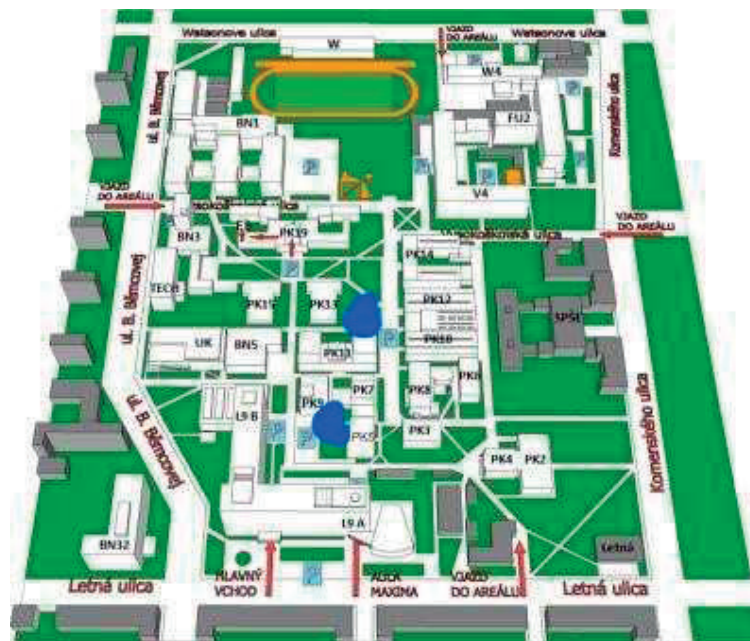


Figure 2. Proposed emplacement of bio retention lakes (blue marks)

Realization will include the following steps:

1. Construction of a bio retention lake in the immediate vicinity of the main TUKE building. With it, the university would be able to capture a sufficient amount of rainwater, which would subsequently be used in the process of irrigating the green roof. Retention ponds are a suitable solution for control and regulation of the quantity and quality of retained rainwater. An underground pipeline network allows the capture and drainage of large amounts of water and regulates its output as needed, maintaining the required level. However, it is necessary to plant natural vegetation, not only from the aesthetic point of view, but mainly to improve the stability of the banks.
2. Installation of vertical vegetation walls. In the exterior on the roof of the main building TUKE, where the green roof is designed, is located an object, so-called observatory, where it is designed within the perimeter wall such a vegetation wall. Additional vegetation walls and green elements are designed in the hall areas of vestibules of the main building.

4. Conclusion

Technical University of Kosice as a leading research and educational institution at the national university level and recognized abroad as an attractive place with a collegial and friendly atmosphere for creative activities of its students and staff, co-creating a cultivated cohesive community, equipped with modern infrastructure, as a confident and attractive center of creativity and innovative actions for the benefit of knowledge and society. Bioretention systems that are not only able to collect water, but also have the ability to self-clean are autonomous elements of the green infrastructure that will be further developed in the future and streamlined. An element of an autonomous rainwater management system will be incorporated into the realization of the lake itself so that it can also provide new perspectives at management and maintenance of such facilities. For this reason, the land of the Technical University of Kosice seems to be a good place to spread new approaches in the thinking of people and especially the young generation of future engineers and designers who can apply such solutions in practice. Also, installation of vertical vegetation walls brings significant positive effects, such as an increase in oxygen production and humidity in the local environment, air cleaning by trapping dust particles, the excellent thermal properties of the system, especially outdoors, will help reduce energy consumption in buildings, soundproofing of the environment.

Acknowledgements

This work has been supported by project of the Ministry of Education of the Slovak Republic ID 20210812131460210: Tvorba zelených zón na TUKE a zvyšovanie povedomia o zmene klímy.

This work has been supported by project of the Ministry of Education of the Slovak Republic VEGA 1/0308/20 Mitigation of hydrological hazards, floods and droughts by exploring extreme hydroclimatic phenomena in river basins.

This work was supported by the Slovak Research and Development Agency under the Contract no. APVV-20-0281.

References:

- [1] Kaya, Y.Z. et al.: Estimation of daily evapotranspiration in Košice City (Slovakia) using several soft computing techniques, *Theoretical and Applied Climatology*, 144, pp. 287–298, 2021.
- [2] Elshafei, G. et al.: Towards an Adaptation of Efficient Passive Design for Thermal Comfort Buildings, *Sustainability*, 13(17), 9570, 2021.
- [3] Zeleňáková, M.: Urban Rainwater and Flood Management, *Water*, 13(7), 974, 2021.
- [4] Finlay, J., Massey, J.: Eco-campus: applying the ecocity model to develop green university and college campuses, *International Journal of Sustainability in Higher Education*, 13(2), pp. 150–165, 2012.
- [5] Longo, M. et al.: Smart mobility for green university campus, *IEEE PES Asia-Pacific Power and Energy Engineering Conference (APPEEC)*, pp. 1–6, 2013.
- [6] Massimo, D.E. et al.: Valuation supports green university: case action at Mediterranea campus in Reggio Calabria, *Procedia – Social and Behavioral Sciences*, 223, pp. 17–24, 2016.

VII Climate Change and Flood Risk Management

ANALYSIS OF THE CHANGE OF PRECIPITATION WITH SHORT DURATION IN MACEDONIA

VIOLETA GJESHOVSKA¹, GOCE TASESKI¹, BOJAN ILIOSKI¹

¹ Ss. Cyril and Methodius University in Skopje, Faculty of Civil Engineering; Republic of North Macedonia
e-mail: violetag@gf.ukim.edu.mk, taseski@gf.ukim.edu.mk, bojanilioski@hotmail.com

Abstract

The change in precipitation has a direct impact on people's lives at different levels. For example, an increase rainfall can cause floods and / or landslides that affect individual homes, cities, and even entire countries. Floods cannot be prevented or accurately predicted, but effective mitigation measures based on their occurrence estimates can significantly reduce their impact. All models for estimating floods are based on precipitation analysis, with special emphasis on short-term precipitation, which is often the cause of catastrophically large floods. Knowing the changes in rainfall over a long period of time guarantees a better prognosis of floods and timely taking appropriate measures to mitigate or to some extent prevent them. Hence, access to up-to-date / new and accurate short-term precipitation data is essential. However, such key data are often unavailable in different parts of the world due to the lack of sufficient measuring stations, but also in the case of raw data. In R.N. Macedonia in practice is still used data on heavy rainfall for the period from 1956 to 1988. The need to update this information with more recent data is more than necessary, given that rainfall is an extremely stochastic phenomenon.

The subject of this paper is updating the precipitation data in Macedonia for the period from 1956 to 2020. The changes of precipitation in the last 30 years in eight measuring stations have been analysed. Existing series for annual maximum precipitation with short duration for the period from 1956-1988, are supplemented with data for precipitation from 1989 to 2020. The procedure of processing pluviographic tapes in order to define the annual maximum precipitation of a certain duration have been done by the method of characteristic (transitional) points or the method of five-minute period of discretization ($\Delta t = 5\text{min}$). The obtained series are statistically analysed, a homogeneity test is performed and the i-D-P (intensity-duration-probability of occurrence) curves are defined. The results are presented in tabular and graphical form.

Keywords: floods, annual maximum precipitation, short duration, i-D-P (intensity-duration- probability of occurrence) curves.

1. Introduction

Precipitation with short duration directly affect the occurrence of floods that can cause serious consequences on people's lives at different levels. Precipitation with short duration and hence floods can not be prevented, but effective mitigation measures based on assessment of their occurrence can significantly reduce the negative effects. All models for estimation of occurrence of floods are based on analysis of precipitation, with special emphasis on short-term precipitation, which is often the cause of catastrophically large floods. Knowing the changes in precipitation over a long period of time guarantees a better prognosis of the occurrence of floods and timely taking appropriate measures to mitigate or prevent them to some extent. Hence, access to up-to-date / new and accurate short-term precipitation data is essential. However, such key data are often unavailable in different parts of the world due to the lack of sufficient measuring stations, but also in the case of raw data.

Rainfall data are very important for climate study, water resources evaluation, drainage design (Desa and Rakhecha 2004; Wang 1987), environmental studies and many other purposes. To have high quality data on measured precipitation at many measuring stations means a higher degree of quality of conducted hydrological analysis. Defining real quantities of flood waters that can be expected in certain small catchment areas is necessary in order to know the possible occurrences of intense rainfall of a short duration. The annual maximum daily rainfall is defined as an extreme instance, with critical duration for a river basin, state or region, with immediate consequences to agriculture, soil conservation, roads, dams and drainage, (P. Willems, et al., 2012), (J.R. Porto de Carvalho, et al., 2014). Rainfall is a fundamental element of climate which is, for several decades, in perpetual mutations. For most regions around the Mediterranean, these changes resulted in significant rainfall deficits (A. Longobardi and P. Villani, 2010), (P.T. Nastos, 2011) accompanied by an increase of exceptional events such as severe droughts and devastating floods, (P. Alpert, T. Ben-Gai, A. Baharad et al., 2002). In the hydrological year, the daily maximum rainfall is the parameter considered

to assess the immediate impact on the hydrological response of streams, flooding cities, soil erosion, dams silting, and agricultural production, (M.J.M. Römkens, K. Helming, and S.N. Prasad, 2002). Observational studies of this variable form a critical line of evidence into how precipitation extremes have changed over the instrumental record, and recent findings are showing that at global or continental scales, extreme precipitation events have been increasing in intensity and/or frequency. For example, Alexander et al. (2006) used gridded precipitation data based on 5948 stations globally and found that precipitation changes exhibited a widespread and significant increase, (Alexander, L.V., et al., 2006). Min et al. (2011), using the same dataset but a different analysis approach, found that 65% of the data-covered areas have positive trends for annual maximum daily precipitation over the period from 1951 to 1999.

In the second half of the eighties of the last century, data on precipitation in the period from 1956 to 1988 were analyzed and intensity, duration and recurrence curves (IDR curves) were defined for the territory of the R.N. Macedonia, (Ž. Shkoklevski, B. Todorovski, 1993). For the last 30 years, intensive precipitations of a short duration have relatively been poorly analyzed in the R. N. Macedonia. Namely, in the period following 1988, the analysis of data on measured precipitation in the territory of our country has been reduced to research that has not fully covered this issue. Therefore, there is a need for complete analysis of the annual maximum daily rainfall precipitation in the period from 1988 till present, in order to define the real intense precipitations and their return periods that will be used for both scientific and professional needs.

This paper deals with analyses of data on measured precipitation at eight measuring stations in the R.N. Macedonia. The existing series of data from the measurements (1956–1988) have been updated with new data and the series for the period from 1956 to 2020 has been completed. This has created a series of 65 data, which represents a sound basis for analysis from a hydrological point of view. The sequences have been tested for homogeneity, statistically processed and defined by the distribution of extreme values and the probability of occurrence for different return periods. The data from the performed analyses are presented on maps in order to show the spatial distribution of the precipitation with a certain return period.

1.1. Study area and available data

Meteorological observations in R.N. Macedonia are performed at 19 main meteorological stations, 7 climatological, 24 phenological, 87 rain gauge stations and 55 automatic meteorological stations (AMS). Within the network of meteorological stations, short-term precipitation is measured by pluviographs at a number of measuring points. Depending on the possibilities, conditions and the need for information, the number of these measuring stations was decreased or increased in the past period. Permanent monitoring of intense rainfall in the R.N. Macedonia is carried out at the meteorological stations shown in Table 1.

Table 1. Overview of analyzed meteorological stations

Station	H [ma.s.l.]	Position		Measurement Period	Notes
		latitude	longitude		
SK-1	240	41°59'	20°28'	1956–1966	stopped working
SK-2	239	41°57'42"	021°37'17"	1967–1975	
SK-3	302	42°00'59"	021°12'59"	1978–1988	with interruption
				1989–2020	
Shtip	336	41°45'13"	022°21'49"	1963–1988	with interruption
				1988–2020	
Prilep	675	41°20'02"	021°13'14"	1959–1988	with interruption
				1989–2020	
Bitola	590	41°02'30"	021°12'13"	1956–1988	with interruption
				1989–2019	with interruption
Ohrid	757	41°06'53"	020°04'50"	1956–1988	
				1989–2020	with interruption
Kriva Palanka	693	42°12'13"	022°21'52"	1959–1988	
				1989–2020	

Demir Kapija	112	41°24'34"	022°21'14"	1957–1979	with interruption
				1987–2020	
Lazaropole	1340	41°32'15"	020°04'45"	1964–1988	with interruption
				1988–2012	with interruption

Pluviographic, short-term, rainfall strips registered at measuring stations Skopje (SK), Shtip (SH), Prilep (P), Bitola (B), Ohrid (O), Kriva Palanka (KP), Demir Kapija (DK) and Lazaropole (L) have been processed and analysed within the investigations presented in this paper. In Skopje, precipitation is measured at three locations: Skopje – Old airport-(SK-1), Skopje-Petrovec (SK-2) and Skopje-Zajchev rid (SK-3). Given the technical possibilities for observations of precipitation by pluviographs, the measurements were performed only in the warm period of the year (from April to November). In winter, the so-called pluviographs with heaters were used (to prevent freezing under negative temperatures), in which case, not one-day pluviograph tapes were used, but mostly seven-day ones. Such records referring to the period from 1956 to 1988 have not been analysed, while those from the period from 1989 to 2020 have been processed and analysed. Based on detailed review of all pluviographic records obtained each year (daily, weekly and monthly) selection of diagrams of all recorded episodes of precipitation and torrents in the course of each month and then in the course of each year has been made. The diagrams with recorded illogical values of precipitation (unreliable diagrams controlled by the UHMR staff) have not been taken into account in the analyses. The procedure of processing pluviographic tapes in order to define the intensity of the maximum precipitation of a certain duration can be done by the method of characteristic (transitional) points or the method of five-minute period of discretization ($\Delta t = 5 \text{ min}$). In the investigations presented in this paper, the second method has been used, i.e., the method of five-minute period of discretization ($\Delta t = 5 \text{ min}$) for which the period of discrediting is constant ($\Delta t = 5 \text{ min}$) and, for the total duration of precipitation, a chronological series of average five-minute intensities of precipitation has been obtained. The maximum values of intensity of precipitation have been obtained by extraction-separation of the largest value in the series of average five-minute precipitation, or the median value of precipitation of a certain duration. An online graphreader tool has been used to read the values from the pluviographic diagrams. For that purpose, all the tapes have, first of all, been scanned, the diagrams have been digitized and the values of the highest precipitation heights with a duration of 5, 10, 20, 40, 60, 90, 150, 300, 720 and 1440 minutes have been determined. Due to the interruptions of the precipitation measurements at certain measuring stations (Bitola, Lazaropole and Ohrid) and for the purpose of completing the series of annual maximum precipitation of a certain duration, the need to supplement the series has been imposed. The completing of the arrays has been done by establishing correlations between the arrays of annual maximum precipitations of a certain duration and the array of maximum daily precipitations which are complete for all stations. When establishing these correlation links, the strength of the connection has been controlled according to the basic criterion for correlation links, i.e., the correlation coefficient (r) has been calculated and controlled.

For the measuring stations Bitola and Ohrid, this coefficient has lower values of precipitation of a shorter duration and higher values of precipitation of a longer duration. For the measuring station Lazaropole, these values have been relatively small, indicating weak connections, wherefore a spatial correlation has been made with the stations: Prilep, Demir Kapija, Ohrid and Bitola. From the comparative analysis of the obtained correlation links, the highest coefficients have been obtained when establishing a correlation relationship of precipitation of a certain duration for m.s. Lazaropole with precipitation of the same duration for m.s. Ohrid.

Based on the previously explained procedure, for the analysed meteorological stations (Skopje, Shtip, Prilep, Bitola, Ohrid, Kriva Palanka, Demir Kapija and Lazaropole), unique series of data on annual maximum precipitations with a duration of 5, 10, 20, 40, 60, 90, 150, 300, 720, 1440 minutes and 24h have been established for the period from 1989 to 2020.

1.2. Defining the functions of probability of heavy rainfall

The statistical processing of the established series of data on annual maximum precipitation of a certain duration for all measuring stations consists of determination of the basic statistical parameters: mean arithmetic value (P_{avr}), mean square deviation (σ), coefficient of variation (C_v), coefficient of asymmetry (C_s). The theoretical probability density function, which is adequate to the empirical frequency, and the probability distribution function apply to the whole population, i.e., the existing arrays of limited data ($n=65$) are treated as arrays of unlimited data ($n=\infty$), which cover all possible future occurrences. Several probability density functions have been analysed: Gumble distribution, Pearson type III, Log-normal two-parameter, and Log-Pearson. By testing the adaptability of these functions to the empirical frequency of the random variable by applying the χ^2 -test at a test significance of $\alpha = 5\%$, the best adjustment has been shown by the Gumble function. The probability of occurrence of maximum intensive precipitation for all rain gauges and duration of precipitation has been defined by applying the Gumble distribution.

The established graphical dependencies between precipitation intensity, duration and probability of occurrence (i-T-p curve) for all measuring stations and short-term precipitation (5, 10, 20, 40, 60, 90, 150, 300, 720, 1440 minutes) are shown graphically, Figure 1.

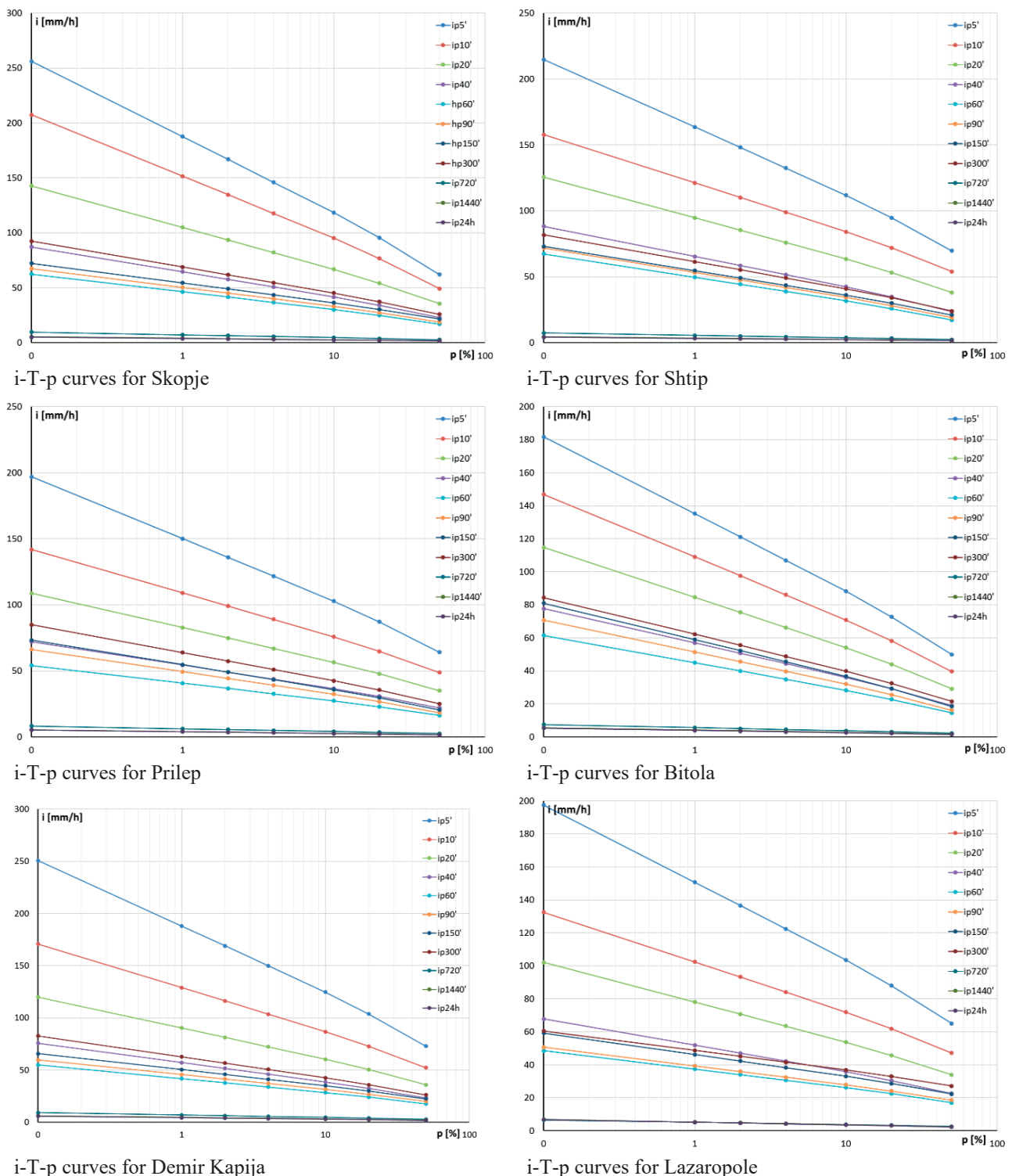


Figure 1. i-T-p curves

2. Results and discussion

If we analyze the calculated values for the intensity of precipitation with a short duration (5, 10, 20, 40, 60, 90, 150, 300, 720, 1440 minutes) for a return period of 10 years for the period 1956 to 2020 with the same data for the period from 1956 to 1988, Figure 2, it can be noted that in Skopje the intensity of rainfall, rainfall with a duration of 5, 10, 20, 40, 60, 90, 150 recorded a decrease, while rainfall with a longer duration of 300, 720, 1440 minutes and 24 hours have increase over the last 30 years. In Shtip, the increase in intensity was observed for precipitation white duration longer than 20 minutes. For the measuring station in Prilep, an increase in the intensity of precipitation with a duration

shorter than 1440 minutes was observed, while a decrease in intensity was observed for precipitation lasting 1440 min and 24h. In Bitola and Ohrid, for all periods of duration of precipitation, a decrease in intensity can be observed in the last 30 years. In Kriva Palanka, there is an increase in the intensity of precipitation with a duration of 40, 60, 90, 150 minutes. In Demir Kapia, there is an increase in precipitation with a duration of more than 300 minutes, while in Lazaropole only for precipitation with a duration of 720 minutes.

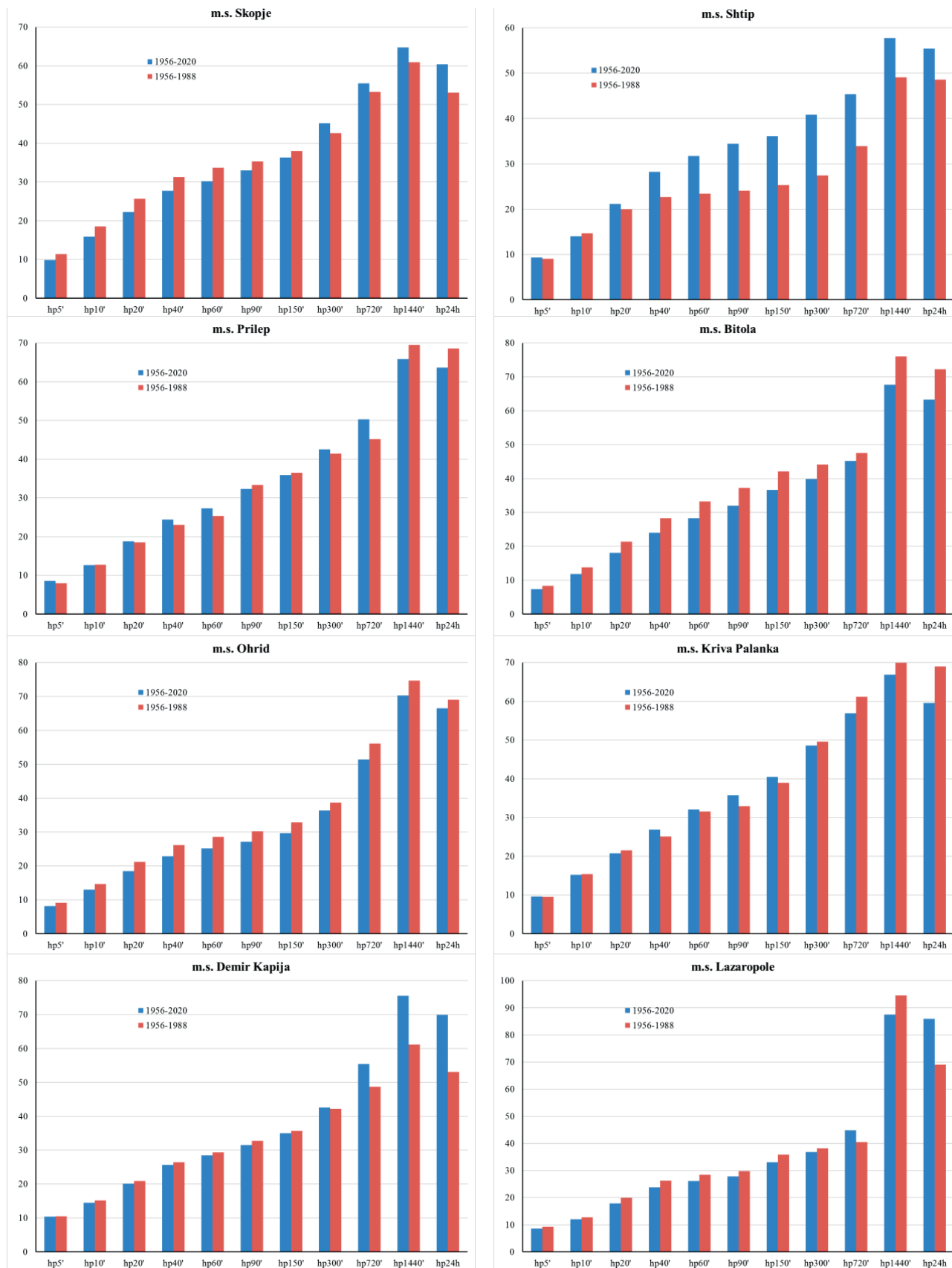


Figure 2. Intensity of short-term precipitation for a return period of 10 years (period 1956–2020 compared to period 1956–1988)

The complex orographic structure of the R.N. Macedonia conditions an uneven spatial distribution of precipitation and affects the pluviometric regime. One of the most important conditions that has an impact on the amount of precipitation is the geographical location of the considered location, i.e., latitude and longitude as well as altitude. The smallest amounts of precipitation occur in the central areas, namely, in Gradsko, Tikvesh and Ovche Pole, which are the driest areas in the territory, with average amounts of precipitation between 400–500 mm per year. The highest amounts of precipitation are registered in the highest mountain massifs in Western Macedonia, amounting to about 1000 mm per year. In other areas in our Republic, an average annual rainfall of 600–1000 mm has been measured for period 1981–2010, Fig. 3, (HMS).

If a comparison is made with the spatial distribution of the calculated extreme values of annual maximum daily precipitation with a return period of 50 years, Fig. 4, the situation is similar. Maximum rainfalls take place in Lazaropole, while the least rainfall is characteristic for Shtip.

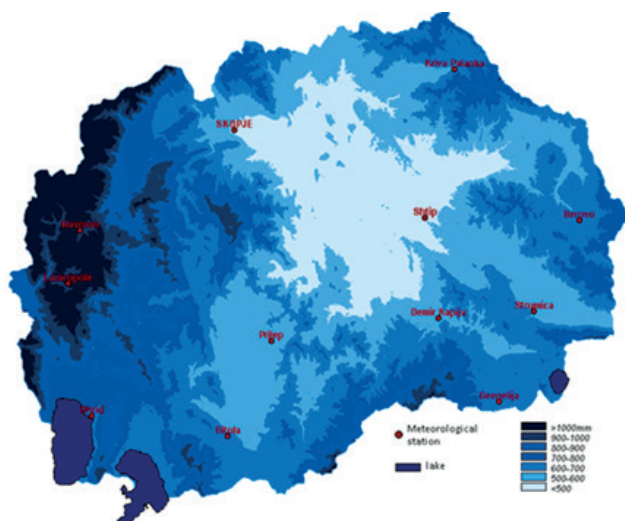


Figure 3. Spatial distribution of average annual rainfall for the period 1981–2010. (Source: HMS)

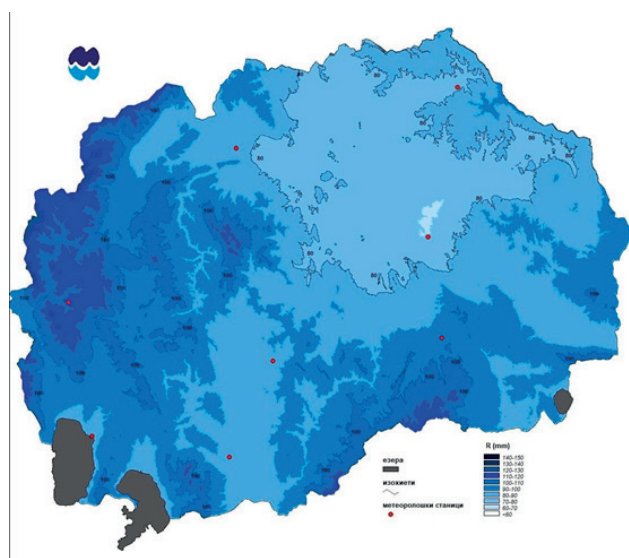


Figure 4. Spatial distribution of maximum precipitation with a return period of 50 years

3. Conclusion

Precipitation as an extremely stochastic phenomenon, variable in time and space, is relevant for analysis in the field of hydrology. These analyses are particularly important given that climate change is evident both globally and regionally. The need for analysis of variations and trend of precipitation with short duration in the R. N. Macedonia is more than necessary, given that such documented analyses were carried out about 30 years ago.

The paper shows analysis of the precipitation with short duration in the R. N. Macedonia based on data measured at eight measuring stations in the period from 1956 to 2020. The analysis of the series of measured data on the precipitation at all eight measuring stations shows logical variability with an increasing trend of precipitation in the last 30 years. Arrays of 65 data have statistically been processed and tested for sequence homogeneity. Extreme values with different return periods have been defined.

The results obtained from these analyses have been compared with those from the analyses carried out based on data measured at the same eight measuring stations in the period from 1956 to 1988 (published in 1993).

The comparative analysis shows that the extreme values of precipitation calculated for different return periods, according to the Gumble's probability distribution, are with an increasing trend.

From the aspect of providing relevant parameters for hydrological studies, it is recommended that these analyses are repeated in shorter time periods in future, at least after each 10 to 15-year period.

Acknowledgements

The analyses presented in this paper were conducted within the scientific research project "Analysis of Intense Rainfall in the Republic of North Macedonia", realized by a team of scientists and collaborators from the Department of Hydraulics, Hydrology and River Engineering at the Faculty of Civil Engineering - Skopje, funded by the Ss. Cyril and Methodius University (UKIM), Skopje. The authors are indebted to Hydro Meteorological Service (HMS) for the data provided.

References:

- [1] P. Willems, et al. (2012). "Climate change impact assessment on urban rainfall extremes and urban drainage: methods and shortcomings", *Atmos. Res.*, 103 pp. 106–118.
- [2] J.R. Porto de Carvalho, et al., (2014). "Annual maximum daily rainfall trends in the midwest, southeast and southern Brazil in the last 71 years," *Weather and Climate Extremes*, vol. 5, no. 1, pp. 7–15.
- [3] A. Longobardi and P. Villani, (2010). "Trend analysis of annual and seasonal rainfall time series in the Mediterranean area," *International Journal of Climatology*, vol. 30, no. 10, pp. 1538–1546.
- [4] P.T. Nastos, (2011). "Trends and variability of precipitation within the Mediterranean region, based on Global Precipitation Climatology Project (GPCP) and ground based datasets," *Advances in the Research of Aquatic Environment*, vol. 1, pp. 67–74, Springer.
- [5] P. Alpert, T. Ben-Gai, A. Baharad et al., (2002). "The paradoxical increase of Mediterranean extreme daily rainfall in spite of decrease in total values", *Geophysical Research Letters*, vol. 29, no. 11, pp. 1–31.
- [6] Bodini, A. and Cossu, Q.A.: (2010). "Vulnerability assessment of Central-East Sardinia (Italy) to extreme rainfall events", *Nat. Hazards Earth Syst. Sci.*, 10, 61–72, <https://doi.org/10.5194/nhess-10-61-2010>.
- [7] M.J.M. Römkens, K. Helming, and S.N. Prasad, (2002). "Soil erosion under different rainfall intensities, surface roughness, and soil water regimes," *Catena*, vol. 46, no. 2–3, pp. 103–123.
- [8] X.-C. Zhang and W.-Z. Liu, (2005). "Simulating potential response of hydrology, soil erosion, and crop productivity to climate change in Changwu tableland region on the Loess Plateau of China," *Agricultural and Forest Meteorology*, vol. 131, no. 3–4, pp. 127–142.
- [9] Bates et al. (2008). "Climate change and water", Intergovernmental Panel on Climate Change Secretariat.
- [10] Field, Christopher B., et al., (2012). "Managing the risks of extreme events and disasters to advance climate change adaptation", Special report of the intergovernmental panel on climate change. Cambridge University Press.
- [11] Min, SK., Zhang, X., Zwiers, F. et al. (2011). "Human contribution to more-intense precipitation extremes". *Nature* 470, 378–381. <https://doi.org/10.1038/nature09763>.
- [12] Alexander, L.V., et al. (2006), "Global observed changes in daily climate extremes of temperature and precipitation", *J. Geophys. Res.*, 111, D05109, doi:10.1029/2005JD006290.
- [13] Ž. Shkoklevski, B. Todorovski, (1993). Intense rainfall in the Republic of Macedonia, Faculty of Civil Engineering, Institute of Hydraulic Engineering, Skopje.
- [14] V. Gjesovska, G. Tasevski, P. Pelivanoski, K. Donevska et al. (2022), Analysis of intense rainfall in the Republic of North Macedonia, Scientific research project, Faculty of Civil Engineering-Skopje, University Ss. Cyril and Methodius, Skopje.
- [15] C. Popovska, V. Gjesovska, (2012). Hidrology- theory with solved problems, Faculty of Civil Engineering-Skopje, University Ss. Cyril and Methodius, Skopje.

VII Climate Change and Flood Risk Management

CLIMATE CHANGE, WATER RESOURCES AND TOURISM

ANTONIO DEKANIĆ¹, BARBARA KARLEUŠA¹, IVANA SUŠANJ ČULE¹

¹ University of Rijeka, Faculty of Tourism and Hospitality Management; Croatia
e-mail: antonio.dekanic0@gmail.com, barbara.karleusa@uniri.hr, isusanj@uniri.hr

Abstract

The impact of climate change on water resources and tourism, the possibility of adapting to climate change in a tourist destination, and mitigation of the impact of tourism activity on the climate change is analysed. Touristic activity seasonality and changes in water demands during the year is addressed. The importance of implementing the process of adaptation to climate change in a tourist destination, possible adaptation measures and opportunities to ensure sustainable management of water resources in order to ensure quality tourism activities but also the quality of life of local inhabitants in the tourist destination are presented.

Keywords: climate change, water resource, tourism, adaptation, mitigation, measures.

1. Introduction

Water resources are one of the key factors for life and development of life on Earth, and thus for humanity. Given the limited water resources, climate change and significant human activity, managing water resources in a sustainable way is an extremely important and very complex task [1]. It has been determined that climate change already has today, and will have even more pronounced and different impacts on water resources in the future. Climate change affects all life on the planet, all resources, including water resources. They also affect all human economic activities (agriculture, fisheries, energy, tourism, etc.) [2].

The need (demand) for water is globally growing due to a number of factors, including population growth, water pollution, economic progress, land use, climate change and others [3]. Drinking water is a strategic resource for socio-economic development and environmental protection, but water scarcity, deteriorating of water quality, droughts and, on the other hand, floods represent current and future challenges in water management, especially with regard to climate change. The effects of climate change are even more pronounced in regions that are already deficient in water resources and where droughts are more frequent, and therefore there is an imbalance between available water resources and water needs [4]. This problem is particularly pronounced in the Mediterranean area, which stands out as a significant tourist destination, where the seasonal (summer) increase in water demand is particularly pronounced, and on the other hand climate change affects the reduction of local and seasonal availability of water resources [5].

The aim of this paper is to analyse the impact of climate change on water resources with an emphasis on tourism and the possibility of adapting to climate change in a tourist destination, but also mitigate the impact of tourism activity on the causes of climate change. The issue of touristic activity seasonality and changes in water demands during the year are emphasized.

The paper analyses the importance of implementing the process of adaptation to climate change in a tourist destination, possible adaptation measures and opportunities to ensure sustainable management of water resources in order to ensure quality tourism activities but also ensure the quality of life of local inhabitants in the tourist destination. The emphasis in this paper is on the touristic destinations in the Mediterranean area especially in the coastal part of the Republic of Croatia.

2. Climate change impact on water resources

The Mediterranean basin, including the Adriatic Sea region, is a region that is very sensitive to climate change, but also to anthropogenic impacts [6]. Since the 1970s, the mean annual temperatures in the Mediterranean region have increased by 0.1°C per decade, and precipitation has decreased by 25 mm per decade [7]. Temperatures are expected to increase by 1.5–2.5°C, and precipitation is expected to decrease by 5% to 20% up to 2050 [8], which could lead to the decrease of freshwater resources throughout the Mediterranean basin (30–50%).

In the Adriatic region, the decrease of 15% of freshwater is expected in northern Italy and the Balkans [8]. Climate changes cause more frequent drought and flood occurrence, while the increase in water demand is expected due to

increasing urbanisation, agricultural production and tourism activities, which leads to the increase in withdrawal of water and pressures on regional water resources [9].

Water resource and supply vulnerability and risk assessments, water scarcity estimates and drought analyses due to climate change impacts are necessary for avoiding future water crises and preparing adaptation measures to mitigate the consequences of such crises [10].

To simulate the impacts of climate change on water resources in future various methodologies have been used [11]: coupling Global Circulation Models (GCMs) with hydrologic models through downscaling techniques, coupling high-resolution Regional Climate Models (RCMs) with hydrologic models and using hypothetical scenarios as inputs to hydrologic models.

The impact of climate change on the water resources in the Mediterranean has been confirmed in different studies [5]. Based on scenarios of varying future temperature and precipitation to analyse the changes in groundwater recharge and in agricultural water demand for the West Bank of the Mediterranean basin, Mizyed [12] concluded that the groundwater recharge could decrease by up to 50%.

Impact of climate change on water resources used for drinking water supply in the Adriatic region has been investigated within the DRINKADRIA project (Adriatic IPA CBC 2007–2013) [5]. As an example of the impact of climate change on water resources for analysed pilot area in northern part of Croatia (where the touristic activity is very high in summer period) for springs Sv. Ivan, Gradole and Bulaž are presented in Figure 1 [6]. The decrease in discharge of springs Sv. Ivan, Gradole and Bulaž can be observed in all historical time series and projected time series of the total lowest average monthly discharge of springs, with accompanying trends, generated using different climate models (REGCM3, ALADIN, and PROMES) for 1961–2050. The island of Corfu in Greece (also pilot area in the Project) is facing rising temperatures and declining rainfall too, especially in the summer months. Although the island of Corfu is located in the western part of the country where precipitation levels are higher than the average in Greece, climate change will negatively affect the availability of water resources [14].

3. Climate change impact and tourism

According to climate modelling results, the Mediterranean region is marked as a “hot spot” with particularly pronounced effects of climate change impact [15]. The Republic of Croatia, which for the most part belongs to that region, will certainly feel the consequences of climate change, and its vulnerability is assessed as high. The vulnerability of some economic sectors is particularly significant: tourism, agriculture, forestry, fisheries and energy, as the success of these sectors depends to a large extent on climate factors. Consequently, the extreme vulnerability of the economy to the effects of climate change can have a negative effect on overall social development. Therefore, the implementation of adaptation measures is the only way to avoid catastrophic consequences for the environment and the economy, which endangers the sustainable development of the society [16].

In the tourism sector, the main expected impacts of climate change are: reduction of tourist demand in the summer months due to high temperatures, increased UV radiation, higher frequency and intensity of extreme weather events; reduction or loss of ecosystem attractiveness and biodiversity as elements of attractiveness in tourism; reduction of water availability and occurrence of problems related to various infrastructure systems (wastewater drainage, solid waste disposal, beach infrastructure, accommodation infrastructure, etc.) and / or their reduced functionality.

Changes in climate will lead to various implications for individual tourist destinations, but they can be both positive and negative. Due to climate change (but also due to its proximity to Western and Northern European guests), the northern parts of Europe could become attractive enough for vacations during the summer months, and the Mediterranean and Croatia could remain attractive (only) for the rest of the year. The tourism sector will be forced to enrich its offer and offer higher quality products, which can have a positive effect on the competitiveness and structure of guests. Favourable climatic conditions in the coastal part of the Republic of Croatia in the off-season and pre-season can have a positive effect on reducing mass tourism in the summer months [17].

At the peak of the touristic season, some tourist destinations and islands have problems with water supply, which will continue in the future due to increased demand for water in this period [18]. The issue of water supply in the context of (oversized) development of island and coastal tourism is highlighted by a considerable number of studies in the Mediterranean area (Mallorca, Malta, Sardinia) [19].

In Croatia the problem is also highlighted on islands and in coastal areas with touristic activity. The impact of tourism on increasing demands for water supply is not only reflected by the seasonal increase of the number of tourists and seasonal workers. Namely, in addition to primary water consumption (drinking, bathing, sanitary water), tourists also encourage secondary consumption for agriculture focused on tourism, swimming pools, green areas, etc. Water consumption increases exponentially with increasing accommodation capacity [19].

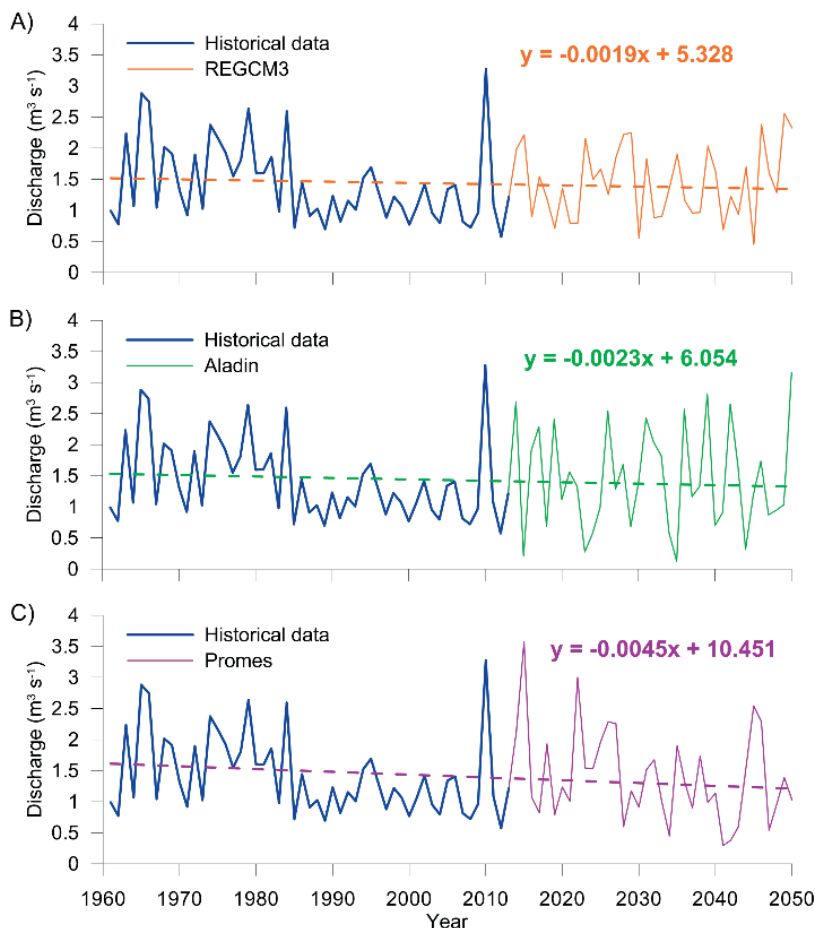


Figure 1. Historical time series and projected time series of the total lowest average monthly discharge of Sv. Ivan, Gradole and Bulaž springs generated using different climate models for 1961-2050 with accompanying trends: A) REGCM3, B) ALADIN, and C) PROMES models [6]

In DRINKADRIA project it was concluded that the decrease of available water resources in the future due to climate change impact (Figure 1) will cause stress during touristic high season period when the demands for water are the highest (even double), and the water resources availability is at the lowest [6]. This can be observed in Figure 2 where the intra-annual distribution of the long-term mean of average monthly overflow discharges and abstracted quantities on the pilot area in Croatia in Istria for springs Sv. Ivan, Gradole and Bulaž are combined together and analysed for the period 1991–2012 [5].

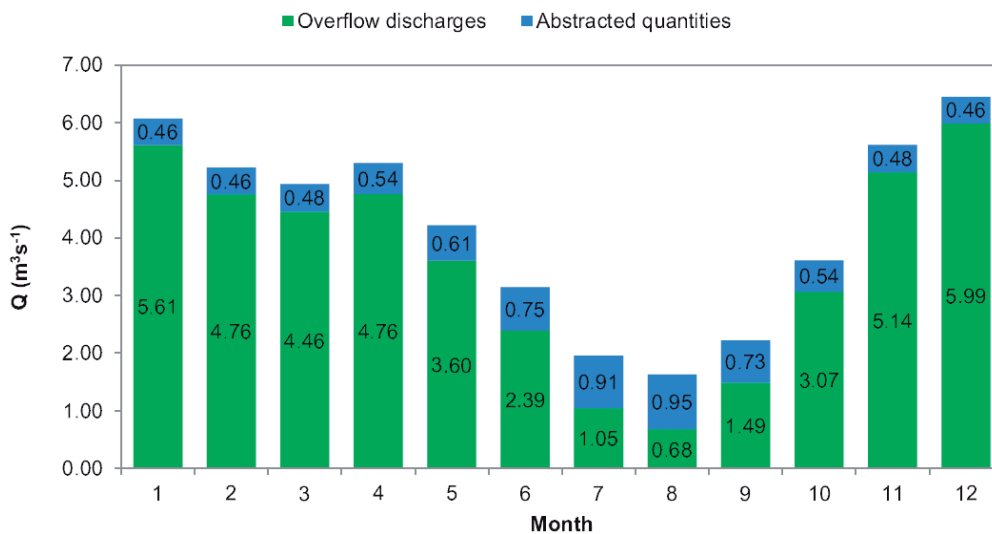


Figure 2. Intra-annual distribution of the long-term mean of average monthly overflow discharges and abstracted quantities for springs Sv. Ivan, Gradole and Bulaž combined together (1991–2012) [5]

When talking about the assumed features of tourism in the coastal part and on the islands, the starting line is usually 3S (Sun, Sea and Sand). Another often assumed basis is sustainable tourism with the fundamental theme that the island, as an eco-paradise, has untouched nature along with the local population and a way of life with low environmental impacts [20]. Tourists are looking for destinations with favourable climatic conditions, and on the other hand, tourism itself contributes to climate change. Addressing climate change is considered a prerequisite for sustainable tourism development, and sustainable water management is important for the quality of life of local inhabitants [19, 21].

4. Adaptation to climate change and mitigation measures

With increasing evidence of the impact of climate change, strategies and plans for climate change adaptation and mitigation have been developed at international, European and national levels. The Paris Agreement on Climate Change obliges the countries of the world to act in two directions: to take urgent measures to reduce greenhouse gas emissions in order to limit the increase in temperature to 1.5°C and 2°C compared to the pre-industrial period, and take measures to adapt to climate change, in order to reduce the damage from climate change (in force since 4 November 2016, confirmed by the EU on 5 October 2016, and by the Republic of Croatia on 17 March 2017, [22]).

The Intergovernmental Panel on Climate Change (IPCC) in 2019 shows that the global trend of temperature rise is +1.1°C and if the concentration of greenhouse gases continues to increase at the current rate, global warming is likely to reach 1.5°C between 2030 and 2052. The UN's 2030 Sustainable Development Goals (SDGs) set 17 global Sustainable Development Goals (SDGs), with a goal 13: taking urgent action to combat climate change and its impacts [22].

The European Commission adopted a new EU strategy for adaptation to climate change on 24 February 2021. The new strategy sets out how the EU can adapt to the inevitable impacts of climate change and become resilient to impending change by 2050. It is necessary to: make adaptation smarter by encouraging action based on reliable data and risk assessment tools, make adaptation more systematic because climate change affects all sectors, make adaptation faster because we already feel the effects of climate change, and step up action internationally because adapting is the cross-sectoral element of EU and Member State action. The Republic of Croatia is obliged to prepare a periodic report to the European Commission on measures to adapt to climate change at the national and local level [22].

The first strategic document that provides an assessment of climate change for Croatia is the Strategy for Adaptation to Climate Change in Croatia for the period until 2040 with a view to 2070 [17] and was adopted by the Croatian Parliament on April 7, 2020. The goal of the Strategy is to raise awareness of the importance and threats of climate change for society and the need to integrate the concept of climate change adaptation into existing and new policies, in order to reduce the vulnerability of the environment, economy and society caused by climate change. The Strategy identifies vulnerable sectors, including hydrology and water resources, and tourism, and prescribes the obligation to take adaptation measures. Table 1 shows the projections of climate parameters in the Republic of Croatia for the period 2041–2070 [17].

Table 1. Projections of climate parameters for the Republic of Croatia according to the RCP4.5 scenario for the period 2041–2070 (prepared by authors based on [17])

Climate parameter	Projections of future climate in Croatia according to scenario RCP4.5 for the period 2041–2070 obtained by climate modelling
Precipitation	Average annual quantity: further decreasing trend (up to 5%) except in the NW parts of Croatia
	Decrease in all seasons (up to 10% mountains and Northern Dalmatia) except winter (increase 5–10% Northern Croatia)
	The number of drought periods will increase
Surface runoff	Reduction of runoff (especially in spring)
Air temperature	Medium: increase 1.5–2.2°C (all seasons, especially in the continental part)
	Max: increase up to 2.2°C in summer (up to 2.3°C on islands)
	Min: the largest increase on the continent in winter 2.1–2.4°C; and 1.8–2°C coastal areas
Mean sea level	2081–2100 32–65 cm (estimation of average means for the Adriatic)

The main expected impacts that can lead to a high degree of vulnerability of water resources are [17]:

- reduction of water quantities in watercourses and springs;
- reduction of groundwater supplies and decline of groundwater levels;
- reduction of water levels in lakes and other dammed natural or built systems;

- rising sea levels, salinization of coastal aquifers and aquatic systems;
- increase in water temperatures accompanied by a decrease in the carrying capacity of receiving water bodies;
- increasing the frequency and intensity of floods in endangered areas;
- increasing the frequency and intensity of torrents;
- increasing the frequency and intensity of floods from rainwater in urban areas;
- increase in sea level, and thus the probability of floods at the mouths of watercourses;
- reducing the efficiency of coastal infrastructure, and
- intensification of salinization of estuaries and coastal aquifers.

The Strategy [17] provides an assessment of the impact of climate change and the vulnerability of the tourism sector on climate change and possible responses to high vulnerability, as shown in Table 2.

Table 2. Overview of the impacts and challenges of climate change adaptation in the tourism sector and possible responses to reducing high vulnerability [17]

Impacts and challenges that cause high vulnerability	Possible responses to reducing high vulnerability
<ul style="list-style-type: none"> – inadequacy of the tourist offer to projected climate change (high temperatures, increased solar radiation, frequency of extreme weather events, etc.), – changing the attractiveness of the area on the coast and in the continental part of the Republic of Croatia, – damage and / or reduced functionality of various infrastructure systems (water supply, drainage, beach infrastructure, horticulture, etc.), – deterioration of ecosystems, biodiversity and cultural heritage important to tourism due to indirect and direct effects of climate change. 	<ul style="list-style-type: none"> – adaptation of the tourism sector to changed business conditions due to the impact of climate change, – aligning tourism activities with projected climate change, – strengthening competences related to impacts and adaptation to climate change of experts directly related to the tourism sector, – inclusion of climate change adaptation measures in all segments of sustainable Croatian tourism, – the revitalisation of tourist offer across the entire territory of the Republic of Croatia and exploitation until now underutilised or untapped potential, – implementation of priority programs for the rehabilitation of cultural assets by including acceptable measures to reduce vulnerability to climate change.

Table 3 provides measures for adaptation to climate change in the tourism sector grouped into categories of very high and high importance and lists the key stakeholders.

Table 3. Climate change adaptation measures in the tourism sector: measures of very high importance (01–04), high importance (05) and key stakeholders [17]

Measure code	Name of the measure	Key stakeholders
T-01	Integrating climate change into the tourism development strategy	Ministry of Tourism, Ministry of Environmental Protection, local and regional self-government units, tourist boards, Croatian Meteorological and Hydrological Service
T-02	Raising awareness of experts involved in the tourism sector about the impact, risks and opportunities for adaptation to climate change	Ministry of Tourism, Croatian Chamber of Commerce, tourist boards, public institutions for the management of protected parts of nature
T-03	Encouraging education of students on climate change	Ministry of Science and Education, Croatian Chamber of Commerce, Croatian Chamber of Crafts
T-04	Strengthening the resilience of tourist infrastructure to various weather extremes	Ministry of Tourism, Ministry of Construction and Physical Planning, Ministry of Environmental Protection, Ministry of the Sea, Transport and Infrastructure, local and regional self-government units, Croatian Meteorological and Hydrological Service
T-05	Strengthening the resilience of local communities in the tourism sector	Ministry of Tourism, local and regional self-government units, tourist boards, Croatian Meteorological and Hydrological Service

In order to respond to the new policy goals for 2030, the existing Sustainable Energy Action Plans (SEAP) were to be upgraded to Sustainable Energy and Climate Action Plans (SECAP). The goal is to reduce CO₂ emissions by at least 40% by 2030, improve energy efficiency, reduce energy consumption and influence the adaptation to climate change. These plans serve as an effective tool for planning climate change mitigation and adaptation measures [23].

In Croatia most cities with prepared SECAP are located in the Primorje-Gorski Kotar and Istria counties (11 cities in total), and these are the cities: Kastav, Opatija and Rijeka (Primorje-Gorski Kotar County), Buje, Novigrad, Pazin, Buzet, Labin, Rovinj, Poreč and Pula (Istria County) [23].

In the field of adaptation to climate change, vulnerability and risk analysis to climate change was conducted, and in the water and tourism sector the risk is moderate or high due to high exposure due to high population density and increase in number of tourists during the touristic season.

These sectors require the timely implementation of climate change adaptation measures. Table 4 gives an example of good practice, i.e. an overview of climate change adaptation measures in the water sector and tourism sector on the example of Croatian Northern Adriatic cities: Rijeka, Kastav, Opatija (Primorje-Gorski Kotar County), Poreč and Labin (Istria County). All these cities are tourist destinations.

In Croatia in 2013, the Institute for Social Research and the Society for Shaping Sustainable Development (Institut za društvena istraživanja and Društvo za oblikovanje održivog razvoja) conducted a survey on citizens' attitudes towards climate change. Even then, 70% of citizens considered climate change a significant problem, and more than 40% of citizens thought that climate change mitigation was more important than current economic development, mostly citizens of coastal regions of the Republic of Croatia [23].

The research conducted in 2019, through the RMPPI (Renewable micro power plant initiative) project confirmed the great interest of citizens in the topic of climate change and considered climate change a significant problem [28].

Climate change is of particular importance for the long-term positioning of tourist destinations on the world market. Some destinations will gain in attractiveness, and there will be more interest in them, while others whose attractiveness will be jeopardized by climate change will have to be repositioned in order to maintain their market position [29].

Table 4. Measures of adaptation to climate change in the water and tourism sector on the example of cities in Primorje-Gorski Kotar County and Istria County (prepared by authors based on [24–27])

Cities	Climate change adaptation measures in the water sector	Climate change adaptation measures in the tourism sector
Rijeka	<ul style="list-style-type: none"> – strengthening the resilience of coastal water-communal infrastructure and coastal water resources, – preparation of project and planning documentation related to water protection infrastructure. 	<ul style="list-style-type: none"> – networking and upgrading the system of monitoring environmental indicators related to climate change.
Kastav and Opatija	<ul style="list-style-type: none"> – economic evaluation of groundwater and springs, – identifying vulnerable groups and critical assets in terms of flood risk, – reconstruction of the water supply network and installation of equipment for smart monitoring of the water supply system in order to reduce water loss in the system, – raising public awareness on the importance of water consumption and the impact of climate change, – rationalization of water consumption, – analysis of the impact of sea level rise, – strengthening the resilience of water and communal infrastructure in coastal areas, – preparation of an analysis of the possibility of recycling wastewater for reuse and rainwater collection. 	<ul style="list-style-type: none"> – increasing resistance to climate change (measuring UV radiation and temperature, availability of drinking water in public places, personal protection from UV radiation), – development and encouragement of tourism activities compatible with resistance to extreme weather conditions (supply diversification), – raising the awareness of tourism workers about the impact, risks and possibilities of adaptation to climate change, – strengthening the resilience of tourist infrastructure to various weather extremes (construction of swimming pools, indoor spa and wellness facilities, refrigerated areas, etc.), – encouraging the education of students of tourism professions on climate change.
Poreč	<ul style="list-style-type: none"> – strengthening capacities for protection against harmful effects of water, stakeholder capacity, measures for protection against harmful effects of water in the event of extreme hydrological conditions (e.g. floods), and resilience of urban areas to anthropogenic pressures caused by climate change. 	<ul style="list-style-type: none"> – development of the concept of sustainable tourism that includes adaptation to climate change, – strengthening the competencies of employees in the tourism sector, – strengthening the resilience of tourist infrastructure to various weather extremes.
Labin	<ul style="list-style-type: none"> – increasing revenues to combat water shortages, – education of the population, – regulations restricting water consumption, especially in dry summer periods, or adopting provisions that promote more rational use of water resources. 	<ul style="list-style-type: none"> – diversification of the tourist offer, – plans and programs related to climate change, – availability of early weather warning systems.

In general, most destinations are chosen by tourists because of the type of climate. In this context, identifying threats to climate change and future perspectives of change are important determinants of likely changes in preferences for travel destinations. Interest and concern about climate change have begun to spread in recent times and have become a global problem, and climate change is receiving significant attention in the field of tourism research [30].

Emphasizing the impact of tourism on the environment (which generates climate change) is a key focus of sustainable tourism development. Namely, the pronounced tourist seasonality affects the development of climate change. The process of adaptation to climate change in a tourist destination requires the interaction of sustainable tourism development and climate change [29].

The future effects of climate change will extend the touristic season. The result of predicting the future climate is greater deseasonalisation of demand, as certain seasons (spring and autumn) will offer greater comfort to tourists and visitors. Higher temperatures in the current main part of the tourist season (July and August) will reduce the number of tourists, thus increasing the number of tourists in other months of the year due to more acceptable temperatures in Mediterranean tourist destinations [18].

This future deseasonal demand in certain tourist destinations will have a positive effect on water supply systems, which have so far been overstressed in the summer months due to a big increase in tourist arrivals in July and August. Tourism is considered among the economic sectors that are least prepared for the risks and opportunities posed by climate change [21].

The development of selective forms of tourism is crucial for adapting the offer to the requirements of tourists who cannot perform normal tourist activities due to unfavourable weather conditions (unbearable heat, UV radiation or rain). The product of the “sun and sea” that is characteristic for Croatia needs to be supplemented with other forms of tourism (health, sports, culture, history, education, entertainment). It is necessary to start applying these measures of adaptation to climate change as soon as possible [31] since it is expected that the cost of investing in adaptation will reduce the cost of repairing possible damages in the future [16].

5. Conclusion

Climate change is affecting, and in the near future it will certainly affect even more intensely, the population of the Earth. This paper presented the impact of climate change with an emphasis on water resources and tourism. The impact of climate change on water resources results mostly in decreasing the available quantities of water in future. The way that tourism responds to climate change is absolutely critical to the sustainability of tourism and if that sector would withdraw from engaging in climate change problematics, it would be to its significant detriment.

For government, NGOs and decision-makers, climate change is a new strategic reality they have to face.

It is clear that there has been a dramatic increase in research in the field of sustainable tourism development and climate change. The pronounced tourist seasonality, that we currently have, negatively affects and burdens water resources and systems in tourist destinations.

Projections of climate parameters for Croatia in the future predict deseasonal touristic demand primarily due to the lower level of comfort that will prevail during the summer months due to too high temperatures. This deseasonalisation, which would redistribute tourist arrivals to the rest of the year, would have a positive impact on water resources and systems, decreasing the stress on water resources that we have now in high season.

The Mediterranean basin area has been identified as one of the most vulnerable regions of the world to climate and anthropogenic change. In this area tourist seasonality is pronounced during the summer months, which is an additional challenge for efficient water management.

High ratings tourists give to destinations with favourable climatic conditions, which are an important element when choosing a destination. Therefore, the climate as one of the most important drivers of tourism, in the future will play an even more important role in choosing a destination. Given that climate is recognized as a key driver of tourism, climate change can have a positive or negative impact on tourism, although tourism itself contributes to climate change. The overall quality of life stems from the sustainability of the tourist destination. This in turn improves the quality of life of the local population and the image and competitiveness of tourist destinations.

Timely adjustments can significantly reduce the future damage and losses caused by climate change in the tourism sector. The SECAP analysis of selected cities in the Northern Adriatic part of Croatia presents concrete and specific measures for adaptation to climate change in the water sector and in the tourism sector, that should be implemented.

The EU is fighting against climate change, so in the last financial period, until 2020, every fifth euro in the European budget was allocated for adaptation to climate change, which is 180 billion euros per year, while in the current financial

period from 2021 to 2027, every fourth euro in the European budget will be allocated for this purpose, which is more than 280 billion euros per year [2].

Another aspect that we are currently adding to our research on climate change impact on water resources and tourism are summer fires in Adriatic coastal areas since the number and fire severity have significantly increased over the past decades [32]. Fires are often consequences of human activities and unfavourable hydrological conditions during summer, have huge impact on the environment and can endanger touristic areas, while additional water resources are needed for fire control and extinguishing.

There is still a lot to be done to raise public awareness about climate change and the impact on natural resources (including water resources). Raising general public awareness about this problem will certainly accelerate further research and implementation of preventive measures. At the same time, from the scientific point of view, the impact of climate change, adaptation and mitigation measures need to be continuously investigated, quantified and included in all spheres of human activities and the environmental management.

Acknowledgements

The research for this article and the publication of this article were funded by the University of Rijeka within the projects “Implementation of Innovative Methodologies, Approaches and Tools for Sustainable River Basin management” (UNIRI-TEHNIC-18-129) and “Hydrology of Water Resources and Identification of Flood and Mudflow Risks in Karst” (UNIRI-TEHNIC-18-54).

References:

- [1] Muhar, A., Đurin B.: Utjecaj klimatskih promjena na vodne resurse u svijetu (Climate change impact on water resources), Zbornik radova Međimurskog veleučilišta u Čakovcu, 9 (1), pp. 46–54, 2018, <https://hrcak.srce.hr/202075> (accessed 14.06.2022.).
- [2] Bebić, M.: Utjecaj globalnih klimatskih promjena na vodne resurse – primjer rijeke Neretve (Climate change impact on water resources – example of river Neretva), Hrvatske vode, 29, pp. 51–56, 2021, <https://hrcak.srce.hr/256260> (accessed 14.06.2022.).
- [3] Koutroulis, A.G., Tsanis, J.K., Daliakopoulos, I.N., Jacob, D.: Impact of climate change on water resources status: a case study for Crete Island, Greece, Journal of Hydrology, 479, pp. 146–158, 2013, <https://doi.org/10.1016/j.jhydrol.2012.11.055>.
- [4] Estrela, T., Pérez-Martin, M.A., Vargas, E.: Impacts of climate change on water resources in Spain, Hydrological Sciences Journal, 57(6), pp. 1154–1167, 2012, doi: 10.1080/02626667.2012.702213
- [5] Karleuša, B., Rubinić, J., Radman, I., Volf, G., Krvavica, N.: Cross-Border Water Resources Management in Present Conditions and for Future Scenarios, International Symposium Cross-border drinking water management: proceedings, University of Rijeka Faculty of Civil Engineering, Rijeka, pp. 59–90, 2016.
- [6] Karleuša, B., Rubinić, J., Radišić, M., Krvavica, N.: [Analysis of Climate Change Impact on Water Supply in Northern Istria \(Croatia\)](#), Technical Gazette, 25 Supplement 2, pp. 366–374, 2018, doi:10.17559/TV-20170809140304.
- [7] Alcamo, J., Henrichs, T.: Critical regions: A model-based estimation of world water resources sensitive to global changes, Aquatic Science, 64(4), pp. 352–362, 2002, <https://doi.org/10.1007/PL00012591>.
- [8] Xoplaki, E., Gonzalez-Rouco, J.F., Luterbacher, J., Wanner, H.: Wet season Mediterranean precipitation variability: influence of large-scale dynamics and trends, Climate Dynamics, 23(1), pp. 63–78, 2004, <https://doi.org/10.1007/s00382-004-0422-0>.
- [9] Milano, M., Ruelland, D., Fernandez, S., Dezetter, A., Fabre, J., Servat, E.: Facing climatic and anthropogenic changes in the Mediterranean basin: What will be the medium-term impact on water stress? Comptes Rendus Geoscience, 344(9), pp. 432–440, 2012, <https://doi.org/10.1080/02626667.2013.774458>
- [10] Collet, L., Ruelland, D., Estupina, V.B., Dezetter, A., Servat, E.: Water supply sustainability and adaptation strategies under anthropogenic and climatic changes of a meso-scale Mediterranean catchment, Science of the Total Environment, 536, pp. 589–602, 2015, <https://doi.org/10.1016/j.scitotenv.2015.07.093>
- [11] Sisto, N.P., Ramirez, A.I., Aguilar-Barajas, I., Magana-Rueda, V.: Climate threats, water supply vulnerability and the risk of a water crisis in the Monterrey Metropolitan Area (Northeastern Mexico), Physics and Chemistry of the Earth, 91, pp. 2–9, 2016, <https://doi.org/10.1016/j.pce.2015.08.015>
- [12] Xu, Z.X., Chen, Y.N., Li, J.Y.: Impact of climate change on water resources in the Tarim River basin, Water Resources Management, 18(5), pp. 439–458, 2004, <https://doi.org/10.1023/B:WARM.0000049142.95583.98>.
- [13] Mizyed, N.: Impacts of climate change on water resources availability and agricultural water demand in the West Bank, Water Resources Management, 23(10), pp. 2015–2029, 2009, <https://doi.org/10.1007/s11269-008-9367-0>.

- [14] Kanakoudis, V., Tsitsifli, S., Papadopoulou, A., Čencur Curk, B., Karleuša, B.: Water resources vulnerability assessment in the Adriatic Sea region: the case of Corfu Island, *Environ Sci Pollut Res*, 24, pp. 20173–20186, 2017, <https://doi.org/10.1007/s11356-017-9732-8>.
- [15] Giorgi, F., Lionello, P.: Climate change projections for the Mediterranean region, *Global and Planetary Change*, 63, pp. 90–104, 2008, <https://doi.org/10.1016/j.gloplacha.2007.09.005>
- [16] [Ministry of Economy and Sustainable Development \(Croatia\): https://prilagodba-klimi.hr/](https://prilagodba-klimi.hr/) (accessed 14.06.2022).
- [17] Strategy for Adaptation to Climate Change in Croatia for the period until 2040 with a view to 2070, Official Gazette of the Republic of Croatia 46/20 (accessed 14.06.2022).
- [18] Perić J., Šverko Grdić Z.: Klimatske promjene i turizam (Climate change and tourism), Faculty of Tourism and Hospitality Management, Opatija, 2017.
- [19] Slavuj, L., Čanjevac, I., Opačić, V.T.: Vodoopskrba kao faktor održivog razvoja turizma otoka Krka (Water Supply as a Factor of Sustainable Tourism Development on the Island of Krk), *Hrvatski geografski glasnik (Croatian Geographical Bulletin)*, 71 (2), pp. 23–41, 2009, <https://doi.org/10.21861/hgg.2009.71.02.02>
- [20] Kelman, I.: Critiques of island sustainability in tourism, *Tourism Geographies*, 23 (3) pp. 397–414, 2021, doi: [10.1080/14616688.2019.1619825](https://doi.org/10.1080/14616688.2019.1619825)
- [21] Scott, D.: Why sustainable tourism must address climate change, *Journal of Sustainable Tourism*, 19(1), pp. 17–34, 2011, doi: [10.1080/09669582.2010.539694](https://doi.org/10.1080/09669582.2010.539694)
- [22] Ministry of Economy and Sustainable Development (Croatia): <https://mingor.gov.hr/o-ministarstvu-1065/djelokrug-uprava-za-klimatske-aktivnosti-1879/prilagodba-klimatskim-promjenama-1965/1965> (accessed 14.06.2022.)
- [23] [Society for Sustainable Development Design \(Croatia\): https://door.hr/](https://door.hr/) (accessed 14.06.2022)
- [24] Akcijski plan energetske i klimatske održivosti razvitka (SECAP) za Grad Rijeku (Sustainable Energy and Climate Action Plan (SECAP) for the city of Rijeka), 2020; <https://www.rijeka.hr/wp-content/uploads/2021/02/Akcijski-plan-odr%C5%BEivog-energetskog-razvoja-i-prilagodbe-na-klimatske-promjene-za-Grad-Rijeku-SECAP.pdf> (accessed 14.06.2022)
- [25] Zajednički akcijski plan energetske i klimatske održivosti razvitka (JOINT SECAP) Grad Kastav, Grad Opatija, te općine Čavle, Matulji i Viškovo (Joint Sustainable Energy and Climate Action Plan (JOINT SECAP) for towns Kastav and Opatija, and municipalities Čavle, Matulji and Viškovo), 2021; <https://kastav.hr/wp-content/uploads/2021/10/1.-Zajednicki-akcijski-plan-energetski-i-klimatski-odrzivog-razvitka-JOINT-SECAP.pdf> (accessed 14.06.2022)
- [26] Strategija prilagodbe klimatskim promjenama Grada Poreča – Parenzo do 2030. godine s prvim petogodišnjim planom provedbe (Municipality of Poreč – Parenzo / Climate change adaptation Strategy (2030.) and Action plan), LIFE 2014 – 2020 – Climate Change Adaptation; http://www.porec.hr/sadrzaj/dokumenti/2019_05_29_Strategija_prilagodbe_klimatskim_promjenama_Grad_Porec_Parenzo.pdf (accessed 14.06.2022).
- [27] Strategija i plan prilagodbe klimatskim promjenama Grada Labina (Strategy and plan for climate change adaptation of the city of Labin), LIFE 2014–2020 – Climate Change Adaptation; <http://www.labin.hr/Files/202110/2.1.%20Strategija%20i%20plan%20prilagodbe%20klimatskim%20promjenama%20Grada%20Labina%20.pdf> (accessed 14.06.2022).
- [28] Renewable micro power plant initiative project, <http://ee.fesb.unist.hr/rmppi/en/project/> (accessed 14.06.2022).
- [29] Racz, A.: Međutjecaj klimatskih promjena i turističke djelatnosti – narativni pregled (Interinfluence between Climate Change and Tourism Industry – a Narrative Review), *Journal of applied health science*, 6(1), pp. 91–115, 2020, <https://doi.org/10.24141/1/6/1/10>
- [30] Farid, H., Hakimian, F., Nair, V., Nair, P.K., Ismail, N.: Trend of research on sustainable tourism and climate change in 21st century, *Worldwide Hospitality and Tourism Themes*, 8(5), pp. 516–533, 2016, <https://doi.org/10.1108/WHATT-06-2016-0032>
- [31] Šverko Grdić, Z., Krstinić Nižić, M., Mamula, M.: Povezanost klimatskih promjena i turizma: multikriterijska analiza ocjenjivanja mjera prilagodbe (Connection between the climate change and tourism: the multi-criteria analysis of assessment of adaptation measures), *Ekonomika misao i praksa*, 1, pp. 171–185, 2017.
- [32] Horvat, B.; Karleuša, B.; Delač, D.; Ožanić, N.; Volf, G.; Kisić, I.: [Spektralni indeks NBR kao temelj za procjenu utjecaja opožarenosti površine na otjecajne karakteristike sliva](#) (Spectral index NBR as a basis to estimate burnt area impact on runoff characteristics), 8. Sabor hrvatskih graditelja (8th Congress of Croatian Builders), HSGI, Zagreb, pp. 171–185, 2021.

VII Climate Change and Flood Risk Management

HYDROLOGIC REGIME OF THE TORYSA RIVER BASIN

PATRIK NAGY¹, MARTINA ZELENÁKOVÁ¹, KATARZYNA BARAŃCZUK², JACEK BARAŃCZUK²

¹Department of Environmental Engineering, Faculty of civil engineering, *Slovakia*,
e-mail: patrik.nagy@tuke.sk

¹Technical University of Kosice, Faculty of Civil Engineering Department of Environmental Engineering; *Slovakia*
e-mail: patrik.nagy@tuke.sk, martina.zelenakova@tuke.sk

²University of Gdańsk, Faculty of Oceanography and Geography, Coastal Cities Living Lab; *Poland*
e-mail: katarzyna.baranczuk@ug.edu.pl, jacek.baranczuk@ug.edu.pl

Abstract

Climate change brings the occurrence of flash floods from extreme rainfall and then the increasingly frequent occurrence of dry periods, which last longer. To mitigate climate change, it is necessary to assess the variability of the flow and take the necessary adaptation measures to mitigate climate change impacts. This paper evaluates the daily average flows in the Torysa river basin in the eastern Slovakia. The graphic method flow duration curves (FDC) were used.

Keywords: Torysa river basin, flow duration curves, discharge, climate change, hydrologic drought.

1. Introduction

Climate change is one of the biggest environmental problems. Climate change refers to extremes in precipitation and increased average air temperature. Lack of rainfall is the main cause of drought. Hydrological drought is caused by a lack of precipitation and is manifested by a lack of surface and underground water [1]. Drought can also be caused by anthropogenic human activity, increased water consumption by industry, agriculture and households. Another cause of climate change is increased surface runoff from the built-up area and overheating of built-up areas [2].

In this paper we focused on the hydrological drought assessment. Daily flows were evaluated using the FDC (Flow Duration Curves) graphical method. FDC show the percentage of time and streamflow value that is equal or exceed during and time period and provide information about the availability and variability of water resources. Their many uses include, for example, the design of water supply systems and run-of-river hydropower plants and ecological studies [3]. FDC is a tool for the management of water resources and is also used in several theoretical studies at river basins. FDCs are the result of complex interactions between climate and geomorphological characteristics of the basin, so they are sensitive to changes in these conditions and can be used for investigation of the impact on water resources. The FDC can give us a view of the hydrological resistance of river regimes, low flow rates and ecological flow integrity [4]. FDC related studies began in the first half of the 20th century [5]. Various approaches were designed for the FDC, the so called parametric and graphic approach [6]. Statistical approaches take into account the characteristics of the basin [7]. Wittenberg estimated the FDC basin based on the parameters of the probability distribution function [8]. There are many other studies that focus on the FDC.

2. Methods and study area

2.1. Study area

The studied territory of the Torysa basin (Fig. 1) is located in eastern Slovakia. It originates in the Levočské hills northwest of the village Torysky. At the beginning it flows to the southwest, later it turns to the north and soon to the east. Near Lipany, it turns to the southeast. In Prešov, its most important tributary, Sekčov river, flows south through the Košice basin. Southeast of Košice, near the village of Nižná Hutka, it flows into Hornád as a left-hand tributary [9]. These hydrological stations were evaluated in the selected river basin. Stations at the Torysa river: Košické Olšany, Prešov, Sabinov and Brezovica and at the Sekčov river: the Demjata hydrological station. Data from hydrological stations were provided by the Slovak Hydrometeorological Institute and are for the period 1972–2020.

Table 1. Basin Torysa data

Hydrologic stations	MAX DAILY Q [m ³ /s]	MIN DAILY Q [m ³ /s]	AVERAGE DAILY Q [m ³ /s]
KOŠICKÉ OLŠANY	292,4	0,89	7,7
PREŠOV	216,4	0,35	4,3
SABINOV	169,4	0,12	3,3
DEMJATA	53,8	0,03	0,7
BREZOVICA	103,7	0,006	1,6

In Tab. 1. are daily maximum flows, daily minimum flows and average daily flows.

Basin Torysa

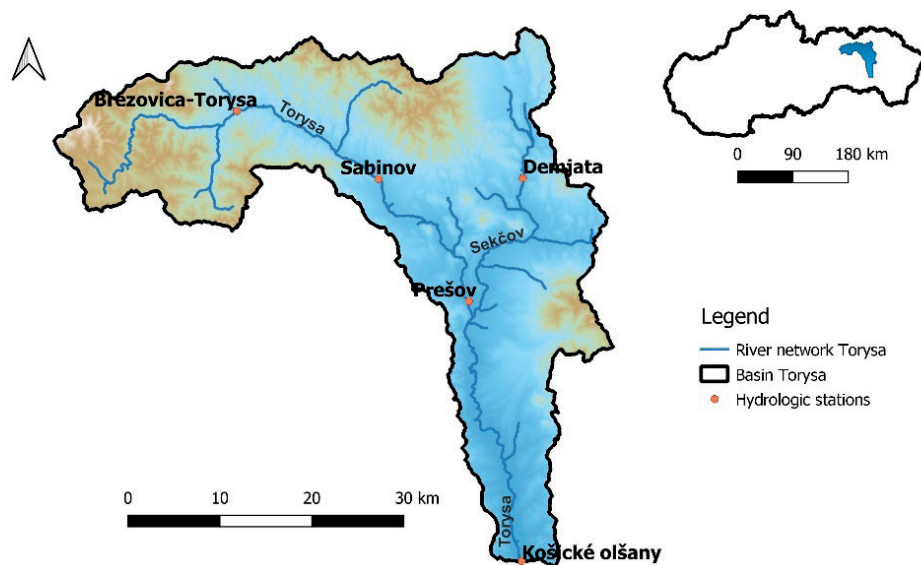


Figure 1. Location of the Torysa river basin and the hydrological stations

2.2. Methods

The FDC graphic method was used, which was processed using the software R. Software R is the environment for statistical calculations and graphics. Daily flows were used to analyze the flow rates, which were divided into fifth periods: 1972–1980, 1981–1990, 1991–2000, 2001–2010, 2011–2020. Lubridate, GGPlot2 and Hydrtsm packages have been used. Using the Rank function, the flow position was assigned in each period and for each station. Then the probability of exceeding $P(1)$.

$$P = 100 * [M/(n + 1)] \quad (1)$$

M = ranked position of the flow, n = total number of observations in data record

The charts were created using the logarithmic function and the GGPlot2 package in R. We chose the type of box-plot graph that is more transparent than Line Graph.

3. Results and discussion

In the 1980s and in the first half of the 1990s, dry conditions were prevailed in Slovakia, which was examined by Fendeková et al. [11]. Flow analysis shows a relatively declining trend of flow in Torysa river basin.

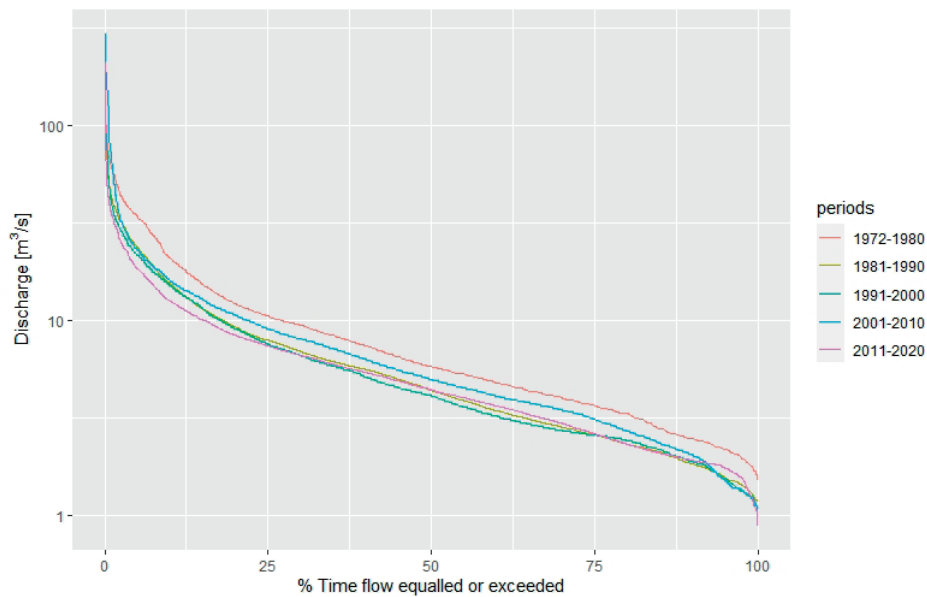


Figure 2. FDC Košické Olšany

In Figure 2 is shown the duration of flows in the Košické Olšany hydrological station, where we can follow the sinusoidal course of the median FDC in the observed periods. In the period 2001–2010, there were large floods, therefore large streamflows were recorded in the Q3 quartile, which affected the FDC. These are the highest flows of the entire observation period in the given station. We see the highest median flows in the period 1972–1980. The median in the period 1981–1990 and 2011–2020 is the same.

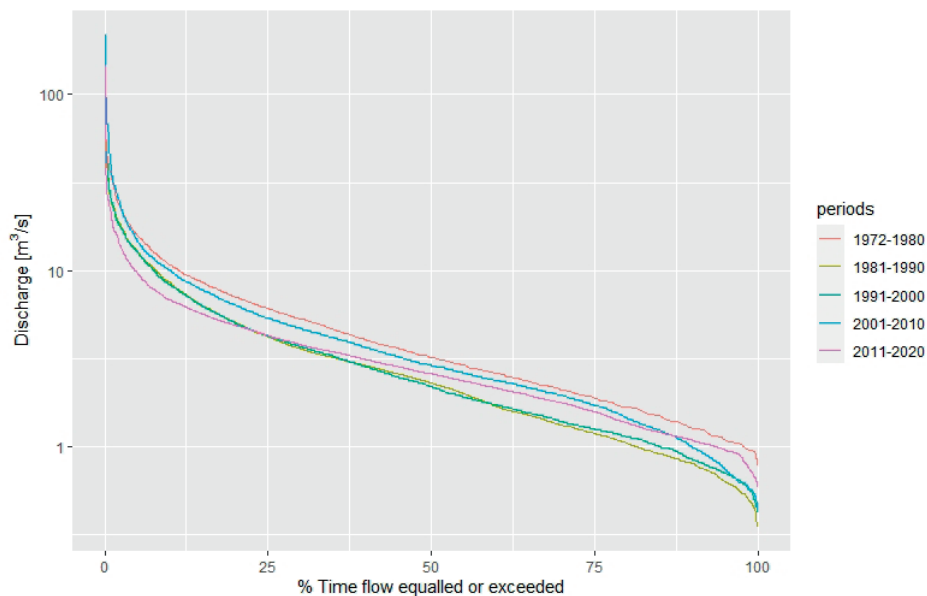


Figure 3. FDC Prešov Torysa

In the Prešov Torysa station, we can observe a significantly dry period in the 80s and 90s, where the value of the median streamflow is also the lowest. In the period 2011–2020, the median value is higher than in the 1980s or 1990s, and the Q2 quartile has the smallest interface than the other periods in the given station (Figure 3).

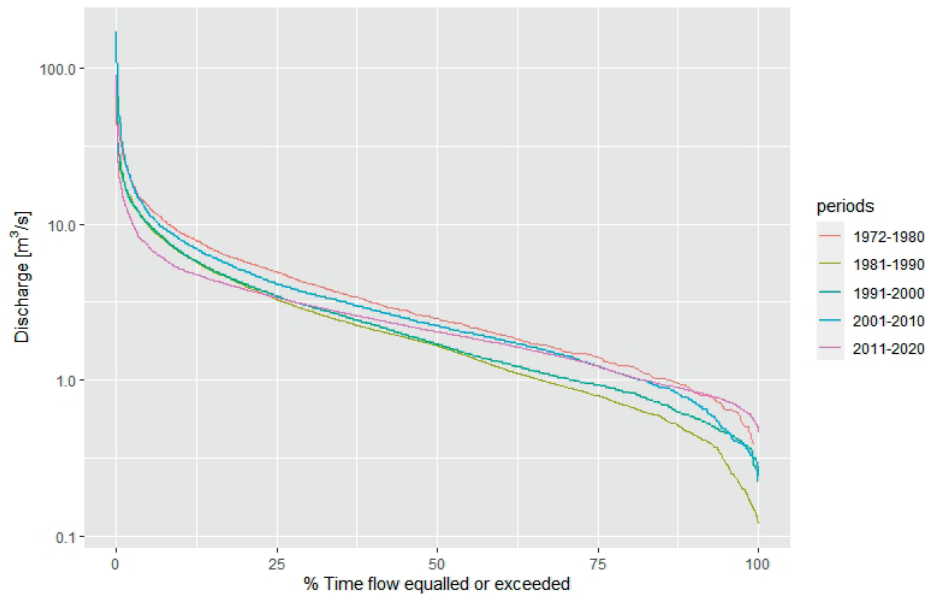


Figure 4. FDC Sabinov

In Sabinov, we can observe a similar course of FDC as in Prešov Torysa station, these stations are not far from each other. But when we compare quartile Q2, in the period 2011–2020 it has the smallest interface, and in quartile Q3 lower flows are observed than in other periods. When we compare the Q1 quartile in the period 2011–2020 and the period 1972–1980 where the value of low flows is similar (Figure 4).

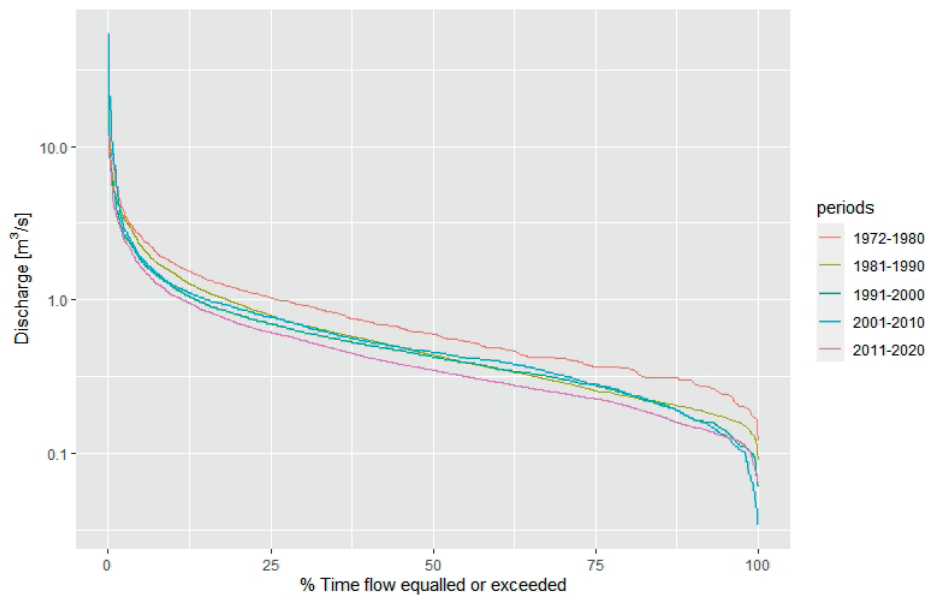


Figure 5. FDC Demjata

At the Demjata station, we observe a decrease in flows over time. The period 2001–2010 is interesting, in quartile Q3 we can observe large flows, but in quartile Q1 we observe the lowest flows in the monitored periods in the given station. Very low flows in quartile Q1 are observed in the period 1991–2000. The average value of the flows is the highest in the period 1972–1980 and the lowest is in the period 2011–2020, approximately the same value of the median is in the periods 1981–1990, 1991–2000 and 2001–2010 (Figure 5).

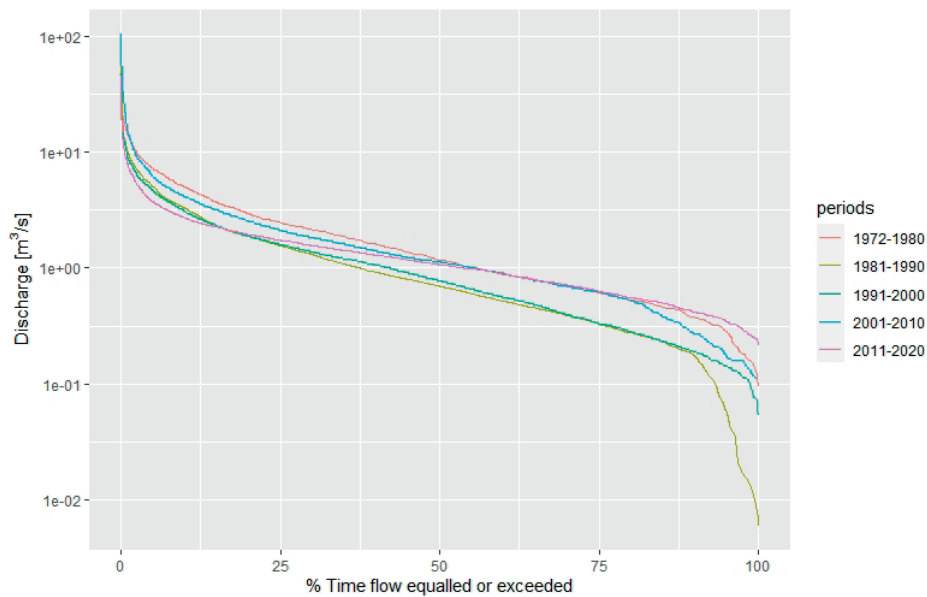


Figure 6. FDC Brezovica

Figure 6 in the Brezovica station we observe very low streamflows in the Q1 quartile in the period 1981–1990, which means that the given decade was dry. In the period 1972–1980, 2001–2010 and 2011–2020, the median value is very similar, but when we compare quartile Q2, the flow interface is larger in the period 1972–1980. In the period 2001–2010, significant large flows were again observed. In the periods 2001–2010 and 2011–2020, higher flows were recorded in the Q3 quartile than in the other periods (Figure 6).

The given graphical results show that there was a hydrological drought in the 1980s, but also the periods 2001–2010 and 2011–2020 in terms of flows are no better, because in the Q2 quartile the streamflow interface is smaller than in the period 1972–2010. But in the last two decades, the Q3 quartile has seen largely high streamflow's.

4. Conclusion

From the results of the study, we can conclude that the flows in the Torisy basin have a decreasing character until the period 2001–2010, when there were large floods in eastern Slovakia. Increased air temperature and less precipitation and more frequent occurrence of dry periods are responsible for the decrease in flows. To mitigate the problems of climate change, adaptation measures to retain water in the country would help, from which it would then be possible to overestimate the flows in the basin during the dry season, but that would be the subject of another study.

Acknowledgements

This work was supported by the Slovak Research and Development Agency under the Contract no. APVV-20-0281, and a project funded by the Ministry of Education of the Slovak Republic VEGA1/0308/20 “Mitigation of hydrological hazards, floods, and droughts by exploring extreme hydroclimatic phenomena in river basins”.

This work has received support from the SCORE (Smart Control of the Climate Resilience in European Coastal Cities) project, funded by the European Union's Horizon 2020 research and innovation programme under grant agreement No 101003534.

References:

- [1] Wilhite, D. A. (2000). Drought as a natural hazard: concepts and definitions.
- [2] Fendeková, M., Gauster, T., Labudová, L., Vrablíková, D., Danáčová, Z., Fendek, M., & Pekárová, P. (2018). Analysing 21st century meteorological and hydrological drought events in Slovakia. *Journal of Hydrology and Hydromechanics*, 66(4), 393–403.
- [3] Smakhtin, V.U. (2001). Low flow hydrology: a review. *Journal of hydrology*, 240(3–4), 147–186.
- [4] Vogel, R.M., & Fennessey, N.M. (1995). Flow duration curves II: A review of applications in water resources planning 1. *JAWRA Journal of the American Water Resources Association*, 31(6), 1029–1039.
- [5] Saville, T., and Watson, J.D. (1933). An Investigation of the flow-duration characteristics of North Carolina Streams. *Eos, Transactions American Geophysical Union*, 14(1), 406–425.

- [6] Castellarin, A., Galeati, G., Brandimarte, L., Montanari, A., & Brath, A. (2004). Regional flow-duration curves: reliability for ungauged basins. *Advances in Water Resources*, 27(10), 953–965.
- [7] Singh, K.P. (1971). Model flow duration and streamflow variability. *Water Resources Research*, 7(4), 1031–1036.
- [8] Wittenberg, H. (1989). Regional analysis of flow duration curves: case studies on river basins in north-west Germany. *IAHS-AISH publication*, (187), 213–220.
- [9] Lehotský, M., Rusnák, M., & Novotný, J. (2022). Short History of Geomorphological Research and Geomorphological Division of Slovakia. In *Landscapes and Landforms of Slovakia* (pp. 1–5). Springer, Cham.
- [10] Fendeková, M., Poórová, J., & Slivová, V. (2018). Hydrologické sucho na Slovensku a prognóza jeho vývoja. *Bratislava: Comenius University. Search in.*

VII Climate Change and Flood Risk Management

SLOPE INSTABILITY FOR DIFFERENT RAINFALL INTENSITIES

BOJAN SUSINOV¹, JOSIF JOSIFOVSKI¹, VLADIMIR VITANOV¹

¹ Ss. Cyril and Methodius University in Skopje, Faculty of Civil Engineering; Republic of North Macedonia
e-mail: susinov@gf.ukim.edu.mk, jjosifovski@gf.ukim.edu.mk, vvitanov@gf.ukim.edu.mk

Abstract

This paper presents the results from the fully coupled flow-deformation analysis of slope stability subjected to different rainfall intensities which correspond to the different probability of occurrence. The main objective was not to define only the influence of the intensive rainfalls on slope stability, but also the changes in saturation and suction for different intensities of a given duration.

A time-dependent analysis was performed using the final element method. Also, widely used constitutive models were used to describe sandy soil's mechanical and hydraulic behaviour.

The results from a hydrological analysis of the intensive rainfalls over the area of the Topolnica tailing dam were used as input parameters for the numerical analysis. A relationship between the probability of occurrence of the maximum monthly intensive rainfall is also plotted in function of the amount of precipitation and characteristic durations. Slope stability analyses were made for rainfall probabilities of 50, 20, 10, 4, 2 and 1%, which correspond to the return period of 2, 5, 10, 25, 50 и 100 months, respectively.

The results show that the wetting front increases when the infiltration rate increases as a result of increased rainfall intensity. The suction profile also changes for different infiltrations. The maximum saturation and suction changes were observed on the slope surface.

Finally, this paper provides information on the influence of extreme rainfall events on slope stability as one of the main trigger factors for landslides or intensive erosion.

Keywords: fully coupled analysis, slope stability, intensive rainfalls, probability, saturation, suction.

1. Introduction

Heavy rainfalls due to climate variations and changes are more often seen as a cause for instabilities, landslides or significant erosion of natural and engineering slopes in both soil and rocky environments. This paper presents examples that confirm this hypothesis, and gives a detailed description of the problems and an advanced concept for the design.



Figure 1. Slope stability problems on Miladinovci – Shtip highway

Figure 1 shows different types of failures occurred on Miladinovci – Shtip highway in the central part of Macedonia. There were examples of shallow landslides above the cut slope, landslides due to water retention on the berm, significant erosion in soft rocks after heavy rainfall in 2020 and continues erosion registered in 2022 [1].

Figure 2 shows the precipitation estimation for the Western Balkan region from last month when more than 20mm/h and 80mm/3h was estimated between Tetovo and Skopje where no weather station was installed yet.

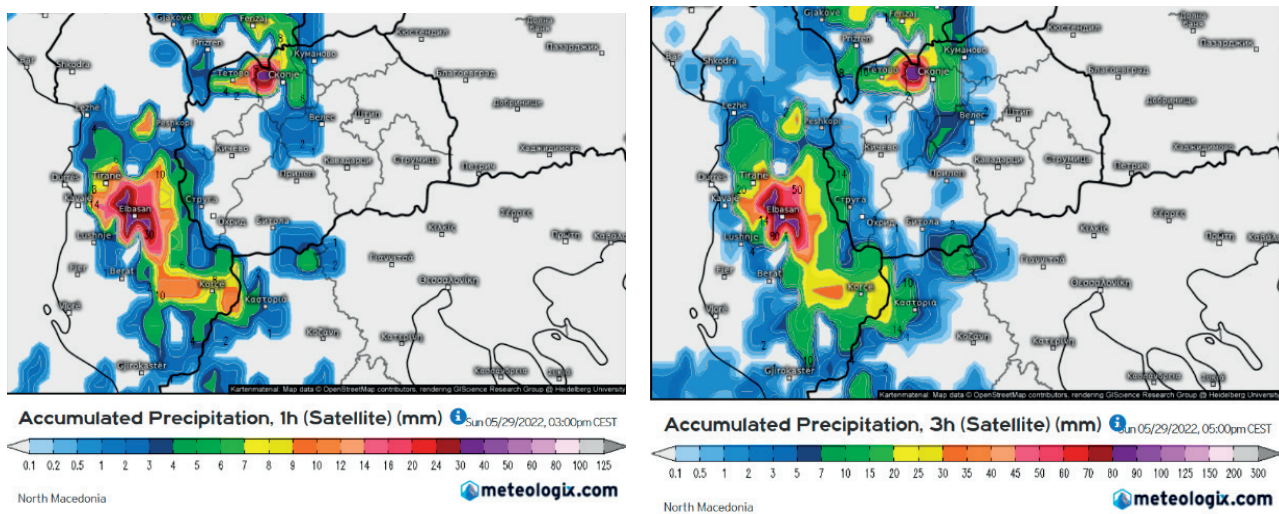


Figure 2. 1-hour and 3-hours precipitation estimation for 29 May 2022

The nearest weather station to the Miladinovci – Shtip highway is Gjurishte weather station where 52 and 43mm/h were measured for two consecutive 12-hours periods on 29 May 2022 [2], see Figure 3.

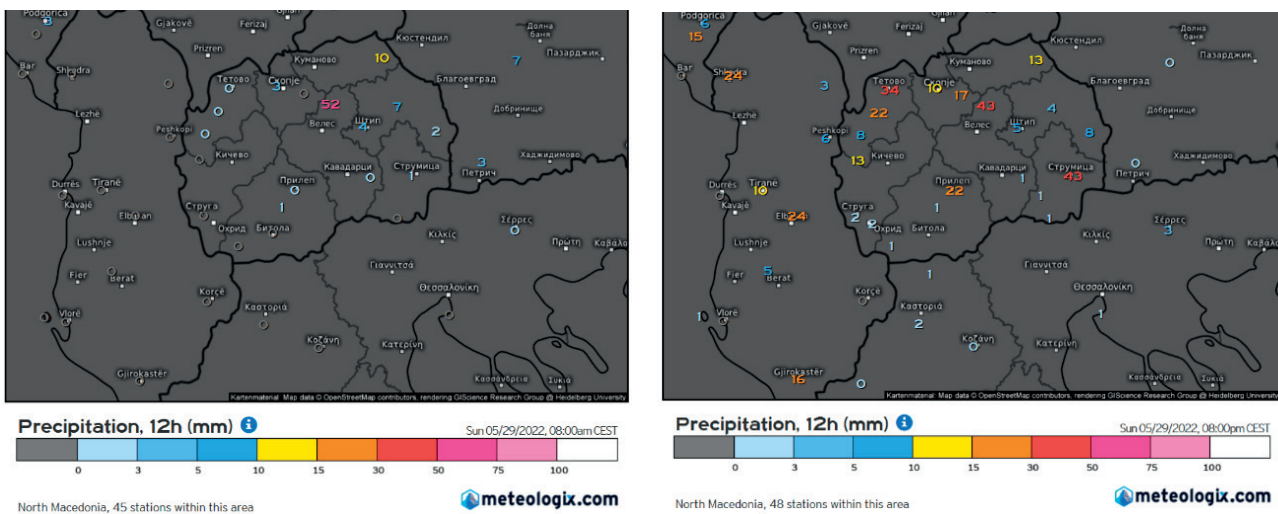


Figure 3. 12-hours measured precipitation for two consecutive measurements on 29 May 2022

The national weather monitoring station [3] measured 25.2mm in one hour and 40.1mm in two hours which causes significant erosion on the slopes presented in Figure 4. The photos was taken between the 2 extreme rainfall events in 24 hours.



Figure 4. Significant erosion on the slopes between the 2 extreme rainfall events on 29 May 2022

This phenomenon is known as slope-atmospheric interaction and often is neglected by the engineers during the design. The aim of this paper is to give one approach for including the rainfall impact on slope stability in the analyses.

2. Methodology, parameters and numerical analysis

The soil-atmospheric interaction is realized through the infiltration of rainwater that infiltrates to the unsaturated zone which increases the natural moisture content and the pore pressure, reduces the suction, thereby reducing the shear strength of the unsaturated soil and increases the risk of sliding.

The hydrostatic equilibrium in stationary flow in unsaturated soils deviates from that in saturated soils depending on whether the water moves down to the groundwater level (infiltration) or upwards (evaporation). In the case of completely saturated soils, that pore pressure is positive due to the absence of air in the pores. In most of the fine-grained soils with very small pores it is negative in case when the moisture is less than the full saturation [4].

In order to include the rainfall in the analysis, it is necessary to use transient coupled analysis which takes into account the mechanical and hydraulically soil behavior in a time-dependent analysis. This is also known as (fully) coupled flow-deformation analysis which can be done in many software based on finite element method [5].

To provide such analysis it is necessary to have precipitation data for the region and its probability of occurrence. Then we should select not only the mechanical model, but also the hydraulic model which can represent the soil behaviour. This can be represented by the relationship between soil suction and water content or saturation degree, so called soil water retention curve – SWRC and Suction-relative permeability relationship.

The rainfall intensity was determined from the previous hydrological analysis of the intensive rainfalls over the area of the Topolnica tailing dam, which is around 50km from the Gjurishte station [6]. After rainfall data series of monthly precipitation were formed, a relationship between the probability of occurrence of the maximum intensive rainfall was plotted in function of the amount of precipitation and characteristic durations, see Figure 5.

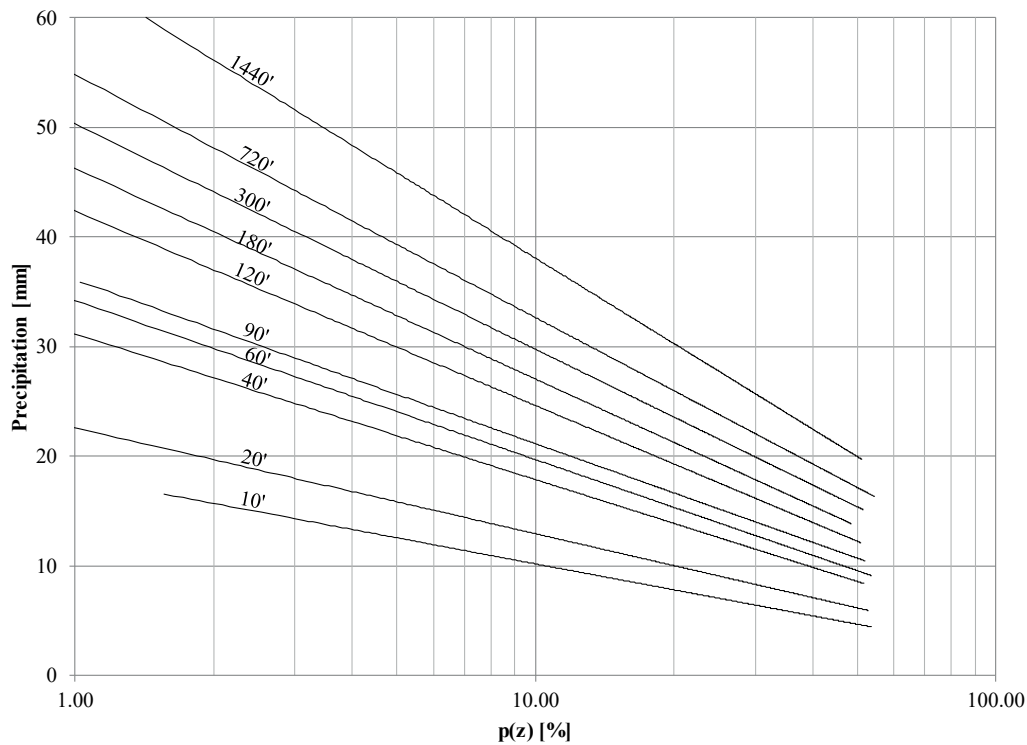


Figure 5. Probability distribution of monthly maximum rainfall data

Table 1. Monthly maximum rainfall [mm] for characteristic probabilities

p(z) [%]	T [months]	10'	20'	40'	60'	90'	120'	180'	300'	720'	1440'
50	2	4.51	5.91	8.09	9.19	10.32	11.76	13.05	14.55	16.55	19.29
20	5	8.10	10.78	14.61	15.83	17.58	20.02	22.10	24.50	26.97	32.06
10	10	11.34	13.33	18.60	21.38	22.45	27.13	29.94	32.89	33.61	38.64
4	25	13.62	17.22	25.68	28.78	29.49	33.89	35.84	39.55	45.83	52.16
2	50	15.72	20.05	28.58	31.25	31.84	38.28	44.09	49.38	52.94	57.47
1	100		22.45	30.02	34.05		43.90	49.45	54.29	56.49	

In this study we used sandy materials with properties given in Table 2.

Table 2. Soil parameters used in the analysis

Material type	Conditions	γ_{unsat} [kN/m ³]	e_{init} [/]	E_{oed} [kN/m ²]	ν [/]	c' [kPa]	φ' [°]	$k_x=k_y$ [m/s]
Sand	Drained	19.0	0.7	8000	0.3	2	28	1×10^{-3}

The mechanical behavior was simulated with Mohr-Coulomb failure criteria [7], while the Van Genuchten hydraulic model for soil behavior was used [8]. The data were taken from the Plaxis database so called Hypres [9]. Figure 6 shows the SWRC and the relationship between suction and relative permeability according to the selected soil type.

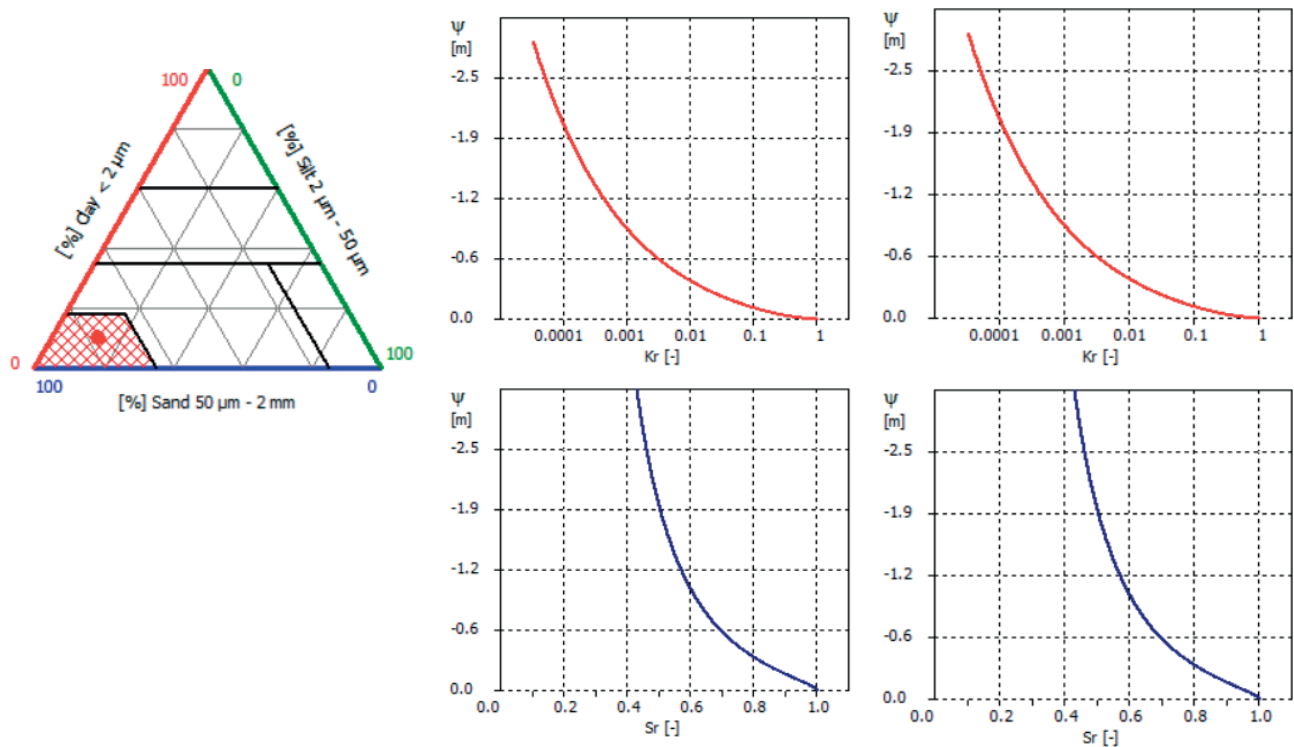


Figure 6. Soil classification and relationship between suction and relative permeability and saturation

Six slope stability analyses were made for different one-hour rainfall intensities and probability of occurrence given in Table 1. The numerical model geometry and boundary conditions (BC) are illustrated in Figure 7.

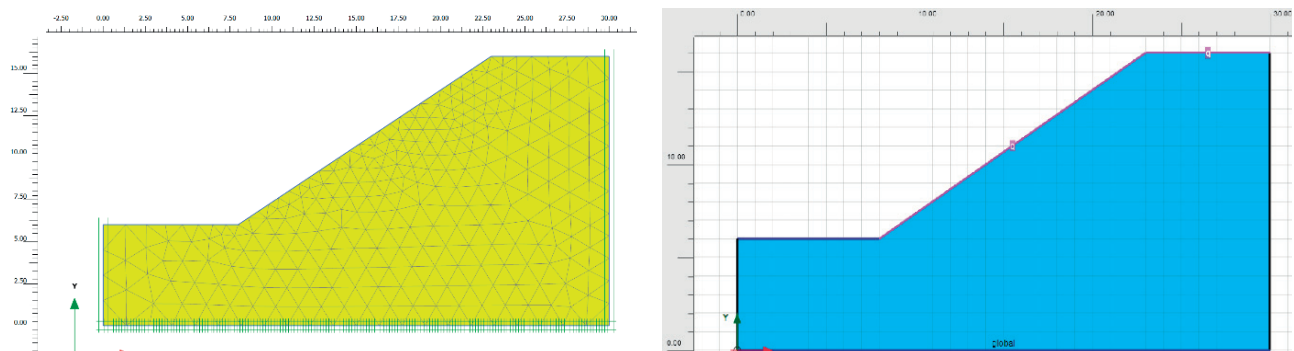


Figure 7. Numerical model geometry and boundary conditions

The slope is 10m height, and 1:2 slope angle. Normal/fully fixed BC was used for the left, right and the bottom side of the model, while infiltration BC were used for the slope crest and slope in order to allow infiltration from the rainfall.

3. Results and discussion

The results from the analyses are presented for the initial and the final phase (maximal rainfall intensity). The change of suction, saturation, deformations and presence of plastic points and points of tension are relevant for such analysis.

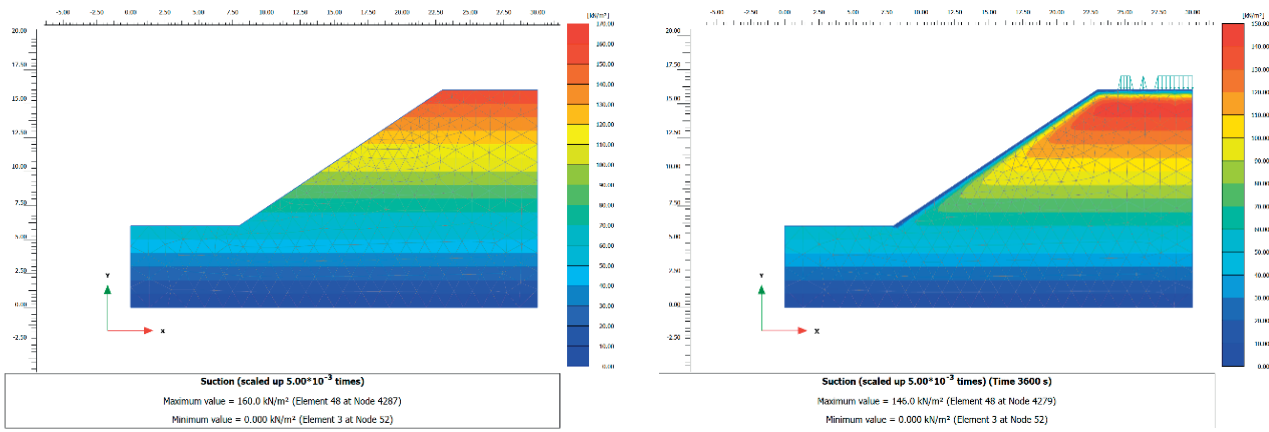


Figure 8. Suction changes in initial phase and after heavy rainfall with maximum intensity

The results show that the maximum suction in the initial phase is 160 kPa and occurs at the top of the slope as a negative pore pressure depending on the groundwater level, while after the rainfall event it decreases to 146 kPa at 2.0 m below the top of the slope. The greatest reduction of the suction occurs on the surface of the slope where the material is saturated due to rainfall influence and it is 0kPa.

The suction is related to the degree of saturation. Figure 9 presents the changes in the degree of saturation before and after the rainfall event.

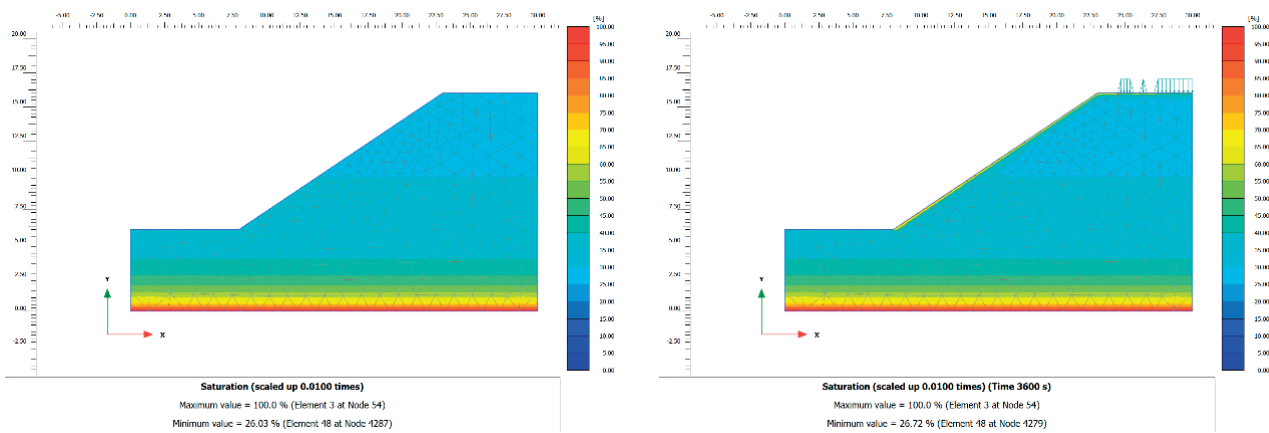


Figure 9. Saturation degree changes in initial phase and after heavy rainfall with maximum intensity

The changes begin immediately after the application of precipitation as a result of infiltration. The minimum degree of saturation occurs in the part where the suction is highest. As the infiltration increases, the unsaturated zone decreases and the surface layer is saturated. After the rainfall, the effect is up to a depth of 1.0 m, while the first 50 cm are completely saturated.

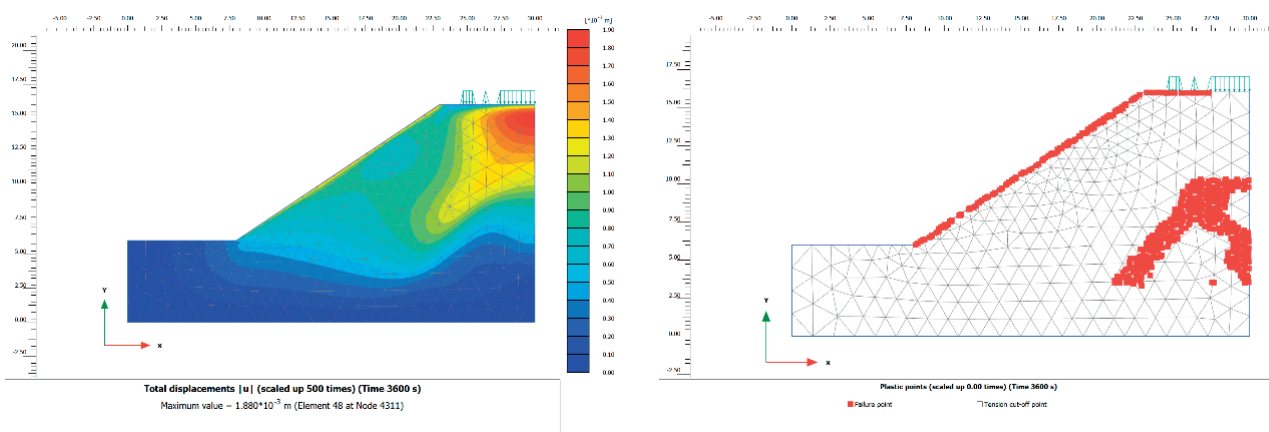


Figure 10. Deformation and plastic points after heavy rainfall with maximum intensity

The maximum deformation is 1.88 mm dominantly vertical inside the model and horizontal on the slope surface.

The results show that the saturation zone increases when the infiltration rate increases as a result of different rainfall intensity. The suction decreases as the rainfall intensity increases. The maximum saturation and suction changes were observed on the slope surface where the rainfall influence is the highest [10].

4. Conclusion

The aim of this paper was to give an overview of the slope stability problems and to introduce an advanced concept for numerical modelling including slope-atmospheric interaction.

The engineering experience show that the standard slope stability analysis is not enough and should include the slope-atmospheric interaction through coupled flow-deformation analysis to prevent slope instabilities due to extreme rainfall events.

The rainfall intensity used in this study was determined from the hydrological analysis of the intensive rainfalls over the area of the Topolnica tailing dam. After rainfall data series of monthly precipitation were formed, a relationship between the probability of occurrence of the maximum intensive rainfall was plotted in function of the amount of precipitation and characteristic durations.

The mechanical behavior was simulated with Mohr-Coulomb failure criteria, while the Van Genuchten hydraulic model for soil behavior was used. The data for SWRC and relationship between suction and relative permeability were taken from the Plaxis database so called Hypres.

The results show that the wetting front increases when the infiltration rate increases as a result of increased rainfall intensity. The suction profile also changes for different infiltrations. The maximum saturation and suction changes were observed on the slope surface and can be concluded that the rainfall has surface influence, but it is a repeating load and can cause intensive erosion, gullies and deeper cracks over time and finally a landslide.

References:

- [1] Susinov, B. & Josifovski, J., 2022. *Slope instability due to atmospheric impact*. Ohrid, Macedonian Association for Geotechnics, pp. 669–678.
- [2] www.meteologix.com, 30.06.2022.
- [3] www.uhmr.gov.mk, 30.06.2022.
- [4] Zhang, L. et al., 2018. *Rainfall-induced soil slope failure: stability analysis and probabilistic assessment*. 1 ed. s.l.:CRC Press
- [5] Susinov, B. & Josifovski, J., 2022. *Numerical modeling of slope instability due to intensive rainfalls*. Ohrid, Macedonian Association for Geotechnics, pp. 559–563.
- [6] Susinov, B., Josifovski, J. & Naumovski, M.: Hydrological analysis of high intensity rainfalls over Topolnica tailing dam. Skopje, Ss. Cyril and Methodius University, Civil Engineering Faculty – Skopje, 2019.
- [7] Bentley Communities, 2022. *PLAXIS Material Models Manual*, s.l.: Bentley Communities.
- [8] Van Genuchten, M.T.: A closed-form equation for predicting the hydraulic conductivity of unsaturated soils. 1. Soil science society of America journal, 44(5), pp. 892–898, 1980.
- [9] Galavi, V.: Groundwater flow, fully coupled flow deformation and undrained analyses in PLAXIS 2D and 3D, s.l.: Plaxis Report, 2010.
- [10] Fredlund, D.G., Rihardjo, H. & Fredlund, M.D., 2012. *Unsaturated Soil Mechanics in Engineering Practice*. Hoboken, NJ: John Wiley & Sons, Inc.